Physicochemical Problems of Mineral Processing

Volume 49, Issue 2

2013

Physicochemical Problems of Mineral Processing

Volume 49, Issue 2, July 1, 2013

Instructions for preparation of manuscripts

It is recommended that the following guidelines be followed by the authors of the manuscripts

- Original papers dealing with principles of mineral processing and papers on technological aspects of mineral processing will be published in the journal which appears twice a year (January 1 and July 1)
- The manuscript should be sent to the journal via manuscript management system (SORPA) available at www.ppmp.pwr.wroc.pl/sorpa
- The manuscript must be written in English
- Contributors whose native language is not English are urged to have their manuscript competently edited prior to submission
- The manuscript should not exceed 10 pages
- There is a 105 EUR fee for printing the paper. No fee is required for the authors participating in the Annual Symposium on Physicochemical Problems on Mineral Processing (Mineral Engineering Conference)
- Additional correspondence regarding the journal should be sent to either jan.drzymala@pwr.wroc.pl or przemyslaw.kowalczuk@pwr.wroc.pl.

CONTENTS

FLOTATION KINETICS AND SEPARATION SELECTIVITY OF COAL SIZE FRACTIONS

Yanfeng LI, Wenda ZHAO, Xiahui GUI, Xiaobo ZHANG

School of Chemical Engineering and Technology, China University of Mining and Technology, Xuzhou 221116, Jiangsu, China. E-Mail: lyf3344@126.com

Abstract: Flotation recovery and kinetics for three size fractions of coal were investigated. Flotation of combustible matter recovery was approximated with the first order kinetic equation while flotation of the ash forming minerals with the second order equation. Next, the equations for each size fraction were combined and a formula was obtained which was used for approximation of the experimental results using the so-called Fuerstenau upgrading curve, which relates the recovery of combustible matter recovery and recovery of ash forming minerals, both in concentrate. The Fuerstenau upgrading plot showed that the best selectivity was obtained for the middle size fraction of 0.25–0.075 mm, while the flotation selectivity of larger 0.5–0.25 mm and smaller –0.075 mm particles was diminished. This finding agrees with many other investigations.

Keywords: coal, flotation rate, combustible matter recovery, ash, particle size

Introduction

China is a country in which coal is the main energy source and in a very long period of time it will not change (Xu, 2003). The fine particle mineral processing technology has become one of the most important development directions in current field of mineral processing (Jameson, 2010; Albijanic et al., 2010; Bhattacharya and Dey, 2008). Flotation is the most widely used and effective method of separation of fine and very fine materials. The principle of flotation is based on different surface properties of mineral matter (Fan et al., 2010; William et al., 2010; Muganda et al., 2011). Very important aspect of flotation is its kinetics. The flotation rate is measured as the recovery change of the floating material in the flotation product per unit time and it is characterized by a rate constant and kinetics order (Vapur et al., 2010; Gui et al., 2011, Brozek and Mlynarczykowska, 2013). It is known that the coal particles of different sizes have different flotation rates. This has been confirmed with industrial data (Song et al., 2001).

Most flotation rate tests show that the fine coal particles can be described by the first order kinetic model and its rate constant changes with the increasing reagents dose (Chelgani et al., 2010; Abkhoshk et al., 2010; Ucurum and Bayat, 2007; Aktas et al., 2008; Brozek and Mlynarczykowska, 2007, 2013). The relationship between flotation rate constant and flotation recovery with particle size was found to be nonlinear (Abkhoshk et al., 2010). Particle size has also a great effect on the attachment/detachment of bubbles and particles (Ireland and Jameson, 2012).

It was shown recently by Drzymala and Luszczkiewicz (2011) as well as Bakalarz and Drzymala (2013) that having kinetics of flotation of the useful component of coal or ore and kinetics of the remaining components in the feed, it is possible directly produce the Fuerstenau upgrading plot. This is so because the Fuerstenau upgrading plot relates recovery of both components while the kinetic curves also relate both recoveries through the time of the process. The aim of this paper is to utilize this approach for coal by taking into account the kinetics of flotation of different size fractions present in ground coal.

Experimental

Analysis of coal sample

Table 1 provides the size composition of the coal sample. As the size becomes smaller, the ash content becomes greater. The ash content in the –0.045 mm size fraction was 30.36%. It is more than 5.60 percent points greater than the average ash content. The yield of dominant 0.25–0.125 mm size fraction is 43.56%.

Table 1. Size analysis data of coal sample

Size fraction, mm	Yield,%	Ash,%	Oversize		Undersize	
			Yield,%	Ash,%	Yield,%	Ash,%
0.50–0.25	21.47	23.25	21.47	23.25	100.00	25.31
0.25–0.125	43.56	23.73	65.03	23.57	78.53	25.88
0.125–0.075	13.97	26.73	79.00	24.13	34.97	28.55
0.075–0.045	11.10	29.22	90.10	24.76	21.00	29.76
–0.045	9.90	30.36	100.00	25.31	9.90	30.36
Total	100.00	25.31	–	–	–	–

From Table 2, one can see that the dominating density fraction of the investigated coal is 1.4–1.5 g/cm^3. Its yield is 37.93% with the ash content of 10.54%. The yield of the -1.5 g/cm^3 density fraction is 57.03% with the ash content of 9.04%. Data for other fractions are given in Table 2. The data show that there is significant amount of ash forming matter in the coal fractions.

Table 2. Density analysis of coal sample

Density, g/cm^3	Yield,%	ash,%	Float accumulation		Sediment accumulation		(Separation density±0.1)	
			Yield,%	ash	Yield,%	ash	Density, g/cm^3	Yield,%
−1.3	0.26	4.21	0.26	4.21	100.00	24.55	1.30	19.10
1.3–1.4	18.84	6.10	19.10	6.07	99.74	24.61	1.40	56.77
1.4–1.5	37.93	10.54	57.03	9.04	80.90	28.92	1.50	58.27
1.5–1.6	20.34	24.49	77.37	13.10	42.97	45.14	1.60	27.08
1.6–1.7	6.74	38.14	84.11	15.11	22.63	63.70	1.70	9.48
1.7–1.8	2.74	54.06	86.85	16.34	15.89	74.54	1.80	3.74
1.8–2.0	1.99	63.60	88.84	17.40	13.15	78.81	1.90	1.99
+2.0	11.16	81.52	100.00	24.55	11.16	81.52	–	–
Total	100.00	24.55	–	–	–	–	–	–

Experimental procedure

Coal was mixed with distilled water and stirred for 120 s. Next collector was added and stirred for 60 s. The foaming agent contact time was 10 s, and then flotation was initiated. The clean coal collection intervals were 30, 30, 60, 60, and 120 s. The total flotation time was 5 min. The obtained six flotation (cleaned coal) products were labeled as concentrates J1, J2, J3, J4, J5 and tailings T. The reagents dosage and other operational parameters were: 320 g/Mg of collector (kerosene), 110 g/Mg of foaming agent (2-octyl alcohol), flotation feed pulp mass concentration was 90 g/dm^3, air flow 0.37 m^3/min, and the stirring speed during flotation was 1800 rpm.

Results and discussion

The flotation kinetics of size fractions of the investigated coal (Table 3 and Fig. 1) can be expressed by the classical first order equation:

$$\varepsilon = \varepsilon_\infty (1 - e^{-k_1 t}) \tag{1}$$

where ε is the combustible matter recovery in concentrate, ε_∞ maximum combustible matter recovery in concentrate, t flotation time and k_1 is the first order kinetics constant. The values of ε_∞ and k_1 were determined with the Matlab software and they are presented in Table 4.

Table 3. Results of coal size fractions flotation

Products	Combustible matter recovery (%)			Ash content (%)		
	0.50–0.25	0.25–0.075	–0.075	0.50–0.250	0.25–0.075	–0.075
J1	79.64	67.87	62.23	10.58	11.05	10.78
J2	14.07	15.36	19.14	11.28	12.06	12.97
J3	1.82	8.60	10.25	13.99	12.48	15.20
J4	0.59	1.82	2.36	15.65	13.50	20.40
J5	0.74	1.93	1.14	44.30	25.26	28.38
T	3.14	4.42	4.88	84.88	83.47	80.75
Total	100.00	100.00	100.00	22.99	25.93	25.23

Figure 1 shows changes of the combustible matter recovery with time. The data were approximated with the first order kinetic equation (Eq. 1). It can be seen from Fig. 1 and Table 4 that the rate of flotation of the combustible matter increases with the particle size. This is so becuse the fine particles exhibit low collision efficiencies due to their low mass and inertial force while the coarse particles have a high degree of heterogeneity. The flotation rate of the 0.5–0.25 mm, 0.25–0.075 mm and –0.075 mm size fractions changes from fast to slow. This agrees with the results of other researchers (Brożek and Mlynarczykowska, 2013; Jameson, 2012; Polat et al., 1993; Gaudin et al., 1931).
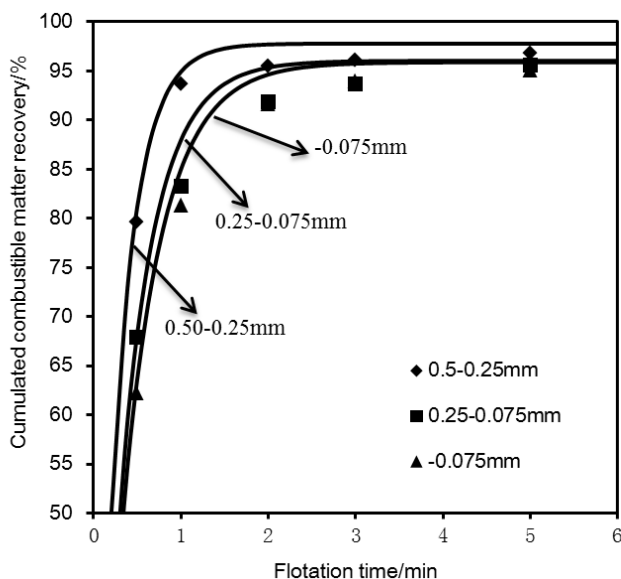
Fig. 1. Relationship between cumulated combustible
matter recovery for different size fractions of investigated coal and flotation time

In the case of the ash forming minerals flotation, the second order kinetic equation was used

$$\varepsilon_a = \frac{\varepsilon_{a\infty}^{2} k_2 t}{1 + \varepsilon_{a\infty} k_2 t} \qquad (2)$$

where ε_a is the ash matter recovery in the concentrate, $\varepsilon_{a\infty}$ maximum ash matter recovery in concentrate, t flotation time and k_2 is the second order kinetics constant. The values of $\varepsilon_{a\infty}$ and k_2 were determined with the Matlab software and they are presented in Table 4.

Table 4. Kinetics of flotation

Kinetic equation	Size fraction/mm	ε_{∞} or $\varepsilon_{a\infty}$	k_1 or k_2	Correlation coefficient
First order (combustible)	0.50–0.25	97.8	3.52	0.998
	0.25–0.075	96.0	2.47	0.988
	−0.075	95.9	2.17	0.998
Second order (ash)	0.50–0.25	41.7	0.16	0.972
	0.25–0.075	38.2	0.09	0.997
	−0.075	43.5	0.05	0.996

Figure 2 shows the change of ash recovery to concentrate and its approximation with the second order kinetic equation presented in Eq. 2. It can be seen from Fig. 2 and
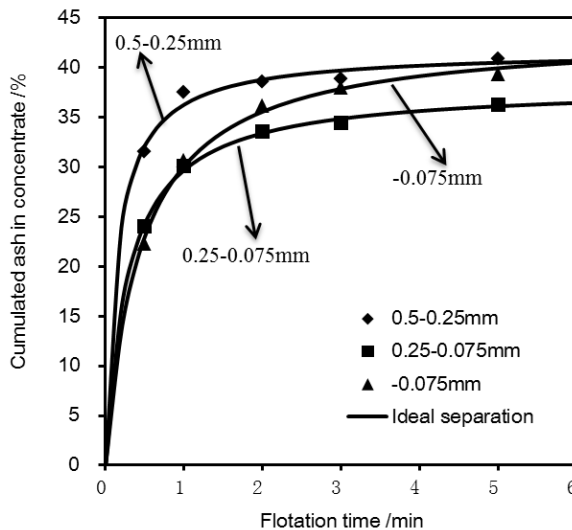
Fig. 2. Relationship between cumulated ash in concentrate
for different size fractions and flotation time

Table 4 that the rate of flotation of ash is different from that of combustible matter because the finest fraction floats better that the 0.25–0.075 mm size fraction and worse than the 0.5–0.25 mm size fraction. This can partly be explained by a combined effect of collision and attachment/detachment sub-processes, dominant for small and large sizes, respectively. The cleaned coal –0.075 mm particles has the most obvious change and the highest cumulated ash content due to a high content of ultrafine ash forming matter. This agrees with the results of other researchers (Brozek and Mlynarczykowska, 2013; Rahman et al., 2012; Vapur et al., 2010; Polat and Chander, 2000; Al Taweel et al., 1986).

As presented recently by Drzymala and Luszczkiewicz (2011) as well as Bakalarz and Drzymala (2013) the flotation kinetics, that is relations between recoveries and time can be combined providing the Fuerstenau upgrading curves (Drzymala and Ahmed, 2005; Drzymala, 2006) relating recovery of the combustible mater and recovery of ash in the concentrate. The Fuerstenau upgrading curves for the investigated size fractions are given in Fig. 3. The experimental points were approximated with the equation

$$\varepsilon = \varepsilon_\infty(1 - e^{\frac{-k_1\varepsilon_a}{\varepsilon_{a\infty}k_2(\varepsilon_{a\infty}-\varepsilon_a)}}) \tag{3}$$

resulting from Eqs 1 and 2 after removing time as the parameter. The obtained equations for each size fraction of the investigated coal are given in Table 5.

Table 5. Upgrading equations used for approximation of data points
of the Fuerstenau upgrading curve for each size fraction

Size fraction/mm	$\varepsilon - t$	$\varepsilon_a - t$	The derived $\varepsilon - \varepsilon_a$
kinetic equation	$\varepsilon = \varepsilon_\infty(1 - e^{-k_1 t})$	$\varepsilon_a = \dfrac{\varepsilon_{a\infty}{}^2 k_2 t}{1 + \varepsilon_{a\infty}k_2 t}$	
0.50–0.25	$\varepsilon_\infty = 97.79$, $k_1 = 3.52$	$\varepsilon_{a\infty} = 41.72$, $k_2 = 0.16$	$\varepsilon = \varepsilon_\infty(1 - e^{\frac{-k_1\varepsilon_a}{\varepsilon_{a\infty}k_2(\varepsilon_{a\infty}-\varepsilon_a)}})$
0.25–0.075	$\varepsilon_\infty = 96.04$, $k_1 = 2.47$	$\varepsilon_{a\infty} = 38.20$, $k_2 = 0.09$	
–0.075	$\varepsilon_\infty = 95.89$, $k_1 = 2.17$	$\varepsilon_{a\infty} = 43.53$, $k_2 = 0.05$	

Figure 3 indicates that the selectivity of flotation is the best for the middle size fraction while both smaller and larger size fractions have diminished selectivity. This observation agrees well with numerous flotation data. For each size fraction, the recovery of combustible matter in concentrate is greater than the recovery of ash in concentrate.
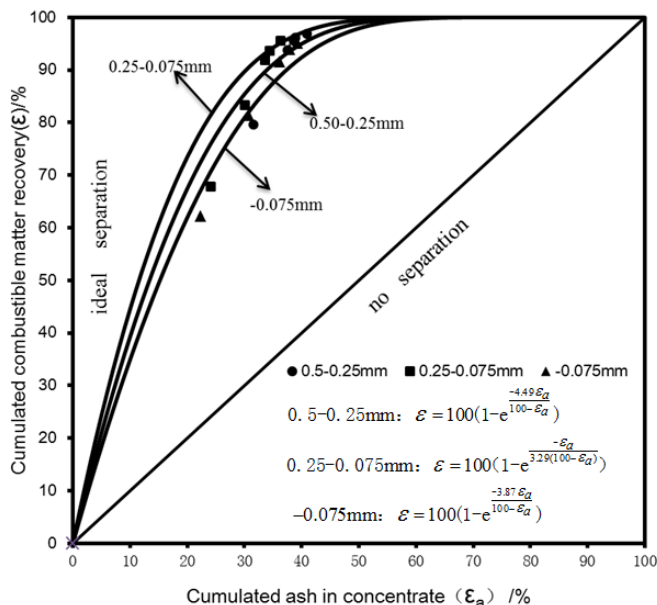
Fig. 3. The Fuerstenau upgrading curve
showing flotation results for different size fractions of investigated coal

Conclusions

According to the tests conducted for coal narrow size fractions, the flotation rate of the 0.5–0.25 mm, 0.25–0.075 mm and –0.075 mm size fractions changes from fast to slow. As the flotation proceeds, the cumulated combustible matter recovery gradually increases and reaches a plateau level at about 95%. The combustible matter recovery in concentrate can be approximated with the first order kinetic equation while the ash matter recovery in the concentrate can be approximated with the second order kinetic equation.

Combination of kinetic equations for combustible and ash matter provides an equation ($\varepsilon = \varepsilon_\infty (1 - e^{\frac{-k_1 \varepsilon_a}{\varepsilon_{a\infty} k_2 (\varepsilon_{a\infty} - \varepsilon_a)}})$) which can be used for approximation of the data points for each flotation size fraction in the recovery-recovery Fuerstenau upgrading curve. The Fuerstenau upgrading curves show that the best selectivity of separation occurs for the middle size fraction of coal.

Acknowledgments

References

ABKHOSHK E., KOR M., REZAI B., 2010. *A study on the effect of particle size on coal flotation kinetics using fuzzy logic*. Expert Systems with Applications, 37(7): 5201–5207.

AKTAS Z., CILLIERS J.J., BANFORD A.W., 2008. *Dynamic froth stability: Particle size, airflow rate and conditioning time effects*. International Journal of Mineral Processing, 87(1–2): 65–71.

AL TAWEEL, A.M., DELORY, B., WOZNICZEK, J., STEFANSKI, M., AN-DERSEN , N., HAMZA, H.A., 1986. *Influence of the surface characteristics of coal on its floatability*. Colloids Surf. 18(1), 9–18.

ALBIJANIC B, OZDEMIR O., NGUYEN A.V., BRADSHAW D., 2010. *A review of induction and attachment times of wetting thin films between air bubbles and particles and its relevance in the separation of particles by flotation*. Advances in colloid and interface science, 159 (1):1–21.

BAKALARZ A., DRZYMALA. J., 2013. *Interrelation of the Fuerstenaua upgrading curves with kinetics of separation*. Physicochemical Problems of Mineral Processing, 49(2), 443–451.

BHATTACHARYA S., DEY S. 2008. *Evaluation of frother performance in coal flotation: A critical review of existing methodologies*. Mineral Processing and Extractive Metallurgy Review, 29(4): 275–298.

BROZEK M., MLYNARCZYKOWSKA A., 2013. *Analysis of effect of particle size on batch flotation of coal,* Physicochemical Problems of Mineral Processing, 49(1): 341–356.

BROZEK M., MLYNARCZYKOWSKA A., 2007. *Analysis of kinetics models of batch flotation*. Physicochemical Problems of Mineral Processing, 41: 51–65.

BROZEK M., MLYNARCZYKOWSKA A., 2013. *An Analysis of Effect of Particle Size on Batch Flotation of Coal. Physicochem. Probl. Miner. Process.* 49(1), 2013, 341−356.

CHELGANI S.C., SHAHBAZI B., REZAI B., 2010. *Estimation of froth flotation recovery and collision probability based on operational parameters using an artificial neural network*. International Journal of Mineral Metallurgy and Materials, 17(5): 526–534.

DRZYMALA J., LUSZCZKIEWICZ A., *Zalety krzywej uzysk–uzysk (Fuerstenaua) do technologicznej analizy i oceny wzbogacania surowców*, Przeglad Gorniczy, 2011, 7/8, 122–128.

DRZYMALA, J., 2006. *Atlas of upgrading curves used in separation and mineral science and technology* . Physicochemical Problems of Mineral Processing, 40: 19–29.

DRZYMALA, J., AHMED, H.A. M., 2005. *Mathematical equations f or approximation of separation results using the Fuerstenau upgrading curves*. Int. J. Miner. Process. 76, 55–65.

FAN M., TAO D., HONAKER R. ET AL., 2010. *Nanobubble generation and its applications in froth flotation (part 2):fundamental study and theoretical analysis*. Mining Science and Technology, 20(2):159–176.

GAUDIN, A.M., GROH, J.O., HENDERSON, H.B., 1931. *Effects of particle size on flotation*. Am. Inst. Min. Metall. Eng., Tech. Publ. 414, 3–23.

GUI X., LIU J., TAO X., WANG, Y., CAO Y., 2011. *Studies on flotation rate of a hard-to-float fine coal*. Journal of China Coal Society, 36(11):1895–1900.(In Chinese)

IRELAND P.M., JAMESON G.J., 2012. *Drag force on a spherical particle moving through a foam: The role of wettability*. International journal of mineral processing, 102:78–88.

JAMESON G. J., 2012. *The Effect of Surface Liberation and Particle Size on Flotation Rate Constants. Minerals Engineering*, 36–38 (2012) 132–137.

JAMESON G.J., 2010. *Advances in Fine and Coarse Particle Flotation*. Canadian Metallurgical Quarterly, 49(4): 325–330.

MUGANDA S., ZANIN M., GRANO S.R., 2011. *Influence of particle size and contact angle on the flotation of chalcopyrite in a laboratory batch flotation cell* .International Journal of Mineral Processing, 98:150–162.

POLAT M., CHANDER, S., 2000. *First-Order Flotation Kinetics Models And Methods For Estimation Of The True Distribution Of Flotation Rate Constants*. INT. J. MINER. PROCESS. 58, 145–166

POLAT, M., ARNOLD, B., CHANDER, S., HOGG, R., ZHOU, R., 1993. *Coal flotation kinetics: Effect of particle size and specific gravity*. In: Parekh, B.K., Groppo, J.G. Eds. , Proc. and Util. of High Sulfur Coals V, Elsevier, 161–171.

RAHMAN R. M., ATA S., JAMESON G.J., 2012. *The effect of flotation variables on the recovery of different particle size fractions in the froth and the pulp*. International Journal of Mineral Processing 106–109 (2012) 70–77.

SONG B., ZHI Y., ZENG D., 2001. *The Investigate of Coal flotation optimal particle size*. Coal Processing and Comprehensive Utilization, 1:16–18. (In Chinese)

UCURUM M., BAYAT O., 2007. *Effects of operating variables on modified flotation parameters in the mineral separation*. Separation and Purification Technology, 55(2): 173–181.

VAPUR H., BAYAT O., UÇURUM M., 2010. *Coal flotation optimization using modified flotation parameters and combustible recovery in a Jameson cell*. Energy Conversion and Management 51, 1891–1897.

VAPUR H.; BAYAT O., UCURUM M., 2010. *Coal flotation optimization using modified flotation parameters and combustible recovery in a Jameson cell*. Energy Conversion and Management, 51(10): 1891–1897.

WILLIAM J.O., ORHAN O., ANH V.N., 2010. *Effect of mechanical and chemical clay removals by hydrocyclone and dispersants on coal flotation*. Minerals Engineering, 23:413–419.

XU Z. 2003. *Electro kinetic study of clay interactions with coal in flotation. International Journal of Mineral Processing*, 68: 183–196.

ANALYSIS OF LARGE PARTICLE SIZES USING A MACHINE VISION SYSTEM

Zelin ZHANG, Jianguo YANG, Xiaolan SU, Lihua DING

School of Chemical Engineering and Technology, China University of Mining and Technology, Xuzhou 221116, Jiangsu, China; zhangzelin3180@163.com; scetyjg@126.com.

Abstract: Many methods based on machine vision were used to estimate coarse particles size distribution in recent years, but comparison of accuracy parameters representing particle size has not been carried out and a related representing analysis has not been yet proposed. Nine parameters were investigated. The results indicated the minor axis of equivalent ellipse and breadth of the best-fit rectangle were the most suitable for representing particle size. The former accuracy ratio was 86.43% and the latter accuracy ratio was 85.39%, while the accuracy of other parameters was less than 70%. A related representing analysis was proposed to explain this phenomenon. This research is instructive and meaningful for the size distribution estimation by machine vision.

Keywords: machine vision, particle size distribution, equivalent ellipse, best-fit rectangle, representing analysis

Introduction

Particle size and size distribution are important variables in many industrial sectors (Tasdemir et al., 2011; Zhang et al., 2012), especially in mining and mineral processes. Most mineral processing operations rely on the size distributions measurement as a key factor in improving process efficiencies (Xia et al., 2012a; Xia et al., 2012b). Sieving has been used to measure particle size distribution traditionally, but it is very time-consuming and cannot be quick enough to provide real-time feedback information to direct production. So machine vision has been used for particle size measurement in the last twenty years.

Many problems such as the way of image acquisition, the algorithm of image segmentation, parameters of particle size and error correction of the system had all been extensively investigated in recent years. However, a comparison of all parameters in accuracy aspect has not been carried out and related representing analysis has not yet proposed. Authors argue that the size parameters extracted from images to represent

sieving particle size should satisfy two demands, i.e., be rotationally-invariant and have a selecting basis.

In image analysis, different ways of measuring particle size, such as equivalent circle diameter (Maerz et al., 1987; Mcdermott et al., 1989; Grannes et al., 1986; Donald and Kettunen, 1996; Maerz et al., 1996; Rholl et al., 1993), maximum size (Montoro et al., 1993; Ord et al., 1989; Kemeny et al., 1994), size of equivalent ellipse (Girdner et al., 1996; Schleifer et al., 1993), Ferret diameter (Kwan et al., 1999; Mora et al., 1998; Mora et al., 2000; Al-Thyabat et al., 2006; Al-Thyabat et al., 2007) and best-fit rectangle (Wang, 2006; Tobias et al., 2012) have been used. All the above parameters are rotationally-invariant, but are optionally selected to estimate size distribution with no representing analysis and selecting basis.

In this paper, 467 coal particles in four size fractions were selected through a strict screening to compare the accuracy of the above mentioned parameters, and a representing analysis combined with a screening principle was proposed to explain the results.

Experiments

Sample preparation

The experiment sample was anthracitic coal from the Tai-Xi coal preparation plant in China. Basically, the sieving operation attempts to divide the coal sample into fractions, each consisting of particles within specific size limits. In China's coal cleaning standards, the mesh apertures are 100, 50, 25, 13, 6, 3, 0.5 mm. When necessary, the mesh apertures can increase or decrease, so a series of sieves with square apertures 3, 6, 13, 25, 50 mm were used in our experiment. As to the coal particles smaller than 3 mm, the outline accuracy by digital image processing is low, and the particles greater than 50 mm are not suitable for experiment and test. For the reasons given above, the particles smaller than 3 mm and greater than 50 mm were discarded. 120 particles (3–6 mm), 146 particles (6–13 mm), 109 particles (13–25 mm) and 92 particles (25–50 mm) were selected to accomplish this research.

Image acquisition and parameters calculation

A high quality picture of the coal particles is needed before any digital image processing is performed. Some researchers noted the shadows cast by the objects, and the interior texture could be confusing to edge detection algorithms (Wang, 2006; Guyot et al., 2004; Casali et al., 2001). A backlit system, shown in Fig. 1A, was built to eliminate these problems. This system was designed as a closed box for avoiding the outside light effect. Digital camera (Nikon S220) was put in the camera hole of this system, and we fixed the height from the hole to the platform as 41.5 cm, just right above of the sample platform. Four fluorescent lamps (TCL 8W) were set equidistantly under the sample platform. Figure 1B is an image of one coal particle taken in the normal daylight, and Fig. 1C is an image of the same coal particle taken in the

backlit system. It is obvious that the image taken in the backlit system can eliminate the shadow and the interior texture, which provide a good basis for extracting features accurately.
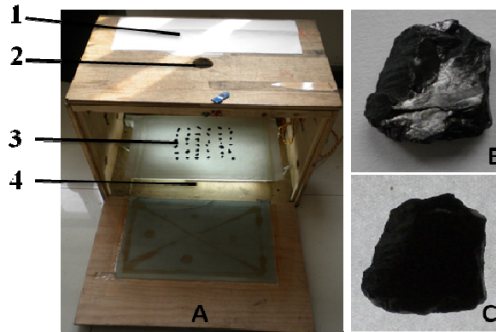
Fig. 1. A – backlit system, B – image of one coal particle taken in normal daylight,
C – image of the same coal particle taken in backlit system; 1 – closed box,
2 – camera hole, 3 – sample platform, 4 – lights

The pixel size of the captured image is 1024×768. The image from Fig. 2 (A) was used to measure the shooting coverage and the conversion ratio between pixel size and actual size. The shooting coverage is 366 mm×274.5 mm, and one pixel is approximately equal to 0.357 mm. When the coal particles are placed on the sample platform, they are carefully spread out, making certain that they are in the stable position and without touching or overlapping each other to insure the accurate edge extraction. Figure 2 (B) is a gray histogram of the image after removing the ruler seen in Fig. 2 (A). The optimal threshold was determined manually as 50 for the twin-peaks method. Sometimes there will be several dirty spots or dust on the platform. In this case the area threshold will be used to remove these isolated micro-regions and filling processes will be used to fill the interior of particles completely. Through the above image processes, all our images can be segmented accurately, like in Fig. 2(C). In this part, some researchers used some methods to segment images, like filtering, dilating, eroding, top-hat, bottom-hat and watershed and so on (Al-Thyabat et al., 2007; Banta et al., 2003). Many morphological processes will cause an inaccurate outline of particles because the regions handled by structure elements chosen in these operations may be changed, especially during dilating and eroding processes. So, we used in our experiments no touching particles and the simple but credible segmentation method to insure the experiment precision.

Nine parameters were investigated. A sketch map of parameters which are easy to express were shown in Fig. 2(D):

D_A – equivalent circle diameter: the circle area is equal to the target area,
D_{max} – maximum size: the maximum distance between two pixels on the perimeter,
D_{major} – major axis of equivalent ellipse: the length of the major axis of the ellipse that has the same normalized second central moments as the target region,

D_{minor} – minor axis of equivalent ellipse: the length of the minor axis of the ellipse that has the same normalized second central moments as the target region,

D_{mean1} – the average of d_{major} and d_{minor},

D_F – Ferret's diameter: the mean value of distances cross the centroid between two parallel tangents which are on opposite sides of the target region in 0°, 45°, 90° and 135°,

D_B – the breadth of best-fit rectangle of target region. The method of best-fit rectangle is a combination of the Ferret method and the least 2nd moments minimization, requiring only calculation of the three moments about the center of gravity, and maximum and minimum co-ordinates in a co-ordinate system oriented in the direction of the axis of the least 2nd moments, and a simple area ratio (Weixing, 2006),

D_L – the length of best-fit rectangle of target region,

D_{mean2} – the average of dB and dL.
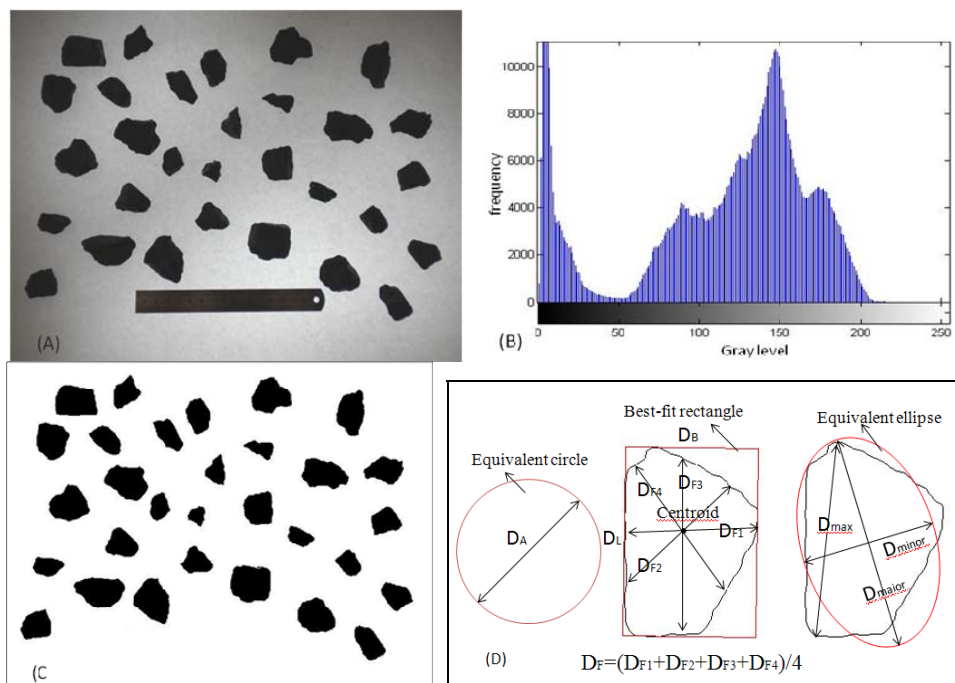
Fig. 2. Image acquisition and processing: (A) coal particles image taken in the backlit system, (B) gray histogram of image after removing ruler in the image (A), (C) binary of image (B) processed by twin-peaks method and removing isolated points, (D) sketch map of D_A, D_F, D_B, D_L, D_{max}, D_{major} and D_{minor}

In order to test and verify the accuracy of this image technique, the length and breadth of best-fit rectangle were used to carry out the comparison. A vernier caliper, minimum range of which is 0.02 mm, was used to measure the actual length and breadth of best-fit rectangle according to the rectangular position after image proc-

esses, like Fig. 3A. Figures 3B and 3C show the actual measurement of breadth and length of one coal particle. Twelve coal particles, three in each size fraction, were chosen randomly to test and verify the accuracy using the above method, and the results were shown in Table 1. The average and variance of absolute value of errors were 0.23 mm and 0.03 mm^2, respectively, indicating that the difference between actual size and estimated size is small. Furthermore, the T-test was used to verify whether the average error is zero. The significance level α is determined as 0.05. The T-value and p-value are 0.4934 and 0.6264, respectively, indicating that the average error can be considered as zero in the above significance level, that is, the errors' fluctuation is normal. All the results show that the accuracy of this image analysis is high and satisfied.
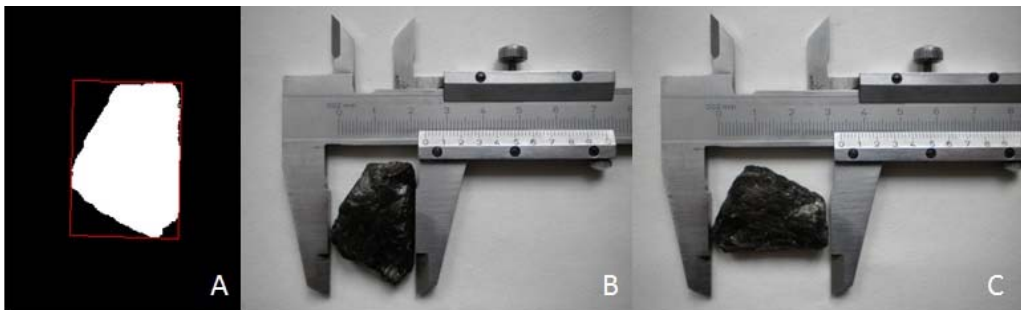
Fig. 3. A. The best-fit rectangle of one coal particle, B. Measuring the actual breadth of this particle best-fit rectangle, C. Measuring actual length of this particle best-fit rectangle, according to the rectangular position of image A

Table 1. Accuracy test of breadth and length of best-fit rectangle by image technique according to actual measurement by vernier caliper

Num	Length of best-fit rectangle, mm			Breadth of best-fit rectangle, mm		
	Actual	Estimation	Error	Actual	Estimation	Error
1	5.10	5.12	−0.02	3.30	3.59	−0.29
2	5.26	5.06	0.2	3.16	3.36	−0.2
3	4.56	4.32	0.24	4.08	3.95	0.13
4	6.58	6.21	0.37	6.00	5.81	0.19
5	10.36	9.95	0.41	8.04	7.88	0.16
6	7.96	7.86	0.1	6.20	5.91	0.29
7	14.02	14.09	−0.07	6.70	6.81	−0.11
8	21.10	21.08	0.02	20.20	20.43	−0.23
9	20.66	20.49	0.17	18.80	18.67	0.13
10	28.54	28.53	0.01	24.40	23.78	0.62
11	33.24	33.17	0.07	23.10	23.54	−0.44
12	44.06	44.51	−0.45	33.30	33.89	−0.59
Average of absolute value of errors, mm	0.23		Variance of absolute value of errors, mm^2		0.03	
t-value	0.4934		p-value		0.6264	

Results and discussion

Totally 467 coal particles in four size fractions were selected through strictly screening to compare the accuracy of the investigated nine parameters. The accuracy ratio of each parameter in each size fraction was calculated as follows:

$$\text{Accuracy ratio} = \frac{\text{Correct number}}{\text{Total number}} \times 100\% . \tag{1}$$

The results shown in Fig. 4 indicate that D_{minor} and D_B were more suitable to represent the real particle size. The mean value of D_B accuracy ratio is 86.43%, and the mean value of D_{minor} accuracy ratio is 85.39%. The others were no more than 70%.

Particle is a 3-D object having length, width and thickness. D_{minor} and D_B were like the width of particles. Width must be smaller than the length. Weixing (2006) indicated that the particle width distribution curve is between the length and thickness curves. Authors verified this phenomenon previously. The real thicknesses of 496 particles were calculated by their real mass, real density and projected area. The width is instead of the breadth of the best-fit rectangle because it is near the real width. Figure 5 shows the results of comparing the real thickness and the breadth of the best-fit rectangle, indicating most particles' thickness are smaller than the width.

In the process of on-line analysis, particles are constantly shaking on the belt, so most particles stand on the stable side, i.e. sit on the biggest bottom area of particle. Of course the collision between particles will also affect the particle standing way. In the laboratory, particles lie mostly on the biggest bottom area, so length and width of the projected area are almost bigger than particle thickness. Thus:

$$\text{Thickness} \leq \text{Width} \leq \text{Length}.$$

When particles pass through a screen hole, according to the screening principle, there are two sizes smaller than the size of the screen hole. Therefore, the width of the particle determines whether this particle can pass through the screen hole. The values of D_{minor} and D_B are near the width of particles, so they are accurate for the analysis.

Conclusion

A set of 496 particles was selected from four size fractions by accurate sieving to compare the accuracy of representing the particle size by nine parameters. Results indicated the D_{minor} and D_B were the most suitable to represent the real particle size. The mean value of D_B accuracy ratio was 86.43%, and the mean value of D_{minor} accuracy ratio was 85.39%. The mean values of others parameters were no greater than 70%. The representing analysis combined with screening principle was proposed to
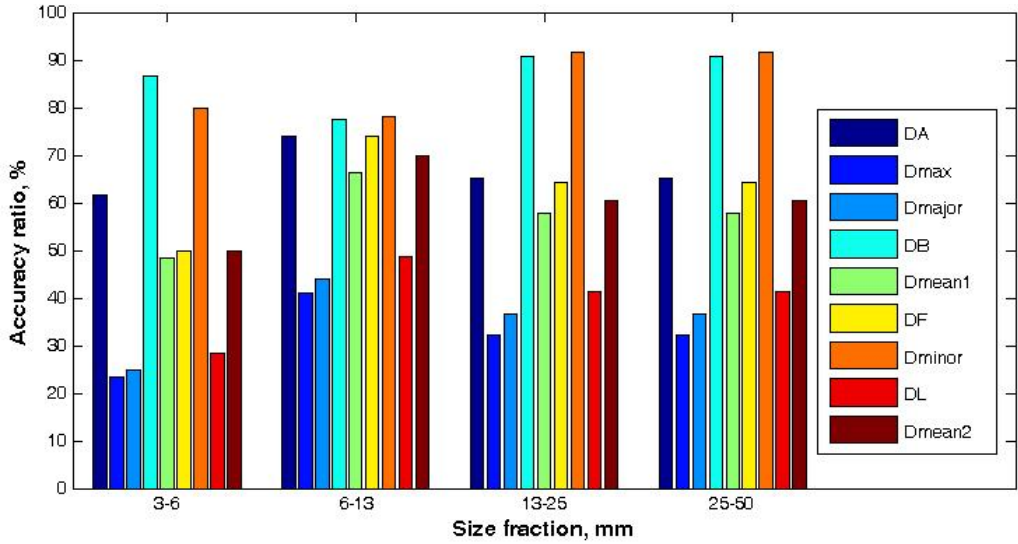
Fig. 4. A comparison of the accuracy of nine parameters in each size fraction
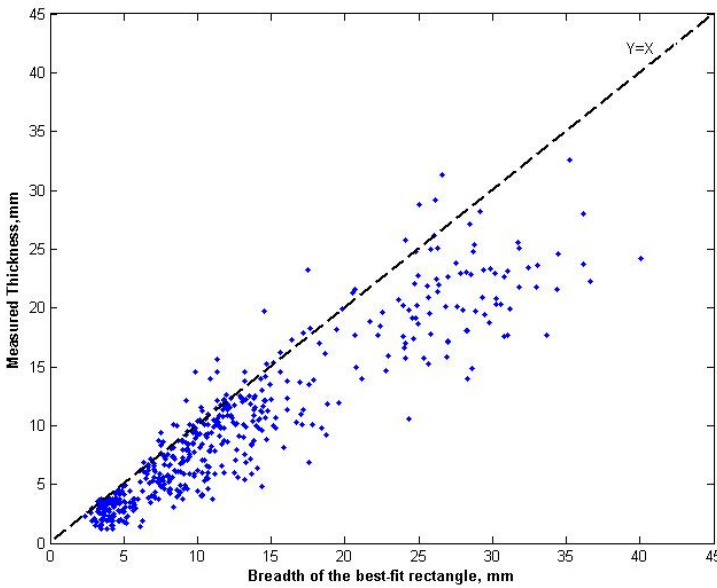
Fig. 5. Real thickness vs. breadth of the best-fit rectangle for the 496-particle sample

explain the results. This research is instructive and meaningful for the size distribution estimation by a machine vision system, especially for the coarse coal particles, based on which the on-line analysis for size distribution can be improved.

Acknowledgments

References

AL-THYABAT S., MILES N.J., 2006. *An improved estimation of size distribution from particle profile measurements*. Powder Technology, 166, 152–160.

AL-THYABAT S., MILES N.J., KOH T.S., 2007. *Estimation of the size distribution of particles moving on a conveyor belt*. Minerals Engineering, 20, 72–83.

BANTA L., CHENG K., ZANIEWSKI J., 2003. *Estimation of limestone particle mass from 2D images*, Powder Technology, 132, 184–189.

CASALI A., GONZALEZ G., VALLEBUON G., PEREZ C., VARGAS R., 2001. *Grindability Softsensors based on Lithological Composition and On-Line Measurements*. Minerals Engineering, 14, 689-700.

DONALD C., KETTUNEN B.E., 1996. *On-line size analysis for the measurement of blast fragmentation*. In: J.A. Franklin, T. Katsabanis (Eds.), *Measurement of Blast Fragmentation*, Rotterdam, Balkema, 175–177.

GIRDNER K.K., KEMENY J.M., SRIKANT A., MCGILL R., 1996. *The split system for analyzing the size distribution of fragmented rock*. In: J.A. Franklin, T. Katsabanis (Eds.), *Measurement of Blast Fragmentation*, Rotterdam, Balkema, 101–108.

GRANNES S.G., 1986. *Determine size distribution of moving pellets by computer image processing*. In: R.V. Ramani (Ed.), *Proceedings of the 19th Application of Computers and Operations Research in Mineral Industry*, Soc. Mining Engineers, Inc., 545–551.

GUYOT O., MONREDON T., LAROSA D., BROUSSAUD A., 2004. *VisioRock, an Integrated Vision Technology for Advanced Control of Comminution Circuits*. Minerals Engineering, 17, 1227-1235.

KEMENY J., 1994. *A practical technique for determining the size distribution of blasted benches, waste dumps, and heap-leach sites*. Mining Engineering, 46, 1281–1284.

KWAN A.K.H., MORA C.F., CHAN H.C., 1999. *Particle shape analysis of coarse aggregate using digital image processing*. Cement and Concrete Research, 29 (9), 1403–1410.

MAERZ N.H., FRANKLIN J.A., ROTHENBURG L., COURSEN D.L., 1987. *Measurement of Rock Fragmentation by Digital Photoanalysis*. 5th. Int. Cong. Int. Soc. Rock Mech., 1, 687–692.

MAERZ N.H., PALANGIO T.C., FRANKLIN J.A., 1996. *WipFrag image based granulometry system*. In: J.A. Franklin, T. Katsabanis (Eds.), *Measurement of Blast Fragmentation*, Rotterdam, Balkema, 91–99.

MCDERMOTT C., HUNTER G.C., MILES N.J., 1989. *The application of image analysis to the measurement of blast fragmentation*. Proceedings of the Surface Mining – Future Concepts, Nottingham University, Marylebone Press, Manchester, 103–108.

MORA C.F., KWAN A.K.H., CHAN H.C., 1998. *Particle Size Distribution Analysis Of Coarse Aggregate Using Digital Image Processing*. Cement and Concrete Research, 28, 921–932.

MORA C.F., KWAN A.K.H., 2000. *Sphericity, shape factor, and convexity measurement of coarse aggregate for concrete using digital image processing*. Cement and Concrete Research, 30, 351–358.

MONTORO J.J., GONZALEZ E., 1993. *New analytical techniques to evaluate fragmentation based on image analysis by computer methods*. Proceedings of the 4th Int. Symposium Rock Fragmentation by Blasting, Vienna, Austria, 309–316.

ORD A., 1989. *Real time image analysis of size and shape distributions of rock fragments*. Proc. Aust. Int. Min. Metall, 294, 28.

RHOLL S.A., 1993. *Photographic assessment of the fragmentation distribution of rock quarry muckpiles*. Proceedings of the 4th Int. Symposium Rock Fragmentation by Blasting, Vienna, Austria, 501–506.

TASDEMIR A., OZDAG H., ONAL G., 2011. *Image analysis of narrow size fractions obtained by sieve analysis. An evaluation by log-normal distribution and shape factors*. Physicochemical Problems of Mineral Processing, 46, 95–106.

TOBIAS A., THURLEY M.J., CARLSON J.E., 2012. *A machine vision system for estimation of size distributions by weight of limestone particles*. Minerals Engineering, 25, 38–46.

WANG, W.X., 2006. *Image analysis of particles by modified Ferret method – best-fit rectangle*. Powder Technology, 165, 1–10.

XIA W., YANG J., ZHAO Y., ZHU B., WANG Y. 2012a, Improving floatability of taixi anthracite coal of mild oxidation by grinding. Physicochem. Probl. Miner. Process. 48 (2), 393–401.

XIA W., YANG J., ZHU B., 2012b. Flotation of oxidized coal dry-ground with collector. Powder Technology, 228, 324–326.

ZHANG Z.L., YANG J.G., DING L.H., ZHAO Y.M., 2012. An improved estimation of coal particle mass using image analysis. doi:10.1016/j.powtec.2012.06.027.

SELECTED MINERAL MATERIALS GRINDING RATE AND ITS EFFECT ON PRODUCT GRANULOMETRIC COMPOSITION

Tomasz P. OLEJNIK

Faculty of Process and Environmental Engineering, University of Technology Lodz, Wolczanska 213, 90-924 Lodz, tomasz.olejnik@p.lodz.pl

Abstract: The article presents investigation on the grinding rate constant. A selection function was measured for different raw materials using a ball mill, and effects of the grinding ball diameter and feed particle sizes on the materials grinding rate constant were investigated. The study was conducted for the mill on a semi-technical scale. The process was carried out periodically using several sets of grinding media. Relations for all investigated materials were expressed by the modified Snow equation. Additionally, the descriptions of the grinding rate was examined. The tendency in the variation of the grinding rate constant with the particle size was similar for all materials used, and was independent of the ball diameter. The author used two selection functions derived theoretically by Tanaka.

Introduction

The industry producing ceramic materials most often uses milling devices, operating principle of which is based on the energy of free grinding media in order to grind the feed. The simplest constructional solution is ball mill with steel or alubit grinding media. Material particles grinding in mills of this type takes place mainly between grinding elements and to a much lesser extent between grinding media and the internal surface of the drum. Ground material particles which are between moving surfaces of the adjacent balls (this movement can result from both progressive and rotary ball motion) are mainly abraded and sheared with a possibility of the crushing mechanism participation. With a cataract ball motion (very desirable in ball mills) there will also occur an impact mechanism of the balls falling down. The ball size and related to it their number also have effect on the contribution of grinding mechanisms. It is obvious that at the same volume of the bed of balls (and at the same time the degree of

filling the drum with balls) the larger are the balls, the smaller will be the number of balls. Larger balls means larger mass of a single ball and higher forces of their mutual interaction. The smaller number of balls related to this means smaller number of contact points, thus reducing mini-areas in which at any given time loads damaging the ground material particles may occur.

Selection of balls diameter depends on the ground material strength as well as the diameter of raw material particles. Generally, for larger particles, which require higher forces to be damaged, larger balls should be used, while in the case of smaller particles (materials weak in strength) better results are obtained by increasing the number of balls' contact points, i.e. by increasing their number at the expense of diameter.

The simplicity of the mill construction is not accompanied by the effectiveness of the grinding process. The low efficiency of the grinding process, caused by the grinding media energy dissipation, forces process engineers to search for such a ball composition for which the decrease of the mean particle dimension is the fastest. This will provide an opportunity to use the operation time of the mill more efficiently.

For many years, the grinding process in ball mills is the subject of statistical analyses and description of kinetics (Epstein 1948; Herbst and Fuerstenau 1968). During grinding in batch ball mills, the mass flow between the separate size classes is analyzed. The selection function, describing the probability of particle grinding, and grinding function, describing the size distribution of raw material ground particles, among others are used for the description of this phenomenon. The mentioned functions enable the description of mass balance for particle size classes by means of an expression (Gaudin and Meloy 1962; Reid 1965):

$$\frac{dm_i(t)}{dt} = -S_i m_i(t) + \sum_{\substack{j=1 \\ j<i}}^{i-1} b_{i,j} S_j m_j(t), \quad i = 1,2,\ldots n, \tag{1}$$

where $m_i(t)$ is the mass of particle fractions from the size range i, S_i is the selection function, $b_{i,j}$ is the rate in which the feed particles from the size range j become particles from the size range i, while t is grinding time. Additionally, it is assumed that in the case of the first size class (particles with the largest size), that is for $i = 1$, the rate of decreasing of this class can be described by the following first order equation:

$$\frac{dm_1(t)}{dt} = -S_1 m_1(t). \tag{2}$$

The form of the selection function S_1 was determined and analyzed by many researchers for ball mills differing in construction, process and equipment conditions, including Kelsall et al. (1968), Austin et al. (1976), Kanda et al. (1978), Zhao and Jimbo (1988), Nomura et al. (1991) or Olejnik (2012). Despite this, the issues of efficiency and rate of the feed comminution process continue to arouse interest. Also

Obraniak and Gluba (2012) used the general form of equation (1) for the description of the granular material granulation rate.

Equation (2) shows that the feed particles disappearance rate decreases. Disappearance in time of the largest feed particles $m_l(t)$ can be described by a dependence:

$$-\frac{dR}{dt} = K_1 R \qquad (3)$$

where R is the mass of the feed contained in the largest size fraction, while K_l corresponds to the constant value of the grinding rate (selection function S_l) for the largest size fraction of particles.

Aim of the study

The author's earlier publications pointed to the dependence between the rate of grinding, the value of partition function and the selection function for batch grinding in a ball mill for variable process parameters. Studies were conducted in a limited range and the obtained results were encouraging enough to undertake further studies and analyses of the process kinetics, with particular emphasis on the rate of grinding the largest particle size fractions (Olejnik 2010, 2011).

Experimental studies

Three rock materials were used for the studies they were: granite, quartzite and graywacke. The value of the batch density and hardness according to the Mohs scale is included in Table 1.

Table 1. Bulk density and mineral hardness

Raw material	Density, $kg \cdot m^{-3}$	Mohs hardness
Granite	1402	6
Quartzite	2315	7
Greywacke	1267	5

Mineral raw materials used in the studies were characterized by various of flexibilities and grindabilities initially were crushed to a give particle size in the range of 5÷8 mm.

Granite is a solid, acidic magma-deep rock, medium or thickly-crystalline of overtly-crystalline structure distinguished by clear symmetry planes, usually in three orthogonal directions (Cappell and White 2001). The bulk density of granite was determined after a free drop and after 10 minutes of shaking of the measurement

sample. The bulk density was, equal to 1394 kg/m^3 and 1410 kg/m^3, respectively, and its average value was equal to 1402 kg/m^3.

   Cambrian sedimentary quartzite was from the Swietokrzyskie Mountains. Majority of the sedimentary quartzite consisted of closely adherent particles bound by silica. Bulk density was, respectively, equal to 1236 kg/m^3 and 1298 kg/m^3, and its average value was equal to 1267 kg/m^3.

   Greywacke is a sedimentary elastic multi-component rock rich in chippings of various finely crystalline rocks (above 25% of dendrite material). Granite is a lithic, acidic, magmatic-intrusive rock, medium or thickly crystalline rock of clearly crystalline structure displaying a visible joint in three perpendicular directions. Greywacke bulk density average value was equal to 1267 kg/m^3.

   The comminution was conducted in a dry mode. The milling kinetics tests were carried out in a semi-technical mill. The internal diameter of the mill's chamber was 0.5 m, whereas its total capacity 0.112 m^3. The mill's rotational frequency was constant and amounted to 0.517 s^{-1}, which constituted 54% of its critical rotational frequency. Filling of the mill (grinding media and feed) was determined for circa 35% of mill capacity. The process of milling was conducted in a periodical mode using balls of different diameters. Ball sets, differing in diameters, are presented in Table 2. Total mass of balls applied for milling was about 40 kg. Feed sampling was performed every 20 minutes, collecting mass of about 0.6 kg for the particle size analysis. The samples were subjected to a particle size analysis using a laser particle size analyzer Analysette 22 (FRITSCH). The analysis of the shape of particles and granulometric composition was carried out with the analyser AWK 3D made by Kamika Instruments. The results of analyses allowed to determine the granulometric composition of the milled material in particular moments of comminution. The particles' shape was determined using the classification according to Zingg (1935).

Table 2. Ball specification for particular compositions

Series	A	B	C	D
Ball diameter, mm		Ball mass, kg		
10	–	6	1	–
20	–	12.3	12.5	11
30	–	12.3	12.5	15
40	–	10	15	15
60	40	–	–	–
Sum	40	40.6	41	41

Results and discussion

In diagrams (Figs 1–4), a dependence between the mass of the fraction of the feed, found on a sieve with the largest size of 3 mm and grinding time for four measurement series, differing in ball composition, is presented. They show almost a linear

dependence in a semi-logarithmic system between the particle composition with the largest size class and grinding time. Therefore, it is possible to determine constant K_l from Eq. 3. The course of curves variation points to the influence of K_l value on the percentage of the feed particles in the largest size fraction. Austin et al. (1976) and Zaho and Jimbo (1988) proposed the following equation to express the relationship between the change in $K_l = S_l$ and the size of the feed particles:

$$S_1 = ax_f^\alpha Q(z) = ax_f^\alpha Q\left(\frac{\ln\left(x_f/\mu\right)}{\ln\sigma}\right)$$

(4)

where a and α are constants. $Q(z)$ is a Gaussian distribution function, x_f describes the value of the feed particles size while z is a dimensionless parameter. The feed particles size for $Q(z) = 0.5$ was labeled with μ, while $\ln \sigma$ determines the standard deviation.
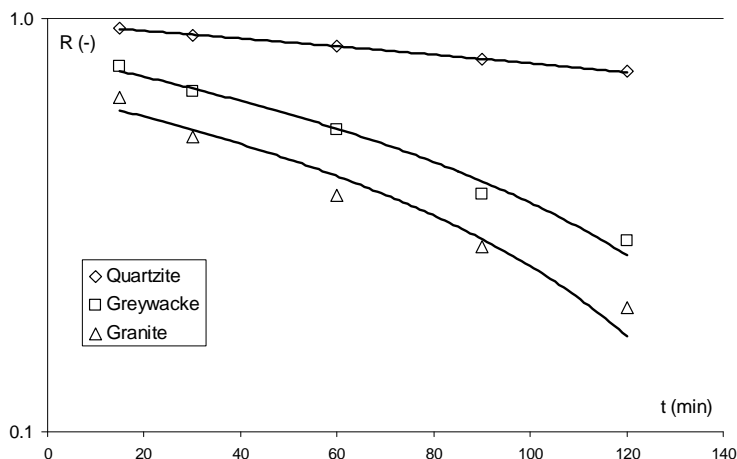
Fig. 1. Dependence between mass of the largest feed particle fraction and grinding time. Ball composition *A*

From the studies of Austin et al. (1976) and Zhao and Jimbo (1988) it resulted that dependence (4) can be used for describing grinding of very fine particles. For big particles (Eq. 4) was not applicable. Snow (1973) citing data of Kelsall et al. (1968) proposed that the dependence between S_l and the feed size can be described by Eq. (5)

$$\frac{S_1}{S_m} = \left(\frac{x_f}{x_m}\right)^\alpha \exp\left(-\frac{x_f}{x_m}\right)$$

(5)

where x_m is the feed size, at which S_1 reaches the maximum value of S_m.

412 T.P. Olejnik

Using the concept of Austin et al. (1976) and assuming that for the feed, equality holds between the constant of grinding, determined from equation Eq. 3, and S_1 for each composition of balls and ground raw materials, the constant of grinding rate was determined.
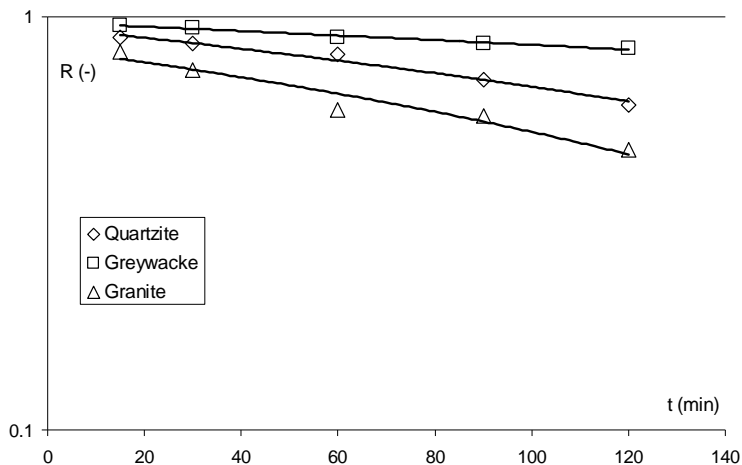
Fig. 2. Dependence between mass of the largest feed particle fraction
and grinding time. Ball composition *B*
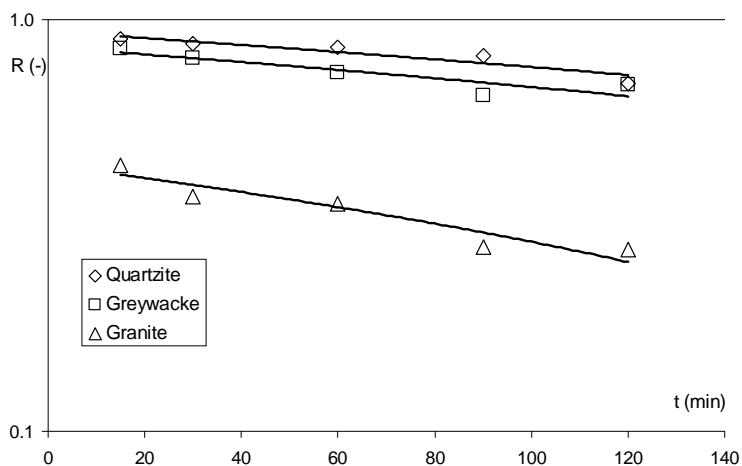
Fig. 3. Dependence between mass of the largest feed particle fraction
and grinding time. Ball composition *C*

Figure 5 contains a dependence between the constant of grinding rate K_l and the feed granulometric composition x_f for grinding of quartzite. The diagram was drawn in the logarithmic form. Different compositions of grinding media were the parameter.
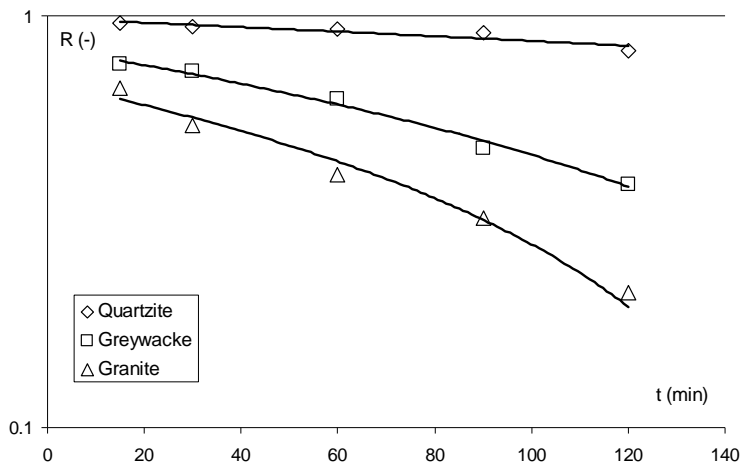
Fig. 4. Correlation between weight of feed particles largest fraction
and grinding time. Balls composition *D*

The feed granulometric composition was determined in terms of weight for separate size fractions after 30 minutes of grinding. A significant effect of the grinding media size on the value of the grinding constant K_1 can be observed for particles above 2 mm.
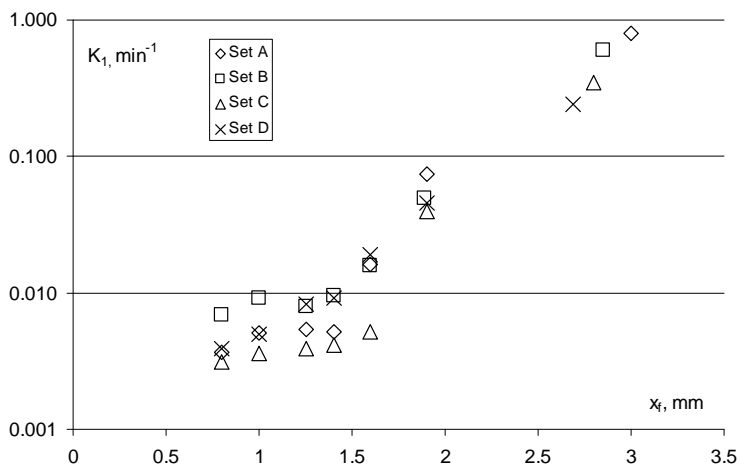
Fig. 5. Change of grinding constant value K_1, with feed granulometric composition
after 30 minutes of grinding of quartzite for four ball sets
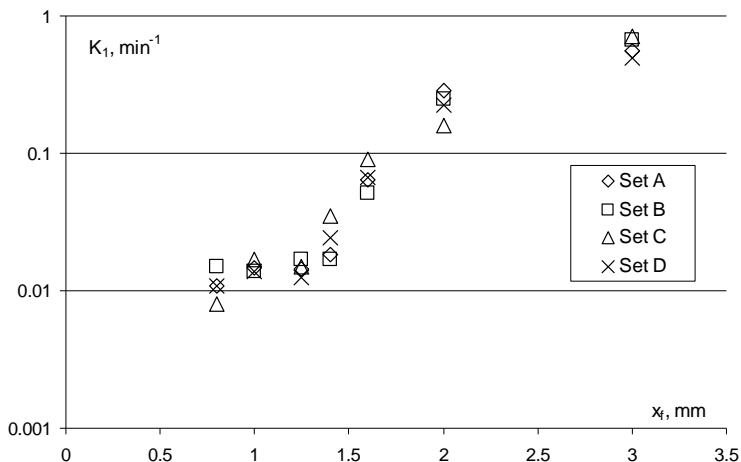
Fig. 6. Change of grinding constant value K_1 and feed granulometric composition
after 30 minutes of grinding for sgreywacke for four ball sets
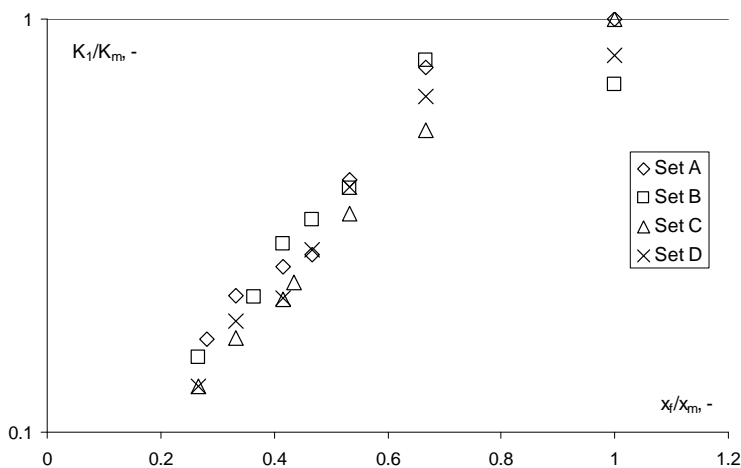
Fig. 7. Change of grinding constant value K_1 and feed granulometric composition
after 30 minutes of grinding of granite for four ball sets

Analysing the course of constant K_1 variability presented in Figs 5–7 it can be stated that they are similar in nature to the three investigated materials. Simultaneously, the course of the dimensionless parameter K_1/K_m value variability presented in Figs 8–10 for the dimensionless feed particle x_f/x_m is arranged along straight lines, while the grinding media diameter had no significant effect on its value. A possible explanation of this intriguing fact can be that in the first grinding stage, the grinding rate depended on the grinding medium diameter determining mechanisms

playing a key role in grinding of the feed particles with the largest size (Notake et al. 2002).
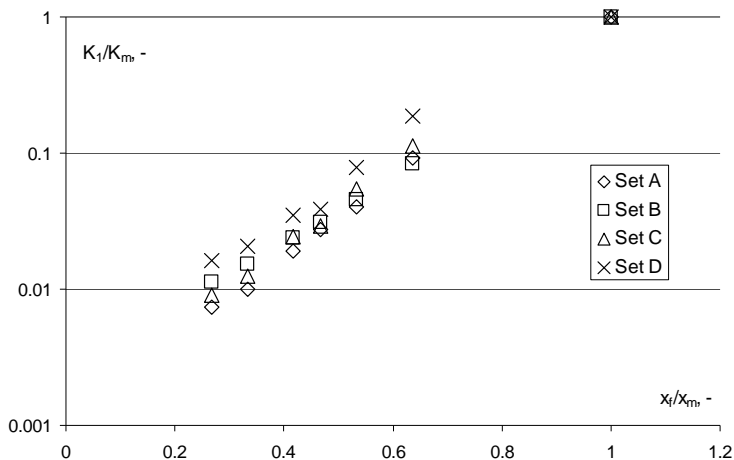
Fig. 8. Change of dimensionless constant of grinding K_1/K_m for quartzite
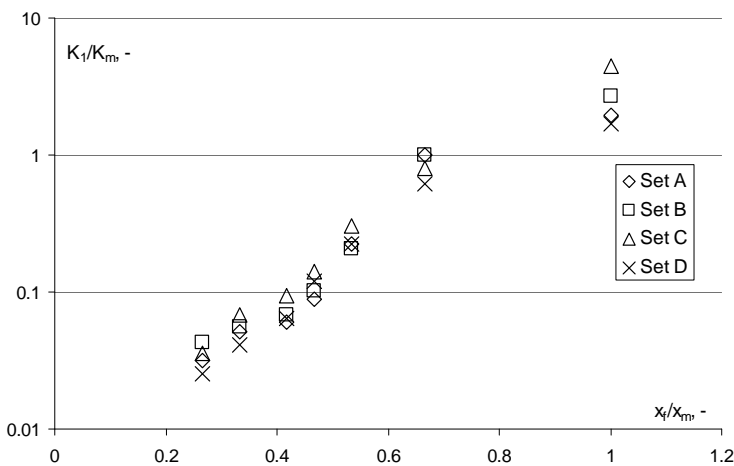
Fig. 9. Change of dimensionless constant of grinding K_1/K_m for greywacke

Figure 11 shows a graphical dependence between the mean particle dimension for the largest size fraction x_m, and the equivalent diameter of grinding media d_B, calculated for each ball set for the three ground materials. The nature of the course of the correlation curves for granite and greywacke is different from the course of the correlation curve for quartzite. Different nature of the course of curves is caused by different morphological structures of raw materials. Quartzite is the material with

almost perfect elastic properties while greywacke and granite are structures with granular structure, characterized by significant grindability.
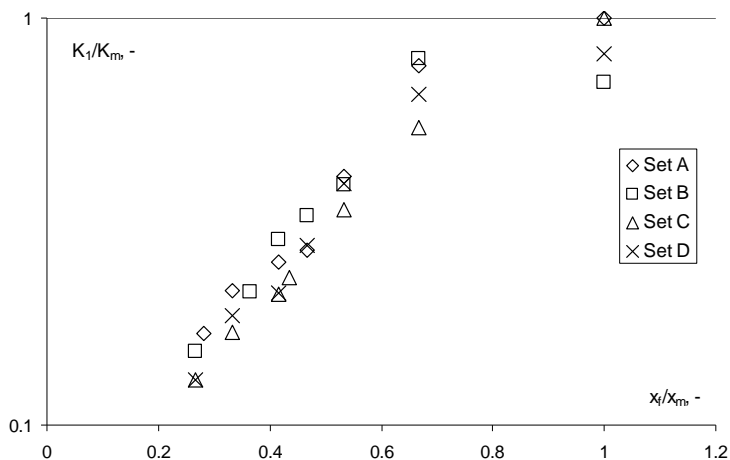
Fig. 10. Change of dimensionless constant of grinding K_1/K_m for granite

Correlation curves, dependencies of the optimum composition of the feed x_m and diameters of grinding media d_B, are described by equations 6-8:

$$x_m(d_B) = 1.7169\, d_B^{0.1456} \text{ (quartzite)} \tag{6}$$

$$x_m(d_B) = 17.267\, d_B^{-0.5304} \text{ (greywacke)} \tag{7}$$

$$x_m(d_B) = 28.983\, d_B^{-0.8222} \text{ (granite).} \tag{8}$$

For the investigated range of ball compositions, in two cases, there is a negative correlation between the ball size and the size of dominating particles contained in the feed. This concerns greywacke and granite. It is assumed that in the considered range of the grinding media variability, for the largest particles of the feed, the relationship between the size and number of balls decides about grinding rate. For grinding media large in size, there is more energy which is used for damaging the internal structure of particles. In the case of raw materials with very heterogeneous particle morphology, also the number of contact points of grinding media with the feed is important. There the ball compositions are differentiated, and with such conditions we had to do in the case of the conducted studies, then with maintaining a constant total mass of grinding media with simultaneous reduction of their size, there is an increase in the probability of finding a particle in the grinding medium impact area. Therefore, for greywacke and granite, grinding media smaller in size enable grinding the feed particles larger in

size. Also abrasive interactions, not only impact interactions, of grinding media decide about the grinding kinetics (constant K_1).
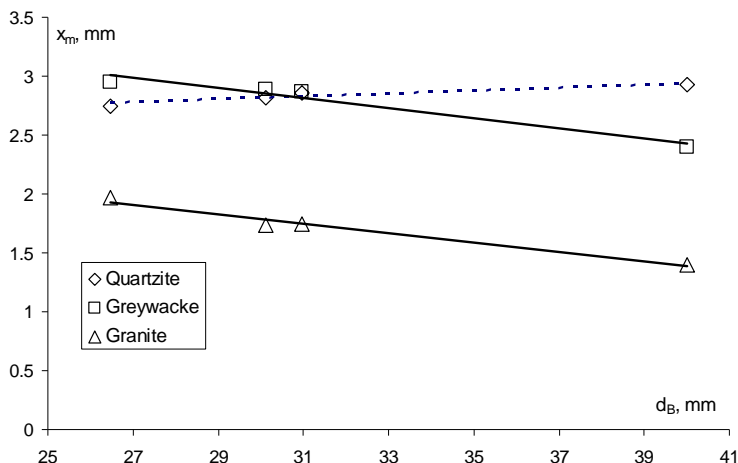
Fig. 11. Correlation between optimum feed size x_m and ball diameter d_B

For quartzite, which is characterised by a high elasticity, the feed particles larger in size must be ground by grinding media larger in size. The direct impact interactions of grinding media decide about rate of the feed grinding K_1. The larger the size, the more energy necessary for damaging the regular quartzite structure. This correlation is consistent with the literature data by Zhao and Jimbo (1988).

Conclusions

The article discusses the results of batch grinding in a ball mill of rock materials such as quartzite, greywacke and granite, and the effect of grinding media composition on the grinding rate constant value (selection function) of the feed particles. Among conclusions concerning the scope of the study, the following should be enumerated:

1. The change in dimensionless parameter describing the grinding rate constant K_1/K_m, depending on the feed particle size, is independent of the size of grinding media.
2. There are correlations between the optimum feed particle x_m and grinding media size as well as between the largest value of the grinding rate constant K_1 and size composition of balls for the three investigated rock materials.
3. The number of contact points, apart from the grinding media size, decides about the grinding rate.

References

AUSTIN L.G., SHOJI K., LUKIE P.T., 1976, *The effect of ball size on mill performance*, Powder Technol. 14, 71–79.

CHAPPELL B.W., WHITE A.J.R., 2001, *Two contrasting granite types: 25 years later*. Australian Journal of Earth Sciences 48, 489–499.

EPSTEIN B., 1948, *Logarithmic-normal distribution in breakage of solids*, Ind. Eng. Chem. 40, 2289–2291.

GAUDIN A.M., MELOY T.P., 1962, *Model and a comminution distribution equation for repeated fracture*, Trans. AIME 223, 43–50.

HERBST J.A., FUERSTENAU D.W., 1968, *The zero-order production of fine sizes in comminution and its implications in simulation*, Trans. AIME 241, 538–549.

KANDA H., GUNJI H., TAKEUCHI K., 1978, *Rate constants of wet and dry ball mill grinding*, J. Soc. Mater. Sci., Jpn. 27, 1978, 663–666.

KELSALL D.F., REID K.J., RESTARICK C.J., 1968, *Continuous grinding in a small wet ball mill*: Part I. *A study of the influence of ball diameter*, Powder Technol. 1, 291–300.

NOMURA S., HOSODA K., TANAKA T., 1991, *An analysis of the selection function for mills using balls as grinding media*, Powder Technol. 68, 1–12.

NOTAKE N., SUZUKI K., ASAHI S., KANDA Y., 2002, *Experimental study on the grinding rate constant of solid materials in a ball mill*, Powder Technology 122, 101–108; PII: S0032-5910(01)00405-3.

OBRANIAK A., GLUBA T., 2012, *Model of energy consumption in the range of nucleation and granule growth in drum granulation of bentonite*, Physicochemical Problems of Mineral Processing, 48 (1), 121-128

OLEJNIK T.P., 2010, *Milling rate of chosen mineral materials in a ball mill under changing apparatus-process conditions*, Proceedings of Comminution'10, CD, s.1-11, 2010.

OLEJNIK T.P., 2011, *Milling kinetics of chosen rock materials under dry conditions considering strength and statistical properties of bed*, Physicochemical Problems of Mineral Processing; 46; s. 145-154, 2011.

OLEJNIK T.P., 2012, *Analysis of the breakage rate function for selected process parameters in quartzite milling*, Chemical and Process Engineering, 2012, 33 (1), 117-129.

REID K.J., 1965, *A solution to the batch grinding equation*, Chem. Eng. Sci. 20, 953–963.

SNOW R.H., 1973, *Gringing mill simulation and scale-up of ball mills*. Proc. 1st Int. Cof. Particle Technol. IITRI, Chicago, p. 28.

ZHAO Q.Q., JIMBO G., 1988, *The effect of grinding media on the breakage rate of planetary mill*, J. Soc. Powder Technol., Jpn. 25, 603–608.

ZINGG T., 1935, *Beitrag zur Schotteranalyse*. Mineralogische und Petrologische Mitteilungen 15, 39–140.

PROCESSING OF IRON ORE FINES FROM ALSWAWEEN KINGDOM OF SAUDI ARABIA

Hussin A. M. AHMED[*], Gamal M. A. MAHRAN[**]

[*] Mining Engineering Dept, Faculty of Engineering, King Abdulaziz University, Saudi Arabia
    Permanent address: Central Metallurgical Research and Development Institute (CMRDI), Helwan, Cairo,
    Egypt (corresponding author e-mail: hussien135@gmail.com)
[**] King Abdulaziz University, Saudi Arabia,
    Permanent address: Alazher University, Qena Branch, Egypt

Abstract: Iron ores located in the Alswaween area (Saudi Arabia) are of finely disseminated nature. They require ultrafine grinding for considerable degree of liberation. In this paper, different upgrading techniques were tried for their processing. The applied upgrading techniques included selective flocculation and column flotation as recent efficient technologies in fines upgrading. Each technique was investigated and optimized separately. Results showed that neither selective flocculation nor column flotation can be successfully used alone to produce high quality iron concentrate especially when using iron ore of size fraction 100% -0.075 mm. The best quality concentrate was found to have 55% Fe and 57% Fe when applying selective flocculation and column flotation, respectively at their optimum operating conditions. Meanwhile, the previously obtained results can be significantly improved when grinding the ore below 45 μm and applying selective flocculation as cleaning step for the concentrate obtained from the column flotation. Thus, it is possible to obtain concentrate having iron content of 63.55% Fe with 52.3% yield, which means an iron recovery in concentrate of ~80%.

Introduction

Iron and its products as steel and cast iron are key players in many industries. The main supply of iron and its products are ores with minor recycled amounts. Consequently, research concerned with the different possible processing techniques of run-of-mine iron ores and iron tailings is in progress (Pradip, 1994; Stephen and Misty 2007; Royand and Das, 2008). Furthermore, the increasing market pressure for improved quality has forced iron concentrate producers to re-examine their process flowsheets and evaluate alternate or supplemental processing routes. For example, the requirement for higher quality pellets imposes that the silica content should be lowered

to levels ranging from 2.0% SiO_2 to below 1.0% SiO_2 (Elmidany and Ahmed, 2008). Thus, it can be said that although there are many typical techniques for upgrading of iron ores (Colombo, 1986; Luo et al., 2005; Elmidany and Ahmed, 2008), the previously mentioned restricted industrial specifications coupled with the depletion of the high-grade ores make it difficult to select suitable upgrading flowsheets. This can be considered as a challenge, knowing that the techniques applied for successful processing of ultra-fine low grade iron ores are limited and require sharp operating conditions (Weissenborn et al., 1994a, 1994b; Ahmed et al., 2007). This challenge is typical in Saudi Arabia. There exist huge reserves of iron ore in the Alsawaween area. The valuable minerals are highly disseminated in the associated gangues. To liberate both components from each other it requires ultrafine grinding. The finely ground ores are usually difficult-to- process with classical upgrading technologies (Stephen and Misty 2007; Royand and Das, 2008). As a result this work aims at applying recent upgrading technologies like selective flocculation and/or column flotation to recover the iron bearing minerals from the gangue minerals of the Alswaween area ore. Selective flocculation and column flotation are considered for that ore because they are among the most efficient techniques applied for treatment and separation of valuable minerals from their associated gangues at high degree of fineness (Iwasaki and Lipp, 1982; Rao et al., 1985; Arol and Iwasaki, 2003; Ahmed et al., 2007). During testing of the ore using such techniques to upgrade the ore, different operating parameters will be investigated. This includes investigating the pH, dose of dispersant (sodium silicate) in addition to the dose and type of flocculant (starch) as parameters affecting selective flocculation technique. On the other hand, parameters considered in studying the column flotation for the same purpose will include collector dose and flotation pH. As a final step in the study, a set of experiments will be implemented to answer the question what will be the effect of the two techniques, that is column flotation and selective flocculation, if they do exist at the same iron processing flowsheet?

Experimental

Iron ore sample preparation

A Saudi iron ore sample from the Alswaween area was selected for this study. The sample was subjected to primary and secondary crushing using jaw and roll crushers, respectively. The secondary crushed product was further ground in a ball mill working in a closed circuit with a 5 cm diameter cyclone rig. The cyclone operating conditions were adjusted to make cut off at 0.075 mm or 0.045 mm size fraction. The purpose of the ball mill close circuit was to yield a 100% -0.075 or 100 % -0.045 mm product that will be considered as a feed for a series of selective flocculation and column flotation laboratory tests. The uppermost liberated sample (100% -45 μm) was upgraded using a sequence of column flotation followed by selective flocculation, applying the predetermined optimum conditions for each of them i.e. when using the 100% -75μm feed, to improve the process recovery, and thus its economics.

Characterization of the iron ore and its concentrates

The considered iron ore sample was physically and chemically characterized. Physical characterization of the sample was conducted by size analyses and petrographic microscope studies in addition to XRD testing to identify the mineralogical distribution and nature of dissemination among the valuable minerals and their associated gangues. However, mineralogical composition of the sample was conducted by X-ray diffraction patterns of the specimen, using X-ray Philips -PW 1010 diffractometer operated with a cobalt radiation target having Fe-filter at 30 kV and 20 mA. During the investigation, characterization was implemented by a routine chemical analysis. In this analysis, Fe was determined using standard method of sample fusion and dissolution (Ahmed et al., 2007).

Selective flocculation tests

In this series of tests, the procedure adopted by Ahmed and his coworkers (2007) was strictly followed. In this procedure, sample dispersibility in aqueous solution was considered as a prerequisite for flocculation. As a result the optimum pH and sodium silicate dosage for highest dispersibility was first investigated. In this series, samples (100% -0.075 mm) were agitated in distilled water for 5 min at 1500 rpm in a 2-dm^3 container (at 0.5 % solid) with the required dosage of sodium silicate at the desired pH (HCl and NaOH as pH regulators). The sample was allowed to settle freely in a 0.5-dm^3 cylinder for 3 minutes. The mass settled after 3 min was then determined. The percent dispersion was calculated by expressing the mass still dispersed after three minutes as mass percent compared to the sample total mass (Ahmed et al., 2007). After determining the optimum dispersion conditions different series of selective flocculation tests were carried out. The series was designed to study effect of starch type and dosage. Different types of starches (potato, corn, wheat, and dextrin) were used as natural polymers. They were freshly prepared as 1% solutions in an alkaline media. A 1% starch solution was prepared by dissolving 1 g of starch and 0.5 g of sodium hydroxide to a volume of 100 cm^3 of distilled water. The resultant solution was heated to 84 ^{o}C and then rapidly cooled to room temperature using ice. The heating and cooling of the solution was carried out within five minutes. In each series the dispersed sample was transferred to a 38 cm in length and 4.7 cm in diameter glass cylinder fitted with side outlets at 4 cm and 11 cm from the bottom. The required dose of flocculants was added from a slow running pipette for further one min. The set-up was inverted 10 times at 180° and then left to settle for 3 min. The non-flocculated fraction (tailing) was withdrawn through the side outlets. Both the flocculated (concentrates) and non-flocculated fractions (tailings) were separately collected, dried, weighed and subjected to necessary chemical analyses as previously mentioned.

Column flotation of iron samples

The column flotation setup used in this study is shown in Fig. 1. For each test, 3 kg of the ground iron ore (100% -0.075 mm feed) was conditioned (for 2 min) in 45-dm^3 tank at 60% solids at alkaline pH for depressing gangue bearing minerals using 0.3 g/Mg sodium silicate. Later on, the pulp was further conditioned for 4 minutes with the targeted dosage of collector. The conditioned pulp was then diluted to 10% solids by weight and the required dose of frother was added. The slurry was next fed into the column by pumping until the pulp level reached a defined fixed height where the rest of the column height was assigned for the mineralized froth. In the whole series of tests, the froth height was kept at approximately 0.25 m. As a result slurry pumping rates as a feed to the column were calibrated to keep constant level allowing froth to form above this level. Air was introduced to the column for 10 minutes. Concentrate was collected and the slurry left in the column and tanks were collected as flotation tailing. Flotation and conditioning parameters (Table 1) were held constant throughout the test unless otherwise stated. Chemicals used in flotation tests were oleic acid as iron collector, sodium silicate as silica depressor, and MIBC as frother. All these chemicals were of reagent grade.

Table 1. Parameters of Alswaween iron ore flotation using column flotation

Conditioning*		Flotation*	
Parameter	value	Parameter	value
Solids %	60%	Solids %	10%
Time (minutes)	4	Flotation time (minutes)	10
pH	11	Wash water	0.2 dm^3/min , (0.019 cm/s)
Impeller speed (RPM)	1200	Collector	Oleic acid dosage (variable)
Solids charge (g)	3000	Froth height (mm)	250
Water type	Tap water	Frother dosage (MIBC) (g/Mg)	0.2

*Operating conditions were selected according to previous studies (Flint et al., 1992; Bhaskar et al., 1993)
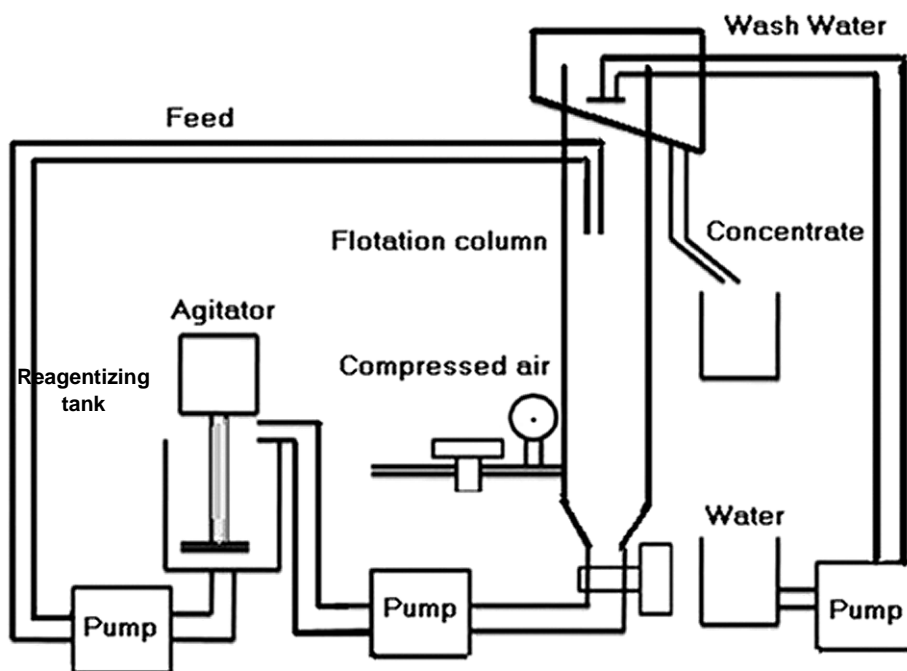
Fig. 1. Experimental setup for column flotation of the tested iron ore

Results and discussion

Sample characterization

Complete chemical analyses of the original iron sample indicate that the sample contains 41.58% Fe. The sample was high in SiO_2 and CaO contents (29% and 4.2%, respectively, Table 2). The contents of MgO, MnO, K_2O, Na_2O, Cl, ZnO, TiO_2, P and Al_2O_3 were minor. On the other hand, the XRD pattern shows that the iron bearing minerals are mainly hematite and magnetite while the main gangue minerals in the sample are quartz and calcite (Fig. 2).

Table 2. Complete chemical analyses of the original investigated iron sample

Constituent	Fet	SiO_2	Al_2O_3	CaO	MgO	Mn	TiO_2
%	41.58	29.1	1.5	4.2	1.5	0.07	0.15

Constituent	S	P	K_2O	Na_2O	V_2O_5	ZnO	
%	0.11	0.31	0.016	0.021	0.002	0.005	
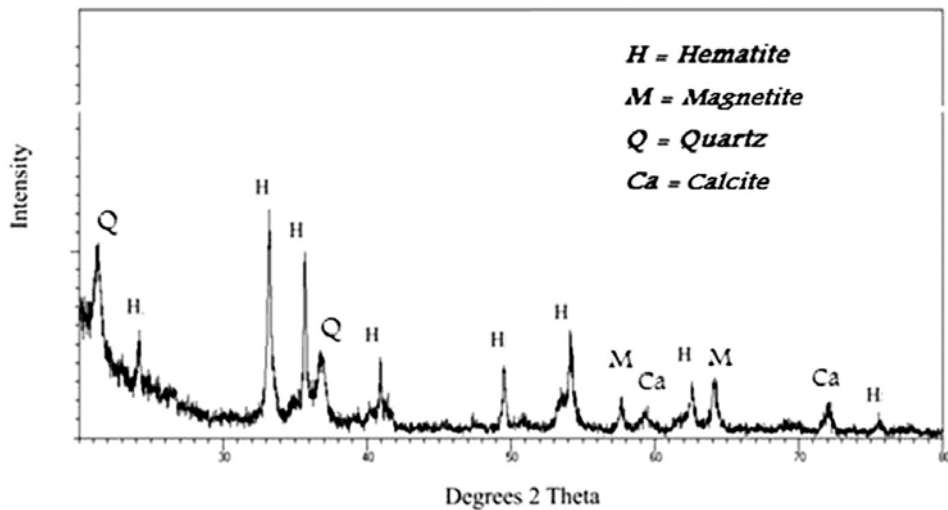
Fig. 2. XRD pattern of the "as received" powdered iron sample

Microscopic liberation analysis (Fig. 3) of the ore shows that in the coarser size fractions percentage of interlocking is very high where the percentage of free iron minerals in the first coarse fractions is less than 35%. However, complex interlocking
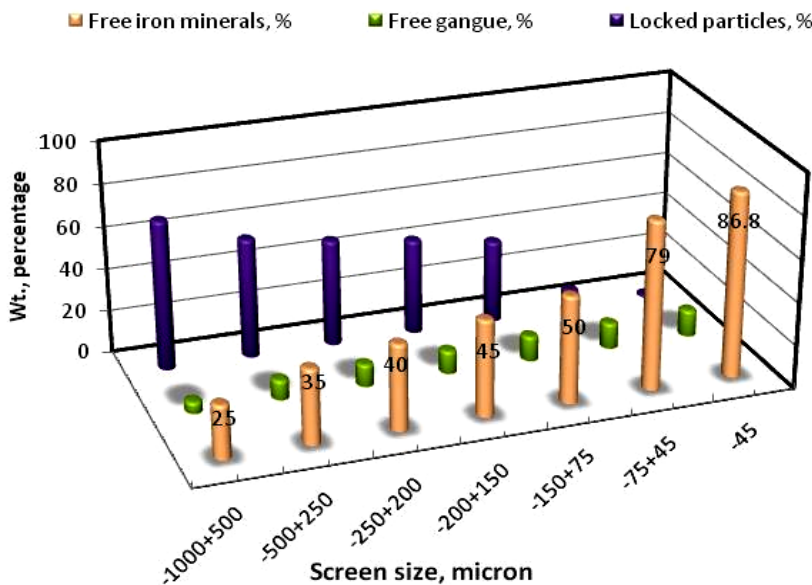
Fig. 3. Liberation pattern of iron minerals in the considered ore

and disseminated nature of the ore can be seen as below 87% of the iron bearing minerals can be liberated below the 45 μm size. Achieving high purity concentrate in beneficiation of this ore is probably quite difficult due to the complexity of interlocking. Proper comminution is required to break the interlocking and attain good liberation in this case.

Iron upgrading applying selective flocculation

Dispersibility tests

Figures 4a and 4b show the effect of pH and sodium silicate dosage on iron dispersibility. Figure 4a indicates that an improvement of the ore dispersibility can be obtained by increasing the pH. The phenomenon can be fitted with a polynomial curve with a correlation coefficient of 0.99. This indicates that the iron dispersibility is directly proportional to the pulp pH with a plateau reached at pH of 10.5−11. On the other hand, at this ideal pH (10.5), an increasing the dose of sodium silicate improves the dispersibility for the whole-investigated pH range (Fig. 4b). Thus, from both Figures 4a and 4b, it can be concluded that the optimum dispersibility conditions are at pH 10.5 and sodium silicate dose of 1 kg/Mg.
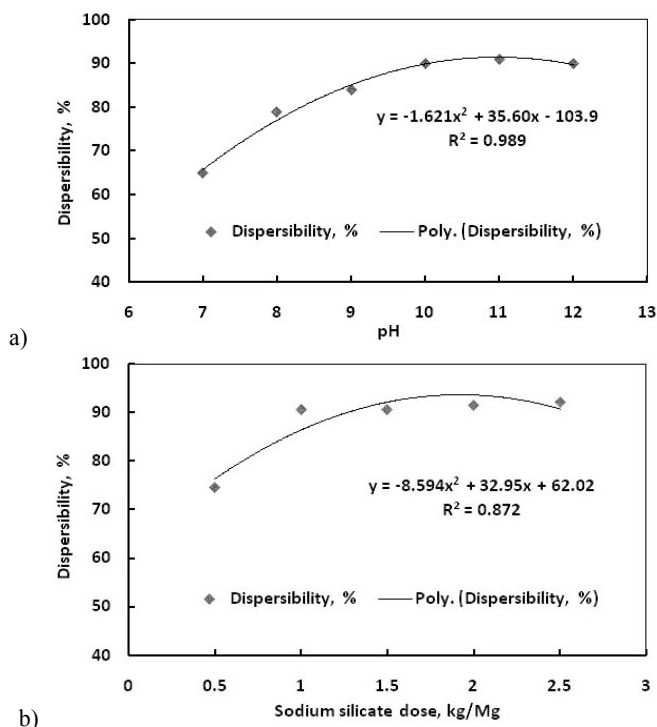
Fig. 4. Effect of pH and sodium silicate on iron ore dispersibility a) effect of pH at sodium silicate dosage of 1 kg/Mg, b) effect of sodium silicate dosage, at pH = 10.5 used feed in both series is 100% – 0.075 mm

Selective flocculation optimization

Effect of flocculant type

Basing on the results presented in Figure 4, several preliminary flocculation tests, using different types of starches as flocculants, were conducted. The operating conditions applied in this series were as follows: pH 10.5, 1 kg/Mg sodium silicate, solid percent 5%, flocculant dose of 1.0 kg/Mg and iron feed size is 100% -0.075 mm. The results of this series show that the different used flocculants return different responses and potato starch provides the best results among the group in reference to the concentrate yield and iron assay and hence the iron recovered in the concentrate fraction (Fig. 5). The iron concentrate obtained when using potato starch was containing ~55% Fe with iron recovery approaching 80% while all other starches returned worse responses. It can be seen that the obtained results are supported with literature interpretations (Subramanian and Natarajan, 1991; Weissenborn et al., 1994 b; Panda et al., 2011), where adsorption of potato starch on the surface of the iron bearing minerals is higher compared to that of other starches at the conditions under investigation.
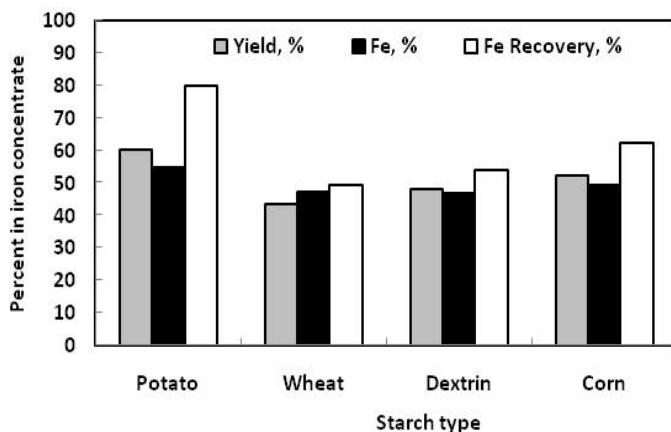
Fig. 5. Effect of starch type on the selective flocculation of iron ore
(feed size 100% – 0.075 mm, pH = 10.5, sodium silicate dose 1 kg/Mg,
flocculation solid percent 5%; and starch dose 1.0 kg/Mg)

Effect of flocculant dose

The hitherto results concluded the preference of potato starch in selective flocculation of the iron sample under investigation. As a result optimization of the potato starch dosage was implemented. Results of such tests are shown in Figure 5. It can be seen that the most pure iron concentrate can be attained at the dosage of potato starch of 1 kg/Mg. This concentrate has iron content approaching 55% Fe with iron recovery of approximately 80%. However, potato starch doses higher than 1 kg/Mg hampers the process selectivity (Table 6). This may be attributed to liberation considerations.
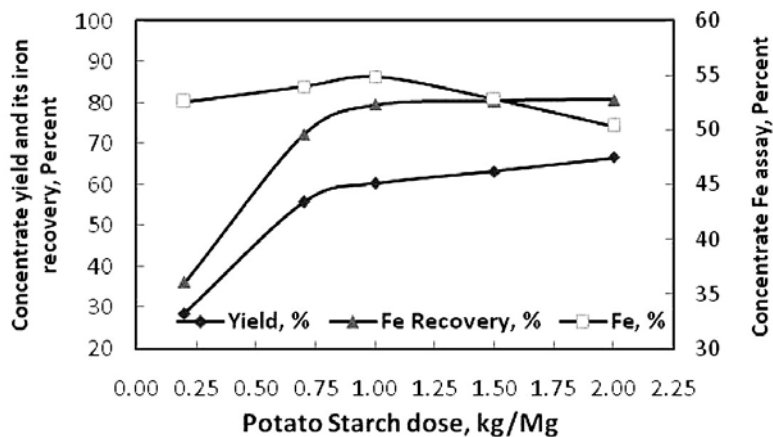
Fig. 6. Effect of potato starch flocculant dose on selective flocculation of iron ore
(feed size, 100% – 0.075 mm, pH = 10.5, sodium silicate dose 1 kg/Mg,
and flocculation S/L ratio = 5)

Column flotation of iron ores

Optimization of selective flocculation, as a technique for processing of the investigated iron ore, lead to the conclusion that it is not possible to obtain iron concentrates of commercial applications. Therefore, the column flotation was adopted as an alternative for selective flocculation. The technique will be investigated regarding the pH values suitable for iron flotation from their gangues besides the most suitable amount of oleic acid collector that should be used.
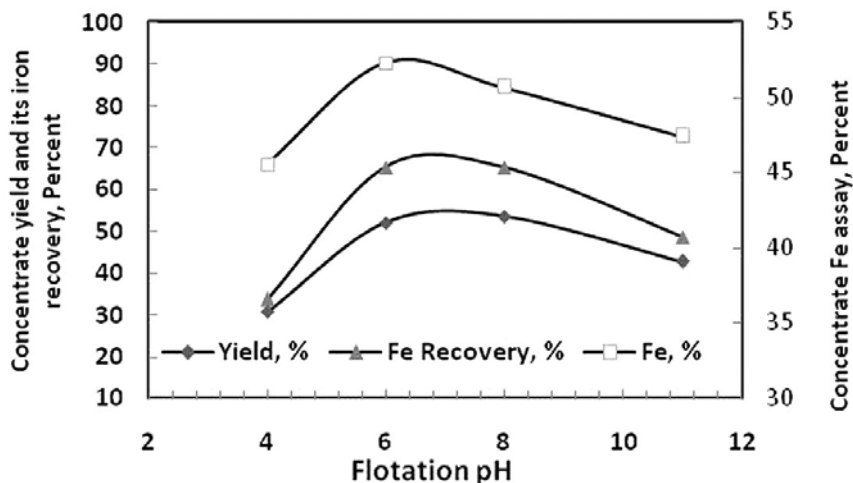
Fig. 7. Effect of flotation pH on the column flotation response of iron ore (feed size,
100% – 0.075 mm, oleic acid collector dosage = 0.5 kg/Mg, MIBC frother dosage 0.2 kg/Mg,
sodium silicate dose as depressant 0.3 kg/Mg, and flotation solid percent 10%)

Effect of flotation pH

The quality and quantity of the iron concentrate obtained when it is floated using oleic acid as collector applying column flotation technique varies with changing flotation pH. In the case of the investigated iron ore, the results show that pH 6 represents the optimum pH (Fig. 7). This is because at this pH the cleanest concentrate was attained. At pH values higher or lower than 6 the iron concentrate obtained have neither good assays nor high recoveries. As a result in the subsequent study pH value of 6 will be considered. In fact this may be attributed to the adsorption of oleic acid collector on the surface of the iron bearing minerals (Flint et al., 1992; Bhaskar et al., 1993; Xinghua et al., 2012).

Effect of collector dose

Considering the results shown in Figure 7, further tests were implemented for the purpose of knowing the most suitable dosage of oleic acid as a collector. Results obtained from this series are presented in Figure 8. It clearly shows that the most clean iron concentrate can be achieved at collector dosage of 1.2 kg/Mg. At this collector dosage a concentrate having iron assay of ~57 % Fe with a recovery of approximately 86% which is much better compared to the purest concentrate achieved in the case of selective flocculation. In spite of the preference of the results obtained when applying the column flotation technique, yet still the obtained concentrate is beyond the commercial application for pellets production. To solve this problem further improvement will be tried by further grinding of the ore for achieving higher degree of liberation.
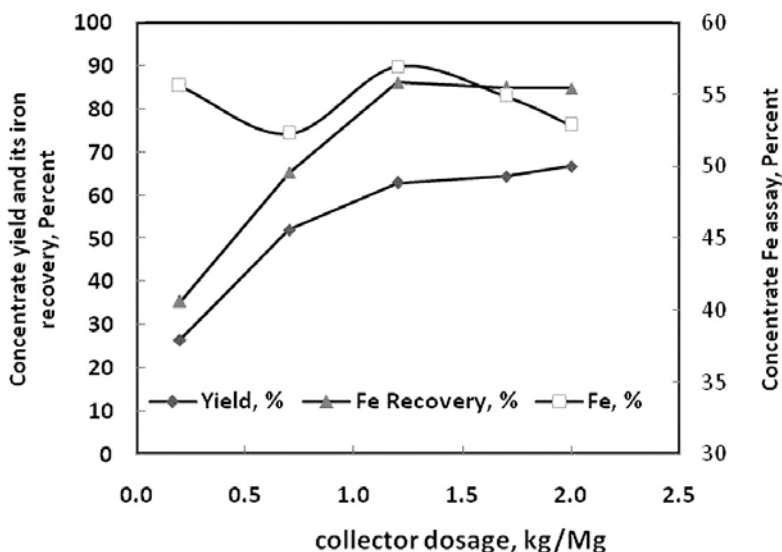
Fig. 8. Effect of oleic acid collector dosage on the column flotation response of iron ore (feed size, 100% – 0.075 mm, pH = 6, MIBC frother dosage 0.2 kg/Mg, sodium silicate dose as depressant 0.3 kg/Mg, and flotation solid percent 10%)

Process further improvement

From the hitherto discussed results, it is obvious that the maximum grade that can be achieved using either selective flocculation or column flotation alone is low i.e. 55% Fe and 57% respectively at the optimum conditions. Even when the floated concentrate was cleaned by selective flocculation, the concentrate quality is still low (Fe% = 58.9%). This is mainly attributed to the low degree of liberation of the considered iron ore. Thus seeking for a higher degree of liberation, the ore was further ground to 100% -45 µm as previously mentioned in the experimental section. Table 3 shows different tests applied for the iron ore sample considered previously obtained results and optimum conditions.

Table 3. Different tests implemented for improvement of iron concentrate specifications to meet commercial applications

Test #	Technique	Operating conditions	Obtained iron concentrate		
			Yield, %	Fe, %	Fe recovery, %
1	Column flotation followed by selective flocculation	−0.075 feed at previously determined optimum conditions	56.3	58.90	79.75
2	Selective flocculation alone	−0.045 feed at previously determined optimum conditions	61.3	55.89	82.40
3	Column flotation alone	−0.045 feed at previously determined optimum conditions	62.7	57.83	87.20
4	Column flotation followed by selective flocculation	−0.045 feed at previously determined optimum conditions	52.3	63.55	79.93

Conclusions

The results of this investigation clearly established that effective separation of iron ore concentrate from finely disseminated iron ore sample of Alswaween area in Saudia Arabia by column flotation and selective flocculation is possible. The effectiveness of separation is greatly influenced by the feed particle size and pH (in both techniques), type of flocculant (in flocculation), collector dosage (in flotation). The separation efficiency is better in case of fine particle size because of liberation considerations of the iron particles from the associated gangues. The results of the investigations showed that it is possible to obtain concentrate having iron content of 63.55% Fe with 52.3% yield, which correspond to an iron recovery in concentrate of ~80% when grinding the ore to below 45 µm and applying selective flocculation for the column flotation concentrate. This product can be utilized in the steel plant as a sinter feed material.

Acknowledgment

References

AHMED H.A.M., EL-MIDANY A.A, ABDEL-KHALEK N.A., 2007, *Statistical optimisation of some parameters affecting flocculation of Egyptian iron ore*, Mineral Processing and Extractive Metallurgy, Trans. Inst. Min Metall. C, Vol. 116, No 4.

AROL A.I, IWASAKI I., 2003, *Effect of sodium silicate on flocculation of hematite with starch in the presence of calcium*, Separation Science and Technology, Vol. 38, No. 3, 647–659.

BHASKAR RAJU G., PRABHAKAR S., SANKARAN C., 1993, *Beneficiation of iron ores by column flotation*, Trans. Ins. Min. Met., Sec. C, 132–135.

COLOMBO A.F., 1986, *Concentration of Iron Oxides by Selective Flocculation-Flotation*, [in:] *Advances in Mineral Processing*, Edited by Somasundaran, P., Published by The Society of Mining Engineers, Inc., Littleton, CO, 695–713.

ELMIDANY A.A., AHMED H.A.M., 2008, *Assessment of a selectivity criterion for upgrading ultrafine iron ores by selective flocculation*, Minerals & Metallurgical Processing Vol. 25, No. 2, 91–96.

FLINT I.M., WYSLOUZIL H.E., DE LIMA ANDRADE V.L., MURDOCK D.J., 1992, *Column flotation of iron ore*, Minerals Engineering, Vol. 5, Issues 10–12, October–December, 1185–1194.

IWASAKI I., LIPP, R.J., 1982, *Flocculation and selective flocculation of iron ores*, Engineering Foundation, 321–341.

LUO LI-QUN; ZHANG JING-SHENG; YU YONG-FU, 2005, *Recovering limonite from Australia iron ores by flocculation-high intensity magnetic separation*, Journal of Central South University of Technology, Vol. 12, No. 6, 682–687.

PANDA L., DAS B., RAO D.S., MISHRA B.K., 2011, *Selective Flocculation of Banded Hematite Quartzite (BHQ) Ores*, The Open Mineral Processing Journal, 2011, 4, 45–51.

PRADIP D., 1994, *Beneficiation of Indian iron ore slimes*, Minerals & Metallurgical Processing, v. 6, No. 3, pp.179-194.

RAO H., K.; NAYAK A.; MAHAPATRA S.N.; NARASIMHAN K.S., 1985, *Selective flocculation for the recovery of iron in Kudremukh tailings*, Transactions of the American Institute of Mining, Metallurgical, and Petroleum Engineers, Society, vol. 278, 1312–1315.

ROY S., DAS A., 2008, *Characterization and processing of low-grade iron ore slime from the Jilling area of India*, Mineral Processing and Extractive Metallurgy Rev., Vol. 29, 213–231.

STEPHEN B.H., MISTY N.D., 2007, *Slon magnetic separator: A new approach for recovering and concentrating iron ore fines*, Montreal Energy & Mines, Montreal, April 29–May 2.

SUBRAMANIAN S.; NATARAJAN K.A., 1991, *Flocculation, filtration and selective flocculation studies on haematite ore fines using starch*, Minerals Engineering, Vol. 4, No. 5–6, 587–598.

WEISSENBORN P.K.; WARREN L.J.; DUNN, J.G., 1994a, *Optimisation of selective flocculation of ultrafine iron ore*, International Journal of Mineral Processing, Vol. 42, No. 3–4, 191–213.

WEISSEBORN P.K., WARREN L.J., DUNN J.G., 1994b, *Selective flocculation of ultra fine iron ore.1.Mechanisim of adsorption of starch into hematite*. Colloids and Surfaces, Vol. 99, 11–27.

XINGHUA L, YONGFU Y, WEN C, XIAOHU Y., 2012, *Effect of selective flocculation desliming on flotation of fine grained Yuanjiacun iron ore*, International Mineral Processing Congress, September 24–28, New Delhi, India.

HYDROMETALLURGICAL PROCESSING
OF EGYPTIAN BAUXITE

Ashraf M. AMER

Environmental Sciences Department, Faculty of Science, Alexandria Egypt, asrafamer0409@yahoo.com

Abstract: A bauxite ore from Um Bogma, Southwestern Sinai, Egypt was mineralogically characterized. It contains 70% gibbsite, 13.2% quartz and 11.0% kaolinite. Beneficiation of the ore reduced the quartz content to 2.4%. Hydrometallurgical processing of the beneficiated gibbsitic bauxite was performed by hot leaching with sodium carbonate and lime in an attritor. Aluminium was converted to soluble sodium aluminate low in SiO_2 (<0.1%) and the recovery was over 95% for a short leaching duration of 30 minutes at 90 °C. The residue was essentially composed of calcium silicate.

Introduction

Bauxite is a chief raw material for aluminum and at present 95% of primary aluminum is produced from this ore. In the last two decades, the discovery of bauxite in Australia, Guinea and Brazil has changed the world bauxite distribution map very significantly. In NE-Africa (Egypt), bauxite laterites are preserved in relictic weathering crusts on the variety of Precambrian basement rocks, as well as on Cretaceous volcanic, and sedimentary type kaolin main periods of lateritic weathering occurred during Early Paleozoic and middle to late Cretaceous times (Andeev et al., 1972).

The Paleozoic and Cretaceous bauxite laterites have in common a complex polystage chemical evolution which comprises either secondary resilication of bauxites or desilication of kaolins. In both cases, the products result in comparably low bauxites or alumina grades. The potential of NE-Africa to supply high-grade bauxites was further reduced due to repeated tectonically induced erosion.

Indigenous non-bauxite materials for alumina production include clays and nepheline syentie, Clays with more than 35% Al_2O_3 are reported to occur in Sinai and Aswan and the estimated reserves are around 35 Tg (million tons). This material is technically suitable for alumina production by sintering as well as acid leaching proc-

esses. Of these, the lime sintering and the nitric acid leaching processes (Scotford and Glastonbory, 1972; Liu et al. 2008) seem to be the most attractive routes. Nepheline syenite with 20% Al_2O_3 and 14% alkali oxides is present in various localities in the Eastern Desert. The estimated reserves is about 25 Tg. These ores are also amenable to processing by lime sintering. However, the alumina production economics have showed that neither of these raw materials would be able to compete with bauxite. This is due to the high investment cost required for their processing which is from 1.5 to 2-fold higher than the conventional Bayer process.

Said et al. (1976) were the first to report the presence of bauxitic material in Egypt in various localities in the Eastern Desert in the weathered crust covering the Nubia complex effusive. Germann et al. (1987) and Fisher et al. (1991) have indicated the possibility of bauxitisation in the southern part of Egypt (south of Kalabsha) and Northern Sudan. Further work was carried out by Segev (1984) on gibbsite mineralization in SW-Sinai.

Among many methods of bauxite processing alkali digestion with NaOH (Cregledi et al., 1981 and Zhao et al. 2010) and acid digestion with HCl have found wider application (Smith, 2009).

The present study deals with mineralogy, beneficiation and hydrometallurgical processing of the Egyptian bauxite deposit. Leaching with sodium carbonate and lime was used in the investigations.

Experimental

Materials and Apparatus

The bauxite sample was obtained from the Um Bogma deposits (Table 1). Pure sodium carbonate and lime were used as leaching and desilication agents, respectively.

Table 1. Chemical analysis of buxite

Component	%
Al_2O_3	50.17
H_2O	27.80
SiO_2	18.22
CaO	1.50
Fe_2O_3	0.32
MnO_2	0.21
MgO	0.12

Leaching experiments were carried out in an attritor – a reactor equipped with high speed stirrer and small balls (Fig.1). The attritor was heated by a thermostatically controlled heating mantle and agitation of the reaction mixture was done mechanically.
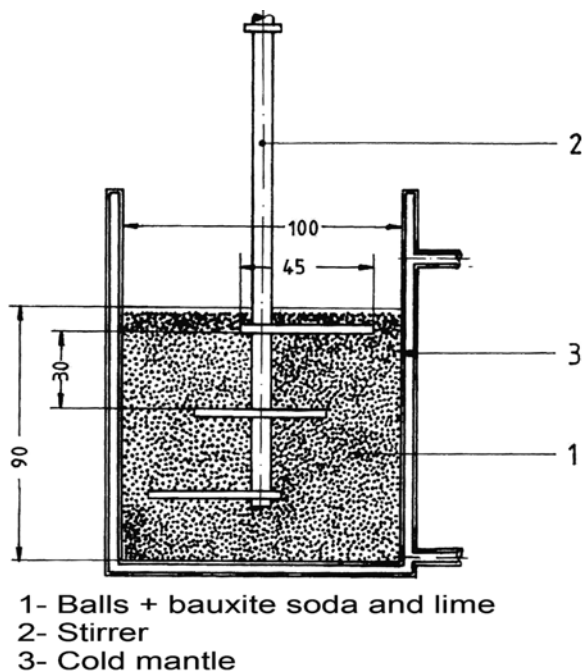
Fig. 1. Sketch of the attritor

Technique of work

Gibbsite and kaolinite were separated from detrital quartz by first pulverizing in a ball mill and then screening through a 63 micron screen. The fines were repulped in water, dispersed thoroughly and then allowed to settle. The suspended fraction was decanted and dried. This fraction contained only 2.4% quartz indicating removal of about 82% quartz.

Calculated amounts of sodium carbonate solution and lime were added in the attritor and heated up. The amount of lime was adjusted to be in stoichiometric proportion to the silica present in the bauxite. On attaining the required temperature calculated amount of bauxite was added under agitation. Samples were withdrawn periodically for analysis of aluminum and silicon in the leach liquor.

Results and discussion

Mineralogy

X-Ray diffraction study

X-ray diffraction analysis of the bauxite sample (Fig. 2) revealed the presence of gibbsite ($Al_2O_3 \cdot 3H_2O$), kaolinite ($Al_2O_3 \cdot 2SiO_2 \cdot 2H_2O$) and goethite ($FeO \cdot OH$).
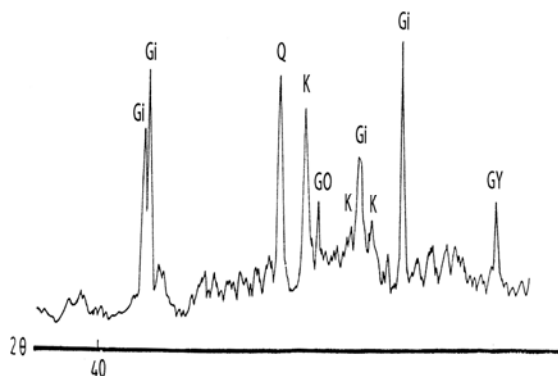
Fig. 2. X-ray diffraction pattern of Um Bogma bauxite
sample using filtered Co Ka radiation.
Gi: gibbsite, Q: quartz, K: Kaolinite, Go: Geothite

Diffraction thermal analysis

From the differential thermal analysis of the bauxite sample (Fig. 3) the following observations are made.

(i)   A small endothermic peak occurs at about 90 ºC due to the loss of surface ad-sorbed water.

(ii) A large endothermic peak is formed at a temperature of about 320 ºC due to the loss of interlayer OH of water which is associated with a significant weight loss of about 17.6 to 21.1% with an average of 19.35%. This peak is characteristic of gibbsite mineral (Belyaev et al., 1964; Cregledi et al., 1981; Kuznetsova et al., 1964).

(iii) A small endothermic peak is seen at a temperature of 550 ºC due to dehydration of kaolinite. The temperature is influenced by the degree of crystallinity of kao-linitic material.

(iv) The re-occurrence, of an endothermic DTA peak at about 950 ºC is seen as the structural peak attributable to the formation of gamma-alumina and tridymite. The complete mineralogical analysis of the bauxite sample is given in Table 2.

Table 2. Mineralogical analysis of studied bauxite sample

Mineral	capacity, %
Gibbsite, $Al_2O_3 \cdot 3H_2O$	70.1
Quartz, SiO_2	13.2
Kaolinite, $Al_2O_3 \cdot 2SiO_2 \cdot 2H_2O$	11.0
Gypsum, $CaSO_4 \cdot 2H_2O$	3.1
Geothite, $FeO \cdot OH$	1.5
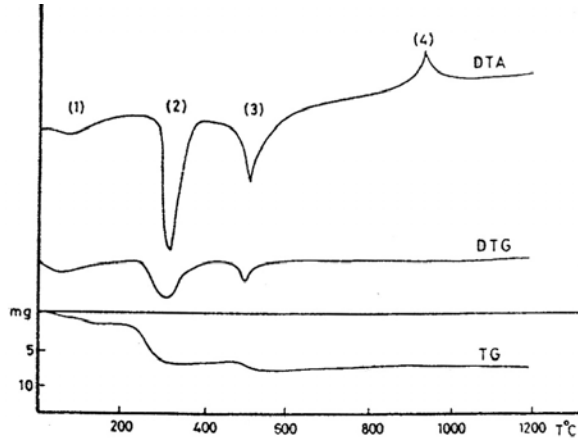
Fig. 3. Derivatogram of representative bauxite sample

Hydrometallurgical processing

The main parameters affecting the efficiency of the leaching process were systematically studied.

Effect of temperature and time

Figure 4 shows the effect of temperature (50–90 $^\circ$C) and time (30–120 min) on the leaching behavior of gibbsitic bauxite. The experiments were carried out using 0.3 M sodium carbonate solution and lime to correspond to CaO/SiO$_2$ ratio of 2.0 at solid content around 30%. Aluminum recovery increases with increasing temperature from 50 $^\circ$C MP to 90 $^\circ$C and time. The optimum Al recovery was >95% for leaching condition of 90 $^\circ$C and 30 min.

Further increase in the leaching time to 40 min had no significant effect on the Al recovery.
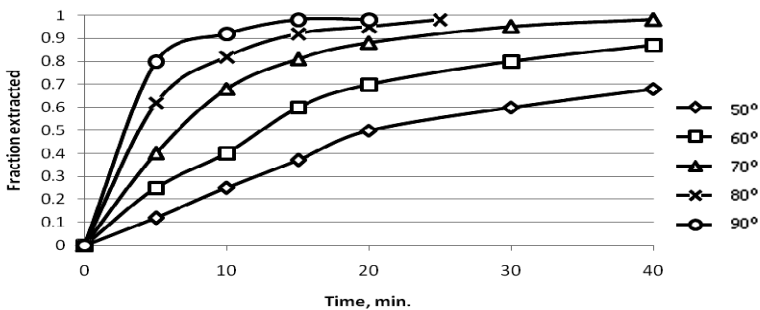
Fig. 4. Effect of temperature on the extraction of aluminum

Effect of sodium carbonate concentration

Figure 5 shows effect of sodium carbonate concentration (0.1–0.9 M) on the Al recovery. Leaching was done under the optimized conditions. It is seen that Al recovery increases with increasing sodium carbonate concentration up to 0.3 M. Further increase in the carbonate concentration did not improve the recovery.
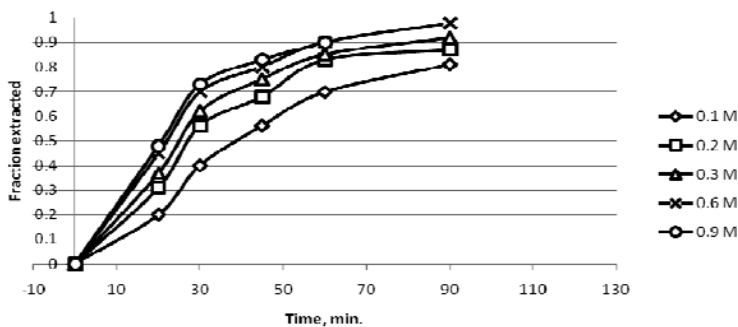
Fig. 5. Effect of sodium hydroxide concentration on the extraction of aluminum

Effect of CaO/SiO$_2$ mole ratio

Figure 6 shows the effect of CaO/SiO$_2$ mole ratio under the optimum leaching conditions. It is noticed that there is a direct proportionality between the aluminum recovery and the CaO/SiO$_2$ ratio in the mole ratio range of 0.5 to 2.0. The optimum Al recovery achieved was 92% at the CaO/SiO$_2$ ratio of 2.0. An increase in the CaO/SiO$_2$ ratio beyond 2.0 led to a significant decrease in the Al recovery, essentially due to the formation of sodium calcium aluminum silicate by the reaction of calcium silicate and sodium aluminate.
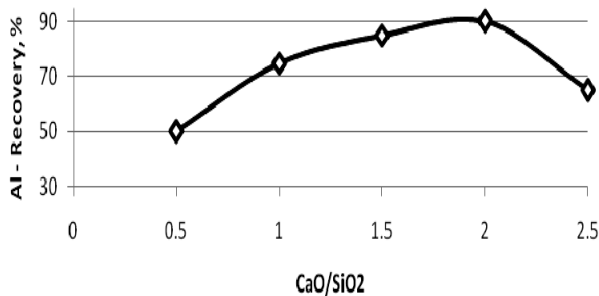
Fig. 6. Effect of ratio of CaO/SiO$_2$ on Al recovery

Table 3. Chemical analysis of leach liquor

Component	%
Al_2O_3	10.010
Na_2O	11.190
SiO_2	0.096
Caustic molar ratio[*]	1.839
Alumina/Caustic ratio, A/C[**]	0.520
Density. g/ml	1.269

[*] Caustic ratio = $(Na_2O, g/dm^3 \times 102) / (Al_2O_3, g/dm^3 \times 62)$
[**] A/C = $(Al_2O_3, g/dm^3) (Na_2O, g/dm^3)$, ($Na_2O$ expressed as Na_2CO_3)

Desilication

The sodium aluminate leach liquor analyzed less than 0.1% silica (Table 3). This is due to the very low reaction rate of silica with sodium carbonate at the leaching temperature (90 °C) 12. Thus, there is no need for a desilication step in the further processing of the leach liquor to produce alumina.

Kinetic aspect

The chemical reactions of gibbsite with sodium carbonate and lime are given bellows:

$$Na_2CO_3 + Ca(OH)_2 \rightarrow 2NaOH + CaCO_3 \tag{1}$$

$$Al_2O_3 \cdot 3H_2O + 2NaOH \rightarrow 2NaAlO_2 + 4H_2O. \tag{2}$$
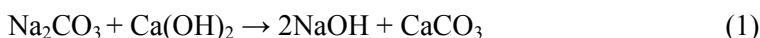
Silica reacts with sodium hydroxide to from sodium silicate, which then reacts with calcium carbonate to form calcium silicate:

$$SiO_2 + 2NaOH \rightarrow Na_2SiO_3 + H_2O \tag{3}$$

$$Na_2SiO_3 + CaCO_3 \rightarrow CaSiO_3 + Na_2CO_3. \tag{4}$$
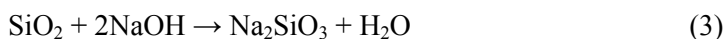
The leaching rate does not increase linearly with the concentration of sodium carbonate above 0.3 M. The rate seems to be limited by the concentration of hydroxide adsorbed on the surface of bauxite. If bauxite reacts with hydroxides already adsorbed on the surface of the bauxite, then the rate of reaction at the surface of sphere of radius r may be expressed as:

$$\frac{dn}{dt} = 4\pi r^2 k C_{Na_2CO_3} \tag{3}$$

where n is the number of bauxite moles in the particle at time t, k is the surface reacting rate constant (taking into account the shape factor and surface roughness), r is the radius of the unreacted core of the particle and $C_{Na_2CO_3}$ is the concentration of hydroxides adsorbed on the surface of the bauxite (mole/unit area).

First-order dependence on $C_{Na_2CO_3}$ was assumed in Eq. (3). The adsorption of hydroxide takes place faster than the leaching rate and the concentration of $C_{Na_2CO_3}$ is much higher than stoichiometry required. Eq. (3) can be integrated to give

$$1 - (1 - \alpha)\ 1/3 = Kt \qquad\qquad (4)$$

where α is the extent of extraction of aluminum, and t is the leaching time. The dependence of grinding time in attritor is illustrated in Fig. 7. The empirical rate constant is compared with the specific surface area of the ground sample in Fig. 8. It is concluded that the rate is a linear function of specific surface area in the interval 1.0–3 m^2/g. Such dependence is quite consistent with the leaching theory. It is also concluded that there is practically no dependence of the rate constant on surface area higher than 3 m^2/g. The formation of agglomerates, as a consequence of grinding may be the reason.
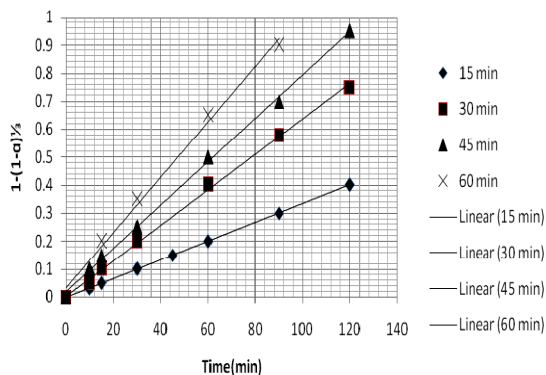
Fig. 7. Linear plots according to the surface reaction model for the effect of grinding time in attritor on leaching rate
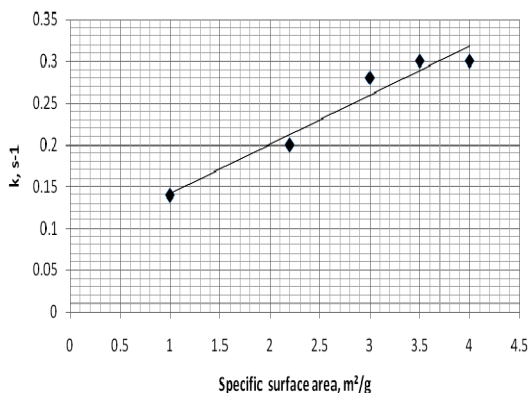
Fig. 8. Dependence of reaction rate (k) on specific surface area of ground bauxite

The surface reaction model was applied to determine the activation energy. The date are presented in Fig. 9. The apparent rate constants were determined from the straight lines of Fig. 9. and plotted according to the Arrhenius equation as shown in Fig. 10.
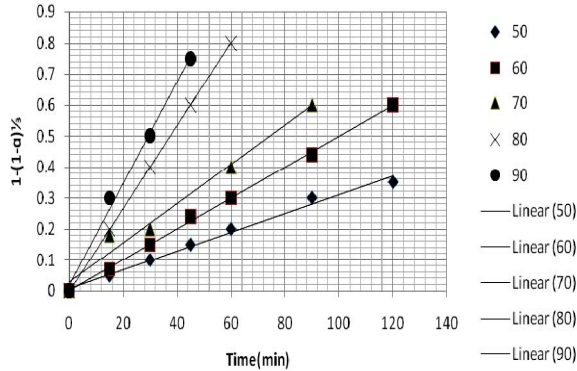
Fig. 9. Linear plots according to the surface reaction model for the effect of temperature on leaching rate. Data are given from Fig.4
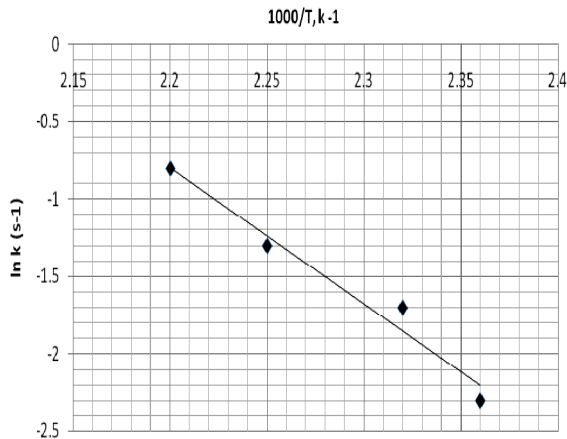
Fig. 10. Arrhenius plot of the apparent rate constants

The activation energy was determined to be 34 kJ/mole and the magnitude of this value confirms the proposed surface reaction control mechanism (Habashi, 1989 and Amer, 1996). The data of Fig. 5, which represents the effect of sodium carbonate concentration on Al recovery, plotted according to Eq. (4), give a linear relationships shown in Fig. 11. The slopes of the straight lines represent the apparent rate constant which are plotted as a function of sodium carbonate concentration in Fig. 12. The apparent rate constant increase and then levels off as the concentration of sodium hydroxide increases. This means that the apparent reaction order with respect to sodium

hydroxide concentration varies from first to zero as the concentration of sodium car-
bonate increases.
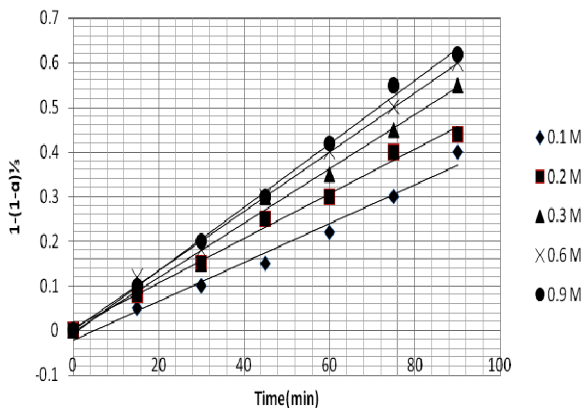
Fig. 11. Linear plots according to the surface reaction model for the effect
of NaCO$_3$ concentration on leaching rate. Data from Fig.6
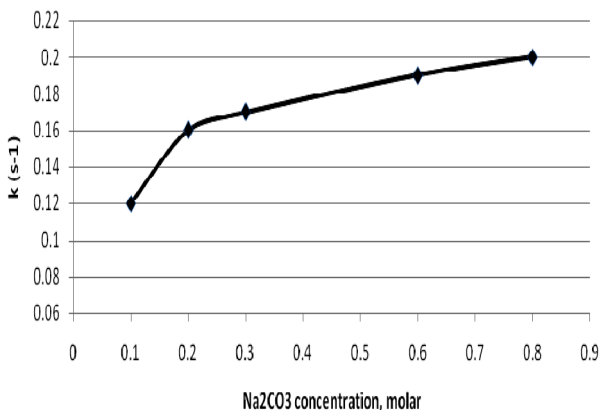
Fig. 12. Variation of the apparent rate constant (k) with Na$_2$CO$_3$ concentration

Conclusions

The bauxite ore from Um Bogma, Southwestern Sinai consists mainly of gibbsite
(70.1%) and kaolinite (11.0%). Beneficiation of the ore has brought down the silica
content from 13.2 to 2.4%. Hydrometallurgical processing of the beneficiated bauxite
in an attritor has given a high Al recovery of 95% for a short leaching duration of 30
min at 90 ºC. The sodium aluminate leach liquor obtained under the above conditions
contains less than 0.1% silica. There is no need for a desilication step in the conver-
sion of the leach liquor to alumina. It can also be concluded that there is practically no

dependence of the rate constant an surface area higher than 3 m^2/g. The activation energy was determined to be 34 KJ/mol and its magnitude confirms the proposed surface reaction control mechanism.

Refrences

AMER A.M. 1996, *Leaching of low grade Egyptian chromite ore*. Hydrometallurgy, 43 (1–3), 307–316

ANDREEV P.A., 1972, *Bauxite Mineral Resources of Industrial Countries and Developing Countries*. The USSR Ministry of Geology. V G F. Moscow. p. 158.

BELYAEV A.I., ZHEMECHUZHINA E.A., 1964, *Leaching of Bauxites at Elevated Pressure and Temperature*. Tr. 3-go Vses. Soveshch. po Khim. i Tekhnol. Glinozema, Erevan, 205-23, P 205 Chem Abstr 63, 7490.

CREGLEDI B., STOKER L., RIEDERAURE S., 1981, *Deironing Technology of Bauxite by Hydrochloric Acid*. Trav D`ICSOBA (International Committee for Study of Bauxites, Alumina and Aluminum), 16, p. 305.

FISHER K, GERMANNT K., SCHWARZ T., 1991, *Origin and properties of laterite – derived deposits in continental basin in upper Egypt and Northern Sudan*. Proc. 7 ME Euro Clay Conf. Dresden 91; 357–362.

GERMANN K, MIRCKE A., DOERING T., FISCKEN K., 1987. *Late cretaceous laterite – derived sedimentary deposits (ooletic ironstone – raolein – bauxite in upper Egypt*, Berliner Geowiss Abh (A) 753: 727–758.

HABASHI F, 1980, *Principles of Extractive Metallurgy. Gordon and Breach*, New York, Vol. 2, p. 59.

KUZNETSOVA S.I., DEREVYANKIN V.A., SHABALINA O.K., 1964, *Behaviour of compounds of Silicon, Titanium, Iron and Organic Substances During Bauxite Leaching*. Tr. 3-go Vses. Soveshch. po Khim. i Tekhnol. Glinozema, Erevan, 225-242.

LIU GUI-HUA, XIAO WEI, PENG ZHI-HONG, 2008, *Sintering process of diasporic bauxite with high iron content low ratioof lime to silica for alumina production the*, Chinese Journal of Nonferrous Metals, 10,

SAID SABET A.H., ZALAT A.A., TENIAKOV V.A., POKRYSHKIN V., 1976, *A Review of theories on the Geological Distribution of Bauxite and their Application for Bauxite prospecting in Egypt*. Annuals of the Geological survey of Egypt. Vol. l, p. 6.

SCOTFORD R.F., GLASTONBURY J.R., 1972, *The effect of temperature on the rates of dissolution of gibbsite and boehmite*. The Canadian Journal of Chemical Engineering, 49, 611–616.

SEGEV A, 1984, *Gibbsite Mineralization and its Genetic Implication for the Um Bogma Manganese Deposit. Southwestern Sinai*, Mineralium Deposita 19, Springer-Verlag, 54.

SMITH P. 2009, *The processing of high silica bauxite – Review of existing and potential resources*, Hydrometallurgy 98 (1–2), pp.162–167.

ZHAO Q., MILLER J.D., WANG X., 2010, *Recent development in the benefication of Chinese bauxite*, Mineral Processing and Extractive Metallurgy Review 31(2), 111–119.

INTERRELATION OF THE FUERSTENAU UPGRADING CURVE PARAMETERS WITH KINETICS OF SEPARATION

Alicja BAKALARZ, Jan DRZYMALA

Wroclaw University of Technology, Wybrzeze Wyspianskiego 27, 50-370 Wroclaw
e-mail: alicja.bakalarz@pwr.wroc.pl; jan.drzymala@pwr.wroc.pl

Abstract: It was shown in the paper that kinetic equations relating recoveries of two components in separation products and time, when combined together to eliminate the time parameter, provide mathematical equations which relate recoveries of the two considered components in concentrate. The obtained one-adjustable-parameter type equations are very useful for approximation of the separation results plotted as the so-called Fuerstenau upgrading curves. Most empirical mathematical formulas presently used for the Fuerstenau plots were derived using various kinetic equations while some are still awaiting for their kinetic derivation.

keywords: *separation, upgrading, kinetics, Fuerstenau curve, beneficiation, recovery, selectivity*

Introduction

Kinetics is one of the most important aspects of separation process (Arbiter, 1951; Arbiter and Harris, 1982; Laskowski, 1989; Wills and Napier-Munn, 2006). The rate of separation determines the time needed for removal of valuable components of ores (Schumann, 1942; Kelly and Spottiswood, 1989). The kinetics of separation is also a basic element of separation models relating components recovery, products grade and properties of the feed. These models can be based on probabilities, energies, forces and their combinations concepts (Drzymala, 2007b). The rate at which a separation process occurs depends on the specificity of the process and process parameters. As a result the kinetic equations relating recovery of an ore component with separation time can assume different mathematical forms (Schumann, 1942; Somasundaran and Lin, 1973; Yuan et al., 1996). Presently more than a dozen kinetic models are available and applied in separation science and technology (for instance Somasundaran and Lin, 1973; Agar et al., 1998; Xu, 1998; Polat and Chander, 2000;

Cilek, 2003; Wills and Napier-Munn, 2006; Brozek and Mlynarczykowska, 2007). The list of selected kinetic equations is presented in Table 1.

In this paper application of kinetic equations for approximation of separation results will be presented. It will be shown that the kinetics of two selected components of the ore provide an equation which can be directly used for construction and interpretation of the recovery–recovery Fuerstenau upgrading curves.

Table 1. Selected kinetic equations (ε – recovery of a component in separation product, ε_{max} – maximum recovery of the same component in separation product, k – rate constant of separation, t – separation time)

Model	Formula	
Zeroth-order model	$\varepsilon = k\,t$	(1)
First-order model	$\varepsilon = \varepsilon_{max}\left(1 - e^{-kt}\right)$	(2)
First-order with rectangular distribution of floatabilities	$\varepsilon = \varepsilon_{max}\left[1 - \dfrac{1}{k\,t}\left(1 - e^{-k\,t}\right)\right]$	(3)
Fully mixed reactor model	$\varepsilon = \varepsilon_{max}\left(1 - \dfrac{1}{1 + \dfrac{t}{k}}\right)$	(4)
Improved gas/solid adsorption model	$\varepsilon = \varepsilon_{max}\left(\dfrac{k\,t}{1 + k\,t}\right)$	(5)
$\dfrac{3}{2}$ -order model	$\varepsilon = \varepsilon_{max}\left(1 - \dfrac{1}{\left(1 + \dfrac{1}{2}k\,t\sqrt{\varepsilon_{max}}\right)^2}\right)$	(6)
Second-order model	$\varepsilon = \dfrac{\varepsilon_{max}^{2}\,k\,t}{1 + \varepsilon_{max}\,k\,t}$	(7)
Second-order model with rectangular of floatabilites	$\varepsilon = \varepsilon_{max}\left\{1 - \dfrac{1}{k\,t}\left[\ln\left(1 + k\,t\right)\right]\right\}$	(8)

Kinetic curves

In minerallurgy the kinetic curves relate recovery of a selected component and time of the process. According to Table 1, the kinetics of separation can assume different mathematical forms. Separation of components according to the first and second order kinetics is presented in Fig.1a. Figure 1a shows the kinetics of separation of one component and also the remaining components of the feed. It has to be emphasized that the sum of the considered and remaining components of the system provides the kinetics of concentrate formation (Fig. 1b).
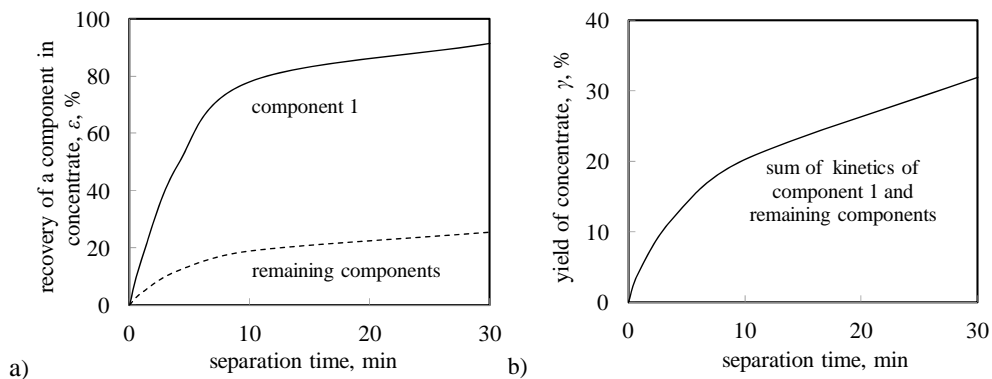
Fig. 1. Separation results plotted as a relationship between recovery of each component in concentrate and separation time (a), yield of components forming concentrate vs. separation time (b)

Separation and upgrading

The characterization of separation results can be accomplished in a number of ways. The most common is upgrading in which quality and quantity of separation products are analyzed (Drzymala et al., 2010; Kowalczuk and Drzymala, 2011). The results of upgrading can be presented either in a tabular or graphical form. Theoretically, there is an infinite number of upgrading curves while in literature about fifty of them can be
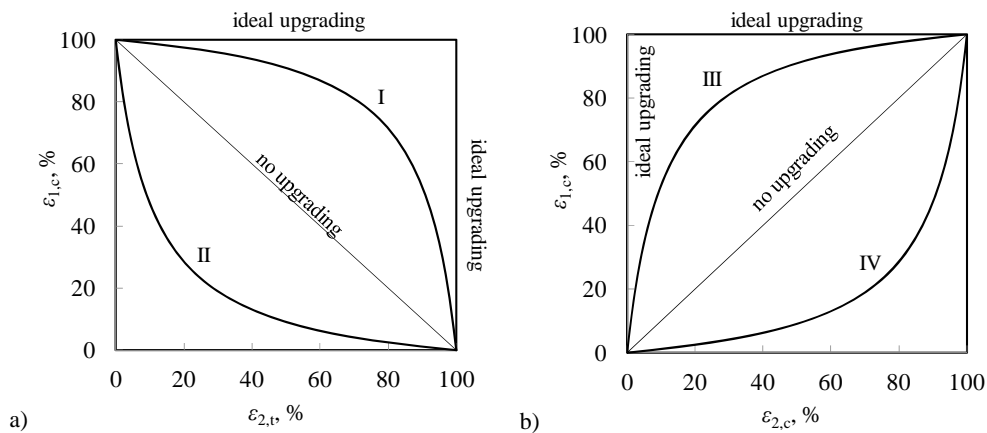
Fig. 2. The Fuerstenau upgrading curves: a) relationship between recovery of a component 1 in concentrate $\varepsilon_{1,c}$ and recovery of a second component in the tailing $\varepsilon_{2,t}$: I - recovery of component 1 in concentrate is greater than recovery of component 2 in concentrate, II - recovery of component 2 in concentrate is greater than recovery of component 1 in concentrate, b) relationship $\varepsilon_{1,c}$ vs. $\varepsilon_{2,c}$: III – recovery of component 1 in concentrate is greater than recovery of component 2 also in concentrate, IV – recovery of component 1 is smaller than recovery of component 2 in the same concentrate (after Drzymala and Ahmed, 2005)

found (Drzymala, 2006, 2007a, 2008). All of them are based on the same data but show the separation elements in different mathematical, graphical an esthetical forms. One of the upgrading curve is the Fuerstenau plot which relates recoveries of two components in the same or different products (Fig. 2). It has been recently quite frequently used because there are simple empirical equations which can be used for the approximation of separation results present as the Fuerstenau graphs (Drzymala and Ahmed, 2005).

The Fuerstenau plot and kinetics of separation

Since the kinetics of separation relates recovery of feed components in products with separation time while the Fuerstenau curve relates recoveries of components, it becomes obvious that elimination of time from the kinetic equations provides the Fuerstenau plot (Fig. 3).
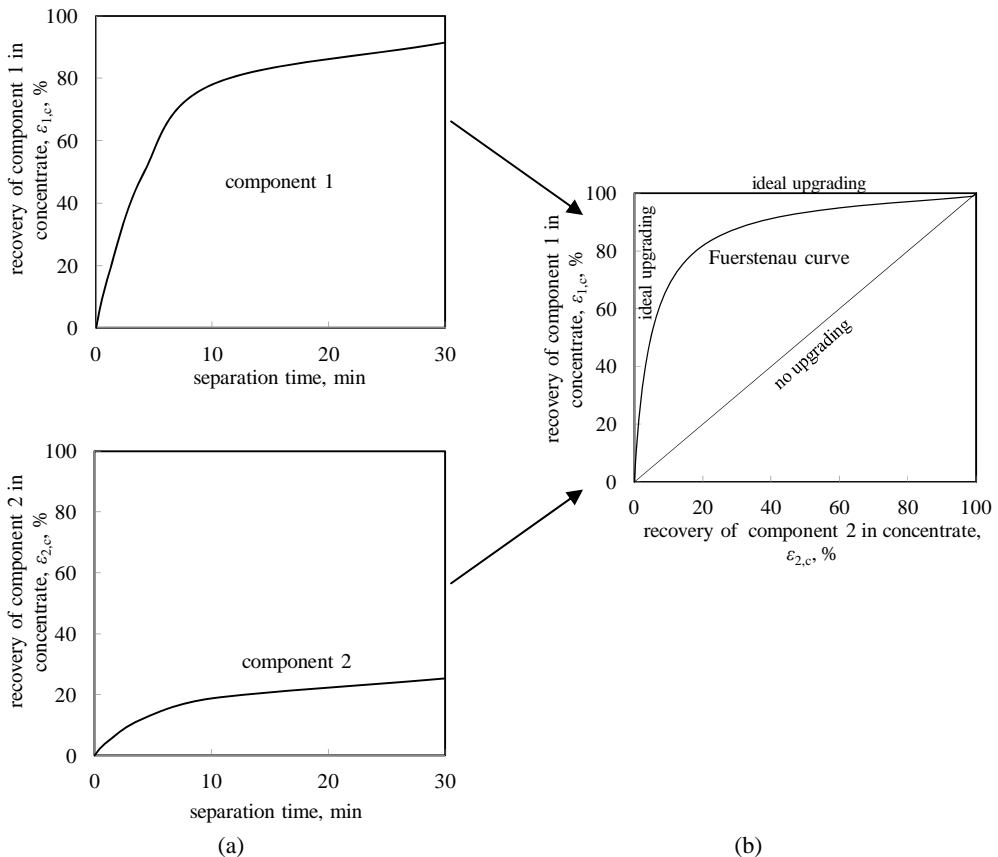
Fig. 3. The kinetics of separation of feed components (a) provide separation results
in the form of the Fuerstenau upgrading curve (b)

Table 2. Kinetic formulas for different combinations of orders (0, 1, 3/2, 2) of separation kinetics
($k = k_1/k_2$, $k' = k_2/k_1$, $\varepsilon_{2,c}$ = component 1 recovery in concentrate, $\varepsilon_{1,c}$ = component 2 recovery in concentrate)

$\varepsilon_{2,c}$ \ $\varepsilon_{1,c}$	0	1	$\frac{3}{2}$	2
0	$\varepsilon_{1,c} = k\,\varepsilon_{2,c}$ Eq. 9 (Fig. 4)	$\varepsilon_{1,c} = -k'\ln\left(\frac{\varepsilon_{2,c}}{100}\right)$ Eq. 10 (Fig. 5)	$\varepsilon_{1,c}=100\cdot\left[1-\frac{1}{(1+5k\,\varepsilon_{2,c})^2}\right]$ Eq. 11 (Fig. 8)	$\varepsilon_{1,c} = \frac{k'\,\varepsilon_{2,c}}{100(100-\varepsilon_{2,c})}$ Eq. 12 (Fig. 6)
1	$\varepsilon_{1,c} = -k\ln\left(\frac{\varepsilon_{2,c}}{100}\right)$ Eq. 13 (Fig. 5)	$\varepsilon_{1,c}=100\cdot\left[1-\left(\frac{100-\varepsilon_{2,c}}{100}\right)^k\right]$ Eq. 14 (Fig. 7)	$\varepsilon_{1,c}=100\cdot\left[1-\frac{1}{\left(1-5k\ln\left(\frac{100-\varepsilon_{2,c}}{100}\right)\right)^2}\right]$ Eq. 15 (Fig. 9)	$\varepsilon_{1,c}=\frac{100^2 k\ln\left(\frac{100-\varepsilon_{2,c}}{100}\right)}{100\,k\ln\left(\frac{100-\varepsilon_{2,c}}{100}\right)-1}$ Eq. 16 (Fig. 12)
$\frac{3}{2}$	$\varepsilon_{1,c}=100\cdot\left[1-\frac{1}{(1+5\cdot k'\,\varepsilon_{2,c})^2}\right]$ Eq. 17 (Fig. 8)	$\varepsilon_{1,c}=100\cdot\left[1-\frac{1}{\left(1-5\cdot k'\ln\left(\frac{100-\varepsilon_{2,c}}{100}\right)\right)^2}\right]$ Eq. 18 (Fig. 9)	$\varepsilon_{1,c}=100\cdot\left[1-\frac{1}{\left(1+\frac{k(10-\sqrt{100-\varepsilon_{2,c}})}{\sqrt{100-\varepsilon_{2,c}}}\right)^2}\right]$ Eq. 19 (Fig. 10)	$\varepsilon_{1,c}=100\cdot\left[1-\frac{1}{\left(1+\frac{k'\,\varepsilon_{2,c}}{20(100-\varepsilon_{2,c})}\right)^2}\right]$ Eq. 20 (Fig. 11)
2	$\varepsilon_{1,c} = \frac{k\,\varepsilon_{2,c}}{100\cdot(100-\varepsilon_{2,c})}$ Eq. 21 (Fig. 6)	$\varepsilon_{1,c}=\frac{100^2 k'\ln\left(\frac{100-\varepsilon_{2,c}}{100}\right)}{100\,k'\ln\left(\frac{100-\varepsilon_{2,c}}{100}\right)-1}$ Eq. 22 (Fig. 12)	$\varepsilon_{1,c}=100\cdot\left[1-\frac{1}{\left(1+\frac{k\cdot\varepsilon_{2,c}}{20\cdot(100-\varepsilon_{2,c})}\right)^2}\right]$ Eq. 23 (Fig. 11)	$\varepsilon_{1,c} = \frac{100\,k\,\varepsilon_{2,c}}{\varepsilon_{2,c}(k-1)+100}$ Eq. 24 (Fig. 13)

Mathematical formulas of the Fuerstenau curves based on kinetic considerations

Since the kinetic equations applied to delineate separation results with time are well known (Table 1), their combinations provide mathematical formulas for approximation of the upgrading results plotted as the Fuerstenau curves. They are collected in Table 2. In all the equations, $k = k_1/k_2$, where k_1 and k_2 are rate constants of component 1 and component 2, respectively. The equations shown in Table 2 are also plotted as the Fuerstenau curves and presented in Table 3 as Figs. 4–13. The shape of each curve depends on the k value. The curves are asymmetrical, except the one shown in Fig. 13, which is symmetrical in relation to the diagonal line of the graph and results from separation of both components according to the second order kinetics.

Table 3. The Fuerstenau plots for different combinations of kinetics of separation ($\varepsilon_{\max} = 100\%$).
Kinetic and separation curves equations are presented in Table 2
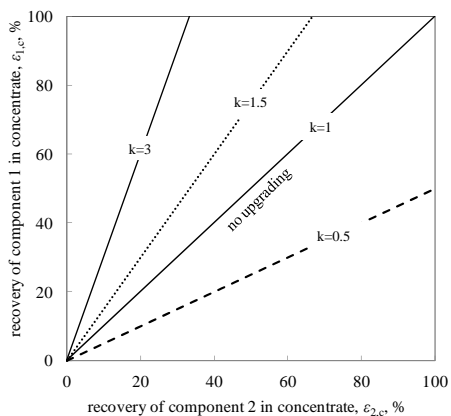
Fig. 4.
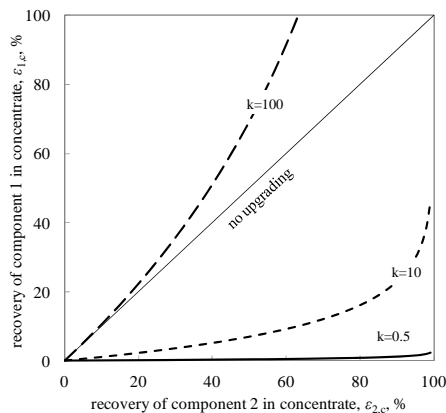
Fig. 5.
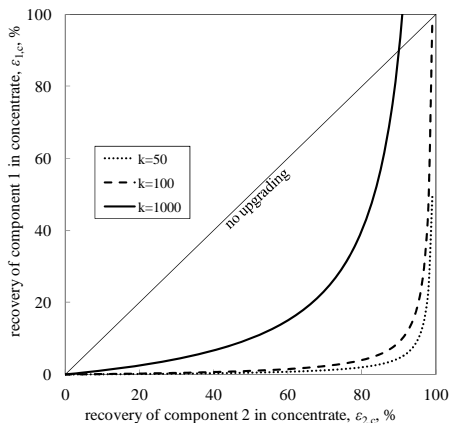
Fig. 6
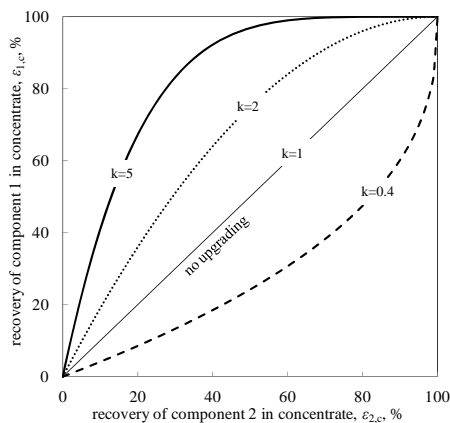
Fig. 7
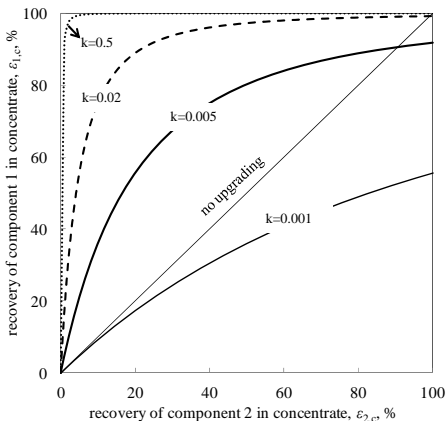
Fig. 8
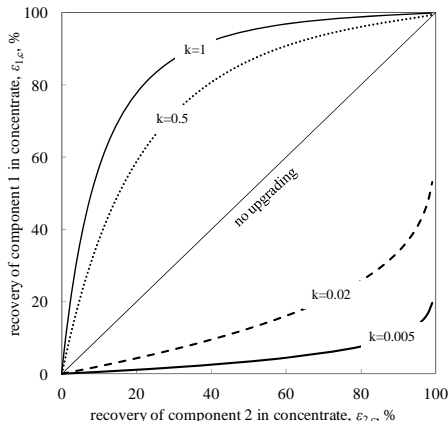
Fig. 9
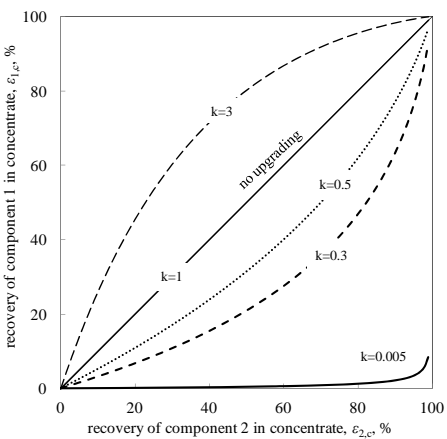
Fig. 10
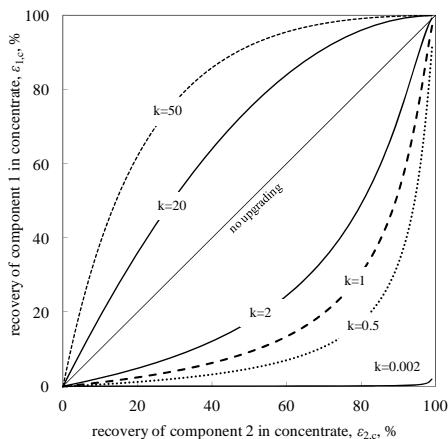
Fig. 11
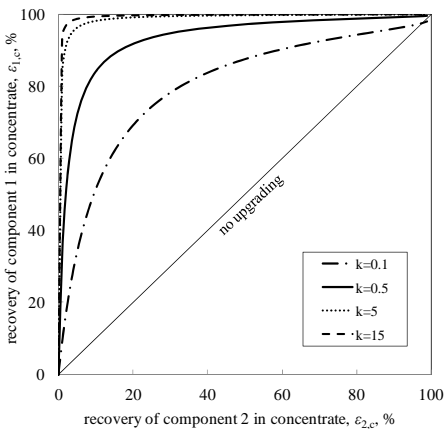
Fig. 12
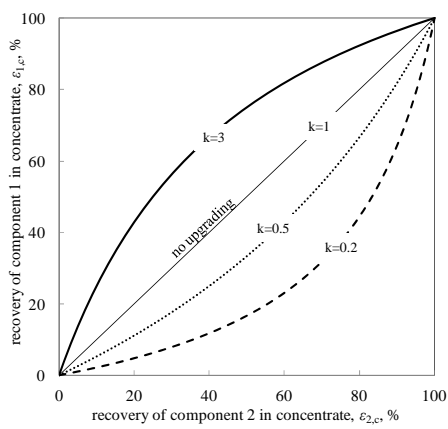
Fig. 13

A comparison of the derived here equations indicates that most empirical equations proposed by Ahmed and Drzymala (2005) can be predicted from the kinetic considerations except equation:

$$\varepsilon_{1,c} = \frac{\varepsilon_{2,c}^{b}}{100^{(b-1)}} \qquad (19)$$

which is awaiting for kinetic justification.

Conclusions

The Fuerstenau upgrading plots relate recovery of components in products. It results from this paper that most mathematical equations that are used for approximation of separation results using the Fuerstenau upgrading curves can be derived from kinetic considerations. Since kinetics relates recovery of a component in a product and time, elimination of time in the kinetic equations for two components provide mathematical equations characterizing separation, which can be plotted as the Fuerstenau curves. The separation curves, including the Fuerstenau upgrading plot, are very useful for approximation, characterization and interpretation of laboratory and industrial results of separation.

Acknowledgements

References

AGAR G.E., CHIA J., REQUIS-C L., 1998. *Flotation rate measurements to optimize an operating circuits*. Miner. Eng., 11(4), 347–360.

ARBITER N., 1951. *Flotation rates and flotation efficiency*. Trans. AIME. Sept., 791–796.

ARBITER N., HARRIS C.C., 1982. *Flotation Kinetics. Froth Flotation*, D.W. Fuerstenau (ed.), AIME, New York, 215.

BROZEK M., MLYNARCZYKOWSKA A., 2007. *Analysis of kinetics models of batch flotation*. Physicochem. Probl. Miner. Process., 41, 51–65.

CILEK E.C., 2004. *Estimation of flotation kinetic parameters by considering interactions of the operating variables*. Miner. Eng., 17, 81–85.

DRZYMALA J., 2006. *Atlas of upgrading curves used in separation and mineral science and technology*. Part I. Physicochem. Probl. Miner. Process., 40, 19–29.

DRZYMALA J., 2007a. *Atlas of upgrading curves used in separation and mineral science and technology*. Part II. Physicochem. Probl. Miner. Process., 41, 27–35.

DRZYMALA J., 2007b. *Mineral Processing. Foundations of theory and practice of minerallurgy*, Oficyna Wyd. PWr., Wroclaw, website: http://www.dbc.wroc.pl/dlibra/docmetadata?id=2070&from= &dirids=1&ver_id=&lp=7&QI.

DRZYMALA J., 2008. *Atlas of upgrading curves used in separation and mineral science and technology*. Part III. Physicochem. Probl. Miner. Process., 42, 75–84.

DRZYMALA J., AHMED H.A.M., 2005. *Mathematical equations for approximation of separation results using the Fuerstenau upgrading curves*. Int. J. Miner. Process., 76, 55–65.

DRZYMALA J., LUSZCZKIEWICZ A., FOSZCZ D., 2010. *Application of upgrading curves for evaluation of past, present, and future performance of a separation plant*. Mineral Processing and Extractive Metall. Rev., 31 (3), 165–175.

KELLY E.G., SPOTTISWOOD D.J., 1989. *Introduction to mineral processing*, 2nd edition, Mineral Engineering Services, Denver.

KOWALCZUK P.B., DRZYMALA J., 2011. *A proposition of symbolism of non-ideal separations followed by analytical procedures for description of separation processes*. Miner. Process. Extr. Metall. Rev. 32(4), 278–288.

LASKOWSKI J.S., 1989. *Thermodynamic and kinetic flotation criteria*. Gordon and Breach Science Publishers, New York, in English.

POLAT M., CHANDER S., 2000. *First-order flotation kinetics models and methods for estimation of the true distribution of flotation rate constants*. Int. J. Miner. Process., 58, 145–166.

SCHUHMANN Jr. R., 1942. *Flotation Kinetics. I. Methods for steady-state study of flotation problems*. J. Phys. Chem., 46(8), 891-902.

SOMASUNDARAN P., LIN I.J., 1973. *Method for evaluating flotation kinetic parameters*. Trans. AIME 254, 181–184.

WILLS B.A., NAPIER-MUNN T., 2006. *Mineral processing technology. An introduction to the practical aspects of ore treatment and mineral recovery*. 7th edition. Elsevier Science & Technology Books.

XU M., 1998. *Modified flotation rate constant and selectivity index*. Miner. Eng., 11(4), 271–278.

YUAN X, M, PALSSON B.I., FORSSBERG K.S.E., 1996. *Statistical interpretation of flotation kinetics for a complex sulphide ore*. Miner. Eng., 9(4), 429–442.

FLUKA MONTE CARLO SIMULATIONS ON NEUTRON INTERACTIONS WITH FeCrP AND FeTiP

Erhan GORMEZ, Turgay KORKUT

Faculty of Science and Art, Department of Physics, Ibrahim Cecen University, 04100, Ağrı, Turkey,
E-mail: turgaykorkut@hotmail.com; tel.: +90 505 874 62 73

Abstract: Andreyivanovite was found in the Kaidun meteorite as individual grains and linear arrays of grains with a maximum dimension of 8 μm within two accumulations of Fe-rich serpentine present in the meteorite. Florenskyite was found as four dispersed grains with a maximum dimension of 14 μm within a single particle of Fe-rich serpentine within the Kaidun meteorite. Their general chemical formulas are FeCrP and FeTiP while stochiometric formulas are $Fe^{0+}Cr_{0.58}Fe^{0+}_{0.15}V^{0+}_{0.1}Ti_{0.08}Ni_{0.06}Co_{0.002}P$ and $Fe^{0+}_{0.98}Ni_{0.13}Ti_{0.85}P$, respectively. We simulated interactions between these two substances and neutron particles (fusion neutrons by reactors, ^{241}Am-Be and ^{252}Cf neutrons used in many scientific investigations and industrial applications). The FLUKA code was used to calculate such interaction parameters as macroscopic cross sections, neutron fluencies and isotope production. Macroscopic cross sections of andreyivanovite and florenskyite are better than concrete (widely used neutron shielding processes). Also radioactive isotopes produced after neutron interactions with these materials are stable. This information may be useful in space and chemistry investigations.

Keywords: *Kaidun meteorite, andreyivanovite, florenskyite, Monte Carlo simulations*

Introduction

The Kaidun meteorite fell on Earth on 3 December 1980 in Yemen (15° 0' N, 48° 18' E). Out of the nearly 60 minerals found within the meteorite, several have not been found in nature, including florenskyite (FeTiP). The meteorite has 842 g of mass and it contains carbonaceous chondrite material. Two phospide based minerals were discovered in the meteorite (Ivanov et al., 2000; Zolensky et al., 2008). They were named andreyivanovite for Andrey Ivanov (Russian geochemist and mineralogist) and florenskyite for Cyrill P. Florensky (Russian geochemist).

Basically, the structure of andreyivanovite consists of Fe, Cr and P elements (Zolensky et al., 2008). Its luster is metallic, transparency is opaque and it has a creamy white color. Crystal system of andreyivanovite is orthorhombic and it belongs

to the dipyramidal class. The density of andreyivanovite is calculated as 6.65 g/cm^3. The empirical formula of andreyivanovite found in the Kaidun meteorite is $Fe^{0+}Cr_{0.58}Fe^{0+}_{0.15}V^{0+}_{0.1}Ti_{0.08}Ni_{0.06}Co_{0.002}P$. Since andreyivanovite is a newly discovered mineral, studies on its properties are limited.

   Elements that form the structure of are iron, nickel, titanium and phosphorus. It is a Fe-rich serpentine like andreyivanovite (Ivanov et al., 2000). The empirical formula of florenskyite found in the Kaidun meteorite is $Fe^{0+}_{0.98}Ni_{0.13}Ti_{0.85}P$.

   There are many studies on the Kaidun meteorite. The studies generally are focused on chronology (Petitat et al., 2011), geochemistry (Ivanov et al., 2010) and space research (Ivanov et al., 2004). Interactions between different Kaidun's minerals and cosmic rays were studied to determine the history of Kaidun meteorite (Kashkarov et al., 1995). It appears that the studies about Kaidun meteorites are inadequate. In this paper we investigated neutron and gamma interactions with andreyivanovite ($Fe^{0+}Cr_{0.58}Fe^{0+}_{0.15}V^{0+}_{0.1}Ti_{0.08}Ni_{0.06}Co_{0.002}P$) or generally FeCrP and florenskyite ($Fe^{0+}_{0.98}Ni_{0.13}Ti_{0.85}P$) or generally (Fe, Ni)TiP.

Monte Carlo simulations

The Monte Carlo method is based on random numbers and mathematical algorithms (Ramírez-López et al., 2011). It can be applied for physical systems, especially in nuclear science. In this study we used FLUKA (Ferrari et al., 2005; Battistoni et al., 2006) as a Monte Carlo simulator. FLUKA is a Monte Carlo package used in interactions between all subatomic particles and matter. It has many advantages in terms of wide energy range. For example, it can simulate neutrons from thermal level to 20 TeV. Also it is useful in many scientific areas (high energy experimental physics and engineering, shielding, detector and telescope design, cosmic ray studies, dosimetry, medical physics and radio-biology). We used the FLUKA Monte Carlo code to simulate neutron and gamma radiation with different materials in our latest studies (Korkut et al., 2010; Korkut et al., 2011; Korkut et al., 2012). In some of these studies we compared FLUKA results with experiments. The FLUKA Monte Carlo Simulation code was used to calculate neutron attenuation coefficients, neutron fluencies and radioisotope productions. These two Monte Carlo packages are open codes and their usage is very simple. Firstly, an input file was created in accordance with experimental conditions. This file includes several parameters as primary beam type and energy, material definitions, geometrical setups, some physical sets (if required), desired outputs (transmission, radioisotope production etc…) and finally total number of particles. And then simulation is run and results are read from the output files.

Simulation setups

We used the 2011.2.8 version of FLUKA. For reactor neutrons 14.1 MeV, for ^{241}Am-Be source a neutron spectrum from 100 keV to 12 MeV and for gamma beam 59.54

keV primary energies were used in the simulations. Number of primary particles was entered as 10^6 in simulations. Andreyivanovite consists of 2.79% Ti, 4% V, 21.99% Cr, 46.27% Fe, 0.08% Co, 2.54% Ni and 22.32% P while florenskyite includes 30.36% Ti, 40.83% Fe, 5.69% Ni and 23.11% P. We used these numbers in our simulations. The shape of sample is cylindrical. Thickness of mineral samples is entered in simulations as 5 cm. Detector area and volume values were taken as defaults of the code. We wanted to get particle transmissions, neutron fluencies and radioisotope production after neutron interactions with mineral samples.

Results and discussions

We have simulated neutron interactions with two meteoritic minerals by the FLUKA Monte Carlo simulation code. Also the FLAIR (Vlachoudis, 2009) tool was used to perform data analysis, simulation geometry and create plots. Simulation results obtained for these two minerals are given below into two sections.

Simulation results for andreyivanovite

Microscopic cross section (σ) is related to probability of interaction of neutrons with the target material. The sum of the microscopic cross sections of the individual nuclei in the target material per unit volume is called the Macroscopic Cross Section (Σ)

$$\Sigma = N\sigma \tag{1}$$

where N is the atomic density of the target. To obtain neutron transmissions by simulations, we used USRBDX score card. Neutron transmission values were used from

$$\Sigma = \frac{\ln T}{x} \tag{2}$$

where x is sample thickness. Neutron transmissions and total neutron macroscopic cross sections for three different three neutron energies are shown in Table 1.

Isotope products after neutron irradiations on mineral samples were calculated by using RESNUCLEI score options in FLUKA. As shown in Tables 2 and 3 different isotopes are formed as a result of interactions. As a result of interactions ^{56}Fe was formed in high amounts for the three neutron energies.

Table 1. Neutron transmissions and total macroscopic cross sections for andreyivanovite

Source	Energy (MeV)	Transmission	Total Macroscopic Cross Section (cm^{-1})
^{241}Am-241	4.5	0.26	0.27
^{252}Cf	2.16	0.32	0.23
Reactor	14.1	0.39	0.19

E. Gormez, T. Korkut

Table 2. Isotope yields after neutron irradiations as a function of mass numbers for andreyivanovite

Am-Be		Cf-252		Reactor	
A	Isotope yield (nuclei/cm3/pr)	A	Isotope yield (nuclei/cm3/pr)	A	Isotope yield (nuclei/cm3/pr)
65	8.38E–08	65	4.94E–08	65	5.31E–09
64	7.18E–06	64	3.36E–06	64	2.42E–06
63	7.82E–09	63	9.96E–08	63	4.17E–06
62	2.09E–05	62	1.11E–05	62	1.33E–05
61	7.78E–06	61	8.82E–06	61	1.50E–05
60	1.62E–04	60	7.90E–05	60	1.11E–04
59	3.06E–04	59	2.25E–04	59	1.53E–04
58	1.43E–03	58	8.40E–04	58	8.16E–04
57	8.77E–03	57	8.22E–03	57	3.79E–03
56	3.13E–01	56	2.25E–01	56	2.43E–01
55	2.83E–05	55	2.77E–05	55	1.08E–01
54	2.10E–02	54	1.03E–02	54	1.23E–02
53	1.22E–03	53	9.73E–04	53	1.94E–02
52	9.25E–03	52	5.08E–03	52	8.88E–03
51	1.35E–04	51	1.06E–04	51	3.55E–03
50	7.84E–04	50	5.34E–04	50	6.38E–04
49	4.36E–04	49	2.09E–04	49	7.48E–04
48	5.77E–03	48	3.83E–03	48	4.21E–03
47	6.21E–04	47	4.75E–04	47	2.05E–03
46	6.71E–04	46	4.47E–04	46	6.48E–04
44	5.62E–06	44	2.33E–07	45	2.71E–04
32	6.21E–07	32	1.46E–06	44	2.89E–05
31	1.02E–03	31	6.62E–04	43	4.26E–05
28	2.47E–06	4	1.41E–06	42	2.33E–06
4	1.16E–04	1	5.80E–04	32	2.30E–07
1	5.24E–03			31	2.64E–04
				30	5.44E–04
				28	1.72E–04
				27	1.91E–05

Fluence is specified as the number of particles traversing a unit surface in a particular point in void per unit time. Neutron fluence means the number of neutrons per unit area (cm^2). We show the neutron fluencies as three different lines plotted in Figs 1-3 for [241]Am-Be, [252]Cf and reactor neutrons, respectively. As can be seen in these figures, andreyivanovite mineral does not produce thermal or epithermal neutrons.

Table 3. Isotope yields after neutron irradiations as a function of atomic numbers for andreyivanovite

Am-Be		Cf-252		Reactor	
Z	Isotope yield (nuclei/cm³/pr)	Z	Isotope yield (nuclei/cm³/pr)	Z	Isotope yield (nuclei/cm³/pr)
28	5.01E–04	28	2.87E–04	28	2.80E–004
27	4.15E–04	27	2.41E–04	27	5.54E–004
26	3.38E–01	26	2.44E–01	26	3.21E–001
25	4.87E–03	25	5.31E–04	25	5.42E–002
24	1.11E–02	24	6.60E–03	24	2.32E–002
23	2.16E–04	23	1.05E–04	23	1.41E–003
22	7.76E–03	22	5.14E–03	22	7.26E–003
21	5.40E–05	21	7.66E–06	21	6.17E–004
20	5.70E–06	20	2.33E–07	20	2.18E–004
15	8.85E–04	15	6.33E–04	15	1.54E–004
14	1.34E–04	14	3.04E–05	14	6.54E–004
13	2.47E–06	2	1.41E–06	13	1.91E–004
2	1.11E–04	1	5.80E–04	2	1.32E–002
1	5.24E–03			1	5.70E–002
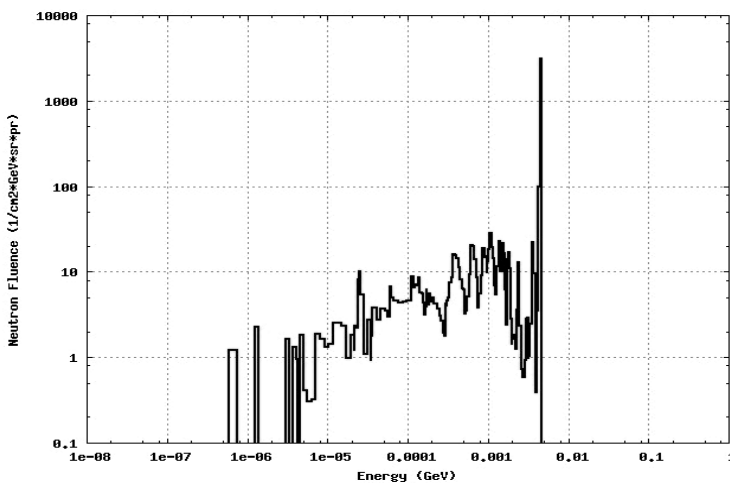
Fig. 1. Andreyivanovite neutron fluence for [241]Am-Be

Simulation results for florenskyite

The same FLUKA Monte Carlo simulations shown above were performed for florenskyite. Neutron transmissions and total macroscopic cross sections are given in Table 4. Radioisotope fragments after neutron irradiation as a function of A and Z are shown in Table 5 and Table 6. Neutron fluencies as a function of energy are illustrated in Figs 4-6 for [241]Am-Be, [252]Cf and reactor energies, respectively.
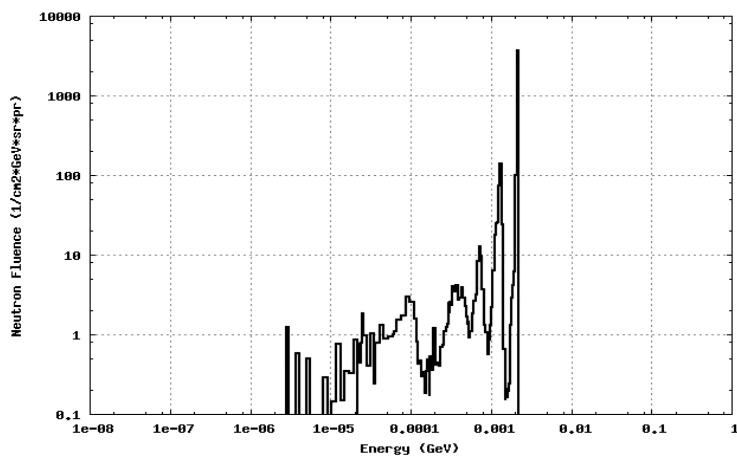
Fig. 2. Andreyivanovite neutron fluence for [252]Cf source
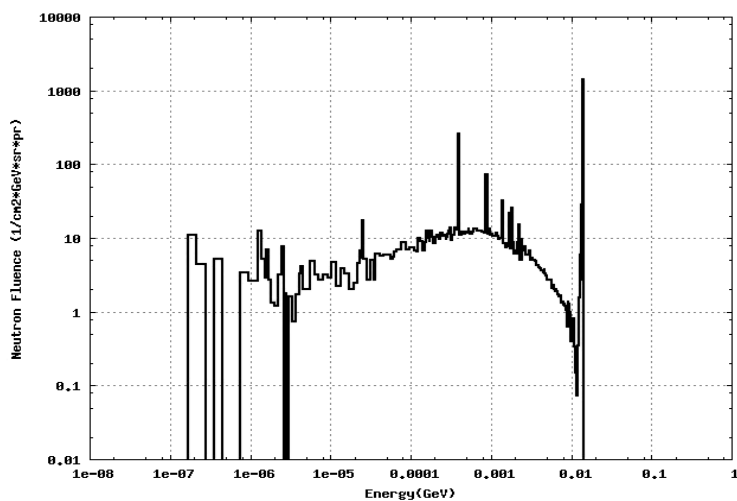
Fig. 3. Andreyivanovite neutron fluence for reactor

Table 4. Neutron transmissions and total macroscopic cross sections for florenskyite

Source	Energy (MeV)	Transmission	Total macroscopic cross section (cm^{-1})
[241]Am-241	4,5	0.27	0.27
[252]Cf	2.16	0.28	0.26
Reactor	14.1	0.41	0.18

Table 5. Isotope yields after neutron irradiations as a function of mass numbers for florenskyite

Am-Be		Cf-252		Reactor	
A	Isotope yield (nuclei/cm^3/pr)	A	Isotope yield (nuclei/cm^3/pr)	A	Isotope yield (nuclei/cm3/pr)
65	1.29E–07	65	3.98E–07	65	7.85E–08
64	1.85E–04	64	7.66E–05	64	7.23E–05
63	1.19E–06	63	2.25E–06	63	1.24E–04
62	7.06E–04	62	3.42E–04	62	3.98E–04
61	2.52E–04	61	2.35E–04	61	4.81E–04
60	5.10E–03	60	2.34E–03	60	3.49E–03
59	1.57E–05	59	3.66E–05	59	1.59E–03
58	1.31E–02	58	6.43E–03	58	7.16E–03
57	3.41E–03	57	3.11E–03	57	7.12E–03
56	1.21E–01	56	8.48E–02	56	9.37E–02
55	3.62E–04	55	2.25E–05	55	4.32E–02
54	8.08E–03	54	3.80E–03	54	4.72E–03
53	1.85E–05	53	2.36E–07	53	7.34E–03
51	5.00E–06	51	1.27E–06	52	1.22E–04
50	4.63E–03	50	2.56E–03	51	5.11E–04
49	6.27E–03	49	2.97E–03	50	3.03E–03
48	8.31E–02	48	5.33E–02	49	5.57E–03
47	8.89E–03	47	6.77E–03	48	6.01E–02
46	9.70E–03	46	6.21E–03	47	2.92E–02
44	8.38E–05	44	2.61E–06	46	9.28E–03
43	5.87E–07	32	1.09E–04	45	3.88E–03
32	5.37E–05	31	4.83E–02	44	4.48E–04
31	7.62E–02	4	1.42E–05	43	6.02E–04
28	1.66E–04	1	3.14E–03	42	3.33E–05
4	6.34E–04			32	1.29E–05
1	1.65E–02			31	1.94E–02
				30	4.07E–02
				28	1.28E–02
				27	1.51E–03
				4	2.37E–02
				3	4.22E–07
				2	9.03E–04
				1	8.82E–02

Table 6. Isotope yields after neutron irradiations as a function of atomic numbers for florenskyite

Am-Be		Cf-252		Reactor	
Z	Isotope yield (nuclei/cm^3/pr)	Z	Isotope yield (nuclei/cm^3/pr)	Z	Isotope yield (nuclei/cm^3/pr)
28	1.54E–02	28	8.67E–03	28	8.67E–03
27	3.55E–03	27	5.46E–04	27	1.01E–02
26	1.32E–01	26	9.18E–02	26	1.25E–01
25	1.88E–03	25	2.00E–04	25	2.11E–02
24	3.14E–05	24	4.13E–07	24	4.92E–03
22	1.12E–01	22	7.17E–02	22	1.00E–01
21	7.66E–04	21	1.06E–04	21	8.72E–03
20	8.59E–05	20	2.61E–06	20	3.16E–03
15	6.59E–02	15	4.62E–02	15	1.10E–02
14	1.04E–02	14	2.29E–03	14	4.92E–02
13	1.66E–04	2	1.42E–05	13	1.43E–02
2	6.34E–04	1	3.14E–03	2	2.37E–02
1	1.65E–02			1	8.91E–02
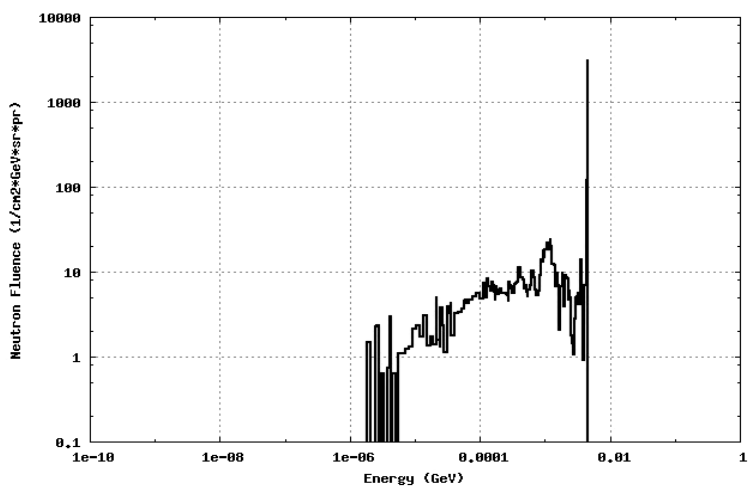
Fig. 4. Florenskyite neutron fluence for [241]Am-Be source
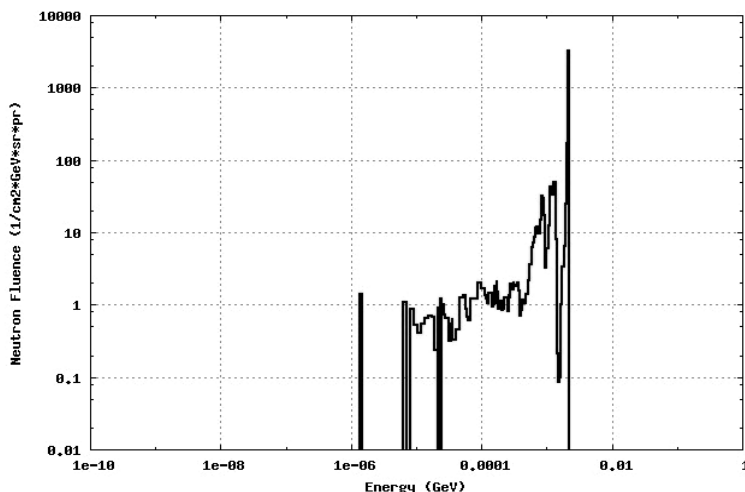
Fig. 5. Florenskyite neutron fluence for ^{252}Cf source
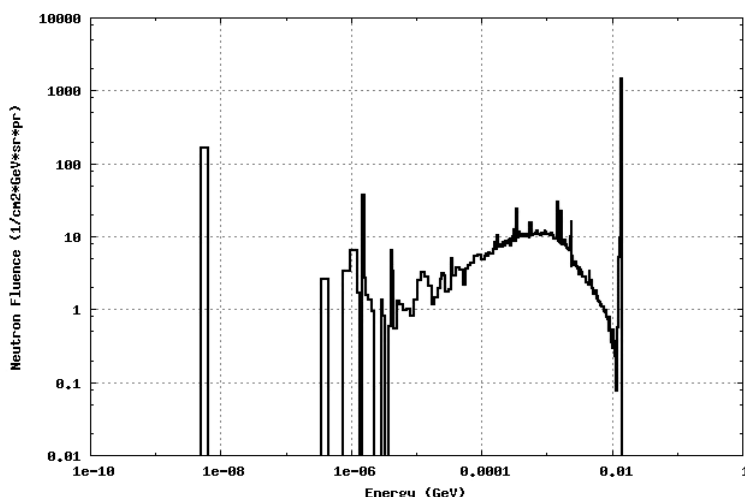
Fig. 6. Florenskyite neutron fluence for reactor

Conclusions

In this paper we calculated several parameters regarding interactions between three different energy neutrons and andreyivanovite and florenskyite, minerals found in the Kaidun meteorite. Kaidun is a meteorite which fallen in the Yemen region in 1980. After this event two new minerals were identified by Ivanov et al., 2000 and Zolensky et al., 2008. It was reported by Ivanov (2004) that Kaidun might originate from Phobos (Martian moon). Therefore, information on interactions between radiation and these compounds may be useful in terms of space research and radiation physics. Also we calculated neutron total macroscopic cross section values for these materials. If

these values are compared with the results by FLUKA ($\Sigma_{Cf\text{-}252}$= 0.149 cm^{-1}, $\Sigma_{Am\text{-}241/Be}$= 0.148 cm^{-1} and $\Sigma_{Reactor}$= 0.120 cm^{-1}), the neutron shielding capacity values for the investigated minerals are satisfactory.

References

BATTISTONI G., MURARO S., SALA P.R., CERUTTI F., FERRARI A., ROESLER S., FASSO` A., RANFT J., 2006. *The FLUKA code: Description and benchmarking*. Proceedings of the Hadronic Shower Simulation Workshop, AIP Conference Proceeding 896, 31.

FERRARI A., SALA P.R., FASSO` A., RANFT J., 2005. *FLUKA: a multi-particle transport code*. CERN-2005-10, INFN/TC_05/11, SLAC-R-773.

IVANOV A.V., ZOLENSKY M.E., SAITO A., OHSUMI K., YANG S.V., KONONKOVA N.N., MIKOUCHI T., 2000. *Florenskyite, FeTiP, a new phosphide from the Kaidun meteorite*. American Mineralogist 85, 1082.

IVANOV A.V., 2004. *Is the Kaidun meteorite a sample from Phobos?* Solar System Research 38(2), 97.

IVANOV A.V., BADYUKOV D.D., KONONKOVA N.N., 2010. *Kaidun meteorite: A fragment of crystalline rock from a new parent body*. Geochemistry International 48(9), 862.

KASHKAROV L.L., KOROTKOVA N.N., SKRIPNIK A.Y., IGNATENKO K.I., 1995. *Radiation-Thermal History of Kaidun Meteorite on Data of Track Study in Silicate Mineral Crystals and Glass Fragments*, Geokhimiya 10, 1409.

KORKUT T., KARABULUT A., BUDAK G., KORKUT H., 2010. *Investigation of fast neutron shielding characteristics depending on boron percentages of MgB_2, $NaBH_4$ and KBH_4.* Journal of Radioanalytical and Nuclear Chemistry, 286, 61.

KORKUT T., KORKUT H., KARABULUT A., BUDAK G., 2011. *A new radiation shielding material: Amethyst ore*, Annals of Nuclear Energy, 38(1), 56.

KORKUT T., KARABULUT A., BUDAK G., AYGÜN B., GENCEL O., HANÇERLIOĞULLARI A., 2012. *Investigation of neutron shielding properties depending on number of boron atoms for colemanite, ulexite and tincal ores by experiments and FLUKA Monte Carlo simulations*. Applied Radiation and Isotopes, 70, 341.

PETITAT M., MARROCCHI Y., MCKEEGAN K.D., MOSTEFAOUI S., MEIBOM A., ZOLENSKY M.E., GOUNELLE M., 2011. *^{53}Mn-^{53}Cr ages of Kaidun carbonates*. Meteoritics & Planetary Science 46 (22), 275.

RAMÍREZ-LÓPEZ A., SOTO-CORTÉS G., GONZÁLEZ-TREJO J., MUÑOZ-NEGRÓN D., 2011. *Computational algorithms for simulating the grain structure formed on steel billets using cellular automaton and chaos theories*. International Journal of Minerals, Metallurgy and Materials, 18(1), 24.

VLACHOUDIS V., 2009. *FLAIR: A Powerful but User Friendly Graphical Interface for FLUKA*, Proc. Int. Conf. on Mathematics, Computational Methods & Reactor Physics (M&C 2009), Saratoga Springs, New York.

ZOLENSKY M., GOUNELLE M., MIKOUCHI T., OHSUMI K., LE L., HAGIYA K., TACHIKAWA O., 2008. *Andreyivanovite: A second new phosphide from the Kaidun meteorite*, American Mineralogist 93, 1295.

DETERMINATION OF LEACHING PARAMETERS FOR THE RECOVERY OF PLATINUM GROUP METALS FROM SECONDARY MATERIALS

Kristian LILLKUNG, Jari AROMAA, Olof FORSEN

Aalto University, School of Chemical Technology, PO Box 16200, 00076 Aalto, Finland,
kristian.lillkung@aalto.fi

Abstract: The leaching parameters for the recovery of platinum group metals were investigated with potentiostatic measurements using wire electrodes. The dissolution rates of Pt, Pd and Rh were measured in concentrated NaCl solution. The parameters inspected were the temperature, redox potential and chloride content. Measurements were done at temperatures 25–94 °C using four different NaCl concentrations, 62.5–250 g/l. Measurements were done at potentials of 950–1250 mV vs. SCE for Pt and Rh and 380–470 mV vs. SCE for Pd. Although higher temperature, potential and chloride content generally increased the dissolution rate, the effect was found to be nonlinear and slightly different for different metals. Based on the results, strongly oxidizing conditions are needed for the leaching process in order to achieve reasonable dissolution rates.

Introduction

Platinum group metals (PGMs) are exploited for many purposes. They are nearly irreplaceable in catalysing reactions.Catalytic converters used for exhaust gas cleaningare one of the most important applications of PGMs. As the requirements for emission levels have become tighter, the demand for the metals has increased. The regulations requiring exhaust gas cleaning have become more stringent in the developing countries, which probably will lead to an even further increase in demand. At the same time, the supply and the number of suppliers of primary PGMs is very low in comparison with many other metals. The main producers are located in South Africa and Russia, which has meant that high amounts of these metals have had to be imported to Europe. The life cycle of the products where PGMs are used is usually relatively short. Therefore an increasing amount of the PGMs is in the scrapped e-waste, catalytic converters etc. The utilization of these secondary sources appears very

attractive, as the concentration of PGMs in secondary material can be in the range of g/kg of scrap material while the concentration in the ores is less than 10 g/Mg (Cawthorn, 1999; Faisal et al., 2008).

The recovery of PGMs from the secondary material has been attempted by several different methods (Marinho et al., 2010), including for example dissolving them in strong acids(Harjanto et al., 2006; Jimenez de Aberasturi et al., 2011), metal vapour treatment (Kayanuma et al., 2004) and carbochlorination (Kim et al., 2000). The hydrometallurgical treatment has appeared to be the most economical alternative. The valuable elements are leached using proper solvent and then recovered from the solution. It has been claimed that aqueous chloride solutions are the only cost-effective medium in which all the PGM can be brought into solution and concentrated (Cleare et al., 1979; Grant, 1989). In general the dissolution of PGM is based on high oxidation potential and effective complexing ions in the solution (Mahmoud, 2003). Some authors have proposed the use of HCl with an oxidant, which appears to be a functioning alternative (Barakat et al., 2006; Harjanto et al., 2006).

The low PGM concentrations become an issue if the whole matrix of the catalytic converter is fed into the leaching process. An attempt to separate the phase containing the PGM particles has been proposed by Liu et al. (2012). They have shown that the PGMs can be separated from the matrix by heating and quenching the catalysts. The separation of extracted PGMs has been attempted by several methods, including solvent extraction (Lee et al., 2010), ion exchange (Shen et al., 2010a; Shen et al., 2010b), chromatographic separation methods (Kokate and Kuchekar, 2010) and molecular recognition methods (Izatt et al., 2012).

The objective of this study was to determine the suitable parameters for preliminary laboratory-scale leaching experiments to recover PGMs from catalytic converter scrap. The parameters considered were the influence of temperature, redox potential and chloride concentration. Metals studied in this research were platinum, palladium and rhodium. The leaching process is planned to work under atmospheric pressure using NaCl solutions. The dissolution behavior of PGMs has to be precisely known in order to determine suitable oxidizing agents and optimal conditions. The dissolution rates were measured using potentiostatic measurements.

Materials and methods

Measurements were conducted using wire electrodes fabricated by mounting the metal wire in glass tubes with epoxy so that only the tip of the wire reacted in the measurements. Wire electrodes were fabricated from platinum (Alfa Aesar Standard grade thermocouple), palladium (Alfa Aesar 99.99%) and rhodium (Alfa Aesar 99.8%). Approximately 20 mm of metal wire was soldered to a copper wire. The diameter of rhodium wire was 0.25 mm while the diameter of palladium was 0.5 mm and platinum 0.508 mm.

Electrochemical measurements were conducted in a three-electrode cell, where a Luggin capillary and solution bridge connected the cell to the reference electrode. The reference electrode used in the experiments was saturated calomel electrode (SCE), type Radiometer REF 401, which was separated from test solution by a KCl salt bridge. The counter electrode used in the experiments was platinum wire.

Measurements were conducted at five different temperatures: 25, 40, 60, 80 and 94 ˚C. The test solutions used were 62.5, 90, 125 and 250 g/l NaCl solutions. Solutions were prepared from distilled water. The volume of the solution in the measurements was 175 ml. The solution was stirred with a magnetic stirrer using a stirring rate of about 500 rpm before the experiments and about 350 rpm during the experiments. The relatively high stirring rate during the experiments was used in order to prevent the bubbles from adhering to the surface of the working electrode. Experiments were conducted in oxygen-free environment. Before the beginning of each measurement oxygen (air) in the cell was removed by using nitrogen purging (purity >99.99%). Purging was conducted through a sintered disk with a constant flow rate one hour before and during the experiments. Nitrogen flow was reduced during the experiments to prevent the bubbles from affecting the results.

Polarization curve measurements were conducted from –50 to 750 mV vs. rest potential for Pd and –50 to 1500 mV for Pt and Rh. Sweep rate was 50 mV/min. The potentiostatic measurements were conducted at potentials of 380, 410, 440 and 470 mV vs. SCE for Pd and at 950, 1050, 1150 and 1250 mV vs. SCE for Pt and Rh. The current density was measured as a function of time in potentiostatic measurements. The initial current density of the dissolution reaction was determined by extrapolating the current density determined during the first few seconds of the measurement back to the start of the experiment. As the dissolution starts, reaction products are formed and the current density changes as a function of time.

Results and discussion

At first, a series of potentiodynamic polarization curve measurements were conducted to understand the overall dissolution behavior of the metals. Based on the curves (example shown in Fig. 1), the dissolution rate of Pt and Rh is significantly higher when they are polarized to over 1000 mV vs. SCE, and Pd when it is polarized to over 400 mV vs. SCE. The current density was found to increase rapidly when these potentials are exceeded.

Based on the potentiostatic measurement series, higher temperature, potential and chloride content generally increased the dissolution rate although the effect was nonlinear and slightly different for different metals. Fig. 2 shows the dissolution rates of palladium at 470mV vs. SCE as a function of temperature and chloride content. At potential of 1250 mV vs. SCE and with the highest chloride content, the dissolution rate of Pt can exceed 1000 µm/h, and Rh 100 µm/h. However, these potentials are so high that some of the measured current density might be caused by the gas evolution

reactions. At the highest tested potential for palladium, 470 mV vs. SCE, a dissolution rate of over 700 µm/h was reached.
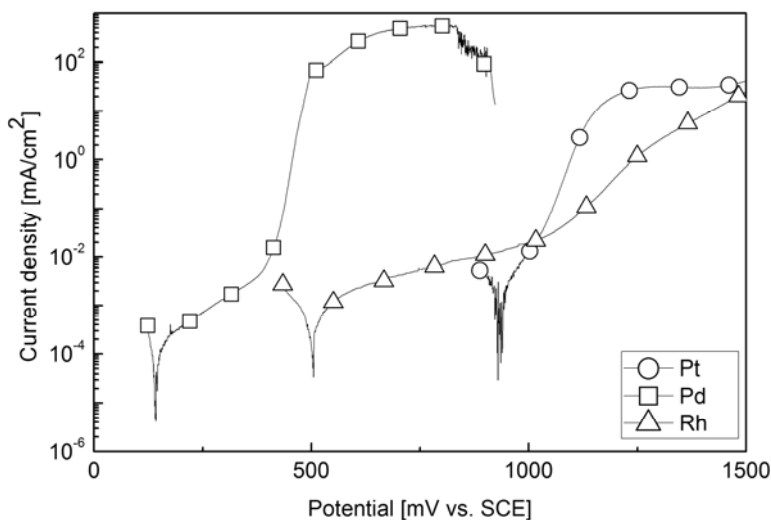
Fig. 1. Polarization curves of platinum, palladium and rhodium
measured in 250 g/l NaCl solution at 25 ˚C.

The effect of temperature
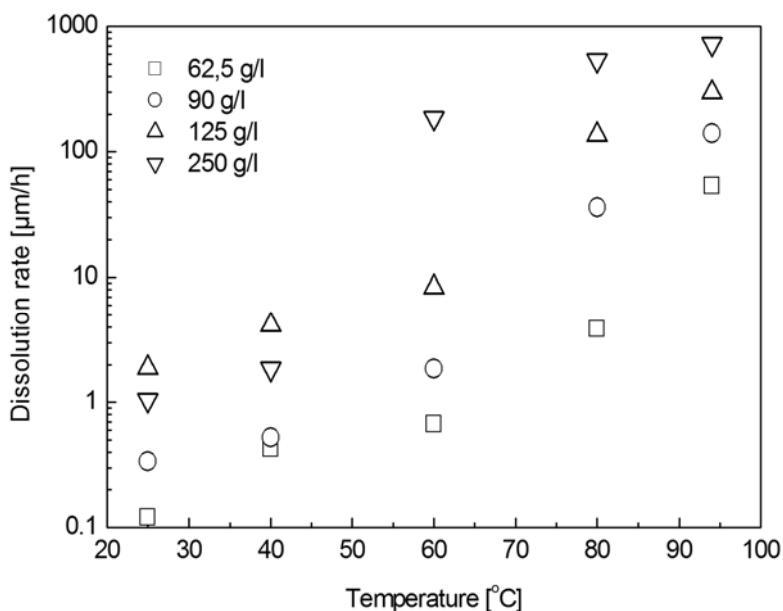
Fig. 2. Dissolution rate of palladium (470 mV vs. SCE) as a function
of temperature and chloride content

The temperature was found to increase the dissolution rate significantly. The effect was found to be different for different metals. The effect was exponential with the measured potentials, as shown in Fig. 3. Therefore the use of temperatures near the water boiling point seems reasonable for the leaching process. However, the effect might be different when an oxidant is used as some of the oxidants degrade at high temperatures.
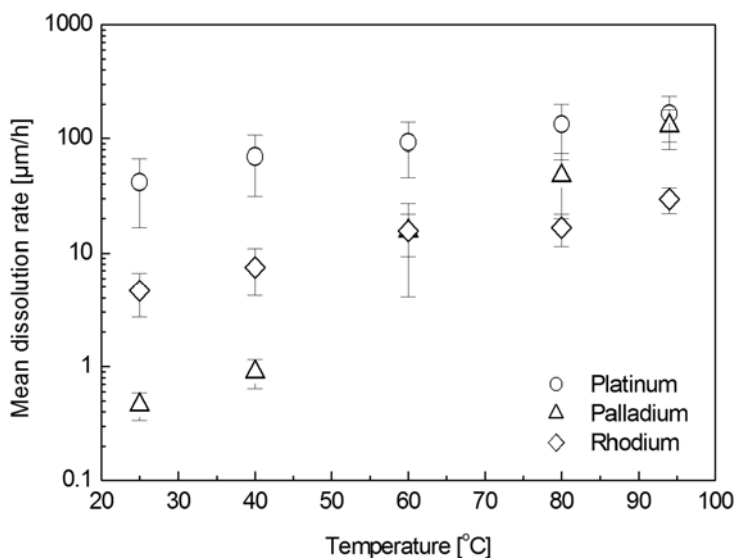
Fig. 3. Temperature dependence of dissolution rates

The effect of redox potential

The effect of redox potential on the dissolution rate appeared to be exponential with the measured potentials, as shown in Fig. 4. The Tafel coefficient for Pd dissolution was 52 mV/decade, which indicates dissolution with a two-electron mechanism. The Tafel coefficient for Pt dissolution was 123 mV/decade, which is in accordance with the one-electron dissolution mechanism. For Rh the value was 284 mV/decade, which cannot be explained by a pure charge transfer. The high value can be explained by the formation of an oxide layer, but this could not be verified. The Rh dissolution reaction follows most likely more complicated reaction mechanism than Pt and Pd. Llopis (1965) has proposed the dissolution to follow a multistep mechanism, where halide ions are first specifically adsorbed on the surface and then dissolved in the second step.

The potential range where the dissolution of Pd starts is relatively low and, hence, there are a variety of possible oxidizers to be used in the actual leaching process. For the leaching of platinum and rhodium the choice of an oxidizer is much more critical, as relatively high potential is needed for economic operation. Barakat et al. (2006)

have proposed the use of hydrogen peroxide as an oxidant, which appears to be a suitable alternative. The effect of different oxidants has to be further experimented in order to define the best alternative.
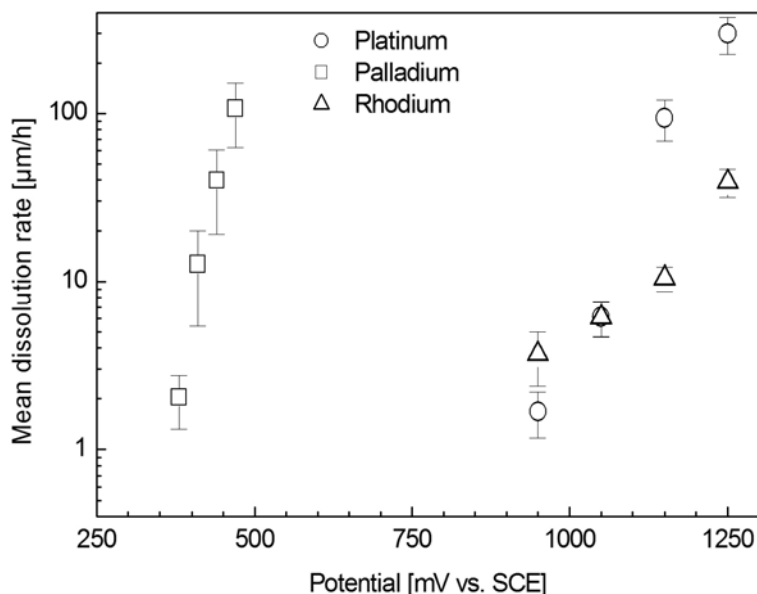
Fig. 4. The effect of redox potential on the dissolution rates

The effect of chloride content

The chloride content increased the dissolution rate relatively linearly, as can be seen from Fig. 5. The higher concentration provided much higher dissolution rates. The optimum concentration for a leaching process appears to be near the NaCl solubility limit.

The reaction order of the dissolution reaction with respect to chloride ion can be calculated from equation 1:

$$n = \frac{\log(rate)}{\log([Cl^-])} \tag{1}$$

where n is reaction order, $[Cl^-]$ is chloride concentration and *rate* is the determined dissolution rate.
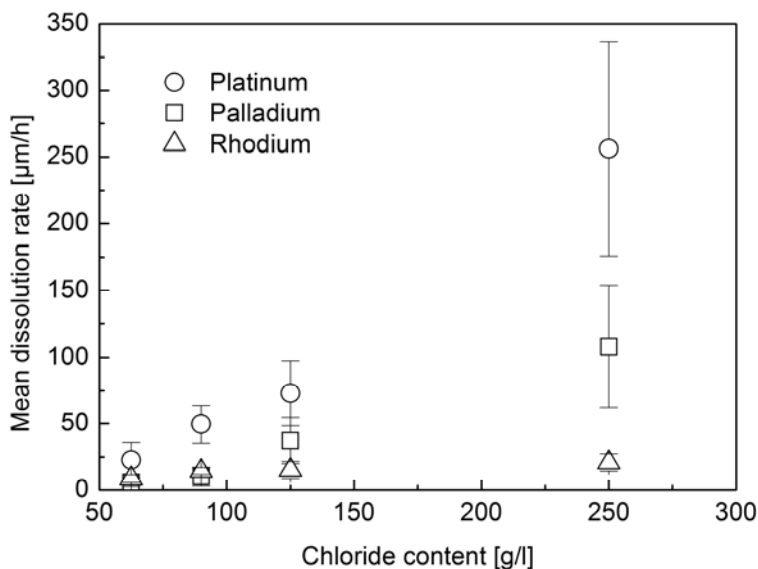
Fig. 5. The effect of chloride content on the dissolution rate

In Fig. 6 are shown the logarithms of dissolution rate of Pt, Pd and Rh as a function of the logarithm of chloride concentration. Based on the results, two chloride ions take part in the dissolution reaction of one platinum or palladium atom. This is in accordance with the dissolution mechanism proposed by Llopis (1969), who proposed that PdCl^{2-} is formed in the primary process and it subsequently reacts with water. Pd and Pt are usually present in the +2 or +4 oxidation states (Cotton, 1997). Unlike Pt and Pd, Rh is usually present in the +3 oxidation state (Benguerel et al., 1996; Cotton, 1997). The results support the mechanism of three chloride ions taking part in the dissolution reaction of Rh. All of the metals are also known to form hexachloro-complexes MeCl$_6^{2-}$ (Cotton, 1997).

Activation energy

The mechanism limiting the reaction rate can be defined by determining the activation energies. These were defined using the Arrhenius law. The activation energies determined from the potentiostatic measurements using steady state current densities are shown in Table 1. Activation energies showed no change with respect to chloride content or potential in the potential range of rapid dissolution. Based on the activation energies shown, it is very likely that the reaction rates are controlled by charge transfer (Peters, 1973). Llopis (1969) has given a value of 84 kJ/mol for the activation energy of Pt in HCl solution. Similarly Baghalha et al. (2009) determined the activation energy of dissolution of Pt in aqua regia to be 72.1 kJ/mol. Although both having a higher value, this also indicates the reaction to be controlled by the electron transfer step.
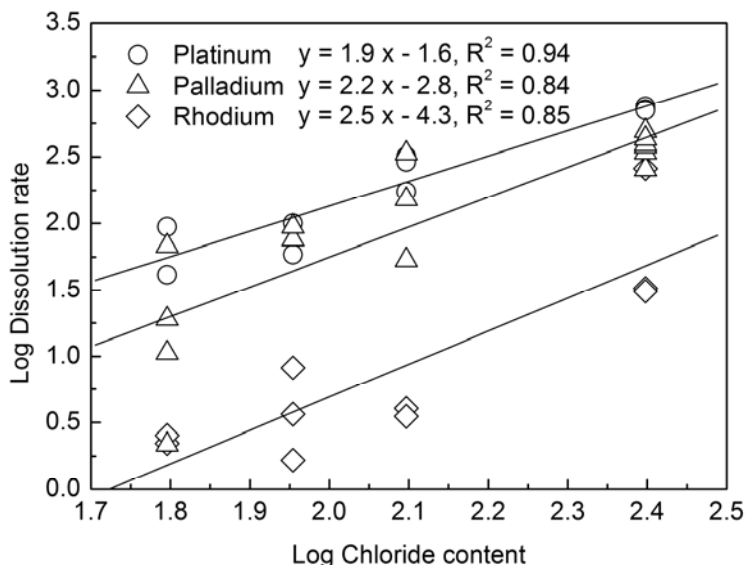
Fig. 6. Logarithm of dissolution rate (Pt 94˚C 1150 mV, Pd 94˚C 470 mV
and Rh 25 ˚C 1250 mV vs. SCE) vs. logarithm of chloride concentration

Table 1.Activation energies determined at the potential range
of rapid dissolution with all measured chloride concentrations

Metal	Activation energy [kJ]
Platinum	59 ± 1
Palladium	68 ± 1
Rhodium	61 ± 1

Conclusions

The results show that strongly oxidizing conditions are needed to achieve reasonable leaching rates of Pt, Pd and Rh in NaCl solutions. The dissolution of Pt and Rh can be assumed to take place at high potential where chlorine and/or oxygen evolution can also occur during the electrochemical testing. Pd dissolves at lower potential than these gas evolution reactions. Pd could be dissolved using chlorine or hydrogen peroxide as an oxidant. A suitable concentration of hydrogen peroxide could provide necessary redox potential also for the leaching of Pt and Rh. The choice of the optimum oxidant requires testing of redox-potential of different possible alternatives before the actual leaching experiments.

The results showed that higher chloride concentration increased the dissolution rate significantly, and therefore highly concentrated chloride solutions should be used in the leaching process. The chloride concentration should be optimized near the NaCl

solubility limit when establishing the leaching process. Increasing temperature increased the dissolution rates. The higher temperature naturally increases the energy cost, so the most economic conditions have to be defined for the actual leaching process. The optimum leaching conditions might also depend on the oxidant used, as some of the oxidants degrade at high temperatures.

According to determined activation energies and similar studies found in the literature, it is suggested that the dissolution processes of the examined platinum group metals in chloride solutions are controlled by the electron transfer step.

Acknowledgements

References

BAGHALHA M., KHOSRAVIAN H., MORTAHEB H., 2009. *Kinetics of platinum extraction from spent reforming catalysts in aqua-regia solutions*. Hydrometallurgy, 95(3–4), 247–253.

BARAKAT M.A., MAHMOUD M.H.H., MAHROUS Y.S., 2006. *Recovery and separation of palladium from spent catalyst*. Applied Catalysis A, General, 301(2), 182–186.

BENGUEREL E., DEMOPOULOS G.P., HARRIS G.B., 1996. *Speciation and separation of rhodium(III) from chloride solutions, a critical review*. Hydrometallurgy, 40, 135–152.

CAWTHORN R.G., 1999. *The platinum and palladium resources of the Bushweld Complex*. South African Journal of Science, 95, 481–489.

CLEARE M.J., CHARLESWORTH P., BRYSON D.J., 1979. *Solvent Extraction in Platinum Group Metal Processing*. J. Chem. Tech. Biotechnol., 29, 210–214.

COTTON S., 1997. *Chemistry of precious metals*. Springer.

FAISAL M., ATSUTA Y., DAIMON H., FUJIE K., 2008. *Recovery of precious metals from spent automobile catalytic converters using supercritical carbon dioxide*. Asia-Pacific Journal of Chemical Engineering, 3(4), 364–367.

GRANT R.A., 1989. *The Separation Chemistry of Rhodium and Iridium*. [In:] L. Manziek (Editor), *IPMI Seminar on Precious Metals Recovery and Refining*. International Precious Metals Institute, Scottsdale, AZ, USA, 7–18.

HARJANTO S., CAO Y., SHIBAYAMA A., NAITOH I., NANAMI T., KASAHARA K., OKUMURA Y., LIU K., FUJITA T., 2006. *Leaching of Pt, Pd and Rh from automotive catalyst residue in various chloride based solutions*. Materials Transactions, 47(1), 129–135.

IZATT S., BRUENING R., IZATT N., 2012. *Some Applications of Molecular Recognition Technology (MRT) to the Mining Industry*. [In:] S. Wang, J. Dutrizac, M. Free, J. Hwang and D. Kim (Editors), *T.T. Chen Honorary Symposium on Hydrometallurgy, Electrometallurgy and Materials Characterization*. Wiley, Orlando, FL, 51–60.

JIMENEZ DE ABERASTURI D., PINEDO R., RUIZ DE LARRAMENDI I., RUIZ DE LARRAMENDI J.I., ROJO T., 2011. *Recovery by hydrometallurgical extraction of the platinum-group metals from car catalytic converters*. Minerals Engineering, 24(6), 505–513.

KAYANUMA Y., OKABE T., MAEDA M., 2004. *Metal Vapor Treatment for Enhancing the Dissolution of Platinum Group Metals from Automotive Catalyst Scrap*. Metallurgical and Materials Transactions B, 35B, 817–824.

KIM C.-H., WOO S.I., JEON S.H., 2000. *Recovery of Platinum-Group Metals from Recycled Automotive Catalytic Converters by Carbochlorination*. Industrial & Engineering Chemistry Research, 39(5), 1185–1192.

KOKATE S.J., KUCHEKAR S.R., 2010. *Reversed phase extraction chromatographic separation of ruthenium(III)*. Journal of Saudi Chemical Society, 14, 41–45.

LEE J.Y., RAJU B., KUMAR B., KUMAR J., PARK H., REDDY B., 2010. *Solvent extraction separation and recovery of palladium and platinum from chloride leach liquors of spent automobile catalyst*. Separation and Purification Technology, 73(2), 213–218.

LIU G., ICHINOSE T., OWADA S., 2012. *Separation of PGMs bearing alumina phase from cordierite in spent automobile catalyst by heating-quenching process*, XXVI International Mineral Processing Congress 2012, New Delhi, India, 2966–2979.

LLOPIS J., 1969. *Corrosion of Platinum Metals and Chemisorption*. Catalysis Reviews, Science and Engineering, 2(1), 161–220.

LLOPIS J., TORDESILLAS I.M., MUNIZ M., 1965. *Anodic Corrosion of Rhodium in hydrochloric acid solutions*. Electrochimica Acta, 10(11), 1045–1055.

MAHMOUD M.H.H., 2003. *Leaching Platinum-Group Metals in a Sulfuric Acid/Chloride Solution*. Journal of the Minerals, Metals and Materials Society, 55(4), 37–40.

MARINHO R.S., AFONSO J.C., DA CUNHA J.W.S.D., 2010. *Recovery of platinum from spent catalysts by liquid-liquid extraction in chloride medium*. Journal of Hazardous Materials, 179(1–3), 488–494.

PETERS E., 1973. *The Physical Chemistry of Hydrometallurgy*. [In:] D.J.I. Evans and R.S. Shoemaker (Editors), *AIME International symposium on hydrometallurgy*, Chicago, 205–228.

SHEN S., PAN T., LIU X., YUAN L., WANG J., ZHANG Y., GUO Z., 2010a. *Adsorption of Rh(III) complexes from chloride solutions obtained by leaching chlorinated spent automotive catalysts on ion-exchange resin Diaion WA21J*. Journal of Hazardous Materials, 179(1–3), 104–112.

SHEN S., PAN T., LIU X., YUAN L., WANG J., ZHANG Y., GUO Z., 2010b. *Adsorption of Pd(II) complexes from chloride solutions obtained by leaching chlorinated spent automotive catalysts on ion exchange resin Diaion WA21J.* Journal of Colloid and Interface Science, 345(1), 12–18.

AN EVALUATION OF A MODIFIED PRODUCT SIZE DISTRIBUTION MODEL BASED ON T-FAMILY CURVES FOR THREE DIFFERENT CRUSHERS

Yakup UMUCU[*], Vedat DENIZ[**], Nazmi UNAL[*]

[*]   Department of Mining Engineering, Suleyman Demirel University, Isparta, Turkey, yakupumucu@sdu.edu.tr
[**] Department of Chemical Engineering, Hitit University, Çorum, Turkey

Abstract: Crushing is a process which is widely used in mineral processing plants, cement factories, aggregates plants and some other industrial plants. Specific fracture energy of the particles is not the only fundamental property that is important: the particle strength also plays a significant role in determining the overall comminution properties of the material. In the drop weight test, a known mass falls through a given height onto a single particle providing an event that allows characterization of the ore under impact breakage. It is known that there are many difficulties and problems in the drop weight and twin pendulum test methods such as being laborious, requiring long test time and requiring a special apparatus. In this study, breakage behavior of slag in different laboratory crushers was investigated. A new size distribution model equation was developed by a t-family value evaluation approach, and the validity of equation was tested.

Keywords: crusher, drop weight tests, t-family, size distribution

Introduction

Comminution concerns the breakage of brittle particles under conditions of applied compressive stress. The nature of the failure mechanisms is governed by material properties of the particulate material and by the nature of the stress field around and within individual particles. The response of the particulate material to the stress field is largely elastic but significant non-elastic behavior occurs, particularly at the tips of growing cracks where large quantities of energy are dissipated when the criteria for fracture are met. The dissipation at the crack tip of the stored elastic energy in the particle turns out to be of critical interest in industrial comminution machines where energy efficiency is of major consequence because of its economic importance. Industrial comminution processes are typically inefficient in their use of energy in the sense that considerably more energy is consumed by the operating equipment than is

actually required to break the particles. In spite of the importance of this observation, it has not been possible to calculate precisely how much energy is actually required.

Crushing is a process which is widely used in mineral processing plants, cement factories, aggregates plants and some other industrial plants. Especially, the demand of crushed stone aggregates has increased from day to day, because of increasing expansion of highway and other construction works and decreasing natural aggregate resources in the world. The crushability of rocks depends mainly on the crusher type and properties, and geological characteristics of rocks. Physico-mechanical properties, mineralogical and textural features, structural properties such as micro cracks, cleavage planes and schistosity are the geological characteristics affecting the rock crushability (Toraman et al., 2010)

Specific fracture energy of the particles is not the only fundamental property that is important. The particle strength also plays a significant role in determining the overall comminution properties of the material. A particle will be broken only if it is stressed beyond its strength which is determined by the intrinsic properties of the material, the presence of micro flaws which act as stress raisers when the particle is under load and the state of stress that is experienced by the particle.

In the drop weight test (Fig. 1) a known mass falls through a given height onto a single particle providing an event that allows characterization of the ore under impact breakage. Although, the drop weight test has advantages in terms of statistical reliability and the potential use of the data from the analysis, it has a number of disadvantages, including necessity of a special apparatus, tiring and particularly the length of time taken to carry out a test. For each drop weight test, 15 samples are tested in five size fractions at three levels of energy input (Tavares, 1999, Tavares et al., 2007, Kingman et al., 2004, Genç et al., 2009).

Narayanan (1986) used a novel procedure for estimation of breakage distribution functions of ores from the t-family of curves. In this method, the product size distribution can be represented by a family of curves using marker points on the size distribution defined as the percentage passing (t) at a fraction of the parent particle size. Thus, t_2 is the percentage passing an aperture of half the size of the parent particle size, t_4 is one quarter and t_{10} is one-tenth of parent particle size.

Narayanan and Whiten (1988) have proposed empirical equations for relating the reference curve data t_{10} with the impact energy.

The t_{10} value is related to the specific comminution energy given by Equation (1):

$$t_{10} = A\ (1 - e^{-bEcs})\qquad\qquad(1)$$

where: t_{10} – percentage passing $1/10^{th}$ of the initial mean size,

Ecs – specific comminution energy (kWh/kg)

A, b – ore impact breakage parameters.

The t_n versus t_{10} relationships can then be used to predict the product size distributions at different crushing times (Sand and Subasinghe, 2004).

Fig. 1. Drop-weight test apparatus

It is known that there are difficulties and problems in drop weight and twin pendulum test methods such as being laborious, requiring long test time and requiring a special apparatus. In this study, the breakage behaviors of the volcanic slag in the different laboratory crushers were investigated. A new size distribution model equation was developed by *t-family* value evaluation approach and validity of the specific energy equation was tested.

Materials and methods

The volcanic slag sample taken from region of Manisa (Turkey) was used as the experimental materials. The chemical properties of the sample were presented in Table 1.

Table 1. Chemical composition of volcanic slag samples used in experiments

Oxides	CaO	SiO_2	Al_2O_3	Fe_2O_3	MgO	SO_3	Na_2O	K_2O	LOI
(%)	8.73	45.74	15.60	10.64	5.98	0.040	5.40	4.98	1.70

2.1. Experimental

About one kg of samples of four mono-size fractions (–30 +20, –20 + 15, –15 + 10, –10 + 6.7 mm) was prepared by screening for determination of the *t-family* curves. The laboratory scale jaw, roller and hammer crushers (Fig. 2), driven by a 1.10 – 2.00 – 11.00 kW motor, respectively, was used in the experiments. Samples were crushed with the laboratory scale crushers, and then the samples were sieved to product size analysis. The modified results of the *t-family* curves versus mean particle size fraction for different crushers were shown in Figs. 3–5.

Fig. 2. Jaw, roller and hammer crushers used in the experiments
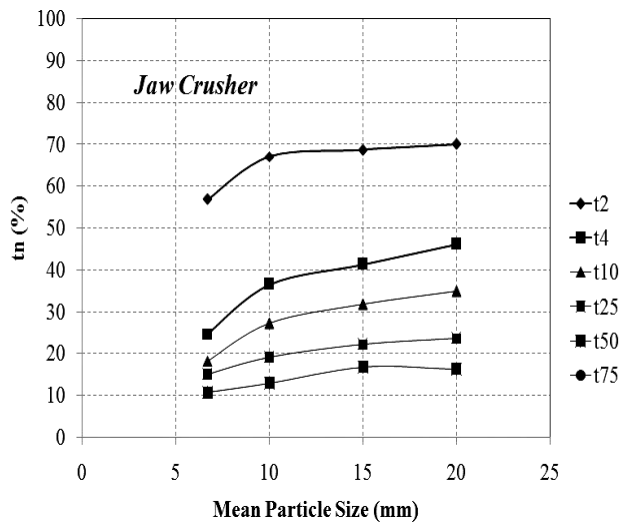
Fig. 3. t_n versus mean size fraction for jaw crusher
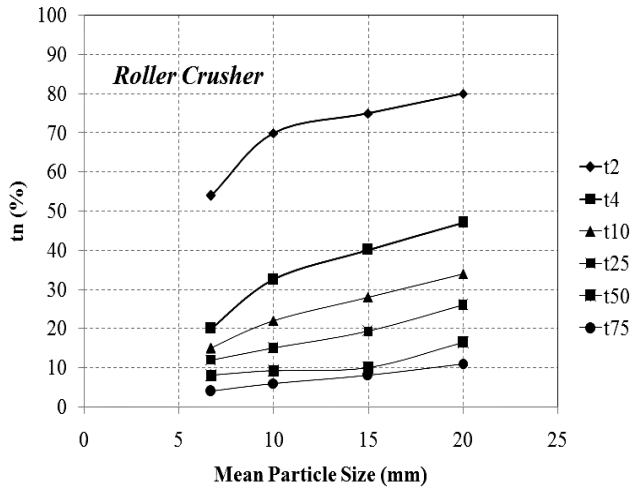
Fig. 4. t_n versus mean size fraction for roller crusher
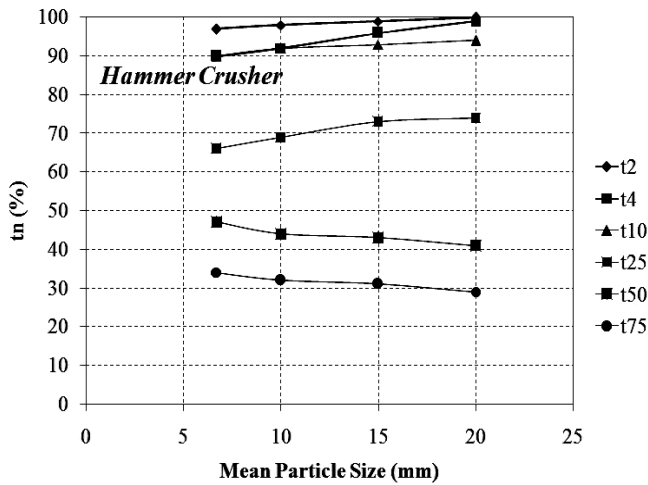
Fig. 5. t_n versus mean size fraction for hammer crusher

Proposed size distribution model equation

King (2002) described a method of presenting product size distributions obtained from the drop weight tests. It is based on the observations made by Narayanan and Whiten (1983) that the cumulative fractions of products passing $1/n^{th}$ of the mean size, denoted as t_n, is related to that passing one-tenth of the parent size denoted by t_{10}. It was also reported that this relationship was applicable to different ore types tested under different impact loading conditions.

In this study, a different size distribution relationship has been found for t_n values of crushing products obtained from different laboratory scale crushers. The following equation is suggested to predict the cumulative percentage passing (t_n), depending on the crushing engine power *(CEP)* and feed particle size (*X*) before crushing:

$$t_n = \left(\frac{56.12}{n^{1.168\, CEP^{-1.274}}} \right) X^{0.30} \qquad (2)$$

and the calculated results obtained by Equation (2) were compared with experimental values obtained from results of Fig. 6. Equation (2) satisfied the experimental values in a wide range of feed size. Equation (2), including a high determination coefficient ($r^2 = 0.79$), is useful, especially when evaluating the particle size distribution in actual operation. Thus, variation of the cumulative percentage passing (t_n) with crushing engine power *(CEP)* and feed particle size (*X*) was empirically described by Eq. (2).
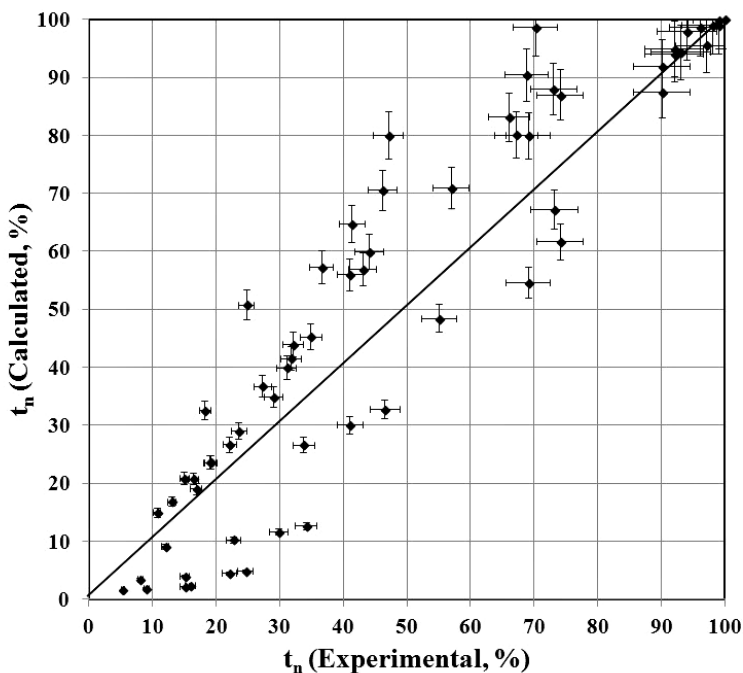
Fig. 6. Comparison of experimental and calculated t_n value for different crushers

Results and discussion

As commonly known, the type of crusher plays an important role in comminution while electrical engine power is important in crusher selection. The modified t-family curves can be used to describe the product size distribution from single-particle

breakage tests. The cumulative percentages passing t_2, t_4, t_{10}, t_{25}, t_{50} and t_{75} are determined by a linear interpolation for the breakage products passing various sieves. However, there are problems by drop weight and twin pendulum tests because of being laborious, requiring long test time and a special apparatus.

Evaluation of single particle breakage data through a single parameter is useful for understanding breakage characteristics, namely the size and input energy level dependency. Breakage characteristics of different size fractions can be examined at various impact energies expressed in kWh/kg or joules/kg by determining the product size distribution of broken particle at any energy level (Genç et al., 2004).

Obtaining the modified *t-family* curves using the twin pendulum device and drop weight apparatus is time consuming and difficult. Therefore, a set of *t-curves* were calculated from different laboratory scale crushers, and a new model was developed. There are only few studies on the effects of work speed, lining design, crusher design and feed dose of materials in crushers, which are widely used in power, cement and mineral processing plants. For this purpose, similar mathematical models can be developed for different work parameters for various materials and various crusher types (Umucu et al., 2013).

Conclusions

The individual particle fracture strengths of materials based on fracture size can benefit from drop weight test results. The models of crushing can be used to results of such tests. An important problem in terms of crushing modeling studies is size-dependent breakage behavior of materials. The breakage data of a single particle broken at an appropriate specific comminution energy level are commonly determined as breakage distributions of the crushing feed materials. In the comminution, the models should define the breakage distribution of each size fraction in the same material.

The effects of feed particle size (X) and electrical crushing engine power on product size distribution were investigated. The proposed model equation which incorporates the self-similar breakage behavior during laboratory comminution could be used as an alternative to the drop weight and twin pendulum tests, as its particle size distributions could be defined more readily and reliably.

The drop weight test allows determining the breakage distribution of materials. The result of comminution, breakage distribution and energy consumed cannot be obtained without laboratory-scale apparatus as the drop weight tests. The experimental work should be done on an industrial scale. The *t*-family curves can characterize comminution products of any crusher. The model proposed in this study can be improved for crushers. In this study, the modified *t-family* model shows easy determination of the product size distribution of any material.

References

DENIZ V., 2011. *A new size distribution model by t-family curves for comminution of limestones in impact crusher.* Advanced Powder Technology, Vol:22 (6), 761–765.

GENC O., BENZER A.H., 2009. *Single particle impact breakage characteristics of clinkers related to mineral composition and grindability*, Minerals Engineering, Vol. 22, 1160–1165.

GENC O., ERGÜN L., BENZER A.H., 2004. *Single particle impact breakage characterization of materials by drop weight testing*, Physicochemical Problems of Mineral Processing, 38, 241–255.

KING R.P., 2002. *Modeling and Simulation of Mineral Processing Systems*, Butterworth–Heinemann Publishers, New York, USA.

KINGMAN S.W., JACKSON K.A., CUMBANE S.M., BRADSHAW N.A., ROWSON R., 2004. *Greenwood, Recent developments in microwave in microwave-assisted comminution*, International Journal of Mineral Processing, Vol.74: 71–83.

NARAYANAN S.S., 1986. *Single particle breakage tests: a review of principles and application to comminution modeling*, Bull. Proc. Austr. Inst. Min. Metall. 291, 49–58.

NARAYANAN S.S., WHITEN W.J., 1983. *Breakage characteristics for ores for ball mill modelling*, in: Proceedings of the Australasian Institute of Mining and Metallurgy, 31–39.

NARAYANAN S.S., WHITEN W.J., 1988. *Determination of comminution characteristics from single particle breakage tests and its application to ball mill scale-up*, Trans. Inst. Min. Metall. (Sec. C). Vol. 97, 115–124.

SAND G.W., SUBASINGHE G.K.N., 2004. *A novel approach to evaluating breakage parameters and modelling batch grinding*, Minerals Engineering, Vol.17, 1111–1116.

TAVARES L.M., 1999, *Energy absorbed in breakage of single particles in drop weight testing*, Minerals Engineering, Vol. 12, 43–50.

TAVARES L.M., CARVALHO R.M., 2007. *Impact work index prediction from continuum damage model of particle fracture*, Minerals Engineering, Vol. 20, 1368–1375.

TORAMAN O.Y., KAHRAMAN S., CAYIRLI S., 2010. *Predicting the crushability of rocks from the impact strength index*, Minerals Engineering, Vol. 23, 752–754

UMUCU Y., DENIZ V., ÇAYIRLI S., 2013. *A new model for comminution behaviour of different coals in an impact crusher* [in:] *Energy Sources, Part A: Recovery, Utilization, and Environmental Effects*, Taylor&Francis, (DOI: 10.1080/15567036.2010.503232).

REMOVAL OF METHYLENE BLUE BY NATURAL AND Ca AND K-EXCHANGED ZEOLITE TREATED WITH HYDROGEN PEROXIDE

Murat CANLI[*], Yuksel ABALI[*], Salih Ugur BAYCA[**]

[*] Faculty of Arts and Sciences, Celal Bayar University, 45140, Manisa, Turkey; murcanli@yahoo.com; yabali@yahoo.com
[**] Soma Vocational School, Celal Bayar University, Soma/Manisa, Turkey; salihbayca@gmail.com

Abstract: A comparison was made of influence of physically adsorbed methylene blue (MB) dye on the physicochemical properties of Manisa-Akdere zeolite (natural zeolite) and zeolite modified with K and Ca (all samples treated with hydrogen peroxide before modification) using batch adsorption technique. After elementary characterization of this adsorbent, the effects were investigated of initial MB concentration, pH, contact time, stirring rate, adsorbent dosage and temperature on the selectivity and sensitivity of the removal process. A larger adsorption of the dye was observed for modified zeolite (42.7 mg/g) than for natural zeolite (28.6 mg/g) per gram of an adsorbent after all zeolite samples treated with hydrogen peroxide. Zeolite treated with H_2O_2 showed higher adsorption capacity than untreated zeolite samples. The Langmuir model (R^2 values between 0.959 and 0.996) fitted the experimental data better than the Freundlich model (R^2 values between 0.804 and 0.988). The adsorption process was found to be slightly influenced by adsorbent dosage, contact time and temperature. Optimum pH for adsorption of MB was found to be at 7. Adsorption equilibrium attained within 30 minutes. The sorption of MB increased slightly with rising temperature. In addition, adsorption values rose with modification Ca-Exchanged (after H_2O_2 treatment) > K-Exchanged (after H_2O_2 treatment) > Zeolite treated with H_2O_2 > Ca-Exchanged >K-Exchanged >Natural Zeolite.

Keywords: dye adsorption, methylene blue, adsorption, isotherms, zeolite, alumino-silicate, hydrogen peroxide

Introduction

Growth in population, oil consumption, exhaust emissions, industrial activities, energy production, and frequently uncontrolled pesticide use resulted in the accumulation of hazardous inorganic and organic pollutants in the environment (Misaelidis, 2011). Moreover, if the concentration of pollutants exceeds certain limits, their presence causes danger to the environment and to human health. In order to minimize such

danger, various precautions should be taken such as waste stabilization and environmental remediation. This can largely be accomplished by extraction of the pollutants from soils or aqueous systems and reduction of their mobility.

The textile and printing industries produce and dump highly colored waste effluents from the use of dyes and pigments, and these wastes cause serious environmental problems. The estimated annual production of more than 10,000 different manufactured dyes is around $7 \cdot 10^8$ kg. These complicated compounds with a high molecular weight resist to biological degradation (Alkan et al., 2007). Even though dyes can be removed from wasters by coagulation, flocculation, biodegradation and oxidation, these methods are expensive and often ineffective (Armagan et al., 2003; Metes et al., 2004).

Therefore, recent studies have been focused on the application of natural mineral clays as low-cost adsorbents to remove colored pollutants (Crini, 2006; Doğan et al., 2009; Fungaroa et al., 2010; Glaysz-Plaska et al. 2000; Gulgonul, 2012; Korkuna et al., 2006; Wang and Peng, 2010). Previous research has shown that several alternative adsorbents have been suggested for MB adsorption like activated carbon or clay minerals, especially, natural and modified zeolites. These aluminosilicates are cheap adsorbents which are widely applied in industry, environment protection, agriculture, medicine, and many other fields (Gümüş and Akbal, 2011; Farhade and Aziz, 2010). The molecular-sieve properties, availability of strongly active surface sites, high resistance to acids and other useful properties of zeolites allow the use of them as catalysts in cracking, hydrocracking, isomerization and other processes (Alzaydien, 2009; Jin et al., 2008). There are several rich reserves of zeolite in Turkey (Albayrak, 2008).

The application of natural zeolites to the environmental remediation is mainly based on their ion-exchange properties (Doğan et al., 2000). It is well-known that ion-exchange in the case of zeolites takes place among cations and they must be modified to provide them with anion sorption properties. Aluminosilicate catalysts are characterized according to their activity, selectivity, stability and their capability of multiple regeneration (Ozdemir, 2008). Natural and modified zeolite are natural minerals composed of the aluminosilicate matrix with a variety of other metal oxides and metal cations embedded (Hernandez et al., 2000; Doğan et al., 2008; Caglar et al., 2009). Zeolite with three 8-membered rings and one 10-membered ring has net negative surface charge which is counterbalanced by monovalent (Na^+, K^+) and divalent (Ca^{2+}) cations. Zeolites can be ion exchanged using metal ions like Fe, Cu, Mn, Ca,and Ba. Zeolites are negatively charged because of the substitution of Si (IV) by Al (III) in the tetrahedral accounts for a negative charge of the structure. The Si/Al ratio determines the properties of zeolites such as ion exchange capacity.

Before applying zeolitic tuff (natural zeolite) to adsorption process, several activation methods are suggested in previous studies for increasing the adsorption capacity of zeolite such as acid activation (Ajemba and Onukwuli, 2013; Kowalczyk et al., 2006), heat activation (Ates et al., 2011), and modification. Even though heat

activation is an effective way to increase the surface area and capacity on an adsorbent, the use of acid activation results in greater increase in surface area and adsorption capacity. Hydrogen peroxide is used for activation of zeolite because of its role as a weak acid. In acidic environments, the oxidation rate of hydrogen peroxide is slow, but faster than basic environments. Modification by metals with mono or bivalent ion also is a way for increasing adsorption capacity of zeolite (Farhade and Aziz, 2010).

The uptake of metal cations from solutions by the zeolites is affected by a variety of factors such as the temperature, the solution pH, the presence of competing cations and complexing agents, the dimensions of the hydrated dissolved species compared to the opening of their channels and the external surface activity (Gurses et al., 2006).

The aim of this article is to show how hydrogen peroxide influences natural and modified zeolite (peroxide applied before modification) in the adsorption of methylene blue. The difference this article from others is that even though H_2O_2 is used in the literature for degredation of MB (Kondru et al., 2009; Slokar and Marechal, 1998; Etaiw and El-Bendary, 2012) and there are several materials already used for activation of zeolite (Ates and Hardacre, 2012; Jia et al., 2009; Hernandez-Ramirez and Holmez, 2008), H_2O_2 was not tried before in activation process of zeolite.

Experimental design

Materials

Natural zeolite samples were obtained from the Demirci-Akdere region, Manisa, Turkey with the general formula of $(K_{2.3} Na_{0.5} Ca_{2.1} Mg_{0.6} Fe(III)_{0.9} Fe(II)_{0.2} Ti_{0.2})$ $(Si_{31.4}Al_{6.5}O_{44})$ $21.8H_2O$ has the chemical composition (in %): SiO_2, 67.29; TiO_2, 0.26; Al_2O_3, 12.32; Fe_2O_3, 1.26; FeO, 0.25; MgO, 0.29; CaO, 3.01; Na_2O, 0.66; K_2O, 2.76; H_2O, 10.90 (see Table 1), whereby the content of the main mineral was 85 ±6%. Methylene Blue, MB (Merck, C.I. = 52015, $C_{16}H_{18}N_3SCl$, FW = 373,86 g/mol] was used as a cationic dye adsorbate (see Fig 1).
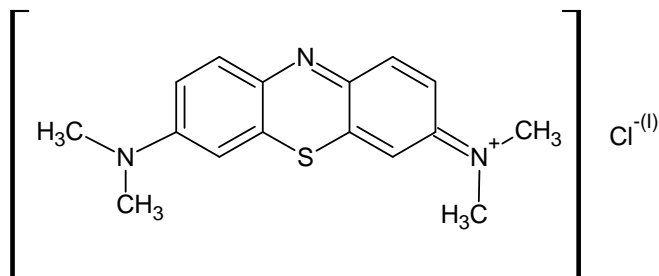
Fig. 1. Chemical structure of methylene blue

Table 1. Physicochemical properties of natural zeolite

Chemical compound	Natural zeolite, %	Zeolite treated with H_2O_2	K-exchanged zeolite	Ca-exchanged zeolite
SiO_2	73.90	74.87	71.46	70.69
Al_2O_3	14.17	16.12	13.28	12.88
Fe_2O_3	1.451	1.116	1.003	1.113
CaO	2.987	2.637	2.514	5.041
MgO	2.465	2.263	2.221	2.201
K_2O	2.939	2.667	6.817	2.438
Na_2O	<0.020	<0.043	0.047	<0.030
CEC	106meq/100g	–	–	–
Particle size	<100 μm	–	–	–
Molecular channel size	7.9 Å × 3.5 Å	–	–	–
S_{BET}	37.95m^2/g	40.34 m^2/g	49.06 m^2/g	54.57 m^2/g
Pore volume	0.11cm^3/g	0.11cm^3/g	0.11cm^3/g	0.11cm^3/g
pH	7.9	7.6	8.7	7.8

Activation and modification of zeolite

Zeolites were transformed into calcium and potassium form after peroxide activation. Before peroxide activation, zeolite was dried in a pre-heated oven at 200 °C for 3 h to get rid of of moisture and other impurities. Acid activation was made by H_2O_2 instead of HCl. 5 g of native solids (particle fraction 100 μm) were applied to 250 ml H_2O_2 (50%, hydrogen peroxide) for 24 h at 25 °C. Mixture was centrifuged and dried in oven at 110 °C. On preparation of Ca-exchanged zeolite and K-exchanged zeolite form of zeolite, 50 ml of each solution 1 M $CaCl_2$ and 1 M KCl mixed with 2 g of zeolite in separate flasks, and then stirred for 24 h. The samples were centrifuged, filtered, washed 10 times with water, dried in oven and ground.

Characterization methods

The specific surface area was calculated using the Brunauer-Emmett-Teller (BET) method and the pore volume (V_p) was determined from low-temperature nitrogen adsorption measured using a Micrometrics Gemini VII analyzer. In determination of the surface area, the samples were degassed at 300 °C before the measurements were taken. The specific surface area was obtained by five points at p/p^0 between 0.1 and 0.99 applying the Brunauer–Emmet–Teller equation to the adsorption data. The phases of the zeolite were determined by X-ray diffraction analyses (XRD) with an automated Philips X'Pert Pro diffractometer with Cu anode using Co Kα radiation at 40 kV and 20 mA over the range (2θ) of 5–80° with a scan time of 1°/min. The chemical composition of zeolite was determined by a Philips X'Pert Pro X-ray fluorescence spectrometer (XRF) equipped with a Rh X-ray tube (operated at 50 kV–60 mA). Scanning Electron micrographs were obtained by using Philips XL-30S FEG scanning

electron microscope (SEM). Thermal analyses were performed by the thermogravimetric analysis (TGA) method (Perkin Elmer Diomand TG/DTA). The types of functionalities of the materials and adsorbed species were determined on the basis of the infrared spectroscopy. The Fourier transform infrared (FT-IR) spectra of natural and modified zeolites (Fig. 3) were recorded in the transmission mode at room temperature on 1725X Perkin-Elmer instrument using KBr pellet technique (1:20) with the resolution 2 cm^{-1}.

Sorption methods

The adsorption was performed by batch experiments. Kinetic experiments were carried out by stirring 100 mL of dye solution of known initial dye concentration (100mg/L) with 0.05 g of zeolite at room temperature (25 °C) at 150 rpm in different 250 ml flasks. After time intervals were completed, solutions were centrifuged at 3500 rpm for 10 min. The concentration in the supernatant solution was analyzed using a UV spectrophotometer (Shimadzu UV-1800) by measuring absorbance at $\lambda_{max} = 664.4$ nm and pH = 7.
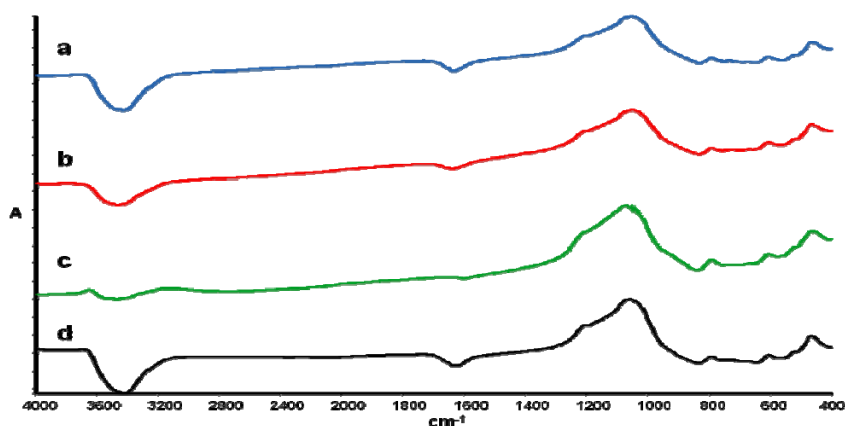
Figure 3. FTIR spectra of ; (a) H_2O_2 treated zeolite, (b) Ca-exchanged zeolite,
(c) K- exchanged zeolite and (d) untreated natural zeolite samples

Results and discussion

Surface areas of zeolite samples are found to be 49.06 m^2/g for K-exc zeolite, 54.57 m^2/g for Ca-exc zeo, and 37.95 m^2/g for untreated zeolite. Besides, activating zeolite with H_2O_2 before modification with K and Ca ions caused the increase in BET surface area. After hydrogen peroxide treatment, the surface area of zeolite has become 44.49 m^2/g. It indicates that the metal chlorides switch with exchangeable ions in zeolite like Ca, Mg and K influenced the surface area in positive way. Bivalent ions like Ca increased the surface area more than monovalent ions like K (Han et al., 2009).
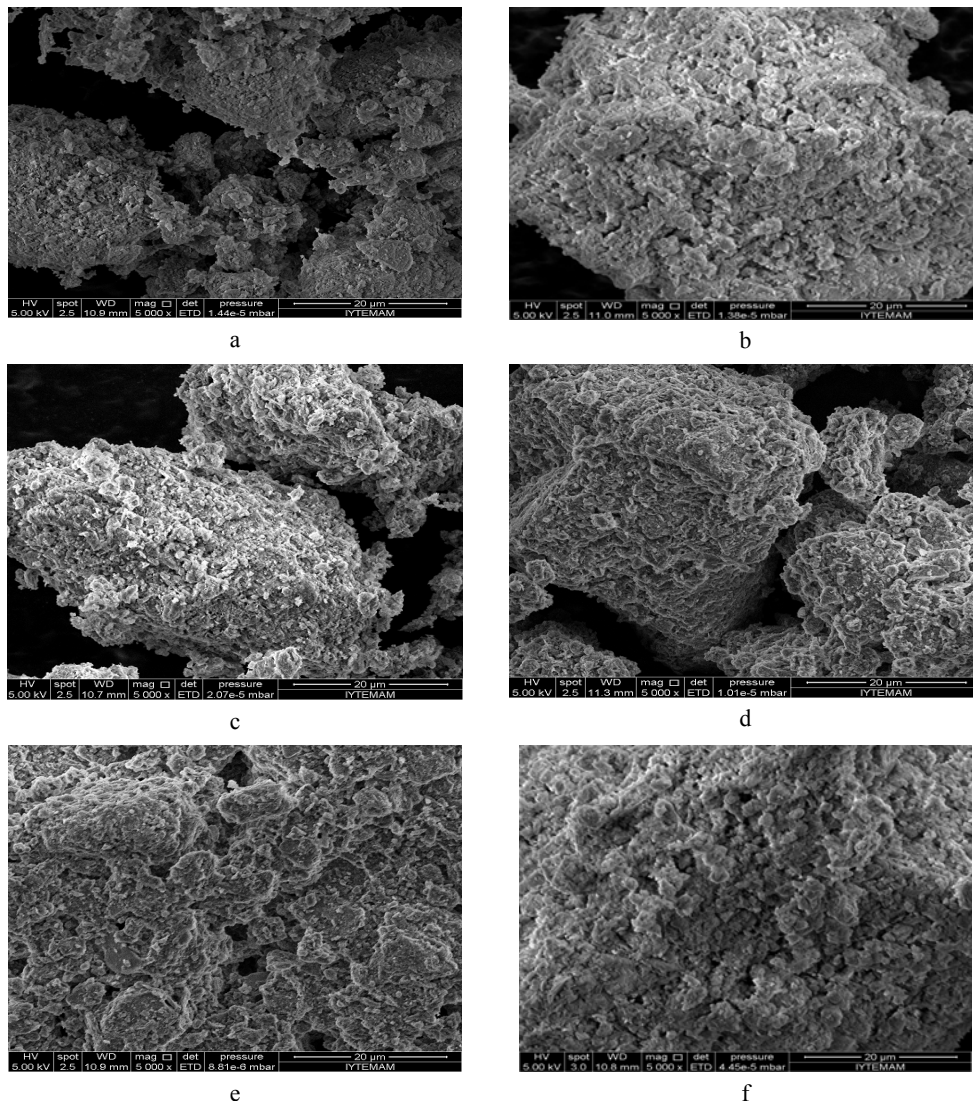
Figure 4. SEM pictures of zeolite samples (a) natural zeolite, (b) zeolite treated with H_2O_2,
(c) K-exchanged zeolite, (d) Ca-exchanged zeolite, (e) Ca-exchanged zeolite after MB adsorption,
and (f) K-exchanged zeolite after MB adsorption

FTIR results presented in Fig. 3 shows that modifying zeolite with Ca and K made change in zeolite structure especially in 3400 and 1680 cm⁻ bands. Chavez et al. (2010) had similar results for Ba adsorption on Ca exchanged zeolite samples. The change in the structure of zeolite samples could be more clearly seen in SEM pictures (see Fig. 4). Activating zeolite with hydrogen peroxide had let more Ca and K ions enter into zeolite surface. The spaces in zeolite structure had been filled with MB by application of modified zeolite on adsorption of MB (see Fig. 4.).

X-ray diffraction patterns of the zeolite samples in (Fig. 5) show that modification of zeolite with solutions did not lead to significant structural changes. The effect of hydrogen peroxide on zeolite appears at decreasing number of peaks because of exchange ions with hydrogen of peroxide. The quantitative XRD analysis demonstrated that the Akdere natural zeolitic tuff consisted of clinoptilolite with minor quantities of quartz, Na-Ca feldspar, mica and opal-CT (Demirhan, 1998). Natural zeolite hardly contains amorphous material. Although, natural zeolite involves both amorphous material which can be seen by means of hump and that of height between 2u is equal to 208 and 308 (Cu Ka) at XRD diagram and opal-CT that is observed by a flat line with the d-spacing of between 4.05 Å and 4.10 Å (cristobalite-tridimite transition). The X-ray diffraction diagrams of the clinoptilolite samples given in Figure 5 show characteristic clinoptilolite peaks at 2u (Cu Ka) = 9.878, 22.48 and 308. As Chavez et al. (2010) stated in their study, XRD results also show the increase in peaks below 10 A° which were caused by Ca and K modification (see Figure 5).
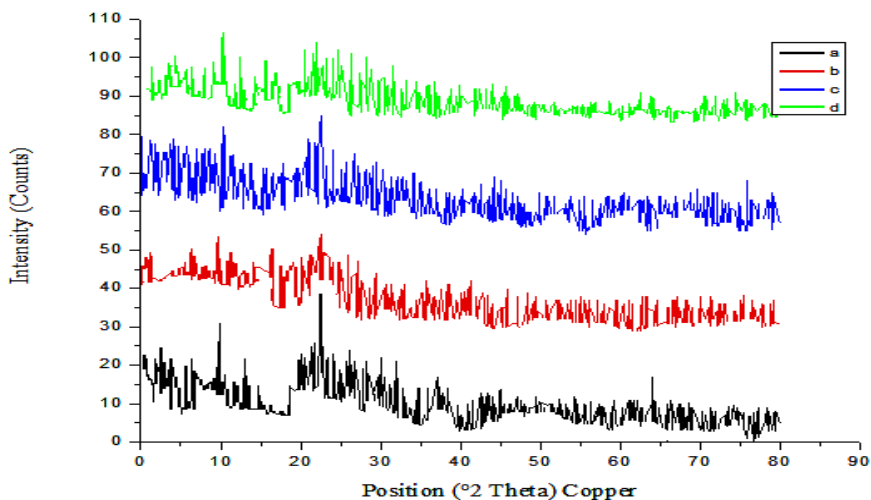
Figure 5. XRD graph of zeolite; a) natural zeolite, b) zeolite treated with H_2O_2, c) K-exchanged zeolite, d) Ca-exchanged zeolite

Table 2 reports the total weight loss for all cation forms determined by TG analysis. The zeolite water loss is higher in the zeolites exchanged with bivalent ion. Thermal analysis results (Table 2) point out the loss of more weight for modified zeolite (Fungaro et al., 2010). In addition, in the monovalent ions, the larger cations have less zeolite water (Table 3). When zeolite samples with and without adsorbed MB were compared, MB adsorbed zeolite samples showed greater weight loss (Fig 6).

Table 2. The results of thermal analysis of natural and modified natural zeolite samples

Sample	Weight Loss (%)
Natural zeolite	12.084
Zeolite treated with H_2O_2	13.734
K- exchanged zeolite	12.974
Ca-exchanged zeolite	14.149

The presence of different exchangeable cations in zeolites changes their temperature at which water is lost from them. TGA curves of natural and modified zeolites are shown in Figure 6. In the temperature range 25–100 °C, the weight loss is due to desorption of physisorbed water. The results vary depending on the type of zeolite and the treatment conditions as Ca-Exchanged > K-Exchanged > Natural Zeolite. After K- and Ca-exchange and H_2O_2 treatment, the amount of water adsorbed decreases, which is a result of the lack of extra framework cations and dealumination.
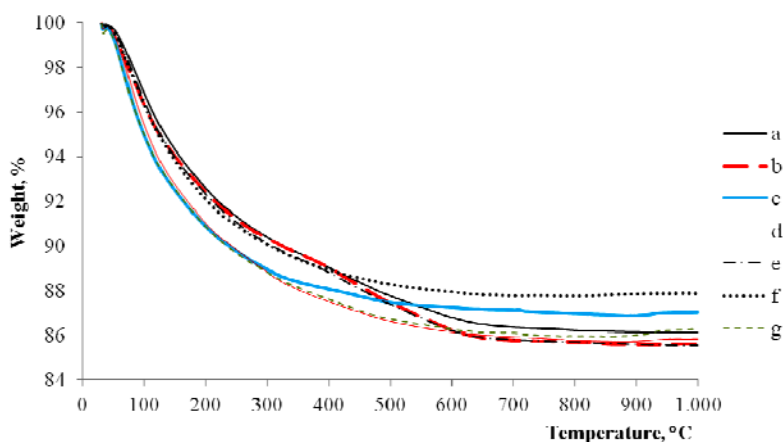
Figure 6. Thermal analysis of zeolite samples: a) MB adsorbed natural zeolite,
b) MB adsorbed zeolite treated with H_2O_2, c) K-exchanged zeolite, d) Ca-exchanged zeolite,
e) MB adsorbed Ca-exchanged zeolite, f) natural zeolite, and g) zeolite treated with H_2O_2

In Ca- and K-exchanged zeolites, the major portions of water molecules are weakly associated with zeolites because of the restriction of water molecules in the defects formed by dealumination. Based on the results mentioned before, the water molecules in zeolites can be classified into three forms as physisorbed water (<100 °C), water associated with extra-framework cations and aluminium (100–400 °C), and water associated with silanol nests (>400 °C). The water exist in clinoptilolite – rich zeolites is more stabile up to 700 °C. However, stability decreases in the zeolites containing mordenite and clinoptilolite. Because of the decrease in the amount of cations after H_2O_2 treatment, the water content in Ca-exchanged zeolite is significantly decreased.

Sorption on natural and modified zeolite

Natural zeolite, zeolite activated with H_2O_2, K-exchanged zeolite activated with H_2O_2, and Ca-exchanged zeolite activated with H_2O_2 were applied to MB solutions. Contact time, initial MB concentration, pH, adsorbent dosage, temperature and agitation speed were the parameters to find out the optimum conditions for the adsorption. To determine equilibrium time in adsorption process, while other variables are kept constant only concentration change depending on stirring time was analyzed. Solutions of 50 mgdm^{-3} concentration of MB prepared from a stock solution at pH = 7 and 300 rpm were mixed with 0.05g zeolite.

As shown in Fig 7a, the adsorption has reached the equilibrium in 30 minutes. q_t is the ratio of adsorbed amount of MB to per gram of zeolite. MB adsorption on zeolite increases with an increase in adsorption time, and come to equilibrium at 30min. At 50 mgdm^{-3} dye concentration and pH 7.0, when the contact time reached from 30min to 240min, the adsorbed amount of MB raised 19.1 mg/g to 21.1 mg/g for natural zeolite, 31.0 mg/g to 32.0 mg/g for K- exchanged zeolite, and 34.0 mg/g to 36.0 mg/g for Ca- exchanged zeolite. The shortest contact time for adsorption was shown as 10 minute in a study by Özdemir (2008) among other studies. However, while Özdemir refers adsorbed amount of MB as 1.25 mg/g, in this study, adsorption comes to equilibrium in 30 minutes with 36 mg/g sorption

Another factor affecting particles adsorbed on dyes is acidity of solution (pH). It is generally expected that adsorption will increase with increasing pH. It is advantage for cationic MB that zeolite surface has negative charge pHs above 6. In Fig.7b, there is no significant change recorded in the amount of MB adsorption at pH between 1 and 8. Increase in adsorption at pHs between 9 and 12 is relatively less than increase in adsorption at pHs between 13 and 14 because of precipitation of MB over pH 8. Therefore, it is decided that there was no contribution made to adsorption amounts by pH over 8, and experiments were set to pH 7. The values for adsorbed amount of MB by zeolite, K-exchanged zeolite and Ca- exchanged zeolite were shifted 20.1 mg/g to 22.4 mg/g, 29.0 mg/g to 35.0 mg/g, and 30.5 mg/g to 38.0 mg/g, respectively when pH increased 3 to 8. Because of the electrostatic attraction force that with increasing pH adsorbed MB onto zeolite surface was increased. It is natural that surface charge of zeolite in alkaline media is negative and cationic MB molecules are kept more on the surface of zeolite at high pH values (Jin et al., 2008). Fungaroa et al. (2010) point out pH for zeolite as 5, but this study shows that best pH value is found 7 because zeta potential value of zeolite is negative over 6 which attracts cationic dyes like MB.

Varying the starting concentration of MB (not shown in Figures) between 50 and 600 mg/dm^3 showed a slight increase in the amount of MB adsorbed. While at 50 mg/dm^3 of C_0 adsorption percentages are 50% for zeolite, 74% for K-exchanged zeolite and 76% for Ca-exchanged zeolite, over 100 mgL^{-1} adsorption percentages dropped clearly as 20% for zeolite, 33% for K-exchanged zeolite and 36% for Ca-exchanged zeolite. This showed that adsorption capacity of zeolite samples for over 100 mg dm^{-3}

initial MB concentration was exceeded, and after 100 mg/dm^3 even modification of zeolite did not affect the adsorption capacity.

For adsorbent dosage, increasing amount of natural and modified zeolite had caused an increase in the amount of adsorbed MB concentration between 0.01g and 0.5g (see Fig.7c). MB adsorption is slightly increased over 0,05g adsorbent added into the mixture. Ozdemir (2012) states that 100 mg/L for initial concentration of MB is optimum same as in this study, while that study finds out adsorbed amount 46.31 mg/g, the adsorbent dosage is used as 0.1 g which is 0.05 g zeolite in this study.
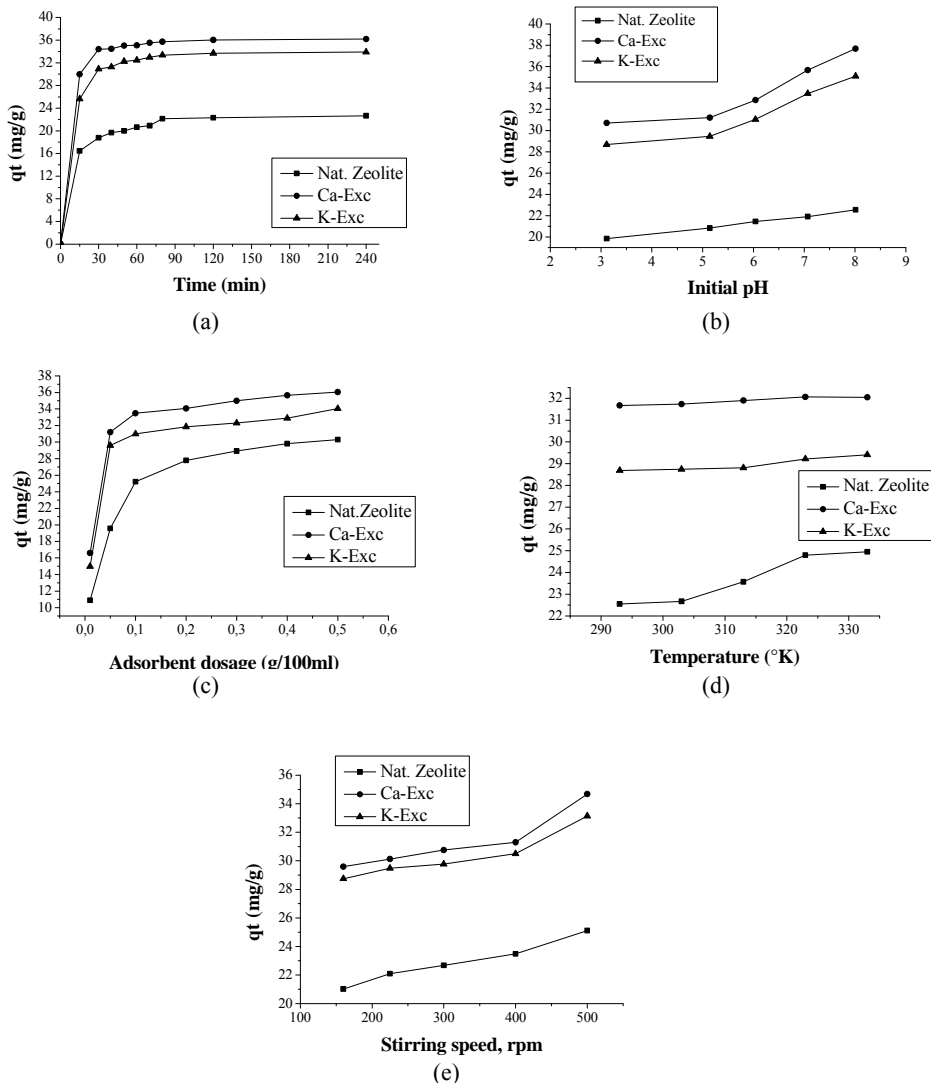
Figure 7. Effects of (a) time, (b) pH, (c) adsorbent dosage, (d) temperature, and (e) stirring speed on MB adsorption by natural zeolite, K-exchanged zeolite, and Ca-exchanged zeolite

Besides the variables considered above, there are also two more variables as temperature and mixture rate used in adsorption. As seen in Fig. 7d, because there is a slight increase in adsorption from 22.0 mg/g toward 26.0 mg/g for natural zeolite, and 29.0 mg/g to 30.0 mg/g for K-exchanged zeolite, 31.0 mg/g to 32.0 mg/g for Ca-exchanged zeolite with increase in temperature from 20 °C to 60 °C. With increase in temperature, MB molecules try harder to get in zeolite pores. Attraction between hydroxyl groups holding on zeolite surface and cationic methylene groups can cause this kind of raise (Bissada et al., 1967). However, in physical adsorption change in temperature does not have influence on increase in adsorption.

In Fig. 7e, it is clear that there is no significant difference in contribution of adsorption percentage with stirring speed at 150, 225, 400 and 500 rpm, respectively. Therefore, the mixture rate is determined as 150rpm. The trend of change with stirring speed pointed out that contacting MB ions with zeolite samples by increasing speed did not cause the raise for adsorption capacity

Table 3. Previous studies on MB adsorption and the maximum amounts adsorbed

Type of adsorbent	Initials conditions	Adsorbed amount of MB (mg/g)	Ref.
Clay	0.1 g; 100 cm^3; 100 mg/dm^3; 60 min	60	Gürses et al. (2006)
Perlite	1 g; 100 cm^3; 93.475 mg/ dm^3; 30 min; pH = 7	7.5	Doğan et al. (2004)
Natural zeolite	2.2434 mg/dm^3; 150 cm^3; 1000 min; 0.01–0.05g	23.6	Farhade and Aziz (2010)
Hazelnut shell	50 cm^3; 0.25 g; 24 h; 959.58 mg/dm^3	96.0	Doğan et al. (2008)
Hazelnut shell	1 g; 2 dm^3; 40 min; 37.39 mg/dm^3; pH = 4.1–4.5	74.8	Doğan (2009)
Zeolite	12.8 mg/dm^3; 100 cm^3; 1 g; 10 min; pH = 5	1.3	Fungaroa et al. (2010)
Melamine-urea resin	13.04 mg/dm^3; 0.3 g; 20 min; 1 dm^3	12.1	Özdemir (2008)
Sepiolite	400.32 mg/dm^3; 2 dm^3; 5 g; 400 rpm; pH = 5–9; 3 h	75.1	Doğan et al. (2007)
(SDBS)- and (SDS)-modified zeolite	25 mg/dm^3; 25 cm^3; pH = 6.43; 0.1 g; 30 min	8.7	Jin et al. (2008)
Tripoli	100 cm^3; 0.5 g; 100 mg/dm^3; pH = 8	17	Alzaydien (2009)
Activated carbon	0.1 g; 50 cm^3; 1–60 min; 100 mg/dm^3	46.3	Ozdemir (2012)
Vineyard pruning waste	25 °C and natural pH; 10 g/2 dm^3; 400 rpm; 60 min	46.1	Ugurlu (2010)
Natural zeolite	0.05 g; 100 cm^3; 30 min, 100 mg/dm^3	28.6	present study
Modified zeolite	0.05 g; 100 cm^3; 30 min, 100 mg/dm^3	42.7	present study

The optimum pH range for adsorption of MB was found to be at 7.0. Adsorption equilibrium attained within 30 minutes. The sorption of MB slightly increased with

rise of temperature. As the zeolite amounts increased, the removal efficiencies increased, but on the other hand, the adsorbed amount on the zeolite decreased with the increasing zeolite amounts. The removal efficiency of natural zeolites is strongly affected by the modification of zeolite. Overall, a comparison of several adsorbents employed for MB adsorption in previous research efforts was presented in Table 3. As it can be seen from Table 3, modified zeolite employed in this work presented higher adsorption capacity when compared with some of adsorbent reported in the literature.

Adsorption equilibrium

The equilibrium adsorption isotherm is fundamental in describing the interactive behavior between solutes and adsorbent, and is important in the design of adsorption system. As shown in Table 4, the adsorption increases with the increasing equilibrium concentration and approaches to equilibrium at higher concentration. Higher temperature slightly results in higher adsorption capacity.

   Two models are commonly used to simulate the adsorption isotherm, the Langmuir and Freundlich isotherms. The well-known expression of the Langmuir model is

$$q_e = \frac{K_L q_{max} C_e}{1 + K_L C_e} \tag{1}$$

where q_e is the equilibrium dye concentration on adsorbent (mg/g), C_e the equilibrium dye concentration in solution (mg/L), q_{max} is the monolayer capacity of the adsorbent (mol/g) and K_L is the Langmuir adsorption constant (dm^3/mg) which relates to the adsorption energy. The Langmuir equation is applicable to homogeneous sorption, where the sorption of each sorbate molecule onto the surface has equal sorption activation energy. On the other hand, the Freundlich equation is

$$q_e = K_F C_e^{1/n} \tag{2}$$

where q_e is the equilibrium dye concentration on adsorbent (mg/g), C_e is the equilibrium dye concentration in solution (mg/L) and K_F (L/g) and n are the Freundlich constants characteristic of the system, indicators of adsorption capacity and adsorption intensity, respectively. The Freundlich equation is employed to describe heterogeneous systems and reversible adsorption and is not restricted to the formation of monolayers.

   The adsorption of MB on zeolite is due to the formation of the hydrogen bonds between surface hydroxyls and dye molecules with participation of water molecules. The non-linear forms of the two isotherms to the experimental data are illustrated in Table 4. The fits for two isotherms are quite similar. Except for K-exchanged zeolite at 50 °C which shows both Langmuir and Freundlich type of isotherm, all other experimental data were well fitted to the Langmuir equation, with good correlation coefficients (Alzaydien, 2009). The correlation coefficients of Ca-exchanged zeolite at both 20 °C and 50 °C and K-exchanged zeolite at 50 °C for two models are greater

than 0.95, indicating that the two models fit the experimental well. For other samples, Langmuir is the only isotherm fits for MB adsorption. For all zeolite samples, Langmuir isotherm correlations belong to 20 °C are higher than the values of 50 °C. This would lead us that temperature does not influence on adsorption. For K_L values, all values decreased with increasing temperature, the highest value was shown for Ca-exchanged zeolite.

The Langmuir model suggests the surface sorption mechanism. The maximum Langmuir equilibrium constant (K_L) calculated from the slope and the intercept of the linear plot were 26.11 mg g^{-1} at 20°C and it belongs to Ca-exchanged zeolite. The value of the monolayer saturation capacity of zeolite was comparable to the adsorption capacities of some other adsorbent materials for MB (Table 4). A direct comparison of literature data obtained using different adsorbents may not be appropriate since experimental conditions are not systematically the same.

Freundlich constant (K_F) and the heterogeneity factor ($1/n$) calculated from the slope and the intercept of the linear plot were changing between 45.42 mg g^{-1} and 722.00 mg g^{-1}, 0.26 and 3.14, respectively. The value of $1/n$ smaller than 1 points out the favorable sorption conditions (Alzaydien, 2009; Chavez et al., 2010). In this manner, Ca-exchanged and K-exchanged zeolite samples were favorable. The Langmuir and Freundlich isotherm constants and linear (R^2) regression coefficients are shown in Table 4.

Table 4. Langmuir and Freundlich isotherms of MB adsorption on natural zeolite, Ca-exchanged and K-exchanged zeolite

	Langmuir Isotherm			Freundlich Isotherm		
	K_L, mg/g	b, L/mg	R^2	$1/n$	K_f, mg/g	R^2
Zeolite (20 °C)	2.845	0.016	0.971	1.891	89.125	0.916
Zeolite (50 °C)	0.053	0.007	0.959	1.748	98.628	0.893
Ca-Exc (20 °C)	26.110	0.568	0.998	0.260	45.420	0.961
Ca-Exc (50 °C)	0.142	0.132	0.996	2.741	221.310	0.973
K-Exc (20 °C)	20.534	0.003	0.988	0.437	87.510	0.804
K-Exc. (50 °C)	0.149	105.68	0.987	3.140	722.000	0.988

Conclusions

The effectiveness of H_2O_2 in activating the natural and modified zeolites to remove methylene blue (MB) ions from aqueous solutions has been presented. It was observed that MB adsorption is partially dependent on the adsorbent amount, particle size, contact time, initial pH of the solution and initial metal concentration.

FTIR, SEM, TG/DTA analyses revealed that Ca- and K-exchanged zeolites have higher surface area and affinity toward MB. Modification after H_2O_2 treatment allowed zeolite samples to adsorb more MB ions than untreated zeolite samples. The effect of activation with H_2O_2, and then modification with KCl and CaCl$_2$ could

significantly improve the adsorption rate and adsorption capacity of MB ions. Adsorption values were arisen with activation and modification as Ca-Exchanged Zeolite (H_2O_2 treatment) > K-Exchanged zeolite (H_2O_2 treatment) > Zeolite treated with peroxide > natural zeolite.

The adsorption of MB on zeolite was found to conform to the Langmuir equation. This study has shown the potential of modified zeolites after H_2O_2 treatment for the removal of MB from wastewater streams due to their relatively low price, abundance in nature, and its easy procedure to modify.

References

ALBAYRAK M., 2008, *Batı Anadolu, Trakya, Kapadokya Yöresi Zeolitleri Mineralojik Veri Kitabı*, MTA Rap., 11053. (in Turkish)

ALKAN M., DEMIRBAS O., DOĞAN M., 2007, *Adsorption kinetics and thermodynamics of an anionic dye onto sepiolite*, Microporous and Mesoporous Materials, 101, 388–396.

ALZAYDIEN A.S., 2009, *Adsorption of Methylene Blue from Aqueous Solution onto a Low-Cost Natural Jordanian Tripoli*. American Journal of Environmental Sciences. 5(3), 197–208.

ARMAGAN B., OZDEMIR O., TURAN M., CELIK M.S., 2003, *The removal of reactive azo dyes by natural and modified zeolites*, Journal of Chemical Technology and Biotechnology. 78, 725–732.

ATEŞ A., HARDACRE C., 2012, *The effect of various treatment conditions on natural zeolites: Ion exchange, acidic, thermal and steam treatments*. Journal of Colloid and Interface Science, 372, 130–140.

ATES A., REITZMANN A., HARDACRE C., YALCIN, H., 2011, *Abatement of nitrous oxide over natural and iron modified natural zeolites*, Applied Catalysis A: General, 407(1–2), 67–75.

AJEMBA R.O., ONUKWULI O.D., 2013, *Adsorptive removal of colour pigment from palm oil using acid activated Nteje clay. Kinetics, equilibrium and thermodynamics*, Physicochemical Problems of Mineral Processing, 49(1), 369−381.

BISSADA K.K., JOHNS W.D., CHENG F.S., 1967, *Cation-Dipole interactions in Clay Organic Complexes*. Clay Minerals, 7, 155–166.

CAGLAR B., AFSIN B., TABAK A., EREN, E., 2009, *Characterization of the cation-exchanged bentonites by XRPD. ATR, DTA/TG analyses and BET measurement*. Chemical Engineering Journal, 149, 242–248.

CHAVEZ M.L., DE PABLO L., GARCIA T.A., 2010, *Adsorption of Ba^{2+} by Ca-exchange clinoptilolite tuff and montmorillonite clay*. Journal of Hazardous Materials, 175, 216–223.

CRINI G., 2006, *Non-conventional low-cost adsorbents for dye removal: A review*. Bioresource Technology, 97, 1061–1085.

DEMIRHAN M., 1998, *Manisa İli-Demirci İlçesi Akdere Köyü ONIR-6645 Ruhsat No'lu Zeolit Sahası Maden Jeolojisi Raporu*, MTA Rap., 10173. (in Turkish)

DOĞAN M., ABAK H., ALKAN M., 2008, *Biosorption of Methylene Blue from Aqueous Solutions by Hazelnut Shells: Equilibrium, Parameters and Isotherms*. Water Air Soil Pollution, 192, 141–153.

DOĞAN M., ABAK H., ALKAN M., 2009, *Adsorption of methylene blue onto hazelnut shell: Kinetics, mechanism and activation parameters*. Journal of Hazardous Materials. 164, 172–181.

DOĞAN M., ALKAN M., OZDEMIR Y., 2000, *Adsorption of Methylene Blue from aqueous solution onto perlite*. Water, Air & Soil Pollution, 120 (3–4), 229–248.

DOĞAN M., OZDEMIR Y., ALKAN M., 2007, *Adsorption kinetics and mechanism of cationic methyl violet and methylene blue dyes onto sepiolite*. Dyes and Pigments, 75(3), 701–713.

ETAIW S.E.H., EL-BENDARY M.M., 2012, *Degradation of methylene blue by catalytic and photo-catalytic processes catalyzed by the organotin-polymer $^3_\infty[(Me_3Sn)_4Fe(CN)_6]$*, Applied Catalysis B: Environmental, 126, 326–333.

FARHADE J., AZIZ H., 2010, *Competitive Adsorption of Methylene Blue and Rhodamine B on Natural Zeolite: Thermodynamic and Kinetic Studies*. Chineese Journal of Chemistry. 28, 349–356.

FUNGAROA D.A., GROSCHEA L.C., PINHEIROB A.S. IZIDOROA J.C., BORRELY S.I., 2010, *Adsorption of methylene blue from aqueous solution on zeolitic material and the improvement as toxicity removal to living organisms*. Orbital Electronic Journal of Chemistry. 2(3), 235–247.

GLADYSZ-PLASKA A., KOWALSKA-TERNES M., MAJDAN M., 2000, *Adsorption of toxic metal ions on zeolites*. Przem Chem. 79:298.

GULGONUL I., 2012, *Evaluation of Turkish Bentonite for Removal of Dyes from Textile Wastewaters*, Physicochemical Problems of Mineral Processing, 48(2), 369–380.

GÜMÜŞ D., AKBAL F., 2011, *Photocatalytic Degradation of Textile Dye and Wastewater*, Water, Air & Soil Pollution, 216, 21–37.

GÜRSES A., DOĞAR C., YALÇIN M., AÇIKYILDIZ M., BAYRAK R., KARACA S., 2006, *The adsorption kinetics of the cationic dye, methylene blue, onto clay*. Journal of Hazardous Materials, 131, 217–228.

HAN R., ZOU L., ZHAO X., XU Y., XU F., LI Y., WANG Y., 2009, *Characterization and properties of iron oxide-coated zeolite as adsorbent for removal of copper (II) from solution in fixed bed column*, Chemical Engineering Journal, 149, 123–131.

HERNANDEZ M.A., CORONA L., ROJAS F., 2000, *Adsorption characteristics of natural erionite, clinoptilolite and mordenite zeolites from Mexico*. Adsorption, 6, 33–45.

HERNANDEZ-RAMIREZ O., HOLMEZ S.C., 2008, *Novel and modified materials for wastewater treatment applications*. Journal of Materials Chemistry, 18, 2751–2761.

JIA A., LOU L., ZHANG C., ZHANG Y., LIU S., 2009, *Selective oxidation of benzyl alcohol to benzaldehyde with hydrogen peroxide over alkali-treated ZSM-5 zeolite catalysts*. Journal of Molecular Catalysis A: Chemical, 306, 123–129.

JIN X., JIANG M., SHAN X., PEI Z., CHEN Z., 2008, *Adsorption of methylene blue and orange II onto unmodified and surfactant-modified zeolite*. Journal of Colloid and Interface Science. 328, 243–247.

KARAOĞLU M.H., UGURLU M., 2010, *Kinetic and equilibrium studies of methylene blue biosorption by vineyard pruning waste*. Fresenius Environmental Bulletin, 19(12b), 3199–3208.

KONDRU A.K., KUMAR P., CHAND S., 2009, *Catalytic wet peroxide oxidation of azo dye (Congo red) using modified Y zeolite as catalyst*. Journal of Hazardous Materials, 166, 342–347.

KORKUNA O., LEBODA R., SKUBISZEWSKA-ZIĘBA, J., VRUBLEVS'KA T., GUŃKO V.M., RYCZKOWSKI J., 2006, *Structural and physicochemical properties of natural zeolites: Clinoptilolite and mordenite*. Microporous Mesoporous Materials, 87, 243–254.

KOWALCZYK P., SPRYNSKYY M., TERZYK A.P., LEBEDYNETS M., NAMIESNIK J., BUSZEWSKI B., 2006, *Porous structure of natural and modified clinoptilolites*, Journal of Colloid and Interface Science, 297, 77–85.

MISAELIDES P., 2011, *Application of natural zeolites in environmental remediation: A short review*, Microporous and Mesoporous Materials, 144, 15–18.

METES A., KOVACEVIC D., VUJEVIC D., PAPIC S., 2004, *The role of zeolites in wastewater treatment of printing inks*, Water Research, 38, 3373-3381.

OZDEMİR C.S., 2012, *Adsorption and desorption kinetics behavior of methylene blue onto actıvated carbon*. Physicochemical Problems of Mineral Processing, 48(2), 441−454.

OZDEMIR F.A., 2008, *Atıksulardan boya giderimi için yeni bir yöntem*. Unpublished Master thesis. Istanbul Tecnical University Institute of Sciences.

SLOKAR Y.M., MARECHAL A.M.L., 1998, *Methods of decoloration of textile wastewaters*. Dyes and Pigments, 37(4), 335-356.

WANG S., PENG Y., 2010, *Natural zeolites as effective adsorbents in water and wastewater treatment*. Chemical Engineering Journal, 156,11–4.

ADVANCED BIOCOMPOSITES BASED ON SILICA AND LIGNIN PRECURSORS

**Lukasz KLAPISZEWSKI, Magdalena NOWACKA,
Karolina SZWARC-RZEPKA, Teofil JESIONOWSKI**

Poznan University of Technology, Faculty of Chemical Technology, Institute of Chemical Technology and
Engineering, M. Sklodowskiej–Curie 2, PL-60-965 Poznan, Poland
E-mail: teofil.jesionowski@put.poznan.pl, phone: +48 616653720, fax: +48 616653649

Abstract: A new method is proposed for obtaining biocomposites based on a combination of silica and lignin precursors. Amorphous silica was produced by two methods: one based on hydrolysis and condensation of tetraethoxysilane (sol–gel method) and the other involving precipitation in a polar medium. Additionally, the commercial silica known under the name of Syloid®244 was used. The silica surface was modified to ensure better affinity of the support to activated lignin. The biocomposites obtained were carefully characterised by determination of their physicochemical and dispersive–morphological properties. Electrokinetic stability of the biocomposites was evaluated on the basis of zeta potential dependence on pH. Thermal stability of the biocomposites and their porous structure parameters (surface area, pore diameter and pore volume) were established. The results indicate that silica/lignin biocomposites are much promising for application in many areas of science and industry.

Keywords: biocomposites, silica, lignin, physicochemical and structural properties

Introduction

Increasing cost of energy and the necessity of the natural environment protection have shifted the interest from production of synthetic materials to their natural biodegradable correspondents. Much attention is paid to materials combining characteristic properties of a few substrates in the form of multifunctional composites. One of such materials undoubtedly is the inorganic–organic system of silica and lignin, showing biocompatibility with the natural environment, relatively low cost of production because of easy availability of the precursors and many other features valuable from the viewpoint of technological use. Lignin, which is a component of wood besides cellulose and hemicellulose, has become an interesting subject of intense research work. Its unique properties have attracted the attention of chemists,

biologists, dieticians and technologists (Kovacs 2011). In wood, lignin plays the role of a scaffold, it stiffens the cell wall, protects wood against pathogens and abiotic factors, such as low or high temperature or the presence of heavy metals. Lignin is also important for the transport of metabolites and water (Novaes 2010).

Lignin makes a three–dimensional inhomogeneous polymer network of unique structure. It is composed of a mixture of organic aliphatic and aromatic compounds, with the greatest contribution of derivatives of *p*-coumaryl, coniferyl and sinapyl alcohols (Ralph 1999, Ek 2009, Collinson 2010). As a natural material being a waste product and hence cheap, it has recently become a subject of great interest. Because of the ease of modification and the possibility of isolation of many compounds from it, lignin has proved to be an excellent raw product for many branches of industry. As shown by Harmita (2009), Sciban (2011) and Brdar (2012), because of low cost and limited solubility in water, lignin can be used for water purification as adsorbent of heavy metals such as zinc, lead, cadmium, copper or nickel. It is also effective for removal of other substances such as dyes, surfactants and organic pollutants. After activation with amine groups (Cotoruelo 2012) lignin can be successfully applied for adsorption of phenols. Lignin being a natural polymer has been also used as an addition to synthetic polymers endowing them with characteristic features (Kunanopparat 2012, Morandim–Giannetti 2012). It is also important in electro-chemistry. When used as an admixture in production of electrodes it shows valuable electrochemical properties following from the presence of electrocatalytic quinone in its structure. Because of low cost and ease of preparation, the electrodes can be used in electrochemical sensors, biosensors, converters and for connecting enzymes acting as bioplatforms (Milczarek 2007, 2009, 2010). The recent work on lignin in electrochemistry (Milczarek 2012) has been directed at production of environmentally friendly devices for electric energy storage.

The other component is silica which is one of the most common mineral on Earth. The most important methods of its production include the hydrolysis of alkoxysilanes based on the Stöber method (Stöber 1968, Ibrahim 2010), precipitation from water solution of sodium silicate in polar systems (Jesionowski 2001) or in nonpolar systems (Jesionowski 2002) and high-temperature combustion of silicon halogens in a gas phase (Wypych 2010). Because of a number of valuable physicochemical properties such as well–developed specific surface area, porosity and hardness, it has been widely used in many branches of industry. Owing to the content of siloxane and silanol groups, silica is an active filler and adsorbent supporting chemically bonded organic substances.

These highly valuable properties and many areas of prospective use have prompted us to make an attempt at combining lignin with inorganic silica support. The intention was to produce a multifunctional biocomposite combining the properties of lignin and silica. Results of this attempt and characterisation of the silica/lignin biocomposites obtained are reported in this paper where we also consider the potential applications of the biocomposites.

Experimental

Synthesis of silica/lignin biocomposites

The silica-lignin biocomposite was obtained in a two-stage process. In the first process a reactor containing dioxane and water (9:1, v/v) was charged with a specific amount of Kraft lignin from Sigma–Aldrich (3, 5, 10, 20, 30, 40, 50 wt./wt. relative to 100 weight parts of silica). Upon continuous stirring with a fast-speed stirrer Eurostar digital IKA-Werke GmbH (1200 rot/min) a water solution of sodium iodate(VII) (Sigma–Aldrich) was introduced in order to activate lignin. The process was performed in the dark for about 30 minutes. In the second stage the lignin solution obtained was introduced at the rate of 5 cm^3/min into a reactor with the earlier prepared silica modified with aminosilane, dispersed in 50 cm^3 of water. Three types of silicas were used: the silica synthesised by the sol–gel method, another one precipitated in a polar system and the third one was a commercial silica Syloid®244.
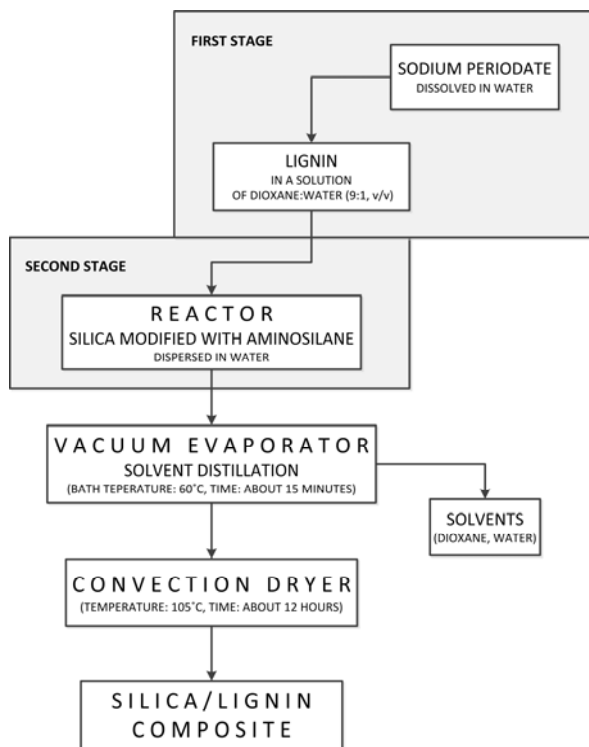
Fig. 1. Preparation of silica/lignin biocomposites – a schematic representation

The silica sample obtained by the modified Stöber method (sol–gel method) was synthesised with the use of tetraethoxysilane – TEOS (Sigma–Aldrich), ethyl alcohol and ammonia (Chempur). The appropriate amount of reagents was placed in a reactor

and carefully dispersed for about 1 h. The second sample was obtained by precipitation in a polar system as a result of reaction between sodium silicate (Vitrosilicon SA) and sulphuric acid (Chempur). A detail description of the process conditions and substrates used is given in (Jesionowski 2002). The sample of commercial product Syloid[®]244 made by W.R. Grace and Company was used for comparative purposes. To activate silica, its surface was functionalised by introducing a modifying mixture of 5 weight parts by mass of *N*-2-(aminoethyl)-3-amino-prophyltrime-thoxysilane in a methanol–water solution of 4:1, v/v). This mixture was dosed into a reactor with a proper silica sample dispersed in water by a peristaltic pump at the rate of 3 cm^3/min. After introduction of the whole portion of the mixture, the contents of the reactor were stirred for about 30 minutes. After modification the silica was introduced into the above described lignin solution and the combined contents were stirred vigorously for about 1 h. After completion of the process the solvent was evaporated at 60 ºC in a vacuum evaporator and the precipitate was dried in a dryer (Memmert) at 105 ºC for about 12 h. A scheme of the process is given in Fig. 1.

Physicochemical evaluation

The silica/lignin biocomposites obtained were subjected to physicochemical and dispersive–morphological characterisation. The particle size distribution was determined by two instruments: Zetasizer Nano ZS (0.6–6000 nm) and Mastersizer 2000 (0.2–2000 µm) employing two measuring methods NIBS and laser diffraction, respectively. Both instruments were made by Malvern Instruments Ltd. The electrokinetic stability of the biocomposites was determined on the basis of zeta potential dependence on pH, using also Zetasizer Nano ZS (Malvern Instruments Ltd.) with an autotitrator attached. Measurements were made in a 0.001M NaCl solution. The thermal stability of biocomposites was evaluated on the basis of thermo-gravimetric measurements on a TG Jupiter STA449F3, made by Netzsch. Colorimetric analysis was made on a colorimeter Specbos 4000 (YETI Technische Instrumente GmbH) to confirm the effectivness of the proposed method of biocomposite synthesis. The samples obtained were also subjected to determination of their specific surface area BET and pore volume and diameter by the method of Barrett, Joyner, Halenda (BJH). The measurements were performed on ASAP 2020, made by Micromeritics Instrument Co.

Results and discussion

Dispersive and morphological characteristics

Table 1 presents results characterising dispersive properties of the biocomposites obtained. The particle size distribution was determined in two ranges of values by two instruments Zetasizer Nano ZS and Mastersizer 2000.

Table 1. Dispersive characteristic of silica/lignin biocomposites

Sample no.	Type of SiO$_2$	Content of Kraft lignin in relation to the silica matrix (wt./wt.)	Range of particle size from Zetasizer Nano ZS (nm)	Particle diameter from Mastersizer 2000 (μm)			
				d(0.1)	d(0.5)	d(0.9)	D[4.3]
1		3	164–255 1280–2300	5.4	18.0	38.4	20.3
2		10	190–220 1480–3090	5.4	17.6	41.7	20.3
3	Stöber silica	20	59–68 825–1280	4.3	15.8	37.1	18.6
4		50	122–164 3580–5560	4.2	17.4	38.9	19.8
5		3	68–79 2670–4800	4.2	17.4	38.9	19.8
6	Hydrated silica	10	106–122 1720–2300	4.9	18.9	42.0	21.5
7		20	59–68 1990–3580	5.4	18.0	38.4	20.3
8		50	142–164 2670–5560	5.6	21.5	47.6	24.4
9		3	712–955	2.5	6.7	28.7	11.8
10	Syloid® 244	10	33–39 2300–3580	2.6	8.2	29.2	12.6
11		20	51–59 1720–3090	2.7	8.8	30.5	13.3
12		50	68–91 1480–3580	2.7	8.3	31.5	13.3

Each product was found to show a tendency towards formation of particle clusters, which is in agreement with the results already reported by Klapiszewski (2012). The plots illustrating particle size distributions (additionally verified by microscopic observations) are given in Fig. 2. The most homogeneous is the sample obtained on the basis of commercial silica Syloid®244 (Fig. 2c). Less homogeneous are the biocomposites based on silica synthesised by the sol–gel method (Fig. 2a) and that precipitated in a polar medium (Fig. 2b).

Figure 3 presents the particle size distribution of biocomposites obtained from 20 weight parts of lignin relative to 100 weight parts of SiO$_2$ to permit a comparison of the products obtained from different silica precursors. The results presented by Klapiszewski (2012) suggested that the presence of small amount of lignin in a biocomposite was beneficial from the viewpoint of dispersive–morphological properties.

(a)   (b)   (c)
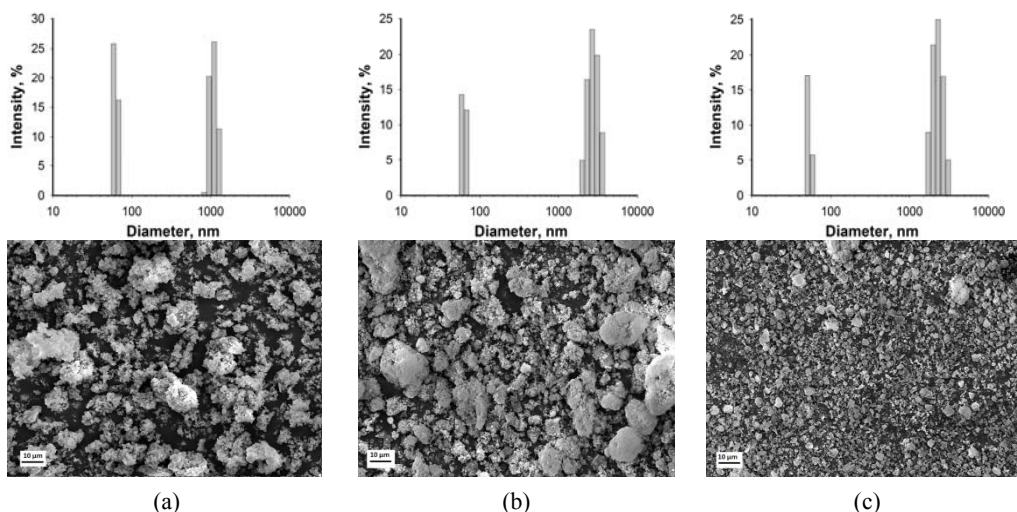
Fig. 2. Particle size distributions (Zetasizer Nano ZS) and SEM microphotographs
of silica/lignin biocomposites containing 20 weight parts by mass of lignin in hybrid matrix
prepared on the basis of silica precursors (a) Stöber silica, (b) hydrated silica, and (c) Syloid®244

For a detail analysis we have chosen the products containing 20 weight parts
by mass of lignin relative to 100 weight parts by mass of SiO_2. As follows from
Fig. 3, the greatest amount of particles in the range of the smallest diameters is
in the biocomposite based on Syloid®244. The plots obtained for the other two
biocomposites (samples 3 and 7) on the basis of Mastersizer 2000
measurements are similar. This result has confirmed the conclusions drawn
from the analysis of Table 1 and Fig. 2.
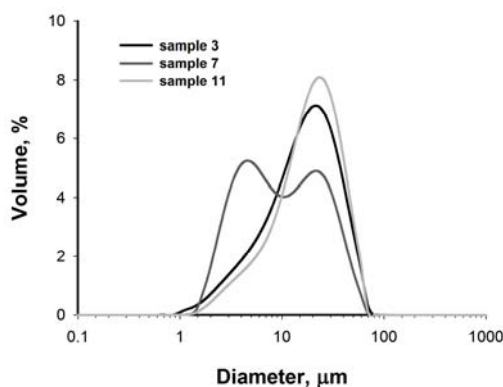
Fig. 3. Particle size distributions (Mastersizer 2000) of selected biocomposites

Electrokinetic characteristic

The electrokinetic potential (zeta) describes the degree of repulsion between the neighbouring particles of similar charges. The value of ζ potential is influenced by many factors of which the most important is pH. The sign and magnitude of zeta potential depends also to a significant degree on the medium in which the particles are dispersed (Weiner 1993, Elimelech 1994, Otterstedt 1998).

(a)   (b)
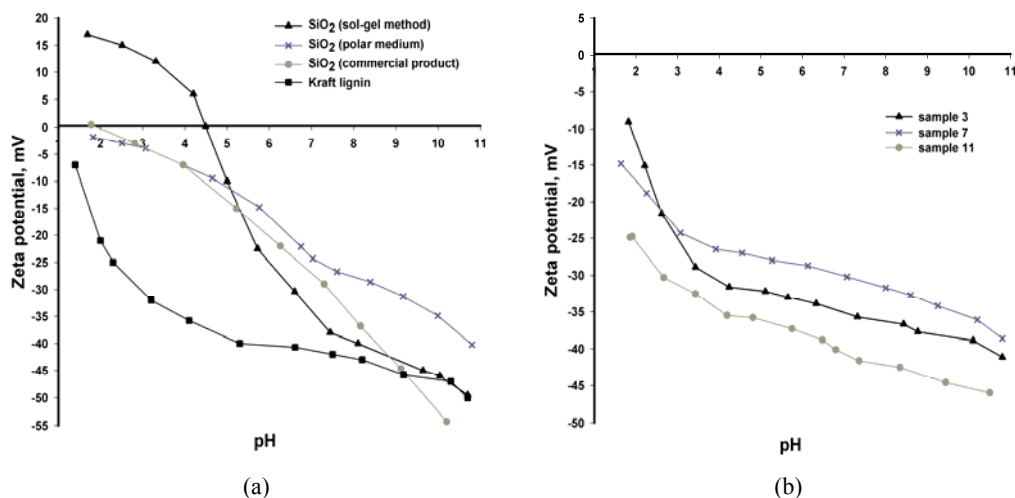
Fig. 4. Zeta potential vs. pH of silicas used and Kraft lignin (a), and
(b) selected biocomposites containing 20 weight parts by mass of lignin in silica matrix

Figure 4 presents the zeta potential as a function of pH for the three types of SiO_2 and Kraft lignin. The measurements were made in a 0.001M NaCl solution in the pH range from 1.7 to 11. The character of the electrokinetic curves presented differs depending on the type of silica used, which has also been reported by Xu (2003) and Jesionowski (2005). For the biocomposites based on Syloid®244 and on silica precipitated in a polar medium the zeta potential values in the acidic pH range were similar. The isoelectric point (i.e.p.) for the biocomposite based on Syloid®244 is noted at pH close to 2, while for the biocomposite based on SiO_2 precipitated in a polar medium no i.e.p. value was reached, but the curve suggests that it would be achieved at pH of about 1.7. Such i.e.p. values are consistent with literature data suggesting that i.e.p. of SiO_2 is reached for pH from 1.7 to 3.5. This implies that in acidic solutions there is a risk of coagulation. The zeta potential in this pH range reaches very low values. In the alkaline pH the commercial silica shows somewhat higher zeta potential so also a better electrokinetic stability. For the biocomposite based on SiO_2 obtained by the sol–gel method, the electrokinetic curve reached i.e.p. at pH close to 4.5. A positive value of surface charge below $pH_{i.e.p.} \sim 4.5$ is not typical of silica but follows from the presence of a small number of $-NH_3^+$ groups

incorporated in the spatial lattice of silica and is related to the method of synthesis applied (Kosmulski 2009).

Kraft lignin shows negative values of zeta potential in the whole pH range studied and the shape of the electrokinetic curve suggests a tendency towards reaching i.e.p. at pH close to 1. Kraft lignin shows negative surface charge in a wide range of pH. The charge is a consequence of ionisation of the surface hydroxyl and acidic groups as a result of lignin dispersion in water solutions (Dong 1996). Kraft lignin has a high electrokinetic stability in pH range from 3 to 11.

Figure 4b presents the zeta potential dependences on pH for the SiO_2/lignin biocomposites. All biocomposites show negative zeta potential in the whole pH range studied and good electrokinetic stability in the pH range from 4 to 11. The character of electrokinetic curves is an indirect confirmation of the effectiveness of the proposed method of SiO_2/lignin biocomposites synthesis.

Colorimetric analysis

Analysis of the colorimetric data has brought another evidence indirectly confirming the effectiveness of the proposed method of silica functionalisation. The colorimetric parameters were determined in the colour space CIE $L*a*b*$.

No significant difference in the colour was detected for the silicas obtained by different methods. Thus, for all silica samples an average value of $L*$ equal to 93.7 was assumed. With increasing content of lignin in the final biocomposite, the value of $L*$ decreases, confirming that the surface functionalisation took place to a satisfactory degree (Fig. 5). Moreover, the values of $a*$ and $b*$ increase, which indicates an increase in the contribution of red and yellow.

An additional parameter that can be of importance in colorimetric analysis is the value of dE factor component describing the total change in colour of particular samples. As expected, this value increases with increasing content of lignin in the biocomposite, which confirms a distinct differences in the colour between the samples containing different amounts of lignin

Thermal analysis

Thermal analysis is the main method for characterisation of thermal properties of chemical substances. Results of thermal analysis provide information on the elementary phenomena taking place and the thermal stability of a substance at elevated temperatures is one of the most important parameters defining the range of prospective application of materials. Such measurements were performed for the silica/lignin biocomposites.

(a)

(b)

(c)
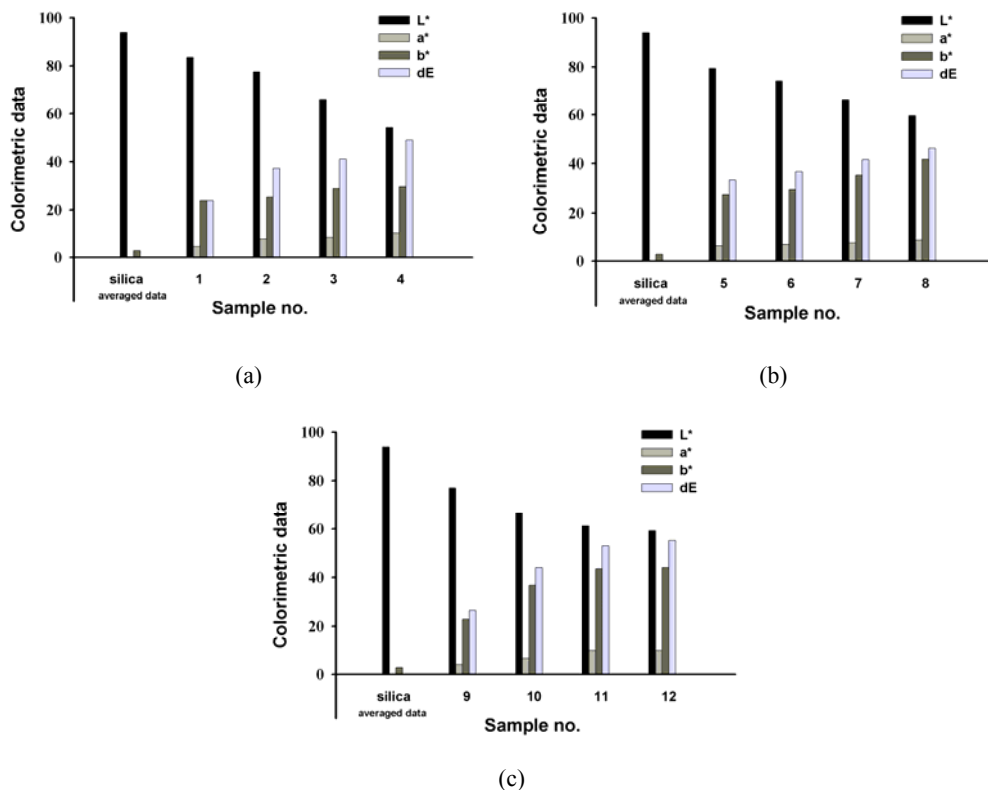
Fig. 5. Colorimetric data of silica and silica/lignin biocomposites obtained on the basis of
(a) Stöber silica, (b) hydrated silica and (c) Syloid[®]244

Figure 6a presents the thermogravimetric curves for the silica and lignin precursors used in the studies. Silica shows high thermal stability and within the temperature range considered its mass loss reaches only 5% (because for all types of silica the course of TG curves was similar, only one curve is presented in the figure). For lignin the mass loss over the temperature range studied was significant and reached 65%. This result confirms the data published in other works, also for the other types of lignin (Rodriguez-Mirasol 1993, Kijima 2011). The most distinct second stage of large mass loss of about 35% takes place in the range 200–600 °C. It corresponds to a complex process of thermal decomposition involving formation of new bonds as a result of crosslinking reactions. The final biocomposites show rather high thermal stability (Fig. 6b) especially samples 7 and 11, which – together with the fact of using a natural precursor – lignin – means that they offer a wide range of prospective applications.
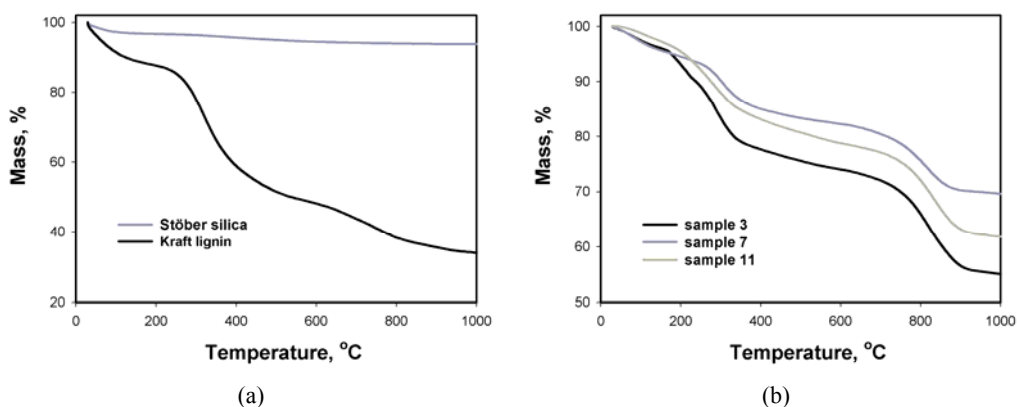
Fig. 6. Thermal analysis of (a) precursors and (b) silica/lignin biocomposites containing
20 wt./wt. of lignin in hybrid matrix

The attractive TG results obtained at this stage of the study suggest that the silica/lignin biocomposites can be used as polymer fillers of new generation. This possibility will be studied in the near future.

Porous structure properties

The structural properties of the biocomposites obtained were characterised on the basis of such parameters as: mean pore diameter, total pore volume and specific surface area BET. Values of these parameters determined for the initial silica samples and selected biocomposites are given in Table 2.

Table 2. Adsorption properties of silicas and silica/lignin biocomposites containing
20 weight parts by mass of lignin per 100 weight parts by mass of silica matrix

Sample Name	BET surface area (m^2/g)	Total volume of pores (cm^3/g)	Mean size of pores (nm)
Stöber silica	7	0.01	6.2
3	4	0.01	7.9
Hydrated silica	129	0,01	3,6
7	115	0.05	3.6
Syloid®244	262	1,2	18,0
11	223	0,9	14,3

The above presented results indicate that the newly proposed silica/lignin biocomposite can be applied as a natural adsorbent. Only the biocomposite based on silica synthesised by the modified Stöber method has a low BET surface area (Table 2). Biocomposites 7 and 11, based on hydrated silica and Syloid®244, had promising values of surface areas of 115 and 223 m^2/g, respectively. The highest

values of the total pore volume and pore diameter were found for Syloid®244 and the biocomposite obtained on its basis (sample 11). The earlier reported results characterising adsorption properties of hydrated silica (Klapiszewski 2012) have been confirmed by the results presented in this work. The adsorption data obtained for the biocomposites studies have shown that their specific surface area BET is large enough to justify the tests of SiO_2/lignin biocomposites adsorption properties towards organic compounds and selected heavy metal ions.

Conclusions

The proposed method for the synthesis of new composites based on silica and lignin has brought promising results from the viewpoint of testing their use as advanced functional materials. The biocomposites obtained show attractive dispersive–morphological properties, especially those containing 10 and 20 weight parts by mass of lignin in silica matrix. With increasing content of lignin in the biocomposite the volume contribution of larger particles increases, leading to formation of aggregates and agglomerates. Results of the studies performed to characterise the obtained materials have proved that the silica/lignin biocomposites have good electrokinetic stability and are promising as polymer fillers or adsorbents of harmful chemical compounds, including heavy metals, thanks to their good thermal and porous structure properties.

Acknowledgements

References

BRDAR M., SCIBAN M., TAKACI A., DOSENOVIC T., 2012, *Comparison of two and three parameters adsorption isotherm for Cr(VI) onto Kraft lignin*, Chem. Eng. J., 183, 108–111.

COLLINSON S.R., THIELEMANS W., 2010, *The catalytic oxidation of biomass to new materials focusing on starch, cellulose and lignin*, Coord. Chem. Rev., 255, 1854–1870.

COTORUELO L.M., MARQUES M.D., DIAZ F.J., RODRIGUEZ–MIRASOL J., RODRIGUEZ J.J., CORDERO T., 2012, *Adsorbent ability of lignin-based activated carbons for the removal of p-nitrophenol from aqueous solutions*, Chem. Eng. J., 184, 176–183.

DONG D., FRICKE A., MOUDGIL B., JOHNSON H., 1996, *Electrokinetic study of Kraft lignin*, Tappi J., 79, 191–197.

ELIMELECH M., CHEN W., WAYPA J., 1994, *Measuring the zeta (electrokinetic) potential of reverse osmosis membranes by a streaming potential analyzer*, Desalination, 95, 269–286.

EK M., GELLERSTEDT G., HENRIKSSON G., 2009, *Wood Chemistry and Biotechnology (Pulp and Paper Chemistry and Technology)*, De Gruyter, Berlin 2009.

HARMITA H., KARTHIKEYAN K.G., PAN X.J., 2009, *Copper and cadmium ions sorption onto Kraft and organosolv lignins*, Bioresour. Technol., 100, 6183–6191.

IBRAHIM I.A.M., ZIKRY A.A.F., SHARAF M.A., 2010, *Preparation of spherical silica nanoparticles: Stöber silica*, J. Amer. Sci., 6, 985–989.

JESIONOWSKI T., KRYSZTAFKIEWICZ A., 2001, *Influence of silane coupling agents on surface properties of precipitated silicas*, Appl. Surf. Sci., 172, 18–32.

JESIONOWSKI T., 2002, *Characterisation of silicas precipitated from solution of sodium metasilicate and hydrochloric acid in emulsion medium*, Powder Technol., 127, 56–65.

JESIONOWSKI T., 2002, *Effect of surfactants on the size and morphology of the silica particles prepared by an emulsion technique*, J. Mater. Sci., 37, 5275–5281.

JESIONOWSKI T., ŻURAWSKA J., KRYSZTAFKIEWICZ A., 2002, *Surface properties and dispersion behavior of precipitated silicas*, J. Mater. Sci., 37, 1621–1633.

JESIONOWSKI T., 2005, *Characterisation of pigments obtained by adsorption of C.I. Basic Blue 9 and C.I. Acid Orange 52 dyes onto silica particles precipitated via the emulsion route*, Dyes Pigments, 67, 81–92.

KIJIMA M., HIRUKAWA T., HANAWA F., HATA T., 2011, *Thermal conversion of alkaline lignin and its structured derivatives to porous carbonized materials*, Bioresour. Technol., 102, 6279–6285.

KLAPISZEWSKI L., MADRAWSKA M., JESIONOWSKI T., 2012, *Preparation and characterisation of hydrated silica/lignin biocomposites*, Physicochem. Probl. Miner. Process., 48, 463–473.

KOSMULSKI M., 2009, Surface Charging and Points of Zero Charge, CRC Press, New York 2009.

KOVACS T.G., MARTEL P.H., O'CONNOR B.I., PARROTT J.L., McMASTER M.E., VAN DER KRAAK G.J., MacLATCHY D.L., VAN DEN HEUVEL M.R., HEWITT L.M., 2011, *Kraft mill effluent survey: progress toward best management practices for reducing effects on fish reproduction*, Environ. Toxicol. Chem., 30, 1421–1429.

KUNANOPPARAT T., MENUT P., MOREL M.H., GUILBERT S., 2012, *Improving wheat gluten materials properties by Kraft lignin addition*, J. Appl. Polym. Sci., 125, 1391–1399.

MILCZAREK G., 2007, *Preparation and characterization of a lignin modified electrode*, Electroanal., 19, 1411–1414.

MILCZAREK G., 2009, *Preparation, characterization and electrocatalytic properties of an iodine|lignin-modified gold electrode*, Electrochim. Acta 54, 3199–3205.

MILCZAREK G., 2010, *Kraft lignin as dispersing agent for carbon nanotubes*, J. Electroanal. Chem., 638, 178–181.

MILCZAREK G., INGANAS O., 2012, *Renewable cathode materials from biopolymer/conjugated polymer interpenetrating networks*, Science, 335, 1468–1470.

MORANDIM–GIANNETTI A.A., AGNELLI J.M., LAN B.Z., MAGNABOSCO R., CASARIN S.A., BETTINI S.H., 2012, *Lignin as additive in polypropylene/coir composites: thermal, mechanical and morphological properties*, Carbohydr. Polym., 87, 2563–2568.

NOVAES E., KIRST M., CHIANG V., WINTER-SEDEROFF H., SEDEROFF R., 2010, *Lignin and biomass: A negative correlation for wood formation and lignin content in trees*, Plant Physiol., 154, 555–561.

OTTERSTEDT J.E., BRANDRETH D.A, 1998, *Small Particles Technology*, Plenum Press, New York 1998.

RALPH J., 1999, *Lignin Structure: Recent Developments*, US Dairy Forage Research Center, USDA–Agricultural Research Service, Madison 1999.

RODRIGUEZ-MIRASOL J., CORDERO T., RODRIGUEZ J.J., 1993, CO_2 – reactivity of Eucalyptus Kraft lignin chars, Carbon, 31, 53–61.

SCIBAN M.B., KLASNJA M.T., ANTOV M.G., 2011, *Study of the biosorption of different heavy metal ions onto Kraft lignin*, Ecol. Eng., 37, 2092–2095.

STÖBER W., FINK A., BOHN E., 1968, *Controlled growth of monodisperse silica spheres in the micron size range*, J. Colloid Interface Sci., 26, 62–69.

WEINER B., TSCHARNUTER W., BRUCE D., FAIRHURST D., 1993, *Zeta potential: A new approach*, Brookhaven Instruments Corporation Holtsville, New York 1993.

WYPYCH G., 2010, *Handbook of Fillers*, Chemical Technology Publishing, Toronto 2010.

XU G., ZHANG J., SONG G., 2003, *Effect of complexation on the zeta potential of silica powder*, Powder Technol., 134, 218–222.

SPECIFIC ION EFFECT OF CHLORIDE SALTS ON COLLECTORLESS FLOTATION OF COAL

Orhan OZDEMIR

Istanbul University, Mining Engineering Department, 34320, Avcilar, Istanbul
orhanozdemir@istanbul.edu.tr

Abstract. Separation of naturally hydrophobic particles, such as coal, by flotation is known to be enhanced with the addition of salt solutions into the system. In this study, the flotation of bituminous coal in the presence of NaCl, KCl, $CaCl_2$ and $MgCl_2$ without use of any flotation chemicals was investigated in detailed. In addition, zeta potential and foam stability tests were performed. The results from this study showed that the flotation behaviour of coal was influenced by these dissolved salts, and determined by the specific effect of these ions, while $MgCl_2$ and KCl solutions showed the highest and the lowest flotation performance improvements, respectively. The ash content of the products also increased with the salt concentration. This can be attributed to the entrainment of the ash minerals in the salt solutions, particularly at higher salt concentrations. Meanwhile, the froth stability tests at 1 M salt concentration also indicated that there is a correlation between the flotation recovery and stability profile of the froth. These results also clearly indicated that Na^+, K^+, Ca^{2+}, Mg^{2+} ions have a strong ion specific effect on the flotation recovery of the coal particles, and there is an optimum salt concentration to produce a clean coal in these salt solutions.

Introduction

High salt concentration has a significant effect on bulk and interfacial water structure, and colloidal interactions between bubbles and particles hence affect flotation of minerals. There are several studies in the literature indicating that dissolved ions in flotation system have a significant effect on the flotation of minerals such as potash, trona and borax in brine solutions, and coal in saline water (Yoon and Sabey 1989; Laskowski 1994; Celik et al. 2002; Ozdemir et al. 2010). Several experimental and modelling techniques for determining solution viscosity and surface tension, bubble-particle attachment time, contact angle, atomic force microscopy, sum-frequency vibrational spectroscopy and molecular dynamics simulation have been used to

provide further information on air-solution and solid-solution interfacial phenomena, especially the interfacial water structure due to the presence of dissolved ions (Ozdemir et al. 2007; Schreithofer and Laskowski 2007; Cheng et al. 2008; Du et al. 2008; Burdukova et al. 2009).

Several flotation plants in the world use process water with high salt content. Meanwhile, the use of process and saline waters in coal flotation has also attracted great interest for many years as the process water can be re-used and the accumulated salt ions available in water can enhance coal flotation. Since the researchers (Majer et al., 1934) discovered in 1934 that that coal could be floated with the increase in salt concentration without use of flotation chemicals (Ratajczak and Drzymala 2003), a number of theories have been proposed to explain the flotation behaviour of coal in salt solutions.

- Klassen and Plaksin 1954 hypothesized that salt ions destabilize the hydrated layers surrounding the coal and hence reduce the surface hydration of the coal (Ratajczak and Drzymala 2003). The destabilization makes the coal more hydrophobic and enhances the bubble-particle attachment. They also concluded that high salt concentration causes a decrease in the hydrophobicity of coal and thus decreases flotation.
- Charlamow 1957 later hypothesized that flotation in salt solutions is only possible for naturally hydrophobic minerals (Ratajczak and Drzymala 2003). Salt flotation significantly depends on the nature of the anions and cations in the salt solution used.
- Klassen and Kovatchev (1959) demonstrated that salt flotation increases with decreasing in zeta potential of particles (Ratajczak and Drzymala 2003).
- First time in the literature, Klassen and Mokrousov 1963 confirmed the discovery of flotation enhancement of naturally hydrophobic particles in salt solutions
- Laskowski (1962 and 1963) proposed that the salt flotation is an electrochemical phenomenon; therefore the presence of electrolytes compresses the electrical double-layer (EDL) between bubbles and particles which corresponds to the reduction of zeta potential of both bubble and particle (Ratajczak and Drzymala 2003).
- Laskowski and Mielecki (1964) later showed that salt flotation is a kinetic phenomenon (Ratajczak and Drzymala 2003).
- Marrucci and Nicodemo (1967) found that the presence of electrolytes in aqueous solution reduced bubble size in the pulp phase when the electrolyte concentration was increased. They proposed that the reduction of bubble coalescence depends upon the valence of the electrolytes as well as the magnitude of the surface tension $(d\gamma/dC)$.
- Laskowski and Iskra (1970) illustrated that contact angle does not change with increasing concentration of salt.
- Li and Somasundaran (1991) showed that efficiency of flotation depends on the degree of bubble coalescence. They later confirmed that while coal flotation decreases at low salt concentration, flotation increased at higher salt

concentrations. For example their studies showed that above 0.1 M NaCl any increase in salt concentration increased the coal floatability. Their studies also showed that the coal flotation decreased with an increase in the salt concentration up to 0.1 M (Li and Somasundaran 1993).

- Reduction of bubble coalescence in salt solutions was also investigated by Craig et al. (1993). Test results showed that there is a definite correlation between the valence of the electrolytes and the transition concentration, where bubble coalescence is reduced by 50%.
- Laskowski (1994) proved that salt ions in the solution destabilize the layer of water around the hydrophobic place as the bridge between the hydrophilic sites.
- Pugh et al. (1997) showed that salt flotation may result from the evolution of hydrophobic micro bubbles on the mineral surfaces. They proposed that salty water contains less dissolved air and thus less cavitations occurs (Paulson and Pugh 1996).
- Ratajczak (2002) also showed that a salt flotation kinetic and thermodynamic phenomenon. And, there is a relationship between contact angle and the energy state of the phase boundaries (Ratajczak and Drzymala 2003).
- Although the studies mentioned above showed that the flotation recovery has a maximum at minimum zeta potentials other studies indicated that the flotation recovery has a maximum at pH values both above and below the isoelectric point (Celik and Somasundaran 1980; Li and Somasundaran 1993).
- However, Harvey et al. (2002) showed that the reduction of zeta potential cannot solely explain the floatability of coal in electrolyte solutions.
- Recently, a study performed by Ozdemir et al. (2009) found that the enhancement of coal flotation in hypersaline water (1 M NaCl) cannot be entirely attributed to the surface chemistry aspects as previously proposed. Their results also proved the previous results by Laskowski and Iskra (1970) that the contact angle of coal in saline water did not change compared with that in de-ionized (DI) water. The atomic force microscopy (AFM) results also indicated that the repulsive force between the bubble and the coal particle was reduced in saline water.

There also have been many studies investigating this mechanism in seawater and saline waters (Yoon 1982; Yoon and Sabey 1989). These studies have brought several mechanisms to explain coal flotation in inorganic electrolyte solutions, and several theories have been suggested to explain the enhancement of coal flotation by salt ions, but the bubble coalescence in salt solutions seems to be a significant factor in coal flotation in saline water. Other available studies have shown that salt ions play an important role in the flotation of soluble minerals and coal (Miller et al. 1992; Hancer et al. 2001; Harvey et al. 2002; Ozdemir et al. 2007). In fact, it is an important issue of using waters containing high salt or sea water due to lack of fresh water in the world. This will also eliminate using flotation chemicals, and therefore, reduce the cost of flotation process. Therefore, it is important to understand how the dissolved ions behave in solutions and at the interfaces.

The literature review shows that little work has done on investigating the effect of salt ions on the ash content of the coal products in the presence of salt solutions. There has been a significant work on the effect and control of various surfactants used in flotation, on bubble size and particle hydrophobicity, however the effect of electrolytes on coal flotation has not been thoroughly investigated in term of ash content of the products. Therefore, the objective of this study is to investigate the effect of various ions (Na^+, K^+, Ca^{2+}, Mg^{2+},) on flotation of coal along with the behaviour of ash minerals in the salt solutions. In this matter, laboratory scale conventional flotation (Denver) experiments were carried out in NaCl, KCl, $CaCl_2$, $MgCl_2$ solutions as a function of salt concentration. Additionally, flotation mechanism of coals in these salt solutions was investigated using zeta potential and froth stability tests.

Materials and methods

Materials

The coal sample used in this study was obtained from Zonguldak, Turkey. The sample was first crushed using jaw and roll crushers to reduce the particle size less than 1 mm. The particle size distribution and ash content of the sample is shown in Fig. (a) and (b). Then, the sample size was reduced down to 212 µm using a ring mill. Finally, the sample was sieved from a 38 µm sieve, and the flotation sample -212+38 µm was obtained. In the case of zeta potential measurements, the sample size was reduced to less than 38 µm using an automatic mortar and pestle.
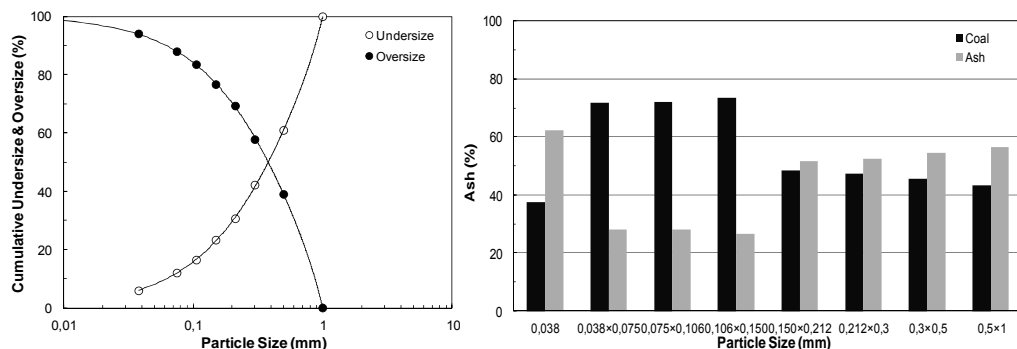
Fig. 1. (a) Particle size distribution, and (b) ash content of the raw coal sample

The flotation studies and the froth stability tests were carried out with analytical grade (> 99%) salts (NaCl, KCl, $CaCl_2$, $MgCl_2$), and they were used without further purification. The salt concentrations used in the experiments were 0.01 M, 0.1 M, 1.0 M, and prepared with mono-distilled water (GFL, Germany). All salt solutions were freshly prepared and used. Additionally, the zeta potential and froth stability tests were performed in de-ionized (DI) water (18 MΩcm) (Milli-Q plus Millipore Ultra Pure

Water system, Millipore Ltd, Molshem, France). The surface tension of the DI water was measured, and found to be about 72.0 mN/m at 23 $^{\circ}$C.

Methods

Zeta potential measurements

The zeta potential measurements of coal particles were carried out using a ZetaPlus instrument (Brookhaven Instruments, Holtsville, NY) to determine the electrophoretic mobility of charged suspensions. First, about 7 g of the sample was dry ground for 15 min using a mortar and pestle. Then, the ground sample was screened through a 38 μm sieve, and the undersize fraction was conditioned in the DI water (solid ratio 1%) using a magnetic stirrer at 500 rpm for 15 min. For pH adjustments, the suspension was mixed for about 5 min in order to reach equilibrium after adding the desired amount of 0.1 M HCl or 0.1 M NaOH. Before each experiment, the suspensions were kept for 5 min to allow the coarse particles to settle down. Then, a small amount of suspension was taken from the top of the suspension, and transferred to the measurement cell. Finally, ten measurements at each pH value were performed, and the average value of the measurements was obtained for the coal particles. An average error of these measurements was about 3%. The experiments were carried out at room temperature (23 $^{\circ}$C).

Flotation experiments

The flotation experiments were carried out with 212×38 μm size fraction using a small laboratory Denver flotation cell (1.5 dm^3). For each flotation experiment, 100 g of a coal sample was added into the cell and mixed with salt solutions at 1000 rpm for 3 min without reagent addition. After 3 min conditioning, air was introduced at a flow rate of 10 dm^3/min into the cell and froth was collected at 1, 3, 7, and 15 min. The impeller speed was kept at 1000 rpm. Feed solid concentration was 10% by weight. After flotation, completed concentrates and tailing were filtered, dried at 80 $^{\circ}$C, and weighted for further processing and analysis. For the ash analysis, an about 5 g of dried sample from each product was first ground using a mortar and pestle. Then, approximately 2 g of a ground sample from each product was burned in an oven at 815 $^{\circ}$C for 2 hr. The ash left over was weighed to calculate the ash content.

Equation 1 was used to calculate the combustible recovery of the flotation experiments:

$$\text{Combustible Recovery (\%)} = [M_C(100 - A_C)/M_F(100 - A_F)] \cdot 100 \qquad (1)$$

where M_C is weight of the concentrate (%), M_F is weight of the feed (%), A_C is the ash content (wt.%) of the concentrate and A_F is the ash content of the feed by weight (%).

Froth stability tests

The froth stability tests were carried out using a 125 cm^3 micro-flotation column cell which was mounted on a magnetic stirrer, and a magnetic stirrer bar was used for

agitation. In this study, 1 g sample (212×38 µm) was used for each test. A suspension of 1% by weight was prepared, and mixed at 500 rpm for 10 min. Finally, the suspension was transferred into the micro-flotation cell, and the froth stability tests were performed at a flow rate of 25, 50, and 100 cm³/min. The froth height was recorded as a function of time at a constant airflow rate until the froth reached to a determined level, and the height was used to calculate the dynamic froth stability.

Dynamic froth stability values were determined using the Bikerman equation, as calculated by Eq. 2 (Johansson and Pugh 1992; Paulson and Pugh 1996; Gourram-Badri et al. 1997; Barbian et al. 2003)

$$DFS = \frac{V_f}{Q} = \frac{H_{max}A}{Q} \qquad (2)$$

where *DFS* is the dynamic froth stability, V_f is the foam volume, H_{max} is the equilibrium height of the froth, *A* is the cross-section area of the cell, and *Q* is the gas volumetric flow rate.

Results and discussion

Results

Zeta potential measurements

Electrokinetic properties of minerals as revealed from zeta potential measurements provide important information for understanding of flotation separation processes. In this regard, zeta potential measurements for the coal were performed to determine the electrophoretic mobility of the sample. Figure 2 presents the zeta potential results of the coal as a function of pH. As seen from Fig. 2, the pzc (point of zero charge) values for the sample were found to be between pH 7 and 8, which agrees with the literature
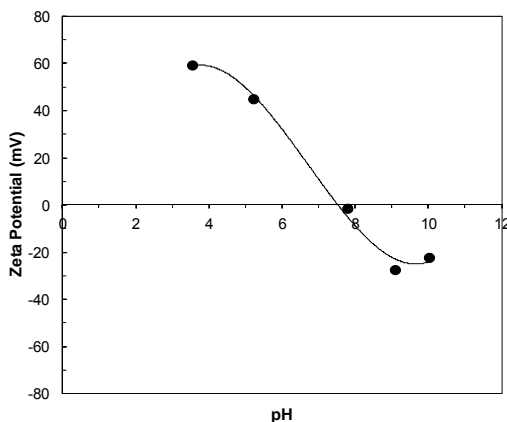
Fig. 2. Zeta potential-pH profile for the coal sample used in this study

data. According to Aplan (1976), the rank of coals can be classified based on their pzc which decreases from bituminous coal to lignite coal. The pzc for low and medium volatile bituminous coals is about pH 8 which indicates that the coal sample used in this study is very hydrophobic.

Flotation experiments

Flotation of coal was carried out in chloride halide salt solutions as a function of salt concentration without a frother or collector, and the results are shown in Figs 3–6. According to the results obtained from coal flotation in NaCl salt solutions, it is possible to produce a coal product with an ash content of 11.17% from the coal sample with an ash content of 52.16% in 10^{-2} M salt concentration in 1 min. If the products are combined after completion of 15 min flotation time, a coal product with an ash content of 17.85% can be obtained with a recovery of 75.6%. With further increase in the salt concentration, the flotation recovery increased to 81.8% and 96.0% for 10^{-1} M and 1 M NaCl, respectively. On the other hand, an increase in salt concentration significantly increased the ash content of the products. For example, it was obtained a coal product with an ash content of 22.35% in 10^{-1} M NaCl, however the ash content of the product at 1 M dramatically increased up to 41.82% for 1 M NaCl. These results clearly indicate that the salt concentration plays an important role in the coal flotation in the salt solutions.
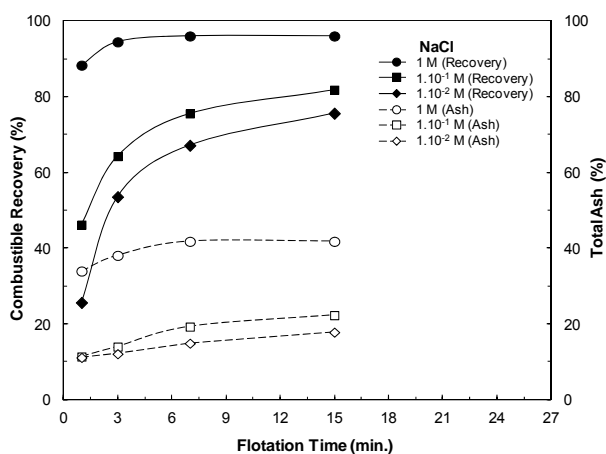
Fig. 3. Coal flotation in NaCl salt solutions

Additionally, a coal product with an ash content of 18.13% was obtained with a recovery of 51.1% after completion of 15 min flotation time in 10^{-2} M KCl salt concentration. An increase in the salt concentration from 10^{-2} M to 10^{-1} M and 1 M increased the flotation recovery to 73.7% and 88.5%, respectively. However, the ash content of the products also increased 31.68% and 41.60% for 10^{-1} M and 1 M KCl, respectively.
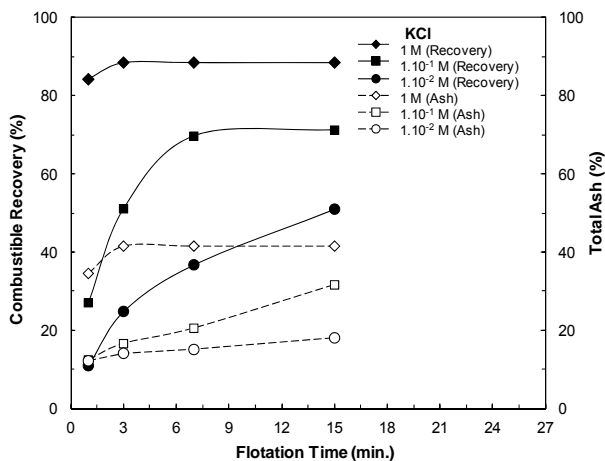
Fig. 4. Coal flotation in KCl salt solutions

The flotation results with $CaCl_2$ showed that a coal product with an ash content of 15.84% was obtained with a recovery of 62.5% after completion of 15 min flotation time in 10^{-2} M salt concentration. A further increase in the salt concentration, the flotation recovery increased to 93.3% and 95.1% for 10^{-1} M and 1 M $CaCl_2$, respectively. An increase in salt concentration also increased the ash content of the products from 34.30% in 10^{-1} M $CaCl_2$ up to 41.24% for 1 M $CaCl_2$.
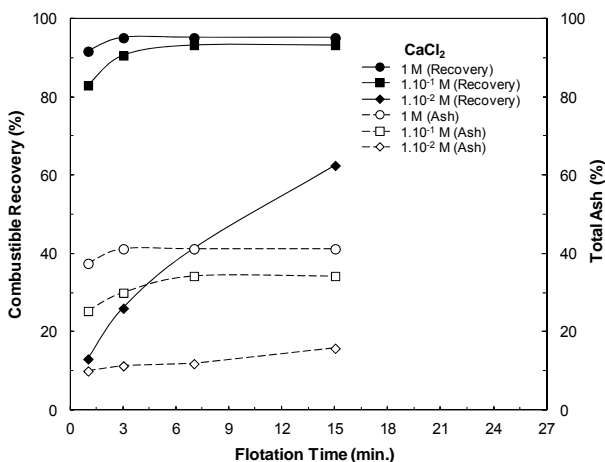
Fig. 5. Coal flotation in $CaCl_2$ salt solutions

Finally, the flotation results with $MgCl_2$ indicated that a coal product with an ash content of 18.23% was obtained with a recovery of 68.1% after completion of 15 min flotation time in 10^{-2} M salt concentration. Additional increase in the salt concentration increased the flotation recovery to 92.5% and 96.9% for 10^{-1} M and 1 M

MgCl$_2$, respectively. An increase in salt concentration also significantly increased the ash content of the products from 34.16% in 10^{-1} M up to 46.83% for 1 M MgCl$_2$.
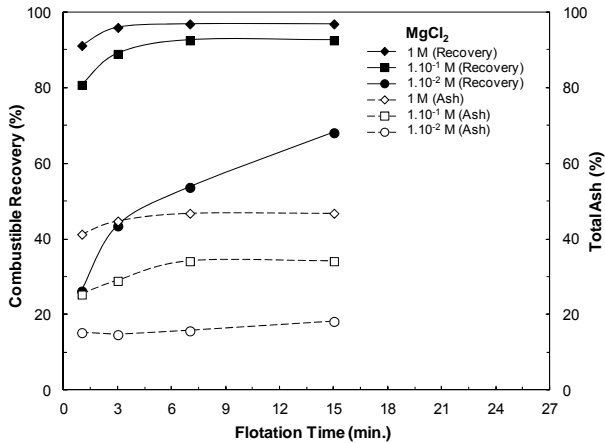
Fig. 6. Coal flotation in MgCl$_2$ salt solutions
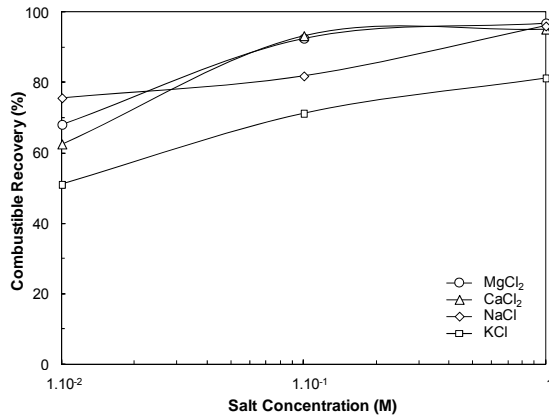
Fig. 7. Coal flotation as a function of salt concentration

Cumulative combustible flotation recovery versus salt concentration shown in Fig. 7 indicates that the flotation recovery increases with increasing salt concentration. As seen from Fig. 7 the increase continues up to 10^{-1} M from 10^{-2} M, then reaches a plateau. According to these results, while MgCl$_2$ produced the highest flotation recovery, KCl gave the lowest flotation recovery. Based on these results, the following trend can be written:

$$MgCl_2 \geq CaCl_2 \geq NaCl > KCl.$$

Froth stability tests

The bubble size distribution of the froth phase is an important performance measure for the flotation system. The experimental results from the froth stability in salt solutions indicated that the same trend can be obtained as shown in Fig. 8

$$MgCl_2 > CaCl_2 > NaCl > KCl.$$

While $MgCl_2$ shows the highest froth stability, KCl gave the lowest stability. Fig. 7 along with Fig. 8 clearly highlights that increased salt concentration solutions to the flotation system can be considered as promoters in the absence of frother as more stable froths form in the system.
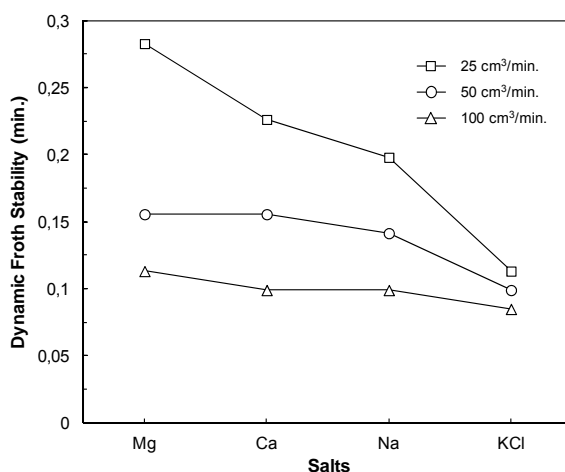
Fig. 8. Dynamic froth stability for coal suspensions
in 1 M salt solutions as a function of amount of air

Discussion

The flotation results suggest that under the present test conditions the coal product can be recovered in chloride salts without using any frother or collector. The coal recovery increases with increasing salt concentration as a function salt concentration. These results also agree with the previous studies (Yoon and Sabey 1989; Li and Somasundaran 1993; Kurniawan et al. 2011).

An inorganic electrolytes, particularly cations such as Na^+ and Mg^{2+}, show a significant influence on the electrokinetic behaviour of the bubbles and particles and reduce the magnitude of zeta potential of bubble and particle (Li and Somasundaran 1991; Paulson and Pugh 1996). In this case, the electrical double-layer is compressed, and hence it will reduce the repulsive interaction between bubbles and particles. For this reason, the hydrophobic force will dominate the system (Yoon and Sabey 1989; Paulson and Pugh 1996; Harvey et al. 2002). The previous experiments also showed

that the flotation recovery reaches maximum at minimum zeta potential (Paulson and Pugh 1996). The atomic force microscopy (AFM) results also indicated that the repulsive force between the bubble and the coal particle was reduced in saline water (Ozdemir et al. 2009). Meanwhile, the results from this study also showed that the contact angle of coal in saline water did not change when compared with that in DI water.

According to the DLVO theory repulsion between bubbles result form a balance of attractive (Van der Waals or dispersive) and repulsive (electrostatic due to negative charge) forces. However, the presence of electrolytes in aqueous solution is known to reduce the occurrence of this process, and a bubble size is reduced in the pulp phase when the electrolyte concentration was increased (Marrucci and Nicodemo 1967). Meanwhile, Craig et al. 1993a; Craig et al. 1993b also showed that there is a definite correlation between the valence of the electrolytes and the transition concentration where bubble coalescence is reduced by 50%. According to this study, the bubble coalescence was inhibited in the presence of some salts such as NaCl, KCl, $MgCl_2$ etc. Transition concentration for each salt is quite different for each salt. For example, the transition concentration of $MgCl_2$ and $CaCl_2$ is 0.02 M, and that of NaCl and KCl is 0,08 and 0,1 M, respectively (Craig et al. 1993a; Craig et al. 1993b). The increase in the flotation recovery from KCl to $MgCl_2$ can be easily attributed to the decrease in bubble coalescence. The previous studies showed that the high number of the bubbles in the system increased the flotation efficiency of coal particles in salt solutions (Kurniawan et al. 2011). These results show the importance of the effect of ion specificity (size and polarizability) at high salt concentrations on bubble coalescence.

The attachment of the coal particles on bubbles depends on the long-range hydrophobic interaction between them. It is well known that a stable froth has a tendency to result in greater recovery values since it holds the mineral particles together for a longer time. It is also noted that liberation of coal particles from gangue increases with decreasing particle size and, therefore, small coal particles are likely more hydrophobic than large particles. Thus, the strong and long-range hydrophobic attraction occurs between the small coal particles and the bubble in salt solutions. As seen from Fig. 9, while salt solutions significantly increased flotation of coal, the ash content of the products also increased. And, this can be attributed to the entrainment of the ash minerals in the salt solutions, particularly at higher salt concentrations. The reason for this is inhibition of bubble coalescence in salt solutions. Hence smaller bubbles occur in the system and cause more stable froth. This also can be linked to the effect of salt type and concentration. For example, in the case of 10^{-2} M salt concentration, which is lower than the transition concentrations for each salt, there is no significant difference among the salts in terms of flotation recovery and ash content of the products (Fig. 9a). However, with increase in salt concentration up to 10^{-1} M, which is higher than the transition concentration of $MgCl_2$ and $CaCl_2$ but lower for NaCl and KCl, the flotation recovery vs. ash content of the products in $MgCl_2$ and $CaCl_2$ solutions exactly shows the same trend compared to NaCl and KCl (Fig. 9b). At

1 M salt concentration which is higher than the transition concentration for each salt the bubble coalescence was completely decreased and eventually prevented, and therefore no significant variation in the flotation recovery was observed for each salt as seen from Fig. 9c. These results clearly indicates that Na^+, K^+, Ca^{2+}, Mg^{2+} ions have a strong ion specific effect on the flotation recovery of the coal particles, and there is an optimum salt concentration to produce a clean coal in these salt solutions.
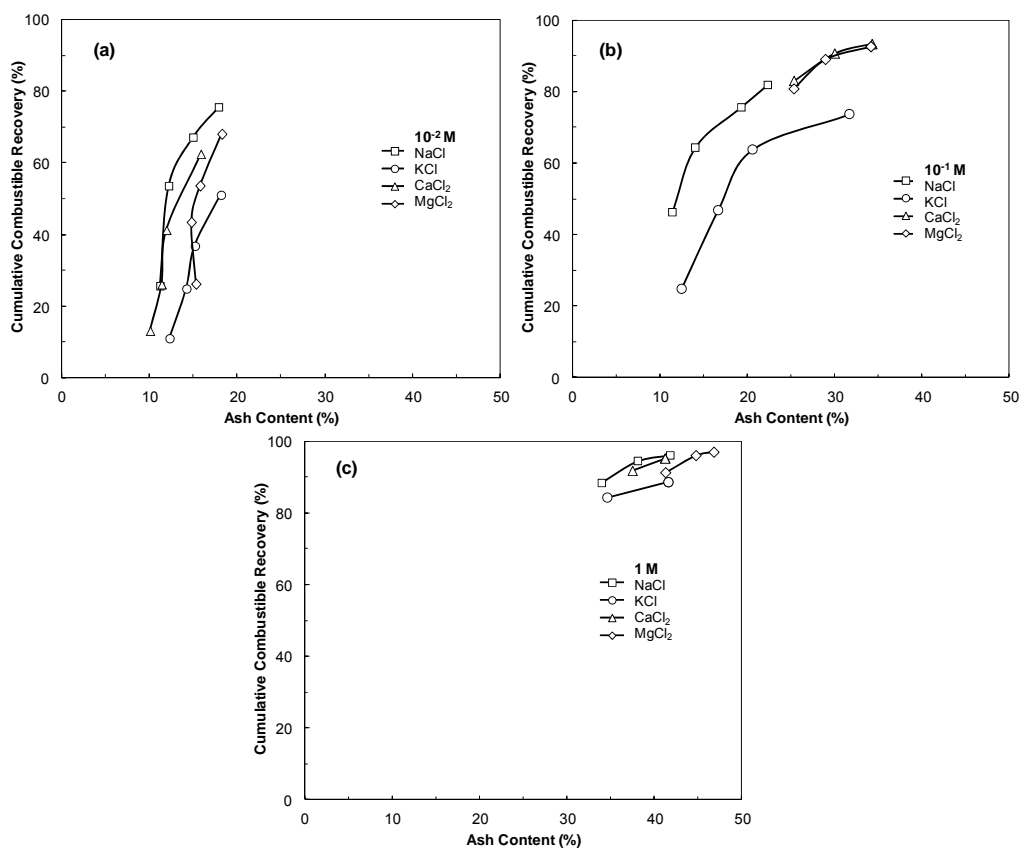
Fig. 9. Cumulative combustible recovery vs. ash content of the products as a function of salt concentration (a) 10^{-2} M, (b) 10^{-1} M, and (c) 1 M

Conclusions

In this study, selected chloride salts, $MgCl_2$, $CaCl_2$, NaCl, and KCl, were used in the experimental program to clarify the mechanism of coal flotation enhancement by ions of inorganic salts. The results from this study showed that the effect of salt on coal recovery depends on the type and the concentration of the electrolyte which significantly affected the froth flotation performance. The experiments also showed

that while the combustible recovery increased with increasing salt concentration, the ash content of the coal products also increased significantly. These results suggest that a coal product with low ash content can be beneficiated with a higher recovery depending on the salt type and concentration.

The results obtained from this study will help to understand the flotation behaviour of many minerals in salt solutions. Furthermore, this will be a fundamental basis for development of improved flotation technology for mineral processing industry.

Acknowledgments

References

APLAN F.F., 1976, *Coal Flotation. Flotation: A.M. Gaudin memorial volume*. M. C. Fuerstenau. New York, AIME: 1235–1264.

BARBIAN N., VENTURA-MEDINA E., CILLIERS, J.J., 2003, *Dynamic froth stability in froth flotation*, Minerals Engineering, 16(11), 1111–1116.

BURDUKOVA E., LASKOWSKI J.S., FORBES G.R., 2009, *Precipitation of dodecyl amine in KCl-NaCl saturated brine and attachment of amine particles to KCl and NaCl surfaces*, International Journal of Mineral Processing, 93(1), 34–40.

CELIK M.S., HANCER M., MILLER J.D., 2002, *Flotation chemistry of boron minerals*, Journal of Colloid and Interface Science, 256(1), 121–131.

CELIK M.S., SOMASUNDARAN P., 1980, *Effect of pretreatments on flotation and electrokinetic properties of coal*, Colloids Surf., 1(1), 121–124.

KHARLAMOV V.S., 1957, *Possible causes of flotation of minerals with electrolytes* (*О возможных причинах вызывающих флотацию минералов електролитами*), Bulletin Mekhanobr Obogashchenie Rud, 2(8), 25–30.

CHENG F.Q., ZHANG Y.N., DU H., LIU J., NALASKOWSKI J., MILLER J.D., 2008, *Surface chemistry features in the flotation of KCl*, In Proceedings of the XXIV International Mineral Processing Congress, Beijing, China

CRAIG V.S.J., NINHAM B.W., PASHLEY R.M., 1993a, *Effect of electrolytes on bubble coalescence*, Nature (London), 364(6435), 317–319.

CRAIG V.S.J., NINHAM B.W., PASHLEY R.M., 1993b, *The effect of electrolytes on bubble coalescence in water*, Journal of Physical Chemistry, 97(39), 10192–10197.

DU H., LIU J., OZDEMIR O., NGUYEN A.V., MILLER J.D., 2008, *Molecular features of the air/carbonate solution interface*, Journal of Colloid and Interface Science, 318(2), 271–277.

GOURRAM-BADRI F., CONIL P., MORIZOT G., 1997, *Measurements of selectivity due to coalescence between two mineralized bubbles and characterization of MIBC action on froth flotation*, International Journal of Mineral Processing, 51(1–4), 197–208.

HANCER M., CELIK M.S., MILLER J.D., 2001, *The significance of interfacial water structure in soluble salt flotation systems*, Journal of Colloid and Interface Science 235(1), 150–161.

HARVEY P.A., NGUYEN A.V., EVANS G.M., 2002, *Influence of electrical double-layer interaction on coal flotation*, Journal of Colloid and Interface Science, 250(2), 337–343.

JOHANSSON G., PUGH R.J., 1992, *The influence of particle size and hydrophobicity on the stability of mineralized froths*, International Journal of Mineral Processing, 34(1–2), 1–21.

KLASSEN V.I., KOVATCHEV K.P., 1959, On mechanism of action of inorganic electrolytes in flotation of minerals (in Russian), DAN SSSR, 129, 6, 1356-1358.

KLASSEN V.I., MOKROUSOV V.A., 1963, *An Introduction to the Theory of Flotation*, Butterworths, London

KLASSEN W.I., PLAKSIN I.N., 1954, *On the mechanism of action of certain chemicals and aeration of the pulp in the flotation of coals* (in Russian), Proceedings of the Academy of Sciences of the USSR, Izv. Acad. Nauk SSSR (известия академии наук СССР, ОТН) 362–371.

KURNIAWAN A.U., OZDEMIR O., NGUYEN A.V., OFORI P., FIRTH B., 2011, *Flotation of coal particles in MgCl₂, NaCl, and NaClO₃ solutions in the absence and presence of Dowfroth 250*, International Journal of Mineral Processing, 98(3–4), 137–144.

LASKOWSKI J., ISKRA J., 1970, *Role of capillary effects in bubble-particle collision in flotation*, Inst. Mining Met., Trans., Sect. C, 79(March), C6–C10.

LASKOWSKI J.S., 1994, *Coal surface chemistry and its role in fine coal beneficiation and utilization*, Coal Prep. (Gordon & Breach), 14(3–4), 115–131.

LASKOWSKI J.S., 1994, *Flotation of potash ores*: Reagents for Better Metallurgy SME, Littleton, USA.

LI C., SOMASUNDARAN P., 1991, *Reversal of bubble charge in multivalent inorganic salt solutions-Effect of magnesium*, Journal of Colloid and Interface Science, 146(1), 215–218.

LI C., SOMASUNDARAN P., 1993, *Role of electrical double layer forces and hydrophobicity in coal flotation in sodium chloride solutions*, Energy Fuels, 7(2), 244–248.

MARRUCCI G., NICODEMO L., 1967, *Coalescence of gas bubbles in aqueous solutions of inorganic electrolytes*, Chemical Engineering Science, 22(9), 1257–1265.

MILLER J.D., YALAMANCHILI M.R., KELLAR J.J., 1992, *Surface charge of alkali halide particles as determined by laser-doppler electrophoresis*, Langmuir, 8(5), 1464–1469.

OZDEMIR O., CELIK M.S., NICKOLOV Z.S., MILLER J.D., 2007, *Water structure and its influence on the flotation of carbonate and bicarbonate salts*, Journal of Colloid and Interface Science, 314(2), 545–551.

OZDEMIR O., JAIN A., GUPTA V., WANG X., MILLER J.D., 2010, *Evaluation of flotation technology for the trona industry*, Minerals Engineering, 23(1), 1–9.

OZDEMIR O., TARAN E., HAMPTON M.A., KARAKASHEV S.I., NGUYEN A.V., 2009, *Surface chemistry aspects of coal flotation in bore water*, International Journal of Mineral Processing, 92(3-4), 177–183.

PAULSON O., PUGH R.J., 1996, F*lotation of inherently hydrophobic particles in aqueous solutions of inorganic electrolytes*, Langmuir, 12(20), 4808–4813.

PUGH R.J., WEISSENBORN P., PAULSON O., 1997, F*lotation in inorganic electrolytes; the relationship between recovery of hydrophobic particles, surface tension, bubble coalescence and gas solubility*, International Journal of Mineral Processing, 51(1–4), 125–138.

RATAJCZAK T., DRZYMALA J., 2003, *Flotacja solna* (*Salt Flotation*), Oficyna Wydawnicza, Wrocław University of Technology, Poland.

SCHREITHOFER N., LASKOWSKI J.S., 2007, *Investigation of KCl crystals/NaCl-KCl saturated brine interface and octadecylamine deposition with the use of AFM*, Canadian Metallurgical Quarterly, 46(3), 285–294.

YOON R.H., 1982, *Flotation of coal using micro-bubbles and inorganic salts*, Mining Congress Journal, 6876–6780.

YOON R.H., SABEY J.B. (1989), *Coal flotation in inorganic salt solution. Interfacial Phenomena in Coal Technology*. G. D. Botsaris and Y. M. Glazman. New York, Marcel Dekker: 87–114.

ROLE OF ORE MINERALOGY
IN SELECTING BENEFICIATION ROUTE
FOR MAGNESITE-DOLOMITE SEPARATION

Ahmed YEHIA[*], Mohamed AL-WAKEEL[**]

[*]   Central Metallurgical R&D Institute, P.O.Box 87, Helwan, Egypt; e-mail:yehia522000@yahoo.com
[**] Faculty of Science, Geological Department, Ain Shams University, Cairo, Egypt

Abstract. Characterization and beneficiation of magnesite-dolomite sample were performed. The role of ore mineralogy in selecting the most adequate concentration method for magnesite-dolomite separation was found to be detrimental. The microscopic analysis showed that dolomite is stained with goethite and lepidocrocite (weakly magnetic minerals), while magnesite is stained with hematite and magnetite (highly magnetic mineral). A dry magnetic separation technique was used to separate dolomite from magnesite. The magnetic separation of the sample resulted in a magnesite concentrate product assaying 1.12% CaO with 46.02% recovery and CaO/SiO_2 molar ratio = 1.62. This magnesite product is suitable for basic refractory. Besides, middling fraction was produced, containing 44.63% magnesite and 10.95% dolomite. This product is suitable for making low-loss forsterite dielectrics.

Keywords: magnetic separation, refractory materials

Introduction

A vast development of heavy and light industries increased the demand for refractories, particularly basic refractory. The basic refractories e.g. magnesite, dolomite, forsterite and their derivatives present great importance for various industries (Girgis and Gag, 1970; Othman and Khalil, 2005). For the forsterite and forsertie-magnesite refractories, carbonate rock, rich in MgO, is considered as a suitable source of raw materials for forsterite brick-making. The presence of impurities, associated with the magnesite ores, reduces its refractoriness. Dolomite, which contains calcium, complicates technical processing during firing of magnesite. Thus, the CaO/SiO_2 molecular ratio is important in determining the quality of magnesite refractoriness, which should not exceed 2. This ratio could be obtained by removing a certain percentage of dolomite, which determines the CaO content, through beneficiation processes. Different methods for magnesite-dolomite separation

have been applied (Chen and Daniel, 2005; Gonglan and Daniel, 2004; Wanzhong et al., 2011). The criteria for the selection of the most adequate concentration method include a series of parameters. The most important is related to ore mineralogy (Araujo et al.2003; Kumar et al. 2010; Upadhyay et al., 2009). There has been considerable interest in recent years in the development of automatic systems for the measurement of mineral composition and texture to solve mineral processing problems. The present work deals with the characterization and beneficiation of magnesite-dolomite ore. The aim was to obtain a magnesite product with a low CaO content to be suitable for refractory industries.

Experimental

Materials

A representative talc-carbonate sample was obtained from the Wadi El-Barramiya locality. It is situated in the Eastern Desert of Egypt and lies between longitudes 33° 44′ 00″–33° 49′ 00″ E and latitudes 25° 03′ 20″–25° 06′ 30″ N. The ore sample, supplied as blocks, was crushed in a 5x6 Denver jaw crusher followed by a "Wedag" rod mill in a closed circuit with a 0.25 mm sieve. The –0.25 mm fraction was passed on a 0.045 mm sieve. The –0.25+0.045 mm size fraction was used in this study. The sample was subjected to flotation using a frother at neutral pH to separate talc from the carbonate fraction (Yehia and Al-Wakeel, 2000). The present study was conducted on the carbonate fraction. Table 1 presents the chemical and mineral composition of the studied sample. It shows that the sample is composed mainly of two minerals, that is magnesite and dolomite. There are other three minerals found in subordinate amounts including talc, serpentine and quartz. The chemical composition of the sample indicates that it is composed mainly of three components: MgO, SiO_2 and Fe_2O_3. It has also relatively high amounts of CaO, which indicates the presence of dolomite.

Table 1. Mineral and chemical composition of the carbonate sample

Mineral composition, %					Chemical composition, %				
Talc	Magnesite	Dolomite	Serpentine	Quartz	SiO_2	MgO	CaO	Fe_2O_3	L.O.I.
2.84	73.58	17.58	1.56	4.89	9.86	33.92	5.73	7.18	40.48

L.O.I. = Loss on Ignition

Methods

Minerals association and characters as well as grain size were investigated by mineralogical examination of hand-picked samples. Identification of minerals by reflected light from polished sections was performed. The polished sections were examined under an "Ortholux Leitz" microscope.

The identification of the composition of the ore sample was possible by studying the X-ray patterns of the specimens using a Philips X-ray diffractometer (PW 1010).

Mg, Ca and Fe were determined using Inductive Couple Plasma Emission Spectrometer. SiO$_2$ was determined gravimetrically. "Carpco" high intensity induced roll magnetic separator, model MIH (13) 111-5, was employed in this investigation as a free fall kind of separator. For efficient separation, the feed material should always be dry, free flowing and free from slimes. In this study, the controlling parameters such as the magnetic field strength and drum speed were modified in such a manner that the recovery-grade relationship could be plotted.

Results and discussion

Petrographic and geochemical analyses

The talc-carbonate rocks of Wadi El-Barramiya are well developed through the alteration of the serpentine rocks by carbon dioxide emanations. This rock is an alteration product of ultra basic rocks such as dunite which is composed of Fe and Mg bearing minerals (olivine and pyroxene). A microscopic examination indicated that magnesite was found in variable crystal sizes ranging from medium to very coarse reaching up to 2.45 mm (Fig. 1). Besides, dolomite occurs in the form of patches and veinlets of microcrystalline, rhombic, and zoned crystals. The carbonate ore shows a brownish tinge of iron-bearing minerals which can be a surface coating or disseminated grains in a matrix of carbonate. It is shown there that dolomite is stained with goethite (α-FeOOH) and lepidocrocite (γ-FeOOH) (weakly magnetic minerals) while magnesite is stained with hematite and magnetite (strongly magnetic mineral). This differential association was controlled by iron oxide precipitation (Kremenetskaya et al., 2009). The source of the iron in the studied ore sample was in the breakdown of ferromagnesium silicates where iron is present in a ferrous form (Ormo et al., 2004). It was suggested that carbonic acid (resulting from dissolving CO$_2$ gas in water) weathered the ferromagnesian minerals to form magnesium-iron-carbonate-rich solution. The released iron from the minerals is oxidized, when exposed to the surface, to form the red coloration of the "red beds". The oxidized ferric iron is highly immobile. The iron needs to be reduced to Fe^{+2} (by donation of electrons) in order to be put into solution and transported.

Previous studies on iron mineralization in the carbonate ore suggested that iron is mobilized and removed by reducing water that moved along conduits (e.g. faults or fractures) and then outwards into adjacent permeable rocks (Beitler et al., 2003; Beitler, et al., 2003; Parry et al., 2004). The fluid is reducing possibly due to the presence of hydrocarbons, methane, organic acids or hydrogen sulfide. When the reducing water (acidic water), carrying iron(II), meets and mixes with shallow, oxygenated ground water (alkaline water), iron is precipitated to form a variety of iron oxides (Grosz et al., 2006). However, hydroxide ions formed from the dissolution of dolomite are almost completely bound to the ferric solution to form
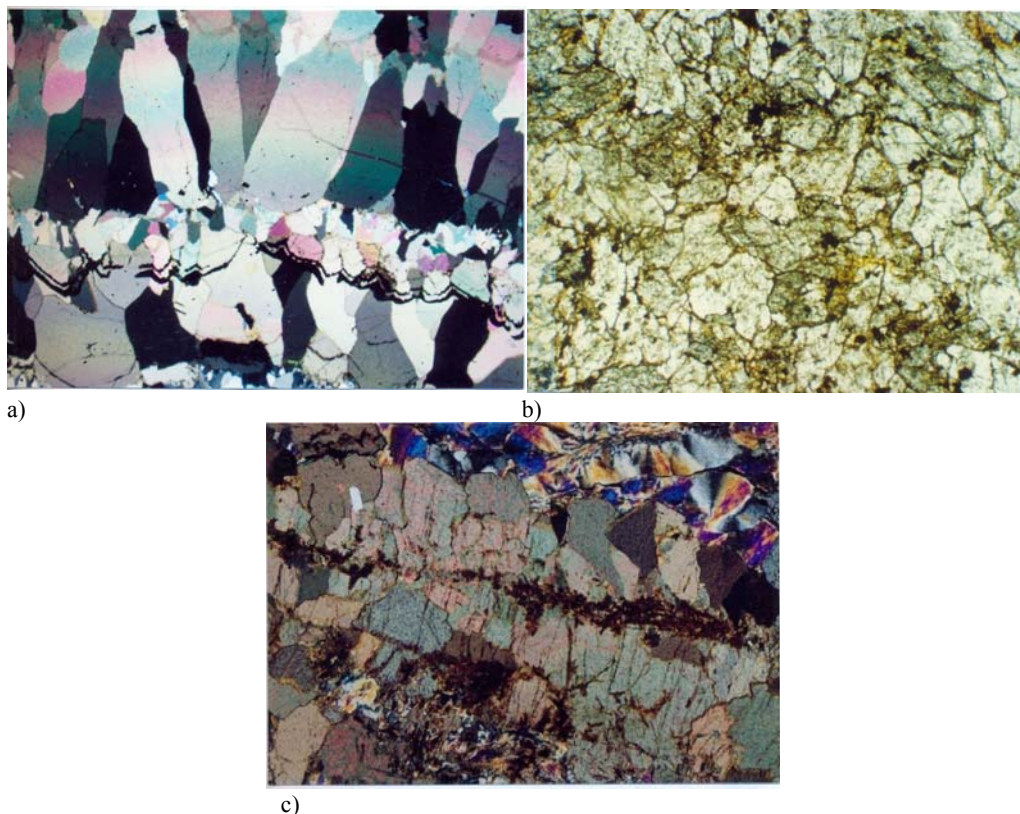
Fig. 1. Carbonate minerals with iron oxyhydroxides. (a) different generations of dolomite crystals separated by goethite bands in its characteristic colloform structure, plane polarized, (b) magnesite with hematite on the crystal boundaries, crossed polar and (c) vein of coarse magnesite crystals stained and bounded by magnetite. Scale-shaped crystals and fine fibers of serpentine in the upper most part

dolomite are almost completely bound to the ferric solution to form hydroxocomplexes of iron. This means that the acidic fluid containing ferric oxides is neutralized on contact with dolomite. This results in goethite precipitation onto dolomite surface. Microscopic analysis of the magnesite-dolomite ore sample indicates that dolomite is stained with goethite while magnesite is stained with hematite and magnetite. Under these conditions neither flotation nor gravity separation can be used to separate dolomite from magnesite. Microscopic investigation revealed that there is a difference in the magnetic properties between dolomite and magnesite which can be separated using a magnetic separation technique. In this case, most of the magnesite which associated with magnetite and hematite minerals will be separated as a strongly magnetic fraction. On the other hand, dolomite stained with goethite and lepidocrocite will be separated as a weakly magnetic fraction. Besides, using such technique, magnesite will be cleaned from the non-magnetic minerals such as quartz and serpentine. However, the aim of this work was to reduce the dolomite

content (represented by CaO) to a minimum value and prepare a magnesite product suitable for basic refractory using magnetic separation technique.

Dry magnetic separation of the carbonate sample

Magnetic separation is a direct physical process based on the difference in magnetic susceptibility for minerals under investigation. Magnetic susceptibility (ξ) is expressed as:

$$\xi = \rho \, \chi \tag{1}$$

where χ is the specific magnetic susceptibility and ρ is the material density. The relevant susceptibilities are as follows:
– strongly magnetic $\xi > 10^{-5}$ m³/kg
– feebly magnetic $\xi = 10^{-6}$ to 0.5×10^{-7} m³/kg
– non-magnetic $\xi < 10^{-8}$ m³/kg.

Table 2 presents the magnetic susceptibility for different minerals found in the studied sample (Schubert, 1978). It is seen that these minerals are amenable to be separated using magnetic separation process. The "Carpco" induced roll magnetic separator with variable speed controller from 0.0 to 100 rpm was used in this study. The generated centrifugal force, with the free fall of the feed, creates favourable conditions for separation using that machine.

Table 2. Magnetic susceptibility for different minerals (Schubert, 1978)

Mineral	Chemical formula	Magnetic susceptibility, $\cdot 10^{-9}$ m³/kg
Magnetite	Fe_3O_4	0.2 to $18 \cdot 10^6$
Hematite	Fe_2O_3	500-3800
Goethite	$FeO(OH)$	250-300
Dolomite	$CaMg(CO_3)$	15
Magnesite	$MgCO_3$	–6.4 to +45
Talc	$Mg_3Si_4O_{10}(OH)_2$	–
Serpentine	$Mg_3Si_2O_5 (OH)_4$	60-1200
Quartz	SiO_2	–5.7

Effect of magnetic field strength

The effective capture of fine particles, using dry high intensity magnetic separation, depends mainly on the magnetic attractive force radially inwards as well as the other competing forces including centrifugal radially outwards and gravitational forces downwards. The magnetic attracting forces acting on a particle are the product of the particle magnetization and the magnetic field gradient (Cohen, 1973; Arvidson, 1995).

The effect of magnetic field strength on the magnesite-dolomite separation was studied at a constant drum speed, 40 rpm (Fig. 2 and Table 3). It is seen that there is

A. Yehia, M. Al-Wakeel

no significant change in CaO until the field intensity of 1.0 Ampere, after which there is a gradual increase in the CaO content in the magnetic fraction (magnesite concentrate). This is due to mechanical entrapment and non-selective magnetic capture of the entrained non-magnetic particles in the clusters of the magnetic particles. However, using magnetic field strength of one Ampere a magnesite concentrate assaying 2.43% CaO with an operational recovery 38.44% was obtained from a feed assaying 5.73% CaO. On the other hand, the wt% of the non-magnetic fraction, mainly dolomite, was decreased with increasing the magnetic field strength. However, it can be seen that the optimum conditions for magnesite-dolomite separation could be achieved at a magnetic field of 1.0 Ampere.
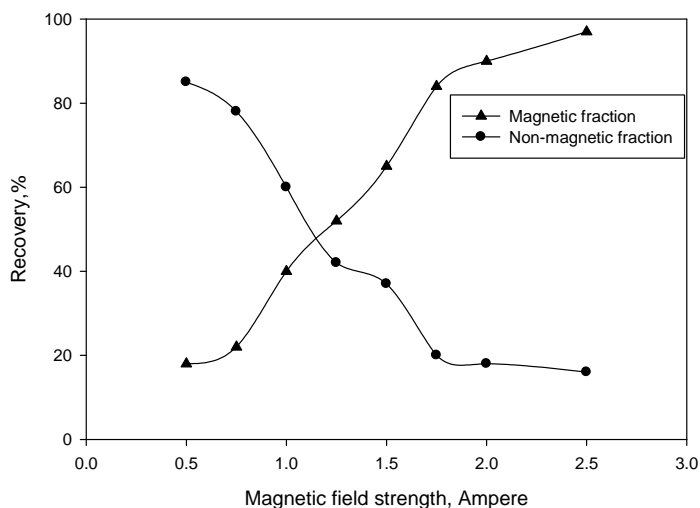
Fig. 2. Effect of magnetic field strength on magnesite-dolomite separation

Table 3. Effect of magnetic field strength on CaO content in magnetic and non-magnetic fractions

Magnetic field strength, Ampere	CaO, %	
	Magnetic	Non-magnetic
0.5	2.21	6.35
0.75	2.33	6.69
1.00	2.43	7.79
1.25	3.38	8.66
1.5	4.56	7.63
1.75	5.46	6.75
2.00	5.43	7.93
2.5	5.59	5.79

Effect of drum speed

The rotation speed of the drum represents the most critical parameter affecting the separation process, since it determines the centrifugal force which affects both the grade and the recovery. The centrifugal force can affect the following:

    – retention time in the magnetic zone

    – separation of the non-magnetic particles with high specific gravity

    – detachment of very fine gangue particles adhering to the drum and to the coarse magnetic grains by residual humidity and electrostatic force.

    Thus, in this case, a precise and effective adjustment between centrifugal and magnetic forces is unequivocal for reaching the equilibrium. Figure 3 and Table 4 present the effect of changing the drum speed on the dolomite-magnesite separation at a constant magnetic field (1.0 Ampere). It is seen that there is a pronounced decrease in the calcium oxide content of the magnetic fraction up to a roll speed of 60 rpm. By increasing the drum speed over this value the CaO content becomes almost constant. The lowering of calcium oxide content in the magnetic fraction with increasing the drum speed was due to the separation of the locked particles with the non-magnetic product.

Table 4. Effect of drum speed on CaO content in magnetic and non-magnetic fractions

Drum speed, rpm	CaO, %	
	Magnetic	Non-magnetic
20	3.81	8.49
40	2.43	7.79
60	1.83	7.23
80	1.82	6.59
100	1.58	6.38
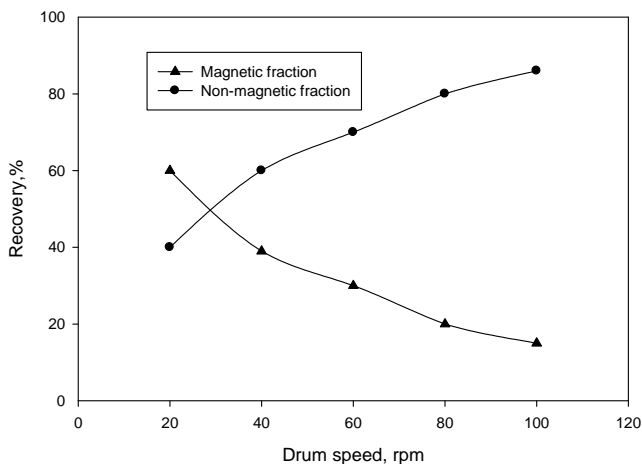
Fig. 3. Effect of drum speed on magnesite-dolomite separation

Under these conditions (60 rpm and 1 Ampere) a magnetic fraction assaying 1.83% CaO with 27.72% recovery was obtained. On the other hand, the recovery and CaO content of the non-magnetic fraction were increased with increasing the drum speed.

Cleaning of the rougher concentrate and evaluation of the separated products

An improvement in the grade of the magnetic concentrate occurs by mechanical cleaning of the rougher magnetic concentrate at 1.0 Ampere and 60 rpm. The decrease in CaO % of the cleaned concentrate, assaying 0.89% CaO, is achieved on the expense of recovery which is only 18.3 %. Two scavenging steps for the non-magnetic fractions were conducted at higher magnetic field strength of 1.25 and 2 Ampere and at 60 rpm drum speed. This step produces a middling product rich in magnesite-dolomite assaying 10.95% CaO with 44.63% recovery. However, blending of the magnetic fraction, obtained from the scavenging step, to the cleaned magnetic concentrate is recommended to achieve a reasonable concentration ratio. This produces a final magnesite concentrate assaying 1.12% CaO with 46.02% recovery (Table 5). The concentrate, with low CaO content and CaO/SiO_2 molar ratio =1.62, is suitable for making basic refractory (Girgis and Gad, 1970; Othman and Khalil, 2005). On the other hand, the middling fraction, called magnesite-dolomite product, can be used for making low-loss forsterite dielectrics. Figure 4 shows different operations used for beneficiation of the carbonate ore.
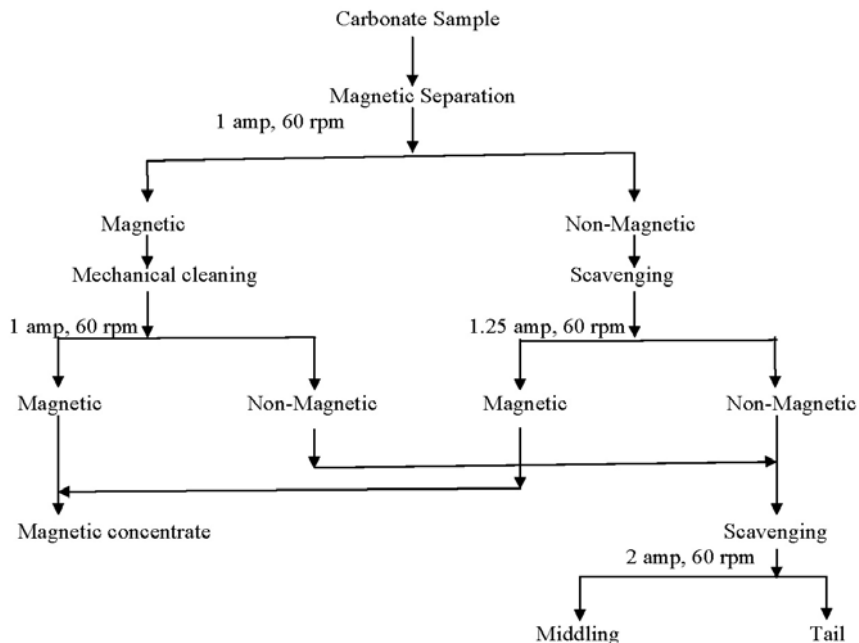
Fig. 4. Suggested flowsheet for the beneficiation of carbonate ore

Table 5. Mineral and chemical composition of the magnetic separation products

Product	Wt%	Mineral composition, %				Chemical composition, %						
		Talc	Magne-site	Dolo-mite	Serpen-tine	Quartz	SiO$_2$	MgO	CaO	Fe$_2$O$_3$	L.O.I.	Total
Concentrate	46.02	0.00	96.49	3.36	0.12	0.00	0.69	46.72	1.12	7.80	43.65	99.98
Middling	44.63	0.27	65.93	32.65	0.65	0.50	4.24	33.45	10.95	7.30	43.258	99.19
Tail	9.35	14.68	48.22	5.62	6.59	25.18	52.28	12.26	4.86	5.70	27.93	99.88
Feed	100	2.84	73.58	17.19	1.56	4.89	11.86	34.26	5.86	7.18	40.48	99.51

L.O.I. = Loss on Ignition

Conclusions

Microscopic analysis of the magnesite-dolomite ore sample indicates that dolomite is stained with goethite (weakly magnetic mineral), while magnesite is stained with hematite and magnetite (strongly magnetic minerals). It is suggested that iron in the ferrous state is produced upon the breakdown of ferromagnesium silicates. The released iron is oxidized when exposed on the surface to form the red coloration of the "redbeds". This iron is reduced by the ground acidic water and precipitates as goethite on dolomite surface. Iron is transported in a reduced state until it precipitates as hematite on magnesite surface when in contact with the oxidized ground water at high pH.

The magnetic technique was selected for magnesite-dolomite separation. The controlling parameters such as magnetic field strength and drum speed were changed in such a manner that the recovery-grade relationship satisfies the objectives of application. Under optimum conditions (1.0 Ampere and 60 rpm) a magnesite concentrate, assaying 1.83% CaO with 27.72% recovery, was obtained. Mechanical cleaning of the rougher magnetic concentrate produced a cleaned concentrate assaying 0.89% CaO with a recovery of 16.26 %. A scavenging step for the non-magnetic fraction was conducted. This step produced a middling product rich in magnesite-dolomite assaying 10.95% CaO with 45.78% recovery. Blending of the magnetic fraction, obtained from the scavenging step, to the cleaned magnetic concentrate is recommended to achieve a reasonable concentration ratio. This produces a final magnesite concentrate assaying 1.12% CaO with 46.02% recovery. The concentrate, with low CaO content and CaO/SiO$_2$ molar ratio=1.62, is suitable for making basic refractories. On the other hand, the middling fraction called magnesite-dolomite product can be used for making low-loss forsterite dielectrics.

References

ARAUJO A.C., AMARANTE S.C., SOUZA C.C., SILVO, R.R., 2003, *Ore mineralogy and its relevance for selection of concentration methods in processing of Brazilian iron ores*, Mineral Processing and Extractive Metallurgy, 112,1, 54–64(11).

ARVIDSON B.R., 1995, *New rare earth magnetic roll separator developments*, Proc. of the XI. Min. Proc. Congress, Berlin, 98.

BEITLER B. PARRY W.T., CHAN M.A., 2003, *Bleaching of Jurassic Navajo Sandstone on Colorado Plateau Laramide Highs: Evidence of exhumed hydrocarbon supergiants?* Geology, 31, 12, 1041–1044.

CHAN M.A., PARRY W.T., BOWMAN J.R., 2000, *Diagenetic hematite and manganese oxides and fault-related fluid flow in Jurassic sandstones, southeastern Utah*. AAPG Bulletin, 84, 9, 1281–1310.

CHEN G.L., DANIEL T., 2005, *Reverse flotation of magnesite by dodecyl phosphate from dolomite in the presence of sodium silicate*, Separation Science and Technology, 39, 2, 377–390.

COHEN H.H., 1973, *Proceedings of the high Gradient Magnetic Separation Symposium*, MJT, Mass.

GIRGIS L.G., GAD G., 1970, *Refractory aspects of some dolomite magnesite rocks*, J. of Applied Chemistry, 20, 8, 234–239.

GONGLAN C., DANIEL T., 2004, *Effect of solution chemistry on floatability of magnesite and dolomite*, Int. J. of Mineral Processing, 74, 1–4, 343–357.

GROSZ S., MATTHEWS A., IIANI S., AYALON A., GARFUNKL Z., 2006, *Iron mineralization and dolomitization in the Paran Fault zone, Israel: implications for low-temperature basinal fluid processes near the Dead Sea Transform*. Geofluids, 6, 137–153.

KREMENETSKAYA I.P., KORYTNAYA O.P., VASIL'AVA T.N., BELYAEVSKII A.T., KADYROVA G.I., AZUKHINA S.I., 2009, *Physicochemical simulation of calcite(dolomite)-FeSO$_4$-H$_2$O open systems*, Russian Journal of Applied Chemistry, vol. 82, no. 10, 1845–1851.

KUMAR V., JADHAV G.N., KHOSLA N.K., MEHROTRA S.P., 2010, *Implication of process mineralogy for beneficiation of low grade iron ore resources containing high alumina from eastern part of India*, Proceeding of the XI International Seminar on Mineral Processing Technology, I, 82–91.

ORMO J., KOMATSU G., CHAN M.A., BEITLER B., PARRY W.T., 2004, *Geological features indicative of processes related to the hematite formation in Meridiani Planum and Aram Chaos, Mars: a comparison with diagenetic hematite deposits in southern Utah, USA*, Icarus, 171, 295–316.

OTHMAN A.G.M., KHALIL N.M., 2005, *Sintering of magnesia refractories through the formation of periclase-forsterite-spinel phases*, Ceramics Int., 31, 8, 117–1121.

PARRY W.T., CHAN M.A., BEITLER B., 2004, *Chemical bleaching indicates episodes of fluid flow in deformation bands in sandstone*. AAPG Bulletin 88, 2, 175–191.

SCHUBERT H. 1978, *Aufbereitung Fester Minerischer Rohstoffe*, VEB Deutscher Verlag für Grundstoffe, 2, Auflage.

UPADHYAY R.K., ROY S., VENKATESH A.S., RAO M.V.S., BANERJEE P.K, 2009, *Relevance of geological aspects and ore mineralogy in selecting beneficiation methods for processing of eastern Indian iron ores*, Mineral Processing and Extractive Metallurgy, 118,1, 49–59.

WANZHONG Y., QIANG L., YINGQIANG M.A., 2011, *Flotation research on dolomite-containing magnesite ore*, Advanced Materials Research, 158, 113–124.

YEHIA A,, Al-WAKEEL M.I. 2000, *Talc separation from talc-carbonate ore to be suitable for different industrial applications, Technical note*, Minerals Engineering, v. 13, no. 1, 111–116.

DETERMINING OPTIMAL CONDITIONS FOR LIGNITE FLOTATION BY DESIGN OF EXPERIMENTS AND THE HALBICH UPGRADING CURVE

Oktay SAHBAZ

Dumlupinar University, Department of Mining Engineering, Kutahya, Turkey, Tel.: +90 537 3862002; Fax.: +90 274 2652066; oktay.sahbaz@dpu.edu.tr

Abstract: In this study conditions for flotation of low rank coal (lignite of Tuncbilek, Turkey) were investigated in detail. The experiments were performed using the 3-variable 2-level (2^3) full factorial experimental design with four base point replicates, and the results were analyzed by the regression model, Fischer test (F-test) and Halbich's upgrading curve for the responses of ash content (or combustible matter grade) and the combustible matter recovery. The results obtained from the analysis indicated that while every factor considerably affected the combustible matter recovery, both collector (kerosene) and frother (AF65) significantly influenced the ash contents of the carbonaceous matter products. The only effective mutual interaction influencing recovery was caused by the kerosene-aeration interaction, while the interaction of kerosene-aeration and kerosene-AF65 and interactions of all factors (kerosene-AF65-aeration) were significant for the ash content of the products. Basing on the grade–recovery Halbich upgrading curve, regression model and a criterion for optimum of flotation results, it was found that a coal product with combustible matter grade of 91.09% and 71% combustible matter recovery can be obtained provided that it is processed at the higher level of kerosene (3 kg/Mg), higher level of frother AF65 (40 ppm) and lower aeration rate level of (0.16 cm/s).

Key words: low rank coal, flotation, design of experiment, upgrading curves

Introduction

Every year in Turkey teragrams of lignite having particle size of finer than 0.5 mm are discharged to the slurry pond after coal processing which not only causes economic losses but also significant environmental problems. Continuous and mechanized mining operations are a source of these fine coal particles which are not easily separated from their gangue minerals by the use of physical separation methods such as heavy media separation, spirals, and screens etc. Meanwhile, flotation process has a great potential for efficient beneficiation of these coals. Additionally, lignite type coals

especially have problematic flotation behavior, not as the high rank coals (Aplan, 1976; Polat et al., 2003). Many studies have been performed to investigate flotation of low rank coals to obtain the optimum working parameters (Naik et al., 2004; 2005; Jia et al., 2000; Mohanty and Honaker, 1999). Some of these studies have also been performed for the Turkish coals (Aktaş and Woodburn, 1995; Ateşok et al., 2001; Cebeci, 2002; Akdemir and Sönmez, 2003, Vapur et al., 2010). All these studies clearly show the importance of chemical factors that are type of collector, frother, and pH on flotation performance. Moreover, some parameters such as aeration, hold-up, and power input can also affect the flotation performance of coals (Kowalczuk et al., 2011; Mohanty and Honaker, 1999).

The parameters and their effects on the combustible matter recovery and other performance characteristics are innumerable. Lately, Kelebek et al. (2008) carried out a study to improve flotation of coal particles obtained from Tuncbilek lignite which is one of the biggest lignite reserves in Turkey. They determined the effect of collector type and pH and stated the necessity for determining the effect of frother (AF65) on Tuncbilek lignite flotation.

The procedure of factorial design of experiments is commonly used to examine the parameters controlling separation processes. The factorial design for performing experiments has many advantages over classical methods of treating one-variable-a-time (Box et al., 1978).The number of experiments and amount of material are reduced and time is saved by the use of factorial design. In addition, the analysis done on the results is easier while the experimental error is reduced. It can also helpful in determination of the optimal condition of the process.

Studies based on statistical approaches usually treat, incorrectly, grade and recovery independently. Therefore, it is necessary to use the so-called upgrading curves (Drzymala, 2006; 2007), that are plotted as quality vs. either quantity or quality of separation products (Drzymala et al., 2012). One of frequently used upgrading curves is the Halbich grade- recovery curve (Drzymala et al., 2012). The Halbich plot is practical and useful as well as has many advantages over other upgrading curves because of using recovery and grade, which are generally used in industrial, liberation, kinetic and theoretical studies (Drzymala et al., 2012).

The aim of this study is to report a procedure of determination of interactions between basic parameters of the process and optimal flotation conditions for the low rank coal of Tuncbilek region by means of factorial design and the Halbich plot.

Materials and methods

Materials

The lignite sample used in this study was obtained from the Tunçbilek underground mine, which is 50 km away from the city centre of Kutahya in Turkey. The sample, which is a sub-bituminous coal (Gülen et al., 2012), was first reduced to finer than 600 μm using a laboratory type jaw crusher and roll mill, respectively. The d_{80} of the

samples was about 450 µm, and the ash content of the sample was found to be 12.13% (87.87% combustible matter). For the flotation tests kerosene, sodium silicate, and Aerofroth 65 (AF65), which is a polygylicol type frother obtained from Cytec and having chemical formula of $H(PO)_{6.5}OH$ (Melo, 2001 and Laskowski et al., 2003) were used as collector, depressant, and frother, respectively. The pH of the coal suspension was 7.5. The experiments were carried out at 23 °C. Local tap water was used in all flotation experiments.

Methods

Flotation tests

The flotation experiments were carried out in the Jameson flotation cell (JFC) which has a 25 mm downcomer equipped with a 6 mm nozzle.

For the flotation experiments, a 500 g sample of coal was added into a conditioning tank, and mixed with tap water at 1300 rpm for 5 min. Then, the desired amount of sodium silicate depressant (700 g/Mg) and kerosene as the collector were added to the conditioning tank and mixed for 10 min. Finally, a desired amount of frother (AF65) was added into the tank and mixed for 1 min. The feed solid concentration was 4% by weight.

After the conditioning process, the slurry was pumped to the nozzle on the top of the downcomer with a high pressure of 110 kPa. The pressure was tried to be fixed at the lowest degree to inhibit turbulence increase in the JFC. The working conditions for the JFC have been explained in detail in studies carried out by Evans et al. (1995) and lately by Şahbaz et al. (2013).

Experimental design

In this study, the flotation tests were performed by using the full factorial center point repeated experimental design. Three important parameters: collector, frother and aeration rate were chosen as independent variables (design factors), and two levels of these variables with their base points were used to generate data for 2^3 factorial design. The variables and their levels are given in Table 1. The 2^3 factorial design including the factors, levels and values are also given in Table 1.

Table 1. Variables and their levels

Flotation Factors	Low level (-1)	Mid Level (0)	High Level (+1)
A, Collector, g/Mg	500	1750	3000
B, Frother, ppm	10	25	40
C, Aeration rate (J_g), cm/s	0.60	0.95	1.30

In the design matrix, the higher level was designated as "+1" while the lower one and mid-point were designated as "–1" and "0", respectively. The following equation (Eq. 1) was used to obtain coded units (X_{coded}) from the actual values (X_{actual}).

$$A_{\text{coded}} = \frac{X_{\text{actual}} - X_{\text{mean}}}{\dfrac{X_{\text{high}} - X_{\text{low}}}{2}} \tag{1}$$

where X_{high} is the highest value of any factor, X_{low} is the lowest value, and X_{mean} is the arithmetic value of X_{high} and X_{low}.

In the study, the combustible matter recovery and the ash content were chosen as responses. The main effect of any factor is the change in response produced by varying the level of the factors. It can be calculated by the below equation:

Main effect of factor X = (Average response at X_{high}) – (Average response at X_{low}) (2)

Additionally, it is very important to find out the interaction effects which occur when the difference in response between levels of any factor is not the same at all levels of the other factor. This effect can only be found by the use of the statistical design given by Eq. 3

$$\begin{aligned}\text{Interaction effects of } X_1 \text{ and } X_2 &= (\text{Average response at } X_1 X_{2high}) \\ &- (\text{Average response at } X_1 X_{2low}) .\end{aligned} \tag{3}$$

A full factorial 2^3 design with four base points can geometrically be shown by a cube. In this case, responses can be placed at the corners and X, Y, and Z axes representing factor A, B and C, respectively. The origin is the center of the cube, and every side of cube is equivalent to two units, +1 and −1. Design expert statistical software (www.statease.com) was used to determine the main and interaction effects with the confidence interval of 95%. The Fisher test and probability values were used to analyze the results statistically. In this analysis, the results were compared according to their F and p-values. The F-value indicates the model significance. It is used for determining the model navigation in the design space. The greater the F-value, the greater is the parameter effect on a response. In addition, the values of p-value is also used to determine the effectiveness of the parameters, and the p-value of less than 0.05 indicates that the model terms are significant at 95% confidence level.

Eight experiments were carried out for this determination using Eq. 4

$$NoE = 2^k, \tag{4}$$

where NoE is the number of the experiments, and k is the number of variables. To supply statistical significance and to estimate the variance (σ^2) and error, additional four experiments were performed at the base level. The variance of the main and interaction effects are given in Eqs 5 and 6 (Kelebek et al., 2008):

$$Variance\ (Effects) = \frac{4\sigma^2}{2^k}, \tag{5}$$

Calculated main or interaction effects / $[Variance\ (Effects)]^{0.5} \geq t_{3,0.025}$,   (6)

The model (regression equation) with the main and interactive terms can be written as following formula:

$$Y = \beta_0 + \beta_1 A + \beta_2 B + \beta_3 C + \beta_{12} AB + \beta_{13} AC + \beta_{23} BC + \beta_{123} ABC \tag{7}$$

where Y is response (recovery or ash content of lignite), β is the coefficients for the main and interaction terms.

Results and discussion

The 2^3 design matrix, which includes the factors and levels, and responses (recovery and ash content) are presented in Table 2. The regression model and its analysis by using the variance of analysis were used to analyses the results of the experimental study.

Table 2. 2^3 factorial design matrix and responses

Run	Coded factors			Response		
	A	B	C	Recovery	Ash	Grade (100 – Ash)
1	−1	−1	−1	39	10.11	89.89
2	1	−1	−1	36	7.98	92.02
3	−1	1	−1	53	7.20	92.80
4	1	1	−1	71	8.91	91.09
5	−1	−1	1	15	7.32	92.68
6	1	−1	1	48	9.30	90.70
7	−1	1	1	37	6.94	93.06
8	1	1	1	61	9.18	90.82
9	0	0	0	57	8.19	91.81
10	0	0	0	49	8.07	91.93
11	0	0	0	48	7.71	92.29
12	0	0	0	53	7.77	92.23

The Pareto Charts for the combustible matter recovery and the ash content of the products are shown in Fig. 1. The charts give the relative importance of the main and interaction effects of AF65, kerosene, and aeration for the flotation recovery. The vertical lines in the charts show the minimum statistically important effect magnitude at the 95% confidence level. If any main or interacting effects exceed the reference line, the effect of parameter will be important for the response. In this case, as seen in Fig.1a, AF65 (B), kerosene (A), aeration (C) and interaction of kerosene-aeration (AC) show an important effect on the combustible matter recovery. In addition, Fig. 1b shows the significant factors of the ash removal. According to Fig. 1b, the most

effective factor is the interaction of kerosene-aeration in the removal of ash (ash content), and it is followed by kerosene-AF65 interaction and triple interaction of the three considered parameters.
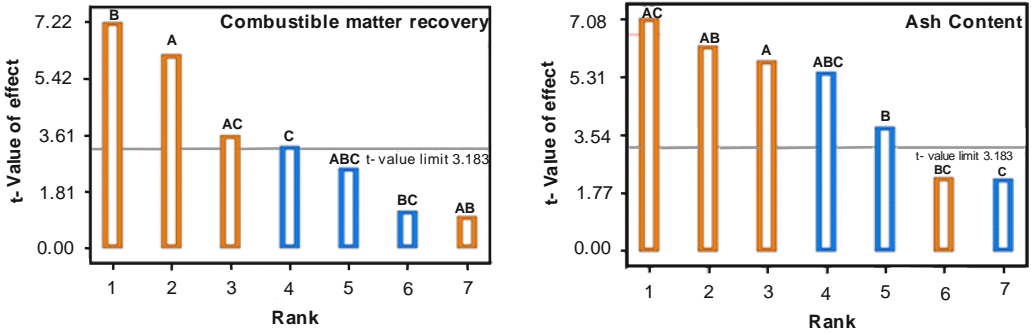
Fig. 1.The Pareto Charts for the parameters affecting recovery and ash content

On the other hand, Fig. 2 is the normal probability plot which is plotted to identify the most effective factors. The significance of the parameters is detected from Fig. 2 by plotting the calculated effects of all factors against a line representing normal distribution. Significance of factors is determined according to their distance from the distribution line in Fig. 2. The effects on the efficiency of the factors on the right side of the line can be described as positive whereas the ones on the left are negative. Accordingly, AF65 (B) is the farthest factor to the normal distribution line with the greatest impact on combustible matter recovery. AF65 is followed by kerosene (A factor), interaction of kerosene-aeration (AC factor), aeration (C factor), and interaction ABC factor for all factors, respectively. The interactions of kerosene-AF65 and AF65-aeration are very close to the normal distribution line. Similar inferences can be made for the ash content as seen in Fig. 2. While the positive effects on the ash content is performed by AC, AB, A and BC, negative effects of the factors can be obtained as ABC, B and C.
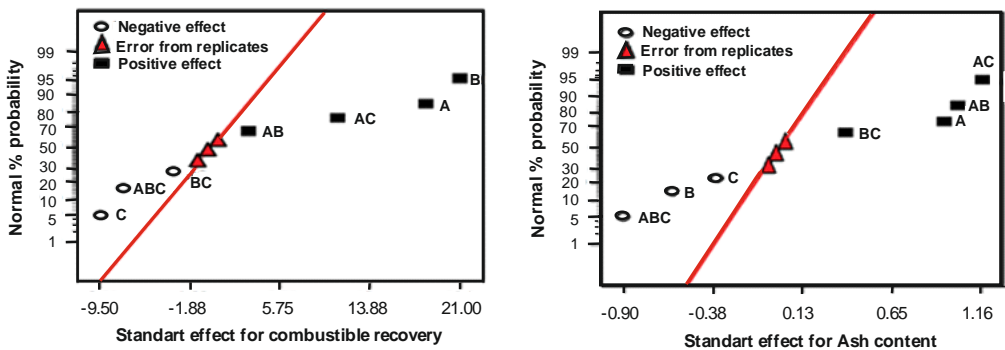
Fig. 2. Normal probability plot for combustible matter recovery and the ash content

Analyses of results

The effects of factors on the combustible matter recovery and the ash content of the lignite sample were determined quantitatively by the use of the F-test at the 95% confidence interval and regression model. The F-test indicates that all parameters significantly affect the combustible matter recovery of the Tuncbilek lignite while only AF65 and kerosene affect the ash content of the lignite (Table 3).

Table 3 includes both F-value of the Fisher-test and p-value for the combustible matter recovery. The model F-value of 17.62 implies that the model is statistically significant. Therefore, the model can be used to navigate the design space. In addition, "Curvature F-value" of 7.18 implies that there is a significant curvature, as measured by the difference between average of the center points and average of the factorial points in the design space. There is only a 7.51% chance that a "curvature F-value" this large could occur due to noise effect. The p-value of curvature in the factorial experiment for the recovery is 0.0751, which is greater than 0.05, indicating an insignificant curvature measured by the difference between the average of the centre points and the factorial points in the design space. An insignificant curvature suggests that the relation between the variables and the response has a linear form.

The main effect of all these factors on the recovery is significant at 95% confidence level (Table 3). According to the variance analyses (Table 3) and the regression equation (Eq. 8) factor A and B, that is kerosene and AF65, is the most effective factors in flotation of Tuncbilek lignite because of the highest F-values (Table 3). The order of main effect is AF65 > kerosene > aeration rate for the recovery and kerosene > AF65 > aeration rate for the ash removal. As Kelebek et al. (2008) suggested AF65 has a great importance for lignite flotation because it increases coal cleaning selectivity by the increase of froth depth and improves the stability of bubbles.

Table 3. Variance analysis for combustible matter recovery and ash content

Source	Combustible matter recovery		Ash content	
	F value	p-value prob > F	F value	p-value prob > F
Model	17.6	0.0192	25.30	0.0114
A-Kerosene	38.3	0.0085	33.61	0.0102
B-AF65	52.1	0.0055	14.32	0.0324
C-Aeration	10.7	0.0469	4.96	0.1123
A B	1.1	0.3782	39.13	0.0082
A C	13	0.0365	50.12	0.0058
B C	1.5	0.3151	5.1	0.1091
A B C	6.7	0.0819	29.83	0.0121
Curvature	7.2	0.0751	9.29	0.0555

The main influences of kerosene and AF65 on ash content are significant at the 95% confidence level. Positive coefficients of kerosene indicate an increase in the ash content, while negative coefficient of AF65 indicates a decrease in the ash content. According to the variance analyses (Table 3) kerosene is the most effective factor for the ash content of the floated product because of the highest F-value (33.61). On the other hand, the interactions of kerosene-AF65 and kerosene-aeration are also significant for the ash content (Table 3). In addition, the interaction between kerosene-AF65-aeration influences significantly the ash content (Table 3). The only insignificant effect is the interaction of AF65-aeration in the given range of parameters. The only statically significant interaction at 95% confidence level is kerosene-aeration for the recoveries while the AF65-kerosene, kerosene-aeration and interactions of all parameters (kerosene-AF65-aeration) significantly affect the ash content of Tuncbilek lignite (Table 3).

The regression equation for the combustible matter recovery (Y_{Cr}) and ash content (Y_{ac}) can be derived from Eq. 7 and has the following forms:

$$Y_{Cr} = 45 + 9A + 10.50B - 4.75C + 1.5AB + 5.25AC - 1.75BC - 3.75ABC \qquad (8)$$

$$Y_{ac} = 8.37 + 0.47A - 0.31B - 0.18C + 0.51AB + 0.58AC + 0.19BC - 0.55ABC. \qquad (9)$$

The regression analyses can be used not only for evaluating the main and interaction effects of factors, but also for evaluating the fitness of Eqs. 8 and 9. In addition, Eqs.8 and 9 can be utilized to determine the combustible matter recovery and ash content of the coal within the experimental conditions limits. In this case, a coefficient of determination, R^2, should be calculated. R^2 is a measure of the amount of variation around the mean value. When the R^2 value is close to 1, it means that predicted values can be appropriately referred to the experimental values. Recovery model (Eq. 8) has $R^2 = 0.9762$ meaning that 97.62% variability in the recovery and the rest 2.38% is attributed to errors. When the differing number of observations in analysis is relatively small, it decreases the R^2 value. Likewise, a smaller number of independent variables increases the R^2 value and vice-versa (Kelebek et al., 2008). Therefore, the modified new value is expressed as an adjusted R^2. The adjusted R^2 of 0.9208 is also satisfactory and verifies the significance of the model. On the other hand, ash content model (Eq. 9) has $R^2 = 0.9833$. It means that 98.73% of the variability is caused by the ash content and the rest 1.27% is attributable to errors. The adjusted $R^2 = 0.9445$ also implies the model significance.

According to the regression models the highest possible recovery (Eq. 8) was obtained as 70.99% at the high level of kerosene (3 kg/Mg), high level of AF65 (40 ppm) and low level of aeration (0.60 cm/s), while the lowest ash content (or highest combustible matter grade) (Eq. 9) was obtained as 6.94% at the high level of AF65 (40 ppm) and aeration (0.26 cm/s) and low level of kerosene (500 g/Mg). These results, taken together are unrealistic as will be shown in the next section of this paper.

This is so because recovery and ash content must be considered together for a given separation process.

Determining the optimal conditions

Statistical software was used to determine the optimal conditions by taking into consideration data and calculations obtained from the factorial design. Combustible matter recovery and grade together were taken as criteria and possible highest points selected for numerical determination of the optimal condition. All levels of factors were chosen in the range of –1, 0 or +1 for the calculations. According to the numerical optimization study, 53% recovery and 92.80% grade were obtained at the low level of kerosene (500 g/Mg), high level of AF65 (40 ppm) and low level of aeration (0.60 cm/s). It should noticed that this kind of statistical approach should be verified by using mineral processing approaches. Therefore, the result must be confirmed and evaluated from the mineral processing point of view.

It is known the best separation results for a series of experiments can be determined by using the so-called upgrading curves, including the grade-recovery plot known as the Halbich curve (Drzymala, 2006). The reason for this is that the Halbich curve has some advantages over other upgrading curves because it considers two essential parameters of separation results which are recovery and grade. These two parameters are widely used in industrial, kinetic and theoretical studies (Drzymala et al., 2012).

The Halbich plot for all 12 experimental points presented in Table 2 is given in Fig. 3. From the point of view of selectivity of the process (Drzymala et al., 2012) the best results are those forming an upgrading line which is the closest to the ideal separation line. This occur for the a1 line which represents flotation results obtained for runs 3 and 4 conducted at increasing amount of collector and constant (higher) level of frother and constant (lower) level of the aeration rate. Other lines denoted as a2, a3 and a4 were plotted by using the experimental data points of runs of 7-8, 5-6 and 1-2. The line for base points was drawn by using the experimental values repeated at centre points of factors (9-10-11-12) (level 0).

According to Kelly and Spottiswood (1982) for a given upgrading line the best result is the one which provides the greatest value of the mathematical product of grade and recovery for the combustible matter. Taking this criterion into account, the best result obtained in this study for the investigated range of parameters was for +1 levels of collector and frother and –1 level of the aeration rate. Thus, the best (optimal) flotation recovery was equal to 91.10% providing 71% of combustible matter in the concentrate at the 3 kg/Mg kerosene, 40 ppm AF65 and 0.16 cm/s aeration rates. It should be noticed the optimum point of separation depends on the criterion imposed on data. Here the criterion is the maximum value of multiplication of grade and recovery values. Thus, the optimal flotation point is not a result as calculated from the factorial design by considering recovery and grade independently (recovery: 70.99% at the high level of kerosene (3000 g/Mg), high level of AF65 (40 ppm) and low level of aeration (0.60 cm/s), ash content or highest combustible matter grade 6.94% at the

high level of AF65 (40 ppm) and aeration (0.26 cm/s) and low level of kerosene (500 g/Mg)).
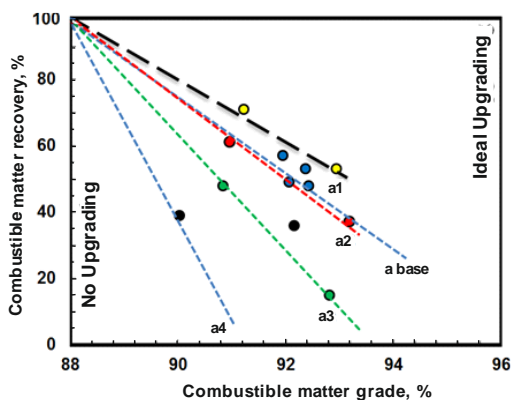
Fig. 3. The Halbich upgrading curve with the results of all experiments. Each straight line connects data points obtained for a constant level of both frother dose and aeration rate and increasing amount of collector. The line denoted as "a base" approximates the data points obtained for experiments conducted four times at the zero level of all parameters

The same conclusion regarding the optimum level of the investigated parameters for Tuncbilek lignite can be obtained using no directly the flotation results but the data points generated with Eqs. 8 and 9 and plotted on the Halbich curve. It means that the 3-variable 2-level (2^3) full factorial experimental design with four base point replicates can be useful not only for determination, expressed in numbers, interactions between parameters, but also optimum flotation conditions for the investigated coal provided that a proper criterion for the optimum is applied. The optimum result obtained from the numerical optimization is also one of the points on line a1 in the Halbich curve.

Conclusions

This study was performed in order to determine, expressed in numbers, interactions between parameters and best conditions for the flotation of Tuncbilek lignite by using both statistical approach and upgrading curves. The flotation experiments were carried out using the 3-variable 2-level (2^3) full factorial experimental design with four base point replicates, and the results were analyzed by using the regression model, F-test and Halbich's upgrading curve for the responses of ash content (or combustible matter grade) and combustible matter recovery. The following findings are obtained from the present study:

- results obtained from this study (Pareto charts and normal probability plot) indicated that the most effective parameters on the combustible matter recovery and the ash content were frother (AF65) and collector (kerosene), respectively.

- the regression and F-test qualitatively showed the main and interaction effect of factors. All parameters investigated in the study indicated a significant influence on the recovery. However, the only significant interaction occurred between kerosene and aeration. On the other hand, except of AF65–aeration interaction, all interactions showed a significant effect on the ash content while only the main significant effects were kerosene and AF65 on the ash content.

- the optimal conditions for the flotation can be determined by taking into account both recovery and grade simultaneously using either the results of the factorial design or the Halbich plot and using criterion of the maximum value of mathematical product of grade and recovery. According to the plot, the best results for the investigated coal can be obtained with the ash content of about 9% and the recovery of 71% at the higher amount of kerosene (3 kg/Mg) and AF65 (40 ppm) with lower aeration rate (0.16 cm/s).

References

AKDEMİR Ü., SÖNMEZ İ., 2003. *Investigation of coal and ash recovery and entrainment in flotation*, Fuel Processing Technology, 82, 1–9.

AKTAS Z., WOODBURN E.T., 1995. *The effect of non-ionic reagent adsorption on the froth structure and flotation performance of two low rank British coal*. Powder Technology, 83,149–158.

APLAN FF., 1976. *Flotation*, In: Fuerstenau MC, editor. AM Gaudin memorial volume. New York: AIME, 1235–64. (From the paper of Yakup Cebeci (2002))

ATESOK G., BOYLU F., ÇELİK M.S., 2001. *Carrier flotation for desulfurization and deashing of difficult-to-float coals*, Minerals Engineering, 14, 661–670.

BOX G.E.P., HUNTER W.G., HUNTER J.S., 1978. *Statistics for Experiments*.Wiley, New York.

CEBECİ Y., 2002. *The investigation of the floatability improvement of Yozgat Ayrıdam lignite using various collectors.* Fuel, 81, 281–289.

DRZYMALA J., 2006. *Atlas of upgrading curves used in separation and mineral science and technology Part I*, Physico-chemical Problems in Mineral Processing, 40, 19–29.

DRZYMALA J., 2007. *Atlas of upgrading curves used in separation and mineral science and technology Part II*, Physico-chemical Problems in Mineral Processing, 41, 27–35.

DRZYMALA J., KOWALCZUK P.B., FOSZCZ D., MUSZER A., HENC T., LUSZCZKIEWICZ A., 2012. *Analysis of separation results by means of the grade-recovery Halbich upgrading curve*, XXVI International Mineral Processing Congress, September 20–24.

EVANS G.M., ATKINSON B., JAMESON G.J., 1995, *The Jameson Cell. Flotation Science and Engineering*, ed. Matis K.A., Marcel Dekker Inc., 331–363.

GÜLEN J., TOPRAK S., PİŞKİN S., 2012. *Batıkömürlerineaitbazıkarakteristiközellikler,* Karaelmas Science and Engineering Journal, 1, 27–33, Turkey.

JIA R., HARRIS G.H., FUERSTENAU D.W., 2000. *An improved class of universal collectors for the flotation of oxidized and/or low-rank coal*, International Journal of Mineral Processing, 58, 99–118.

KELEBEK Ş., DEMIR U., SAHBAZ O., UCAR A., CINAR M., KARAGUZEL C., OTEYAKA B., 2008. *The effects of dodecylamine, kerosene and pH on batch flotation of Turkey's Tuncbilek coal*, Int. Journal of Mineral Processing, 88, p65–71.

KELLY E.G., SPOTTISWOOD D. J., 1982. Introduction to Mineral Processing, Wiley, New York

KOWALCZUK P. B., SAHBAZ O., DRZYMALA J., 2011, *Maximum size of floating particles in different flotation cells,* Minerals Engineering, 24, 766–771.

LASKOWSKİ J.S., TLHONE T., WILLIAMS P., DING K., 2003. *Fundamental Properties of the polyoxypropylene alkyl ether flotation frothers*, International Journal of Mineral Processing, 72, 289–299.

MELO F., 2005.*Fundemental Properties of flotaiton frothers and their effect on flotation*, Master of Applied Science Thesis, The University of British Columbia, Canada.

MOHANTY M.K., HONAKER R.Q., 1999. *A comperative evaluation of the leading advanced flotation technologies.* Minerals Engineering, 12, 1–13.

NAIK P., REDDY P.S.R., MISRA N., 2004. *Optimization of coal flotation using statistical technique*, Fuel Processing Technology, 85, 1473–1485.

NAIK, P., P.S.R. REDDY and N. MISRA, 2005. *Interpretation of interaction effects and optimization of reagent dosages for fine coal flotation*, International Journal of Mineral Processing, 75, p. 83–90.

POLAT M., POLAT H., CHANDER S., 2003. *Physical and chemical interactions in coal flotation*, International journal of Mineral Processing, 72, 199–213.

ŞAHBAZ O., UCAR A., OTEYAKA B., 2013.*Velocity gradient and maximum floatable particle size in the Jameson cell.* Minerals Engineering, 41, 79–85.

VAPUR H., BAYAT O., UÇURUM M.,, 2010. *Coal flotation optimization using modified flotation parameters and combustible matter recovery in a Jameson cell.* Energy Conservation and Management, 51, 1891–1897.

LEACHING OF ZINC FROM LOW GRADE OXIDE ORE USING ORGANIC ACID

Mehdi IRANNAJAD[*], Mohammad MESHKINI[**], Amir Reza AZADMEHR[*]

[*] Department of Mining and Metallurgical Engineering, Amirkabir University of Technolog., Tehran, Iran, iranajad@aut.ac.ir

[**] IranianAcademic Center for Education, Culture and Research(ACECR), Branch of Amirkabir, Iran

Abstract: The leaching of low grade zinc oxide mining tailings by organic acid as a leaching agent was investigated. Zinc was extracted successfully from sample by citric acid leaching. The effects of solid-to-liquid ratio, acid concentration, reaction time, temperature and ore particle size on the leaching efficiency were studied. The results obtained showed that particle sizes and reaction time had not any significant effect on the leaching recovery of zinc from smithsonite in the sizes range of 40-350 μm. Under conditions: temperature of 80ºC, reaction time of 60 min, citric acid concentration of 0.5 mol/L, and solid to liquid ratio of 1:10, 82% of zinc could be recovered.

Introduction

Zinc is one of the most important base metals in the galvanizing, cosmetic, die casting and manufacturing industries. Zinc is extracted mostly from zinc sulfide ores. Zinc sulfide ores especially sphalerite are suitable and useful sources for the production of zinc because they could easily be separated and concentrated by flotation from the gangue (Espiari et al., 2006; Qing et al., 2010). In this respect, the increasing demand of zinc and zinc compounds, and therefore new sources of zinc such as low grade oxide ores have been considered. The leaching of low grade ore is attracted considerably in recent years. One of the most important sources of low grade ores in zinc mineral processing is zinc mining tailings. Smithsonite ($ZnCO_3$), hydrozincite ($2ZnCO_3·3Zn(OH)_2$), zincite (ZnO), willemite ($ZnSiO_4$), gahnite ($ZnAl_2O_4$), descloizite ($PbZnVO_4OH$), hardystonite ($Ca_2ZnSi_2O_7$) and hemimorphite ($Zn_2SiO_3·H_2O$), are mostly zinc oxide ores, an abundance of which include smithsonite and hemimorphite (Jones, 1987). Zinc oxide ores in Iran are abundant and are mainly found in the center and in northwest part of Iran (Espiari et al., 2006). Both

hydrometallurgical and pyrometallurgical methods have been used for extraction of zinc from ore or residual (Chen et al., 2009). Recently there are some reports stating that zinc oxide ores can be treated by flotation (Onal et al., 2005; Ejtemaei and Irannajad, 2008; Irannajad et al., 2009; Ejtemaei et al., 2011) and by biohydrometallurgical methods (Meshkini et al., 2011b). Although the results obtained by these methods showed that the efficiency is comparable with usual methods the technology certainly needs further follow-up.

Many studies on leaching of zinc oxide ores by acid and basic solution have been published. In recent years the leaching of zinc ores containing oxidized minerals such as carbonates or silicates with sulfuric acid and its kinetics have been investigated. He et al. (2010) Cun-xiong et al. (2010) and Xu et al. (2010) focused on pressure leaching. The amount of zinc extraction in sulfuric acid solution is high in comparison with other methods and the concentration of silica and other unwanted elements are low. In these studies, the effects of temperature, concentration of sulfuric acid, ore particle size, air pressure, leaching time and solid to liquid ratio were investigated and optimum conditions were established. Espiari et al. (2006) studied the zinc dissolution kinetics of smithsonite and hemimorphite in the lead flotation tailings by sulfuric acid. Zhao and Stanforth (2000) produced zinc powder by use of the alkaline leaching process on smitsonithe. They extracted over 85% of both Zn and Pb, and less than 10% of aluminum using 5 M NaOH solution as a leaching agent in which zinc, lead and aluminum come into solution as $Zn(OH)_4^{-2}$, $Pb(OH)_4^{-2}$, and $Al(OH)_4^{-1}$. Similarly to this study Chen et al. (2009) investigated the parameters affecting the process like ore particle size, temperature, leaching time, alkali concentration and solid to liquid ratio to leach refractory hemimorphite $[Zn_4(Si_2O_7)(OH)\cdot H_2O]$ zinc oxide ores with NaOH solution. The optimum conditions determined were: particle size of 65–76 μm, 2 h leaching time at 85 °C in the presence of 5 mol/dm^3 sodium hydroxide and solid to liquid ratio of 1:10. The maximum zinc extraction in optimum conditions was reported to be 73% of zinc content of ore. Ju et al. (2005) studied the dissolution kinetics of smithsonite ore in ammonium chloride solution. The effect of stirring speed, ore particle size, reaction temperature, and concentration of ammonium chloride on zinc dissolution rate was investigated. The results showed that at the optimum leaching conditions about 91.2% of zinc could be recovered under conditions: ore particle size of 84–110 μm; reaction temperature of 90 °C, 240 min reaction time and ammonium chloride concentration 5 mol/dm^3. In recent years the studies on zinc oxide leaching by organic acids were initiated. Hursit et al. (2009) studied the dissolution kinetics of smithsonite ore in aqueous gluconic acid solutions using the parameters such as temperature, acid concentration, ore particle size and stirring speed. On the other hand organic acids can be produced by microbial processing (Papagianni et al., 1999; Sankpal et al., 2001). There are many studies showing that zinc oxide sources were treated by organic acids produced by microorganism (Schinner and Burgstaller, 1989; Burgstaller et al., 1992; Castro et al., 2000; Meshkini et al., 2011b).

Moreover, there are few reports on leaching of zinc oxide ores with organic acid reagents. The aim of this work was to investigate the extraction of zinc from Iranian low grade zinc ore by hydrometallurgical techniques using organic acid as a leaching agent. The effect of important variable parameters such as solid to liquid ratio, acid concentration, reaction time, temperature and particle size on zinc leaching has been investigated.

Materials and methods

The sample of the ore came from mining tailings of Angoran lead-zinc mine, Iran. X-ray diffraction analysis indicated that the mineralogical constituents were smithsonite, small amounts of other zinc minerals such as hemimorphite, gangue minerals of quartz and some clay minerals (Meshkini and Irannajad, 2011a). Results of XRF analysis are given in Table 1. Citric acid was purchased from Merck and used without further purification.

Table 1. Chemical analysis of the ore sample

Component	Wt%
ZnO	16.1
Al_2O_3	8.0
SiO_2	21.2
CaO	21.3
Fe_2O_3	3.59
Impurities	5.37
L.O.I	24.44

Ore samples were crushed and sieved to size fractions of $-400+300$ µm (350 µm), $-300+180$ µm (240 µm), $-180+88$ µm (134 µm), $-88+44$ µm (66 µm) and $-44+37$ µm (40.5 µm). The entire experiment was performed in a 500 cm^3 round-bottomed flask with a condenser and was placed in a thermostatically controlled water bath to prevent evaporation loss. For each experiment 100 cm^3 volume of citric acid was poured into the flask at a definite concentration and heated to the required temperature. Then the ore sample of required size fraction was added and agitated with the stirrer at 350 rpm. At the end of each experiment the solution was analyzed by Atomic Absorption Spectrometry (AAS) to determine the zinc content. Zinc recovery (R_{zn}) was calculated according to the following equation:

$$R_{Zn} = \frac{c \cdot v}{c_0} \cdot 100 \tag{1}$$

M. Irannajad, M. Meshkini, A. R. Azadmehr

where, c (mg/dm^3) is the metal concentration of leaching solution, v (l) the leaching solution volume and c_0 (mg) is the amount of zinc in the ore sample.

X-ray diffraction (XRD) spectra and X-ray fluorescence analysis of the sample were obtained using a Philips X-ray diffractometer 1140 (Cu$_\alpha$=1.54 Å, 40 kV, 30 mA, calibrated with Si-standard) and a Philips X-ray fluorescence apparatus Xunique II (80 kV, 40 mA, calibrated with Si-standard), respectively. Determination of zinc concentration was done using a Unicam Atomic Absorption Spectrometry (AAS).

Results and discussion

The reaction between citric acid and smithsonite ore can be presented as follows:

$$C_6H_8O_7 \leftrightarrow 2H^+ + C_6H_6O_7^{2-} \tag{2}$$

$$ZnCO_3 + 2H^+ \rightarrow Zn^{2+} + CO_2 + H_2O \tag{3}$$

$$ZnCO_3 + C_6H_8O_7 \rightarrow Zn^{2+} + C_6H_6O_7^{2-} + CO_2 + H_2O \tag{4}$$
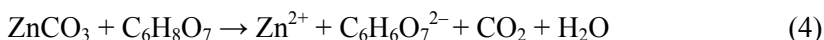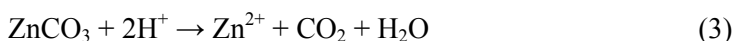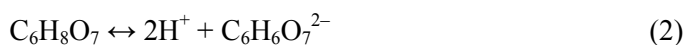
The sum of reactions (2) and (3) is reaction (4). Citric acid is a weak acid and it seems that the coordination of citrate with zinc ions causes the increase of smithsonite solubility.

Effect of solid to liquid ratio

Figure 1 presents the results of leaching with different solid to liquid ratio that was studied in the range of 1:5 to 1:30. The leaching rate of the ore sample increased with the decreasing solid to liquid ratio. According to a definite concentration of initial citric acid, the increasing of solid to liquid ratio reduces the zinc recovery. It decreases from 67% at S/L= 1:30 to 20% at S/L= 1:5. When solid to liquid ratio was increased,
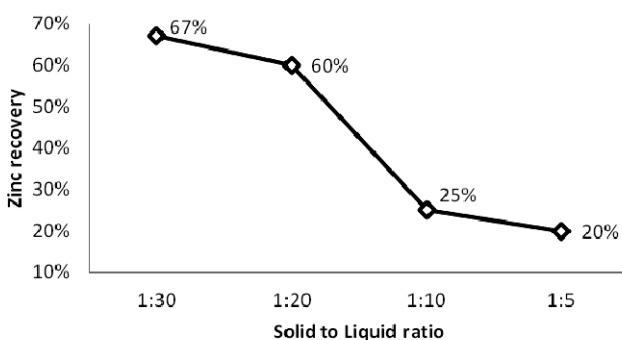
Fig. 1. Effect of solid to liquid ratio on zinc recovery at 25 °C,
0.5 M citric acid and 60 min reaction time

the amount of dissolved ore per unit liquid increase consequently the recovery decreases (Bayrak et al., 2010). Those are consistent with the results of Chen et al. (2002) and Espiari et al. (2006) in the treatment of the zinc oxide ore by alkaline and acidic leaching respectively.

Effect of acid concentration

The effect of acid concentration was investigated for a leach time of 60 min at 25 °C for solid to liquid ratio of 1:10, 1:20 and 1:30. As observed in Fig. 2, by increasing acid concentration the zinc recovery is increased in both 1:20 and 1:30 solid to liquid ratios. In the 1:10 solid to liquid ratio experiments showed that the zinc recovery increases by increasing the acid concentration up to 0.5 M of citric acid concentration and further increase in the acid concentration causes the decrease of zinc recovery. These results are partly similar to the results obtained by Hursit et al. (2009) using the gluconic acid as leaching reagent. It seems that the increase in acid concentration in the leaching medium caused the acid saturation near the solid particles (Hursit et al., 2009). Conversely, this behaviour cannot be seen in alkaline or non-organic acid leaching of zinc oxides. For this reason the constant concentration value was fixed as 0.5 M in the experiments. Additionally, for economy reasons the solid to liquid ratio was maintained constant at 1:10.
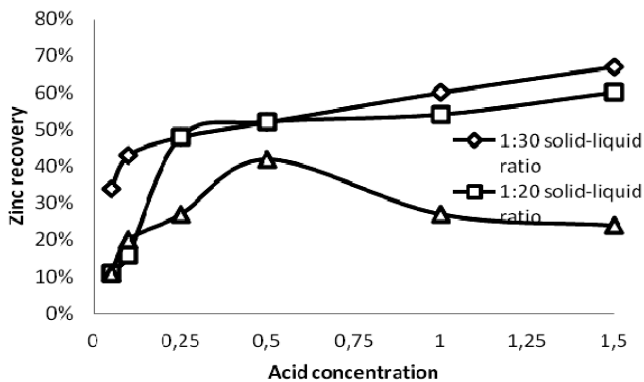
Fig. 2. Influence of acid concentration atvarious solid
to liquid ratioon zinc recovery at 25 °C

Effect of reaction time

The results obtained in leaching tests under different reaction times at temperature of 25°C using 0.5 M citric acid and 1:10 solid-to-liquid ratio are presented in Fig. 3. The reaction time does not affect zinc recovery positively. These results are similar to the results of alkaline and acidic leaching of zinc oxide ore studied by Chen et al. (2002), He et al. (2010) and Xu et al. (2010), respectively.
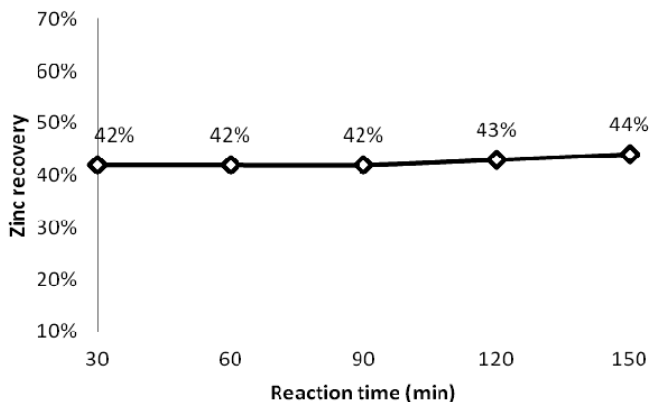
Fig. 3. Effect of reaction time on zinc recovery at 25 °C,
0.5 M citric acid and 1:10 solid-to-liquid ratio

Effect of temperature

Four batch leach tests were performed to determine the optimum temperature of zinc extraction. The effect of temperature was investigated in the range of 25–80 °C for a reaction time of 60 min in 0.5 M citric acid and 1:10 solid-to-liquid ratio. As observed in Fig. 4, the zinc recovery increased as the temperature increased. This is similar to the previous results reported by Santos et al. (2010) investigating the leaching of a zinc silicate ore. He reported that increasing the temperature from 70 °C to 90 °C caused the increase in zinc extraction from 36 to 90%.
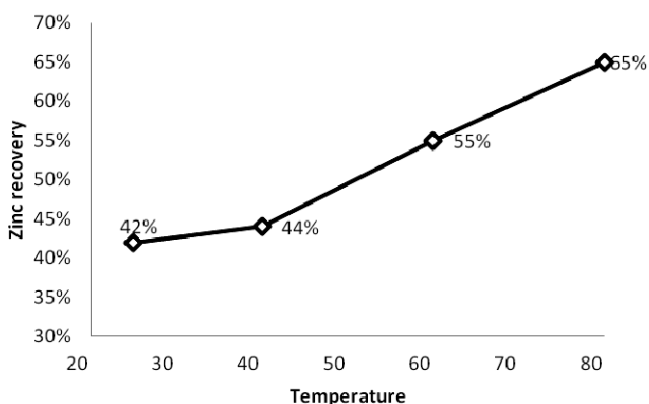
Fig. 4. Effect of temperature on zinc recovery at 0.5 M concentration
of citric acid, 1:10 solid-to-liquid ratio and 60 min reaction time

Effect of particle size

The experiments were performed with different particle size at 25 °C using 0.5 M citric acid and 1:10 solid-to-liquid ratio. Figure 5 shows that particle size had not a significant effect on zinc recovery. However the increase in particle size increases zinc recovery and the best results were obtained with particle size of 350 μm. The result is similar to one obtained in the work by Chen et al. (2002) in which zinc was extracted by alkaline leaching. However other works (Santos et al., 2010; Hursit et al., 2009) showed that the increaseof particle size caused the decrease in zinc recovery attributed to the decrease of the contact surface in the case of larger particle size.
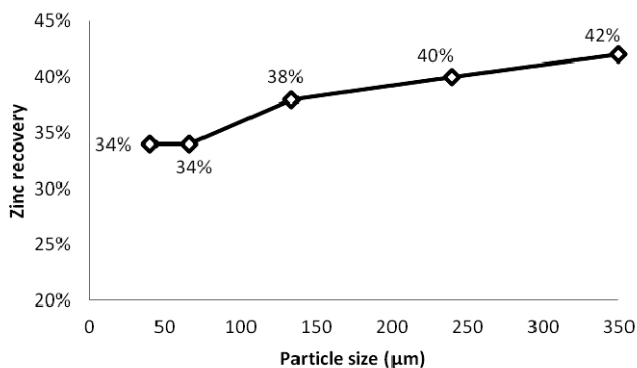
Fig. 5. Effect of particle size on zinc recovery at 25 °C, 0.5 M citric acid,
1:10 solid to liquid ratio and 60 min reaction time

Final optimisation experiment

By optimizing the leaching parameters as summarized in Table 2 the final tests showed that it was possible to extract 82% of zinc content.

Table 2. The results of leaching under optimum process conditions at a solid-to-liquid ratio of 1:10

acid concentration (M)	reaction time (min)	Temperature (°C)	particle size (micron)	Recovery (%)
0.5	60	80	350	82

Conclusions

This study demonstrates that zinc can be successfully recovered from mining tailings by citric acid leaching. Particle size and reaction time had an insignificant effect on the leaching recovery of zinc from smithsonite in the size range of 40–350 μm. When the ore sample of 350 μm size were leached for 60 min at 80° C in the presence of 0.5 mol/dm^3 citric acid and 1:10 solid-to-liquid ratio, more than 80% of zinc from the oxide ore can be extracted.

References

BAYRAK B., LACIN O., SARAC H., 2010, Kinetic study on the leaching of calcined magnesite in gluconic acid solutions. Industrial and Engineering Chemistry, 16, 479–484.

BURGSTALLER W., STRASSER H., WOBKING H., SCHINNER F., 1992, Solubilization of zinc oxide from filter dust with Penicillium simplicissimum: bioreactor leaching and stoichiometry. Environ Sci Technol, 26(2), 340–346.

CASTRO I., FIETTO J., VIEIRA R., TRO´PIA M., CAMPOS L., PANIAGO E., BRANDAO R., 2000, Bioleaching of zinc and nickel from silicates using Aspergillus niger cultures. Hydrometallurgy, 57, 39–49.

CHEN A., ZHAO Z. W., JIA X., LONG S., HUO G., CHEN X., 2009, Alkaline leaching Zn and its concomitant metals from refractory hemimorphite zinc oxide ore. Hydrometallurgy, 97, 228–232.

CUN-XIONG L., HONG-SHENG X., ZHI-GAN D., XING-BIN L., MING-TIN L., CHANG W., 2010, Pressure leaching of zinc silicate ore in sulfuric acid medium. Transaction of Nonferrous Metals Society of China, 20, 918-923.

EJTEMAEI M., IRANNAJAD M., 2008, Recovery of Zinc Oxide Minerals from Angooran Mining Tailings by Flotation. MSc Thesis, Amirkabir University of Technology (Tehran Polytechnic), Iran.

EJTEMAEI M., IRANNAJAD M., GHARABAGHI M., 2011, Influence of important factors on flotation of zinc oxide mineral using cationic, anionic and mixed (cationic/anionic) collectors. Minerals Engineering,24.1402-1408.

ESPIARI S., RASHCHI F., SADRNEZHAAD S., 2006, Hydrometallurgical treatment of tailings with high zinc content. Hydrometallurgy,82, 54–62.

HE S., WANG J., YAN J., 2010, Pressure leaching of high silica Pb–Zn oxide ore in sulfuric acid medium. Hydrometallurgy, 104, 235–240.

HURSIT M., LACIN O., SARAC H., 2009, Dissolution kinetics of smithsonite ore as an alternative zinc source with an organic leach reagent. Taiwan Institute of Chemical Engineers, 97, 6–12.

IRANNAJAD M., EJTEMAEI M., GHARABAGHI M., 2009. The effect of reagents on selective flotation of smithsonite–calcite–quartz. Minerals Engineering, 22, 766–771.

JONES M., 1987. Applied mineralogy: a quantitative approach. Graham & Trotman, London, p. 22.

JU S., MOTANG T., SHENGHAI Y., YINGNIAN L., 2005, Dissolution kinetics of smithsonite ore in ammonium chloride solution. Hydrometallurgy, 80, 67–74.

MESHKINI M., IRANNAJAD M., 2011 a, Zinc Recovery from Angoran Mining Tailing by Biohydrometallurgical Method. MSc Thesis, Amirkabir University of Technology (Tehran Polytechnic), Iran.

MESHKINI M., IRANNAJAD M., AZADMEHR A., ABASI ROHALLAHI A., 2011 b, Extraction of Zinc from Low Grade Zinc Oxide Ores using Bacteria. Second National Conference of Applied Microbiology. Tehran, Iran.

ONAL G., BULUT G., GUL A., KANGAL O., Perek K., Arslan F., 2005, Flotation of Aladag oxide lead–zinc ores. Minerals Engineering, 18, 279–282.

PAPAGIANNI M., MATTEY M., KRISTIANSEN B., 1999, The influence of glucose concentration on citric acid production and morphology of Aspergillus niger in batch and culture. Enzyme and Microbial Technology, 25, 710-717.

QING L., YOU-CAI Z., GUO-DONG Z., 2010, Thermodynamics of Zn(II)-NaOH-H2O system. Shanghai Univ, 14(5), 332–336.

SANKPAL N., JOSHI A., KULKARNI B., 2001, Citric acid production by Aspergillus niger immobilized on cellulose microfibrils: influence of morphology and fermenter conditions on productivity. Process Biochemistry, 36, 1129–1139.

SANTOS F. M., PINA P. S., PORCARO R., OLIVEIRA A. V., SILVA C. A., LEÃO V. A., 2010, The kinetics of zinc silicate leaching in sodium hydroxide. Hydrometallurgy, 102, 43–49.

SCHINNER F., BURGSTALLER W., 1989, Extraction of Zinc from Industrial Waste by a Penicillium sp. Applied and Enviromental Microbiology, 55, 1153–1156.

XU H., WEI C., LI C., FAN G., DENG Z., LI M., LI X., 2010, Sulfuric acid leaching of zinc silicate ore under pressure. Hydrometallurgy, 105, 186–190.

ZHAO Y., STANFORTH R., 2000, Production of Zn powder by alkaline treatment of smithsonite Zn–Pb ores. Hydrometallurgy, 56, 237–249.

PRODUCTION OF HIGH QUALITY MAGNESIUM CHLORIDE FROM RECYCLED WASTE MAGNESITE POWDER

Necmettin ERDOGAN[*], Erkan YERSEL[**], Cengiz CELEBI[***], Nevzat KAVAKLI[***], Turan BATAR[****]

[*]   Aksaray University, Department of Mining Engineering, Aksaray, Turkey
      nerdogan@aksaray.edu.tr
[**]   Canakkale Onsekiz Mart University, Department of Mining Engineering, Canakkale, Turkey
[***] Ministry of Energy and Natural Resources, Ankara, Turkey
[****] Gediz University, Faculty of Engineering and Architechure, Izmir, Turkey

Abstract: This study investigates the production of high-quality $MgCl_2$ from recycled waste magnesite powder with an average particle size of d_{50} 0.079 mm using the HCl acid leaching method. The experimental parameters were, leaching temperature, leaching time, amount of the acid, liquid-to-solid ratio, scale-up factor, acid concentration, particle size and mixing speed. The experiments were performed under reproducible conditions. The results showed that optimum leaching parameters were: temperature of 70 °C, 180 min leaching time, 130 cm^3 acid consumption, 3.6 cm^3/g liquid-to-solid ratio, scale-up factor of 1, 10.17 M acid concentration, 0.079 mm average particle size and a mixing speed 60 rpm. Under these optimum conditions, the leaching yield was 96.72%. The produced $MgCl_2$ solution contained 0.04% SiO_2, 0.36% CaO, 0% Fe_2O_3, 0% Al_2O_3, 46.73% $MgCl_2$, 52.87% L.O.I. and 99.60% $MgCl_2$+L.O.I. (= $MgCl_2 \cdot 6H_2O$). These results indicated that high-quality magnesium chloride can be produced from waste magnesite powder.

Keywords: waste magnesite powder, leaching hydrochloride acid, magnesium chloride, $MgCl_2$

Introduction

Magnesite ($MgCO_3$) is a primary source for the production of magnesium and its compounds. Natural magnesite theoretically contains 47.6% MgO and impurities such as silicon dioxide, iron and calcium. It is the basic raw material for the manufacture of alkaline refractory products and used in iron-steel, cement, glass, sugar, lime and paper industries as well as the paint and ink industry, the pharmaceutical industry as an anti-acid, and in the production of many magnesium chemicals (Abali at al., 2006).

Shaped and unshaped magnesite refractories have been used for many years as high strength hot-face refractories in a wide range of furnaces.

They have important applications where high degrees of refractoriness or resistance to basic environments are required, such as steel making vessels and rotary cement kilns (Shikano, 1998; Palco at el., 2002).

Chou et al. (1989) investigated the dissolution of various carbonates (including calcite, magnesite and dolomite) in HCl solutions at 25 °C using a continuous fluidized bed reactor and samples of a relatively coarse particle size. Ozbek et al. (1999) investigated the dissolution kinetics of magnesite with Cl_2 gas in water. They found that the diffusion was controlled through the fluid layer. Harris et al. (1988) studied the production of magnesium from concentrated magnesium chloride solutions. In addition, Abali et al. (2006) investigated the optimum conditions for the dissolution of magnesite with H_2SO_4 solutions. They reported that the optimum conditions were 65 °C, 5/100 g/cm^3, 2M, 60 min and 300 rpm. Abdel-aal et al. (1996) analyzed Egyptian magnesite ore (43.32% MgO) from the Eastern Desert leached with aqueous hydrochloric acid. They reported that the optimum conditions of leaching were: ore particle size -0.5 mm, temperature 60 °C, leaching time 15 min, HCl-to-MgO molar ratio 1.06, and liquid/solid ratio of 2.5:1 cm^3/g. These conditions led to a recovery of approximately 99.1% MgO. Abali et al. (2011) also investigated the Taguchi method to determine the optimum conditions for leaching dolomite ore in hydrochloric acid solutions. The experimental parameters were leaching temperature, solid-to-liquid ratio, acid initial concentration, leaching time and stirring speed. The optimum leaching parameter levels were found to be temperature 50 °C, solid-to-liquid ratio 2%, acid concentration 20 g/cm^3 (2 mol/dm^3), stirring speed 450 rpm, leaching time 5 min. Under the optimum process conditions, the dolomite ore leaching efficiency was approximately 83%. Ozdemir et el. (2009) investigated the recovery of magnesium from magnesite tailings in aqueous hydrochloric acid solutions with acid leaching in a batch reactor using hydrochloric acid solutions. Subsequently, they also investigated production of magnesium chloride hexahydrate ($MgCl_2 \cdot 6H_2O$) from leaching solution. The parameters were the effects of temperature, acid concentration, solid-to-liquid ratio, particle size and stirring speed on the leaching process. According to Ozdemir et al. (2009), the pseudo-second-order reaction model seems to be appropriate for the magnesium leaching.

The aims of this study are firstly to investigate the use of recycled waste magnesite powder to produce high-quality magnesium chloride. For this purpose, the acid leaching method was used to determine the optimum leaching conditions and parameters. The experimental plan was based on parameters and their levels to determine the leaching rate of waste magnesite powder in HCl solutions. To determine the optimum conditions the parameters of signal-noise graphics were drawn. The maximum leaching performance of the waste magnesite powder was predicted from the calculation of the optimum conditions. The produced $MgCl_2$ solution comprised: 0.04% SiO_2, 0.36% CaO, 0% Fe_2O_3, 0% Al_2O_3, 46.73% $MgCl_2$, 52.87% L.O.I. and

99.60% $MgCl_2$+L.O.I. (= $MgCl_2 \cdot 6H_2O$). These result shows that high-quality magnesium chloride was successfully produced from waste magnesia powder. Thus, waste magnesite powder produced in the electrofilter installation of the ore processing plants can be recycled thus saving money. In addition, the waste powder is prevented from damaging the environment.

Experiment

Material

For the experiments the waste magnesite powder was obtained from the electrofilter output of the ore processing plant of the Kütahya Magnesite Enterprises Company, Turkey. In order to determine the properties of waste magnesite powder sample the chemical, physical and mineralogical tests were carried out. A wet chemical analysis method was used according to the ASTM C574-78 standard and the results were given in Table 1. In order to determine the particle size distribution of the waste magnesite powder, sieve analysis was carried out. Of the material 80% was of d_{80} size and the average grain size was considered to d_{50}. The results are given in Table 2. In order to determine the d_{80} and d_{50}, a cumulative undersize graph was drawn to analyze sieving results. The cumulative undersize chart is presented in Fig. 1, d_{80} and d_{50} are equal to 0.165 mm and 0.079 mm, respectively. In order to determine the mineralogical structure of the sample, X-Ray Diffraction (XRD) analysis was carried out and analysis of the results is given in Fig. 2. The leaching agent, purchased from Detsan, was 32% acid grade hydrochloric acid (10.17 M) having 1.159 g/cm^3 density.
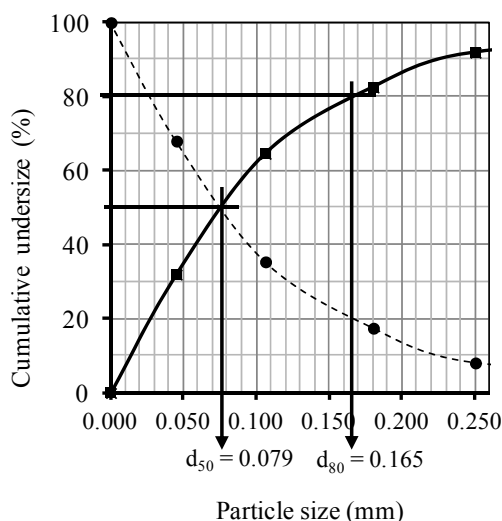
Fig. 1. d_{80} and d_{50} of the waste magnesite powder

Table 1. Chemical analysis of the waste magnesite powder

Compounds	Weights %
MgO	43.80
SiO_2	13.32
CaO	2.13
Fe_2O_3	2.35
Al_2O_3	0.65
L.O.I	37.75
Total	100.00

Table 2. Sieve analysis of waste magnesite powder

Size fraction (mm)	Weights (%)	Cumulative undersize (%) $\Sigma\uparrow$	Cumulative oversize (%) $\Sigma\downarrow$
−1+0.5	1.97	100.00	1.97
−0.5+0.250	6.15	98.03	8.12
−0.250 +0.180	9.38	91.88	17.50
−0.180+0.106	17.92	82.50	35.42
−0.106+0.045	32.60	64.58	68.02
−0.045+0	31.98	31.98	100.00
Total	100.00		
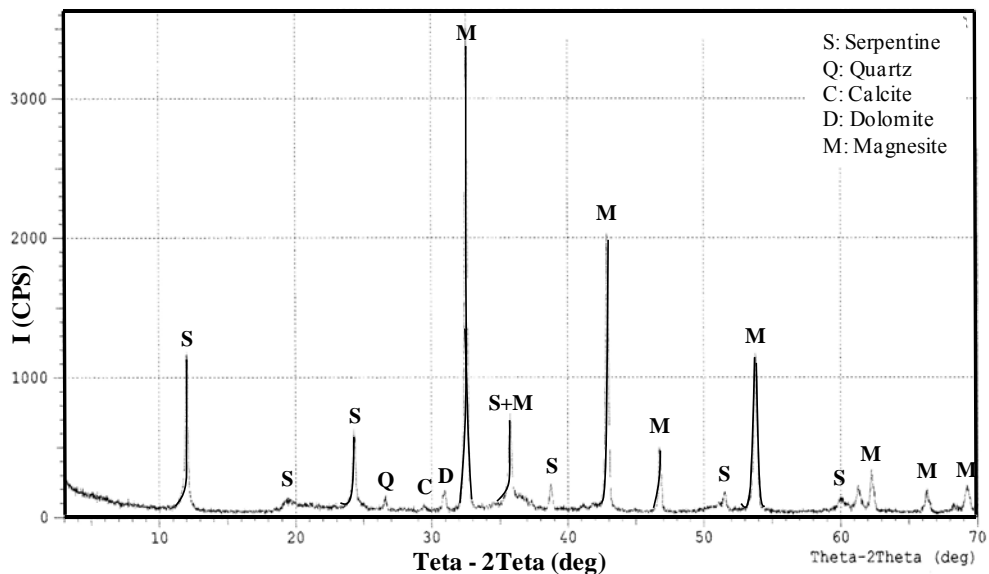
Fig. 2. XRD of the waste magnesite powder

Method

The HCl acid leaching method was used for the production of high-purity $MgCl_2$. The leaching experimental setup is shown in Fig. 3, and the leaching flow-chart is presented in Figure 4. The experimental parameters are leaching temperature, leaching time, amount of the acid, liquid-to-solid ratio, scale-up factor, acid concentration, particle size and mixing speed as shown in Table 3. The variable leaching parameters are: leaching temperature 30–40–50–60–70 °C, leaching time 60–120–180–240–300 min, amount of acid 100–110–120–130–140 cm^3, liquid–solid ratio 3.0/1–3.3/1–3.6/1 g/cm^3, and the scale–up factor 1–2–3–4–5. The acid concentration of 10.17 M, the average grain size 0.079 mm, the mixing rate of 60 rpm were determined and were applied as fixed leaching parameters. The required quantity of the waste magnesite powder and acid for leaching were calculated according to the stoichiometric formula and weighed. Water, waste magnesite powder and acid were fed sequentially into the leaching tank. The leaching tank was heated indirectly. At the end of the leaching process, the $MgCl_2$ solution was produced by separating the soluble and insoluble minerals using a filter paper. The optimum leaching conditions were determined as a result of the experiment. In order to determine the quality of magnesium chloride in optimum leaching conditions, chemical analysis was performed by wet chemical analysis method according to the ASTM C574-78 standard.

Results and discussion

Waste magnesite powder was received from the electro-filter of the ore processing plant in the Kütahya Magnesite Enterprises Company of Turkey. The results of chemical analysis of sample are given in Table 1. The amount of SiO_2 was 13.32%. The particle size of the sample was analyzed and the results are given in Table 2. Exactly 80% of the material passed through the sieve was d_{80} and d_{50} was the average grain size. The d_{80} and d_{50} were measured as 0.165 mm and 0.079 mm, respectively, and the results are given in Fig. 1. In order to determine the mineralogical structure of the sample, X-Ray Diffraction (XRD) analysis was made, and the results of the analysis are given in Fig. 2. According to the XRD chart the major mineral in the waste magnesite powder is magnesite, and minor minerals are serpentine, calcite, dolomite and quartz. The experimental setup of the magnesium chloride production is given in Fig. 3, and the flow chart is given in Fig. 4. Variable and fixed leaching experiment parameter values are given in Table 3.

In order to determine the quality of the magnesium chloride, chemical analysis was undertaken using a wet chemical analysis method according to the ASTM C574-78 standard. According to the results of the chemical analysis given in Table 5, the solution of magnesium chloride contained 0.04% SiO_2, 0.36% CaO, 0% Fe_2O_3, 0% Al_2O_3, 46.73% $MgCl_2$, 52.87% L.O.I. and 99.60% $MgCl_2$+L.O.I. (= $MgCl_2 \cdot 6H_2O$). Thus, the results show that high-purity magnesium chloride was produced from the waste magnesite sample.

N. Erdogan, E. Yersel, C. Celebi, N. Kavakli, T. Batar
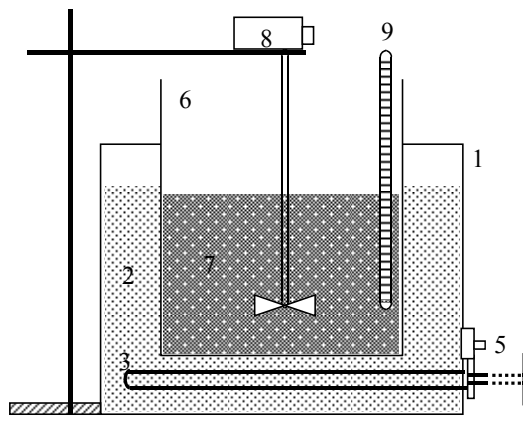
Fig. 3. Leaching experimental setup: 1 – water bath, 2 – water, 3 – heater, 4 – power supply,
5 – thermostat, 6 – glass beaker, 7 – solution, 8 – mixer, 9 – thermometer
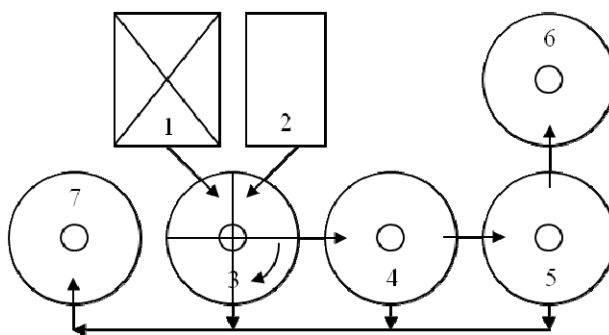
Fig. 4. Leaching flow sheet: 1 − waste magnesite powder tank, 2 – HCl acid tank,
3 – leaching tank, 4 – solution settling tank, 5 – solution settling tank,
6 – clean solution tank, 7 – waste (minerals) collection tank

Table 3. Parameters of leaching experiment

	Temperature change	Time change	Amount of acid change	Scale-up change
Leaching temperature ($^{\circ}$C)	30-40-50-60-70	70	70	70
Leaching time (min)	180	60-120-180-240-300	180	180
The amount of acid (cm^3)	130	130	100-110-120-130-140	130
Liquid-to-solid ratio (cm^3/g)	3.6/1	3.6/1	3.0/1; 3.3/1; 3.6/1	3.6/1
Scale-up factor	1	1	1	1-2-3-4-5
Acid concentration (M)	10.17	10.17	10.17	10.17
The average particle size; d_{50} (mm)	0.079	0.079	0.079	0.079
Mixing speed (rpm)	60	60	60	60

Table 4. Optimum leach parameters

Parameters	values
Leaching temperature ($^{\circ}$C)	70
Leaching time (min)	180
The amount of acid (cm^3)	130
Liquid-to-solid ratio (cm^3/g)	3.6/1
Scale-up factor	1
Acid concentration (M)	10.17
The average particle size; d_{50} (mm)	0.079
Mixing speed (rpm)	60
Leach yield (%)	96.72

Table 5. Chemical analysis results of the magnesium chloride solution

Compounds	Weights %
$MgCl_2$	46.73
SiO_2	0.04
CaO	0.36
Fe_2O_3	0
Al_2O_3	0
L.O.I.	52.87
Total	100.00
$MgCl_2$+L.O.I. = $MgCl_2.6H_2O$	99.60
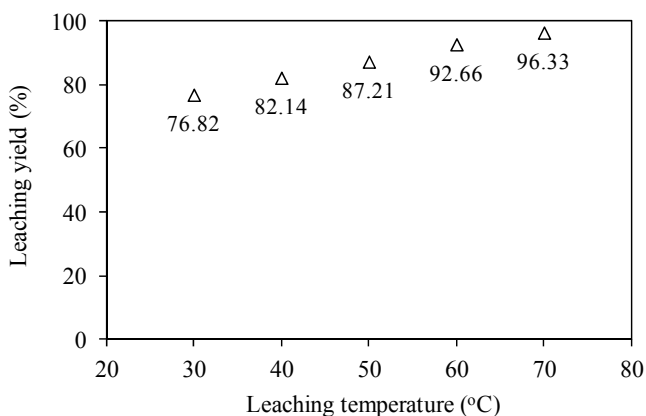
Fig. 5. Leaching yield in relation to leaching temperature
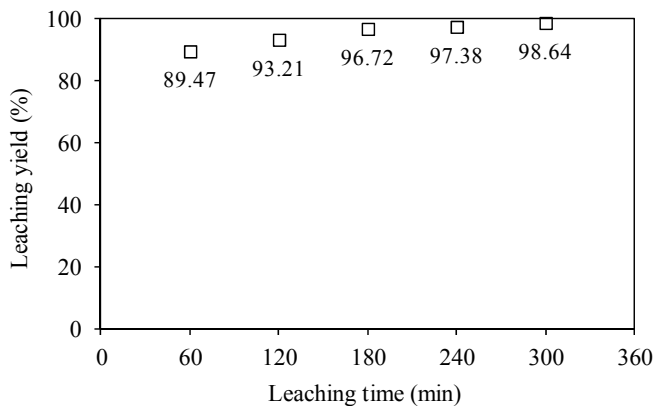
Fig. 6. Leaching yield in relation to leaching time
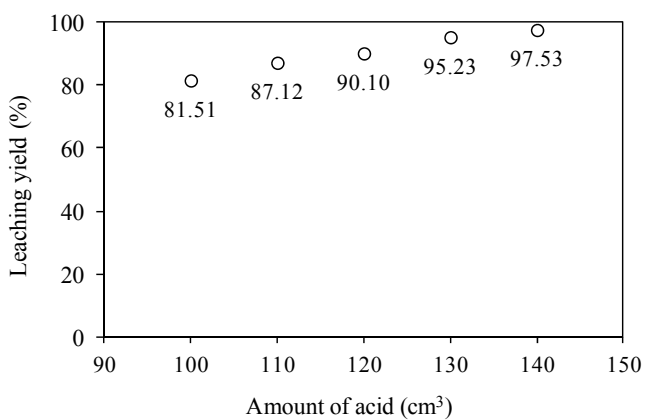
Fig. 7. Leaching yield in relation to amount of acid
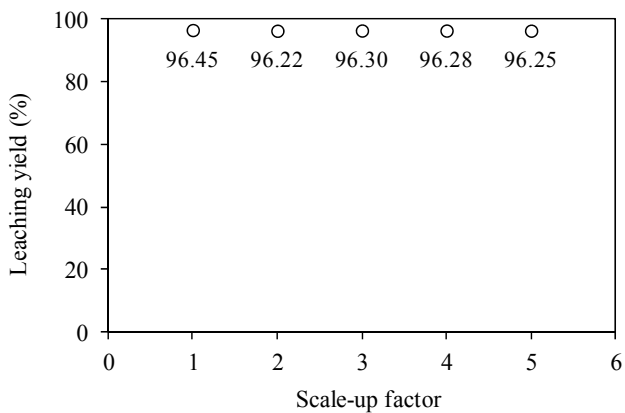
Fig. 8. Leaching yield in relation to the scale-up factor

Chou et al. (1989) investigated the dissolution of various carbonates (including calcite, magnesite and dolomite) in HCl solutions at 25 °C using coarse particle size samples. However, in this study a fine particle sample of waste magnesite was analyzed at 70 °C. Abali et al. (2006) investigated the optimum conditions for dissolution of magnesite with H_2SO_4 solutions. They reported that the optimum conditions were found to be 65 °C, 5/100 g/cm^3, 2M, 60 min and 300 rpm. In the current study the optimum conditions were; leaching temperature 70 °C, leaching time 180 min, the amount of acid 130 cm^3, liquid-to-solid ratio 6.3 cm^3/g, the acid concentration 10.17 M and a mixing speed of 60 rpm. Abdel-aal at el. (1996) analyzed Egyptian magnesite ore (43.32% MgO) from the Eastern Desert leached with aqueous hydrochloric acid. They reported that the optimum conditions of leaching were ore particle size –0.5 mm, temperature 60 °C, leaching time 15 min, HCl to MgO molar ratio 1.06, and liquid/solid ratio of 2.5:1 cm^3/g, recovery 99.1% MgO. By contrast, in this study optimum conditions were; average particle size 0.079 mm, temperature 70 °C, leaching time 180 min, liquid-to-solid ratio 6.3 cm^3/g, recovery 99.60% $MgCl_2$+L.O.I (= $MgCl_2 \cdot 6H_2O$).

In the current study from very fine waste material $MgCl_2 \cdot 6H_2O$ was produced with the yield of 99.60% containing no Al_2O_3 and no Fe_2O_3.

Conclusions

The aim of this study was to investigate the optimization of waste magnesite powder using leaching in hydrochloric acid solutions, to produce high-quality magnesium chloride, and thus, recycle waste magnesite powder. The experimental parameters were: leaching temperature, leaching time, amount of acid, liquid-to-solid ratio, scale-up factor, acid concentration, particle size and mixed speed. The experiments were carried out under reproducible conditions. On completion of the experiments, the optimum leaching parameter levels were found to be temperature 70 °C, leaching time 180 min, amount of acid 130 cm^3, liquid-to-solid ratio 3.6 cm^3/g, scale-up factor 1, acid concentration 10.17 M, average particle size 0.079 mm and mixing speed 60 rpm. Under the optimum leaching conditions, the yield was 96.72% and pH 8. The produced $MgCl_2$ solution consisted of 0.04% SiO_2, 0.36% CaO, 0% Fe_2O_3, 0% Al_2O_3, 46.73% $MgCl_2$, 52.87% L.O.I. and 99.60% $MgCl_2$+L.O.I. (= $MgCl_2 \cdot 6H_2O$). These results show that high-quality magnesium chloride can be successfully produced by recycling waste magnesite powder. In addition to protecting the environment by reducing the amount of waste this process has economic benefits.

Acknowledgments

References

ABALI Y., COPUR M., YAVUZ M., 2006, *Determination of the optimum conditions for dissolution of magnesite with H_2SO_4 solution*, Indian Journal of Chemical Technology, Vol 13, July 2006, 391–397.

ABALI Y., BAYCAN S., ARISOY K., VAIZOGULLAR A., 2011, *Optimization of Dolomite Ore Leaching in Hydrochloric Acid Solutions*, Physicochem. Probl. Miner. Process. 46 (2011) 253–262.

ABDEL-AAL E. A., IBRAHIM I. A., RASHAD M. M., ISMAIL A. K., 1996, *Hydrometallurgical processing of Egyptian magnesite ore*, Physicochemical Problems of Mineral Processing, 30 (1996) 207–216.

ATAK S., 1982, *Flotasyon uygulamaları ve ilkeleri* (in Turkish), ITU, Istanbul.

BREUSCH, F. L., ULUSOY, E., 1987, Genel ve Anorganik Kimya, (in Turkish), İstanbul.

CHOU L., GARRELS R. M., WOLLAST R., 1989, *Comparative study of the kinetics and mechanism of dissolution of carbonate minerals*, Chem. Geology, 78: 269–282.

DONMEZ B., DEMIR F., LACIN O., 2009, *Leaching kinetics of calcined magnesite in acetic acid solutions*, Journal of Industrial and Engineering Chemistry 15 (2009), 865–869.

ERDOGAN N., 2002, *Kumas Elektro-Filtre Manyezit Tozu Artıklarından Magnezyum Bilesikleri (Magnezyum Oksit, Magnezyum Hidroksit, Magnezyum Klorür ve Magnezyum Diborit) Üretimi*, (in Turkish) PhD, Osmangazi University, 180, Eskisehir, Turkey.

HARRIS G. B., PEACEY J. G., MONETTE S., 1988, *Manufacture of concentrated magnesium chloride solution from magnesite for production of magnesium*, Chem. Abst., 109: 24855c.

KAYA M., 1993, *Magnezit ve Bazik Refrakter Teknolojisi*, (in Turkish), Publications of Anadolu University, 450, Eskisehir, Turkey, p. 290

OZBEK H., ABALI Y., ÇOLAK S., CEYHUN I., KARAGOLGE Z., 1999, *Dissolution kinetics of magnesite mineral in water saturated by chlorine gas*, Hydrometallurgy, 51: 173.

OZDEMIR M., CAKIR D., KIPCAK I., 2009, *Magnesium recovery from magnesite tailings by acid leaching and production of magnesium chloride hexahydrate from leaching solution by evaporation*, Int. J. Miner. Process. 93 (2009), 209–212.

PALCO S., RIGUAD M., 2002, *Metallurgy refractories and environment conference*, Slovakia: Technical University of Kosice, p. 275

SHIKANO H., 1998, *Refractories handbook*, Japan, Technical Association of Refractories, p. 127.

A STUDY ON HEAVY METALS MOBILITY FROM ZINC PLANT RESIDUES IN IRAN

Davood MORADKHANI[*]**, Shahla ESKANDARI**[*]**, Behzad SEDAGHAT**[**]**, Majid RAJAIE NAJAFABADI**[**]

[*] Faculty of Engineering, Zanjan University, Zanjan, Iran, sh_eskandari8@yahoo.com (S. Eskandari)
[**] R&D Center, Research & Engineering Co. for Non-ferrous Metals (RECo), Zanjan, Iran

Abstract: The transport of heavy metals from mining disposal site to groundwater and surface water is one of the most serious environmental problems in the world. The transport of heavy metals such as Zn, Cd and Mn from leaching filter cake in RECo, Zanjan, Iran was examined by using column leaching. Parameters studied included: flow rate, pH of input solution and leaching time. In this study, the maximum dissolution percents of Zn, Cd and Mn in input solution pH of 5 were 45.50 %, 53.97% and 19.94%, respectively. To statistically analysis the experimental results, SPSS14 software was employed. The results of SPSS 14 indicated that for the Zn, Cd and Mn dissolution, time and flow rate were found respectively, the effective parameters for the pollution in zinc leach residues.

Keywords: heavy metals, zinc leaching plant, leaching filter cake, column leaching

Introduction

Metals are released into the environment at increasing rates by mining, industry, and agriculture, causing serious problems for environmental and human health (Li et al, 2000; Tang and Zhao, 2005).

Large areas of agricultural soils are contaminated by heavy metals that originate mainly from former or current mining activities, industrial emissions, or the application of sewage sludge. Elevated heavy metal concentrations in the soil can lead to enhanced crop uptake. Excessive metals in human nutrition can be toxic and can cause acute and chronic diseases (Geldmacher, 1984).

Cadmium and zinc for example, can lead to acute gastrointestinal and respiratory damage and acute heart, brain, and kidney damage (Friberg et al., 1986).

The production of non-ferrous metals from primary and secondary material results in the generation of a wide variety of wastes and residues. They are a result of the metals separation that is necessary for the production of pure metals from complex

sources. These wastes and residues arise from the different stages of processing as well as from the off-gas and water treatment systems (Florijn and Van Beusichem, 1993; Hatch Associates Ltd., 2000; Ross, 1994; Wentz, 1989).

The transfer of heavy metals from soils to plants is dependent on three factors: the total amount of potentially available elements (quantity factor), the activity as well as the ionic ratios of elements in the soil solution (intensity factor), and the rate of element transfer from solid to liquid phases and to plant roots (reaction kinetics) (Brümmer et al., 1986).

A leach-electrolysis process for zinc production is practiced in zinc plant located in Zanjan, Iran. In that process a lot of filter cakes as by-product are generated daily. These wastes are retained for valuable elements recovery in the future and dumped in open stockpiles where they may cause heavy metal pollution problems. In these plants three types of wastes were produced: leaching filter cake, cobalt purification filter cake and Ni-Cd purification filter cake. All of the filter cakes have a high percent of heavy metal (Hakami, 2005).

In this study the metal releasing potential of zinc production by-products was investigated. The aim of this study is to discuss the leaching behavior of heavy metal in zinc plant residue (leaching filter cake) with special attention to the effects of input pH, input flow rate and leaching time on leachability of zinc, cadmium and manganese.

Materials and methods

Materials

Leaching filter cake for this study was obtained from Research & Engineering Co. for Non-ferrous Metals, Zanjan, Iran. After drying, the filter cake was ground and sieved to +200 mesh (74 μm). The chemical analysis was carried out by Perkin-Elmer AA300 model atomic absorption spectrophotometer. The analytic results were given in Table 1.

Table 1. Chemical analysis of leaching filter cake

Component	Zn	Pb	Fe	Mn	Co	Ni	Cd	Ca	Mg
Wt.%	7.55	8.13	2.35	0.14	0.02	0.02	0.09	7.67	0.27

Also XRD analysis of the sample was done and the results are shown in Fig. 1. Sulfuric acid was used to adjust the solution pH as required. Figure 2 demonstrates the process in which the leaching filter cake is produced.
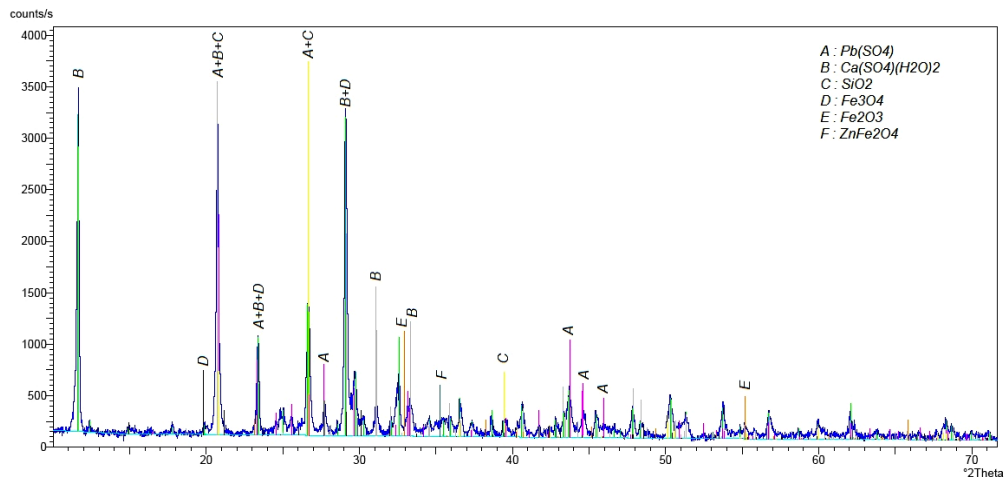
Fig. 1. X-ray diffraction analysis of the leaching filter cake used in the study
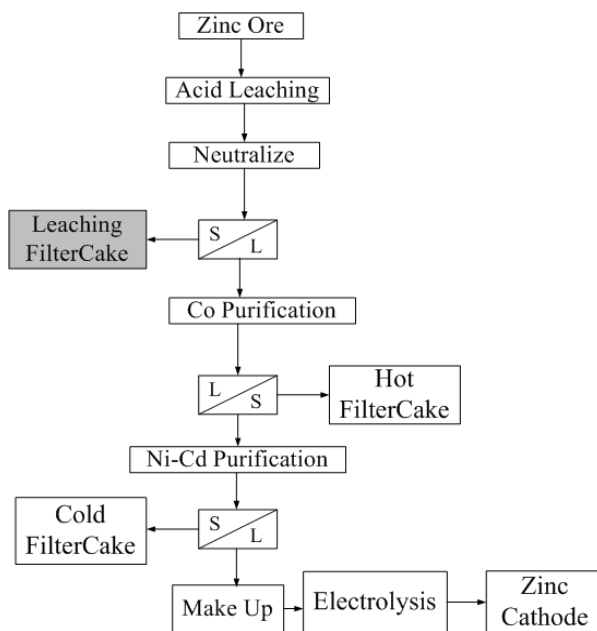
Fig. 2. Flow diagram of Filter Cake production in zinc plant used in this study

Experimental method

For experimental design and determining the important factors which affect the leach-ability of residual, the conventional method was used. In this study columns with 6 cm diameter and 50 cm length from Plexy glass were employed. A 2–4 cm layer of washed and dried sand with a Whatman paper was put at the end of each column.

About 875 g of dried leaching filter cake was placed. To attain uniform distribution of leaching solution a layer of fiber-glass between two Whatman papers were used in the top of each column. Process variables were pH of input solution, rate of input solution and leaching time. Table 2 shows the variation intervals for these parameters. Acid sparking time was 24 hours a day. During this time output solution was collected in a container to prepare reagent samples for measurements of Zn, Cd and Mn concentration after 2, 4, 6, 10, 15 and 20 days.

Table 2. Variation intervals of experimental parameter for the filter cake leaching

Parameter	Value					
Flow rate(cm^3/min)	0.5	1	2	–	–	–
Input pH	5	6	7	–	–	–
Leaching time (days)	2	4	6	10	15	20

Results and discussion

Effect of pH of input solution

The effect of input solution pH on the dissolution of Zn, Cd and Mn are shown in Figs 3, 5 and 7. Based on the pH of rain water in Zanjan city, three input solution pHs of 5, 6 and 7 were selected. The maximum dissolution of Zn, Cd and Mn was observed after two days with the input solution pH of 5 and the flow rate of 1 mm/min. They were equal to 26554.6 mg/dm^3, 365.5 mg/dm^3 and 232.7 mg/dm^3, respectively. The results shown in Figs 3, 5 and 7 indicate that the concentration of above mentioned metals decrease with increasing leaching time up to 20 days then reaches constant rate.
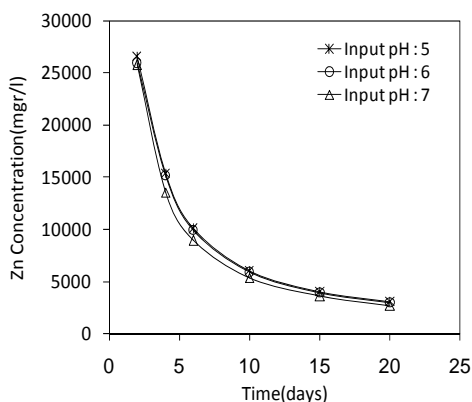
Fig. 3. Effect of input pH on the Zn dissolution
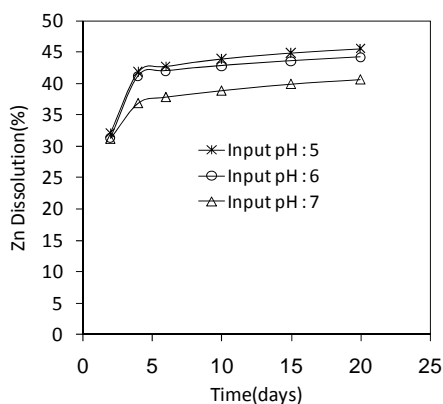
Fig. 4. Zn dissolution percentage
at three different input pH
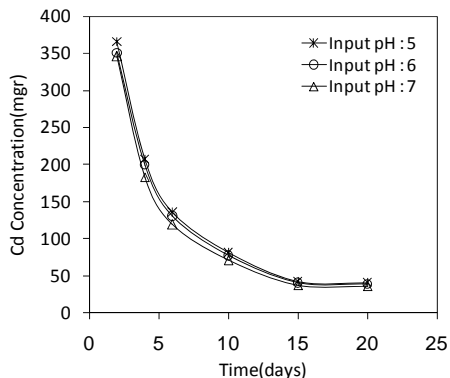
Fig. 5. Effect of input pH on the Cd dissolution
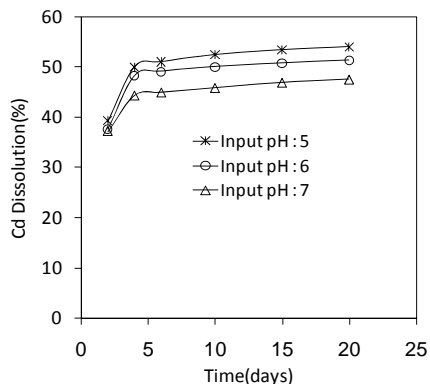
Fig. 6. Cd dissolution percentage
at three different input pH
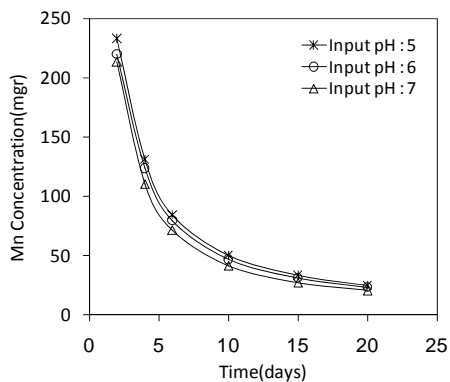
Fig. 7. Effect of input pH on the Mn dissolution
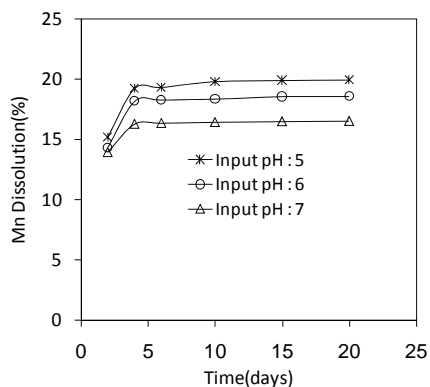
Fig. 8. Mn dissolution percentage
at three different input pH

Figs 4, 6 and 8 show that the maximum dissolution percentages of Zn, Cd and Mn in input solution were attained at pH 5 and were 45.50%, 53.97% and 19.94%, respectively. The batch experiments showed that the dissolution percentage of Zn, Cd and Mn increased with increasing leaching time to 4 days, whereas the mentioned metals dissolution percentage did not change significantly with leaching time to 20 days.

Effect of input flow rate

Figures 9, 11 and 13 illustrate the effect of flow rate on the dissolution of Zn, Cd and Mn. Three flow rates of 0.5, 1 and 2 cm^3/min were selected. The maximum dissolution of Zn, Cd and Mn was achieved after two days with the flow rate of 0.5 ml/min and pH of 5 and amounted to 40527.3 mg/dm^3, 548.6 mg/dm^3 and 314.5 mg/dm^3, respectively.
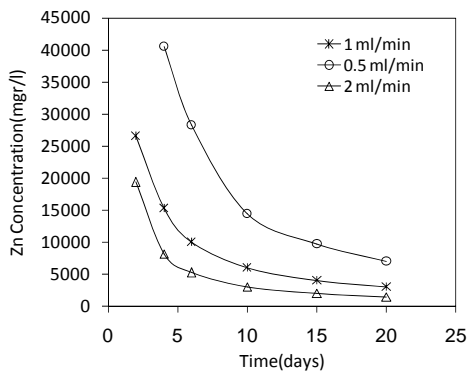
Fig. 9. Effect of flow rate on the Zn dissolution
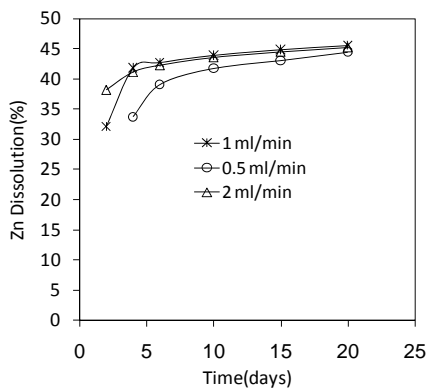
Fig. 10. Zn dissolution percentage
at three different flow rates
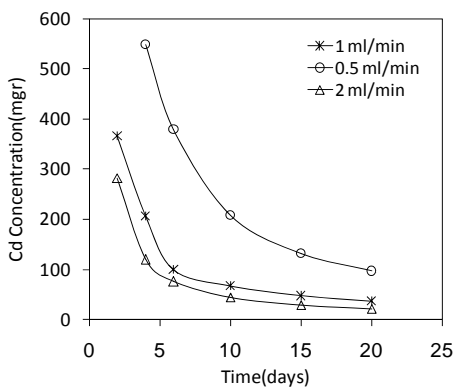
Fig. 11. Effect of flow rate on the Cd dissolution
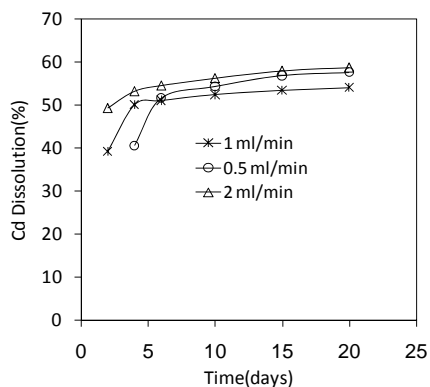
Fig.12. Cd dissolution percentage
at three different flow rates
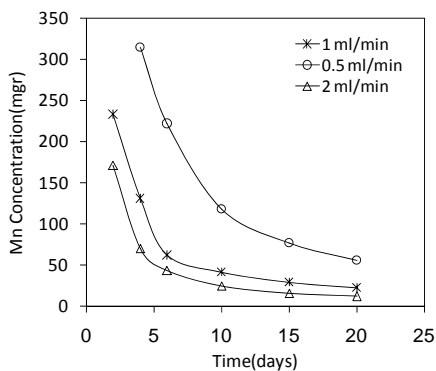
Fig. 13. Effect of flow rate on the Mn dissolution
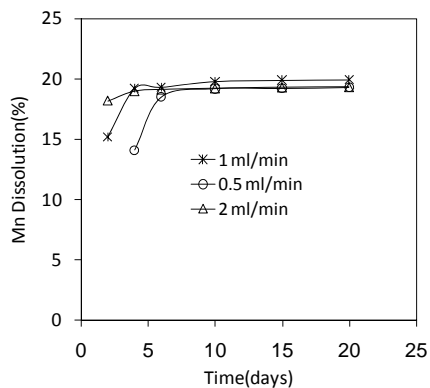
Fig. 14. Mn dissolution percentage at three
different flow rates

As can be seen in Figs. 10,12 and14 the maximum dissolution percentages of Zn, Cd and Mn were attained at the flow rate of 1 ml/min and were 45.50%, 53.97% and 19.94%, respectively. As shown in those figures the results indicate that the dissolution percentages of above mentioned metals increase with increasing leaching time up to 4 days and then reaches a constant rate.

Experimental equation for estimation of dissolution percentage

The volume of solutions obtained from the columns in sampling days was determined. Zn, Cd and Mn content of each solution was measured. Basing on equation (1) the dissolution percentages of Zn, Cd and Mn were calculated

$$D = \frac{\text{volume of output solution} \times \text{element concentration}}{\text{weight of sample} \times \text{grade}} \times 100 . \tag{1}$$

The influence of flow rate, input pH and leaching time on the dissolution percentage was statistically analyzed by SPSS14 software using a multi-variable linear model. The relation between the dissolution percentages of elements and mentioned factors such as input pH, flow rate and leaching time was investigated.

The equation for dissolution percentage of zinc is given below:

$$D_{Zn} = -0.053H + 0.266Q + 0.528t \tag{2}$$

where H is input pH, Q is flow rate and t is leaching time.

For the dissolution percentage of cadmium the equation is:

$$D_{Cd} = -0.151H + 0.318Q + 0.508t. \tag{3}$$

The equation for dissolution percentage of manganese is:

$$D_{Mn} = -0.163H + 0.268Q + 0.412t. \tag{4}$$

As can be seen in the equations (2)–(4) the effective parameters governing transport of Zn, Cd and Mn to the environment are time and flow rate.

Conclusion

Experiments were carried out to investigate the effect of input pH, input flow rate and leaching time on the leaching behavior of heavy metals such as zinc, cadmium and manganese from zinc plant residue (leaching filter cake) to environment. A maximum dissolution of zinc, cadmium and manganese was obtained at following condition: flow rate of 1 ml/min, input pH 5 and leaching time 4 days. In this study, the most important parameters for dissolution of zinc, cadmium and manganese are time and flow rate, respectively, in range studied.

Acknowledgements

References

BRÜMMER G., GERTH J., HERMS U., 1986, Heavy *metal species, mobility and availability in soils*, Z. flanzenernaehr. Bodenkd. 149, 382–398.

FLORIJN P.J., VAN BEUSICHEM M.L., 1993, *Uptake and distribution of cadmium in maze inbred lines*, Plant Soil 150, 25–32.

FRIBERG L., NORDBERG G.F., VOUK V.B., 1986, *Handbook on toxicology of metals*, 2nd ed. Elsevier, Amsterdam.

GELDMACHER V.M., 1984, *Meaning of the heavy metals in the toxicology (In German)*, Fresenius' Z. Anal. Chem. 317, 427–432.

HAKAMI A.R., 2005, *Report of zinc production in R&D center*, IZMDC, Report No.224, 1–10.

HATCH ASSOCIATES LTD, 2000, *Review of Environmental Releases for the Base Metals Smelting Sector*, prepared for Environment Canada, PR36242.002

LI X.D., WAI O.W.H., LI Y.S., COLES B.J., RAMSEY H., THORNTON I., 2000, *Heavy metal distribution in sediment profiles of the Pearl River estuary*, *South China*, Appl. Geochem. 15, 567–581.

ROSS S.M., 1994, *Toxic metals in soil–plant systems*, John Wiley & Sons, Chichester, UK.

TANG X., ZHAO L., 2005, *The development of sludge disposal strategy*, Environ. Sci. Manag. 30, (68–70) 90.

WENTZ C.A., 1989, *Hazardous Waste Management*, McGraw-Hill, New York.

THE EFFECT OF ZETA POTENTIAL
ON THE SEDIMENTATION BEHAVIOR
OF NATURAL STONE PROCESSING EFFLUENT

Haldun KURAMA[*], Cengiz KARAGUZEL[**]

[*] Eskişehir Osmangazi University, Mining Engineering Department, e-mail: hkurama@ogu.edu.tr
[**] Dumlupınar University, Mining Engineering Department

Abstract: One of the main problems for the natural stone industry is treatment of huge amount of waste sludge resulting from the cutting and polishing of them to produce slabs or tiles. The effective treatment of this sludge is very important for reducing of the sludge volume and overall operating costs. Previous studies showed that settling rate and water clarity of the supernatant solution can be increased by flocculation process. In this study, detailed electrokinetic studies were performed on the travertine samples received as natural and slurry form. The natural form of the sample was supplied from a travertine quarry while the slurry was taken from the cutting and polishing process wastewater collector pool of the processing plant. The electrokinetic measurements were conducted to find out the effect of suspension pH and the solid content on the surface potential of solid particles show that zeta potential (ζ) of travertine is positive at pH 9.76 over the all solid contents studied in this work. However, ζ of the particles become negative at lower pH values for 1% solid weight content. In contrast, for travertine slurry (6.73% solid weight), different potential variations were determined. The particles were negatively charged between pH 6 and 8. The results highlighted the effect of dissolved specific ions in the waste slurry and sensitivity of ζ to the ionic strength of the solution. The ζ measurements for a raw travertine sample, performed with different amounts of NaCl additions into the solutions, confirmed the above findings. An addition of low amounts of NaCl decreases ζ of the solid surface. Finally, the ζ measurements in the presence of polymer concentration of 0.001% to 0.1 % (wt/vol) clearly indicated that the flocculant molecules are adsorbed extensively on the travertine particles, and increase the surface potential of the particles with increasing reagent concentration.

Keywords: travertine, environment, stone industry, zeta potential

Introduction

The natural stone industry is one of the oldest in the world. The history of natural stone usage goes back to the ancient time. In fact, two of the Seven Wonders of the Ancient World were built by using Turkish natural stone (Çelik and Sabah 2008). In

recent years, although much of the international attention in the natural stone industry has been centered on China and India, Turkey is still an important player in the market with a capable of producing over 5 million m^3 of natural stone block. The color and texture qualities compared to other producers and higher travertine reserves provide many advantages to Turkey in the world travertine market. Especially, the Denizli travertine is a very special natural stone mined in limited number of countries in the world (Çobanoğlu and Çelik 2012; Barutçu 2008).

Nowadays, one of the main problems for the natural stone industry in Turkey is the treatment of huge amount of waste sludge resulting from the cutting and polishing of them to produce slabs or tiles. The presence of fine particles in recycled water due to inefficient solid–liquid separation of waste sludge causes several problems. An effective treatment of the sludge is very important for reducing the sludge volume, obtained water quality and overall operating costs. Previous studies concerned the sedimentation of fine particles in waste effluents, for both travertine and marble, showed that settling rate and water clarity of supernatant solution can be increased by using anionic polyelectrolytes. The efficiency of the flocculation process is strongly affected by flocculation pH and the anionic degree of polymers (Bayraktar et al. 1996; Seyrankaya et al. 2000; Arslan et al. 2005; Ersoy et al. 2009). In a recent study performed by Taşdemir and Kurama, (2012), it was confirmed that the solid content, particle size and flocculation polymer type are effective parameters in settling of the suspended particles. However, it was reported that the origin of the slurry and chemical composition of natural stones, especially travertine samples, strongly affect the sign and magnitude of surface potential, and hence sedimentation rate of the solid particle present in the effluents. Therefore, in this study, detailed electrokinetic studies were performed on travertine samples in natural and slurry form. The development of surface charge was discussed taking into account dissolved species, solid content, suspension pH and polymer concentration.

Material and method

Material

Raw and travertine slurry samples used in this study were supplied by Nasip Marble Company (Denizli, Turkey). The natural form of the sample (NT) was supplied from a travertine quarry while the slurry was taken from the cutting and polishing process wastewaters collector pool of the processing plant. The tile and slab production capacity of the processing plant is 250.000 m^2 per year. The Denizli basin is an important region not only in Turkey but also in the world. In the early 1980s, Denizli had only a few quarries, but today the city became an important travertine production and marketing place with approximately 82 travertine and marble processing plants. These plants process a variety of travertine and marbles supplied from their quarries.

The raw travertine sample was firstly crushed and ground in a porcelain ball mill in order to decrease its size for electrokinetic measurements. The chemical composition,

determined by the X-Ray fluorescence (XRF), and the physical properties of representative sample is given in Table 1. As can be seen from Table 1, the raw sample mainly consists of $CaCO_3$ with a little amount of MgO, SiO_2 and Fe_2O_3.

The solid content of the slurry was determined by filtering the sample through blue band filter paper. The separated solid was then dried in an oven at 100 ^oC and weighted to calculate the solid weight %. The solid weight content and the turbidity of the slurry were determined as 6.73% solid weight and >2000 NTU, respectively. The particle size distribution analysis of the particles present in slurry was performed using a Malvern Mastersizer 2000. It was found that 50% of particles were smaller than 40 μm.

Table 1. Chemical and physical analysis results of travertine

Component	%	Property	
MgO	0.56	Specific bulk density, g/cm^3	2.339
SiO_2	0.32	Specific gravity, g/cm^3	2.73
SO_3	0.28	Porosity, %	0.28
CaO	55.00	Water absorption, %	5.51
Fe_2O_3	0.17	Surface area-(BET), $m^2 \, g^{-1}$	3.22
LOI	43.67		

Experimental procedures

Electrokinetic measurements of the samples were performed by the electrophoretic method using Zetasizer Nano ZS (Malvern Inst, UK). In each measurement, the suspension was prepared by placing predetermined amount of solid sample, 1, 3, 5, and 10% solid weight, into the 100 cm^3 beaker or for slurry sample, a 50 cm^3 of suspension was placed on a magnetic stirrer, stirred for 10 min and kept for 2 min to allow the coarser particles to settle. Then, 2 cm^3 of solution was taken from the upper part of the beaker, transferred to a closed measurement cell and the zeta potential (ζ) was measured.

In flocculation measurements anionic polymer SPP510 of high molecular weight was used as flocculant. A 1 dm^3 portion of the flocculant stock solution was prepared with distilled water and pre-determined amounts were added to the sample solutions.

Results and discussion

Solubility and gravity settling of travertine particles in waste slurry

The term travertine generally means carbonate rocks (limestone) deposited by supersaturated alkaline mineral waters. Calcium carbonate is poorly soluble in pure water, however, if the pH of the solution decreases, solubility increases due to the increasing carbonic acid concentration in the solution (Lide, 2005).

$$CaCO_3 (s) \leftrightarrow Ca^{2+}(aq) + CO_3^{-2}(aq) \quad Ksp = 5.10^{-9} \quad (1)$$

$$H_2O + CO_2 \leftrightarrow H_2CO_3 \quad (2)$$

$$CaCO_3 + H_2CO_3 \leftrightarrow Ca^{2+} + 2\, HCO_3^-. \quad (3)$$
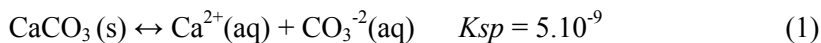
The solubility test performed with a supernatant consisting of 5 to 15% solid showed that Ca^{2+} and Mg^{2+} ion concentrations of solutions slightly increase with increasing solid content and contact time, however, in general, it can be concluded that the concentrations of calcium and magnesium ions are independent of the solids content.

The movement of the sludge zone as a function of settling time is given in Figure 1. It was found that sedimentation of fine particles in waste slurry completed within 10 min of setting time. Although the sedimentation process is considered as rapid, the turbidity measurement of the upward water zone shows that it still contains suspended particles, 455 NTU.
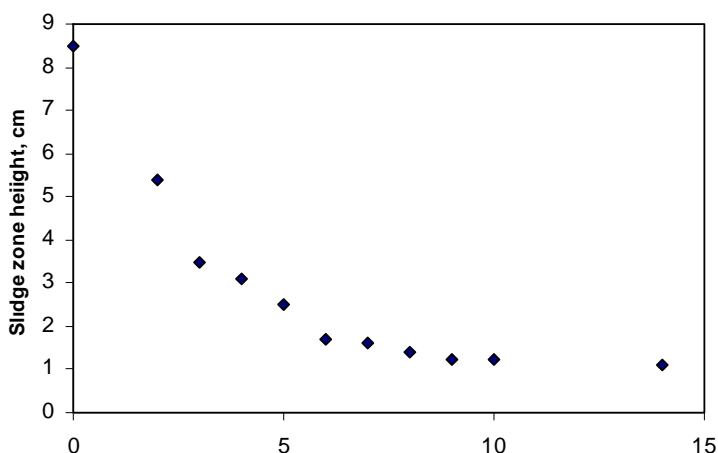
Fig. 1. Gravity settling of travertine particles in waste slurry as function of settling time

Electrokinetic measurements

The effect of the solid content and the pH variation of the solution on ζ potential of the raw travertine sample are given in Fig. 2 and Fig. 3, respectively. It was found that the ζ potential of travertine particles is positive over the whole solid contents range at pH 9.76. The values of ζ potential increase, with increasing solid content from 2.64 mV, to 7.62 mV (for 5% solid weight). A further increase in solids content, resulted in a slight decrease of ζ potential. This could be attributed a small variation of the equilibrium condition of $CaCO_3$ in water with increased solid content.
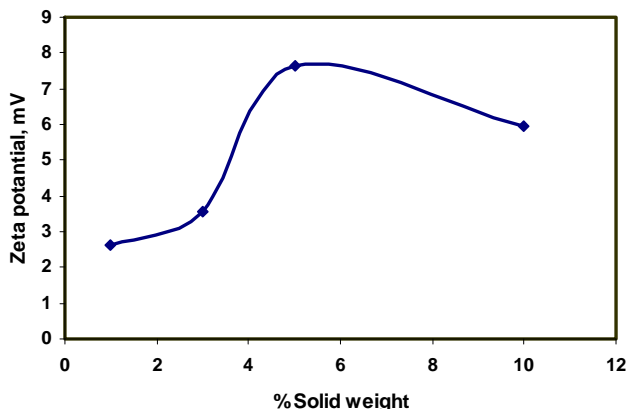
Fig. 2. Zeta potential variation of travertine sample against to solid percent at pH 9.76

The electrokinetic behavior of the $CaCO_3$-water system has been widely studied in literature. It was pointed out that the dissolution of $CaCO_3$ in water (Eq. 1) is affected by small difference in equilibrium condition, modification of solution pH and the hydrolyzing reactions of the dissolved ions. These effects cause variations of both sign and magnitude of ζ potential according to the possible reactions which can be given as follows

$$CO_3^{2-} (aq) + H_2O \leftrightarrow HCO_3^- (aq) + OH^- (aq) \quad K = 10^{-3.7} \tag{4}$$

$$Ca^{2+} (aq) + H_2O \leftrightarrow Ca(OH)^+ (ag) + H^+ (aq) \quad K = 10^{-12.9} \tag{5}$$

$$Ca^{2+} (aq) + HCO_3^- (ag) \leftrightarrow CaHCO_3^+ (aq) \quad K = 10^{1.1}. \tag{6}$$
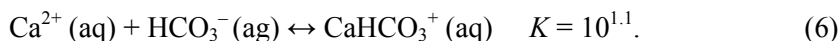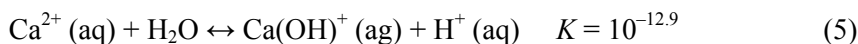
The Ca^{2+}, CO_3^{2-} and hydrated or hydroxylated species of these ions, such as HCO_3^-, $Ca(OH)^+$, and $CaHCO_3^+$ are considered the major potential determined ions (PDI) while H^+ and OH^- ions are secondary PDI and act as a regulator of concentration of particular anions (Eriksson et al., 2007). Except the above parameters, the measurement methods also play an important role in determine the ζ potential of surface. Recently, Moulin and Roques (2003) reviewed previous findings obtained by different researchers and concluded that the sign of the measured ζ potential is positive, negative, or variable, depending on the measurement conditions, contribution of solubility products, hydrolyzing reactions and availability of foreign ions.

The electrokinetic results given in Fig. 3 indicated that ζ potential of travertine particles have two isoelectrical points (IEP) and the potential values changed between -3 to $+3$ mV as a function of the solution pH. The ζ potentials slightly move to lower potentials (as negative) with increasing OH^- concentration of the solution. It is approaching the second IEP at about pH 9.4 and than further increase with solution pH leading to positively charged surface.
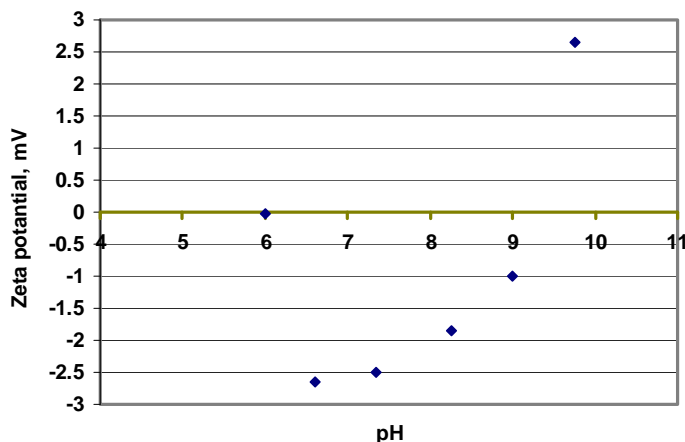
Fig. 3. Variation of zeta potential of travertine sample against solution pH
at a solid content of 1%

The decrease of negative potential with increases of pH may be attributed to the possible reaction given below. With increasing pH the surface charge becomes more negative and ζ potential has to decrease. The positive sign can be due to the adsorption of protons. However, we should consider the contribution of foreign cations and anions or organic impurities adsorbed on the particle surface generally observed for natural travertine and calcite samples.

$$CO_3H^-_{surface} + H^+ \leftrightarrow CO_3H^{+2}_{surface} \quad \text{(Moulin and Roques, 2003)} \qquad (7)$$

The previous study performed by Vdovic (2000) dealing with the electrokinetic behavior of both natural and synthetic forms of calcite showed that synthetic calcite has positive ζ potential at pH of pH_{IEP} 8.4, which decreases with either the increase or decrease of pH. Natural calcite, in contrast, has negative ζ potential throughout the investigated pH range of 6–10.

On the other hand, a slight decrease of the negative ζ potential of surface at lower pH values can be attributed to the adsorption of the hydrated carbonate ions in the electric double layer which are closer to the surface of the mineral (inner the Helmholz layer), while calcium ions remain in the outer layer as previously reported by Siffert and Fimbel (1984). When the dispersed mass of $CaCO_3$ in solution is increased, the surface contact with the water phase becomes sufficiently large to ensure rapid equilibrium. Under this condition, certain surface Ca^{2+} cations hydrate until the equilibrium in solution is attained. The surface Ca^{2+} ions are smaller than CO_3^{2-} ions and impart a positive charge to the surface. If dissolution process is still in progress, the absolute values of ζ potential could be a consequence of non-simultaneous detachment of the constituent ions from the surface. Higher loss of $CaOH^+$ than CO_3H^- during dissolution of calcite could explain more negative surface when the system has not yet reached the equilibrium (Stipp and Hochella, 1991).

Rather than the above conclusions, the effect of shrinkage of solid particle and the diminution of the surface on the potential variations with dissolution process, especially lower amount of sample is used, could also be concerned. Calcite or travertine grains in contact with water tend to reach the equilibrium by releasing a certain amount of their constituent ions in the solution. If a smaller quantity of sample is used or if the pH decreases than the IEP, the dissolution will cause a diminution of grains, and consequently the diminution of the available surface area, and ζ- potential of the surface becomes more negative (Moulin and Roques, 2003) .
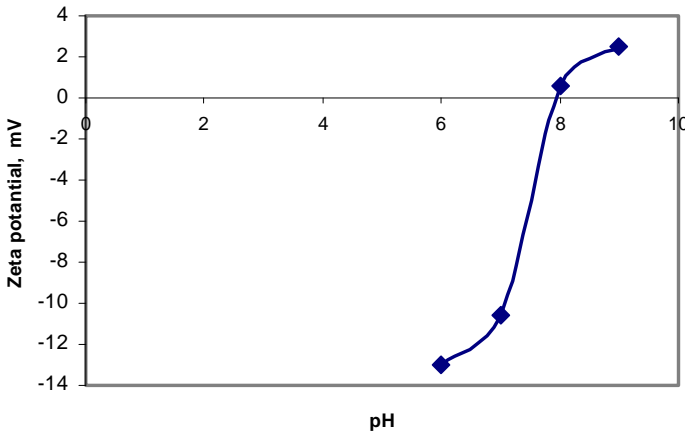
Fig. 4. Variation of zeta potential of travertine slurry as a function of solution pH

Figure 4 shows that the ζ potential profile of the solid particles present in the travertine slurry. Differently from the above findings, the particle surface is negatively charged even at lower pH values. This could be attributed to higher concentrations of dissolved specific ions and organic impurities that are found in the waste slurry. The surface properties of travertine are expected to be same as $CaCO_3$. However, greater porous structure and adsorbed or detached organic and inorganic impurities on the surface make it completely different from the solid form (Vdovic and Kralj, 2000).

In order to examine the effect of these ions on surface potential, the ζ-potential measurements were also performed with different amounts of NaCl additions in measurement solutions (Fig. 5). The result confirmed the ζ potential of the particle is sensitive to the ionic strength of the solution. In general, ζ potential of the surface increases with increasing NaCl concentration. However, compared to electrolyte-free solution, addition of a lower amount of NaCl to the solution decreases ζ potential of particles. For 0.002 M NaCl addition, ζ-potential of the solid surface decreases from 2.64 mV to -1.34 mV.
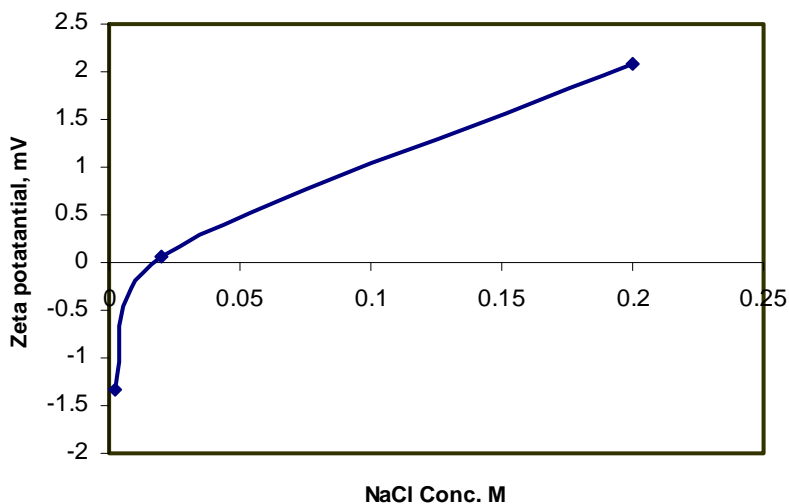
Fig. 5. Zeta potential variation of 1% solid content suspension
as a function of NaCl concentrations at pH 9–10

The positive values measured above 0.1 M NaCl addition may be attributed to the ion-ion interactions and ion-surface interactions of the structure-making cations and structure breaking anions or foreign ions that are present in the solution and the difficulties of measuring ζ potential above 0.1 mol dm^{-3}. As previously discussed by Kosmulski and Rosenholm (1996), the electric field around a colloidal particle could hardly be measured at electrolyte concentrations above 0.1 mol dm^{-3} using traditional equipment. At low ionic strengths, the electrolytes of alkali halides (1-1) show common properties. The isoelectric point of oxides and many other solids does not depend on the nature and concentration of these salts. However, for the electrolytes involving multivalent ions, in contrast, the isoelectric points are shifted. The direction and magnitude of the shift depends on the nature and concentration of the electrolyte. At higher ionic strengths, far fewer water molecules per ion are available, and due to this water deficit, some ions experience partial dehydration. This dehydration allows the ions to approach closer to the surface. Moreover, the hydration shell is distorted and finally the individual properties of particular ions and salts are displayed in ion-ion interactions or in ion-surface interactions that are not important under lower ionic strength conditions. When the ionic strength exceeds a critical value, which is below 0.1-mol dm^{-3} for common 1-1 salts, the iep starts to shift gradually toward higher pH values with increasing ionic strength. Finally, when the ionic strength exceeds a second critical value, there is no iep and the ζ potentials are positive over the entire measured pH range.

Kosmulski et al. (2003) studied the electrokinetic potentials of mineral oxides and calcium carbonate in artificial seawater, and released a relatively same conclusion. It was reported that ζ potentials of concerned materials are depressed in the presence of

a high salt concentration. In case of calcium carbonate, measured ζ potential equal to 1.91 mV by electroacoustic method at pH 8 in artificial seawater (at high ionic strengths) is substantially lower than the previously published results at low ionic strengths. Within the studied pH range of 7–9, calcium carbonates showed pH independent ζ potentials potential.

The variation of zeta potentials as a function of polymer concentration for flocculation process is given at Fig. 6.
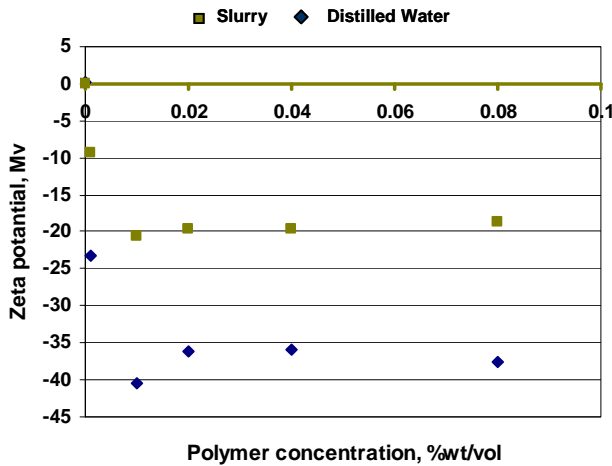
Fig. 6. Zeta potential variation of 1% solid content travertine suspension as a function of polymer concentrations (0.001%–0.08% wt/vol). pH 8–8.5

It is clearly indicated that the flocculant molecules adsorbed extensively on the travertine particles, and lower amount of reactive addition is sufficient to increase the surface potential of the particles to fall into the stabile region. ζ potential of the particle surface sharply increases from –8.4 mV to –36.7 mV for the solution consisting of 1% with polymer addition of 0.05% wt/ vol. and a further increase of the flocculant concentration does not cause any considerable effect on the ζ potential values. In the case of the slurry sample, this increase is negative (from 0.6 mV to –16 mV).

This conclusion can be supported by the results from the previous paper in which ζ potential of calcite in the presence of organic acids was investigated. Positive surface charge of calcite was reduced by introduction of fulvic acid to the solution. The high affinity of fulvic acid molecules for calcium carbonate surface is due to electrostatic attraction between positively charged surface sites and the negative charge (Vdovic and Kralj, 2000).

For the coagulation or coagulation + flocculation aid sedimentation processes the measurement of ζ potential is accepted as an effective tool for coagulation control because the changes in zeta potential indicate changes in the repulsive force between

colloids. The magnitude of zeta potential gives an indication of the potential stability of the colloidal system. If all the particles in suspension have a large negative or positive zeta potential then they will tend to repel each other and there will be no tendency for the particles to come together. On the other hand, if the particles have low zeta potential values, then there will be no force to prevent the particles coming together and coagulation. Therefore, the first step for effective coagulation is the destabilization of the suspension by eliminating these repulsive forces. Either compressing the double layer through pH control or addition of electrolytes can overcome the energy barrier between particles. Double layer compression involves adding salts to the system. As the ionic concentration increases, the double layer and the repulsion energy curves are compressed until there is no longer an energy barrier. Particle agglomeration occurs rapidly under these conditions because the colloids can just about fall into the van der Waals "trap" without having to surmount an energy barrier (Somasundaran and Das, 1998, www.zeta-meter.com). In practice, a large amount of electrolyte addition alone is an impractical technique for water treatment. However, usage of dual flocculant or coagulation + flocculation can help to increase flocculation efficiency. As discussed previously, although the solubility of the travertine particles in suspension is very low, a relatively high concentration of Ca^{2+} and Mg^{2+} ions in waste slurry, 360.72 mg Ca^{2+}/dm^3 and 340 48 mg Mg^{2+}/dm^3 at pH of 7.75, leads to decreasing ζ potential of particles and approaching the surface charge the isoelectric point (Fig. 4). The availability of such ions in solution improves the binding of the anionic polymer segments onto the negatively charged surface (Hiemenz and Rajagopalan, 1997). Such ions act as "bridges-with bridges" to induce flocculation.

Conclusion

According to the experimental finding discussed above, the following conclusion can be drawn. The electrochemical measurement results showed that the surface charges of the travertine particles in distilled water are strongly affected by the suspension pH and the solid content of solution. It was found that the surface potential of solid particles is positive at pH 9.76 over the all solid contents studied. However, ζ potential of the particles becomes slightly negative values at lower pH values for 1% solid weight content. For travertine slurry, different potential variations were determined. The particle surfaces are negatively charged between pH values of 6 and 8 due to the higher concentrations of dissolved specific ions i.e. Ca^{2+} and Mg^{2+} in the waste slurry. These results highlight the importance of influence of the source of the slurries on the surface charge or the magnitude of potential of particles and confirmed that ζ potential of the particle surface is sensitive to the ionic strength of the solution. Furthermore, it can also propound that availability of such ions in the solution allows the elimination of repulsive forces between particles and destabilizes the suspension to effective adsorption of polymer molecules to each particle.

References

ARSLAN E. I., ASLAN S., IPEK U., ALTUN S., YAZIOĞLU S., 2005, *Physico-chemical treatment of marble processing wastewater and recycling of its sludge.* Waste Management Research 23, 550–559.

BARUTÇU S., 2008, *Porters five forces analysis for natural stone industry and competitive strategies.* Journal of Global Strategic Management 03, 57–67.

BAYRAKTAR I., ONER M., KARAPINAR N., SAKLAR S., 1996, *Wastewater treatment in the marble industry*. In M. Kemal, V. Arslan, A. Akar, & M. Canbazoğlu (Eds.), 1996 Proceedings of the 6th International Mineral Processing Symposium, 24-26 September, Kuşadası, 673–677, Rotterdam, NL: Balkema.

CELIK M.Y., SABAH E., 2008, *Geological and technical characterization of Iscehisar (Afyon-Turkey) marble deposits and the impact of marble waste on environmental pollution.* Journal of Environmental Management, 87, 106–116.

COBANOGLU I., CELIK S. B., 2012, *Determination of strength parameters and quality assessment of Denizli travertines (SW Turkey)*. Engineering Geology 129–130, 38–47.

ERIKSSON R., MERTA J., ROSENHOLM J. B., 2007, *The calcite/water interface I. Surface charge in indifferent electrolyte media and the influence of low-molecular-weight polyelectrolyte*. Journal of Colloid and Interface Science 313, 184–193

ERSOY B., TOSUN I., GUNAY A., DIKMEN S., 2009, *Turbidity removal from wastewaters of natural Stone processing by coagulation/flocculation method*s. Clean 37, 225–232.

HIEMENZ C. P., RAJAGOPALAN R., 1997, *Principles of colloid and surface chemistry* (3rd edition), New York, NY: Marcel Dekker Inc.

LIDE D. R., 2005, *CRC Handbook of Chemistry and Physics* (86th Ed.). Boca Raton (FL): CRC Press. ISBN 0-8493-0486-5.

KOSMULSKI M, MACZKA E., BOCZKOWSKA M-K., ROSENHOLM J.B., 2003, *Electrokinetic potentials of mineral oxides and calcium carbonate in artificial seawater*, Marine Pollution Bulletin 46, 120–122.

KOSMULSKI M., ROSENHOLM J.B., 1996, *Electroacoustic study of adsorption of* i*ons on anatase and zirconia from very concentrated electrolytes* J. Phys. Chem.**,** 100, 11681–11687.

MOULIN P., ROQUES H., 2003, *Zeta potential measurement of calcium carbonate,* Journal of Colloid and Interface Science 261, 115–126.

SOMASUNDARAN P., DAS K.K., 1998, *Flocculation and selective flocculation-An overview.* In S. Atak, G. Önal, M.S. Çelik, (Eds.), Preceding of the 7th International Mineral Processing Symposium, Istanbul, 15–17 September, 81–91, Rotterdam, NL: Balkema.

SEYRANKAYA A., MALAYOGLU U., AKAR A., 2000, *Flocculation conditions of marble from industrial wastewater and environmental consideration,* In G.Özbayoğlu (Ed.), Proceedings of the 8th International Mineral Processing Symposium, 645–652, Rotterdam, NL: Balkema.

SIFFERT B., FIMBEL P., 1984, *Parameters affecting the sing and the magnitude of the electrokinetic potential of calcite*. Colloids and Surfaces, 11, 377–489.

STIPP S.L., HOCHELLA M.F. JR., 1991*, Structure and bonding environments at the calcite surface as observed with X-ray photoelectron spectroscopy (XPS) and low-energy electron diffraction (LEED)*. Geochimica et Cosmochimica Acta 55, 1723–1736.

TASDEMIR T., KURAMA H., 2012, *Fine particle removal from natural stone processing effluent by flocculation*, Environmental Progress & Sustainable Energy, DOI 10.1002/ep.

VDOVİC N., 2001, *Electrokinetic behaviour of calcite—the relationship with other calcite properties*, Chemical Geology 177, 241–248.

VDOVIC N., KRALJ D., 2000, *Electrokinetic properties of spontaneously precipitated calcium carbonate polymorphs: the influence of organic substances*, Colloids and Surfaces A: Physicochemical and Engineering Aspects 161, 499–505.

http://www.zeta-meter.com. *Everything you want to know about coagulation & flocculation*, 4th Edition, 1993.20.4.2012.

KINETIC MODELING OF CHROMIUM(III) EXTRACTION WITH ALIQUAT 336 FROM ALKALINE AQUEOUS SOLUTIONS CONTAINING CHLORIDES

Barbara WIONCZYK

Institute of Leather Industry, Zgierska 73, 91-462 Lodz, Poland, wionczyk@ips.lodz.pl, phone: +48 422536132

Abstract: The effects of time, composition and history of preparation of the aqueous phase on the liquid-liquid extraction of chromium(III) with Aliquat 336 from the aqueous alkaline solutions containing chlorides were studied. At time far from the equilibrium the yield and initial rate of the chromium(III) extraction depend on NaOH concentration, ionic strength of the aqueous phase and the way of its preparation. At the constant composition of the feed solution, rate of the Cr(III) extraction in approach to the equilibrium is higher when chromium(III) is extracted from the alkaline aqueous phase freshly prepared by direct dissolution of a weighted sample of CrCl₃ than from that obtained by dilution of aged stock solution of CrCl₃. Kinetic analysis by the mathematical models showed that within the whole period of time needed to reach the equilibrium, the rate of the Cr(III) extraction is limited by the second-, and third-order chemical reaction towards Cr(III), irrespective of composition and preparation history of the aqueous phase. The three-dimensional diffusion and chemical reaction at phase boundary substrate-product (the contracting volume) models have a significant effect on the chromium(III) extraction within the initial extent of the process.

Introduction

Different industrial processes apply chromium compounds as dyes, paint pigments, for metal plating and in the leather processing as a tanning agent. In such industrial processes, besides the final products, various wastes containing chromium compounds are generated. Chromium(III) basic sulfate is the most frequently and widely applied as a tanning agent in the leather industry because it allows to produce leathers of very high quality. However, many chemical and mechanical operations (chromium tanning, splitting and shaving of chromium-tanned leathers), which are made during processing of raw animal hides/skins into finished leathers, generate large quantities of liquid and solid wastes containing chromium(III).

Total quantities of these wastes depend on applied technology and on type of leathers produced. Generally, solid tannery wastes containing chromium(III) can constitute from 18 to 57% of the total amount of all solid wastes produced by tanneries. About 40% of Cr(III) compounds, which were not uptaken by hides during tanning operation, remain in spent tanning liquors and these baths are the main source of chromium(III) in tannery effluents. Such wastes create an environmental hazard and moreover, a risk for the human health when they are inadequately treated and/or discharged without purification into the landfill or rivers. It is known that the trace quantities of chromium(III) are needed for the proper functioning of the human organism (Senczuk, 1999; Indulski, 1992). However, oxidation of chromium(III) to carcinogenic chromium(VI) in surface water and soils under favourable conditions (acid rains and the presence of some oxidants like MnO_2) should be taken into account (Kabata-Pendias and Pendias, 1993; Ciszewski and Baraniak, 2006; Apte et al., 2005). Besides, in the natural environment interconversion Cr(III) $\Leftrightarrow$ Cr(VI) is observed and controlled by different factors, e.g. concentration and kind of chromium species, presence of oxidizing or reducing agents, electrochemical potentials of oxidation and reduction reactions, pH, ambient temperature, light, presence of complexing agents (Kimbrough et al., 1999).

A worldwide legislation exists on chromium limits for discharge of tannery effluents into water bodies and sewers (Bosnic et al., 2000). Many of these regulations distinguish between the limit of chromium(III) and chromium(VI) compounds. However, generally, the typical limit for total chromium concentration in tannery effluents is within the range 2–4 mg/dm³ (Gauglhofer, 1991; Bosnic et al., 2000).

The recovery of chromium(III) from the tannery effluents and wastes is justifiable both ecologically and economically. First of all, it reduces a risk of contamination of environment by compounds of chromium. Second, such activities may prevent loses of chromium compounds which could be reused in other industrial processes.

From literature data it comes that various methods have been examined for removing and recovering of chromium(III) compounds from aqueous solutions and tannery floats/wastewaters. These methods are based on adsorption (Liu et al., 2010; Papandreou et al., 2011), biosorption (Karaoglu et al., 2010; Sundar et al., 2011), ion exchange (Gode and Pehlivan, 2006), and various membrane techniques such as ultrafiltration (Korus and Loska, 2009; Labanda et al., 2009), micellar enhanced ultrafiltration (Auodia et al., 2003), nanofiltration (Religa et al., 2011), reverse osmosis (Hintermeyer et al., 2008) and transport through the bulk, supported, emulsion and polymer inclusion liquid membranes with application of various carriers (Gawronski and Religa, 2007; Buonomenna, 2006; Ochromowicz and Apostoluk, 2010; Alguacil et al., 2009; Konczyk et al., 2010).

One of the most efficient methods for concentration and separation of different metal species including chromium is the liquid-liquid extraction which is economically feasible when flow rates are high and concentrations of contaminants are greater than 0.5 g/dm³ (Kentish and Stevens, 2001).

Studies described earlier in literature, concerning the liquid-liquid extraction of Cr(III), indicate that both cationic and anionic species of chromium(III) (formed with ethylenediaminetetraacetic acid (EDTA)) are extracted mainly from acidic and neutral aqueous solutions with acidic extractants (Apostoluk and Bartecki, 1985; Islam and Biswas, 1979; Pandey et al., 1996) and with trioctylmethylammonium chloride (Aliquat 336) (Irving and Al-Jarrah, 1973). Wionczyk and Apostoluk (2004a; b) have showed for the first time that quaternary ammonium compounds effectively extract anionic hydroxocomplexes of chromium(III) which can be formed in the model alkaline solutions prepared from an aged stock solution of $KCr(SO_4)_2$ and NaOH. Wionczyk and co-workers (Wionczyk and Apostoluk, 2005; Wionczyk, 2009) have determined the effects of various parameters and electrolytes on the chromium(III) extraction. This method was examined for the removal of chromium(III) from some industrial spent tanning liquors (Wionczyk et al., 2006) and from protein hydrolyzate obtained by alkaline hydrolysis of wastes of chromium-tanned leathers (Wionczyk et al., 2011a; 2011b).

From the other side, taking into account available literature data, it can be found out that the extraction of chromium(III) from alkaline media is a problem still recognized very scarcely and it is also interesting and important issue with an environmental studies approach.

Recently, Wionczyk et al. (2011c) have reported studies on the kinetics and equilibria of the liquid-liquid extraction of chromium(III) with Aliquat 336 from alkaline aqueous solutions, containing anions of various complexing abilities and hydration properties, which were freshly prepared by dilution of the aged stock aqueous solutions of various chromium(III) salts (nitrates, perchlorates, or sulfates).

Consequently, as a development of the all investigations mentioned above, in this paper the studies are reported on the liquid-liquid extraction of chromium(III) with Aliquat 336 from alkaline solutions containing chloride ions. The effects of extraction time, composition and history of preparation of the aqueous phases (directly from weighted sample of $CrCl_3$ or by dilution of aged solution of $CrCl_3$) are presented. The kinetic models with application of mathematical rate equations and a discussion on the estimation of factors limiting the chromium(III) extraction under examined conditions are given. Moreover, results described in this paper are compared with those reported recently by Wionczyk et al. (2011c).

Experimental

Reagents

The initial aqueous phases were freshly prepared alkaline solutions of composition: chromium(III) – 0.005 mol/dm³, sodium hydroxide – 0.3 mol/dm³ or 0.5 mol/dm³, chloride ions – 0.015 mol/dm³. These aqueous phases were prepared immediately before the extraction in the following two different ways: (WS) – by direct dissolution of a weighted sample of $CrCl_3 \cdot 6H_2O$ and appropriate alkalization with

NaOH; (AQ) – by direct dilution and alkalization of the aged (for several months) stock aqueous solution of chromium(III) chloride. All compounds with high purity were obtained from POCh (Poland). Distilled water was used in the studies.

Solution of Aliquat 336 (90% of trioctylmethylammonium chloride, for synthesis Merck-Schuchardt) in heptane (p.a., Chempur, Poland) at concentration 0.05 mol/dm^3 modified with 1% (v/v) of 1-decanol (>99% for synthesis, Merck-Schuchardt) was used as the initial organic phase.

Extraction of chromium(III)

The equal volumes of the aqueous and organic phases were shaken mechanically in thermostatic water bath shaker type Elpin 357 (Poland) with constant speed (140 rpm) at constant temperature (25 ± 0.5 ºC) for appropriate period of time varying within the range from 0.5 to 360 minutes. Then, the phases were transferred to separation funnels and were left to clarify and separate for 3 h.

The distribution of chromium(III) in both phases was determined spectro-photometrically with 1,5-diphenylcarbazide after oxidation of Cr(III) to Cr(VI). The concentration of chlorides in the aqueous phase was estimated by Volhard's method.

Kinetic models and calculations

The studies on the kinetics of heterogeneous processes can be carried out using the isothermal method in which observations of an extent of process/reaction (α) within a period of time (t), are made at constant temperature. In general, this method is more appropriate for kinetic analysis of the slowest processes and is based on the determination of a rate equation according to the mathematical model which the most precisely explains the systematic changes of α with time and describes mechanism of process/reaction. Values of α vary from 0 at the beginning of process to 1 when it is over.

An extent/progress of the chromium(III) extraction in the presented system was measured by dimensionless fraction (α) of Cr(III) extracted to the organic phase after any period of the extraction time and it was as follows:

$$\alpha = \frac{c_o^t}{c_a^0} \tag{1}$$

where c_a^0 stands for initial concentration of chromium(III) in the aqueous phase at the beginning of process and c_o^t denotes concentration of chromium(III) extracted to the organic phase at time t of the process duration. The yield of chromium(III) extraction (%E) from the aqueous to the organic phase was calculated as follows:

$$\%E = \alpha \cdot 100. \tag{2}$$

The rate of heterogeneous process under conditions far from the equilibrium can be kinetically described by the following general equation in the differential form (Perez-Maqueda et al., 2005):

$$\frac{d\alpha}{dt} = k_T \cdot f(\alpha) \tag{3}$$

where k_T is temperature-dependent rate constant, $f(\alpha)$ a term describing the relation between the rate of process/reaction and its mechanism.

After introduction to Eq. (3) of the following designation

$$\int_0^\alpha \frac{d\alpha}{f(\alpha)} = g(\alpha) \tag{4}$$

the total integral form of Eq. (3) is:

$$g(\alpha) = k_T \cdot t . \tag{5}$$

The various rate equations (kinetic models) describing the mechanism of a heterogeneous process are proposed in literature (Galwey and Brown, 1998). Some of the integral forms of the rate equations, which were selected for the kinetic analysis of the experimental results received in the examined extraction system, are specified in Table 1.

Table 1. Some of the most important rate equations (models) proposed for kinetic analysis of heterogeneous processes (Galwey and Brown, 1998)

Kind of kinetic model	Symbol	Mechanism	Integral form $g(\alpha) = k_T \cdot t$
Geometrical models	R2	phase boundary controlled reaction (contracting area)	$1 - \sqrt{(1-\alpha)}$
	R3	phase boundary controlled reaction (contracting volume)	$1 - \sqrt[3]{(1-\alpha)}$
Diffusion models	D1	one-dimensional diffusion	α^2
	D2	two-dimensional diffusion	$(1-\alpha)\ln(1-\alpha) + \alpha$
	D3	three-dimensional diffusion (Jander equation)	$[1-(1-\alpha)^{1/3}]^2$
	D4	three-dimensional diffusion (Ginstling-Brounshtein equation)	$[1-(2\alpha \cdot 3^{-1})]-(1-\alpha)^{2/3}$
'Order of reaction' models	F1/ A1	first order /Avrami-Erofeev equation, $n = 1$	$-\ln(1-\alpha)$
	F2	second order	$(1-\alpha)^{-1} - 1$
	F3	third order	$(1-\alpha)^{-2} - 1$

Results and discussion

The effect of extraction time, composition and history of preparation of the aqueous phase

The relationships between the yield of chromium(III) extraction and the contact time of phases (aqueous and organic) for various composition and history of preparation of the initial aqueous phase (WS or AQ methods given in 2.1.) in the tested system are showed in Fig. 1. They indicate that an elongation of extraction time and reduction of NaOH concentration in the initial aqueous phase from 0.5 mol/dm^3 to 0.3 mol/dm^3 affect positively the extraction of chromium(III) from the alkaline aqueous solutions of chlorides, irrespective of the mode of preparation of the feed aqueous solutions. Namely, at 0.3 mol/dm^3 of NaOH in the aqueous phase, chromium(III) is extracted almost completely with the high yield equal to 98-99% after 2 hours, while at 0.5 mol/dm^3 of sodium hydroxide, the extraction of chromium(III) attains the maximum 89–90% only after 5 hours of the phase contact. The lower concentration of NaOH in the aqueous phase the shorter time is needed to achieve the equilibrium of the chromium(III) extraction under examined conditions. The negative effect of the increasing concentration of NaOH on the efficiency of Cr(III) extraction from the alkaline chloride solutions is attributed to the negative influence of the ionic strength of the aqueous phase as it can be expected according to the findings of our previous studies (Wionczyk and Apostoluk, 2005; Wionczyk, 2009).
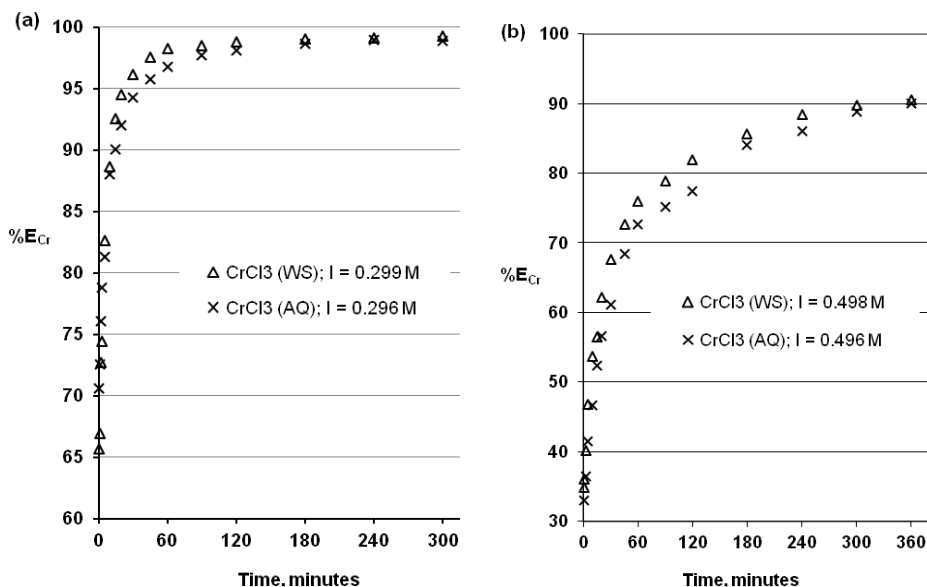
Fig. 1. Effect of time and preparation history (WS and AQ) of the initial aqueous phases on the extraction of Cr(III) (%E) from the aqueous solutions of chlorides in: (a) 0.3 M; (b) 0.5 M NaOH.
I – denotes the initial ionic strength of the aqueous phase

The results given in Fig. 1 shows that extraction of chromium(III) in the studied system depends also on the history of preparation of the initial aqueous phases (WS or AQ). Namely, at constant contact time of phases and at constant initial composition of the aqueous phase, the yield of extraction of Cr(III) from the fresh aqueous alkaline solution prepared from sample of CrCl$_3$·6H$_2$O (WS) is slightly higher than this from the diluted aged stock solution of chromium(III) chloride (AQ). However, these differences between Cr(III) extraction are observed only at the time far from the equilibrium of extraction. It means that yield of chromium(III) extraction depends on the way of preparation of the feed alkaline aqueous solution (WS or AQ). It may be discussed in terms of different Cr(III) complex species which can be present in the fresh and/or aged aqueous solutions of chromium(III) chlorides. The percent of Cr(III) extraction at the equilibrium is constant and its value does not depend on the history of preparation of the initial aqueous phase.

The rate of chromium(III) extraction in an approach to the equilibrium state

Depending on the possibilities of hydrodynamic control of an examined extraction system, different techniques used for determination of the rate of the extraction of an individual component can be divided as follows:

- methods in which measurements are made at constant interfacial area of the organic and aqueous phases, e.g. the method using a modified Lewis cell,
- methods in which there is a lack of the constant interfacial area because both organic and aqueous phases are vigorously mixed which leads to their mutual dispersion.

In the present work all experiments concerning the effect of time on the chromium(III) extraction were made under constant processing conditions (temperature, volume ratio of phases, shaking speed of phases, time of phase separation). Then, the results of those experiments were treated in accordance with the one of the methods for determination of the rate of liquid-liquid extraction in which interfacial area of aqueous and organic phases is not constant.

The liquid-liquid extraction is a complex process consisting of various chemical reactions and several processes, e.g. diffusion, mass transfer and distribution. Its total rate is limited by the rate of its slowest stage. A total equilibrium of the extraction can be described by one general equation at the assumption that side reactions do not proceed in the aqueous and organic phases. Then, like the velocity of an elementary chemical reaction, the rate of the extraction of component can be determined by the measurements of changes of its concentration in a unit of time at constant temperature.

Consequently, by analogy to the elementary chemical reaction, the integral forms of the first-order ($\ln c_{Cr_a} = k_1 t$) and the second-order ($1/c_{Cr_a} = k_2 t$) kinetic equations, usually used to define the order of a chemical reaction (Jones and Atkins, 2009), were applied to examine which of the kinetic relations precisely describes the changes of chromium(III) concentration in the aqueous phase (c_{Cr_a}) with time (t) during progress of the Cr(III) extraction. The fits of the experimental data obtained from the studies on

the extraction of chromium(III) with Aliquat 336 under the all tested conditions to these first-order and second-order kinetic equations are graphically demonstrated in Fig. 2a, b.

(a)   (b)
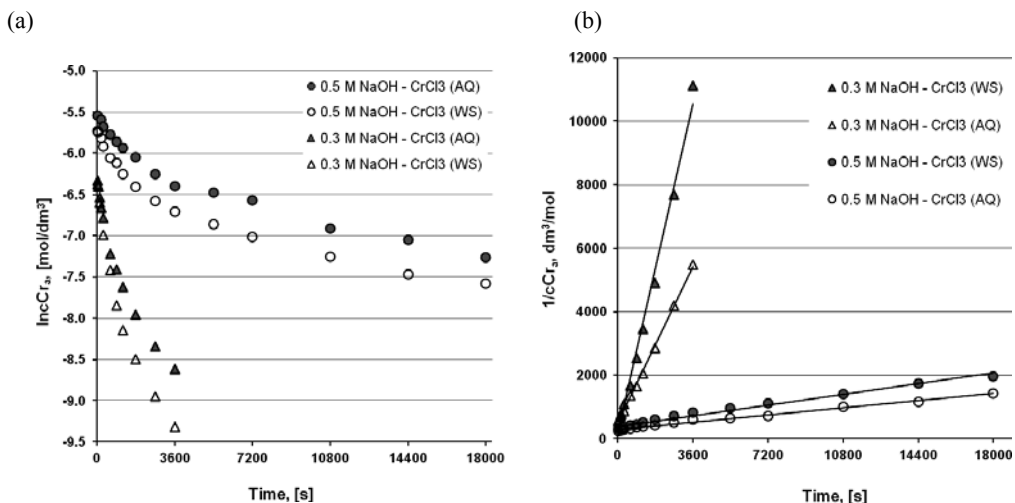
Fig. 2. The fits of experimental data to (a) the first-order, (b) the second-order kinetic equations determined in the systems $CrCl_3$-NaOH-0.05 M Aliquat 336 with the aqueous phases of various compositions and history of preparation (WS and AQ)

From Fig. 2a, it is evident that under each studied conditions the experimental points deviate from straight lines of the kinetic relation $\ln c_{Cr_a} = k_1 t$ within the whole periods of time needed to attain the equilibrium of chromium(III) extraction. Then, it may be supposed that at time far from the equilibrium, the rate of the extraction of chromium(III) in the tested system cannot be expressed by the first-order kinetic equation. However, for the extraction of Cr(III) from the aqueous phases at 0.5 mol/dm³of NaOH, it is possible to find such range of the extraction time, 0.5-30 minutes, within which more than three experimental points will be well fitted to this kinetic equation giving the linear dependence. At concentration of NaOH equal to 0.3 mol/dm³, it is difficult to select such range of the initial extraction time within which more than three experimental points will be precisely fitted to the dependence $\ln c_{Cr_a} = k_1 \cdot t$. Moreover, it should be noted that after 30 seconds of the phase contact, which corresponds to the first experimental points in Fig. 1, the yield of extraction of chromium(III) from the feed chloride solution at 0.3 mol/dm³ of NaOH exceeds 65%, irrespective of the way of preparation of the aqueous phases. Then, to test of linearity of the relation $\ln c_{Cr_a} = k_1 \cdot t$ in the system with lower concentration of NaOH, several experimental points should be obtained at the initial extraction time shorter than 30 seconds. However, this is practically impossible under the applied experimental conditions.

From Fig. 2b it comes that within the periods of time (60 and 300 minutes) which are necessary to reach the equilibrium of extraction, the changes of reciprocal of Cr(III) concentration in the aqueous phases with time of the extraction create precisely the linear dependences typical for the second-order kinetic equation ($1/c_{Cr_a} = k_2 t$). These straight lines are characterized by various slopes (k_2) which depend on the concentration of NaOH and on the preparation history of the alkaline Cr(III) feed solutions. Equations of the straight lines plotted in Fig. 2b, and consequently, the values of their slopes (k_2) were determined using the method of regression analysis. Moreover, the quality of mathematical fit of the experimental data to the second-order kinetic relationship ($1/c_{Cr_a} = k_2 \cdot t$) was evaluated applying the statistical criteria (determination coefficient R^2; standard deviation of estimate and of the slope of regression line S.D.; Fisher-Snedecor test function F). Those parameters and values of slopes (k_2) of the straight lines (in Fig. 2b), which correspond to the rate constants of the chromium(III) extraction under each examined conditions, are given in Table 2. The number of experimental points, N, and the ranges of the extraction time, within which the kinetic equation was tested, are also specified in this Table.

The values of statistical criteria (Table 2) reveal that the all relations ($1/c_{Cr_a} = k_2 t$) presented in Fig. 2b are of very good statistical quality. Then, it can be accepted that the rate of the extraction of chromium(III) with Aliquat 336 from the alkaline aqueous solution containing chlorides may be described by the second-order kinetic equation towards Cr(III), irrespective of the initial concentration of NaOH and on the way of preparation of the aqueous phases. Values of the rate constants (k_2) prove that chromium(III) is extracted with the highest rate from the feed aqueous solution prepared directly from the sample of $CrCl_3 \cdot 6H_2O$ (WS) at 0.3 mol/dm^3 of NaOH. Moreover, the rate constant (2.96 dm^{3}mol^{-1}s^{-1}) determined under these conditions is about twice higher than that (1.37 dm^{3}mol^{-1}s^{-1}) established for the aqueous phase prepared by dilution of the aged stock solution of $CrCl_3$ (AQ). From Table 2 it also comes that the effect of the way of preparation of the feed aqueous solution (WS or AQ) on the rate of chromium(III) extraction at higher concentration of NaOH is already lower though the velocity of the Cr(III) extraction in the system with the aqueous phase obtained directly from the sample of $CrCl_3 \cdot 6H_2O$ (WS) is still higher.

Taking these findings into account it can be accepted that the observed differences (Table 2) between the rate of the extraction of chromium(III) from the aqueous alkaline solutions containing chlorides may be attributed to the various kind of complexes of chromium(III) which are probably present in the aqueous phases of different concentration of NaOH and history of their preparation (WS or AQ).

Table 2. The rate constants (k_2) and their statistical assessment determined from the second-order kinetic equation, $1/c_{\mathrm{Cr}_a} = k_2\,t$, (Jones and Atkins, 2009) for the extraction of chromium(III) in the studied system $CrCl_3$ – NaOH – Aliquat 336 with the aqueous phases of different composition and history of preparation (WS or AQ). The statistical symbols are explained in text

c_{NaOH}^0, mol/dm^3	History of preparation of the aqueous phase	(k_2 ± S.D.), dm^{3}mol^{-1}s^{-1}	R^2	S.D.	F	N	Range of the extraction time, min
0.3	CrCl$_3$ (WS)	2.958 ± 0.067	0.9948	345	1933	11	0.5–60
0.3	CrCl$_3$ (AQ)	1.369 ± 0.017	0.9984	65	6325	11	0.5–60
0.5	CrCl$_3$ (WS)	0.093 ± 0.003	0.9845	67	889	15	0.5–300
0.5	CrCl$_3$ (AQ)	0.063 ± 0.002	0.9888	39	1151	14	0.5–300

The results received in our previous typical extraction studies (Wionczyk et al., 2011c) were taken to compare the effect of different kind of anions (sulphates, nitrates, perchlorates, and chlorides) on the rate of the extraction of chromium(III) in the systems with Aliquat 336 from the alkaline aqueous phases freshly prepared by dilution of the aged stock solutions of different chromium(III) salts ($KCr(SO_4)_2$, $Cr(NO_3)_3$, $Cr(ClO_4)_3$, and $CrCl_3$). The experiments relating to the effect of time on the Cr(III) extraction were carried out in our previous (Wionczyk et al., 2011c) and present studies under the same conditions. Consequently, the quality of fitting of the results obtained previously in work Wionczyk et al. (2011c) to the relation $1/c_{\mathrm{Cr}_a} = k_2\,t$ and the rate constants (k_2) for those earlier examined systems were determined. The all values of the rate constant (k_2) established from the second-order kinetic equations ($1/c_{\mathrm{Cr}_a} = k_2\,t$) in the extraction systems with sulphates, nitrates, perchlorates, and chlorides as well as their statistical criteria are presented in Table 3.

From Table 3 it is evident that at concentration of NaOH equal to 0.5 mol/dm^3, the rate of the chromium(III) extraction in the examined systems depends on the type of anions present in the aqueous phases and increases according to the increasing negative values of free energy of hydration of tested anions. However, at 0.3 mol/dm^3 of NaOH, the rate of chromium(III) extraction increases in the other sequence of anions. Namely, under these conditions, the extraction of Cr(III) in the system with chlorides ($\Delta G_{\mathrm{hydr}} = -346$ kJ/mol, Marcus, 2004) reached the equilibrium faster than in the system with sulfates, i.e. anions of higher free energy of hydration ($\Delta G_{\mathrm{hydr}} = -1090$ kJ/mol, Marcus, 2004).

That effect of anions (Table 3) may be discussed in term of the different kind of Cr(III) complexes which could form in the alkaline aqueous phases in the presence of examined anions. On the other hand, the aggregation of Aliquat 336 (Vandegrift et al., 1980; Wionczyk and Apostoluk, 2005; Oliveira and Bertazzoli, 2007), and consequently, the formation of emulsion in the studied extraction system may be taken into account. As it is known, quaternary ammonium salts aggregate and interact with molecules of solvent in aqueous and non-aqueous solution to form association colloid

such as micelles and microemulsions (Jakubowska, 2012a). Moreover, from literature data it follows that anions of the lyotropic (Hofmeister) series, dependently on their position in that sequence, affect strongly micellization, micellar structure, micellar transitions, and micellar growth of the surfactants (Abezgauz et al., 2010; Muller et al., 2013; Jakubowska, 2012b).

Table 3. The rate constants (k_2) determined from the second-order kinetic equation ($1/c_{Cr_a} = k_2 t$) for the extraction of chromium(III) with Aliquat 336 from the alkaline aqueous phases prepared by dilution of the aged solutions of different Cr(III) salts. Values of k_2 for the Cr(III) extraction in the systems with sulfates, nitrates, and perchlorates were established on the base of results obtained by Wionczyk et al. (2011c)

c_{NaOH}^0, mol/dm^3	Anions present in the aqueous phase	($k_2 \pm$ S.D.), dm^{3}mol^{-1}s^{-1}	R^2	S.D.	F	N	Range of extraction time, min	ΔG_{hydr}, kJ/mol (Marcus, 2004)
0.3	ClO_4^-	0.571 ± 0.022	0.9911	65	672	7	5–60	−214
0.3	NO_3^-	0.811 ± 0.041	0.9852	119	401	7	5–60	−306
0.3	SO_4^{2-}	1.037 ± 0.059	0.9906	121	634	7	5–60	−1090
0.3	Cl^-	1.369 ± 0.017	0.9984	65	6325	11	0.5–60	−347
0.5	ClO_4^-	0.040 ± 0.001	0.9915	23	1165	11	5–300	−214
0.5	NO_3^-	0.044 ± 0.001	0.9897	27	1056	12	5–300	−306
0.5	Cl^-	0.063 ± 0.002	0.9888	39	1151	14	0.5–300	−347
0.5	SO_4^{2-}	0.118 ± 0.002	0.9964	44	2770	11	5–300	−1090
0.5	ClO_4^-	0.043 ± 0.003	0.9728	9	215	7	5–60	−214
0.5	NO_3^-	0.053 ± 0.002	0.9880	7	494	7	5–60	−306
0.5	Cl^-	0.095 ± 0.002	0.9971	6	2707	9	0.5–60	−347
0.5	SO_4^{2-}	0.142 ± 0.005	0.9922	15	768	7	5–60	−1090

Kinetic modeling of the extraction of chromium(III) from the aqueous alkaline phases containing chlorides

In order to examine the correctness of the findings in Section 3.2. (the rate of the extraction of chromium(III) under studied conditions can be expressed by the kinetic equation of the second-order chemical reaction and also to estimate some factors limiting the extraction rate) the kinetic models (Table 1) used usually for the kinetic analysis of heterogeneous processes were applied to these aims.

The quality of mathematical fit of the experimental data received in the studied extraction system with CrCl$_3$, NaOH and Aliquat 336 to the integral forms, g(α), of the each geometrical (R2, R3), diffusion (D1-D4) and the order of chemical reaction (F1-F3) kinetic models was examined using the method of multiple regression

analysis. Values of statistical parameters (R^2, S.D., F) were used as a measure of precision of the fitting of the obtained results to the each of kinetic models given in Table 1.

Table 4. Fittings of α-time experimental data to the selected kinetic models (given in Table 1) for the extraction system 0.005 M CrCl$_3$ – 0.3 M NaOH – 0.05 M Aliquat 336, with the aqueous phases of different history of preparation

Model	Alkaline aqueous phase from							
	Sample of CrCl$_3$ (WS) $\alpha = 0.657$–0.983 $t = 0.5$–60 minutes				Aged solution of CrCl$_3$ (AQ) $\alpha = 0.706$–0.968 $t = 0.5$–60 minutes			
	$(k_T \pm$ S.D.$)10^{-3}$ [s^{-1}]	R^2	F	N	$(k_T \pm$ S.D.$)10^{-3}$ [s^{-1}]	R^2	F	N
R2	0.127 ± 0.022	0.7540	32	11	0.099 ± 0.016	0.8002	41	11
R3	0.125 ± 0.019	0.8037	42	11	0.096 ± 0.013	0.8364	52	11
D1	0.144 ± 0.032	0.6515	20	11	0.117 ± 0.022	0.7215	27	11
D2	0.175 ± 0.032	0.7371	29	11	0.141 ± 0.022	0.7919	39	11
D3	0.134 ± 0.016	0.8797	74	11	0.100 ± 0.011	0.8962	87	11
D4	0.059 ± 0.010	0.7900	39	11	0.046 ± 0.007	0.8314	50	11
F1	0.861 ± 0.092	0.8965	88	11	0.620 ± 0.064	0.9026	94	11
F2	15.23 ± 0.31	0.9959	2446	11	7.622 ± 0.007	0.9992	13061	11
F3	715.8 ± 85.0	0.8764	71	11	219.9 ± 15.4	0.9535	205	11

The rate constants (k_T) and statistical criteria determined for the studied extraction system with the aqueous phases prepared in the different ways (WS or AQ) from CrCl$_3$ and NaOH at concentration equal to 0.3 mol/dm^3 and to 0.5 mol/dm^3 are given in Tables 4 and 5, respectively. The ranges of α and periods of the extraction time within which the kinetic models were tested are also given in Tables 4 and 5.

Parameters of the statistical assessment shown in Table 4, determined in the system with 0.3 M NaOH, reveal that the best fitting of α-time data was obtained to the kinetic model F2. Therefore, within the examined period of extraction time (0.5–60 minutes), far from the equilibrium, which corresponds to the range of α equal to 0.66–0.98, the rate of chromium(III) extraction from the alkaline aqueous solution containing chlorides is limited mainly by the second-order chemical reaction (F2), irrespective of the way of preparation of the aqueous phase (WS or AQ). What is more, under these conditions, the quality of fitting of the changes of α with time to the geometrical (R2, R3) and to the diffusion rate equations (D1-D4) is rather poor. However, the contracting volume (R3) from among the geometrical models and the three-dimensional diffusion rate equation (D3) from among the diffusion models may be taken also into account as models describing the behaviour of chromium(III) during the extraction.

Table 5. Fittings of α-time experimental data to the selected kinetic models (given in Table 1) determined for the extraction system 0.005 M CrCl$_3$ – 0.5 M NaOH – 0.05 M Aliquat 336, with the aqueous phases of various history of preparation

Model	Alkaline aqueous phase from							
	Sample of CrCl$_3$ (WS) $\alpha = 0.349$–0.897 $t = 0.5$–300 minutes				Aged solution of CrCl$_3$ (AQ) $\alpha = 0.330$–0.888 $t = 0.5$–300 minutes			
	$(k_T \pm$ S.D.$)10^{-3}$, s^{-1}	R^2	F	N	$(k_T \pm$ S.D.$)10^{-3}$, s^{-1}	R^2	F	N
R2	0.026 ± 0.004	0.7538	44	15	0.025 ± 0.003	0.8057	55	14
R3	0.021 ± 0.003	0.7890	53	15	0.021 ± 0.002	0.8369	68	14
D1	0.037 ± 0.006	0.7442	42	15	0.036 ± 0.005	0.8040	54	14
D2	0.033 ± 0.004	0.8197	65	15	0.032 ± 0.003	0.8706	88	14
D3	0.015 ± 0.001	0.9050	134	15	0.014 ± 0.001	0.9396	203	14
D4	0.009 ± 0.001	0.8521	82	15	0.009 ± 0.001	0.8976	115	14
F1	0.101 ± 0.011	0.8550	84	15	0.096 ± 0.009	0.8935	110	14
F2	0.459 ± 0.016	0.9825	786	15	0.398 ± 0.012	0.9886	1130	14
F3	4.915 ± 0.113	0.9927	1892	15	3.789 ± 0.155	0.9787	599	14
	$\alpha = 0.349$–0.676 $t = 0.5$–30 minutes				$\alpha = 0.330$–0.684 $t = 0.5$–45 minutes			
	$(k_T \pm$ S.D.$)10^{-3}$ [s^{-1}]	R^2	F	N	$(k_T \pm$ S.D.$)10^{-3}$ [s^{-1}]	R^2	F	N
R2	0.136 ± 0.013	0.9394	109	8	0.095 ± 0.008	0.9477	128	8
R3	0.103 ± 0.009	0.9471	109	8	0.072 ± 0.006	0.9560	153	8
D1	0.193 ± 0.015	0.9572	157	8	0.134 ± 0.009	0.9670	206	8
D2	0.138 ± 0.009	0.9725	248	8	0.097 ± 0.005	0.9821	386	8
D3	0.046 ± 0.002	0.9854	473	8	0.032 ± 0.001	0.9932	1026	8
D4	0.035 ± 0.002	0.9777	308	8	0.025 ± 0.001	0.9869	528	8
F1	0.398 ± 0.030	0.9610	174	8	0.279 ± 0.018	0.9706	232	8
F2	0.877 ± 0.036	0.9885	604	8	0.620 ± 0.017	0.9950	1386	8
F3	3.989 ± 0.134	0.9922	890	8	2.863 ± 0.115	0.9887	616	8

The results obtained for the system with 0.5 M NaOH (Table 5) indicate that within the whole period of time (0.5–300 minutes) needed to reach the extraction equilibrium, for which $\alpha = 0.33$–0.90, the best linearity fittings of α-time experimental data to the kinetic rate equations were obtained for the F2 and F3 models, irrespective of the history preparation of the aqueous phases. Therefore, the rate of chromium(III) extraction under these conditions is limited both by the second-order and third-order chemical reactions. The assessment of the results in Table 5 indicates that within the period of 0.5–300 minutes, the fittings of experimental data to the geometrical (R2, R3) and to the diffusion models (D1–D4) are of lower importance and statistical quality. However, the model D3 with the determination coefficient R^2 higher than 0.90 may be taken into account as a factor limiting the Cr(III) extraction under these conditions. Moreover, data obtained (Table 5) across the similar extent of the

chromium(III) extraction (α = 0.33–0.68), which corresponds to the shorter initial periods of time (0.5–30 minutes and 0.5–45 minutes) reveal that the all tested geometrical (R2, R3), diffusion (D1-D4) and the reaction order models (F1–F3) give acceptable fittings to the changes of α-time. However, the best linear relations of the α-time data are obtained by the fittings to the F2, F3, and D3 kinetic models.

Then, it can be concluded that within the whole period of time necessary to attain the equilibrium, the extraction of chromium(III) with Aliquat 336 from the fresh alkaline aqueous solutions containing chlorides is limited by the second-order chemical reaction towards Cr(III), irrespective of the NaOH concentration and of the history of preparation of the aqueous phase. However, at NaOH concentration equal to 0.5 mol/dm³, the rate of the Cr(III) extraction is also limited by the third-order chemical reaction. Moreover, within the shorter initial period of the extraction time the effect of the three-dimensional diffusion (D3) and the chemical reaction at phase boundary (R2) on the rate of chromium(III) extraction is visible.

From Tables 4 and 5 it also comes that values of the rate constants determined from the best fitted kinetic models (F2 and/or F3) for the extraction of chromium(III) in the tested system depend on the NaOH concentration and on the history of preparation of the aqueous phases (WS or AQ) as it was found from the relation $1/c_{Cr_a} = k_2 \cdot t$ in Section 3.2. At constant concentration of NaOH, the extraction equilibrium is reached faster when chromium(III) is extracted from the alkaline aqueous phase freshly prepared by direct dissolution of a weighted sample of CrCl₃ than from that obtained from the aged stock solution of CrCl₃.

Table 6. The rate constant (k_T) determined from the F2 and F3 kinetic models for the extraction of Cr(III) in the system with Aliquat 336 and with the alkaline aqueous phases prepared by dilution of the aged stock solutions of different Cr(III) salts. Values of k_T for the systems with sulphates, nitrates, and perchlorates were taken from Wionczyk et al. (2011c)

c_{NaOH}^0, [mol/dm³]	Anions in the aqueous phase	Model F2 ($k_T \pm$ S.D.)·10^{-3} [s⁻¹]	Model F3 ($k_T \pm$ S.D.)·10^{-3} [s⁻¹]	Range of extraction time [min]	Range of α
0.3	ClO_4^-	2.95 ± 0.12	44.4 ± 4.5	5–60	0.642–0.949
0.3	NO_3^-	4.41 ± 0.12	85.4 ± 11.0	5–60	0.693–0.986
0.3	SO_4^{2-}	6.40 ± 0.16	130 ± 16	5–60	0.733–0.959
0.3	Cl^-	7.62 ± 0.01	220 ± 15	0.5–60	0.706–0.968
0.5	ClO_4^-	0.23 ± 0.01	1.14 ± 0.05	5–300	0.310–0.794
0.5	NO_3^-	0.22 ± 0.01	1.42 ± 0.02	5–300	0.325–0.807
0.5	Cl^-	0.40 ± 0.01	3.79 ± 0.16	0.5–300	0.330–0.888
0.5	SO_4^{2-}	0.68 ± 0.01	10.2 ± 0.6	5–300	0.439–0.928
0.5	ClO_4^-	0.23 ± 0.01	1.14 ± 0.05	5–1200	0.310–0.673
0.5	NO_3^-	0.30 ± 0.01	1.32 ± 0.07	5–90	0.325–0.670
0.5	Cl^-	0.62 ± 0.02	2.86 ± 0.12	0.5–45	0.330–0.684
0.5	SO_4^{2-}	0.91 ± 0.08	4.68 ± 0.26	5–30	0.439–0.683

A comparison between the rate constants of the Cr(III) extraction determined in the present and in the earlier studies (Wionczyk et al., 2011c) from the best fitted F2 and F3 kinetic models ($R^2 > 0.90$) in the systems with Aliquat 336 and with the alkaline aqueous phases prepared from the aged aqueous solutions of different Cr(III) salts (CrCl$_3$, or KCr(SO$_4$)$_2$, or Cr(NO$_3$)$_3$, or Cr(ClO$_4$)$_3$) is given in Table 6. These results confirm findings from Section 3.2, that the velocity of the chromium(III) extraction depends on concentration of NaOH and on the kind of anions present in the aqueous phase. On the other hand, values of the rate constant determined from F2 and F3 models varying with hydration properties of anions present in the aqueous phase, i.e. with their free energy of hydration in order like that established from relation $1/c_{Cr_a} = k_2 \cdot t$ (Section 3.2, Table 3). Moreover, Table 6 shows that at constant composition of the aqueous phase, the values of the rate constants determined from the F3 model are considerably higher than those calculated from the second-order kinetic model (F2).

Taking into account the all kinetic considerations presented in this paper, it can be assumed that the extraction of chromium(III) in the studied system with chlorides may be described as follows:

$$[R_4N]Cl_{(o)} + Cr(OH)_{4(a)}^- = [R_4N][Cr(OH)_4]_{(o)} + Cl^-_{(a)} \tag{6}$$

$$2[R_4N][Cr(OH)_4]_{(o)} = [R_4N][Cr_2(OH)_7]_{(o)} + [R_4N]OH_{(o)} \tag{7}$$

$$[R_4N]OH_{(o)} + Cr(OH)_{4(a)}^- = [R_4N][Cr(OH)_4]_{(o)} + OH^-_{(a)} \tag{8}$$

and summing up

$$\begin{aligned} 2[R_4N]Cl_{(o)} + 3Cr(OH)_{4(a)}^- &= [R_4N][Cr(OH)_4]_{(o)} \\ &+ [R_4N][Cr_2(OH)_7]_{(o)} + 2Cl^-_{(a)} + OH^-_{(a)}. \end{aligned} \tag{9}$$
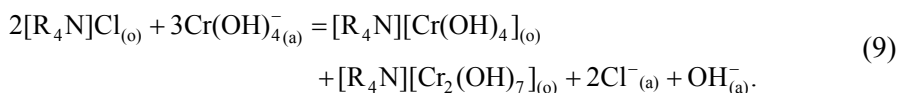
Further studies are planned with the application of some instrumental techniques, for instance spectroscopy UV-VIS, to confirm the above assumptions and to explain the differences in kinetic behavior of chromium(III) during the extraction with Aliquat 336 from the alkaline aqueous solutions of different composition and history of their preparation.

Conclusions

It was demonstrated that within time far from the equilibrium, the extraction of chromium(III) with Aliquat 336 from the aqueous alkaline feed solution containing chlorides depends on composition and history of preparation of the aqueous phase. A reduction in the initial NaOH concentration from 0.5 mol/dm^3 to 0.3 mol/dm^3 and

thus, the ionic strength of the aqueous phase, affect positively the yield and the rate of chromium(III) extraction under studied conditions.

At constant composition of the feed aqueous solution the equilibrium of the chromium(III) extraction is attained faster when chromium(III) is extracted from the aqueous phase freshly prepared by direct dissolution and alkalization of a sample of $CrCl_3 \cdot 6H_2O$ than from that freshly prepared from the aged (several months) stock aqueous solution of $CrCl_3$.

The kinetic analyses of the experimental data by the mathematical models and by the method of multiple regression analysis reveal that within the whole period of time needed to attain the equilibrium, the initial rate of chromium(III) extraction is limited mainly by the second-order and also by the third-order chemical reaction towards chromium(III), irrespective of composition and the preparation history of the aqueous phase. However, within the shorter initial period of time which corresponds to the smaller extent of the extraction, the three-dimensional diffusion and the chemical reaction at phase boundary substrate-product (the contracting volume) models can have a significant effect on the rate of chromium(III) extraction.

It can be also concluded that the extraction of chromium(III) with Aliquat 336 from the alkaline aqueous phases, prepared by dilution of the aged stock solutions of chromium(III) salts, depends on a kind of anions present in the aqueous phase, and exactly, on their hydration properties. Namely, at concentration of NaOH in the feed aqueous solution equal to 0.5 mol/dm^3, the rate constants of Cr(III) extraction increase with the increasing negative values of free energy of hydration of anions present in the aqueous phase according to the following order: perchlorates < nitrates < chlorides < sulfates. At 0.3 mol/dm^3 of NaOH, the effect of these anions on the rate of Cr(III) extraction is varying in the different sequence: perchlorates < nitrates < sulfates < chlorides.

Acknowledgements

References

ABEZGAUZ L., KUPERKAR K., HASSAN P.A., RAMON O., BAHUDUR P., DANINO D., 2010, Effect of Hofmeister anions on micellization and micellar growth of the surfactant cetylpyridinium chloride, J. Colloid Interface Sci. 342, 83–92.

ALGUACIL F.J., ALONSO M., LOPEZ F.A., LOPEZ-DELGADO A., 2009, *Application of pseudoemulsion based hollow fiber strip dispersion (PEHFSD) for recovery of Cr(III) from alkaline solutions*, Sep. Purif. Technol. 66 , 586–590.

AOUDIA M., ALLAL N., DJENNET A., TOUMI L., 2003, *Dynamic micellar enhanced ultrafiltration: use of anionic (SDS)–nonionic(NPE) system to remove Cr^{3+} at low surfactant concentration*, J. Membrane Sci. 217, 181–192.

APOSTOLUK W., BARTECKI A., 1985, *Extraction of chromium(III) from sodium chloride solutions by means of carboxylic acids*, Hydrometallurgy 15, 191–202.

APTE A.D., VERMA S., TARE V., BOSE P., 2005, *Oxidation of Cr(III) in tannery sludge to Cr(VI): Field observations and theoretical assessment*, J. Hazard. Mater. B121, 215–222.

BOSNIC M., BULJAN J., DANIELS R.P., 2000, *Pollutants in tannery effluents. Definitions and environmental impact. Limits for discharge into water bodies and sewers*, UNIDO Report US/RAS/92/120. Regional Programme for Pollution Control in the Tanning Industry in South-East Asia, 9 August.

BUONOMENNA M.G., ORANGES T., MOLINARI R., DRIOLI E., 2006, *Chromium(III) removal by supported liquid membranes: a comparison among D2HEPA, DNNSA, and a novel extractant as carriers*, Water Environ. Res. 78, 69–75.

CISZEWSKI A., BARANIAK M., 2006, *Chemical and Electrochemical Activity of Elements in Aqueous Medium*, Edition by Poznan University of Technology, Poznan, 258–275.

GALWEY A.K., BROWN M.E., 1998, *Kinetic background to thermal analysis and calorimetry*, Chapter 3 in: Handbook of Thermal Analysis and Calorimetry, Vol. 1: Principles and Practice, M.E. Brown (Ed.), Elsevier, 147–224.

GAUGLHOFER J., 1991, *Chromium in tannery effluents and its impact on the environment*, J. Soc. Leather Technol. Chem. 75 (3), 103–106.

GAWRONSKI R., RELIGA P., 2007, *Transport mechanism of chromium(III) through the unmixed bulk liquid membrane containing dinonylonaphthalenesulfonic acid as a carrier*, J. Membr. Sci. 289, 187–190.

GODE F., PEHLIVAN E., 2006, *Removal of chromium(III) from aqueous solutions using Lewatit S 100: The effect of pH, time, metal concentration and temperature*, J. Hazard. Mater. B136, 330–337.

HINTERMEYER B.H., LACOUR N.A., PEREZ-PADILLA A., TAVANI E.L., 2008, *Separation of the chromium(III) present in a tanning wastewater by means of precipitation, reverse osmosis and adsorption*, Latin Am. Appl. Res. 38, 63–71.

INDULSKI J.A. (Ed.), 1992, *Environmental Health Criteria*, Edition by Institute of Labour Medicine, Łódź, 133–142.

IRVING H.M.N.H., AL-JARRAH R.H., 1973, *The extraction of the chromium(III)-EDTA complex by solutions of Aliquat 336 in various organic solvents*, Anal. Chim. Acta 63, 79–84.

ISLAM F., BISWAS R.K., 1979, *The solvent extraction of chromium(III) with bis-(2-ethyl hexyl) phosphoric acid in benzene and other solvents*, J. Inorg. Nucl. Chem. 41, 229–233.

JAKUBOWSKA A., 2012a, *Surfactants – application and micelle formation*, Wiad. Chem. 66, 209–226.

JAKUBOWSKA A., 2012b, *Ion binding to interfaces and specific ion effects*, Wiad. Chem. 66, 193–208.

JONES L., ATKINS P., 2009, *Chemistry. Molecules, Matter, and Change*, (fourth edition translated in Polish by J. Kuryłowicz) Edition by Wydawnictwo Naukowe PWN, Warszawa, 599–652.

KABATA-PENDIAS A., PENDIAS H., 1993, *Biogeochemistry of Trace Elements*, PWN, Warszawa, 242–251.

KARAOGLU M.H., ZOR S., UGURLU M., 2010, *Biosorption of Cr(III) from solutions using vineyard pruning waste*, Chem. Eng. J. 159, 98–106.

KENTISH S.E., STEVENS G.W., 2001, *Innovations in separations technology for the recycling and reuse of liquid waste streams*, Chem. Eng. J. 84, 149–159.

KIMBROUGH D.E., COHEN Y., WINER A.M., CREELMAN L., MABUNI C., 1999, *A critical assessment of chromium in the environment*, Critical Reviews in Environmental Science and Technology 29 (1), 1–46.

KONCZYK J., KOZLOWSKI C., WALKOWIAK W., 2010, *Removal of chromium(III) from acidic aqueous solution by polymer inclusion membranes with D2EHPA and Aliquat 336*, Desalination, 263, 211–216.

KORUS I., LOSKA K., 2009, *Removal of Cr(III) and Cr(VI) ions from aqueous solutions by means of polyelectrolyte-enhanced ultrafiltration*, Desalination 247, 390–395.

LABANDA J., KHAIDAR M.S., LLORENS J., 2009, *Feasibility study on the recovery of chromium(III) by polymer enhances ultrafiltration*, Desalination 249, 277–581.

LIU Y., GUO L., ZHU L., SUN X., CHEN J., 2010, *Removal of Cr(III, VI) by quaternary ammonium and quaternary phosphonium ionic liquids functionalized silica materials*, Chem. Eng. J. 158, 108–114.

MARCUS Y., 2004, *Principles of Solubility and Solutions*, in: Solvent Extraction Principles and Practice, Rydberg, J., Cox, M., Musikas, C., Choppin, G.R., (Eds.), Dekker, M., New York, 27–80.

MULLER W., DEJUGNAT C., ZEMB T., DUFRECHE J.F., DIAT O., 2013, *How do Anions Affect Self-assembly and solubility of cetylpyridinum surfactants in water*, J. Phys. Chem B 117, 1345–1356.

OCHROMOWICZ K., APOSTOLUK W., 2010, *Modelling of carrier mediated transport of chromium(III) in the supported liquid membrane system with D2EHPA*, Sep. Purif. Technol. 72, 112–117.

OLIVEIRA B., BERTAZZOLI R., 2007, *On role of the surfactant aliquat® 336 on the kinetics of oxygen reduction reaction and on the rate of hydrogen peroxide electrosynthesis*, J. Electroanal. Chem. 611, 126–132.

PANDEY B.D., COTE G., BAUER D., 1996, *Extraction of chromium(III) from spent tanning baths*, Hydrometallurgy 40, 343–357.

PAPANDREOU A.D., STOURNARAS C.J., PANIAS D., PASPALIARIS I., 2011, *Adsorption of Pb(II), Zn(II) and Cr(III) on coal fly ash porous pellets*, Minerals Engineering 24, 1495–1501.

PEREZ-MAQUEDA L.A., SANCHEZ-JIMENEZ P.E., CRIADO J.M., 2005, *Kinetic analysis of solid-state reactions: precision of the activation energy calculated by integral methods*, Int. J. Chem. Kinet. 37, 658–666.

RELIGA P., KOWALIK A., GIERYCZ P., 2011, *Application of nanofiltration for chromium concentration in the tannery wastewater*, J. Hazard. Mater. 186, 288–292.

SENCZUK W., (Ed.), 1999, *Toxicology*, third edition, PZWL, Warszawa, Chapter 13.4, 448–454.

SUNDAR K., MUKHERJEE A., SADIQ M., CHANDRASEKARAN N., 2011, *Cr(III) bioremoval capacities of indigenous and adapted bacterial strains from Palarriver basin*, J. Hazard. Mater. 187, 553–561.

VANDEGRIFT G.F., McCARTY LEWEY S., DYRKACZ G.R., HORWITZ E.P., 1980, *Interfacial activity of liquid/liquid extraction reagents-II. Quaternary ammonium salts*, J. Inorg. Nucl. Chem. 42, 127–130.

WIONCZYK B., 2009, *Effect of temperature on the extraction of chromium(III) from alkaline aqueous solution with trioctylmethylammonium chloride (Aliquat 336)*. Solvent Extr. Ion Exch. 27, 423–446.

WIONCZYK B., APOSTOLUK W., 2004a, *Solvent extraction of chromium(III) from alkaline media with quaternary ammonium compounds*. Part I. Hydrometallurgy 72, 185–193.

WIONCZYK B., APOSTOLUK W., 2004b, *Solvent extraction of chromium(III) from alkaline media with quaternary ammonium compounds*, Part II. Hydrometallurgy 72, 195–203.

WIONCZYK B., APOSTOLUK W., 2005, *Equilibria of extraction of chromium(III) from alkaline solutions with trioctylmethylammonium chloride (Aliquat 336)*, Hydrometallurgy 78, 116–128.

WIONCZYK B., APOSTOLUK W., CHAREWICZ W.A., 2006, *Solvent extraction of chromium(III) from spent tanning liquors with Aliquat 336*, Hydrometallurgy 82, 83–92.

WIONCZYK, B. APOSTOLUK W., CHAREWICZ W.A., ADAMSKI Z., 2011a, *Recovery of chromium(III) from wastes of uncolored chromium leathers*. Part I. *Kinetic studies on alkaline hydrolytic decomposition of the wastes*, Sep. Purif. Technol. 81, 223–236.

WIONCZYK B., APOSTOLUK W., CHAREWICZ W.A., ADAMSKI Z., 2011b, *Recovery of chromium(III) from wastes of uncolored chromium leathers*. Part II. *Solvent extraction of chromium(III) from alkaline protein hydrolyzate*, Sep. Purif. Technol. 81, 237–242.

WIONCZYK B., CIERPISZEWSKI R., MOL A., PROCHASKA K., 2011c, *Studies on the kinetics and equilibrium of the solvent extraction of chromium(III) from alkaline aqueous solutions of different composition in the system with Aliquat 336*, J. Hazard. Mater. 198, 257–268.

COMPARISON OF CHEMICAL AND BIOLOGICAL LEACHING OF SULFIDE TAILINGS

Jari AROMAA[*]**, Jarno MAKINEN**[**]**, Henri VEPSALAINEN**[*,***]**,**
Tommi KAARTINEN[**]**, Margareta WAHLSTROM**[**]**, Olof FORSEN**[*]

[*]   Aalto University, Department of Materials Science. P.O. Box 16200, FI 00076 Aalto, Espoo, Finland,
      jari.aromaa@aalto.fi
[**] VTT, Waste Technology and Recycling. P.O. Box 1000, FI 02044 VTT, Espoo, Finland
[***] Present address OutotecOyj, P.O. Box 86, FI 02200, Espoo, Finland

Abstract: Sulphidic tailings from Finnish Hitura nickel mine and Pyhäsalmi multi-metal mine were leached using sulphuric acid and bioleached. The aim was to recover minor amounts of valuable Cu, Ni, Zn and Mn. Both tailings consisted mainly of iron and magnesium-containing minerals and acid neutralizing minerals. The solution after chemical leaching tests contained mostly iron and magnesium, in Hitura up to 11 g/dm^3 Fe and 38 g/dm^3 Mg while in Pyhäsalmi 8–9 g/dm^3 Fe and 4 g/dm^3 Mg. Amount of these metals was 20–100-fold larger than amount of valuable metals, which were typically 100-300 mg/dm^3. Problems in chemical leaching were high consumption of acid and poor selectivity. Bioleaching using iron and sulphur oxidizing bacteria was more selective towards the valuable metals. Both in leaching and bioleaching the high concentration of iron and magnesium in solution will make metals recovery challenging.

Introduction

The tailings from mining and extraction contain metals whose dissolution is an environmental risk. In Finland, mining activities utilise mainly sulphidic ores, containing only minor amounts of neutralizing carbonate minerals. This leads to a situation where sulphidic tailings may oxidize spontaneously in tailing ponds and generate Acid Rock Drainage (ARD). Metal rich in the ARD may leak from pond to surrounding environment, causing heavy stress to large areas (Moncur et al. 2005).The tailings are also considered as sources of valuable metals (Xie et al. 2005, Antonijevic et al. 2008). Yearly in Finland about three teragrams (Tg, million tons) of mining wastes containing valuable metals are stored at dump sites. Currently only 20% of

these wastes are reused. Especially tailings from mineral processing contain valuable metals but they appear in so small concentrations that processing them would be difficult with traditional methods.

Bioleaching is a rapidly growing technique for extraction of various metals from ores and mineral concentrates. Traditionally industrial scale applications have been related to copper extraction from sulphidic minerals, but lately promising results have also been acquired with recovery of gold, uranium, nickel and zinc. As bioleaching is relatively low-cost technology, it may also be utilised for poor ores and mine site wastes, like tailings (Bosecker 1997, Rawlings 2002). Bioleaching is based on certain bacteria's ability to oxidize ferrous iron (Fe^{2+}) to ferric iron (Fe^{3+}), and/or to oxidize reduced sulphur compounds to sulphuric acid (H_2SO_4). Produced Fe^{3+} and H^+ can both attack sulphide minerals and release valuable metals to surrounding solution. Due to generation of sulphuric acid, pH of the surrounding solution decreases rapidly to values like 1–3, maintaining valuable metals in oxidized and solubilised form suitable for recovery process (Sand et al. 2001).

This work studies hydrometallurgical and biological methods for processing sulphidic tailings. It focuses on recovery of copper, nickel and zinc from sulphide tailings. Hydrometallurgical and bioleaching test series were done for two mineral processing tailings, which had been taken from the Finnish Hitura and Pyhäsal mine. Hitura is a nickel and Pyhäsalmi is a multi-metal mine, and both are located in North Ostrobothnia. Hitura produces nickel concentrate, which contains small amounts of copper, cobalt, platinum and palladium. Pyhäsalmi produces three different copper, nickel and pyrite concentrates.

Experimental

The purpose of the work was to clarify, which leaching conditions should be used to recover as much as possible of the valuable copper, nickel and zinc metals. Tailings from the Hitura and Pyhäsalmi mines were collected in years 2010–2011 and stored under water. Freeze-dried and homogenized samples were analysed by the ICP-AAS. The results are shown in Table 1. Attention must be paid to the facts that the Hitura tailings contained some zinc and Pyhäsalmi tailings contained little nickel. Sands contained a ten-fold, or greater, amount of iron compared to the wanted metals.

Table 1. Average metal concentrations in Hitura and Pyhäsalmi tailings

Material	Cu, g/kg	Ni, mg/kg	Zn, mg/kg	Mg, g/kg	Mn, g/kg	Fe, g/kg
Hitura tailing	1.20	2775	70	41.60	1.27	111.00
Pyhäsalmi tailing A	1.56	25	2185	9.64	1.14	205.00
Pyhäsalmi tailing B	0.52	16	738	6.96	0.40	764.00

The Hitura tailings consist mainly serpentinite $Mg_3(OH)_4Si_2O_5$ (52.6%), chlorite $(Mg,Fe)_5Al(Si_3Al)O_{10}(OH)_8$ (12.8%), and tremolite or antofyllite $Ca_2(Mg,Fe)_5Si_8O_{22}(OH)_2$ and $(Mg,Fe)_7Si_8O_{22}(OH)_2$, (10.4%). In addition, the Hitura tailings contained calcite $CaCO_3$(0.4%) and some sulphide minerals of which pyrrhotite ($Fe_{0.83-1}S$) is the most common. The Hitura tailings contain acid producing sulphide minerals, but very little neutralizing carbonates. On the other hand, the serpentinite is an alkaline and acid-neutralizing mineral. Pyhäsalmi tailings A and B consist mainly of pyrite FeS_2 (38.4–83.6%) and barite (3.1–19.6%). It contains also some pyrrhotite (2.2%), sphalerite $(Zn, Fe)S$ (0.2%) and chalcopyrite $CuFeS_2$ (0.1%). The Pyhäsalmi tailings contain a lot of acid-producing sulphates but only little neutralizing carbonates and silicate minerals. As shown in Table 1, the composition of Pyhäsalmi tailings A and B varies greatly, illustrating the heterogenic and time dependent nature of tailings (Toropainen and Heikkinen 2006).

Chemical leaching experiments were done as batch leaching tests with Hitura and Pyhäsalmi tailings A, which contained more valuable metals than Pyhäsalmi tailings B. Constants in experiments were volume of acid 700 cm^3, amount of solid 250 g, speed of stirrer 200 rpm and gas flow rate 1 dm^3/min. Experiment time was 120 minutes. During the test samples were taken from the solution and the values of pH and redox potential were followed. The 15 cm^3 of samples were taken at 5, 15, 30, 60 and 120 minutes from the beginning of experiment. Before sampling stirring and gas purging were stopped and solution was allowed to settle. The solution sample was taken from the surface of the solution, and immediately filtered and stabilized. pH and redox potential values were measured at 0, 5, 10, 20, 30, 40, 60, 80, 100 and 120 minutes. Factorial testing with three variables and three levels was done for both materials. Factors were pH that had levels 0, 1 and 3, temperature at levels 25 °C, 50 °C and 75 °C and redox potential, which was controlled by purging with oxygen, air or nitrogen. Table 2 shows the factor levels and combinations used in factorial testing. Note that for acid concentration the highest level is the highest acid concentration that

Table 2. Randomized order of experiments and factor combinations

Std Order	Run Order	pH	T, °C	Redox
4	1	0	75	Nitrogen
9	2	1	50	Air
6	3	0	25	Oxygen
2	4	0	25	Nitrogen
10	5	1	50	Air
1	6	3	25	Nitrogen
8	7	0	75	Oxygen
3	8	3	75	Nitrogen
5	9	3	25	Oxygen
7	10	3	75	Oxygen

numerically means lowest pH-value. When the variables had been chosen, the 2^3 test series with center point was planned using the MINITAB 16 software. In Table 2 the column Run Order is the order of tests and Std Order is the order used for the analysis. The same test program of ten tests was done for both tailings. Factorial analysis of the variables was made with the MINITAB 16 statistic calculation software. Three major analyses were conducted. Pareto analysis shows the significance of the factor to the measured response. The main factor analysis shows the effect of each individual factor on the measured response. An interaction plot shows how two factors effect on the response together.

For bioleaching experiments the VTT (VTT Technical Research Centre of Finland) mixed acidophilic culture was cultivated in duplicate 500 cm^3 Erlenmeyer flasks with a working volume of 250 cm^3. Cultivations were incubated at 28 °C with shaking at 150 rpm. Sterile growth medium contained deionized water (ddH$_2$O), mineral salts and trace elements (Table 3) and it was supplemented with sterile S^0 (1% w/v) and FeSO$_4$ (4.5 g/dm^3 Fe^{2+}). Vitality of the cultivation was monitored by pH, Oxidation Reduction Potential (ORP) and dissolved Fe^{2+} measurements, and by microscoping (Zeiss Axioskop II and Zeiss Axio Imager). New medium was made every fortnight.

Table 3. Concentration of growth medium

Chemical formula	Concentration, mg/dm^3	Chemical formula	Concentration, mg/dm^3
$(NH_4)_2SO_4$	2160	H_3BO_3	1.4
K_2HPO_4	36	$MnSO_4 \cdot H_2O$	1.4
$MgSO_4 \cdot 7H_2O$	360	$Na_2MoO_4 \cdot 2H_2O$	0.6
$Ca(NO_3)_2$	7.2	$CoCl_2 \cdot 6H_2O$	0.4
$FeCl_3 \cdot 6 H_2O$	7.9	$ZnSO_4 \cdot 7H_2O$	0.6
$CuSO_4 \cdot 5 H_2O$	0.4	Na_2SeO_4	0.07

Bioleaching experiments were done as batch leaching tests with Hitura and Pyhäsalmi tailings B. As Pyhäsalmi tailings B contained less valuable metals than Pyhäsalmi tailings A, it was seen more suitable for cost effective bioleaching technique. Preliminary bioleaching experiments were done to clarify optimal conditions for scaled up reactor experiments. Bioleaching experiments were conducted in duplicate 250 cm^3 Erlenmeyer flasks containing mineral salts medium and trace elements (Table 3) with a total working volume of 100 cm^3. Flasks were inoculated with 10% (v/v) VTT's mixed acidophilic culture and incubated at 28 °C with shaking at 150 rpm. Examined parameters were addition of S^0 (0–1% w/v) and/or FeSO$_4$ (0– 4.5 g/dm^3 Fe^{2+}), pH fixation with strong H$_2$SO$_4$ to pH 2, and pulp density of tailings (1–10% w/v). Progress of bioleaching was monitored by pH, ORP and dissolved Fe^{2+} measurements. Liquid samples were taken to analyse dissolved metals and anions after

experiments. Samples were filtered with 0.45 µm filter paper and stabilized with strong HNO_3 (0.25 cm^3 / 50 cm^3 of sample). Tailings were bioleached for 20 days.

Scaled up bioleaching reactors were run in batch mode in 3 dm^3 Continuously Stirred Tank Reactors (CSTR) with a total working volume of 2 dm^3. Reactors were equipped with mixers and 10 cm diameter propellers. Stirring speed was 100 rpm. The aeration was supplied from the bottoms at 1.5 dm^3/min. The air bubble size was reduced with a choke. Temperature of reactors was maintained at 28°C with heated water circulations. The leaching solution contained mineral salts, trace elements, ddH_2O (Table 4) and 10% (v/v) of VTT's mixed acidophilic culture. The experiment with Hitura tailings was supplemented with S^0 (1% w/v) and $FeSO_4$ (4.5 g/dm^3 Fe^{2+}). Also pH was fixed to 2 with strong H_2SO_4. Experiment with Pyhäsalmi tailings B had no S^0 or $FeSO_4$ additions, and pH was not fixed. Both tailings were bioleached for 20 days. Progress of bioleaching was monitored by pH, ORP and dissolved Fe^{2+} measurements. Liquid samples were taken to analyse dissolved metals and anions after experiments. Samples were filtered with 0.45 µm filter paper and stabilized with strong HNO_3 (0.25cm^3 / 50 cm^3 of sample). Also solid reject was analysed. Tailings were bioleached for 20 days.

Results

Chemical leaching tests

The leaching kinetics of different metals was estimated by solution analyses. The recovery of metals was calculated using solution and tailing analyses. The leaching tests showed that dissolution of metals is most efficient in the most acid solutions. Examples of dissolution kinetics of the Hitura tailings are shown in Figs. 1 and 2. Figure 1 shows that iron and magnesium concentrations in the leach solution are much higher than those of valuable metals. This results from the raw material composition, where iron and magnesium compounds dominate. The iron concentrations in the most successful tests were 4–11 g/dm^3 and magnesium concentrations 7–38 g/dm^3. Figure 2 shows that the contents of the valuable metals were typically only a hundredth of the contents of iron or magnesium. The Cu, Ni and Mn concentrations were in the range of 100–300 mg/dm^3 in the most successful experiments.

The recoveries from the Hitura tailings are shown in Table 4. The most successful leaching tests were 7, 3, 4 and 1, even though copper was not recovered in the last one. Table 4 shows that recovery of magnesium is greater than that of other metals. The recovery of iron is often of the same order as the recovery of the valuable metals. No preferential dissolution of valuable metals was found. In tests 1 and 7 with low pH and high temperature, magnesium recoveries were over 100%, which must be an analytical error. Leaching tests with the Hitura tailings dissolved mainly magnesium and iron.
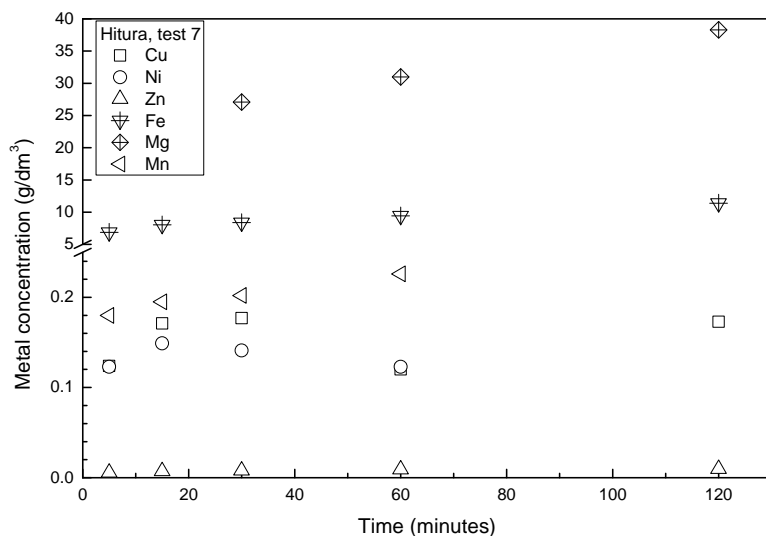
Fig. 1. Metal concentration as function of time in Hitura tailings test 7 (pH = 0, T = 75 °C, O_2)
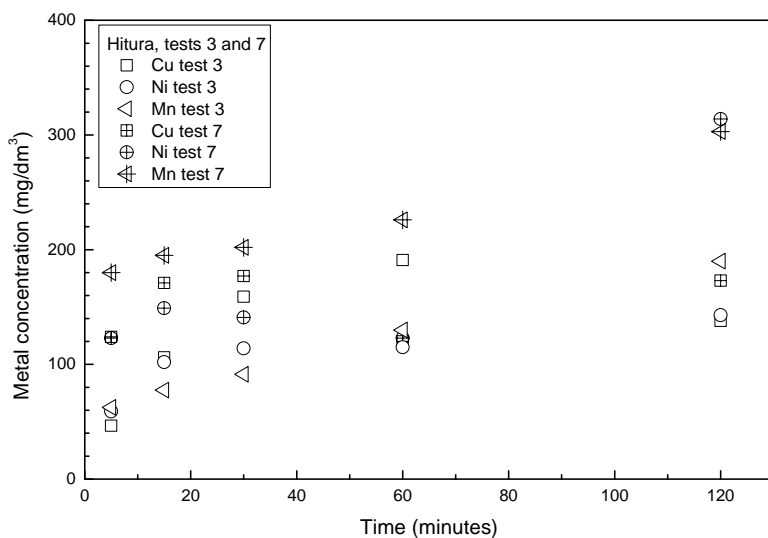
Fig. 2. Dissolution of Cu, Ni and Mn from Hitura tailings
in tests 3 (pH = 0, T = 25 °C, O_2) and 7 (pH = 0, T = 75 °C, O_2)

Examples of dissolution kinetics in leaching tests with the Pyhäsalmi tailings are shown in Figs. 3 and 4. Also in these tests most efficient dissolution was found in tests with highest acidity. In the Pyhäsalmi tailings tests iron concentrations were 2–8 g/dm^3 and magnesium concentrations 1.5–4 g/dm^3 in the most successful tests (Fig. 3). The

valuable metal concentrations were 20-80 mg/dm^3 Cu, 200–500 mg/dm^3 Zn, and 100–200 mg/dm^{3}Mn.

Table 4. Recoveries from Hitura tailings based on analyses after 120 minutes of leaching

Test, RunOrder	pH	T, °C	Redox	Cu, %	Zn,%	Ni, %	Fe, %	Mg, %	Mn,%
1	0	75	N_2	0.14	25.9	18.6	17.5	173	46.8
2	1	50	Air	0.00	0.08	3.07	0.01	8.83	8.31
3	0	25	O_2	27.7	10.5	12.4	12.8	81.4	35.9
4	0	25	N_2	13.1	8.81	5.85	6.36	38.6	14.0
5	1	50	Air	0.01	0.17	3.36	0.01	7.27	8.37
6	3	25	N_2	0.00	0.02	0.04	0.00	1.89	0.15
7	0	75	O_2	34.7	33.0	27.2	24.6	220	57.3
8	3	75	N_2	0.00	1.03	0.02	0.01	1.23	0.15
9	3	25	O_2	0.01	0.02	0.19	0.00	2.09	0.18
10	3	75	O_2	0.02	0.09	0.10	0.00	3.16	0.29
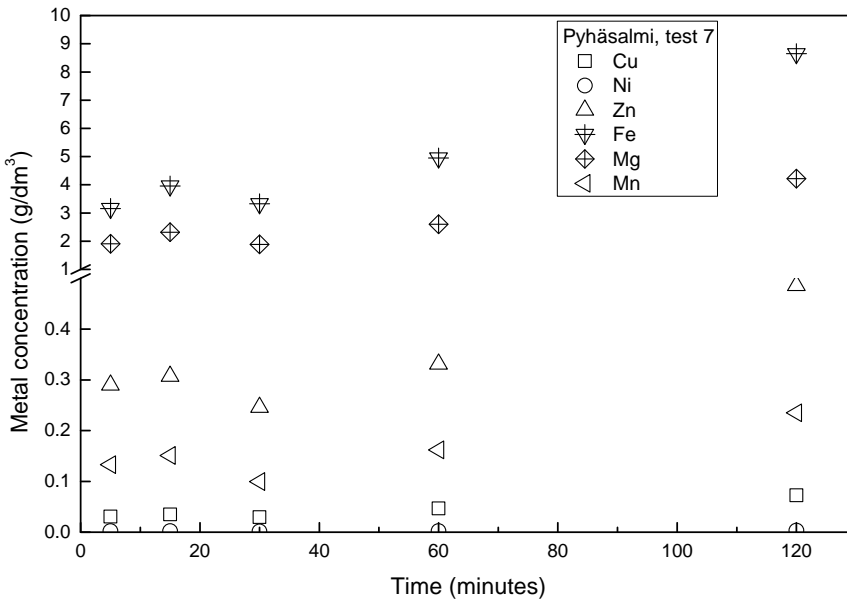
Fig. 3. Metal concentration as a function of time
in Pyhäsalmi tailings test 7 (pH = 0, T = 75 °C, O_2)
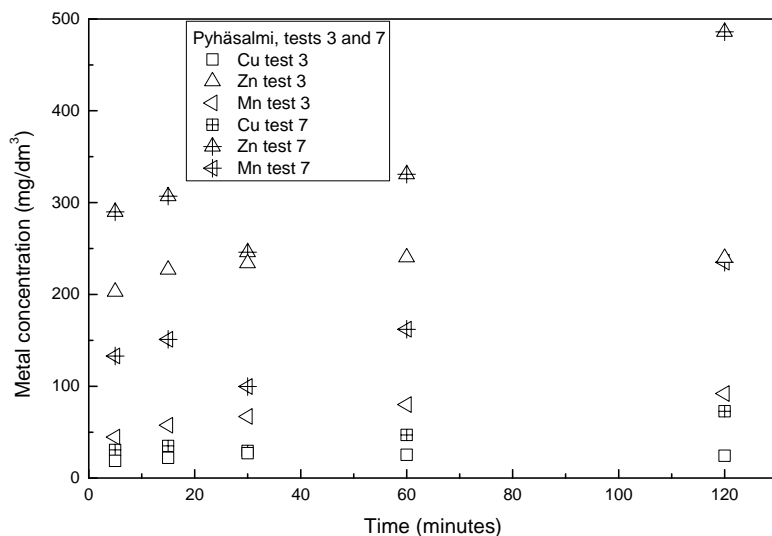
Figure 4. Dissolution of Cu, Zn and Mn from Pyhäsalmi tailings
in tests 3 (pH = 0, T = 25 °C, O_2) and 7 (pH = 0, T = 75 °C, O_2)

The recoveries from the Pyhäsalmi tailings are shown in Table 5. The most successful tests were again the tests with highest acidity 7, 4, 3 and 1. Dissolution of valuable metals Cu, Zn and Mn in other tests was very small. The solution concentrations of iron and magnesium were also in Pyhäsalmi tests much higher than concentrations of the valuable metals. In Pyhäsalmi tests iron recovery was often smaller than that of valuable metals but magnesium extraction was again high. The Pyhäsalmi tests showed slightly better preferential dissolution of valuable metals than the Hitura tests.

Table 5. Recoveries from Pyhäsalmi tailings based on analyses after 120 minutes leaching

Test, RunOrder	pH	T, °C	Redox	Cu, %	Zn,%	Ni, %	Fe, %	Mg, %	Mn,%
1	0	75	N_2	12.8	46.4	32.9	9.03	90.6	41.3
2	1	50	Air	0.34	26.9	17.9	1.07	17.0	13.7
3	0	25	O_2	3.75	26.4	19.7	2.75	36.6	19.4
4	0	25	N_2	3.66	26.7	19.4	2.81	37.1	19.6
5	1	50	Air	0.90	19.7	11.9	0.82	12.9	10.0
6	3	25	N_2	0.00	0.01	0.14	0.00	1.47	0.20
7	0	75	O_2	11.2	53.4	31.1	10.1	105	49.5
8	3	75	N_2	0.00	0.01	0.08	0.00	3.44	0.26
9	3	25	O_2	0.00	0.02	0.18	0.00	1.64	0.23
10	3	75	O_2	0.00	0.02	0.11	0.00	3.31	0.38

The effect of leaching factors were analysed using the Minitab 16 software. The main effects of the Hitura tailings leaching were strong increased dissolution of Cu, Ni and Mn and also of Fe and Mg with increasing acidity and redox potential and low increase with increasing temperature. The increase in acidity had positive interaction with temperature and redox potential for all metals. All tested factors were significant for all metals. The main effects of the Pyhäsalmi A tailings leaching were increased dissolution of Cu, Zn and Mnas well as Fe and Mg with increasing acidity and temperature and low increase or even decrease with increasing redox potential. The increase in acidity had positive interaction with temperature for all metals. Tested factors were significant for Cu, Mn, Fe and Mg but not for Zn, possibly due to highly scattered results.

Bioleaching tests

Figure 5 presents monitored parameters of bioleaching of the Hitura tailings in a 3 dm^3 reactor. At the beginning of the experiment, pH tends to rise, mainly due to acid-neutralizing serpentinite. However, after addition of H_2SO_4 (95 cm^3 95% H_2SO_4 / 1 kg of Hitura tailings), biological sulphuric acid production outmatched neutralization capacity and pH decreased to 1.4. At the same time, sulphate concentration rose from 13 to 37 g/dm^3, illustrating the activity of sulphur oxidizing bacteria and sulphide mineral dissolution. Dramatic changes in both ORP (E_h) and concentration of dissolved Fe^{2+} illustrate the activity of iron oxidizing bacteria. Dissolved Fe^{2+} concentration is quickly decreased by bacteria.
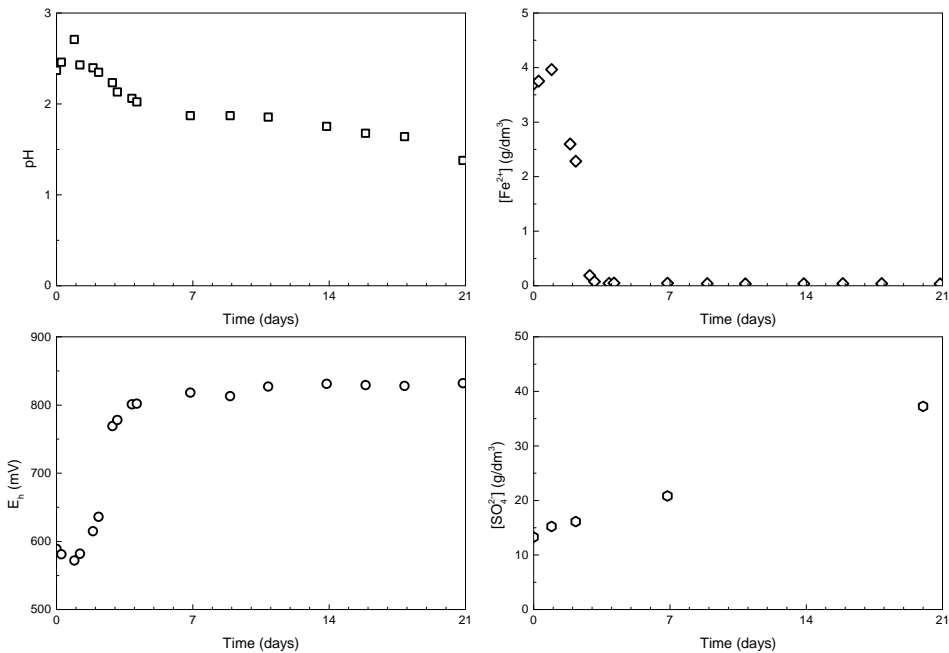
Fig. 5. Monitored parameters in bioleaching reactor of Hitura tailings

The leaching kinetics of different metals was estimated by solution analyses, presented in Fig. 6. Concentrations of all valuable metals were increasing steadily, as predicted. Mg followed also this trend, rising from 0.2 g/dm^3 to 3.4 g/dm^3. However, concentration of iron remained rather constant at ~ 5 g/dm^3, mainly due to addition of $FeSO_4$ (4.5 g/dm^3 Fe^{2+}). Table 6 shows the recoveries of metals. The recovery were calculated using solution and tailing analyses.
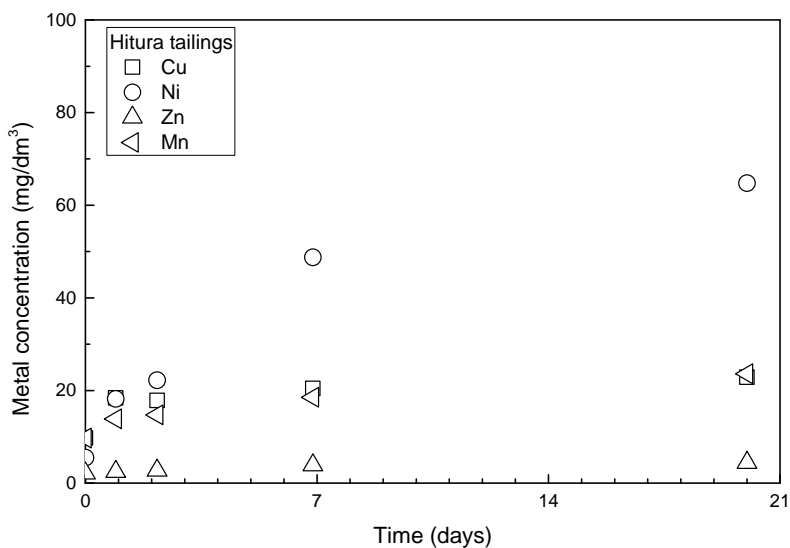
Fig. 6. Metal concentration as function of time in Hitura tailings bioleaching reactor, S^0 = 1% (w/v), Fe^{2+} = 4.5 g/dm^3, fixed pH $\leq$ 2, pulp density 2.5% (w/v)

Table 6. Recoveries from Hitura tailings based on the analyses after 20 days of bioleaching

Hitura tailings	Cu, %	Zn,%	Ni, %	Fe, %	Mg, %	Mn,%
Recovery	76.5	100[1]	93.3	-[2]	100[1]	74.3

[1]Over 100 % recovery, due to error in ICP analyses

[2]$FeSO_4$ added to reactor, iron recovery cannot be calculated

Figure 7 presents monitored parameters of bioleaching of Pyhäsalmi tailing B in the 3 dm^3 reactor. pH began to decrease immediately and end up at pH 1.4. At the same time sulphate concentration rose from 3 to 101 g/dm^3. This illustrates the activity of sulphur oxidizing bacteria and efficient sulphide mineral dissolution. Dramatic changes in the ORP (E_h) and low Fe^{2+} concentration during the experiment illustrate the activity of iron oxidizing bacteria.
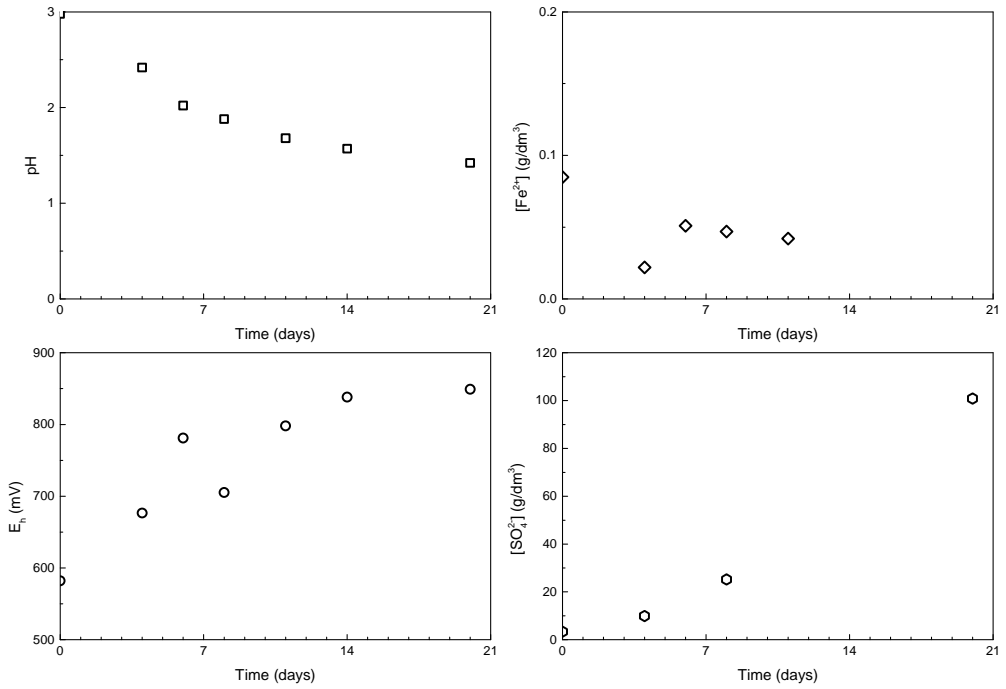
Fig. 7. Monitored parameters in bioleaching reactor of Pyhäsalmi B tailings
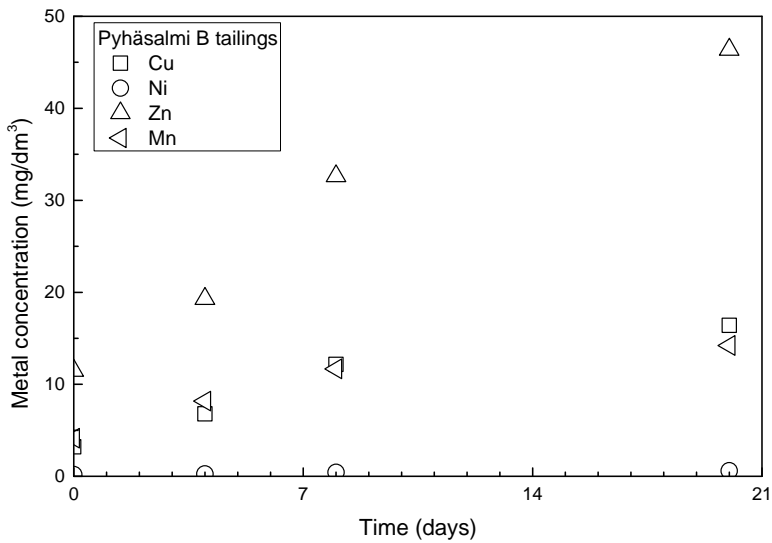
Fig. 8. Metal concentration as function of time in Pyhäsalmi B tailings
bioleaching reactor (no chemical additives, pulp density 5% (w/v))

The leaching kinetics of different metals was estimated by solution analyses (Fig. 8). Concentrations of all valuable metals were increasing steadily, as predicted. Magnsium and Fe followed also this trend, rising from 0.07 g/dm^3 to 0.26 g/dm^3 and 0.1 to 6.0 g/dm^3, respectively. As $FeSO_4$ was not added, iron was completely dissolving from the mineral matrix. Table 7 shows the recoveries of metals. The recoverys were calculated using solution and tailing analyses.

Table 7. Recoveries from Pyhäsalmi tailings B based on the analyses after 20 days of bioleaching

Pyhäsalmi tailing B	Cu, %	Zn,%	Ni, %	Fe, %	Mg, %	Mn,%
Recovery	71.3	100[1]	85.2	17.6	83.3	79.1

[1] Over 100 % recovery, due to error in the ICP analyses

Composition of leached tailings

Leached tailings were analysed with ICP-AAS for residual metals. The results are shown in Table 8. The results indicate that bioleaching can be more selective towards the wanted metals.

Table 8. Residual metals in leached tailings

Material	Cu, mg/kg	Ni, mg/kg	Zn, mg/kg	Mg, g/kg	Mn, mg/kg	Fe, g/kg
Hitura tailing (chem. leaching, test 7)	439	1533	62	59.85	412	61.75
Hitura tailing (bioleaching reactor)	369	404	30	75.90	513	119.40[1]
Pyhäsalmi tailing A (chem. leaching, test 7)	1600	29	1490	8.26	559	163.50
Pyhäsalmi tailing B (bioleaching reactor)	286	9	112	2.96	153	442.00

[1] $FeSO_4$ added to reactor

Discussion

Both tailings gave similar results in the chemical leaching tests. All variables had effect for leaching metals. High temperature and redox potential and low pH gave best results. Both tailings contained minerals that neutralize acid. The tailings had also much iron and magnesium containing minerals. The solution after chemical leaching tests contained mostly iron and magnesium. The Hitura tailing contained up to 11 g/dm^3 Fe and 38 g/dm^3 Mg and Pyhäsalmi tailing 8–9 g/dm^3 Fe and 4 g/dm^3 Mg. Due to tailings composition, the amount of these metals was 20–100-fold larger than the amount of valuable metals, which was typically 100–300 mg/dm^3. The iron and magnesium compounds dissolve easily and no preferential dissolution of valuable metals was achieved. High acid consumption and high Fe and Mg levels will make valuable metals recovery difficult with conventional methods. Also it must be emphasized that the leached tailings contained still relatively high concentrations of valuable metals making utilisation or disposal challenging.

In bioleaching experiments it was seen that bacteria were able to grow in the presence of both tailings when low pulp densities (2.5–5.0% w/v) were used. The

Hitura tailings contained plenty of acid-neutralizing minerals (e.g. serpentinite), which caused the need for external acid addition alongside the biological acid production. When there were minor amounts of suitable substrates in the Hitura tailings (e.g. FeS_2), S^0 and $FeSO_4$ were added to the reactor. With a 20-day bioleaching, the majority of valuable metals were leached to the solution, but as Fe and Mg levels were magnitudes higher, recovery from solutions is challenging. Pyhäsalmi tailing B was seen as more suitable material for bioleaching technique as it contained lower amount of acid neutralizing minerals. Moreover, the Pyhäsalmi tailing B consisted mainly of FeS_2, which was used itself as a substrate for iron and sulphur oxidizing bacteria and no S^0 or $FeSO_4$ additions were needed. Valuable metals were leached efficiently and also residual metal concentrations in solid reject were lower. However, the recovery processes will still face challenges due to high Fe and Mg concentrations in produced liquid.

Conclusions

Sulfidic tailings were leached using sulfuric acid and bacteria. The tailings consisted mainly of iron and magnesium containing minerals as well as acid neutralizing minerals. The concentrations of valuable metals like Ni, Cu, Zn and Mn were orders of magnitude lower than those of Fe and Mg. This caused high consumption of acid and poor selectivity in chemical leaching. Bioleaching using iron and sulphur oxidizing bacteria was more selective towards the valuable metals. Even though the reaction rates and valuable metal concentrations in bioleaching were lower than in chemical leaching, the selectivity and lower processing costs make bioleaching more attractive. Both in chemical leaching and bioleaching the high concentration of iron and magnesium in solution will make metals recovery challenging.

Acknowledgements

References

ANTONIJEVIĆ M.M., DIMITRIJEVIĆ M.D., STEVANOVIĆ Z.O., SERBULA S.M., BOGDANOVIC G.D., 2008, *Investigation of the possibility of copper recovery from the flotation tailings by acid leaching*. Journal of Hazardous Materials158, 1, 23–34.

MONCUR M.C., PTACEK C.J., BLOWES D.W., JAMBORJ L., 2005, *Release, transport and attenuation of metals from an old tailings impoundment*. Applied Geochemistry 20, 3, 639–659.

TOROPAINEN V., HEIKKINEN P., 2006, *Mineralogical and chemical composition of the tailings and waste rock samples of Pyhäsalmi, Hitura, Talvivaaraand Ihalainen ore deposits*. GTK Report S49/0000/2006/3.

XIE Y., XU Y., YAN L., YANG R., Recovery of nickel, copper and cobalt from low-grade Ni–Cu sulfide tailings. Hydrometallurgy 80(2005) 1–2, 54–58.

BOSECKER K., 1997, Bioleaching: metal solubilization by microorganisms. FEMS Microbiology reviews 20, 591–604.

RAWLINGS D.E., 2002, *Heavy metal mining using microbes*. Annual Review of Microbiology 56, 65-91.

SAND W., GEHRKE T., JOZSA P-G., SCHIPPERS A., 2001, *(Bio)chemistry of bacterial leaching – direct vs. indirect bioleaching.* Hydrometallurgy 59, 159–175.

REMOVAL OF HAZARDOUS AIR POLLUTANTS BASED ON COMMERCIAL COAL PREPARATION PLANT DATA

Gulhan OZBAYOGLU

Atilim University, Faculty of Engineering, Incek, Golbasi, Ankara, Turkey, e-mail: gulhan@atilim.edu.tr

Abstract: This paper investigates the concentration, distribution, and rejection of hazardous air pollutants, specifically identified by the US Clean Air Act Amendments of 1990, based on commercial coal preparation plant data obtained on-site. The samples were collected from the products of the different cleaning circuits of the operating plant. The concentrations of twelve potentially hazardous trace elements, including As, Cd, Co, Cr, Hg, Mn, Ni, Pb, Se, Th and U in those samples were determined. Compared with the average concentration of the trace elements in Turkish coals, the run-of-mine coal fed to the existing plant appears to contain higher concentrations of Cd, Hg, Mn, Th and V. However, the concentrations of As, Cd, Cr, Mn, Se, Th, U and V of the run-of-mine coal are above the world averages. Cd, Cr, Hg, Mn, Pb and Th concentrations of run-of-mine coal were easily removed at commercial coal preparation plant refuse in the range of 51.8% to 77.4 %, while only a small reduction was achieved for U and V as they were concentrated in clean coals. The present study reveals that conventional coal preparation technologies could significantly reduce hazardous air pollutants concentrations in coal.

Key words: hazardous air pollutants, coal preparation, Turkish lignites, trace elements rejection, dense medium separation

Introduction

General

Many of the potentially hazardous air pollutants (HAP's for short) occur as trace elements in run-of-mine coals. The growing awareness of environmental issues has increased the attention on these elements (Coal Trading Blog, 2011; Gürdal, 2008; Pesek et al., 2005; Swaine, 1998). As coal will continue to be a major energy source to generate electricity worldwide, the trace elements which may cause hazardous emissions upon combustion of the coal have also become an increasingly important concern for those involved in the industry. The US Clean Air Act Amendments of 1990 specifically identifies As, Be, Cd, Cr, Co, Hg, Mn, Ni, Pb, Sb, Se and U as potential HAP's (Demir et al., 1998). These trace elements are known to be toxic and

have adverse effects on humans, plants and animals. Table 1 summarizes the average concentrations of a number of trace elements in Turkish coal samples compared against world averages (Tuncali et al., 2002).

Table 1. Potential hazardous air pollutants in Turkish lignites and the world (ppm)

Trace Elements	As	Be	Cd	Co	Cr	Hg	Mn	Ni	Pb	Se	Th	U	V
Average	53	1	1	9.4	109	0.1	123	126	12	2	6	13	87
Minimum	2	0.2	0.01	1	7	0.03	5	3	0.1	0.1	1	0.4	6
Maximum	686	7	45	55	580	0.7	691	1700	286	26	29	132	287
World average	10	2	0.5	5	20	-	70	20	20	1	4	2	40

As seen in Table 1, the concentration of these trace elements have a wide range of variation, and their amounts vary considerably from seam to seam and, in some cases, even within the same seam. During combustion at electrical utilities, trace elements may be released to the atmosphere as solid compounds with the fly-ash and, in the vapor phase, with the flue-gas (Yasushi et al., 2003; Esenlik et al., 2006; Zevenhoven et al., 2005; Ward, 2002). To control toxic air emissions, post-combustion and/or pre-combustion methods can be used (Vejahati et al., 2010; Gupta, 2006; Vassilev et al., 2001; Akers et al., 2000). Elements such as Sb, Be, Cd, Co, Pb and Mn are believed to be removed with fly-ash by applying post-combustion methods – that is, by electrostatic precipitators. On the other hand, trace elements such as As, Cl, Hg and Se have the potential to volatilize/vaporize and, consequently, cannot be controlled as effectively by conventional post-combustion techniques. However, coal cleaning, when applied before combustion to remove ash in coal, is effective in reducing the level of most of the trace elements, but the degree of removal of ash and trace elements are dependent on the coal, the degree of liberation of the trace elements bearing mineral matters, and the cleaning method of coal itself (Davidson, 1998). Although, physical cleaning may provide limited improvement in the quality of run-of-mine coal, it has been considered an economical and effective technique in minimizing environmental problems (Dangyu et al., 2007; Weng and Peng, 2003; Wang et al., 2009).

Unfortunately, there are limited information concerning of trace elements removal during coal washing in the world (Wang et al., 2009; Wang et al., 2003). Similarly, very limited data is available on the subject of trace elements removal from Turkish coals by coal preparation techniques (Özbayoğlu, 2010; 2011).

As stated before, coal preparation is used commercially to improve the quality of coal by removing ash and sulfur. During the removing of ash, the trace elements which are associated with inorganic matter would be rejected autogenously, since there is a general relationship between overall ash removal and trace elements

rejection. Therefore, the objective of this investigation is to determine the HAP's partitioning and rejections that would be achieved in different coal cleaning circuits of an existing coal preparation plant in Turkey. Although, the Imbat coal preparation plant was chosen for this study, trace elements reduction would be expected similarly in different ranges in the other coal preparation plants depending on coal, modes and occurrences of trace elements and cleaning methods used.

Coal preparation plants in Turkey

Coal is the main raw material to generate power for electricity in Turkey with a total reserve of about 12.88 petagrams (Pg or billion tons), of which 11.56 Pg is lignite and 1.32 Pg is bituminous coal. The Turkish coal sector produces both hard coal and lignite primarily used for power generation. Currently, there are around 45 coal preparation plants in operation in Turkey, with capacities ranging from 50 to 1000 mega grams per hour (tph), 12 to treat bituminous coal, and the rest to cover about 40% of the country's lignite production. Most of the lignite coal preparation plants are based on dense medium separation facilities. Static (drums, baths, vessels) and dynamic heavy medium (cyclones) equipment are used to treat coarse coal (+18 mm) and fine coal (0.5–18 mm), respectively. In this investigation, both the distribution and the possibility of the removal of trace elements are addressed in different cleaning circuits of the commercial Imbat coal preparation plant, whose flowsheet has been simplified in Fig. 1. This plant has a capacity of 350 Mg per hour, and it treats the coal coming from underground operations.

As seen from the flow sheet, the run-of-mine coal is crushed to 50 mm top-size before processing and, then, screened through 18 mm to separate the coal into coarse (+18 mm) and fine (−18 mm) size fractions. Drewboy is used for cleaning coarse size coal into two steps. The first Drewboy cleans the coal at a density of 1.80 g/cm^3 to remove coarse shale, followed by the second Drewboy working at 1.55 g/cm^3 density to produce clean coal and middling. Magnetite is used in the preparation of dense medium. The fine pieces (−18 mm) are deslimed at about 0.5 mm, and the 0.5–18 mm fraction is cleaned in dense medium cyclones at 1.55 g/ cm^3. The clean coals are screened through 10 mm and 0.5 mm screens to produce clean coals in sizes of 10–18 mm and 0.5–10 mm according to the market specifications. The –0.5mm-size coal is passed through hydrocyclones to recover the 0.1–0.5mm fraction and to remove the slime. Dewatering of the coarse and fine coal fractions is done in vibrating and screen-bowl centrifuges. Eventually, the products of +18 mm middling and hydrocyclones U/F are mixed together to be burnt in power plants.

There, at the coal preparation plant, the main problem is the clay, which clogs the openings of the screen surfaces causing an inefficient screening and mixing of clay particles to the bath of Drewboy. This condition has a diverse impact on both the performance and the capacity of the plant.
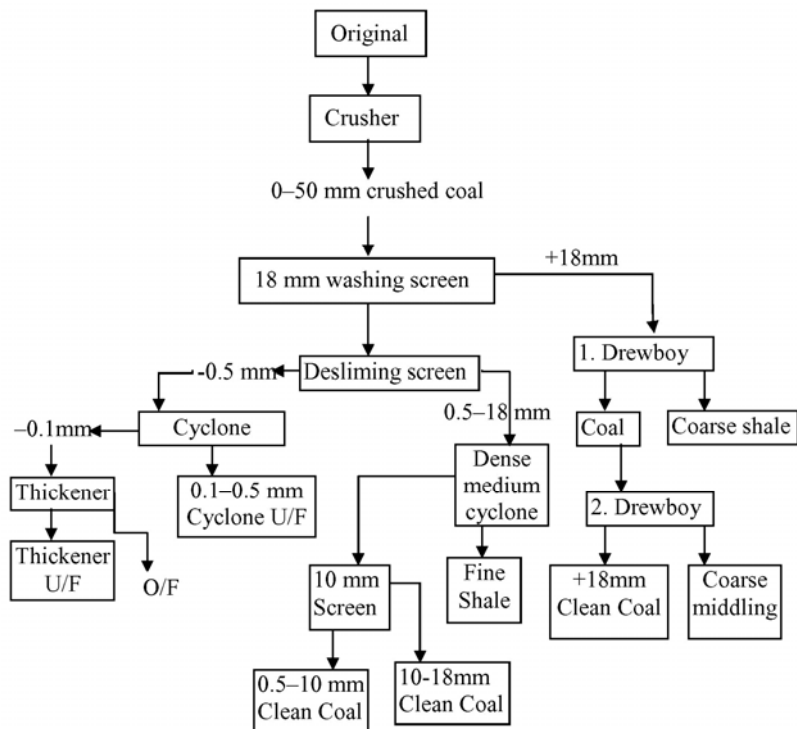
Fig. 1. Simplified flow sheet of Imbat Coal Preparation Plant

Materials and method

Systematic samples were collected from the run-of-mine coal (r.o.m.), the coarse and fine clean coals, coarse shale and middling of Drewboy and fine shale of dense medium cyclones, and the U/F of hydrocyclones and that of the tailing pond of the Imbat Coal Preparation Plant. The samples obtained were collected incrementally within 60-minute intervals in one day from the cleaning equipments. The trace elements analysis was carried out on dried representative samples of the mentioned products using the XRF and ICP-OES techniques.

For each trace element, the enrichment ratio – the ratio of the grade of concentrate (products) to that of the run-of-mine coal – was calculated. Also, the contents and distributions of trace elements in each cleaning circuit were determined. Finally, the rejection of trace elements was calculated.

Results and discussions

The proximate analysis and trace elements (hazardous air pollutants) contents of the run-of-mine coal and plant products were determined as illustrated in Tables 2 and 3.

Table 2. Proximate analysis of the samples (on dry basis)

Samples	Weight, %	Ash, %	Volatile Matter, %	Low Heat Value, MJ/kg	Total sulfur, %	Sulfur in ash %
+18mm clean coal	17.16	17.56	40.25	23.58	1.16	0.60
10–18mm clean coal	4.46	15.44	40.93	24.37	1.16	0.55
0.5–10mm clean coal	14.75	13.60	41.20	25.21	1.19	0.52
0.1–0.5mm cyclone U/F	2.92	30.94	37.13	18.59	1.05	0.74
Coarse middling	9.82	34.75	38.21	16.27	0.61	0.54
Coarse shale	28.67	62.70	36.98	1.49	1.03	0.23
Fine shale	17.96	64.16	35.92	1.54	0.24	0.57
Thickener U/F	4.26	44.53	25.24	6.17	0.96	0.43
Feed (run-of-mine)	100.00	42.54	38.08	11.90	0.69	0.46

Table 3. Trace elements contents of the samples (ppm)

Trace elements	As	Cd	Co	Cr	Hg	Mn	Ni	Pb	Se	Th	U	V
+18 mm clean coal	45.1	2.0	3.0	26.8	0.7	149.8	14.6	7.9	1.2	3.8	18.1	104.8
10–18 mm clean coal	46.7	2.0	3.0	27.5	1.0	71.3	15.0	7.4	1.1	3.8	17.8	132.1
0.5–10mm clean coal	51.2	0.5	3.0	30.8	1.0	58.7	16.5	8.3	1.1	4.1	18.6	165.2
0.1–0.5mm cyclone U/F	45.0	2.0	3.0	36.8	1.0	128.1	19.0	15.4	1.2	6.2	15.1	134.7
Coarse middling	44.8	2.0	5.4	35.2	0.6	50.9	16.5	12.9	1.1	5.6	14.5	117.6
Coarse shale	31.2	2.0	3.0	41.3	1.0	360.4	12.8	12.3	1.1	8.3	3.8	45.4
Fine shale	23.7	2.0	3.0	37.2	1.0	349.1	15.6	12.8	0.9	7.0	3.4	53.9
Thickener U/F	30.1	2.0	5.8	51.6	0.5	180.3	23.4	18.6	1.0	14.6	14.3	103.6
Feed (run-of-mine)	37.6	1.8	3.3	35.6	0.9	214.5	15.2	11.2	1.1	6.4	10.8	90.8

According to the results, the ash content of the run-of-mine coal treated in the conventional Imbat Coal Preparation Plant is high with a concentration level of

42.54% because of the underground operations. However, its total sulfur content is very low (0.69%).

The ash content of +18 mm clean coal is high as 17.56% due to the mixing and floating of undispersed clay particles with the coal. The ash content decreases with the decrease in coal size. When these three clean coals are mixed together, the combined products will have a weight percentage of 36.37% with an average ash content of 15.69% and average low heat value of 24.34 MJ/kg according to metallurgical balance calculations. By similar calculation, the total plant shale, which is a mixture of coarse and fine shale, will have 46.63% weight with a total ash removal 69.4%.

It can be observed that, among the hazardous air pollutants of the run-of-mine coal, Cd, Mn, Th, V and Hg contents are above the Turkish coal averages; yet, Co, Cr, and Ni contents are much lower. On the other hand, As, Cd, Cr, Mn, Se, Th, U and V contents of the run-of-mine coal are above the world averages as seen in Table 1. The enrichment ratios of the trace elements detected within the plant products are tabulated in Table 4.

As seen in Table 4, U and V enrichments almost appear in clean coal samples, while Mn and Th are enriched in the shale. Also, 0.1–0.5 mm slimes collected in U/F of cyclone and slimes precipitated in the thickener U/F are enriched in Cd, Cr, Ni, Pb, U and V. Among all the examined products, the highest enrichment is found for Th at 2.28, and the second highest enrichment for Co at 1.76, at the thickener U/F.

Table 4. Enrichment ratio of the products

	As	Cd	Co	Cr	Hg	Mn	Ni	Pb	Se	Th	U	V
+ 18 mm clean coal	1.20	1.11	0.91	0.75	0.78	0.70	0.96	0.71	1.09	0.59	1.68	1.15
10–18 mm clean coal	1.24	1.11	0.91	0.77	1.11	0.33	0.99	0.66	1.00	0.59	1.65	1.45
0.5–10mm clean coal	1.36	0.28	0.91	0.87	1.11	0.27	1.09	0.74	1.00	0.64	1.72	1.82
0.1–0.5mm cyclone U/F	1.20	1.11	0.91	1.03	1.11	0.60	1.25	1.38	1.09	0.97	1.40	1.48
Coarse middling	1.19	1.11	1.64	0.99	0.67	0.24	1.09	1.15	1.00	0.87	1.34	1.30
Coarse shale	0.83	1.11	0.91	1.16	1.11	1.68	0.84	1.10	1.00	1.30	0.35	0.50
Fine shale	0.63	1.11	0.91	1.04	1.11	1.63	1.02	1.14	0.82	1.09	0.31	0.59
Thickener U/F	0.80	1.11	1.76	1.45	0.56	0.84	1.54	1.66	0.91	2.28	1.32	1.14

The trace elements contents and distributions of the plant products are calculated, and the extents of the removal of hazardous air pollutants are indicated in Table 5. Here, the trace elements retained in the clean coals and the ones which can be

removed with the shale can be seen. Summarized in the bottom row are the total amount of clean coal produced and the total amount of hazardous air pollutants rejection with the shale.

Table 5. Trace elements rejections (%) in different products

Trace elements	As	Cd	Co	Cr	Hg	Mn	Ni	Pb	Se	Th	U	V
+18mm clean coal	20.6	19.3	15.3	12.9	13.5	5.7	16.4	12.1	19.1	10.2	28.7	19.8
10–18mm clean coal	5.5	5.0	4.0	3.4	5.0	1.2	4.4	2.9	4.5	2.6	7.3	6.5
0.5–10mm clean coal	20.1	4.2	13.2	12.8	16.6	3.5	16.0	10.9	15.0	9.4	25.4	26.8
Middling[*]	15.2	14.3	18.4	12.7	9.9	8.6	14.2	15.3	13.3	11.4	17.2	17.0
Coarse shale	23.8	32.2	25.6	33.2	32.3	48.2	24.1	31.4	29.2	37.1	10.1	14.3
Fine shale	11.3	20.2	16.1	18.8	20.2	29.2	18.4	20.4	15.0	19.6	5.7	10.7
Thickener U/F	3.4	4.8	7.4	6.2	2.4	3.6	6.5	7.0	3.9	9.7	5.6	4.9
Total clean coals[**]	46.2	28.5	32.5	29.1	35.1	10.4	36.8	25.9	38.6	22.2	61.4	53.1
Total refuse[***]	35.1	52.4	41.7	52.0	52.5	77.4	42.5	51.8	44.2	56.7	15.8	25.0

[*]   Mixture of coarse middling and cyclone U/F
[**]   Mixture of +18mm, 10–18mm, 0.5-10mm clean coals
[***] Mixture of coarse and fine shales

Parallel to the achievement in Table 4, Table 5 showed that among the twelve trace elements examined, six of them – namely, Cd, Cr, Hg, Mn, Pb and Th – were rejected between 51.8% and 77.4 % together with the refuse. These trace elements demonstrate affinity to the inorganic matter, and are concentrated in the sink products. On the other hand, 61.4% of U and 53.1% of V retained in the clean coal, because U and V have a strong association with organic matter and is difficult to remove by coal preparation methods.

It can be concluded that in a conventional coal preparation plant, without any advanced size reductions, it is possible to minimize the harmful effects of hazardous air pollutants once the ash is removed. Although advanced coal cleaning processes are often more successful in removing a higher proportion of trace elements, the economics may not be attractive in that they are relatively expensive and can result in rather wet and fine coal product, thus making it difficult to handle and transport.

Conclusions

The run-of-mine coal treated at the Imbat Coal Preparation Plant contains potential hazardous air pollutants – namely, As, Cd, Co, Cr, Hg, Mn, Ni, Pb, Se, Th, U and V –

identified by the US Clean Air Act Amendments of 1990. These trace elements are known to be toxic and have adverse effects on humans, plants, and animals.

The conventional Imbat Coal Preparation Plant with a capacity of 350 Mg per hour, cleans the coal obtained from underground coal operations containing 42.54% ash, 38.08% volatile matter and 0.69% total sulfur in dry basis with 11.90MJ/kg low heating value. The trace elements of As, Cd, Cr, Mn, Se, Th, U and V within the run-of-mine coal are above the world averages while Cd, Mn, Th,V and Hg grades are above the Turkish coal averages. The plant produces 36.37% by weight total clean coal with 15.69% ash and 24.34 MJ/kg low heat value. The total ash rejection from the plant is 69.4%.

The trace elements in the run-of-mine coal, namely Cd, Cr, Hg, Mn, Pb and Th, all of which are associated with the inorganic portion of the coal were easily removed at Imbat Coal Preparation Plant. The highest rejection was obtained for Mn (77.4%), which was more than the plant ash rejection.

During the 69.34% of ash removal from coal, six trace elements mentioned above are rejected within a range of 51.8% to 77.4 % with the ash. However, 15.8% and 25.0% reductions were achieved for U and V, respectively due to their strong association with organic matrix.

Although conventional coal preparation processes in use today may not make up for a complete removal of any trace elements, it was proven that they are effective in reducing the concentration of many trace elements without any further size reduction, especially those present at relatively high concentrations. For further rejection, it is necessary to reduce the top size of the feed and to grind middling to enhance the liberation of trace elements as well as to improve the cleaning circuits by applying advanced coal cleaning technologies. Advanced coal cleaning technologies may offer better trace elements removal than conventional cleaning.

Acknowledgements

References

AKERS D.J., ALUKO M.E., EKECHUKWU K.N., LEBOWITZ H.E., 2000, *Process for removal of hazardous air pollutants from coal*, US Patent No: 6156281.

COAL TRADING BLOG 2011, *Significance of trace elements in coal. An overview*, http://bestcoaltrading.blogspot.com/2011/significance-of-trace-elements-in-coal.htmp.

DANGYU S., YONG Q, JUNYING, Z., WENFENG, W, CHUGUANG, Z., 2007, *Concentration and distribution of trace elements in some coals from Northern China*, International Journal of Coal Geology, Vol. 69, Issue 3, 179–191.

DAVIDSON R., 1998, *Coal cleaning to remove trace elements. A review*, Coal Preparation, Vol.19, 159–176.

DEMIR I., RUCH R.R., DAMBERGER H.H., HARVEY R.D., STEELE J.D., HO K.K., 1998, *Environmentally critical elements in channel and cleaned samples of Illinois coals*, Fuel, Vol. 77, Issues 1–2, 95–107.

ESENLIK S., KARAYIGIT A.İ., BULUT Y., QUEROL X., ALASTUEY A., FONT O., 2006, *Element behaviour during combustion in coal-fired Orhaneli power plant*, Bursa-Turkey, Geologica acta, vol. 4, Issue 4, 439–449.

GUPTA R., 2006, *Advanced coal characterization: A review*, Presented at the Sino-Australia Symposium on Advanced Coal Utilization Technology, July 12–14, Wuhan, China.

GURDAL G., 2008, *Geochemistry of trace elements in Çan coal (Miocene)*, Çanakkale, Turkey, International Journal of Coal Geology, vol. 74, Issue 1,3, 28–40.

OZBAYOGLU G., 2011, *Partitioning of Major and trace elements of a Turkish lignite with size and density*, Physicochemical Problems of Mineral Processing, 47, 5160.

OZBAYOGLU G. 2010, *Potential of removing trace elements from a Turkish lignite*, International Journal of Coal Preparation and Utilization, 30, 322–333.

PESEK J., BENCKO V., SYKOROVA I., VASICEK M., MICHNA O., MARTINEK K., (2005), *Some trace elements in coal of the Czech Republic, environment and health protection implications*, Cent.Eur.J.Public Health, 13(3).153–158.

SWAINE D.J., 1998, *Trace elements during the mining and beneficiation of coal*, Coal Preparation, Vol. 19, 177–193.

TUNCALI E., CIFTCI B., YAVUZ N., TOPRAK S., KOKER A., GENCER Z., AYCIK H., SAHIN N., 2002, *Chemical and Technological Properties of Turkish Lignites*, General Directorate of Mineral Research and Exploration (M.T.A.), Ankara, Turkey.

WANG W., QIN Y., SONG D., 2003, *Cleaning potential of hazardous elements during coal washing, Journal of Fuel Chemistry and Technology*, DOI: cnki:ISSN:0253-2409.0.2003-04-002.

WANG W., QIN Y., WANG J., LI J., 2009, *Partitioning of hazardous trace elements during coal preparation*, The 6th. International Conference on Mining Science and Technology, Procedia Earth and Planetary Science 1, 838–844.

WARD C.R., (2002), *Analysis and significance of mineral matter in coal seams*, International Journal of Coal Geology, 50, 135–168.

WENG L., PENG S., 2003, *Effectiveness of coal preparation in removing hazardous trace elements in air*, Environmental Science and Technology, DOI: CNKI:SUN:FJKS. 0.2003-01-003.

VASSILEV S.V., ESKENAZY G.M., VASSILEVE C.G., 2001, *Behaviour of elelements and minerals during preparation and combustion of the Pernik coal*, Bulgaria, Fuel Processing Techology, Vol.72, Issue 2, 103–129.

VEJAHATI F., XU Z., GUPTA R., 2010, *Trace elements in coal: Associations with coal and minerals and their behavior during coal utilization – A review*, Fuel 89, 904–911.

YASUSHI S., KUNIHISA S., MIO O., EIICHI K., MASAHIKO M., 2003, *The release behavior of trace elements from coal during high temperature process*, Nippon Enerugi Gakkai Sekitan Kagaku Happyo Ronbunshu, vol.40. 136–137 (Japanese).

ZEVENHOVEN R., SAVOLAHTI J., VERHOVEN L., 2005, *Partitioning of mercury and other trace elements from coal and waste-derived fuels during fluidized bed pyrolysis*, 18th International Conference on Fluidized Bed Combustion, Toronto, Ontario, Canada.

CALCIUM CARBONATE MINERALIZATION. PART 1: THE EFFECT OF POLY(ETHYLENE GLYCOL) CONCENTRATION ON THE FORMATION OF PRECIPITATE

Izabela POLOWCZYK, Anna BASTRZYK, Tomasz KOZLECKI, Zygmunt SADOWSKI

Wroclaw University of Technology, Faculty of Chemistry, Department of Chemical Engineering, Wybrzeze Wyspianskiego 27, 50-370 Wroclaw, Poland, izabela.polowczyk@pwr.wroc.pl

Abstract: In this study, the role of polymer in precipitation has been examined by studying the effect of poly(ethylene glycol) (PEG) on the formation of calcium carbonate particles. The $CaCO_3$ particles were characterized by several techniques, such as FTIR, XRD, SEM, and particle size distribution analysis. In the absence of polymer, the mixing of reagents in an aqueous solution led to the formation of calcite crystals. Introduction of poly(ethylene glycol) molecules reduced the rate of crystallization process, and the effect was concentration dependent. In the presence of 0.05, 0.1, and 0.5 % of PEG, after 5 minutes of precipitation initiation, vaterite microspheres appeared in the system and which were transformed into calcite crystals after 24 hours. The calcium carbonate obtained with PEG was characterized by smaller sized particles in comparison with the ones without polymer.

Key words: calcium carbonate, calcite, vaterite, mineralization, PEG

Introduction

The crystallization of calcium carbonate ($CaCO_3$) is of considerable importance in numerous industrial applications as well as in biology. Hence, it is widely used by nature as an inorganic components in exoskeletons and tissues of many mineralizing organisms, giving them strength and shape (Voinescu et al., 2007). There are six $CaCO_3$ mineral polymorphs including calcite, aragonite, vaterite, $CaCO_3$ monohydrate, $CaCO_3$ hexahydrate and amorphous $CaCO_3$ (Manoli and Dalas, 2000; Li et al., 2010). It has been found that calcite and aragonite have stable thermodynamic structures, while vaterite is thermodynamically unstable so that it is easily transformable to calcite or aragonite in aqueous solution (Li et al., 2010). The

precipitation and stabilization of these polymorphs depend upon the precipitation condition such as degree of supersaturation, pH, ionic medium, and concentration and type of additives (Amjad et al., 2007). The biological system uses organic molecules that function variously as nucleators, cooperative modifiers and as matrices or molds for minerals (Manoli et al., 2002). These organic components are polyanionics and polyacids, which have a high calcium affinity. Avian eggs shells present a unique and interesting model for exploring the process of biomineralization, in which $CaCO_3$ layers are created by selective nucleation and deposition of calcite crystal by protein. The active sites on the protein recognize calcium ions and induce nucleation of specific polymorph of $CaCO_3$ and control of the morphology of mineral phase (Lakshminarayanan et al., 2002). Synthesized polymers have also been used in mineralization process. It has been shown that special functional low molecular weight and polymeric additives, such as block copolymers, poly(ethylene glycol) (PEG), polyelectrolyte, polyacrylamide and cellulose, exhibit large influence on the crystallization of $CaCO_3$ (Xie et al., 2006; Xu et al., 2008; Xu et al., 2011, Sadowski et al., 2010; Su et al., 2010). Among various templates, PEG is of particular interests because its molecules contain hydrophilic groups, which can act as a donor to metal ions to form metal complexes with diverse conformation (Xu et al., 2003). However, up to date the effect of these compounds in precipitation of calcium carbonate is not well understood.

The aim of this paper is to investigate the effect of high molecular weight poly(ethylene glycol) of various concentrations on the crystal growth of $CaCO_3$.

Materials and methods

Calcium carbonate precipitation

The poly(ethylene glycol) having an average molecular weight of 5 megagrams/mol from BDH Chemicals was used. Calcium chloride dihydrate (purity > 99%) and disodium carbonate were purchased from Sigma Aldrich. All chemicals used in these syntheses were applied without further purification. The preparation of calcium carbonate was performed according to the method reported in our earlier paper (Sadowski et al., 2010). The solutions of sodium carbonate and calcium chloride (0.1M) with PEG 5000000 (0.01-1%) were prepared one day before the calcium carbonate synthesis and have been stirred overnight. The precipitation experiments were carried out in the Erlenmeyer flasks by mixing a sodium carbonate solution with calcium chloride at the speed of the magnetic stirrer of 300 rpm. After 5 minutes or 24 hours the precipitate was removed from solution by centrifugation. The deposit was collected and washed twice with 100 cm^3 of deionized water and dried at 30ºC. The experiments were conducted at ambient temperature.
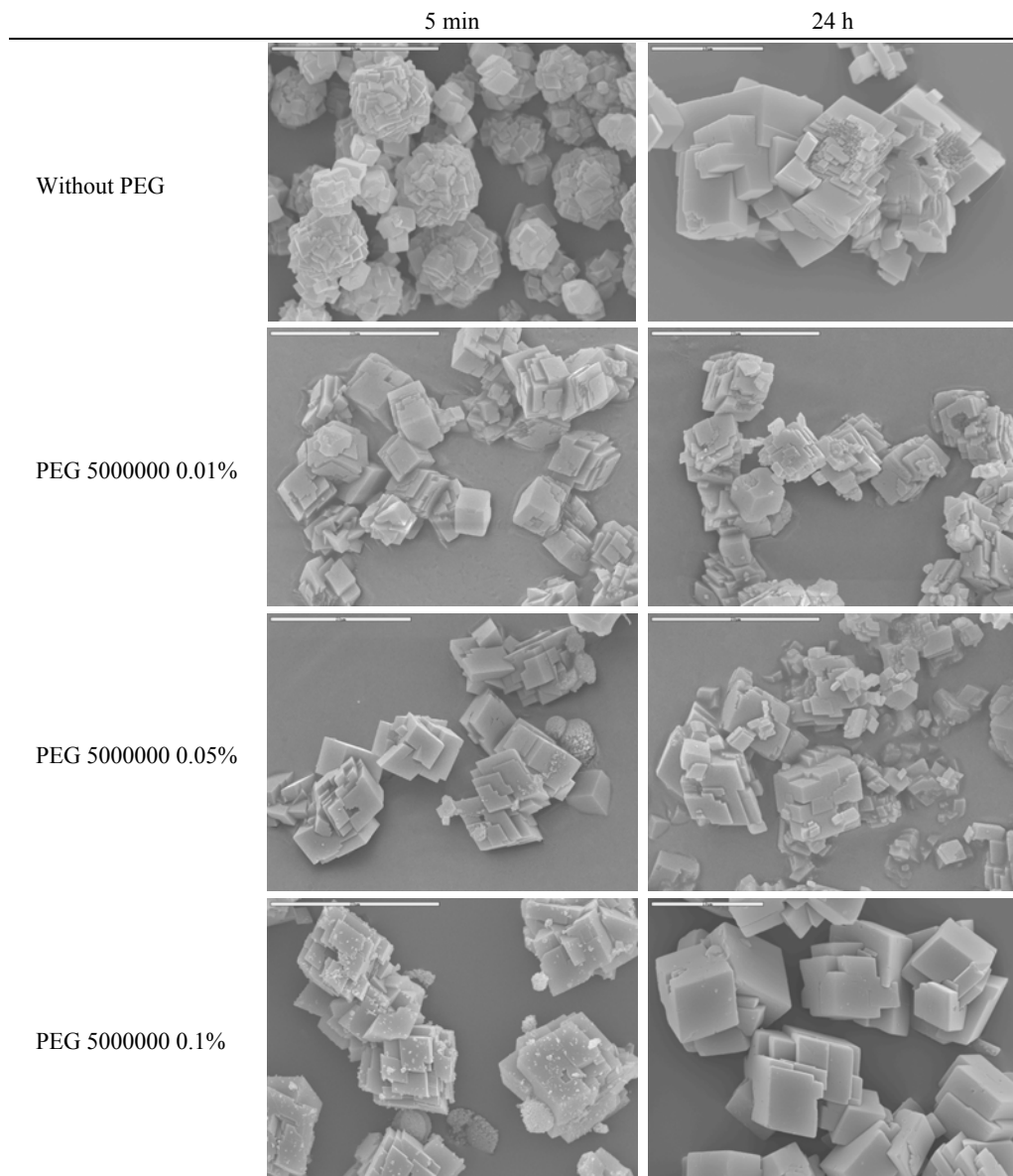
Particle characterization

The microstructure of precipitate was observed using a JSM 5800 LV scanning electron microscope (JEOL). The crystallographic structure of calcium carbonates was determined by using an Advance 8D (Bruker) X-ray powder diffractometer with CuKα radiation. Fourier transform infrared spectroscopy (FTIR) was carried out using PE 1600 FTIR spectrometer (Perkin Elmer). The samples were mixed with KBr powder. The spectra were recorded in a reflection mode from 4000 to 400 cm^{-1} at a resolution of 2 cm^{-1}. Particle size analysis were realized using a Mastersizer 2000 laser diffractometer, equipped with HydroMu dispersion unit (Malvern). These measurements were carried out without and afterwards under operation of ultrasounds in a dispersion unit, so the agglomerates of calcium carbonate could have been broken. The surface area of the samples were measured by the BET method with helium/nitrogen mixture using FlowSorbII apparatus (Micromeritics).
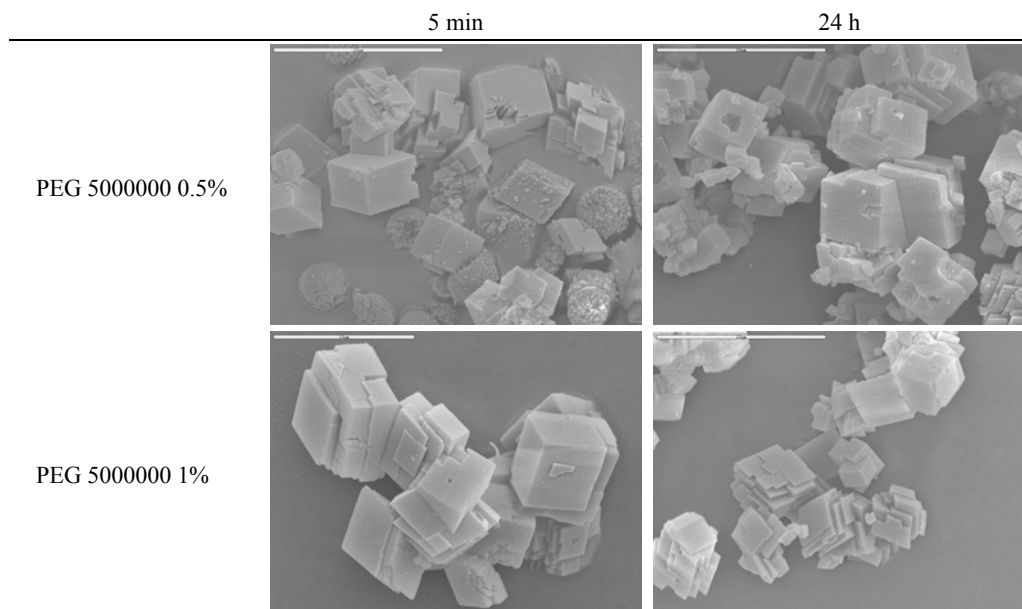
Result and discussion

The morphology and sizes of obtained $CaCO_3$ precipitates were characterized by the SEM analysis and particle size distribution measurements. In Table 1, the SEM images of calcium carbonate precipitated with the addition of PEG 5000000 and without any additive were collected. The volume median diameters (d_{50}) and quantiles (d_{10} and d_{90}) of particles along with the results of BET specific surface area measurements are shown in Table 2. From these tables one can conclude that $CaCO_3$ mineralized without PEG polymer formed rhombohedral calcite crystals of an average size of 12.5 and 21.5 μm after 5 min and 24 h of incubation, respectively. Precipitation of calcium carbonates in the presence of various polymer concentration resulted in slight changes of particles diameter after 5 minutes of incubation. In contrast, $CaCO_3$ precipitates obtained in the presence of PEG but collected after 24 hours of incubation exhibited particles with diameters ranging from 13.4 to 15.9 μm. The slight increase in the particle size observed at a high polymer concentration may be caused by the flocculation effect. The particle formed agglomerates of crystal linked by the polymer molecules, as it can be seen in Table 1. These results indicate that the presence of poly(ethylene glycol) inhibits the growth of $CaCO_3$ particles in the system. It is known that low and high molecular weight additives can stabilize nonequilibrium morphologies by changing the relative growth rates of different crystal faces through molecular, specific interactions with certain surfaces that modify the surface energy or growth mechanism, or both (Xie et al., 2006). Xie and co-workers (2006) showed that the PEG molecules are able to stabilized and modified crystals. The main cause of the influence of organic additives on the nucleation and crystal growth rates is considered to be the specific adsorption of polymers on the forming faces of calcium carbonate crystals, and the differences in strength of this adsorption interaction because of the nature of polymers (the number and nature of functional groups, including polar ones,

and the molecular weight) determine the final form of the calcium carbonate precipitate (Shestak et al., 2011).

Table 1. SEM images of calcium carbonate particles precipitated in the presence of various concentration of poly(ethylene glycol) after 5 minutes and 24 hours

	5 min	24 h
Without PEG		
PEG 5000000 0.01%		
PEG 5000000 0.05%		
PEG 5000000 0.1%		

	5 min	24 h
PEG 5000000 0.5%		
PEG 5000000 1%		

The PEG is a polymer with the hydrophilic groups ($–CH_2CH_2O–$) which exert the ability to bind calcium as a nucleation site of $CaCO_3$ and induce the formation of $CaCO_3$ crystal to adsorption on the special face and inhabitation the crystallization on the orientation (Xie et al., 2006). Additionally, from the SEM images (Table 1), one can see that after 5 minutes of precipitation, regular plate-like structure particles were produced in the presence of PEG 5000000 with at the concentration of 0.01%. At a higher polymer concentration, 0.05, 0.1 and 0.5%, spherical morphologies of carbonates appeared in the system. These microspheres are known as vaterite. Literature data reveal that the individual microsphere of vaterite consists of much smaller nanoparticles and is characterized by high porosity (Kim and Park, 2010). The BET specific surface area results confirm this finding; significantly larger surface areas were obtained for the samples where the vaterite phase were found. From the SEM images it can be observed that the needle-shape structures are also present under that condition. This observation is in agreement with earlier experimental data published in literature. Xie and co-workers (2006) observed that at higher polymer concentrations, the interplay of nucleation and growth becomes more complicated, because the polymorph that is most efficiently nucleated is also the one for which the growth is most effectively stopped. This is why we observe at 0.05 % concentration of polymer a large amount of vaterite in the system.

Figure 1 compares the infrared spectra of $CaCO_3$ precipitates collected at 5 minute and 24 hours of mineralization in the presence of poly(ethylene glycol) molecules at a concentration of 0.01, 0.05, 0.1, 0.5 and 1.0%. In Figure 1, the spectrum taken at 5 minute exhibits a split in the band around 1320 and 1419 cm^{-1}. The two split carbonate

I. Polowczyk, A. Bastrzyk, T. Kozlecki, Z. Sadowski

Table 2. Specific surface areas BET and diameters of calcium carbonate particles precipitated
in the presence of various concentration of poly(ethylene glycol)

| Sample name	Time	BET S.A. [m^2/g]	d_{10} [μm] no-ultrasounds/ ultrasounds	d_{50} [μm] no-ultrasounds/ ultrasounds	d_{90} [μm] no-ultrasounds/ ultrasounds
Without PEG	5min	0.99	9.8/6.6	22.7/12.5	47.2/23.2
	24h	0.74	16.4/7.9	32.6/21.5	59.3/40.4
PEG 5000000 0.01%	5min	0.73	7.7/6.2	17.4/12.7	36.5/23.1
	24h	0.71	8.9/6.5	20.4/13.4	39.4/24.5
PEG 5000000 0.05%	5min	1.19	9.5/8.2	18.8/14.7	33.7/24.4
	24h	0.74	9.2/6.0	19.3/13.6	40.6/25.1
PEG 5000000 0.1%	5min	1.37	8.7/7.0	21.0/15.7	41.4/29.1
	24h	0.56	11.0/8.2	23.6/15.6	44.5/28.0
PEG 5000000 0.5%	5min	1.39	6.9/7.6	15.6/13.6	30.2/23.9
	24h	0.56	9.9/7.9	21.0/15.8	44.8/30.8
PEG 5000000 1%	5min	0.52	7.8/6.3	17.9/12.7	81.2/23.4
	24h	0.62	8.4/6.8	18.3/14.9	35.3/30.4
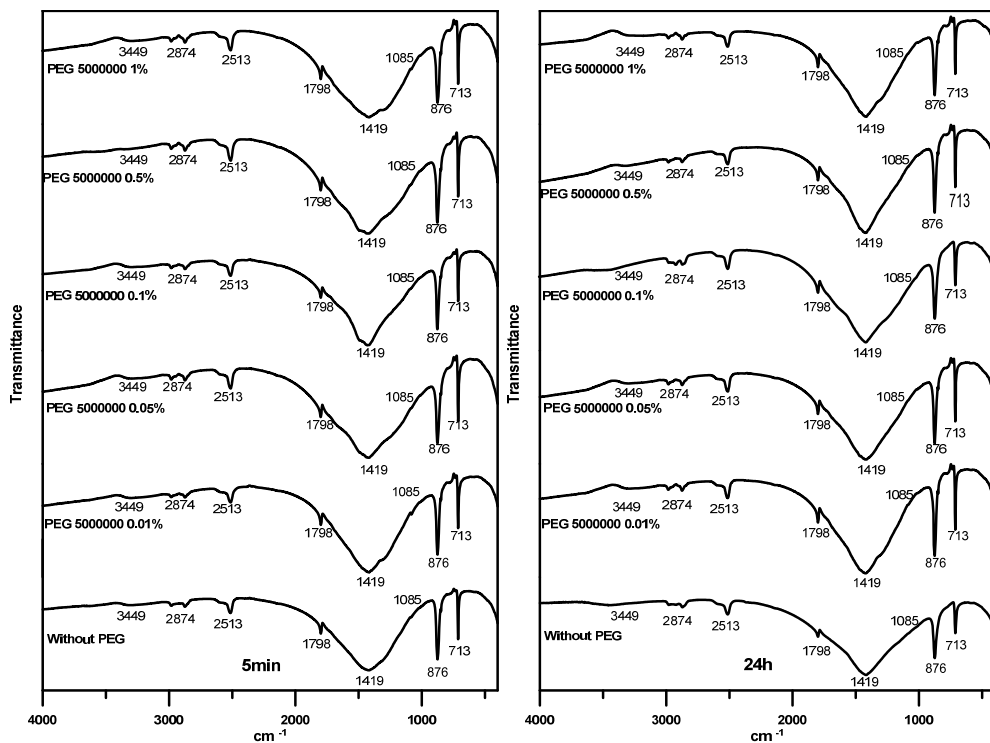
Fig. 1. FTIR spectra of calcium carbonate precipitated after 5 minutes and 24 hours
in the presence of various concentration of poly(ethylene glycol)

absorptions appear in ACC or the vaterite phase by an asymmetric stretch of carbonate ions, according to literature data (Addadi et al, 2003; Kim and Park, 2010). These results suggest that the addition of polymer preserves the vaterite phase transition into calcite. The FTIR spectrum of calcium carbonate obtained after 24h revealed a characteristic spectrum of calcite crystal based on the in-plane band and on the out-plane band at ~712 and ~875 cm^{-1} respectively, and anti-symmetry stretch at ~1420 cm^{-1} characteristic of calcite (Menahem and Mastai, 2008; Xu et al., 2011; Wang et al., 2009).

The powder diffraction patterns presented in Figure 2 also evidenced calcite phase creation, mostly. With the elliptical marks, the small vaterite picks appearing in the calcium carbonate precipitated within 5 min in the presence of 0.05–0.5% of PEG concentration were distinguished. Without the addition of poly(ethylene glycol) as well as at very high (1%) concentration, only calcite was formed. Also leaving the particles in solution for one day resulted in vaterite phase extinction.
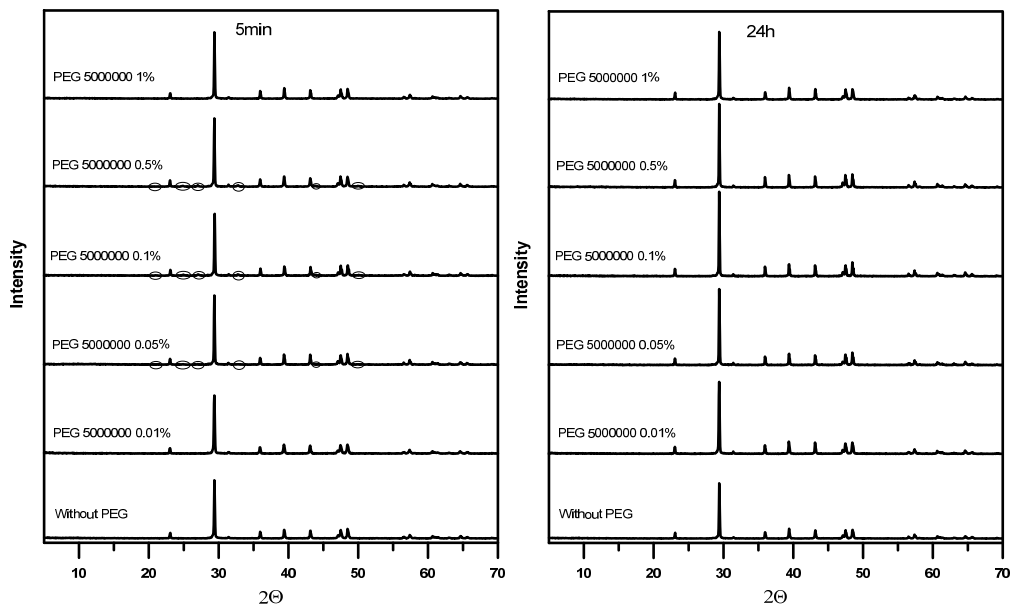

Fig. 2. XRD patterns of calcium carbonate crystals obtained at various concentration of poly(ethylene glycol) after 5 minutes and 24 hours precipitation

The quantitative analysis of powder diffraction data has been performed using the ReX ver. 0.7.0 computer program (Bortolotti et al., 2009). The software is free for personal and non-commercial use, and along with a short tutorial and is available at http://www.rexpd.com. The results of analysis for calcium carbonate precipitates after 5 minutes are shown in Table 3. Calcite was the only phase found in calcium carbonate after 24 h.

Table 3. Calcite and vaterite contents in calcium carbonate precipitated after 5 minutes
in the presence of various concentration of poly(ethylene glycol)

Sample name	$CaCO_3$ form	vol.%	wt.%
Without PEG	calcite	100	100
	vaterite	0	0
PEG 5000000 0.01%	calcite	100	100
	vaterite	0	0
PEG 5000000 0.05%	calcite	98.6	97.0
	vaterite	1.4	3.0
PEG 5000000 0.1%	calcite	94.8	89.4
	vaterite	5.2	10.6
PEG 5000000 0.5%	calcite	95.5	90.8
	vaterite	4.5	9.2
PEG 5000000 1%	calcite	100	100
	vaterite	0	0

Conclusions

The calcium carbonate crystals precipitated in the presence of PEG polymer are predominantly calcite. Small amount of vaterite phase has been obtained at the concentration of polymer 0.05–0.5%. Without polymer addition only calcite phase was formed. PEG 5000000 can affect the morphology of $CaCO_3$ crystals as well as a size distribution of precipitate. The smallest particles were obtained in the presence of 1% of the polymer in the solution. The largest surface areas have been obtained for samples having the vaterite phase. The possible mechanism of formation of calcium carbonates crystals is proposed below. In the aqueous solution, Ca^{2+} and CO_3^{2-} firstly form ACC, which quickly transforms into vaterite and calcite within minutes. At the same time the polymer molecules adsorb on the surface of the particles. They inhibit the growth of crystal during the process resulting in formation small particles. This mechanism is similar to that described in literature in the presence of other polymer such as pluronic (Zhao et al., 2012). Both polymers possess the same functional group, ethylene oxide (EO), which can interact with calcite surface.

Acknowledgements

References

ADDADI L., RAZ S., WEINER S., 2003, *Taking Advantage of Disorder: Amorphous Calcium Carbonate and Its Roles of Biomineralization*, Adv. Mater. 15, No. 12, 959–970.

AMJAD Z, ZUHL R.W., 2007, *Calcium Carbonate Precipitation in the Presence of Inhibitors*, Materials Performance. October, 42–47.

BORTOLOTTI M., LUTTEROTTI L., LONARDELLI I., 2009, *ReX: a computer program for structural analysis using powder diffraction data*, J. Appl. Cryst. 42, 538–539.

KIM S., PARK C.B, 2010, *Dopamine-Induced Mineralization of Calcium Carbonate Vterite Microspheres*, Langmuir. 26, 14730–14736.

LAKSHMINARAYANAN R., KINI R.M., VALIYAVEETTIL S., 2002, *Investigation of the role of ansocalcin in the biomineralization in goose eggshell matrix*, Proc. Natl. Acad. Sci. USA. 99, 5155–5159.

LI W., LIU L., CHEN W., YU L., LI W., YU H., 2010, *Calcium carbonate precipitation and crystal morphology induced by microbial carbonic anhydrase and other biological factors*, Process Biochemistry 45, 1017–1021.

MANOLI F., DALAS E., 2000, *Spontaneous precipitation of calcium carbonate in the presence of chondroitin sulfate*, J. Cryst. Growth. 217, 416–421.

MANOLI F., KANAKIS J., MALKAJ P., DALAS E., 2002, *The effect of aminoacids on the crystal growth of calcium carbonate*, J. Cryst. Growth. 236, 363–370.

MENAHEM T., MASTAI Y., 2008, *Controlled crystallization of calcium carbonate superstructures in macroemulsions*, J. Cryst. Growth. 310, 3552–3556.

SHESTAK I.V., VOROB'EV P.D., CHEREDNICHENKO D.V., VOROB'EVA E.V., BONDAREVA G.V., STRNADOVA N., 2011, *Effect of Polyacrylic Acid and Polyethylene Glycol on the Crystallization of Calcium Carbonate in the Presence of Magnesium Ions*, Russ. J. Inorg. Chem. Vol. 56, No. 2, 176–180.

SU Y., YANG H., SHI W., GUO H., ZHAO Y., WANG D., 2010, *Crystallization and morphological control of calcium carbonate by functionalized triblock copolymers*, Colloid Surf A. 355, 158–162.

SADOWSKI Z., POLOWCZYK I., FRĄCKOWIAK A., KOŹLECKI T., CHIBOWSKI S., 2010, *Bioinspired synthesis of calcium carbonate colloid particles*, Physicochem. Probl. Miner. Process. 44, 205–214.

VOINESCU A.E., TOURAUD D., LECKER A., PFITZNER A., KUNZ W., NINHAM B.W., 2007, *Mineralization of CaCO$_3$ in the Presence of Egg White Lysozyme*, Langmuir. 23, 12269–12274.

WANG X., KONG R., PAN X., XU H., XIA D., SHAN H., LU J.R., 2009, *Lysozyme mediated calcium carbonate mineralization*, J. Phys. Chem. B. 113, 8975–8982.

XIE A.J., ZHANG C.Y., SHEN Y.H., QUI L.G., XIAO P.P. HU Z.Y., 2006, *Morphologies of calcium carbonate crystallites grown from aqueous solutions containing polyethylene glycol*, Cryst. Res. Technol. 41, 967–971.

XU F., XIE Y., ZHANG X., WU C.Z., XI W., HONG J., TIAN X., 2003, *From polymer-metal complex framework to 3D architectures: growth, characterization and formation mechanism of micrometer-sized α-NiS*, New J. Chem. 11, 1331–1335.

XU X.-R., CAI A.-H., LIU R., PAN H.-H., TANG R.-K., CHO K., 2008, *The roles of water and polyelectrolytes in the phase transformation of amorphous calcium carbonate*, J. Cryst. Growth. 310, 3779–3787.

XU X., ZHAO Y., LAI Q., HAO Y., 2011, *Effect of Polyethylene Glycol on Phase and Morphology of Calcium Carbonate*, J. Appl. Polym. Sci. 119, 319–324.

ZHAO Y., WANG X., JIAO J., WANG R., YU L., 2012, *The preparation of calcium carbonate crystals in pluronic F68 solution*, J. Molecular Liquids. 169, 144–151.

HYDROMETALLURGICAL RECOVERY OF COBALT(II) FROM ACIDIC CHLORIDE SOLUTIONS BY TRANSPORT THROUGH POLYMER INCLUSION MEMBRANES

Beata POSPIECH

Department of Chemistry, Czestochowa University of Technology, Armii Krajowej 19, 42-200 Czestochowa, Poland, e-mail: b.pospiech@wip.pcz.pl

Abstract: In this work a selective transport of Co(II) and Li(I) ions from acidic chloride solutions through polymer inclusion membranes (PIMs) with Cyanex 301 has been studied. The effect of composition of the polymer membrane has been investigated. The obtained results show that around 98% of Co(II) was transported from the source phase containing 0.01 M Co(II) and 0.01 M Li(I) at pH 4.0 through PIM after 12 h into 3.0 M HCl. The membrane containing 18 wt.% cellulose triacetate (CTA), 32 wt.% Cyanex 301 and 50 wt.% o-nitrophenyl octyl ether (ONPOE) showed very good stability, suggesting that there is a possibility of application of the membrane for Co(II) recovery from acidic leach liquor solutions of spent lithium ion batteries (LIBs).

Keywords: cobalt(II), lithium(I), Cyanex 301, polymer inclusion membrane, lithium ion batteries

Introduction

The polymer inclusion membranes (PIM) belong to liquid membranes. One of the important aspects of the PIM is distribution of organic carriers in the polymer matrix, which determines their transport efficiency. The transport processes across liquid membranes are a good alternative to conventional solvent extraction due to their advantages such as high selectivity, operational simplicity, low solvent inventory, low energy consumption, as well as combination of extraction and stripping into one single stage (Pospiech, 2012; Kozlowski and Walkowiak, 2007; Ines et al., 2012; Pospiech and Walkowiak, 2005). The transport of Co(II) ions across liquid membranes containing organophosphorous extractants in the role of ion carriers was only investigated by a few researchers. The separation of Co(II) and Li(I) ions from a model leach liquor of spent lithium ion batteries (LIBs) in the process of transport through supported liquid membrane extraction (SLM) was studied by Swain et al.,

(2007). Cyanex 272 (bis(2,4,4-trimethylpentyl)phosphinic acid) was used as an ion carrier. The synergistic effect of Cyanex 272, DP-8R (bis(2-ethylhexyl)phosphoric acid) and Acorga M5640 (2-hydroxy-5-nonylbenzaldehyde oxime) on the separation factor of Co(II) and Li(I) from aqueous sulphate solutions was investigated by Alguacil et al. (2005, 2011) and Swain et al. (2010). Sürücü et al. (2010) reported separation of Co(II) from acidic media, containing both equimolar and nonequimolar mixtures of Co(II) and Ni(II) using the SLM with Alamine 336 as a mobile carrier. Kozlowski et al. (2006) studied competitive transport of trace radionuclides ions (Co-60, Sr-90 and Cs-137) from nitrate aqueous solutions through the PIM containing organophosphorous acids (D2EHPA, Cyanex 272, Cyanex 301, Cyanex 302). The correlation between permeability of metal ions and pK_a of ion carriers was linear, and any increase in pK_a caused a decrease in the permeability coefficients of Co(II). Recently, Kagaya et al. (2011) showed extraction of Co(II) from solutions containing various concentrations of lithium chloride and hydrochloric acid using a poly(vinyl chloride) (PVC)-based polymer inclusion membrane with Aliquat 336 as a carrier.

The present work examines the possibility of recovery of Co(II) ions from a simulated acidic leach liquor of lithium ion batteries (LIBs) by transport through the PIMs with Cyanex 301 as the mobile carrier. The model leach liquor was an equimolar chloride solution containing 0.01 M Co(II) and Li(I). Lithium ion battery (LIB) industry waste contains $LiCoO_2$ and the leach liquor of spent LIBs contains Co(II) and Li(I) in equimolar amounts (Zhang et al., 1998). Cyanex 301 was used as the ion carrier due to its efficiency of Co(II) ions separation from acidic solutions. Besides, Cyanex 301 may be a useful carrier for metals removing from acidic process streams where pH adjustment is not economical (Rickelton and Boyle, 1988).

Experimental

Reagents

Inorganic chemicals, i.e. $CoCl_2 \cdot 6H_2O$, LiCl and HCl were of analytical grade (purchased from POCh, Gliwice, Poland). Aqueous solutions were prepared with deionized water. The synthetic leach liquor of lithium ion battery containing 0.01 M Co(II) and 0.01 M Li(I) was used in this study.

Organic reagents bis(2,4,4-trimethylpentyl)dithiophosphinic acid (Cyanex 301) of 85 % purity, cellulose triacetate (CTA), dichloromethane, *o*-nitrophenyl octyl ether (ONPOE), tris(2-ethylhexyl)phosphate (TEHP), bis(2-ethylhexyl) adipate (DEHA) of analytical reagent grade (purchased from Fluka) were used without further purification.

Polymer inclusion membrane preparation

Solutions of cellulose triacetate (CTA), the ion carrier (Cyanex 301), and the plasticizer (i.e. *o*-nitrophenyl octyl ether (ONPOE), tris(2-ethylhexyl)phosphate

(TEHP) or bis(2-ethylhexyl) adipate (DEHA)) in dichloromethane were prepared. A portion of this solution was poured on a flat- bottom glass Petri dish (7.0 cm in diameter) which was kept on the leveled surface. The organic solvent was allowed to evaporate over a period of 12 h. After solvent evaporation, the obtained membrane was peeled off from the Petri dish by immersion in cold water. This membrane was soaked for 12 h in distilled water to achieve its homogeneity before use. The membrane contained 2.7 cm^3 plasticizer per 1 g of CTA. The thickness of the membrane was measured using a digital ultrameter (MG-401, Elmetron).

Transport studies

A membrane module was used to transport Co(II) and Li(I) across the PIM. Both aqueous phases were pumped with a peristaltic pump (PP1B-05A type, Zalimp, Poland) working at a speed of 100 cm^3/min from tanks containing both source and receiving phases. The diagram of the transport experiments across the PIM can be found in Kozlowski (2006). The effective membrane area which was exposed to both phases was 12.56 cm^2. The volumes of the source and the receiving phases were 100 cm^3. The both phases were stirred by a magnetic stirrer at 200 rpm. The permeation of metal ions was monitored by sampling the aqueous phases (0.1 cm^3 each) at different time intervals, which was analyzed by an atomic absorption spectrophotometer (Solaar 939, Unicam) to determine cobalt(II) and lithium(I) concentrations. The source phase acidity was controlled by pH-meter (CX-731, Elmetron) with pH electrode (Hydromet, Poland). The aqueous source phase (model solution) containing 0.01 M of each metal ions, it is Co(II), Li(II) at pH 4.0, was used in all experiments. The pH was kept constant by adding few mm3 of 2 M NaOH. The PIM transport experiments were conducted at room temperature (23-25 ºC).

The kinetics of the PIM transport process is described by a first-order reaction in metal ion concentration (Danesi, 1984):

$$\ln\left(\frac{c}{c_i}\right) = -kt \tag{1}$$

where c is a metal ion concentration (M) in a source phase at some given time, c_i the initial metal ion concentration in the source phase (M), k the rate constant (s^{-1}), t time of transport (*s*). The k value can be calculated from a $\ln(c/c_i)$ versus time plot. The rate constant value for the duplicate transport experiment is averaged and standard deviation is calculated. The permeability coefficient *(P)* is calculated as follows:

$$\ln\left(\frac{c}{c_i}\right) = -\frac{A}{V}Pt , \tag{2}$$

where V is volume of the aqueous source phase (m^3), and A is an effective area of membrane (m^2). The initial flux *(J$_i$)* is determined as:

$$J_i = P c_i . \tag{3}$$

The selectivity coefficient S is defined as the ratio of the initial fluxes for Co(II) and Li(I) ions:

$$S = \frac{J_{i,\text{Co(II)}}}{J_{i,\text{Li(I)}}} . \tag{4}$$

The recovery factor (RF) of metal ions from the source phase into receiving phase is given by:

$$RF = \frac{c_i - c}{c_i} \cdot 100\% . \tag{5}$$

Results and discussion

Effect of membrane composition on transport of Co(II)/Li(I)

The carrier concentration in the membrane plays a significant role during the permeation of metal ions in transport processes across the PIM. In this work, the influence of Cyanex 301 concentration on the permeation of Co(II) and Li(I) ions was investigated. Cyanex 301 is a phosphinic acid which contains two sulphur donor atoms and thus is a "soft" (class-b) ligand. It is therefore expected to extract the later 3d transition metal ions more efficiently than Cyanex 302 (Jakovlijec et al., 2004). Cyanex 272, 301 and 302 extract metal ions by a cation exchange mechanism (Tait, 1992):

$$M_a^{n+} + (n+X)(RH)_o \rightarrow (MR_n \cdot xRH)_o + nH_a^+ \tag{6}$$

where M^{n+} is the n-valent metal cation, RH is the organic acid, the subscripts 'a' and 'o' represent the aqueous and organic phases, respectively.

Figure 1 shows that concentration of Cyanex 301 varied from 0.5 $\text{mol} \cdot \text{dm}^{-3}$ to 4.0 $\text{mol} \cdot \text{dm}^{-3}$ (on volume of plasticizer). The plasticizer concentration was 2.7 cm^3 per 1.0 g of the CTA. The transport of Co(II) was slow at low concentration of the ion carrier. The permeability coefficient (P) increases with increasing carrier concentration up to 2.0 $\text{mol} \cdot \text{dm}^{-3}$, and then decreases for higher Cyanex 301 concentration (Fig. 1.). This concentration of Cyanex 301 represents probably a critical value above which the permeability of the PIM decreases. The maximum transport of Co(II) ions was obtained by using the membrane containing 0.065 g of Cyanex 301 (2.0 $\text{mol} \cdot \text{dm}^{-3}$ on volume of plasticizer). The highest flux of Co(II) was 72.2 $\mu\text{mol} \cdot \text{m}^{-2} \cdot \text{s}^{-1}$. The resulting membrane contained 18 wt.% CTA and 32 wt.% Cyanex 301 and 50 wt.% ONPOE. Increase of the carrier concentration in the membrane phase caused decrease of metal ion flux. It is probably due to limited solubility of carrier in ONPOE. This effect can also be attributed to the membrane

saturation by the metal-ion carrier complex. An increase of the carrier ion concentration in membrane phase resulted in increased thickness of the membrane, which affected the transport rates. For higher carrier concentration, the membrane became more viscous. Therefore, the diffusion of the ion-carrier complexes in the membrane was reduced. In turn, Arous (2004) showed that for low carrier concentration value, the ion carrier penetrates well inside the CTA matrix. However, higher concentration of ion carrier caused inhibition of the diffusion of metal ions through membrane due to the formation of a multilayer in membrane.
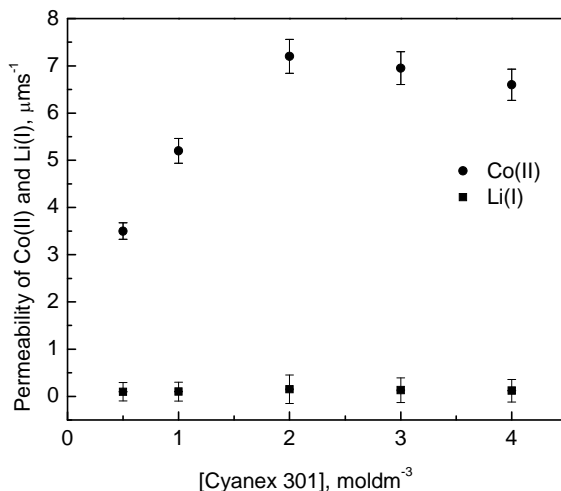

Fig. 1. Effect of Cyanex 301 concentration in PIM on the permeability of Co(II) and Li(I);
PIM: 0.0375 g CTA, 2.7 cm^3 ONPOE/1 g CTA; the source phase: 0.01 M CoCl$_2$,
0.01 M LiCl; the receiving phase 3.0 M HCl

Plasticizers play dual role in behavior of the PIM as the plasticizing the polymer matrix and as a solvent for the ion carrier in the membrane. The plasticizer in the PIM improves the chemical and mechanical properties, stability of membrane, and membrane softness and flexibility. The type of plasticizer is very important to obtain membranes with suitable physical characteristics. The membrane permeability may be improved by selecting an appropriate plasticizer. In order to study the influence of the type of plasticizers on the PIM containing 0.065 g Cyanex 301 in transport process of Co(II) and Li(I) ions were investigated. The PIMs were prepared by using different plasticizers. The plasticizers used in the preparation of the PIM were: *o*-nitrophenyl octyl ether (ONPOE), bis(2-ethylhexyl) adipate (DEHA) and tris(2-ethylhexyl)-phosphate (TEHP). Table 1 lists the values of viscosity and the dielectric constants of the plasticizers used in the present work (Kebiche-Senhadji et al., 2010; Arous et al., 2010). ONPOE belongs to *o*-nitrophenyl alkyl ethers which are frequently used plasticizers in PIMs. DEHA is an ester of 2-ethylhexanol and adipic acid. TEHP belongs to phosphate esters and can be used as an extractant. Solutions of the

plasticizers in dichloromethane were prepared. The concentration of these plasticizers in the membrane was 2.7 cm^3 per 1 g of CTA. The membranes thickness with ONPOE, DEHA and TEHP were 45 μm, 48 μm and 46 μm, respectively. These PIMs were examined for transport of Co(II) and Li(I) from aqueous source phase at pH 4.0 into 3.0 M HCl as the receiving phase. Co(II) and Li(I) fluxes for the experiments conducted with the membranes containing different plasticizers are shown in Fig. 2. As can be observed that the removal of Co(II) from the source phase was more effective for ONPOE as the plasticizer than for TEHP or DEHA. In the case of the membranes with TEHP and DEHA, the fluxes of Co(II) and Li(I) were comparable. These experiments indicated a decrease in initial fluxes in the following order of plasticizers: ONPOE>TEHP~DEHA.

Table 1. Kinetic parameters for Co(II) and Li(I) transport across PIM depending on the type of the plasticizers. PIM: 0.0375 g CTA, 0.065 g Cyanex 301 (2.0 M), 2.7 cm^3 plasticizer/1 g CTA; the source phase: 0.01 M CoCl$_2$, 0.01 M LiCl; the receiving phase: 3.0 M HCl

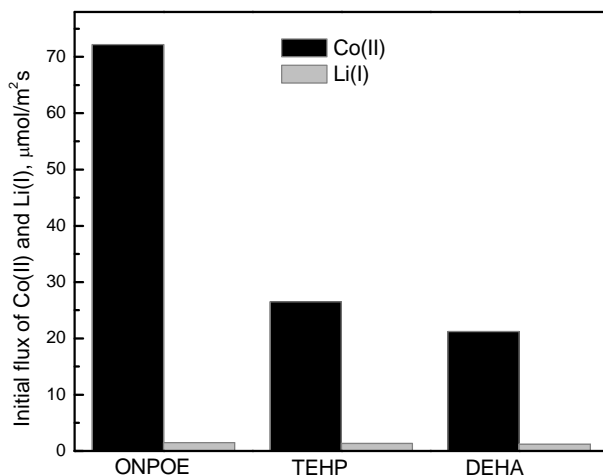| Type of plasticizer	Dielectric constant, ε	Viscosity, (cP)	Metal ions	Permeability coefficient, P ($\mu m \cdot s^{-1}$)
ONPOE	23.1	12.8	Co(II)	7.22
			Li(I)	0.15
DEHA	5.1	13.7	Co(II)	2.12
			Li(I)	0.12
TEHP	4.8	10.2	Co(II)	2.67
			Li(I)	0.14

Fig. 2. Effect of the type of plasticizer on the initial flux (J_0) of Co(II) and Li(I); PIM: 0.0375 g CTA, 2.7 cm^3 plasticizer/1g CTA; the source phase: 0.01 M CoCl$_2$, 0.01 M LiCl; the receiving phase 3.0 M HCl

Table 1 shows the variation of permeability of Co(II) and Li(I) versus the type of plasticizer. This behavior can be explained by the properties of used plasticizers, especially values of the dielectric constant determining the stability of metal ions complexes formed in the membrane phase. Unlike ONPOE, both DEHA and TEHP have low dielectric constants. It can be seen that high value of dielectric constants of ONPOE as plasticizer preferred the Co(II) transport through the PIM with Cyanex 301. The polarity of the plasticizer had a greater influence on the diffusion of the complex in the membrane compared with the viscosity.

Stability of PIM in transport process of Co(II)/Li(I)

The stability of the PIM containing 32% Cyanex 301, 50% ONPOE and 18% CTA was evaluated on the basis of the permeability coefficients values obtained from four sequential experiments. The membrane was used under the following experimental conditions: pH of the source phase was 4.0, concentration of metal ions 0.01 M, the receiving phase: 3.0 M HCl. The membrane was removed from the cell and washed in deionized water. Four membrane transport experiments with the same membrane were conducted. The permeability coefficient of Co(II) and Li(I) ions varied slightly after four cycles of 12 h each. Table 2 shows the changes of permeability coefficient of Co(I) and Li(I) observed during all four experiments. It can be seen from Table 2 that the permeability coefficients for Co(II) and Li(I) decreased from 7.22 to 6.93 $\mu m \cdot s^{-1}$ and from 0.150 to 0.125 $\mu m \cdot s^{-1}$, respectively. This observation confirms low tendency to leach the Cyanex 301 from the membrane matrix. This membrane is stable. The results show that the PIM shows good term integrity. In view of the high stability of the PIM under given experimental conditions, the membrane can be used for separation of Co(II) and Li(I) from acidic solutions, it is leach liquor of lithium ion battery.

Table. 2. Effect of number of cycles for Co(II) and Li(I) transport across PIMs on initial total ions transport flux. PIM: 0.0375 g CTA, 2.7 cm^3 ONPOE/1 g CTA, 2.0 M Cyanex 301; the source phase: 0.01 M CoCl$_2$, 0.01 M LiCl, the receiving phase: 3.0 M HCl

Cycle number	Permeability coefficient, P ($\mu m \cdot s^{-1}$)	
	Co(II)	Li(I)
1	7.22	0.150
2	7.15	0.142
3	7.10	0.138
4	6.93	0.125

Conclusions

The polymer inclusion membranes (PIMs) with Cyanex 301 as ion carrier and o-nitrophenyl octyl ether (ONPOE) as the plasticizer provide an attractive alternative to conventional solvent extraction methods for the separation of Co(II) and Li(I) ions. The results showed that Co(II) can be effectively recovered from aqueous acidic chloride solutions containing Li(I) in hydrometallurgical process of transport across the PIM with Cyanex 301. The PIM containing Cyanex 301 as the carrier, did not leak out organic carrier into the aqueous receiving phase, giving a long-term stability and good durability. The highest flux of cobalt(II) ions was obtained by transport through the PIM containing 32 wt.% Cyanex 301, 50 wt.% ONPOE and 18 wt.% CTA into 3.0 M hydrochloric acid as the receiving phase. The obtained results showed that recovery of Co(II) ions reached 98% after 12 h. Finally, the developed in this work system can be useful for recovery of Co(II) from acidic aqueous solutions containing Li(I) ions.

References

ALGUACIL F.J., ALONSO M., LOPEZ F.A., LOPEZ-DELGADO A., 2011, *Active transport of cobalt(II) through a supported liquid membrane using the mixture DP8R and Acorga M5640 as extractant*, Desalination 281, 221–225.

ALGUACIL F.J., ALONSO M., 2005, *Separation of zinc(II) from cobalt(II) solutions using supported liquid membrane with DP-8R (di(2-ethylhexyl) phosphoric acid) as a carrier*, J. Membr. Sci. 41, 179–186.

AROUS O., KERDUOUDUJ H., SETA P., 2004, *Comparison of carrier-facilitated silver(I) and copper(II) ions transport mechanisms in a supported liquid membrane and in a plasticized cellulose triacetate membrane*, J. Membr. Sci. 241, 177–185.

AROUS O., AMARA M., TRARI M., BOUGUELIA A., KERDUOUDUJ, H., 2010, *Cadmium (II) and lead transport in a polymer inclusion membrane using tributyl phosphate as mobile carrier and CuFeO$_2$ as a polarized photo electrode*, J. Hazard. Mater.180, 493–498.

DANESI P.R., 1984, *Separation of metal species by supported liquid membranes*, Sep. Sci. Technol. 19, 857–894.

INES M., ALMEIDA G.S., CATRALL R.W., KOLEV S.D., 2012, *Recent trends in extraction and transport of metal ions using polymer inclusion membranes (PIMs)*, J. Membr. Sci. 415–416 (2012) 9–23.

JAKOVLIJEC B., BOURGET C., NUCCIARONE D., 2004, *Cyanex 301 binary extractant systems in cobalt/nickel recovery from acidic chloride solutions*, Hydrometallurgy 75, 25–36.

KAGAYA S., CATTRALL R.W., KOLEV S.D., 2011, *Solid-phase extraction of cobalt(II) from lithium chloride solutions using a poly(vinyl chloride)-based polymer inclusion membrane with Aliquat 336 as the carrier*, Anal. Sci. 27, 653–657.

KEBICHE-SENHADJI O., TINGRY S., SETA P., BENAMOR M., 2010, *Selective extraction of Cr(VI) over metallic species by polymer inclusion membrane (PIM) using anion (Aliquat 336) as carrier*, Desalination 258, 59–65.

KOZLOWSKI C.A., WALKOWIAK W., 2007, *Competitive transport of cobalt-60, strontium-90, and cesium-137 radioisotopes across polymer inclusion membranes with DNNS*, J. Membr. Sci. 297, 181–189.

KOZLOWSKI A.C., KOZLOWSKA J., PELLOWSKI WALKOWIAK W., 2006, *Separation of cobalt-60, strontium-90, and cesium-137 radioisotopes by competitive transport across polymer inclusion membranes with organophosphorous acids*, Desalination 198, 141–148.

POSPIECH B., WALKOWIAK W., WOZNIAK M., 2005, *Application of TBP in selective removal of iron(III) in solvent extraction and transport through polymer inclusion membranes*, Physicochem. Probl. Miner. Process. 39, 89–98.

POSPIECH B., 2012, *Separation of silver(I) and copper(II) from aqueous solutions by transport through polymer inclusion membranes with Cyanex 471X*, Sep. Sci. Technol. 47:9, 1413–1419

RICKELTON W.A., BOYLE R.J., 1988, *Solvent extraction with organophosphines – commercial & potential applications*, Sep. Sci. Technol. 23, 1227–1250.

SURUCU A., EYUPOGLU V., TUTKUN O., 2010, *Selective separation of cobalt and nickel by supported liquid membranes*, Desalination 250, 1155–1156.

SWAIN B., JEONG J., LEE J., LEE G., 2007, *Extraction of Co(II) by supported liquid membrane and solvent extraction using Cyanex 272 as an extractant: A comparison study*, J. Membr. Sci. 288, 139–148.

SWAIN B., JEONG, J. LEE, J., LEE G., SOHN J., 2007, *Hydrometallurgical process for recovery of cobalt from waste cathodic active material generated during manufacturing of lithium ion batteries*, J. Power Sources 167, 536–544.

SWAIN B., JEONG J., YOO K., LEE J., 2010, *Synergistic separation of Co(II)/Li(I) for the recycling of LIB industry wastes by supported liquid membrane using Cyanex 272 and DP-8R*, Hydrometallurgy 101, 20–27.

TAIT B. K., 1992, *The extraction of base metal ions by Cyanex 301, Cyanex 302 and their binary extractants mixtures with Aliquat 336*, Solv. Extr. Ion Exch. 10, 799–809.

EFFECT OF HEAT TREATMENT ON BREAKAGE RATE FUNCTION OF ULEXITE

Halil IPEK, Haydar SAHAN

Osmangazi University, Engineering Faculty, Mining Engineering Department, Eskisehir, Turkey
hipek@ogu.edu.tr, Tel : +90 2222393750, Fax: +90 222 239 36 13

Abstract: The kinetics of batch grinding and heat treated of ulexite using different size fractions (–3350+2360, –2360+1700, –1700+1180, 1180+850, –850+600, –600+425, –425+300, –300+212 and –212+150 micrometers was determined using a standard Bond ball mill. It was found that breakage of ulexite follows the first order behavior for all feed sizes with the correlation coefficients equal to approximately 98%. The dry grinding of the single-sized fraction and heat treatment of ulexite showed that heat treatment samples were ground much faster than the original ulexite samples.

Keywords: ulexite, grinding, ball milling, breakage rate function, heat treatment, micro wave

Introduction

About 70% of world's known boron reserves are in Turkey. A great portion of Turkish commercially recoverable boron reserves are colemanite, ulexite and tincal. Ulexite has a triclinic crystal structure with a chemical formula of $NaCaB_5O_9 \cdot 8H_2O$ (hydrated sodium calcium borate). It has many important uses such as in the production of glass, agriculture goods, textiles, nuclear fiberglass, and insulators in the cellulose industry (Mobbs, 2010)

Size reduction of minerals by grinding is widely used in the preparation of raw materials for the manufacturing. As it is known that a significant amount of energy which is used in grinding, turns into heat and cannot be efficiently used in grinding. It is possible to obtain more effective grinding by setting up more effective grinding systems which consumes less energy (Bozkurt and Ozgur, 2007, Ipek and Goktepe, 2011).

The design and scaling-up of ball mills are important issues in the size reduction process. Therefore, various models are used for predicting the behavior of large industrial-scale mills. An analysis of grinding in ball mills uses the concepts of selection and cumulative breakage distribution functions. The selection function (specific rate of

breakage) is defined as the fraction by weight of particles of a given size i which are selected and broken per unit time of grinding. This value varies with size and is denoted S_i. The cumulative breakage distribution function, $B_{i,j}$, is defined as the fraction by weight of breakage products from size j which falls below size i, where $i \leq j$ (Austin and Bagga, 1981; Austin et al., 1984).

When ulexite is subjected to heat treatment, internal thermal reactions occur. First, mineral loses its crystallization water followed either by the production of amorphous material or recrystallization into new phases. According to Sener et al. (2000) ulexite does not decrepitate. Instead, it only exfoliates due to gradual removing of water vapor and the structure becomes amorphous with numerous microcracks and interstices. This product is weak and can be easily ground to powder (Sener et al, 2000).

The objective of this study is to analyze the effect of heat treatment of ulexite on its breakage rate function.

Theoretical background

Austin and Bagga (1981) analyzed the variation of specific rates of breakage during batch grinding of several materials to fine sizes. They found that the normal region could be defined by the first-order breakage:

Rate of breakage of size $\qquad 1 = S_1 w_1(t) W,$ $\hfill (1)$

where S_1 is the specific rate of breakage of feed size 1 material, and $w_1(t)$ is the mass fraction of the total charge, W, at time t of grinding.

Assuming that S_1 does not change with time due to the first order breakage process, this equation integrates to

$$\log [w_1(t)] = \log[w_1(0)] - S_i t/2.3. \qquad (2)$$

Plotting experimental values of $w_1(t)$ versus t using log-linear scales enables to determine the S_1 values for the top size interval of material being tested. The equation for the variation of the specific rate of breakage S_i with particle size is

$$S_i = a_T x_i^{\alpha}. \qquad (3)$$

If S_i passes through a maximum at a certain size

$$S_i = a_T (x_i/x_1)^{\alpha} Q_i \qquad (4)$$

$$Q_i = [1/(1+(x_i/\mu)^{\Lambda})] \qquad (5)$$

where x_i is the upper limit of the size interval indexed by i. x_1 is 1 mm, a_T and α are model parameters that depend on the properties of the material and the grinding conditions while Q_i is a correction factor. According to Austin et al. (1981, 1984) the specific rate of breakage varies with particle size. While Q_i assumes the value of 1 for

fine size particles, it becomes smaller with increasing size. μ is the particle size at which the correction factor is 0.5 and Λ is a positive number which show how rapidly the rates of breakage fall as size increase and the higher Λ values show that the more rapidly the values decrease.

Materials and experimental methods

Material

The -125+25 mm size fraction of ulexite washed concentrate, obtained from Etibank Mining Co., was used. The density of ulexite, measured with a pycnometer, was 1.95 g/cm^3 basing on seven measurements and Moh's hardness of ulexite, measured by a hardness pen, was 1. All samples were rewashed to separate from clay minerals and then they were crushed below 5 mm. Approximately a 100 kg cleaned sample was crushed with a jaw crusher and classified into nine different mono sized fractions for kinetic tests. The chemical analyses of these test material are given in Table 1.

Table 1. Chemical composition of investigated ulexite sample

B_2O_3 (%)	SiO_2 (%)	Al_2O_3 (%)	Fe_2O_3 (%)	CaO (%)	MgO (%)	Na_2O (%)	SO_3 (%)	SO_4 (%)
38.1	3.1	0..05	0.02	16.5	1.4	3.9	0.02	0.02

Grinding Tests

In order to determine the breakage rate function, one size fraction technique was used (Austin et al., 1984). In this technique, nine different mono sized fractions which are $-3350+2360$, $-2360+1700$, $-1700+1180$, $-1180+850$, $-850+600$, $-600+425$, $-425+300$, $-300+212$ and $-212+150$ micrometers were prepared. In each case, the mill was loaded in such a way that 100% of the interstitial void volume of the ball charge was filled with the mono-sized material at the beginning of the experiments. This load was 2263 g and it was calculated with the following formulas (Sahan, 2010):

$$N_c = \frac{42.3}{\sqrt{D-d}}$$

$$J = \left(\frac{\text{mass of balls/ball density}}{\text{mill volume}} \right) \times \frac{1.0}{0.6}$$

$$f_c = \left(\frac{\text{mass of powder/powder density}}{\text{mill volume}} \right) \times \frac{1.0}{0.6}$$

$$U = \frac{f_c}{0.4 J}.$$

The characteristics of the Bond mill used in grinding tests and test conditions are outlined in Table 2.

Table 2. Mill characteristics and test conditions

Mill	Diameter, D, cm	30.5				
	Length, L, cm	30.5				
	Volume, V, cm^3	22272				
	Speed, rpm	70				
	Critical speed, N_c	86.55				
Media charge	Diameter, d, mm	38.10	31.75	24.50	19.05	12.70
	Number	43	67	10	71	94
	Total mass, g	22603				
	Specific gravity g/cm^3	7.79				
	Fractional ball filling, J	0.22				
Material charge	Fractional powder filling, f_c	0,09				
	Powder-ball loading ratio, U	1,00				

Results and discussion

Determination of specific rate of breakage

In order to determine the breakage rate parameters of original and heat treated ulexite samples, which were classified into eight different mono-size fraction, were ground dry for 0.25, 0.5, 1, 2 , 3, 4, and 5 minutes separately. The heat treatment process was performed at 400 °C and 600 °C for 30 minutes in a Lenton brand furnace and also at 850 W for 10 minutes in a Siemens brand household microwave oven. The mono-sized samples were entered to the furnace after the furnace reached the target tempera-ture of 400 °C and 600 °C. The mono-sized samples were entered into the microwave after the microwave worked for 5 minutes at 850W. The feed sample weight was 275 g for all heat treatment tests because of the capacities of the furnace and the micro-wave oven. Average weight losses were 15.00%, 30.06%, 10.24%, and ranging be-tween 14.40–15.80, 29.15–30.94, 9.24–11.09 for 400 °C, 600 °C and 850 W respec-tively. Average weight losses of all feed sizes are shown in Fig. 1.

After the heat treatment, the samples were resized. The mono-sized feed samples consisted of approximately 96% in the top size interval ($w_2(0) = 0.04$). Test charge of the mono-sized feed samples were 2263 g, as mentioned above, and were constant during all the grinding tests.
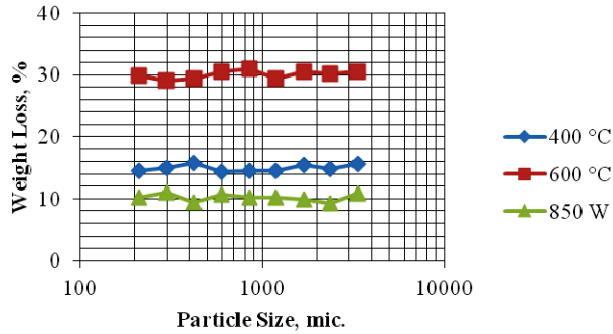
Fig. 1. Average weight losses versus all feed sizes

Figures 2-4 show the initial grinding results of ulexite plotted as first order process for the eight different mono-sized fractions. It can be seen that the breakage process follows the first order behavior for all the feed sizes. The values of correlation coefficient are listed in Table 3. The S_i values are determined from the average slopes of plots (Fig. 2–4) represented mathematically by Eq. 2.
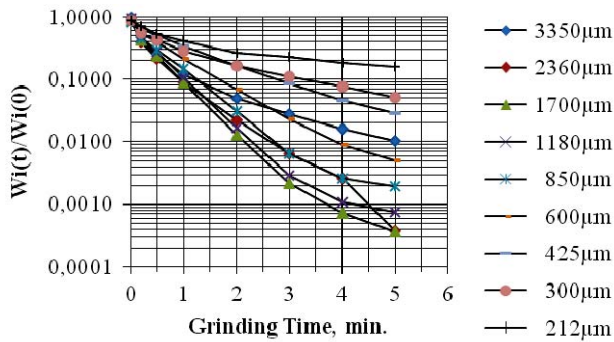

Fig. 2. First order plot for dry grinding of different feed sizes of ulexite
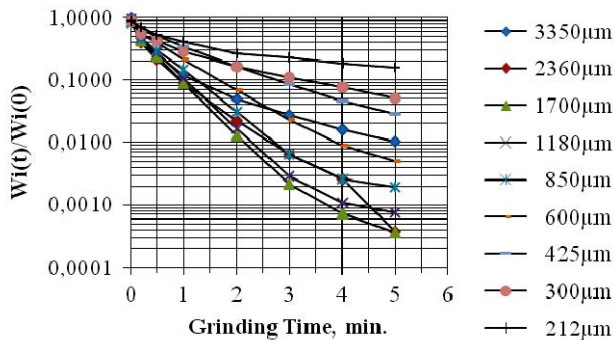
Fig. 3. First order plot for dry grinding of different feed sizes heat treated ulexite at 400 °C for 30 minutes in a furnace
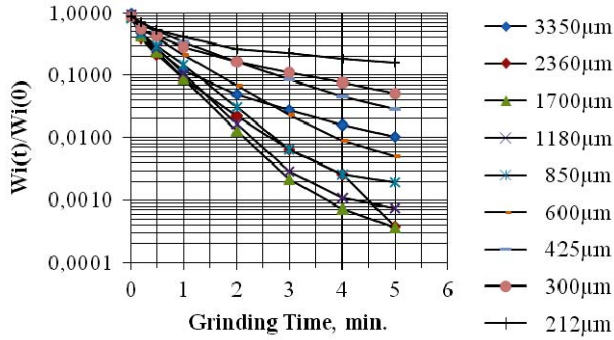
Fig. 4. First order plot for dry grinding of different feed sizes of heat treated
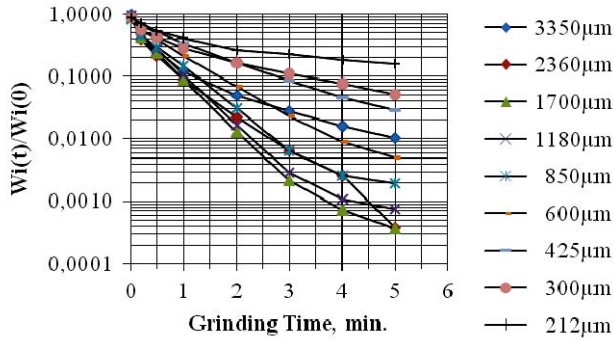at 600 °C ulexite for 30 minutes in furnace

Fig. 5. First order plot for dry grinding of different feed sizes of 850 W
heat treated ulexite for 10 minutes in microwave

Table 3. Values of correlation of the first order plots for dry grinding of ulexite samples

Feed Size microns	Original	400 °C	600 °C	850 W
−3350+2360	0,9901	0,9837	0,9893	0,9865
−2360+1700	0,9991	0,9778	0,9908	0,9700
−1700−1180	0,9969	0,9852	0,9926	0,9938
−1180+850	0,9952	0,9913	0,9928	0,9945
−850+600	0,9864	0,9917	0,9962	0,9931
−600+425	0,9884	0,9899	0,9621	0,9883
−425+300	0,9955	0,9716	0,9719	0,9831
−300+212	0,9975	0,9770	0,9770	0,9780
−212+150	0,9992	0,9018	0,9771	0,9559

As shown in the charts above, the heat treated samples were broken very fast, up
to 2 minutes of grinding. After that, a slowing down effect was observed. Therefore,

the S_i values of the heat treated ulexite were determined for two minutes of grinding while the grinding time of the original sample was 5 minutes.

Figure 6 shows that the variation of the specific rate of the breakage with the feed sizes. It is clearly seen there that the values increase sharply until 1700 micrometers and then they sharply decrease for 400 °C heat treatment and 850 W microwaved ulexite samples. Also the values increase sharply until 2360 micrometers and then decrease sharply for 600 °C while the Si values increase sharply for 1180 micrometers and then smoothly decrease for original ulexite sample. This was due to the inefficiency of the largest particle sizes that were not nipped properly in the mill. The variations of the S_i values with the particle sizes were fitted with Eqs 4 and 5. The specific rate of breakage parameters a_T, α, μ and Λ depend on the properties of the material. As can be seen in Table 4, the grinding conditions were calculated by non–linear regression techniques.
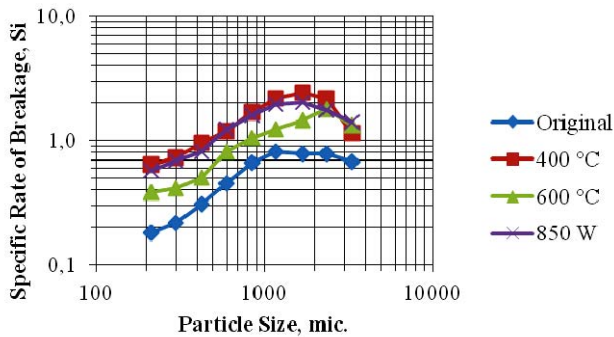

Fig. 6. Variation of S_i values of original and heat treated samples of ulexite with particle size

Table 4. Specific rate of breakage parameters

	αT	α	μ	Λ
Original	0.72	0.92	2.42	2.62
400 °C	1.90	0.79	2.55	4.34
600 °C	1.13	0.77	3.26	3.99
850 W	1.75	0.76	2.55	3.03

Conclusion

The grinding of ulexite samples obeys the first order breakage kinetics for all feed sizes both for the original and heat treated ulexite. Dry grinding of the single–sized fraction of ulexite and heat treated ulexite showed that heat treated samples were ground much faster than the original ulexite samples. Contrary to expectations, the breakage rate of the 600 °C heat treated ulexite sample is slower than that of 400 °C and 850 W heat treated ulexite samples. The a_T parameters show this situation clearly. As mentioned in the Sener (2000) study, ulexite samples recrystallize at 600 °C.

References

AUSTIN L.G., BAGGA P., 1981, *An analysis of fine dry grinding in ball mills*, Powder Tech., 67, 277–286.

AUSTIN L.G., KLIMPEL R.R., LUCKIE P.T., 1984, *The process engineering of size reduction*, SEM, New York.

BOZKURT V., OZGUR I., 2007, *Dry grinding kinetics of colemanite*, Powder Technology, 176, 88–92.

IPEK H., GOKTEPE F., 2011, *Determination of grindability characteristics of zeolite*, Physicochem. Probl. Miner. Process. 47, 183–192.

MOBBS P.M., 2010, *Boron*, USGS Minerals Yearbook

SAHAN H., 2010, *Determination of grindability properties of ulexite*, M. Sc. Thesis, Osmangazi University, Eskisehir, Turkey (Turkish Text).

SENER S., OZBAYOGLU, DEMIRCI S., 2000, *Changes in the structure of ulexite on heating*, ThermochimicaActa, 362, 107–112.

EXPERIMENTAL STUDY ON ELECTROKINETIC OF KAOLINITE PARTICLES IN AQUEOUS SUSPENSIONS

Fanfei MIN, Qing ZHAO, Lingyun LIU

Anhui University of Science and Technology, School of Materials Science and Engineering, Huainan 232001, China

Abstract. Influence of aqueous phase properties and process parameters on kaolinite particle zeta potential was quantified by electrophoresis experiments. The results indicated that pH strongly altered the zeta potential of kaolinite and it decreases at the beginning and then increases in the range of pH = 2–13. The activity of different cations changes the zeta potential and has the following tendency of $Al^{3+} > Ca^{2+} > Mg^{2+} > Na^+$ and the zeta potential increases due to heterocoagulation of different mineral particles in suspension. It was found that the zeta potential of kaolinite particles increases after the suspension was stirred and decreases at the beginning, and then increases with soaking time. The FTIR results showed that the zeta potential takes into account ion adsorption and the change of Si–O, Al–O and Al–OH groups on the surface of the kaolinite particles.

Keywords: kaolinite, zeta potential, pH, immersion time, electrophoresis

Introduction

In recent years, with the improvement of coal mining mechanization degree and geological conditions change, a lot of reject enters coal and increases ash in raw coals in China. The raw coal which includes much reject will produce a lot of slimes in water of the coal washing process. The slime contains a considerable amount of ultrafine particles such as clay particles. The removal of ultrafine particles from the slurries is usually slow and incomplete because the colloidal particles are extremely small（Zbik et al., 2008). In addition, the surfaces of these colloids usually have the same charge, which causes repulsion forces and prevents aggregation. Investigations showed that kaolinite particles, which are one of the predominant minerals in coal slime, are commonly generated in mineral processing at neutral to high pH and they are always charged negative in the process water. The kaolinite particles tend to form stable dispersions with poor dewatering characteristics (Kihc and Hosten, 2010) .

Dai et al. (2010) found that the zeta potential of the mixed metal layered hydroxide-kaolinite suspension system decreased with increasing pH values. Yang and Fan (2010) have shown that ferric-polysilicate can change the zeta potential of kaolin from negative to positive and polymers of ferric-polysilicate ion in polysilicate iron has a strong neutralize effect with its positive charge. Gan and Liu (2008) reported that kaolinite carried negative charges in the entire pH range tested from 3 to 12. The zeta potential increased in the negative direction with increasing pH from 4 to 8 and stabilized at about –50 mV above pH 8. The zeta potential of kaolinite in the presence of Ca^{2+} became much less negatively charged between pH 6 and 12. The zeta potential of kaolinite in the presence of Mg^{2+} closely followed that in Ca^{2+} solutions from pH 6 to 10. However, above pH 10, the zeta potential increased sharply and reached zero at pH 10.4, then moved into positive region. Hou *et al.* (2010) have studied interaction of the diffuse layers of electric double layer between negatively charged kaolinite particle and positively charged particles of goethite, gibbsite, hematite and found the interaction of the diffuse layers increases with the increase in the ratio of kaolinite to Fe/Al oxides and decreases with the rise of system pH. Electrokinetic studies, mostly in terms of electrophoretic mobility measurements (some electroacoustic or dielectric spectroscopy measurements have also been performed), have been done for kaolinite (Williams,1978; Smith and Narimatsu,1993; Hussain et al., 1996; Chassagne et al., 2009; Alkan et al., 2005; Rao et al., 2011; Duman et al., 2012) .

From the forgoing review, it can be seen that the surface electric potential characteristics of kaolinite particles in single mineral system has been studied extensively. Few studies investigated the effects of different mineral particles and process operating conditions on zeta potential of kaolinite particles in the coal slime water. The major objectives of this study are to investigate the difference of zeta potential between the single system of kaolinite and the binary systems containing kaolinite and coal or quartz, and to discuss the effects of stirring intensity, immersion time, pH, electrolyte and mineral on the change of kaolinite particles zeta potential.

Materials and methods

Minerals and chemicals

The coal-associated kaolinite sample was supplied by Huainan Mining Industry Co..Ltd., Huainan, China, which was used for zeta potential measurements. Chemical analysis and X-ray diffraction indicated that the kaolinite sample contained about 87% kaolinite and 10% quartz (see Fig. 1). The FTIR analysis of the sample (see Fig. 2) shows that 3698 cm^{-1}, 3617 cm^{-1} is –OH stretching vibration, 1200 to 1000 cm^{-1} the Si–O stretching vibration; 1000 to 900 cm^{-1} the Al-OH bending vibration; the majority of absorption peaks of 500 ~ 400 cm^{-1} the vibration of Si–O or Al–O on the surface of the sample. Particle size analysis by SALD-7101 (Shimadzu Corporation, Japan) showed that the sample particle size is less than 5 μm and the average particle size is 0.74 μm.
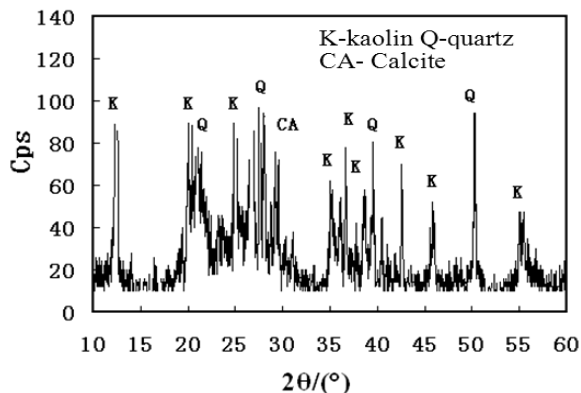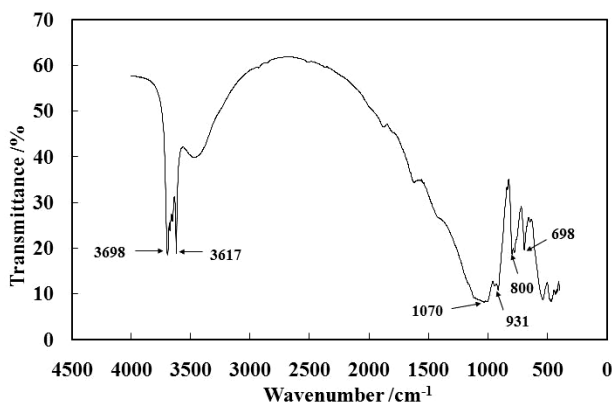
Fig. 1. XRD trace of kaolinite

Fig.2. The FTIR spectra of kaolinite

The bituminous coal sample was provided by Huainan Mining Industry Co. Ltd., Huainan, China. The bituminous coal sample was crushed to less than 75 μm. The results of bituminous coal sample proximate analysis in air dry basis are moisture 2.15%, ash 8.33%, volatile matter 29.30%, fixed carbon 60.22%. The bituminous coal sample was mixed with kaolinite sample for zeta potential measurements.

The quartz sample was purchased from sub-Sheng Chemical Co. Ltd., Wuxi, China. The diameter of the quartz particles is less than 110.00 μm with a median diameter (d_{50}) of 49.98 μm. The quartz sample was mixed with kaolinite sample for zeta potential measurements.

The chemicals used in this study were certified A.C.S. grade reagents and purchased from Shanghai Reagent Company, Shanghai, China. NaCl (>99%), CaCl$_2$ (>99%), MgCl$_2$ (>98%), and AlCl$_3$ (>98%) were used as sources of Na$^+$, Ca^{2+}, Mg^{2+} and Al^{3+}. NaOH (99.0%) and HCl (36.5–38%, solution) were used as pH regulators. All solutions used in this study were prepared using distilled water made by a glass still.

Experimental methods

Preparation of stock suspensions for zeta potential measurement

Stock suspension of kaolinite was prepared by dispersing 20 g of the kaolinite sample in 1 dm^3 of deionized water. For the binary colloid suspensions, kaolinite/coal or kaolinite/quartz were placed in the same container according to their different quantitative ratio. The suspension was mildly stirred with a agitator (JJ-1, made in China) at 300 rev/min for 10 min at 25 ºC. The pH of the suspension was controlled at 7.0 adjusted with HCl or NaOH. Next, the suspensions were equilibrated for another 30 min before zeta potential determination.

Determination of zeta potential

The zeta potential of the kaolinite and other samples were measured at 25±0.5 ºC with a JS94G + micro-electrophoresis apparatus made in China. The zeta potential for each sample was determined by taking the average of 6 runs. The standard deviation for the 6 runs was within ±3 mV. The colloid suspension was agitated and transferred to the electrophoresis vessel after wetting the electrode to avoid any disturbance due to air bubble. The values of zeta potential were calculated using the computer with the specific software.

Other measurements

The different types of functional groups on kaolinite samples were identified by the Fourier Transform Infrared (FTIR) Spectroscopy in the range of 4000–400 cm^{-1}. BRUKER Vector33 was employed to study the infrared spectroscopy of the sample. The samples were first dried at 50 ºC and mixed with KBr and then pressed into pellets which contained approximately 0.5 wt. % samples.

In X-ray diffraction analysis (XRD) a Rigaku's D/Max-3B XRD X-ray spectrometer diffractometer was used. All the analyses were done using Cu Kα radiation with Cu/Ni electrodes and goniometer speed of 2°/min, sampling interval: 0.02°. X-Ray Diffraction (XRD) allows identification and quantification of unknown phases in a mixture by using search/match software.

Results and discussion

The effect of agitation on zeta potential of kaolinite particle surface

Zeta potentials of kaolinite at different agitating speeds were presented in Fig. 3a. The infrared spectroscopy results of kaolinite samples agitated at different speeds were shown in Fig. 3b.
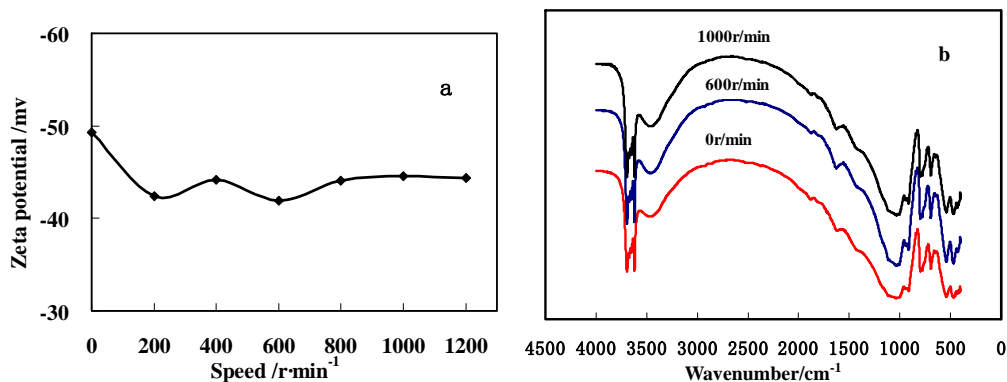
Fig. 3. Zeta potential (a) and FTIR spectra (b) of kaolinite at different agitating speeds

It can be seen from Fig. 3a that as the agitating speed increases the absolute value of zeta potential of kaolinite particles surface first decreases, then slightly increases and when agitating speed reaches 800 rpm, the zeta potentials get stability around –44 mV. At low agitating speed, some metal cations, such as Ca^{2+}, Mg^{2+} and other cations dissolute from kaolinite samples (see Table 1), and these cations will be adsorbed on the negatively charged surface of kaolinite particles, the multivalent metal cations would theoretically reduce the thickness of the electric double layers of kaolinite (edges) and the reduced electric double layer thickness means that the zeta potential of the particles would be lower and lead to lower electrostatic repulsion. As the agitating speed increases, the kaolinite particles turns into fine particles, which leads to producing a number of new breaking bonds of Al–O and Si–O negatively charged on the particle surface, so the absolute value of the zeta potential of kaolinite particles surface increases. As can be seen from Fig. 3b that the intensity of –OH stretching vibration in 3698 cm^{-1}, 3617 cm^{-1} and Al–OH bending vibration in 1000 to 900 cm^{-1} increases with the agitating speed increases. The results indicate that there are a certain number of Si–OH and Al–OH generated on fine kaolinite particles surface which is caused by Al–O and Si–O bond adsorption of H^{+} (Yang et al., 2001).

Table 1. Ion composition of kaolinite suspensions

Ions	Ca^{2+}	Mg^{2+}	$Na^{+}+K^{+}$	Cl^{-}	SO_4^{2-}	CO_3^{2-}	HCO_3^{-}
Concentration, mg/dm^3	12.02	1.21	55.00	62.03	7.20	0.00	61.02

The effect of pH value on zeta potential of kaolinite particle surface

pH is an important factor influencing the zeta potential value of kaolinite. The effect of pH value on the zeta potential of kaolinite is shown in Fig. 5a. It can be seen that the absolute value of zeta potential gradually increases and reaches its maximum at pH 8 and then tends to decrease with the pH value increasing. It agrees with the result gotten of Gans and Liu (2008). The isoelectric point is a pH value at which the total

amount of positive charge on the surface of solid is equal to the total amount of negative charge on it. The amount of net surface charge of solid or zeta potential value is zero at the isoelectric point. The isoelectric point is a characteristic property of solid particles. Therefore, it is important to know the isoelectric point of clay and surface charge of the clay particles for the adsorption or flotation processes (Duman et al., 2012). Figure 5a shows that kaolinite has no isoelectric point in range of 2–13 pH value, which indicates that the isoelectric point of kaolinite is lower than pH 2. The result is agreement with the result gotten by Duman et al. (2012) and Yang et al. (2001), which is lower than the literature value (Hu and Liu, 2003; Alkan et al., 2005). The low isoelectric point of kaolinite may be because the sample is coal-associated kaolinite containing quartz and other minerals. Besides, the number of solid particles facilitate the surface charge generation by producing the ionic species at the solid/liquid interface, kaolinite concentration in the suspension and this also can affect the zeta potential value of the suspension (Tunc and Duman, 2008).

The absolute values of kaolinite zeta potential in colloid suspensions are the largest when the pH value reaches about 8. The pH value of coal slurry is usually about 8, so the negativity of slime kaolinite particles surface is the largest, which causes repulsion forces and prevents aggregation.

Kaolinite is a 1:1 layer mineral, in which one layer consists of an alumina octahedral sheet (termed as O-face) and another consists of silica tetrahedral sheet (termed as T-face), as shown in Fig. 4. The two layers share a common plane of oxygen atoms, and the repeating layers are bound together by hydrogen bonds between hydroxyl groups of O-face and the highly electronegative oxygen of the T-face (Ma and Eggleton, 1999). It is an acceptable fact that the isomorphic substitution in the tetrahedral sheet results in permanent negative charges at the T-face (which is pH-independent), and the protonation/deprotonation of the silanol and aluminol groups at the edges leads to the results that surface charges vary with the medium (which is pH-dependent). The O-faces behave the same characteristics of surface charges as the edges, as reported elsewhere (Tombacz and Szekeres, 2006).
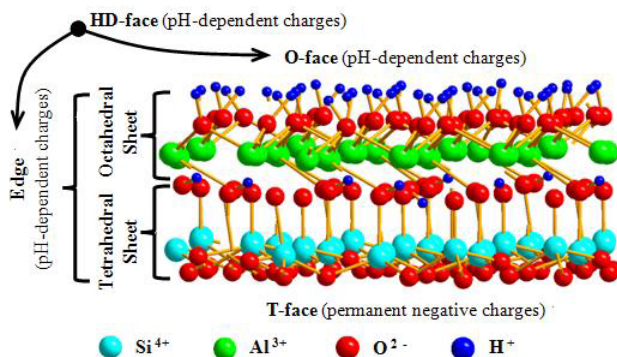

Fig. 4. Molecular structure of kaolinite layer

Kaolinite splits easily along the level parallel direction, and produces a number of negatively charged breaking bonds of Al–O and Si–O bond on the particle surface. The particle surface easily forms large number of Al–OH and Si–OH groups. As it is known, the surface charges of oxide mineral particles are originated from the protonation and deprotonation of the surfaces as follows:

$$M–OH + H^+ \rightarrow M–OH_2^+$$

$$M–OH + OH^- \rightarrow M–O^-$$
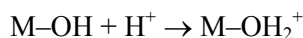
where M represents metal, such as Al and Si in this case. At low pHs, the protonation of the surfaces leads to be positively charged, while at high pHs the deprotonation results in negative charges. The value of the surface charge on oxide minerals (or zeta potential) closely correlates with pH value of the mineral suspension. It will affect the surface charge density or electric potential (Yin et al., 2006). In acidic medium, H^+ and the particle surface-OH can have neutralization reaction to compress particle surface electric double layer, so the absolute value of zeta potential with the acidic enhancement becomes smaller and smaller. In alkaline medium, due to complexation reactions, the particle surface have a large number of OH⁻ to make particle surface charge negatively, so the electronegativity of kaolin particles surface increases.

Figure 5b shows that when pH is neutral or acidic, the stretching vibration intensity of -OH in the range of 3700～3600 cm⁻¹ is stronger, which indicates that there are a large number of –OH groups generated on kaolinite particle surface in acidic and neutral aqueous media. When the pH value is about 13, the stretching vibration intensity of –OH in the range of 3700～3600 cm⁻¹ weaken, and the stretching vibration intensity of Al–O and Si–O bonds is significantly enhanced, which shows
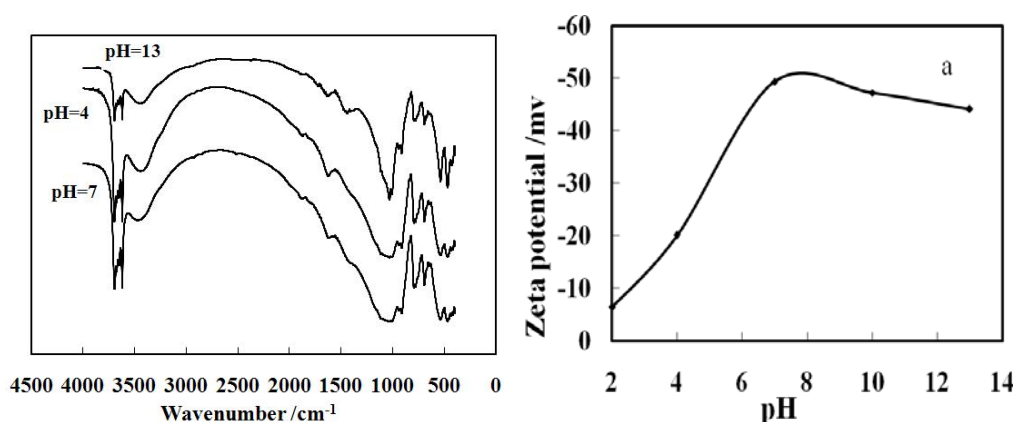

Fig. 5. Zeta potential (a) and FTIR spectra (b) of kaolinite at different pH values

that the –OH on particle surface has complexation reactions with the –OH in alkaline medium to increase the electronegativity of kaolin particles surface. However, when pH value is larger than 8, the absolute values of zeta potential trend to decrease. The DLVO theory (Hu et al., 2001) shows that the excess NaOH added to the solution to adjust the pH has increased the concentration of ions in the solution, and these ions compress particle surface electric double layer leading to reducing the potential value of the particle surface.

The effect of immersion time on zeta potential of kaolinite particle surface

Zeta potentials of kaolinite at different immersion times are presented in Fig. 6a. The infrared spectroscopy results of kaolinite samples soaked in different time are shown in Fig. 6b.
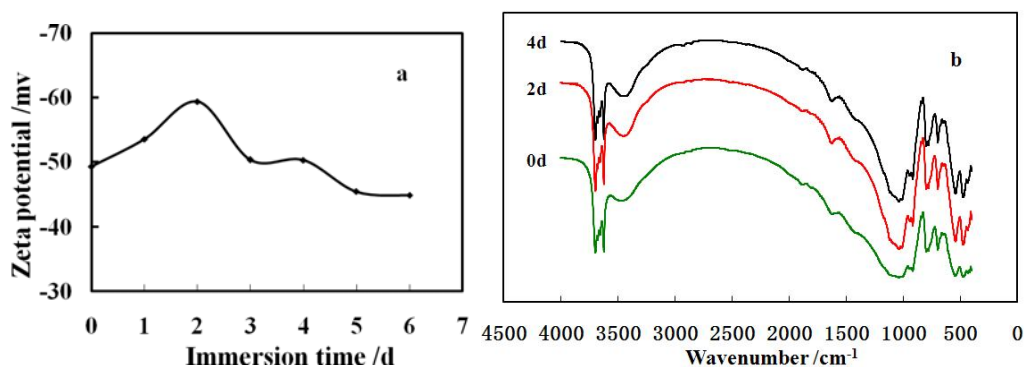

Fig. 6. Zeta potential (a) and FTIR spectra (b) of kaolinit with different immersion times

As shown in Fig. 6a, the absolute value of zeta potential increases with immersion time prolonging and the absolute value reaches the maximum 59.37 mV in the second day, and then the zeta potential absolute value gradually decreases with the extension of immersion time. Water will gradually undermine the cohesiveness between the mineral particles of kaolinite in saturated state and enter the pores between the chip-shaped particles resulting in uneven inner-stress and a lot of micropores in mudstone and induce softening and degradation (Huang and Che, 2007). Kaolinite breaks into fine particles within a certain immersion time which would produce new bonds of $-SiO^-$ and $-AlO^-$. With the further extension of the immersion time, some salts mixed internally in particles more easily dissolve into the solution along with ionization of Ca^{2+} and Mg^{2+} and other cations. The adsorption of these cations onto the the $-SiO^-$ or $-AlO^-$ groups on the surface of kaolinite will compress particle surface electric double layer to reduce the potential value of the kaolin particle surface. Duman et al. (2012) reported that the adsorption of H^+ ions in water onto the negatively charged kaolinite surface leads to increasing pH value.

Figure 6 b shows that the stretching vibration intensity of -OH group in the range of 3700–3600 cm^{-1} is stronger when the soaking time is 2 days. The stretching vibration intensity of –OH in the range of 3700–3600 cm^{-1} will weaken after the kaolinite sample soaked for 4 days.

The effect of cation on zeta potential of kaolinite particle surface

The zeta potentials of kaolinite at pH 7 as a function of Ca^{2+} concentration are shown in Fig. 7a. The zeta potentials of kaolinite at pH 7 in the presence of 86 mg/dm^3 multivalent metal cations (0.00374 mol/dm^3 Na$^+$, 0.00215 mol/dm^3 Ca^{2+}, 0.00358 mol/dm^3 Mg^{2+} or 0.00319 mol/dm^3 Al^{3+}) were measured and results are presented in Fig. 7b.

As can be seen from Fig. 7a, with Ca^{2+} concentration increasing, the absolute value of the surface zeta potentials of kaolinite gradually decrease. When Ca^{2+} concentration reaches 0.00215 mol/dm^3, the absolute value of zeta potential is decreased by 51.66%, and then tends to balance, the absolute value of zeta potential does not change significantly. This proofs that the adsorption of Ca^{2+} to kaolinite particle tends to be stability and saturation (Zhang et al., 2011). It can be seen from Fig. 7b that the zeta potential absolute value decreases with the increase of metal cationic valence.
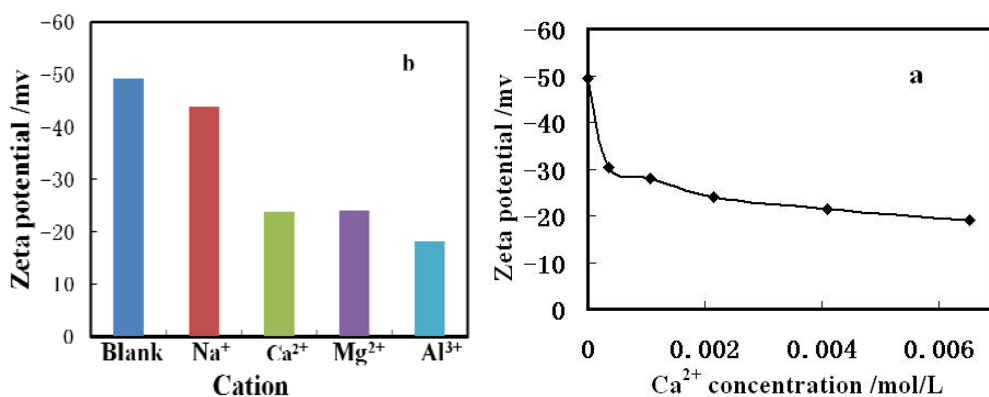

Fig.7 Zeta potential of kaolinite in the presence of Na$^+$, Ca^{2+}, Mg^{2+}, Al^{3+}

The strong zeta potential change in the presence of the metal ions was likely due to two reasons. The first was the compression of the electrical double layer by the multivalent metal cations. Taking Mg^{2+} as an example, the addition of 10^{-3} mol/dm^3 divalent Mg^{2+} cations would theoretically reduce the thickness of the electric double layers of kaolinite from 9.6 nm (with 10^{-3} mol/ dm^3 KCl as supporting electrolyte) to 5.6 nm (Gan and Liu, 2008; Zhang et al., 2008; Wang and Hu, 1988). If the surface potential is unchanged, the reduced electric double layer thickness means that the zeta potential of the particles would be lower. The second was the hydrolysis and adsorption of the metal-hydroxyl species on kaolinite. At above pH 8, these metal cations were hydrolyzed. The positively charged hydrolyzed species such as CaOH$^+$,

MgOH$^+$, and AlOH^{2+} could adsorb on the deprotonated surface kaolinite edges. This "charge-neutralization" effect of the multivalent metal ions has been widely reported in water treatment (Duman et al., 2012; Gan and Liu, 2008). The high valence cation has more positive charge under the same concentration conditions. Its compression capacity to the particle surface electric double layer is stronger, and for the unit positive charge, Ca^{2+} and Mg^{2+} have greater impact than Al^{3+} on the electric potential of kaolin particle surface. The Ca^{2+} has better compression capacity to the particle surface electric double layer, so the absolute value of the zeta potential decreases more, which relates to their different capacity of adsorption to the surface of kaolin particles.

Change of zeta potential and interaction between kaolinite particles and other mineral particles

Figure 8 shows the comparison of the zeta potential at pH 7 between the single system of kaolinite (named K) or quartz (named Q) and the binary-system with different quantitative ratio of kaolinite to bitumen.
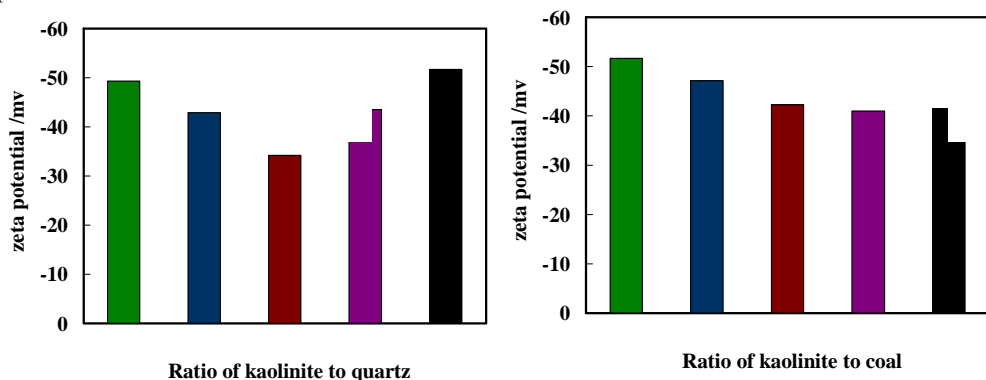

Fig. 8. Zeta potential curves in single systems of kaolinite and quartz (a) and coal and binary systems containing kaolinite and quartz or kaolinite and bitumen (b)

It can be seen that the absolute value of zeta potential in binary-system was lower than that in single kaolinite or quartz system, when the ratio of kaolinite to quartz is about 1:1. The absolute value of the surface potential of binary-system reaches the minimum, which suggested that the presence of quartz decreased the absolute value of zeta potential of the binary-system containing kaolinite and quartz. When kaolinite and quartz exist simultaneously in the same colloid suspension system, the electrostatic attraction makes the particle of kaolinite close to the particle of quartz, the interaction of the diffuse layers on oppositely charged particles decreases the value of effective charge density on kaolinite and quartz, and thus the zeta potential in the mixed charge system moves to the positive value side compared to the single kaolinite system (Hou et al., 2007; Lu and Hon, 1992; Gupta et al., 2011). In addition, the average particle size of the quartz samples used in the test is approximately 48.264 μm, the average particle size of kaolinite samples is about 0.735 μm. Since the

large difference between the two samples particle size, both of them are prone to mutual coagulation, in which the kaolinite particle owning the size of less than 1μm tend to coagulate. The quartz particles which size is larger than 1μm tend to participate in mutual coagulation (Lu and Hon, 1992; Gupta et al., 2011).

In a slightly acidic solution, the kaolinite edge is positively charged through protonation of surface hydroxyl groups. On the other hand, bituminous coal particles are a mixture of hydrocarbons containing carboxylic and phenolic groups. These groups exposed to the aqueous phase are ionized at basic pH and thus carry negative charges (Gan and Liu, 2008). Thus, the kaolinite particles and bituminous coal particles can interact with negatively charged coal particles droplets through electrostatic attraction, which induced the absolute value of zeta potential decrease.

The surface interaction mechanism of mixed mineral particles can be analyzed using the classical DLVO theory. The general formula of total energy (V_T) between the mineral particles can be expressed (Tombacz and Szekeres, 2006) as:

$$V_T = V_R + V_A \tag{1}$$

where V_T is the total energy, V_R and V_A are the electrostatic and van der Waals energy between the particles. The potential energy of the electrical double layer interaction between two homogeneous spheres can be expressed (Rao et al., 2011; Duman et al., 2012) by:

$$V_R = \left(\frac{\pi \varepsilon_a r_1 r_2}{r_1 + r_2} \right) \left(\psi_{01}^2 + \psi_{02}^2 \right) \left(\frac{2\psi_{01}\psi_{02}}{\psi_{01}^2 + \psi_{02}^2} p + q \right) \tag{2}$$

where r_1 and r_2 are the radius of kaolinite and quartz particles, ε_a the permittivity, ψ_{01} and ψ_{02} outer Helmholtz plane (OHP) potential or zeta potential of kaolinite and quartz particles, p and q can be expressed (Rao et al., 2011 ; Duman et al., 2012) by:

$$p = \ln \frac{1 + \exp(-\kappa h)}{1 - \exp(-\kappa h)} \tag{3}$$

$$q = \ln\left[1 - \exp(-2\kappa h)\right] \tag{4}$$

where h is the shortest separation between two particles and κ the Debye reciprocal length, which is given (Tombacz and Szekeres, 2006) by:

$$\kappa^2 = 1000 e^2 N_A / \varepsilon k_B T \sum_i z_i^2 M_i \tag{5}$$

where N_A is the Avogadro's number, Z_i and M_i are the valence of and the molar concentration of ions I, k_B the Boltzmann constant, T absolute temperature, e the elementary charge, Z the valence of determining ion;

The van der Waals interaction between two homogeneous particles is expressed (Rao et al., 2011; Duman et al., 2012) by:

$$V_A = -\frac{A_{132}}{6h}\left(\frac{r_1 r_2}{r_1 + r_2}\right) \tag{6}$$

where A_{132} is the Hamaker constant of particles 1and particles 2 in medium 3, which may be obtained (Rao *et al.*, 2011; Duman *et al.*, 2012) by:

$$A_{132} \approx \left(\sqrt{A_{11}} - \sqrt{A_{33}}\right)\left(\sqrt{A_{22}} - \sqrt{A_{33}}\right) \tag{7}$$

where A_{11}, $A_{22}$and A_{33} are the Hamaker constants of particles 1, particles 2 and medium 3 in vacuum, respectively.
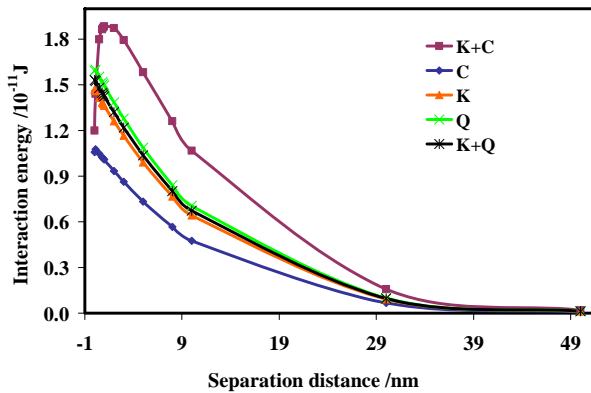
Fig. 9. Interaction energy profiles for different surface interactions
of kaolinite and other mineral particles

Based on the DLVO theory, the total potential energy of interaction between particles in aqueous solutions as a function of distance between the particles was calculated. The results are presented in Fig. 9.

As can be seen, the interaction energy between the particles of different mineral is repulsive at the pH 7 due to the strong electrostatic repulsion between negatively charged particles faces. The repulsion order is as follows: (K+C) (repulsion between kaolinite and coal particles) > Q (repulsion between quartz particles) > (K + Q) (repulsion between quartz and kaolinite particles) > K(repulsion between kaolinite particles) > C(repulsion between coal particles). However, the order of the absolute value of the mineral particle surface zeta potential is $zeta_Q > zeta_K > zeta_{(K+C)} > zeta_C > zeta_{(K+Q)}$, and the result is vary with the classical DLVO theory, which may be the reason why the particles tend to occur mutual coagulation phenomen to cause the repulsion energy between the particles has been reduced.

It can be seen from Fig. 3a that as the agitating speed increases, the absolute value of zeta potential of kaolinite particles surface first decreases.

Conclusions

The absolute value of zeta potential reaches its maximum and then tends to decrease with increasing immersion time. With the pH value increasing, the absolute value of zeta potential gradually increases and reaches its maximum at pH 8. No isoelectric point was found in the experimental range of 2–13 pH value, which may be because the sample contains other heterogeneities and kaolinite suspension concentration also can affect the zeta potential value of the suspension.

The order of the ability to reduce the zeta potential of kaolin particles surface under the conditions of the different valences of cations in the same concentration is that $Al^{3+} > Ca^{2+} > Mg^{2+} > Na^{+}$.

The suspension particle surface ion adsorption and the change of surface bonds of Si–O, Al–O and Al–OH are the underlying reasons to change surface zeta potential of kaolin suspension particle.

The repulsion of different mineral particles in the mixed suspension liquid of kaolinite with quartz and coal is in dominant position, and that the existence of mutual coagulation role in the different mineral particles makes the absolute value of the zeta potential of the particle surface to reduce.

Acknowledgements

References

ALKAN M., DEMIRBAS Ö., DOĞAN M., 2005. *Electrokinetic properties of kaolinite in mono-and multivalent electrolyte solutions*. Micropor. and Mesopor. Mat. 83, 51–59.

CHASSAGNE C., MIETTA F., WINTERWERP J.C., 2009. *Electrokinetic study of kaolinite suspensions*. J. Colloid Interf. Sci. 336, 352–359.

DAI X.N., WANG X.F., 2002. *Effect of pH on the zeta potential of MMH-kaolinite suspensions*. J. Dezhou College. 18,42–45.

DUMAN O., TUNC S., CETINKAYA A., 2012. *Electrokinetic and rheological properties of kaolinite inpoly(diallyldimethylammonium chloride), poly(sodium 4-styrene sulfonate) and poly(vinyl alcohol) solutions*. Colloids and Surfaces A: Physicochem. Eng. Aspects. 394, 23-32.

GAN W. B., LIU Q., 2008. *Coagulation of bitumen with kaolinite in aqueous solutions containing Ca2+,Mg2+ and Fe3+: Effect of citric acid*. J. Colloid Interf. Sci.. 324, 85–91.

GUPTA V., HAMPTON M. A., STOKES J. R., 2011. *Particle interactions in kaolinite suspensions and corresponding aggregate structures*. J. Colloid Interf. Sci. 358, 95–103.

HOU T., XU R. K., ZHAO A. Z.,2007. I*nteraction between electric double layers of kaolinite and Fe/Al oxides in suspensions*. Colloids and Surfaces A: Physicochem. Eng. Aspects. 297(2007), 91–94.

HU H. M., CHEN X. Z., WANG Y., 2001. *The application of dynamic potential in determining the coal dressing wastewater*. Enviro. Protect. Sci. 104, 14–15.

HU Y., LIU X., 2003. *Chemical composition and surface property of kaolins*. Miner. Eng. 8, 1279–1284.

HUANG H.W., CHE P., 2007. *Research on micro-mechanism of softening and argillitization of mudstone*. J. Tongji Univ. 35, 866–870.

HUSSAIN S. A., DEMIRCI S., ÖZBAYOĞLU G., 1996. *Zeta potential measurements on three clays from Turkey and effects of clays on coal flotation*. J. Colloid Interf. Sci. 184, 535–541.

KIHC M.G., HOSTEN C., 2010. *A comparative study of electrocoagulation and coagulation of aqueous suspensions of kaolinite powders*. J. Hazard. Mater. 176, 735–740.

LU S. C., HON D., 1992. *Interface separation principle and application*. Beijing: Metallurgical Industry Press.

MA C., EGGLETON R. A., 1999. *Surface layer types of kaolinite: a high resolution transmission electron microscope study*. Clays Clay Miner. 47, 181–191.

RAO F., RAMIREZ-ACOSTA F. J., SANCHEZ-LEIJA R. J., SONG S.X., LOPEZ-VALDIVIESO A., 2011. *Stability of kaolinite dispersions in the presence of sodium and aluminum ions*. Appl. Clay Sci. 51, 38–42.

SMITH R.W., NARIMATSU Y., 1993. *Electrokinetic behavior of kaolinite in surfactant solutions as measured by both the microelectrophoresis and streaming potential methods*. Miner. Eng., 7, 753–763.

TOMBACZ E., SZEKERES M., 2006. *Surface charge heterogeneity of kaolinite in aqueous suspension in comparison with montmorillonite.* Appl Clay Sci. 34, 105–124.

TUNC S., DUMAN O., 2008. *The effect of different molecular weight of poly(ethylene glycol) on the electrokinetic and rheological properties of Na–bentonite suspensions*. Colloids Surf. A. 317,93–99.

WANG, D. Z., HU Y. H.,1988. *Flotation solution chemistry*. Changsha: Hunan Science and Technology Press.

WILLIAMS D. J. A., WILLIAMS K. P., 1978. *Electrophoresis and zetapotential of kaolinite*. J. Colloid Interf. Sci. 65, 9–87.

YANG H.L., FAN M.Q., 2010. *Relationship between iron consumption, silicon consumption and flocculation characteristics of PFS*. J. Enviro. Eng. 4, 2789–2792.

YANG S. J., SHEN Z. Y., YING Y. Y., 2001. *Distribution of electric charge on crystalline grain surface of kaolinite and its industrial significance.* Non-Metal. Miner. 24, 196–198.

YIN H. R., WU L. H., FU F. C., 2006. *Research and application of nano-kaolin*. Mater. Rev. 20, 196–199.

ZBIK M.S., SMART R.S.C., MORRIS G.E., 2008. *Kaolinite flocculation structure*. J. Colloid Interface Sci. 328, 73–80.

ZHANG M. Q., LIU J. T., WANG Y. T., 2008. *Effects of water hardness on the dispersion of fine coal and kaolinite in coal slurry*. J. China Coal Soci. 9, 1058–1062.

ZHANG Z. J., LIU J.T., FENG L., 2011. *A prediction model based on langmuir theory for equilibrium adsorption amount*. J. Northeastern Univ. 32, 749–756.

PREPARATION AND CHARACTERIZATION OF SiO$_2$/SILANE/POSS FUNCTIONAL HYBRIDS

**Karolina SZWARC-RZEPKA, Tomasz SZATKOWSKI,
Filip CIESIELCZYK, Teofil JESIONOWSKI**

Poznan University of Technology, Faculty of Chemical Technology, Institute of Chemical Technology and
Engineering, M. Sklodowskiej-Curie 2, PL-60-965, Poznan, Poland, e-mail: Teofil.Jesionowski@put.poznan.pl

Abstract: Novel SiO$_2$/silane/POSS functional hybrids have been synthesized via an immobilization method. Hybrid materials were obtained through a connection of emulsion silica with defined dispersive and morphological properties with (3-isocyanatepropyl)triethoxysilane and selected mono- or octasubstituted POSS compounds in organic solvent. Modification effectiveness of the obtained SiO$_2$/silane/POSS hybrid systems was confirmed with the use of the Fourier transform infrared spectroscopy (FTIR). In order to determine the influence of bifunctionalization on coverage degree of the selected POSS compounds, elemental analysis (C, H, N contents) was performed. Moreover, parameters of porous structure of the obtained products were determined: BET surface area, total volume and mean size of pores. During analysis the thermal stability of silsesquioxanes cage, unmodified silica support, and hybrid systems have been investigated. For this purpose dispersive and morphological characterization (particle size distribution and TEM images) was performed.

Keywords: SiO$_2$/silane/POSS hybrids, silica support, silsesquioxanes cage, bifunctionalization process

Introduction

Nanotechnology is a modern science, which is focused mainly on designing and creation of structures, of which at least one dimension is in nanometric scale (Swiderski, 2008; Szwarc-Rzepka, 2013). Among nanofillers particularly interesting are various silica products, silsesquioxanes, fullerens and carbon nanotubes. Those compounds are especially susceptible to various kinds of modifications (Zurawska, 2003).

One of the most popular modifiers, next to silane coupling agents (Andrzejewska, 2004; Jesionowski, 2003; Jesionowski, 2010; Karim, 2012), are polyhedral oligomeric silsesquioxanes (POSS) (Wu, 2009). POSS is a group of compounds build of inorganic and organic part. The inorganic core is made of silicon-oxygen cage. On the

other hand, organic fragments, located at the corners of the cage, might be composed of alkil, alkylen, epoxy, hydroxyl, acryl, methacrylate or other organic groups and their derivatives (Kuo, 2001; Li, 2001; Ipoh, 1995). Usually, oligomeric silsesquioxanes are colorless, crystalline substances in the 1–100 nm particle size range (Zhang, 2009; Iyer, 2007; Utracki, 2004). They crystallize from solution usually in form of white powders. However, they might also appear in form of colorless oil or waxes (Ye, 2006; Kickelbick, 2007).

Dynamic development of nanotechnology have had a significant influence on a formation of novel synthesis method of functionalized nanofillers. Addition of materials of particle size lower than 100 nm to organic, as well as inorganic matrix is often a reason for improvement or maintaining constant properties of final components (Thostenson, 2005).

Bianchini and Galland (2005) have modified surface of silica with polyhedral oligomeric silsesquioxanes, where amines are part of side functional groups. Goal of the research was to point at catalytic properties of metallocene and POSS modified silica in ethylene polymerization process. Equally interesting examples were obtained by Carniato et al. (2008). They have dealt with problems concerning surface bifunctionalization of an ordered mesoporous silica (SBA-15), and unordered silica (SiO_2-Dav). For modification purpose (3-isocyanatepropyl)triethoxysilane and monosubstituted POSS with amine group, have been used. Obtained hybrid systems were utilized as a heterogenic catalysts in a limonene epoxydation reaction.

In this paper grafting of traditional inorganic support, namely silica, with well known silane proadhesive compound, and modern modifying agents, that is cage silsesquioxanes, was performed on the basis of the bifunctionalization process. Due to the fact, that single cubic structure T_8 is able to attach as much as eight reactive organic groups (Lee, 1998), properties of the obtained compounds, such as thermal stability, mechanical strength, catalytic activity etc., are improved.

Experimental

Materials

The material studied was SiO_2 filler precipitated in the emulsion system, in analogy to previously described procedure by Jesionowski (2009).

The inorganic filler surface was grafted with selected alkoxysilane (purchased from Sigma-Aldrich) (Table 1) and also with Methacryl POSS[®] Cage Mixture and AminoethylaminopropylIsobutyl POSS[®] (purchased from Hybrid Plastics[®] Co.) (Table 2) in the amounts of 3, 5 or 10 weight parts by mass of SiO_2.

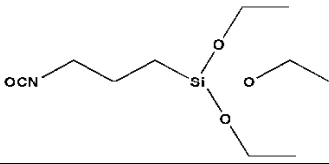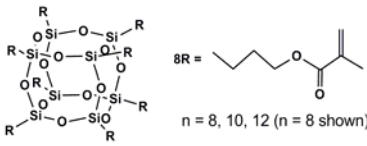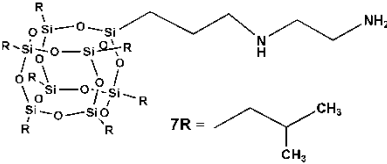Table 1. Alkoxysilane used for inorganic filler surface grafting

Name	(3-isocyanatepropyl)triethoxysilane
Formula	$(C_2H_5O)_3Si(CH_2)_3NCO$
Structure	
Molecular weight	247.36
Form	liquid
Density (g/cm^3)	0.999 (temperature 25 °C)
Color	transparently

Table 2. POSS compounds used for inorganic filler surface functionalization

Name	Methacryl POSS® Cage Mixture	AminoethylaminopropylIsobutyl POSS®
Formula	$C_{56}H_{88}O_{28}Si_8$	$C_{33}H_{76}N_2O_{12}Si_8$
Structure		
Molecular weight	1433.97	917.65
Form	liquid (oily)	powder
Density (g/cm^3)	1.200 (temperature 20 °C)	1.170 (temperature 20 °C)
Color	transparently	white

SiO₂/silane/POSS hybrids synthesis

Silica filler was submitted to the bifunctionalization via immobilization in organic solvent method. Schematic diagram of the bifunctionalization process has been presented in Fig. 1.

The process consisted of two stages. To a four-necked flask, supplied with a high-speed stirrer and mounted in a water bath, an appropriate fraction of emulsion silica was introduced into organic solvent – toluene. Nitrogen has been introduced in order to ensure inert atmosphere. When temperature in water bath reached 50 °C, modification process started. With the use of a peristaltic pump, a proper amount of

organosilane (3, 5 or 10 weight parts by mass of silica) was dosed into toluene with rate equal to 1 cm^3/min (1). Afterwards, selected POSS compound in organic solvent has been introduced into the system (2) with set rate of dosing.
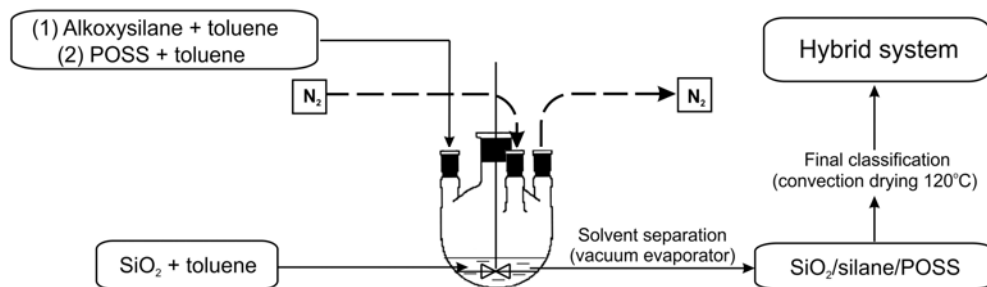

Fig. 1. Schematic diagram of SiO$_2$/silane/POSS hybrid systems preparation

After that time mixture remained in the reactor for 2 h under stirring (ca. 800 rpm). Then, the organic solvent was separated by distillation. Obtained powders has been dried in a convectional dryer in temperature as high as 120 °C for 48 h.

Evaluation of physicochemical properties

The final products were characterized by a number of methods. The effectiveness, degree of bifunctionalization of SiO$_2$ with silane and selected POSS compounds were estimated using the FTIR IFS 66v/S spectrophotometer made by Bruker.

The chemical composition of the functionalized SiO$_2$ systems were determined using a Vario EL Cube apparatus (Elementar Analysensysteme GmbH).

For selected hybrid systems the nitrogen adsorption/desorption isotherms were recorded using an ASAP 2020 analyzer, made by Micromeritics Instrument Co. On the basis of BET equations the specific surface area BET (S_{BET}) was calculated and the pore size (D_P) and total pore volume (V_P) were found from the BJH algorithm.

Thermogravimetric analyses were performed using a Jupiter STA 449 F3 (Netzsch GmbH). Samples weighing approximately 10.0 mg were placed in an Al$_2$O$_3$ crucible, and heated at a rate of 10 ºC/min from 30 to 1000 ºC in a nitrogen atmosphere.

The particle size distributions of the samples were measured using Zetasizer Nano ZS made by Malvern Instrument Ltd., enabling measurements in the range 0.6–6000 nm (NIBS method). Microstructure of the samples was analyzed by using the transmission electron microscopy images (Joel 1200 EX II).

Results and discussion

In the first stage of investigation Fourier transform infrared spectroscopy has been performed.

Figure 2 shows the FTIR spectra of emulsion silica (ES) and the hybrid obtained after silica modification with 5 weight parts by mass of isocyanatesilane, and 10 weight parts by mass of methacryl POSS compound (HS-I5.M10). The spectra presented prove a high efficiency of modification and change in the chemical character of the SiO_2 surface. Emulsion silica presents two characteristic absorptions bands at 1100 and 595 cm^{-1}, which are assigned to Si–O–Si stretching vibration, respectively. The spectrum of unmodified silica also shows adsorption band around 1640 cm^{-1}, which is assigned to the bending mode of physically adsorbed water molecules, in analogy to (Hong, 2007). Additionally, the intensity of the band at 3600–3200 cm^{-1}, assigned to the stretching vibrations of –OH groups, is coming from physically adsorbed water.
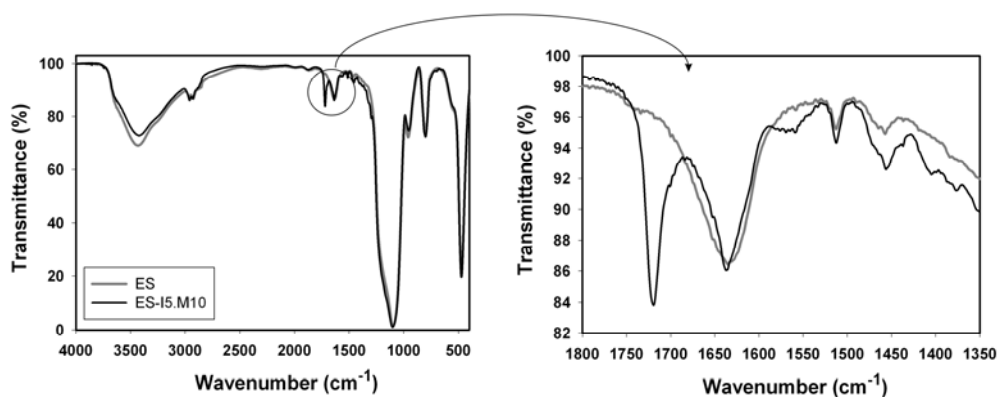

Fig. 2. FTIR spectra of unmodified emulsion silica (ES) and the hybrid obtained via modification with 5 weight parts by mass of (3-isocyanatepropyl)triethoxysilane and 10 weight parts by mass of Methacryl POSS® Cage Mixture (ES-I5.M10)

As a result of the performed bifunctionalization process a change in the band intensity at 3700–3200 cm^{-1} in the spectrum of the ES-I5.M10 sample has been observed and assigned to the stretching vibrations of –OH group, which might be related to changes in the hydrophilic–hydrophobic properties of the specimen. Moreover, the reduction of the intensity of this band confirms a chemical bonding of the modifier to silica surface and an effective substitution of double vicinal groups by its molecules. Besides, spectrum of the produced hybrids contains the stretching vibration band ν(C–H) in the range of 2950–2850 cm^{-1}. The band at 1720 cm^{-1} arises from the carbonyl stretching vibrations (ν(=C=O)) which corresponds to isocyanatesilane and methacrylate groups. Noteworthy is the presence of a weak

absorption band at 1550 cm^{-1}, which most likely relate to appearing of ν(C=C). Finally, absorption band corresponding to the stretching vibration of N=C=O group at 2250 cm^{-1} for the hybrid was not observed, because these groups have been effectively substituted by molecules of POSS with methacrylate groups. Analogical situation and suggested mechanism of SiO$_2$/modifier interactions, has been presented in our earlier work (Ciesielczyk, 2013).

Additionally, in Fig. 3 FTIR spectra of the ES and the hybrids obtained as a result of the bifunctionalization of silica support with 5 weight parts by mass of isocyanatesilane and 10 weight parts by mass of AminoethylaminopropylIsobutyl POSS$^{®}$ (ES-I5.N10). A change in the band absorption intensity characteristic for physically adsorbed water molecules has been observed. Moreover, because of masking effect of the intensive band sourcing from –OH group, absorption band characteristic for stretching vibrations of N–H in 3500–3250 cm^{-1} range has not been observed. Additionally, raise in band intensity of ν(C–H) bonds in the range of 2950–2850 cm^{-1} has been noted. Moreover, a formation of a very weak band assigned to secondary and primary amines has been also confirmed (Fig. 3).
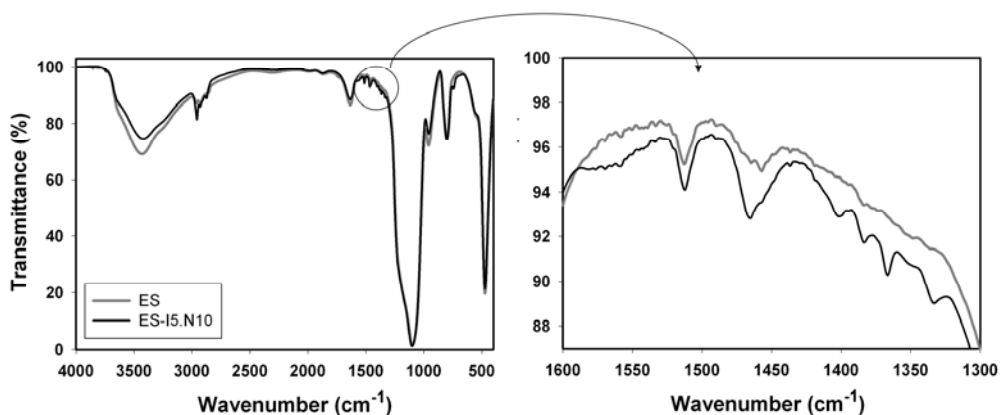

Fig. 3. FTIR spectra of unmodified emulsion silica (ES) and the hybrid obtained by their modification with 5 weight parts by mass of (3-isocyanatepropyl)triethoxysilane and 10 weight parts by mass of AminoethylaminopropylIsobutyl POSS$^{®}$ (ES-I5.N10)

Furthermore, chemical composition of the obtained materials was determined using elemental analysis (Table 3). The procedure was performed in order to verify the effectiveness of the modification process and to calculate the surface coverage degree of the silica support with (3-isocyanatepropyl)triethoxysilane and selected POSS compounds. The degree of coverage was calculated from the Berendsen and de Golan equation (1978).

As a result of the silica supports bifunctionalization with silane and Methacryl POSS$^{®}$ Cage Mixture, the content of carbon and hydrogen was found to increase with rising the applied amounts of POSS modifier (in weight parts by mass). Since the

degree of coverage depends on the specific surface area of the initial support, lower values were obtained for emulsion silica modified with 5 weight parts by mass of the organosilane and 3, 5, 10 weight parts by mass of the methacryl POSS compound, i.e. 0.505 μmol/m^2, 0.548 μmol/m^2, and 0.717 μmol/m^2, respectively (Table 3). In the case of hybrid systems made from emulsion silica modified with 5 weight parts by mass of (3-isocyanatepropyl)triethoxysilane and 3, 5 or 10 weight parts by mass of AminoethylaminopropylIsobutyl POSS®, the content of carbon, hydrogen, and nitrogen also was found to increase with the applied amounts of POSS modifier. The obtained values of the coverage degree are as high as 0.927 μmol/m^2, 1.078 μmol/m^2, and 1.690 μmol/m^2.

Table 3. Elemental content of carbon, nitrogen and hydrogen and parameters of the porous structure of unmodified silica and silica-based fillers grafted with alkoxysilane and different amounts of Methacryl POSS® Cage Mixture and AminoethylaminopropylIsobutyl POSS®

Acronym	Elemental content (%)			Degree of coverage (μmol/m^2)	Parameters of porous structure		
	N	C	H		S_{BET} (m^2/g)	V_P (cm^3/g)	D_P (nm)
ES	–	2.398	1.227	–	77	0.23	8
ES-I5.M3	–	4.875	1.712	0.505	76	0.18	9
ES-I5.M5	–	5.075	1.762	0.548	55	0.16	10
ES-I5.M10	–	5.838	1.885	0.717	46	0.12	11
ES-I5.N3	0.289	5.374	1.939	0.927	77	0.18	8
ES-I5.N5	0.315	5.824	2.026	1.078	75	0.17	9
ES-I5.N10	0.459	7.560	2.366	1.690	55	0.14	10

In a further part of the research, an attempt to interpret the parameters of porous structures, such as specific surface area (S_{BET}), total pore volume (V_P) and mean size of pores (D_P) of unmodified emulsion silica, as well as alkoxysilane and POSS modified silica filler has been undertaken. Investigation results have been set in Table 3. Additionally, adsorption/desorption isotherms of nitrogen and pore size distribution of selected samples have been determined. Obtained results of selected powders have been presented in Fig. 4. Analysis of the data shown in Table 3 allows to state, that the obtained emulsion silica can be characterized with relatively high value of specific surface area equal to 77 m^2/g, taking under consideration spherical shape of the particles. The product can be included into mesoporous adsorbents group. Pores volume equal to V_P = 0.23 cm^3/g, and pores diameter D_P = 8 nm serves as a confirmation for the statement. From these data one can conclude that the process of emulsion silica bifunctionalization with use of silanes and oligomeric silsesquioxanes, caused significant changes in basic adsorption parameters. For samples bifunctionalized with 3, 5 or 10 weight parts by mass of methacryl POSS compound a decrease in pores volume has been noted, and reached values equal to 0.18 cm^3/g,

0.16 cm^3/g, and 0.12 cm^3/g, respectively. For the hybrids obtained with the use of amino POSS compound, smaller changes have been noted in comparison to final silica filler. Worth mentioning is also fact, that the kind and amount of used modifier, undoubtedly have impact on adsorption properties of the produced hybrid systems.

Analyzing data in Fig. 4 it has been stated that from isotherms set-up, according to IUPAC, are of type IV type with the hysteresis of type H3. It has been observed, that amount of adsorbed nitrogen on surface of the non-modified emulsion silica (Fig. 4a) slightly raises, until it reaches the value of relative pressure equal to 0.6. After exceeding the value of characteristic pressure rapid increase in adsorbed nitrogen has been observed, reaching maximum value as high as 122 m^2/g at p/p_0 = 1. For the presented hybrid systems functionalized with 3 or 10 weight parts by mass of POSS compounds (see Figs. 4b and 4c) an analogical dependence has been observed.
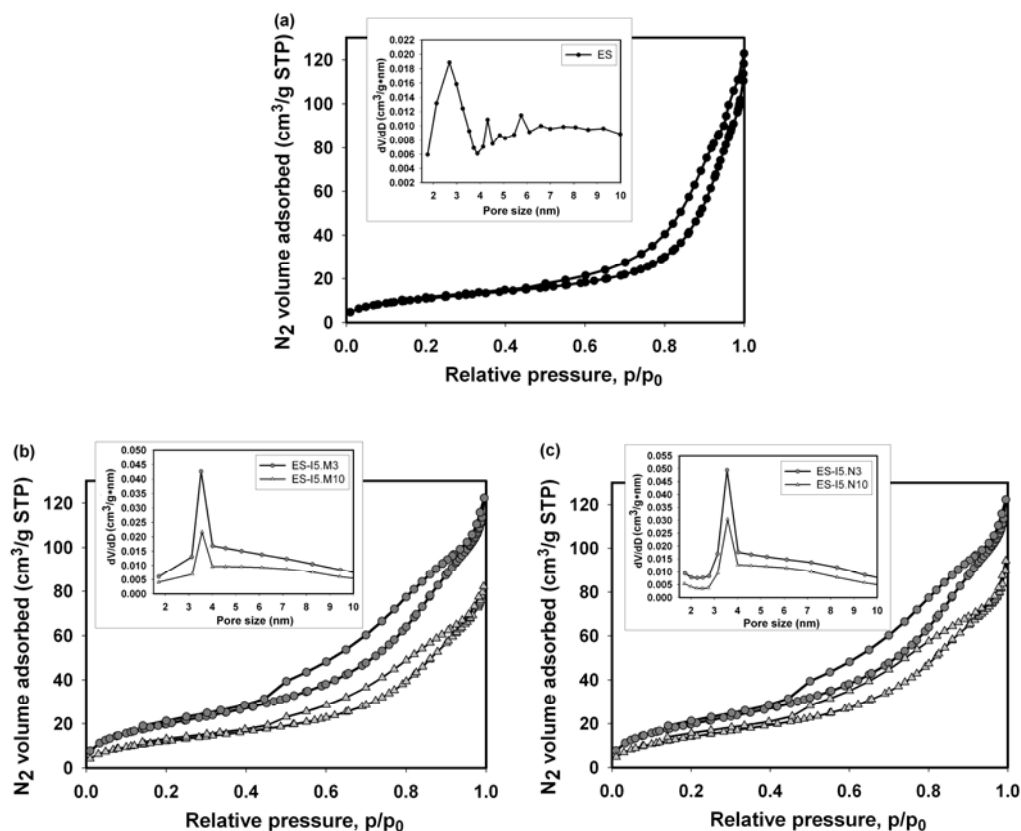

Fig. 4. Nitrogen adsorption/desorption isotherms and pore size distributions for
(a) unmodified emulsion silica and hybrid systems obtained using 5 weight parts by mass of
the (3-isocyanatepropyl)triethoxysilane and (b) 3 or 10 weight parts by mass of the Methacryl POSS®
Cage Mixture (ES-I5.M3, ES-I5.M10), and (c) 3 or 10 weight parts by mass of
the AminoethylaminopropylIsobutyl POSS® (ES-I5.N3, ES-I5.N10)

Up to the value of relative pressure equal to $p/p_0 = 0.4$, a slight increase in the amount of adsorbed nitrogen has been noted. After exceeding this value, the amount of adsorbed nitrogen rises rapidly. When value of relative pressure reached its maximum, i.e. 1.0, the amount of adsorbed gas molecules was equal to 122 cm^3/g for ES-I5.M3 (Fig. 4b), 85 cm^3/g for ES-I5.M10 (Fig. 4b), 122 cm^3/g for ES-I5.N3 (Fig. 4c), and 95 cm^3/g for sample ES-I5.N10 (Fig. 4c).

Examination of the bifunctionalization process effectiveness has been broaden by thermal analysis TG/DTA (Fig. 5) of the pure POSS compounds, final silica support, and selected hybrid materials. The results from TG/DTA analysis allowed to estimate temperatures range, which correspond to important chemical and structural transitions of the obtained hybrids.

Figure 5a shows a TGA thermograms of pure silsesquioxanes used for the hybrids obtained. As it can be seen, the TGA curve of pure Methacryl POSS® Cage Mixture revealed a mass loss of about 43% at 550 °C. The process continued until total degradation of the methacrylate groups substituted at the silicon atoms of the POSS skeleton. The rapid mass changes are accompanied by exothermic effects in temperature range from 300 to 700 °C. In the case of AminoethylaminopropylIsobutyl POSS® a two-stage degradation process has been observed. At the first stage an insignificant mass loss is most likely related to humidity evaporation, which has been captured by the compound as a result of heating process. The second change begins at 400 °C, and is accompanied by strong exothermic effect. At temperature as high as 500 °C sample mass stabilizes, and further increase in temperature does not cause considerable mass change. Total mass loss is equal to ~95%.
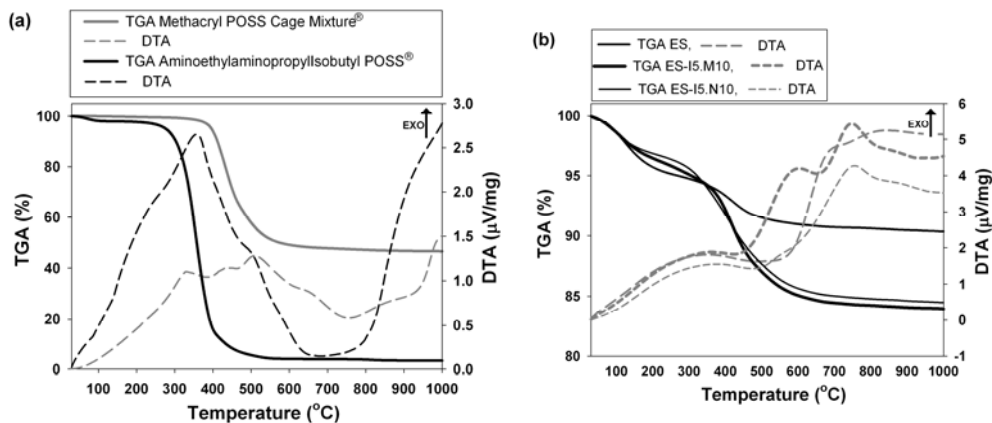

Fig. 5. Thermograms of (a) pure Methacryl POSS® Cage Mixture and AminoethylaminopropylIsobutyl POSS® and (b) unmodified emulsion silica, and hybrids functionalization with 5 weight parts by mass of isocyanatosilane and 10 weight parts by mass of selected POSS compounds

Figure 5b shows TGA thermograms of the unmodified emulsion silica and hybrids obtained by silica functionalization with 5 weight parts by mass of

isocyanatesilane, and 10 weight parts by mass of the selected POSS compounds. Analysis of the hybrid systems has been performed in order to determine thermal stability. The obtained thermograms were compared with curves characteristic for pure POSS modifiers. In case of the unmodified silica filler first mass loss is observable in temperature range from 30 to 300 °C, and most likely corresponds to loss of physically and chemically bound water. At this point mass loss is slightly above 10%. The mass change is also connected with endothermic effect. In further part of thermogram mass loss equal to 7% is observable, which is reflected by exothermic effect on the DTA curve (Fig. 5b). Observable thermal effect in the temperature range 300–700 °C corresponds to a loss of constitutional water. Afterwards only slight mass loss have been registered. For the selected hybrid systems (ES-I5.M10 and ES-I5.N10) two-stage degradation process has been observed as well. First mass loss for both systems is somewhat smaller and equal to ~8%. Additionally, the change is accompanied with endothermic effect. Second change characterize with exothermic effect (from 300 to 700 ^{o}C), and likely corresponds to degradation of the organic substituents, which appears in the corners of silsesquioxane. Noteworthy is fact, that no significant changes in the thermogravimetric curves, resulting from change of the cage modifier, have been observed. As can be noted for this example, mass loss for sample functionalized with AminoethylaminopropylIsobutyl POSS® (ES-I5.N10) is slightly lower in comparison to the hybrid bifunctionalized with methacryl POSS compound, and is equal to 16% of total mass sample.

Moreover, for the final support and SiO_2/silane/POSS functionalized hybrids dispersive and morphological characteristics have been performed. These parameters determine potential application of such systems, e.g. as a polymers filler. The particle size distribution according to volume contribution obtained for the unmodified SiO_2 is presented in Fig. 6a. One band covering the particle diameters from 342 to 712 nm with the maximum volume contribution of 32.2% comes from particles of 459 nm in diameter.
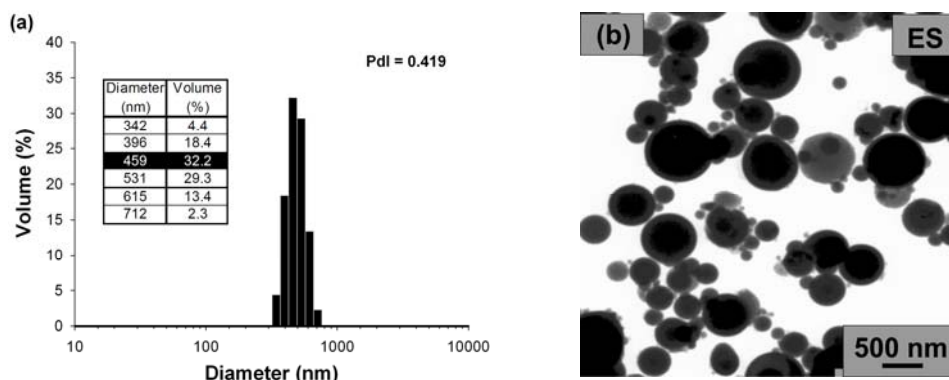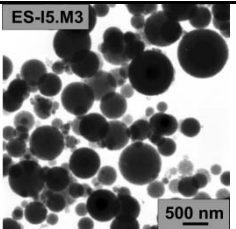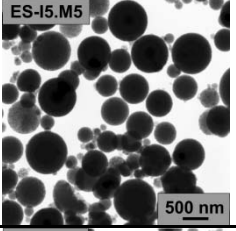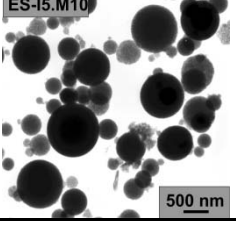

Fig. 6. PSD (a) and TEM microphotograph (b) of the unmodified SiO_2
precipitated in the emulsion system

The polydispersity index (PdI) of this filler is equal to 0.419. The TEM microphotograph of the studied sample is presented in Fig. 6b. The picture serves as a confirmation for the presence of particles with small diameters (corresponding to those indicated in the particle size distributions), significant homogeneity, spherical shape, and showing low tendency to form agglomerate structures.
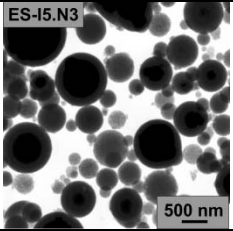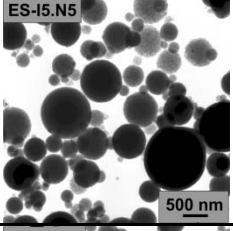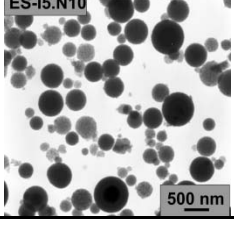
Table 4 presents dispersive and morphological characteristics of hybrids obtained as a result of SiO_2 modification with 5 weight parts by mass of organosilane and Methacryl POSS® Cage Mixture in different amounts. The results prove that the bifunctionalization has caused significant changes in dispersive character of the hybrid systems obtained.

Table 4. Dispersive and morphological characteristics of hybrid fillers obtained after SiO_2 modification with (3-isocyanatepropyl)triethoxysilane and Methacryl POSS® Cage Mixture in different amounts

Acronym	Amounts of modifiers (weight parts by mass)		Dispersive properties			TEM microphotograph
	Silane	POSS	Diameters range (nm)	Dominant particles diameter (nm)	PdI	
ES-I5.M3		3	396–955; 1110–2300	712 (18.5%)	1.000	
ES-I5.M5	5	5	459–955	712 (33.6%)	0.647	
ES-I5.M10		10	531–1280	825 (28.6%)	0.674	

Analyzing data collected and set-up in Table 4 it has been concluded that filler obtained after 2-hour functionalization with use of 5 weight part (3-isocyanate-propyl)triethoxysilane, and various amounts of the methacryl POSS compound can be described with different particles sizes. All samples presented in Table 4 show high tendency to particles agglomeration. For presented systems an increase in the polidispersity index in comparison to the final support has been observed. For instance, sample modified with 5 weight parts by mass of the silane and 3 weight parts by mass of POSS with methacrylate groups has PdI value equal to 1.

Table 5. Dispersive and morphological characteristics of the hybrid fillers obtained after SiO_2 modification with (3-isocyanatepropyl)triethoxysilane and AminoethylaminopropylIsobutyl POSS® in different amounts

Acronym	Amounts of modifiers (weight parts by mass)		Dispersive properties			TEM microphotograph
	Silane	POSS	Diameters range (nm)	Dominant particles diameter (nm)	PdI	
ES-I5.N3		3	295–955; 1110–6440	396 (18.8%)	1.000	
ES-I5.N5	5	5	825–2300	1280 (31.4%)	0.897	
ES-I5.N10		10	255–825	456 (17.3%)	0.714	

The most attractive dispersive parameters are observed for the hybrid synthesized with use of 5 weight parts by mass of Methacryl POSS® Cage Mixture. Data analysis

suggests that the sample is characterized with the monomodal particle size distribution in particles diameter range 459–955 nm and with volume fraction maximum equal to 33.6% pointing at particles with diameter as high as 712 nm, its polidispersity index is equal to 0.647.

Furthermore, Table 5 presents data of systems obtained with use of 5 weight parts by mass of (3-isocyanatepropyl)triethoxysilane and Aminoethylamino-propylIsobutyl POSS® in different amounts. The bifunctionalization contribute to a significant rise of analyzed particles size, with exception for sample ES-I5.N10, modified with 10 weight parts of amino POSS, which shows the most analogous dispersive character to the unmodified emulsion silica (see Fig. 6a). Analysis of the presented results let us to notice a monomodal particles size distribution in the diameter range of 255–6440 nm for SiO$_2$ modified with 5 weight parts by mass of silane, and 10 weight parts by mass of POSS. The highest volumetric fraction (17.3%) in the sample corresponds to particles diameter equal to 456 nm and the PdI of these sample was 0.714.

Conclusions

As a result of the investigation, novel SiO$_2$/silane/POSS functional hybrids have been obtained. It was stated that proposed modification route is an effective process, and it significantly contributes to changes in their physicochemical parameters. It was confirmed by the presented FTIR results.

Bifunctionalization of emulsion silica with POSS compounds increases coverage degree along with an increase in the applied amounts of the POSS modifiers. This was confirmed by the content of carbon and hydrogen. Higher values of the coverage degree were obtained in case of utilization of monosubstituted POSS, i.e. AminoethylaminopropylIsobutyl POSS®.

Examined parameters of porous structure of hybrid materials synthesized with utilization of N-POSS are higher than values noted for the hybrid obtained with use of Methacyl POSS® Cage Mixture.

SiO$_2$/silane/POSS hybrids acquired via immobilization in organic solvent are characterized with small shift in thermal stability. However, a change in the bifunctionalized samples mass loss, in comparison to native silsesquioxane cage, has been observed.

Performed process of the emulsion silica bifunctionalization with organofunctional silane and POSS modifier have contributed to a change in dispersive character of the obtained fillers.

Acknowledgements

References

ANDRZEJEWSKA A., KRYSZTAFKIEWICZ A., JESIONOWSKI T., 2004, *A study of the influence of solvents on the dispersive characteristics of silica, modified with 3-aminopropyltriethoxysilane, as filler for plastic and paint systems,* Pigment and Resin Technology 33, 142–151.

BANEY R.H., ITOH M., SAKAKIBARA A., SUZUKI T., 1995, *Silsesquioxanes,* Chemical Reviews 95, 1409–1430.

BERENDSEN G.E., de GOLAN L., 1978, *Preparation and chromatographic properties of some chemically bonded phases for reversed-phase liquid chromatotography*, Journal of Liquid Chromatography 1, 561–586.

BIANCHINI D., GALLAND G.B., DOS SANTOS J.H.Z., WILLIAMS R.J.J., FASCE D.P., DELL'ERBA I.E., QUIJADA R., PEREZ M., 2005, *Metallocene supported on a Polyhedral Oligomeric Silsesquioxane-modified silica with high catalytic activity for ethylene polymerization*, Journal of Polymer Science: Part A: Polymer Chemistry 43, 5465–5476.

CARNIATO F., BISIO CH., BOCCALERI E., GUIDOTTI M., GAVRILOVA E., MARCHESE L., 2008, *Titanosilsesquioxane anchored on mesoporous silicas: A novel approach for the preparation of heterogeneous catalysts for selective oxidations,* Chemistry - A European Journal 14, 8098–8101.

CIESILECZYK F., SZWAR-RZEPKA K., JESIONOWSKI T., 2013, *Evaluation of physicochemical properties of a new group of SiO₂/silane/POSS hybrid materials,* Surface and Interface Analysis, in press: DOI 10.1002/sia.5199.

HONG R.Y., FU H.P., ZHANG Y.J., LIU L., WANG J., LI H.Z., ZHENG Y., 2007, *Surface-modified silica nanoparticles for reinforcement of PMMA*, Journal of Applied Polymer Science 105, 2176–2184.

IPOH M., SAKAKIBARA M., SUZUKI T., 1995, *Silsesquioxane,* Chemical Reviews 95, 1409–1430.

IYER S., ABU-ALI A., DETWILER A., SEHIRALDI A., 2007, *Transparent polymer – Polyhedral Oligomeric Silsesquioxane composities*, ACS Symposium Series (*Science and technology of silicones and silicone-modified materials*), Cleveland, 964, 313–325.

JESIONOWSKI T., ZURAWSKA J., KRYSZTAFKIEWICZ A., POKORA M., WASZAK D., TYTUS W., 2003, *Physicochemical and morphological properties of hydrated silicas precipitated following alkoxysilane surface modification*, Applied Surface Science 205, 212–224.

JESIONOWSKI T., 2009, *Preparation of spherical silica in emulsion systems using the co-precipitation technique*, Materials Chemistry and Physics 113, 839–849

JESIONOWSKI T., CIESIELCZYK F., KRYSZTAFKIEWICZ A., 2010, *Influence of selected alkoxysilanes on dispersive properties and surface chemistry of spherical silica precipitated in emulsion media*, Materials Chemistry and Physics 119, 65–74.

KARIM A.H., JALIL A.A., TRIWAHYONO S., SIDIK S.M., KAMARUDIN N.H.N., JUSOH R., JUSOH N.W.C., HAMEED B.H., 2012, *Amino modified mesostructured silica nanoparticles for efficient adsorption of methylene blue*, Journal of Colloid and Interface Science 386, 307–314.

KAWAKAMI Y., 2007, *Structural control and functionalization of oligomeric silsesquioxanes,* Reactive and Functional Polymers 67, 1137–1147.

KICKELBICK G., 2007, *Hybrid materials. Synthesis, characterization and applications*, WILEY – VCH Verlag GmbH and Co. KGaA, Weinheim, 1–48, 225–254.

KRYSZTAFKIEWICZ A., RAGER B., WIECZOREK W., 1996, *Metody modyfikacji powierzchni napełniaczy mineralnych stosowanych w tworzywach sztucznych,* Physicochemical Problems of Mineral Processing 30, 107–117.

KUO S-W., CHANG F-C., 2001, *POSS related polymer nanocomposites*, Progress in Polymer Science 36, 1649–1696.

LEE A., LICHTENHAN J.D., 1998, *Viscoelastic responses of polyhedral oligosilsesquioxane reinforced epoxy systems,* Macromolecules 31, 4970–4974.

LI G., WANG L., NI G., PITTMAN JR. CH. U., 2001, *Polyhedral Oligomeric Silsesquioxane (POSS). Polymers and copolymers: a review*, Journal of Inorganic and Organometallic Polymers 11, 123–154.

SWIDERSKI F., ROBAK-WASZKIEWICZ B., 2008, *Nanotechnologia – korzyści i zagrożenia zdrowotne,* Bromatologia i Chemia Toksykologiczna 3, 202–208.

SZWARC-RZEPKA K., MARCINIEC B., JESIONOWSKI T., 2013, *Immobilization of multifunctional silsesquioxane cage on precipitated silica supports,* Adsorption, 19, 483–494.

THOSTENSON, E.T., LI, CH., CHOU, T.W., 2005, *Nano-composites in context,* Composites Science and Technology 65, 491–516.

UTRACKI A.L., *Clay – containing polymeric nanocomposites – Volume 1*, Rapra Technology Limited, Crewe 2004, 35–72.

WU J., MATHER P.T., 2009, *POSS Polymers: Physical properties and biomaterials applications,* Journal of Macromolecular Science®, Part C: Polymer Reviews, 49, 25–63.

YE Y-S., CHEN W-Y., WANG Y-Z., 2006, *Synthesis and properties of low-dielectric-constant polyimides with introduced reactive fluorine polyhedral oligomeric silsesquioxanes,* Journal of Polymer Science Part A: Polymer Chemistry 44, 5391–5402.

ZHANG H., JUNG M., SHIN Y., YOON K., LEE D., 2009, *Preparation and properties of ethylene/POSS copolymer with rac-Et(Ind)$_2$ZrCl$_2$ catalyst,* Journal of Applied Polymer Science 111, 2697–2702.

ZURAWSKA J., KRYSZTAFKIEWICZ A., JESIONOWSKI T., 2003, *Physicochemical properties, surface morphology and particle size distribution of precipitated silicas,* Surface and Interface Analysis, 35, 914–921.

EXPANDED PERLITE AGGREGATE CHARACTERIZATION FOR USE AS A LIGHTWEIGHT CONSTRUCTION RAW MATERIAL

Atila Gurhan CELIK[*] , Ahmet Mahmut KILIC[**], Gaye Ozgur CAKAL[***]

[*] National Boron Research Institute, Dumlupınar Bulvari, No: 166-10, 06520 Ankara, Turkey, agce_1@hotmail.com
[**] Mining Engineering Department, Cukurova University, 01330 Adana, Turkey
[***]Ankara University, Institute of Nuclear Sciences, 06100 Tandoğan, Ankara, Turkey

Abstract: The purpose of this study is to investigate the use of İzmir (Menderes-Cumaovası) expanded perlite as a construction raw material by determining its characteristic properties, as well as its physical properties at different temperatures (up to 600°C). The perlites, having glassy, porous structure, were found to contain 70.68% SiO_2 and 13.04% Al_2O_3. The physical properties of the perlites changed with temperature. The highest surface area, 524 m^2/g, was obtained at 400°C. The physical properties were found to have high statistical relation. It was concluded that expanded perlite aggregates could be used as a construction raw material.

Keywords: perlite, lightweight aggregate, characteristic property, physical property, temperature, construction raw material

Introduction

Perlite, which is obtained from pumice, contains 2–5% water and has a glassy form of rhyolitic or dacitic magma. The commercial product, commonly designated as expanded perlite, is produced by heating the material to 760–1100 °C, thereby converting its indigenous water to vapor and causing the material to expand to 4 to 20 times its original volume while forming lightweight high-porosity aggregates (Dogan and Alkan, 2004; Harben and Bates, 1990). The heating process does not change the perlite density (2.2–2.3 kg/dm^3) but the bulk density decreases to 60–80 g/dm^3. During the thermal treatments, a structural transition from amorphous to crystalline occurs, accompanied by increased cation exchange capacity (CEC) from 20–30 to 35–50 cmol/kg, as a result of the multiplication of broken edges, and increased specific surface area from 1.2 to 2.3 m^2/g (Dogan and Alkan, 2004).

   Perlite is basically the mineral obsidian. Perlite mineral deposits exist in many countries of the world, but the expanded product is only available in countries which have commercial expanding plants (Topcu and Isıkdag, 2007). The world reserves of perlite are estimated as 700 million tons. In 2011, 1.7 million tons had been produced, mostly by Greece (500.000 Mg), United States (375.000 t) and Turkey (220.000 Mg); however, no information for China, leading producer, was available (Bolen, 2011). Turkey's 160.000 tons of probable perlite reserves are located in Menderes, İzmir. Although our country has rich resources and capacity of perlite, domestic demand is very limited and most of the produced perlite is imported.

   Perlite is used in various areas such as construction materials, agriculture, medical and chemical industry. Moreover, expanded perlite aggregate (EPA) has been used within the constructional elements such as brick, plaster, pipe, wall and floor block; however has not been industrially utilized in concrete yet. EPA is a heat and sound insulator, and lightweight material which ensures economic benefits in constructions (Topcu and Isıkdag, 2008). Many researchers have studied the characteristic properties of the perlites and their use as construction materials (Singh and Garg, 1991; Demirboga et al., 2001; Demirboga and Gul, 2003; Lanzon and Garcia-Ruiz, 2008; Sari et al., 2009; Sengul et al., 2011; Çelik, 2010). In these studies, mainly the use of perlite as a thermal insulator in lightweight concrete and brick production was examined.

   The aim of this study is to determine the characteristic properties of Menderes expanded perlite aggregate and investigate changes in their physical properties depending on temperature. Also, the analyses, to determine the use of EPA as a raw material for construction, are performed. This study will be the basis of the forthcoming studies in which Menderes expanded perlite aggregate is used as a construction raw material.

Materials and method

Expanded perlite was obtained from Menderes-Cumaovası Perlite Processing Plant of Eti Mine Works (İzmir, Turkey). Perlites were expanded to 0.2-2 mm size and 150-300 kg/m^3 density at 1000 °C by using high-temperature furnaces at Eti Mine Menderes Works.

   To determine the characteristic properties of the expanded perlite at ambient temperature, chemical analysis, petrographic analysis, qualitative mineralogical analysis (XRD); scanning electron microscopy (SEM) analysis, energy dispersive X-ray spectroscopy (EDS) analysis, thermo-gravimetric/differential thermal (TG-DTA) analysis, and surface area measurements were performed. At the same time, to find out some of the important physical properties of the expanded perlites at ambient temperature and temperatures up to 600 °C, specific gravity, bulk density, porosity, water absorption and compactness ratio analyses were carried out on five different samples. The sieve analysis, fine matter analysis, organic matter content and loss on

ignition analyses were also performed to determine the use of expanded perlite as a construction raw material. Analyses were performed at Mining Technical Research Institute (MTA), Ankara, Turkey and Middle East Technical University (METU) Chemical Engineering Department, Ankara, Turkey.

Petrographic analysis was done by Olympus BH-2 microscope. Chemical analysis of the 105 °C dried samples was performed by using the Siemens SRS 300 X-ray Fluorescence Spectrometer (XRF) instrument. XRD of the powdered samples was carried by using Rigaku XRD Geigerflex equipped with Cu X-ray tube. XRD patterns were recorded from $20° < 2\theta < 60°$ with step of 0.02°. Images and elemental composition of the samples were obtained by SEM instrument using FEI Quanta 400 MK2 equipped with EDAX Genesis XM 4i detector. Proportional elemental distribution was found by EDS analyzer. The amount of weight loss of the perlite samples were determined by TG-DTA using TG/DTA 6300 S11 EXSTAR 6000. The measurements were performed up to 1000 °C under air flow using uniform heating rate of 20 °C/min. The sample holder was cylindrical-shaped platinum crucible having a diameter of 6 mm and height of 10 mm.

BET (Brunauer, Emmett and Teller) surface area measurements were performed by Nova Instruments Quantochrome 2200. To determine the bulk densities, the samples were grinded, sieved through 16 mesh sieves (1 mm sieve opening) and impurities were removed. The bulk density analyses were done according to TS 3529 and ASTM C-127-42 standards. Specific gravities were determined by means of a pycnometer in accordance with TS 1114 EN13055-1 standards. Porosity measurements were performed by Autopore IV 9220 mercury porosimeter. Before the above mentioned analyses, the samples were put into the furnace at the preset temperature for two hours.

Water absorption properties of the particles smaller than 4-8 mm were found according to TS 1114 EN 13055-1 and ASTM C 127-42 standards. The compactness ratio was determined in accordance with ASTM C 127-42 and 128-57 standards.

The sieve analysis and fine matter analysis, which was done to determine the usability of EPA as a construction material, was performed according to TS 1114 EN 13055-1 standards. Organic matter content was determined according to TS EN 1744-1, in which expanded perlite aggregate having 2-4 mm size was exposed to 3-6% NaOH for 24 hours. The presence of organic matter after 24 hours was determined according to the light yellow, dark brown or red color of the aggregates. The loss on ignition analysis of expanded perlite aggregates were carried out according to TS 1114 EN 13055-1 standards.

Results and discussion

Mineralogical and petrographic analyses of EPA

Perlite, in terms of color and chemical composition, resembles mostly to pumice. The most effective way of separating perlite from diatomite, pumice and other volcanic originated rocks is their mineralogical and petrographic analyses. The chemical analysis results are given in Table 1. As a result of the chemical analysis, it was observed that perlite has an average SiO_2 and Al_2O_3 amount of 70.68% and 13.04%, respectively, which is compatible with the literature (Topcu and Isıkdag, 2007; Tekin et al., 2010). Also as a result of the XRD analysis (Figure 1), perlite samples were found to consist of amorphous silica and opal-CT (98%) and trace amounts of feldspar and quartz. A similar XRD pattern was also found by Sodeyama et al. (1999).

Table 1. Chemical analysis and loss on ignition analysis results of EPA samples (%)

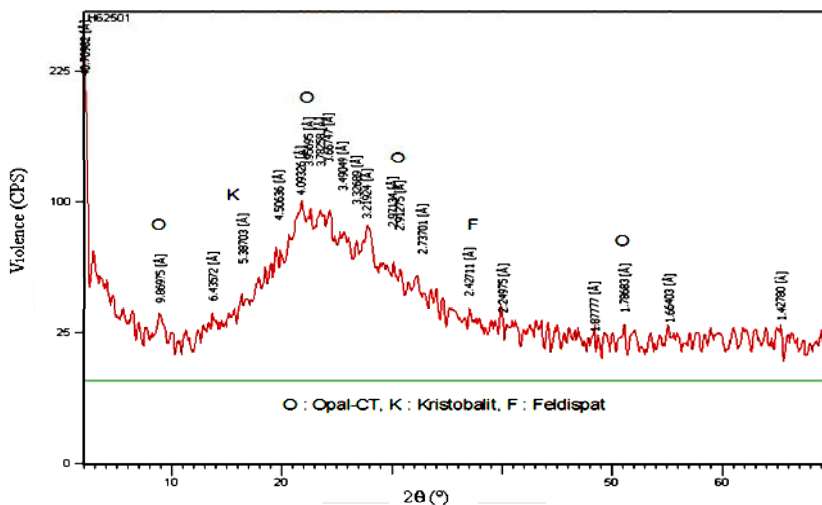| Sample No	SiO_2	Al_2O_3	Na_2O	K_2O	Fe_2O_3	CaO+MgO	*LoI
1	70.7	13.0	3.6	4.6	0.8	3.9	3.1
2	69.8	12.1	3.3	4.2	1.1	3.5	3.0
3	71.4	13.8	3.8	3.9	1.6	3.6	3.2
4	70.4	13.4	3.5	4.4	1.0	3.9	3.1
5	71.1	12.9	3.5	4.6	0.7	4.0	3.0
Average	70.68	13.04	3.54	4.34	1.04	3.78	3.08

*LoI: Loss on ignition

Fig. 1. XRD analysis of EPA

The petrographic investigation on the expanded perlite is given in Figure 2. As seen from the microphotograph, perlite had a glassy and porous structure. There was countless number of pores, each having different micron sizes. This structure of the perlite makes it lighter, while providing a big advantage in terms of heat and sound transmission. In the analysis, the presence of opal-CT, feldspar, mica, illite and quartz minerals were determined within the perlite structure (Figure 2).
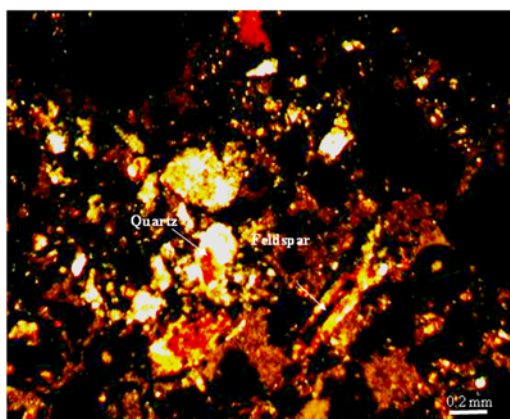

Fig. 2. Microphotograph showing feldspar and quartz in EPA

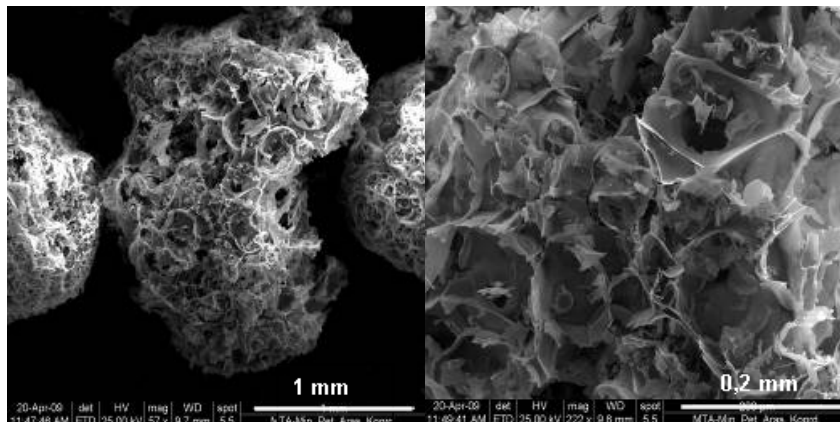Fig. 3. SEM images of EPA

SEM images of EPA, Figure 3, also had a crystal-like porous and glassy structure. SEM images are similar to the image given by Sarı et al. (2009). The proportional distribution of the elements, determined by EDS analysis (Figure 4), showed that within the expanded perlite samples, silicon (45.13%), oxygen (38.91%), aluminum (8%), potassium (5.58%) and sodium (2.37%) were present.
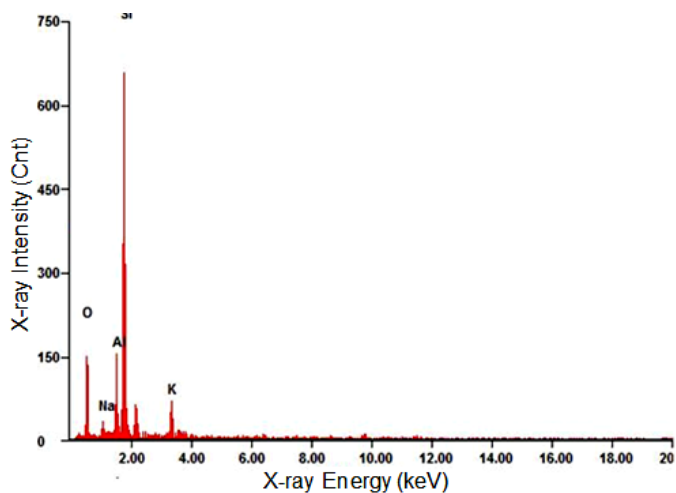
Fig. 4. EDS analysis of EPA

Thermal analyses of EPA

From the TGA analysis (Figure 5), it was found that the perlite sample lost all its moisture till 200°C and had a weight loss of 1.4% at 450 °C. At temperatures above 500°C, no considerable weight loss (0.3%) was observed. At 1000 °C, perlite had a total weight loss of 1.8%, which shows that it can be used at high-temperature applications. Roulia et al., 2006 also found that expanded perlite retains 1.6–1.9 wt% water for all studied temperatures (till 950°C). The dehydration in perlites is divided to three temperature ranges by Roulia et al., 2006: 0–250°C, 250–550°C and 550–950°C. In the first temperature range, the molecular water bound loosely either superficially or adsorbed in pores are released. In the second temperature range molecular water trapped into the inner pores of the material is released. At the last temperature range – OH groups associated to the oxygen atoms through strong hydrogen bonding are released.

Besides, DTA curve gave an exothermic peak at 250 °C. This broad peak corresponds to the release of water either bound loosely or trapped into the inner pores of expanded perlite. The exothermic peak can also be attributed to the glass compression and internal surface area diminution. Roulia et al. (2006) also found an exothermic peak in the DTA curve for expanded perlite at around 250°C. The phase change started in the temperature range of 500-600 °C and completed at 1000 °C.
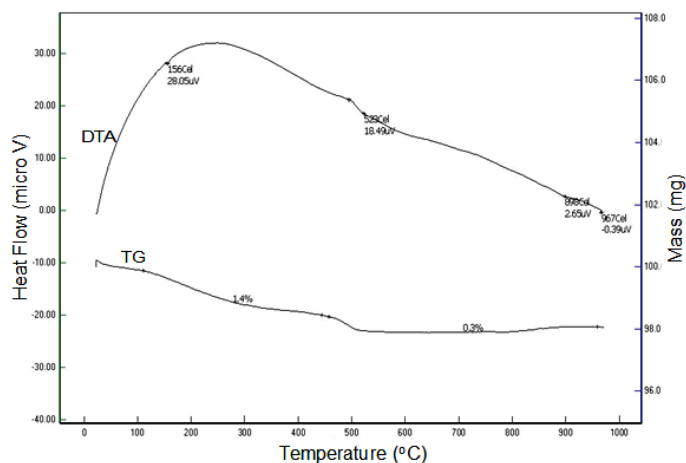
Fig. 5. TG-DTA curves of EPA (heating rate = 20 °C/min.)

To determine the mass loss of expanded perlite with heat, loss on ignition test was performed and the results are given in Table 1. As seen in Table 1, the loss on ignition of EPA was less than 5% (3.08±0.09%). This result confirms that EPA can be used as a construction raw material when tested according to TS 1114 EN 13055-1 standard.

Variation of physical properties of EPA with temperature

Surface area, bulk density, specific gravity, porosity, water absorption and compactness ratio values of EPA were determined at different temperatures and given in Table 2. The highest surface area (523.8±18.5 m^2/g) was obtained at 400 °C which decreased with the increase in temperature. As temperature was increased above 400°C, thermolysis began and the perlite samples started to decompose. At temperatures above 600 °C, the decomposition of perlite samples was practically

Table 2. Physical properties of EPA at different temperatures

Temperature (^{o}C)	Surface area (m^{2}g^{-1})	Specific gravity (kg/m^3)	Bulk density (kg/m^3)	Porosity (%)	Water absorption (%)	Compactness ratio
Ambient	108.7±7.1	1973±90	230±10	79±1.30	71.1±1.0	0.12±0.04
100	295.4±4.3	1958±50	220±20	68±1.90	67.8±0.9	0.11±0.07
200	308.5±11.2	1936±95	210±20	56±2.00	63.7±0.9	0.11±0.03
300	442.9±16.7	1922±60	190±10	48±1.10	59.8±0.7	0.10±0.01
400	523.8±18.5	1905±80	150±40	43±1.10	51.5±0.8	0.08±0.04
500	265.5±8.9	1886±40	100±10	36±0.95	48.5±0.6	0.06±0.01
600	73.0±6.4	1845±60	85±10	30±0.85	44.5±0.6	0.05±0.01

finished and the surface area decreased. Bulk density, specific gravity, porosity and compactness ratio values decreased depending on the temperature. The highest values were reached at 100 °C, whereas the lowest values were attained at 600 °C. EPA has a specific gravity of 1973 ± 90 kg/m^3 and bulk density of 230 ± 10 kg/m^3 at 100°C, whereas these values decreased to 1905 ± 80 kg/m^3 and 150 ± 40 kg/m^3 at 400°C, respectively. The porosity, water absorption and compactness ratio of EPA decreased from $79.00\pm1.30\%$ to $43.00\pm1.10\%$, $71.1\pm1.0\%$ to $51.5\pm0.8\%$, and $0.12\pm0.04\%$ to $0.08\pm0.04\%$ at 400°C, respectively.

Sieve, fine matter and organic content analyses

Sieve analysis, fine matter analysis and organic matter content analyses were performed to investigate if EPA could be used as a construction raw material. From the sieve analysis (Figure 6), performed according to TS 1114 EN 13055-1 standards, it was observed that EPA was within the standard range. So it can be concluded that it can be used during the production of construction materials.
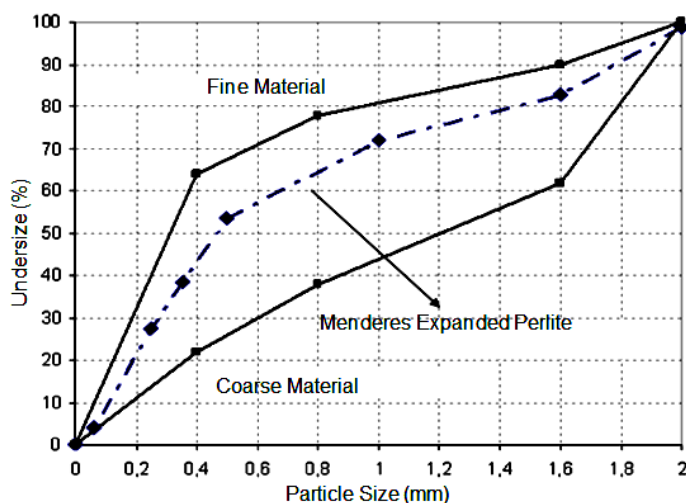

Fig. 6. Sieve analysis curve

Fine matter analysis of EPA, given in Table 3, was performed to determine the suitability of 0-4 mm particle size to TS 1114 EN 13055-1 standard. The fine matter analysis defined in the standard was the percent ratio of the oversized material to the undersized residue when 0.063 mm sieve opening was used. The evaluation of the results showed that fine matter content was less than 5% ($3.68\pm0.07\%$) as specified in the standard. Presence of organic matter in EPA is inconvenient and unfavorable. According to the experimental criteria given in TS EN 1744-1 standard, no organic matter formation was detected in EPA. These analyses together with mass loss on ignition analysis showed that EPA can be used as a construction raw material.

Table 3. Fine matter amounts of EPA (0-4 mm sieve opening)

Sample No	1	2	3	4	5
Dry weight (g)	1030	1050	1100	1050	1000
0.063 mm – Oversize weight (g)	480	456	502	483	448
1.0+0.5 mm – Oversize weight (g)	212	198	225	211	204
1.6+1 mm – Oversize weight (g)	146	165	174	150	142
2+1.6 mm – Oversize weight (g)	106	119	111	124	109
4+2 mm – Oversize weight (g)	44	73	52	49	56
Total oversize material weight (g)	988	1011	1064	1017	958
Total undersize residue weight (g)	42	39	36	33	42
Fine matter ratio (%)	4.07	3.71	3.27	3.14	4.20
Average (%)			3.68		

Comparison of characteristic properties

When the characteristic properties of perlite were examined, it was observed that chemical analysis, petrographic analysis, XRD, SEM and EDS analysis results support each other. TG-DTA analysis showed changes in direct proportion to the mass loss on ignition. Besides, significant statistical relations exist between the physical properties of the perlite; especially between specific gravity and bulk density ($R^2 = 0,9252$) (Fig. 7), bulk density and porosity ($R^2 = 0,9246$) (Figure 8), water absorption and specific gravity ($R^2 = 0,9501$) (Figure 9), compactness ratio and specific gravity ($R^2 = 0,9297$) (Fig. 10). It can also be seen that although there exists sets of relationships between the physical properties of the expanded perlite, they also decrease with temperature.
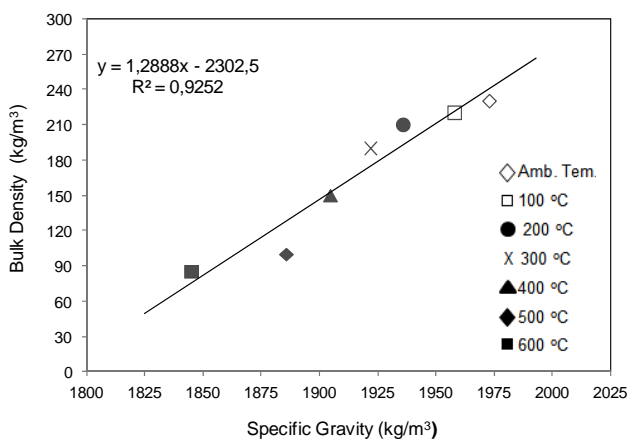

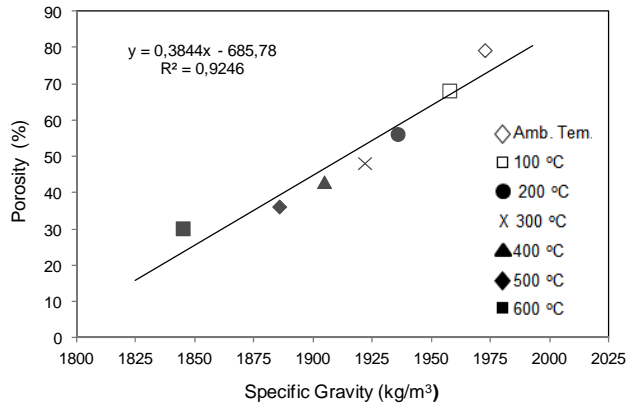Fig. 7. Relationship between specific gravity and bulk density

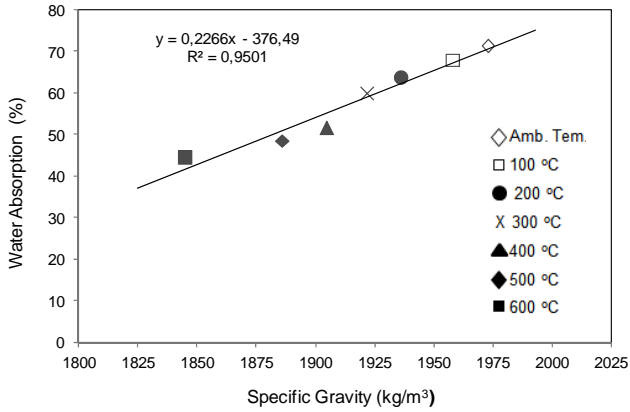Fig. 8. Relationship between specific gravity and porosity

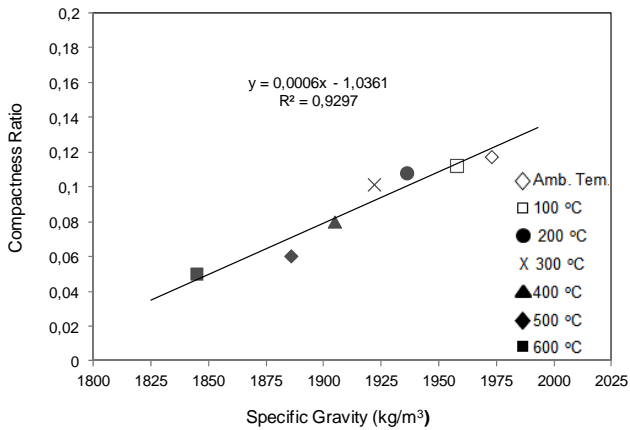Fig. 9. Relationship between specific gravity and water absorption

Fig. 10. Relationship between specific gravity and compactness ratio

Conclusions

During the studies aiming to investigate characteristic properties of EPA and find its suitability as construction raw material, many of its properties were determined. The chemical composition of the expanded perlite was found to consist of 70.68% SiO_2 and 13.04% Al_2O_3. The petrographic observations showed presence of opal-CT, feldspar, mica, illite, and quartz in the perlite structure. SEM images showed a crystal like porous and glassy structure. EDS analysis showed the presence of 45.13% silicon and 38.91% oxygen within the EPA structure. A weight loss of 1.8% at 1000 °C was found from the TG-DTA analysis meaning that expanded perlite can be utilized at high temperature applications. Although specific gravity, bulk density, porosity, water absorption and compactness ratios differ at different temperatures, they were found to have high statistical relation. In addition, surface area was also affected by temperature. To determine whether EPA could be used as a construction raw material or not, sieve analysis, fine-matter content and mass loss on ignition analysis and organic matter content were performed and it was found that EPA was appropriate to be used as a lightweight construction raw material.

Acknowledgements

References

ASTM-C 127-42 *Standard Test Method for Specific Gravity and Absorption of Coarse Aggregates.*

ASTM C 128-57 *Standard Test Method for Specific Gravity and Absorption of Fine Aggregates.*

BOLEN P. W., 2011. *USGS Mineral Commodity Summaries 2011. U.S.* Department of the Interior, U.S. Geological Survey, Reston, Virginia-USA.

CELIK A.G., 2010. *Production of lightweight bricks from boron added perlite mixtures and determination of technological properties*. Ph.D. Dissertation, Çukurova University, Department of Mining Engineering, Adana.

DEMIRBOGA R., ORUN I., GUL R., 2001. *Effects of Expanded Perlite Aggregate and Mineral Admixtures On The Compressive Strength of Low-Density Concretes.* Cement Concrete Res. 31(11), 1627–1632.

DEMIRBOGA R., GUL R., 2003. *The Effects of Expanded Perlite Aggregate, Silica Fume and Fly Ash on The Thermal Conductivity of Lightweight Concrete.* Cement Concrete Res. 33 (5), 723-727.

DOGAN M., ALKAN M., 2004. *Some Physicochemical Properties of Perlite As An Adsorbent.* Fresenius Environmental Bulletin. 13, 252–257.

HARBEN P. W., BATES R.L., 1990. *Industrial Minerals Geology and World Deposits.* Metal Bulletin Inc., London.

LANZON M., GARCIA-RUIZ P.A., 2008. *Lightweight Cement Mortars: Advantages and Inconveniences of Expanded Perlite and Its Influence on Fresh and Hardened State and Durability.* Construction and Building Materials. 22, 1798-1806.

ROULIA M., CHASSAPIS K., KAPOUTSIS J.A., KAMITSOS E.I., SAVVIDIS T., 2006. *Influence of Thermal Treatment on the Water Release and the Glassy Structure of Perlite.* J Mater Sci. 41, 5870-5881.

SARI A., KARAIPEKLI A., ALKAN C., 2009. *Preparation, Characterization and Thermal Properties of Lauric Acid/Expanded Perlite As Novel Form-Stable Composite Phase Change Material.* Chemical Engineering Journal. 155, 899–904.

SENGUL O., AZIZI S., KARAOSMANOGLU F., TASDEMIR M., 2011. *Effect of Expanded Perlite on The Mechanical Properties and Thermal Conductivity of Lightweight Concrete.* Energy and Buildings. 43, 671–676.

SINGH M., GARG M., 1991. *Perlite-Based Building Materials A Review of Current Applications.* Construction and Building Materials. 5(2), 75-81.

SODEYAMA K., SAKKA Y., KAMINO Y., SEKI H., 1999. *Preparation of Fine Expanded Perlite.* Journal of Materials Science. 34, 2461-2468.

TEKIN N., DINCER A., DEMIRBAS O., ALKAN M., 2010. *Adsorption of Cationic Polyacrylamide (C-PAM) on Expanded Perlite.* Applied Clay Science. 50, 125-129.

TOPCU I.B., ISIKDAG B., 2007. *Manufacture of High Heat Conductivity Resistant Clay Bricks Containing Perlite.* Building and Environment. 42, 3540–3546.

TOPCU I.B., ISIKDAG B., 2008. *Effect of Expanded Perlite Aggregate on The Properties of Lightweight Concrete.* Journal of materials processing technology. 204, 34–38.

TS 1114 EN 13055-1, 2004. *Lightweight Aggregates - Part 1: For Use In Concrete, Mortar And The Juice.*

TS 3529, 1980. *Determination of Specific Gravity and Water Absorption Ratio in Concrete Aggregates.*

TS EN 1744-1, 2000. *Tests for Chemical Properties of Aggregates-Part 1: Chemical Analysis.*

PREPARATION AND CHARACTERISATION OF UNMODIFIED AND POLY(ETHYLENE GLYCOL) GRAFTED MAGNESIUM HYDROXIDE

Agnieszka PILARSKA[*]**, Magdalena NOWACKA**[*]**, Krzysztof PILARSKI**[**]**, Dominik PAUKSZTA**[*]**, Lukasz KLAPISZEWSKI**[*]**, Teofil JESIONOWSKI**[*]

[*] Poznan University of Technology, Faculty of Chemical Technology, Institute of Chemical Technology and Engineering, M. Sklodowskiej-Curie 2, PL-60-965 Poznan, Poland; teofil.jesionowski@put.poznan.pl

[**] Poznan University of Life Science, Faculty of Agriculture and Bioengineering, Institute of Biosystems Engineering, Wojska Polskiego 50, PL-60-637 Poznan, Poland

Abstract: The method for the synthesis of either unmodified magnesium hydroxide or functionalised with poly(ethylene glycols) of different molecular weights and physicochemical properties of the products are presented. Magnesium hydroxide was obtained by the precipitation method under well defined conditions from ammonia solution and different magnesium salts. Dispersive properties of the products were characterised by polydispersity index, particle size, as well as SEM images. Crystalline structure of magnesium hydroxide samples were determined by the WAXS method. To confirm the presence of functional groups introduced by appropriate modifiers the samples were subjected to spectroscopic analysis. Electrokinetic stability of the studied samples was determined on the basis of zeta potential dependence vs. pH measurements. The modification has resulted in reduction of particle diameters in some $Mg(OH)_2$ samples.

Introduction

$Mg(OH)_2$ is usually precipitated from solutions of magnesium salts by a precipitating agent which usually is a strong base such as NH_4OH (Fellner 2011, Wang 2007; 2011) or NaOH (Pilarska 2011, Song 2011, Veldurthi 2012). The most often used precursors of magnesium are inorganic salts such as $MgCl_2$, $MgSO_4$ and $Mg(NO_3)_2$. Sometimes organic compounds of magnesium are used, e.g. $Mg(CH_3CO_2)_2$ (Alvarado 2000). Parameters of the process have a considerable influence on the structure and morphological−dispersive properties of the products. For this reason the choice of

optimum conditions of the process that would lead to obtaining products of target properties has been of profound interest to many research groups.

Most often the influences of the rate and direction of reagent dosing, their concentrations, mass and volume contributions, temperature of precipitation and calcination, and methods of drying have been studied (Wang 2005, Wang 2007, Yun 2009).

According to the recent literature data, the final properties of materials, in particular their morphology, are strongly related to the types of precursor and precipitating agents applied (Wang 2011; Pilarska 2012). Recently, besides the main reagents increasingly often the modifying compounds are involved in syntheses of chemical compounds. Modification of the reaction system by introducing an additional organic or inorganic chemical substance, leads to changes in the properties of the products including those in the product surface. The purpose of such modification of the original properties of the reaction products is first of all to increase the activity and selectivity of catalysts based on $Mg(OH)_2$. Modification can also bring improvement in the dispersion and insulating properties of sintered ceramic materials, and sometimes in development of surface area of the material modified (Azhari 2010; Tang 2011). Introduction of organic modifying compounds is particularly important when inorganic compounds such as magnesium hydroxide should be bound to organic compounds such as polymers. The modification results in changing the hydrophilic character of the surface into hydrophobic, which improves the compatibility of the composite components and has beneficial influence on its mechanical properties (Wei 2008; Chen 2009). Organic modifying compounds are also applied to help reduce the magnesium hydroxide particle size and develop their surface area. The majority of the hitherto used modifiers have been relatively expensive. Recently much interest has been paid to the use of PEG type compounds as modifiers PEG (Wang 2007; Wang 2011). Poly(ethylene glycols) are not only cheap but they also have a beneficial effect on the microstructure and surface character of magnesium hydroxide (Pilarska 2012).

One of the parameters characterising functional properties of chemical materials is zeta potential. It is a measure of electrostatic interactions between molecules/partilces and permits estimation of stability of colloidal dispersion of a system that is a tendency to coagulation of particles limited by the repulsive forces between them. This also informs about the magnitude of electric charge in direct vicinity of the solid state surface and has been widely used for quantitative evaluation of the electric charge on the double electric layer (Kosmulski 2001; Jesionowski 2003).

The aim of the study presented is analysis of the influence of the modifiers applied on the dispersive and physicochemical properties of $Mg(OH)_2$ samples obtained in precipitation reaction and discussion of their potential use.

Experimental

The substrates used for the synthesis of magnesium hydroxide were: hydrated magnesium sulphate ($MgSO_4 \cdot 7H_2O$, analytical grade), magnesium chloride ($MgCl_2 \cdot 6H_2O$), magnesium nitrate ($Mg(NO_3)_2 \cdot 6H_2O$, analytical grade), ammonium hydroxide (NH_4OH, analytical grade) as a precipitating agent (all made by POCh SA.) and non-ionic compounds from the group of poly(ethylene glycols): PEG 200, PEG 8000 and PEG 20000 (purchased from Sigma-Aldrich), as 2% solutions. Magnesium hydroxide was obtained from a 5% solution of a given magnesium salt and ammonia solution prepared with the excess of the stoichiometric amounts of the reactants, where salt/NH_4OH = 1:1.5. Reaction of magnesium hydroxide precipitation was carried out in a reactor of 500 cm^3 in capacity, equipped with a fast rotating stirrer made by Eurostar digital IKA-Werke (1800 rpm.). The reaction system was thermostated in a bath made by MP14 Julabo. The process was conducted at 80 ºC. The reagents were dosed simultaneously into the water system containing PEG. The use of a peristaltic pump (Ismatec ISM833A type) ensured a constant flow rate of the reagents (2.3 cm^3/min). On completion of reagents introduction, the reaction system was stirred for about 30 min. The precipitate of magnesium hydroxide was filtered off, washed out and dried in a dryer (Memmert) at 105ºC for about 6 h. A technological scheme of the process is shown in Fig. 1.
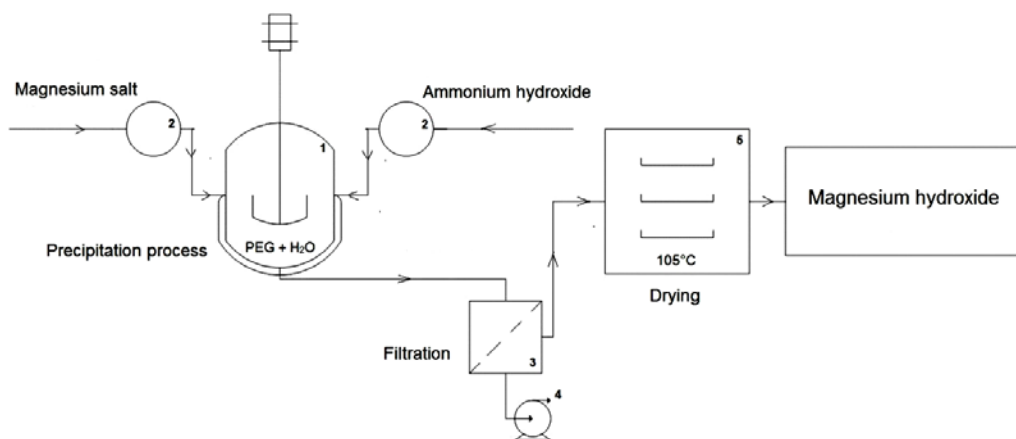
Fig. 1. Preparation of magnesium hydroxides – a technological scheme:
1 – reactor, 2 – peristaltic pomp, 3 – pressure filter, 4 – vacuum pomp, 5 – drier

The magnesium hydroxides obtained were subjected to physicochemical and dispersive-morphological characterisation. The particle size distribution was determined by two instruments Zetasizer Nano ZS (0.6–6000 nm) and Mastersizer 2000 (0.2–2000 μm) employing two measuring methods NIBS and laser diffraction, respectively. Both instruments were made by Malvern Instruments Ltd. The morphology and microstructure of the products were characterised on the basis of

observations by a scanning electron microscope Zeiss EVO 40. The crystalline structure of selected magnesium hydroxide samples was determined by WAXS. The X-ray diffractograms were recorded by a computer-controlled horizontal diffractometer, equipped with a HZG-3 type goniometer. The magnesium hydroxides were also subjected to FT-IR spectral analysis (using an IFS 66v/S made by Bruker). Here the materials were analysed in tablet form, made by pressing a mixture of anhydrous KBr (ca. 0.1 g) and 1 mg of the tested substance in a special steel ring under a pressure of approximately 1000 MPa. The electrokinetic stability of the products was determined on the basis of zeta potential dependence on pH, using a Zetasizer Nano ZS (Malvern Instruments Ltd.) with an autotitrator attached. Measurements were made in a 0.001M NaCl solution in the range of pH from 2 to 12.

Results and discussion

Dispersive and morphological characteristics

Table 1 presents results characterising dispersive properties of magnesium hydroxide samples unmodified and modified by PEG (2% solution) of different molecular mass: PEG 200, 8000, 20000. All magnesium hydroxide samples were obtained using 5% solutions of particular magnesium salt (magnesium sulphate, chloride and nitrate) with an excess of ammonium hydroxide with respect to its stoichiometric amount of 1:1.5 (salt/NH_4OH), at 80 °C. The particle size distribution was determined in two ranges of values by two instruments Zetasizer Nano ZS and Mastersizer 2000.

Pilarska (2012) reported results of dispersion study and other measurements for magnesium hydroxide samples obtained from the same substrates but under different process conditions, that is at the stoichiometric rate of the reagents and at 60°C. For the products obtained in this process the authors have not observed the modification applied to improve the dispersive properties. The smallest particles (59–142 nm) were obtained for the sample precipitated from a solution of magnesium sulphate and modified by PEG 400.

The particle size distributions in the scale extended to 0.2−2000 μm (Mastersizer 2000) of magnesium hydroxide samples obtained in this study evidence the effectiveness of application of ammonium hydroxide in excess amount, in particular in preventing formation of large agglomerates (S-NH_3-unmod., N-NH_3-unmod., Cl-NH_3-unmod, Table 1). Thus the excess of ammonium hydroxide produced a different effect than the excess of sodium hydroxide in the reactions with the same magnesium salts for which a undesirable microstructural changes were observed (Myerson 2002; Pilarska 2010). The best example illustrating the positive effect of the excessive amount of ammonium hydroxide on dispersive properties of the product is the sample S-NH_3-unmod., obtained from a solution of magnesium sulphate and having particles of diameters from the range 160−190 nm and a low polydispersity index of 0.154.

Table 1. Dispersive characteristic of unmodified magnesium hydroxide
and grafted with 2% solution of appropriate PEG

Sample No.	Precipitation process conditions			Dispersive properties			
	Type of salt	Mean molecular weight of PEG	PdI	Range of particle size from Zetasizer Nano ZS (nm)	Particle size from Masteriszer 2000 (nm)		
					d(0.1)	d(0.5)	d(0.9)
S–NH$_3$–unmod.	magnesium sulphate	–	0.154	160–190	3.53	20.58	29.42
1S–NH$_3$–mod.		200	0.641	79–1720	7.78	21.79	39.70
2S–NH$_3$–mod.		8000	0.521	68–531	13.28	20.20	31.00
3S–NH$_3$–mod.		20000	0.437	51–459	3.46	16.84	30.61
N–NH$_3$–unmod.	magnesium nitrate	–	0.496	4800–5560	3.16	7.80	15.97
1N–NH$_3$–mod.		200	0.708	44–5560	5.58	15.46	32.34
2N–NH$_3$–mod.		8000	0.543	51–5560	3.29	8.91	18.27
3N–NH$_3$–mod.		20000	0.582	79–5560	2.81	8.30	17.19
Cl–NH$_3$–unmod.	magnesium chloride	–	0.397	190–615	8.38	14.66	24.57
1Cl–NH$_3$–mod.		200	0.686	59–5560	3.09	6.60	11.76
2Cl–NH$_3$–mod.		8000	0.435	51–1480	4.32	12.24	26.43
3Cl–NH$_3$–mod.		20000	0.205	91–190	7.05	11.67	19.13

Of significant importance is the type of magnesium salt used (Pilarska 2011). It has been shown on the basis of dispersion studies that the salts of higher water solubility, such as magnesium sulphate and magnesium chloride, have beneficial effect on the product dispersion. The results evidencing better properties of samples labelled S and Cl than those obtained for the sample synthesised with the use of magnesium nitrate (sample N) are shown in Table 1. The diameters of particles in sample N often reached values close to 6 μm, and the relatively high values of the polydispersity index determined for this sample, 0.496–0.708, suggest heterogeneous character of this sample. The elevated temperature of precipitation and the use of a salt of good water solubility, like magnesium sulphate, favours formation of particles of smaller sizes.

In general, only in some modified samples the particles had smaller sizes than in their unmodified correspondents. On the basis of measurements by Zetasizer Nano ZS, a considerable improvement in the dispersive properties was noted for sample 3Cl–NH$_3$-mod (Fig. 2). The particle size distribution (Fig. 2a) confirms that the modified sample has particles of significantly smaller diameters, reduced from 459 to 142 nm. The SEM images presented in Figs. 2b, c, clearly reveal the differences in dispersive properties between the unmodified and modified samples. The sample of magnesium hydroxide obtained with the use of PEG 20000 is homogeneous (PdI = 0.205) and small particle sizes, while in the unmodified sample the particles form smaller and

larger agglomerations. Restricted tendency towards formation of secondary agglomerates was also noted for the sample 1Cl–NH$_3$-mod. (PEG 200). For the other samples no significant improvement in the dispersive properties was observed upon modification.
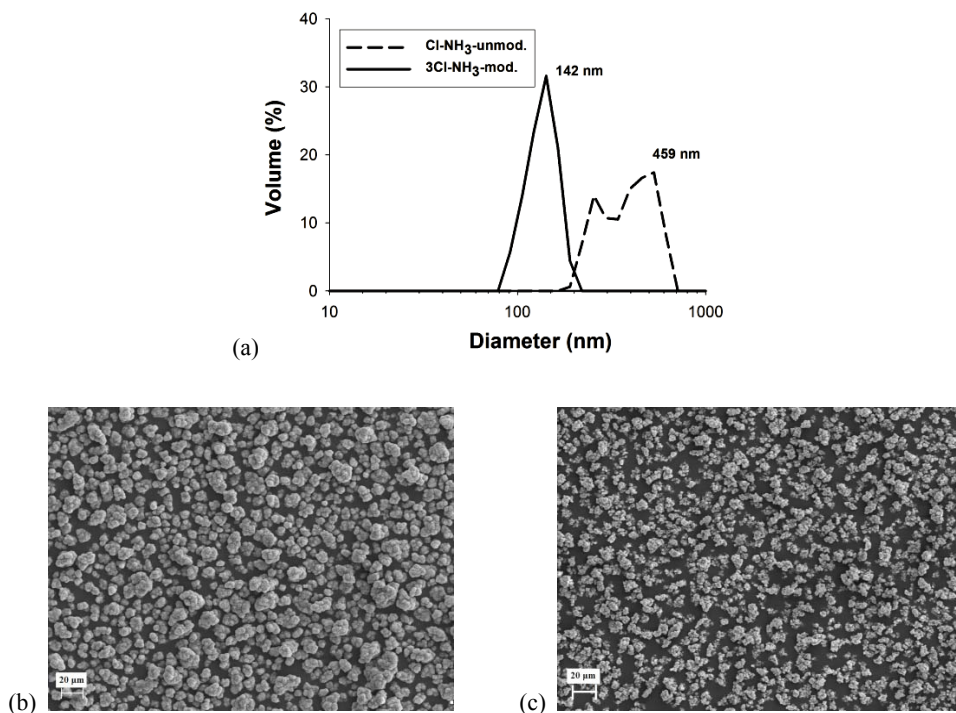

(a)

(b)

(c)

Fig. 2. (a) Particle size distributions (Zetasizer Nano ZS) and (b), (c) SEM images of magnesium hydroxides Cl-NH$_3$-unmod., 3Cl-NH$_3$-mod.

WAXS analysis

Physicochemical characterisation of the magnesium hydroxide samples obtained was supplemented with X-ray studies. Exemplary X-ray patterns are presented in Fig. 3 and show the maxima characteristic of the crystalline structure of Mg(OH)$_2$ brucite. Figure 3a shows the X-ray patterns of unmodified samples precipitated with the use of three different magnesium salts. In the samples Cl–NH$_3$-unmod. and N–NH$_3$-unmod., the crystalline structure was much better developed than in S–NH$_3$-unmod., as follows from the shape and intensity of peaks. These observations confirm that the type of magnesium salt used as magnesium precursor affects the development of crystalline structure. For instance when magnesium sulphate is used, the crystallites of magnesium hydroxide are poorer developed and irregular, which is reflected in the properties (e.g. adsorptive or catalytic) of magnesium hydroxide produced (Climent 2007; Pilarska 2012).
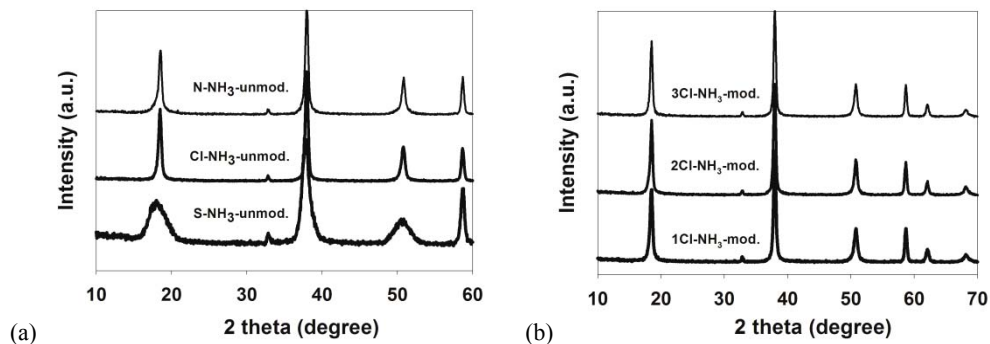
Fig. 3. X-ray diffraction patterns of magnesium hydroxides obtained with the use of
(a) magnesium sulphate, chloride and nitrate (unmodified); (b) magnesium chloride
and modifiers of different molecular weights of poly(ethylene glycols)

According to literature (Lv 2004) the crystalline structure characteristic of brucite does not change, despite the differences in the particles morphology. According to literature, the parameters of the method of synthesis of magnesium hydroxide e.g. temperature, time of reaction, time of maturation of the post-reaction mixture (Alvarado 2000; Meshani 2009), also have no effect on the crystalline structure. As follows from the X-ray patterns of the modified samples precipitated with the excess of ammonia solution and magnesium chloride, Fig. 3b, also the type and amount of the modifier have no effect on the crystalline structure.

FT-IR analysis

In order to confirm the presence of functional groups introduced by the modifiers (poly(ethylene glycols)), the samples of magnesium hydroxide precipitated in solutions of different salts were subjected to FT-IR analysis. The studies were performed for
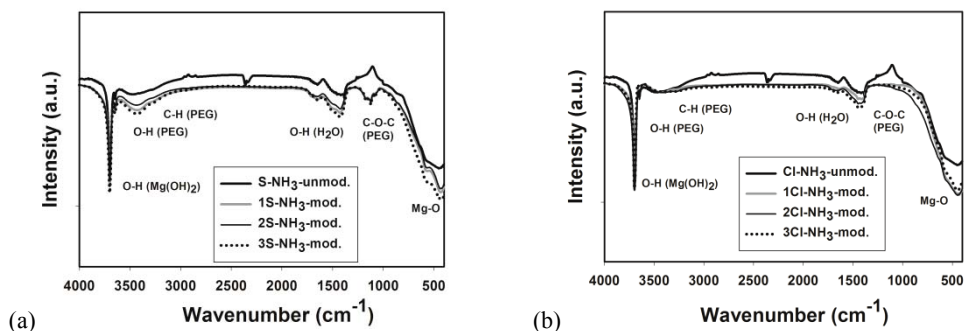

Fig. 4. FT-IR spectra of magnesium hydroxide samples precipitated (a) without and with modifiers of
PEGs and magnesium sulphate (b) without and with modifiers of PEGs and magnesium chloride

both unmodified samples and those modified with PEG 200, 8000, 20000. The FT-IR spectra presented in fig. 4 prove the presence of functional groups introduced from PEG grafted to $Mg(OH)_2$. In the spectra of the samples obtained with the use of magnesium sulphate as a precursor of magnesium the bands assigned to the functional groups O–H (PEG) and C–H (PEG) have significantly higher intensities. Small and rather insignificant changes in the character of the FT-IR spectra of all modified samples imply incorporation of similar amounts of the modifiers in the samples.

The first absorption maximum, of pointed shape and high intensity at 3700 cm^{-1} is assigned to the asymmetric stretching vibrations of –OH groups from $Mg(OH)_2$. The band at 1650 cm^{-1} is assigned to the stretching vibrations of –OH groups from water. The broad peak at 3430 cm^{-1} corresponds to the adsorbed –OH PEG groups, while the low-intensity bands at 2930 cm^{-1} and 2860 cm^{-1} are assigned to the methylene groups –CH$_2$ (stretching vibrations of PEG). The broad peak at 1400 cm^{-1} is also assigned to –CH$_2$ groups from PEG (bending−scissoring vibrations). The band at 1115 cm^{-1} corresponds to the asymmetric stretching vibrations of ether groups C−O−C PEG. The last intense and broad maximum at 440 cm^{-1} corresponds to the stretching vibrations of Mg–O. The assignment is in agreement with literature data (Hsu 2005; Wang 2011).

Electrokinetic characterisation

Figure 5 presents zeta potential versus pH for unmodified magnesium hydroxide samples obtained with the use of magnesium sulphate (S-NH$_3$-unmod., Fig. 5a) and magnesium nitrate (N−NH$_3$-unmod., Fig. 5b) and for these samples modified with PEG 200, 8000, 20000. In the analysed pH range, the electrokinetic curves reach zeta potential values from the range −5÷62 mV. The unmodified samples S−NH$_3$-unmod., N-NH$_3$-unmod. show electrokinetic stability in a relatively wide range from pH 2 to 9, while their modified correspondents are stable in a narrower range of pH, from 1 to 6.5.
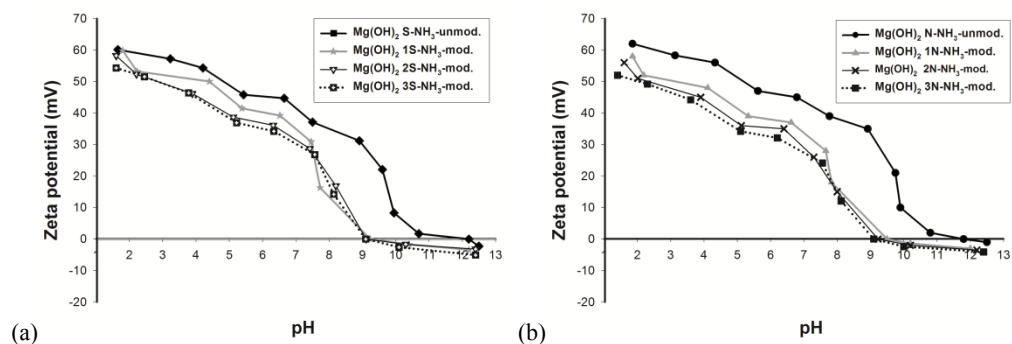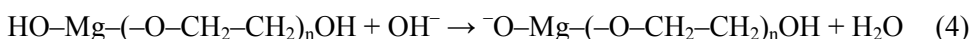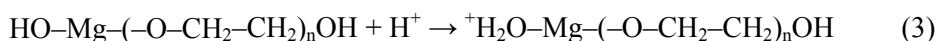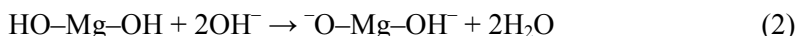

Fig. 5. Zeta potential vs. pH for $Mg(OH)_2$ samples unmodified and modified with PEGs and precipitated with the use of (a) magnesium sulphate, (b) magnesium nitrate solutions

According to the DLVO (Deriaguin, Landau, Verwey, Overbeek) theory, stability of colloidal systems at particular values of zeta potential is determined by overlapping of double electric layers that protect two approaching each other molecules from colliding. In other words, the sample is stable until the electrostatic (repulsive) forces overcome the attractive van der Waals forces (Kosmulski 2009).

The proposed method for the synthesis of magnesium hydroxide in the presence of poly(ethylene glycol) has slightly reduced the pH range of electrokinetic stability of the analysed samples. The small changes in stability of magnesium hydroxide samples after introduction of PEGs are arguments for the use of such modifiers. According to literature data (Saravanan 2005) poly(ethylene glycol) shows electrokinetic stability in two pH ranges, from 2 to 6.5 and from 10 to 12. Probably, if PEGs were applied in higher concentrations, the electrokinetic curves measured for the modified samples would be shifted towards much smaller potential values (below –30 mV). Because of a number of attractive properties of PEG, such as nontoxicity or biocompatibility, this compound has been often used as an adhesive in the ceramic industry, as a plasticiser, as a stabiliser of oxide ions (*PEG protects iron oxide nanoparticles, PEG-PIONs*) or as a modifier of a layered double hydroxides, LDHs of multifunctional use, e.g. in polymer coatings (Ujii 2011; Li 2011). The isoelectric points of unmodified hydroxides (S-NH$_3$-unmod., N-NH$_3$-unmod., Figs. 5a, b) occur at pH of about 11, which fully correlates with literature data (Schott 1981). Zeta potential of a colloidal system is a parameter directly related to its pH. The reactions of dissociation of unmodified and modified products in acidic environment (HCl) and alkaline environment (NaOH) (1–4), were proposed to occur according to the scheme:

$$HO\text{–}Mg\text{–}OH + 2H^+ \rightarrow {}^+H_2O\text{–}Mg\text{–}OH_2{}^+ \tag{1}$$

$$HO\text{–}Mg\text{–}OH + 2OH^- \rightarrow {}^-O\text{–}Mg\text{–}OH^- + 2H_2O \tag{2}$$

$$HO\text{–}Mg\text{–}(\text{–}O\text{–}CH_2\text{–}CH_2)_nOH + H^+ \rightarrow {}^+H_2O\text{–}Mg\text{–}(\text{–}O\text{–}CH_2\text{–}CH_2)_nOH \tag{3}$$

$$HO\text{–}Mg\text{–}(\text{–}O\text{–}CH_2\text{–}CH_2)_nOH + OH^- \rightarrow {}^-O\text{–}Mg\text{–}(\text{–}O\text{–}CH_2\text{–}CH_2)_nOH + H_2O \tag{4}$$

In the acidic environment (HCl) in which zeta potential takes the most beneficial values, proton is attached to the –OH group and generates charge thanks to which the surface of the products becomes more reactive (1, 3) and their colloids much more stable. It should be noted that thanks to the electrostatic interactions in acidic media, a reaction between MgOH$_2$$^+$ and ethoxyoxgen from PEG of small negative electric charge, which makes the modification with these reagents even more effective. The negative charge appearing upon the reaction of the products in an alkaline medium (NaOH) causes a decrease in zeta potential, leading to total destabilisation of the system at certain pH values (reactions 2, 4). For modified samples of Mg(OH)$_2$, reactions with the –OH groups from PEG are also possible both in acidic and alkaline media.

The knowledge of zeta potential of a given substance permits a selective use of its properties, so the interest in its determination has substantially increased, also in industry. On the basis of the known zeta potential it is possible to indentify the mechanisms and conditions of adsorption or separation (flotation) of dispersed solids for which isoelectric point determination is essential (Fuerstenau 2005; Kosmulski 2001). The same is true for $Mg(OH)_2$ both that obtained from minerals and by synthesis.

Conclusions

No particularly beneficial changes in the dispersive properties have been noted as a result of functionalisation of precipitated magnesium hydroxide samples with PEG compounds. Only for a few samples modified with PEG 20000 (3S-NH_3-mod., 3N-NH_3-mod., 3Cl–NH_3-mod), the formation of particles of smaller size was evidenced. As confirmed by the WAXS study, modification with PEGs had no effect on the crystalline structure that remained to be typical of brucite. However, differences in the degree of development of this structure were observed, depending on the magnesium salt used as magnesium precursor. In the samples obtained with the use of magnesium sulphate the structure was irregular and poorly developed. The results of FT-IR analysis confirmed the presence of functional groups coming from PEG in the modified samples. The zeta potential measurements proved that the samples obtained were electrokinetically stable in a wide range of pH, from 2 to 9. The isoelectric points detected corresponded to the pH values being in full agreement with the literature data. Modification with PEG compounds only slightly reduced the pH of electrokinetic stability of the samples studied (to 1−6.5).

Acknowledgements

References

ALVARADO E., TORRES-MARTINEZ L.M., FUENTES A.F., QUINTANA P., 2000, *Preparation and characterization of MgO powders obtained from different magnesium salts and the mineral dolomite*, Polyhedron, 19, 2345–2351.
AZHARI A., SHARIF Sh.M., GOLESTANIFARD F., SABEERI A., 2010, *Phase evolution in Fe2O3/MgO nanocomposite prepared via a simple precipitation method*, Mat. Chem. Phys., 124, 658–663.
CHEN J., LIN L., SONG Y., SHAO L., 2009, *Influence of KOH on the hydrothermal modification of Mg(OH)2 crystals*, J. Cryst. Growth, 311, 2405–2408.
CHEN X., YU J., GUO S., LU S., LUO Z., HE M., 2009, *Surface modification of magnesium hydroxide and its application in flame retardant polypropylene composites*, J. Mater. Sci., 44, 1324–1332.
CHEN X., YU J., GUO S., LU S., LUO Z., HE M., 2009, *Effects of magnesium hydroxide and its surface modification on crystallization and rheological behaviors of polypropylene*, Polym. Compos., 30, 941–947.

CLIMENT M.J., CORMA A., IBORRA S., MIFSUD M., 2007, *MgO nanoparticle-based multifunctional catalysts in the cascade reaction allows the green synthesis of anti-inflammatory agents*, J. Catal., 247, 223–230.

FELLNER P., HIVES J., KHANDL V., KRALIK M., JURISOWA J., LIPTAJ T., PACH L., 2011, *Preparation of magnesium hydroxide from nitrate aqueous solution*, Chem. Pap., 65, 454–459.

FUERSTENAU D.W., PRADIP, 2005 *Zeta potentials in the flotation of oxide and silicate minerals*, Adv. Colloid Interface Sci., 114–115, 9–26.

HSU J.P., NACU A., 2005, *Preparation of submicron-sized Mg(OH)$_2$ particles through precipitation*, Colloids Surf. A: Physicochem. Eng. Asp., 262, 220–231.

JESIONOWSKI T., 2003, *Influence of aminosilane surface modification and dyes adsorption on zeta potential of spherical silica particles formed in emulsion system*, Colloids Surf., A: Physicochem. Eng. Asp., 222, 87−94.

KOSMULSKI M., *Chemical Properties of Material Surfaces*, Marcel Dekker, New York 2001.

KOSMULSKI M., 2009, *Zeta potentials in nonaqueous media: how to measure and control them*, Colloids Surf., A: Physicochem. Eng. Aspects,159, 277−281.

KOSMULSKI M., 2009, *Surface Charging and Points of Zero Charge*, CRC Press, New York.

LI D., XU X., XU J., HOU W., 2011, *Poly(ethylene glycol) haired layered double hydroxides as biocompatible nanovehicles: Morphology and dispersity study*, Colloids Surf. A: Physicochem. Eng. Aspects, 384, 585– 591.

LV J., QIU L., QU B., 2004, *Controlled growth of three morphological structures of magnesium hydroxide nanoparticles by wet precipitation method*, J. Cryst. Growth, 267, 676–684.

MESHANI F., REZAI M., 2009, *Facile synthesis of nanocrystalline magnesium oxide with high surface area*, Powder Technol., 196, 85–88.

MYERSON A.S., GINDE R., 2002, *Crystals, crystal growth, and nucleation*, in: Myerson A.S. (Ed.), Handbook of Industrial Crystallization, 2nd ed., Butterworth- Heinemanm, 33–66.

PILARSKA A., KLAPISZEWSKI Ł., JESIONOWSKI T., 2011, *Wpływ parametrów strącania na właściwości fizykochemiczne Mg(OH)$_2$ i jego wybranych kalcynatów*, Przem. Chem., 90, 983–987.

PILARSKA A., MARKIEWICZ E., CIESIELCZYK F., JESIONOWSKI T., 2011, *The influence of spray drying on dispersive the and physicochemical properties of magnesium oxide*, Dry. Technol., 29, 1210−1218.

PILARSKA A., LINDA I., WYSOKOWSKI M., PAUKSZTA D., JESIONOWSKI T., 2012, *Synthesis of Mg(OH)$_2$ from magnesium salts and NH$_4$OH by direct functionalisation with poly(ethylene glycols),* Physicochem. Probl. Miner. Process, 48, 631 – 643.

PILARSKA A., PAUKSZTA D., CIESIELCZYK F., JESIONOWSKI T., 2010, *Physico-chemical and dispersive characterisation of magnesium oxides precipitated from the Mg(NO$_3$)$_2$ and MgSO$_4$ solutions*, Pol. J. Chem. Technol., 12, 252–256.

SARAVANAN L., SUBRAMANIAN S., 2005, *Surface chemical studies on the competitive adsorption of poly(ethylene glycol) and ammonium poly(methacrylate) onto alumina*, J. Colloid Interface Sci., 284, 363–377.

SCHOTT H., *Electrocinetic studies of magnesium hydroxide*, 1981, J. Pharm. Sci., 70, 486–489.

SONG X., SUN S., ZHANG D., JIN WANG J., YU J., 2011, *Synthesis and characterization of magnesium hydroxide by batch reaction crystallization*, Front. Chem. Sci. Eng., 5, 416–421.

REZAI M., KHAJENOORI M., NEMATOLLAHI B., 2011, *Preparation of nanocrystalline MgO by surfactant assisted precipitation method*, Mater. Res. Bull., 46, 1632–1637.

TANG L., YAMAGUCHI D., WONG L., BURKE N., CHIANG K., 2011, *The promoting effect of ceria on Li/MgO catalysts for the oxidative coupling of methane*, Catal. Today, 178, 172–180.

UJII K., KANAYAMA N., ASAI K., KISHIMOTO M., OHARA Y., AKASHI Y., YAMADA K., HASHIMOTO S., ODA T., OHKOHCHI N., YANAGIHARA H., KITA E., YAMAGUCHI M., FUJII H., NAGASAKI Y., 2011, *Preparation of highly dispersible and tumor-accumulative, iron oxide nanoparticles. Multi-point anchoring of PEG-b-poly(4-vinylobenzylphosphonate) improves performance significantly*, Colloids Surf. B: Biointerfaces, 88, 771–778.

VELDURTHI S., SHIN C.H., JOO O.S., JUNG K.D., 2012, *Synthesis of mesoporous MgO single crystals without templates*, Microporous Mesoporous Mater., 152, 31–36.

WANG B.H., ZHANG W.B., ZHANG W., MUJUMDAR A.S., HUANG L.X., 2005, *Progress in drying technology for nanomaterial*, Drying Technol., 23, 7–32.

WANG B.H., ZHANG W.B., ZHANG W., YU C.Y., WANG G., HUANG L.X., MUJUMDAR A.S., 2007, *Influence of drying processes on agglomeration and grain diameters of magnesium oxide nanoparticles*, Drying Technol., 25, 715–721.

WANG P., LI C., GONG H., WANG H., LIU J., 2011, *Morphology control and growth mechanism of magnesium hydroxide nanoparticles via a simple wet precipitation method*, Ceram. Int., 37, 2061–2066.

WANG W., QIAO X., CHEN J., LI H., 2007, *Facile synthesis of magnesium oxide nanoplates via chemical precipitation*, Mater. Lett., 61, 3218–3220.

WEI L., QI-MING F., LE-MING O., KUN L., 2008, *Surface modification of magnesium hydroxide by γ-aminopropyltriethoxysilane*, J. Cent. S. Univ. Tech., 15, 318–323.

YUN L., WANG B.H., JING D., LV X., YU C.Y., WANG G., HUANG L.X., MUJUMDAR A.S., 2009, *Drying kinetics of magnesium hydroxide of different morphological micro nanostructures,* Dry. Technol, 27, 523–528.

FLOTATION AFTER A DIRECT CONTACT OF FLOTATION REAGENTS WITH CARBONATE PARTICLES PART 1. MODEL INVESTIGATIONS

Hussin A.M. AHMED[*], Mohamed S. ALJUHANI[**], Jan DRZYMALA[***]

[*] King Abdulaziz University, P.O. Box 80204-Jeddah 21589, Kingdom of Saudi Arabia (permanent address: Central Metallurgical R&D Institute, Helwan, Cairo, Egypt
[**] University of Tabuk, Tabuk 71491, P.O. Box 74, Kingdom of Saudi Arabia
[***]Wroclaw University of Technology, Wybrzeze Wyspianskiego 27, 50-370 Wroclaw, Poland, jan.drzymala@pwr.wroc.pl

Abstract: Carbonate fluorapatite (francolite), calcite and dolomite separately, as well as their model mixtures, were subjected to flotation after conditioning the particles with microemulsion consisting of 20% of Custafloat AR27 (collector, blend of fatty acid soaps and sulfates), 55% fuel oil #5 and 25% water at 70% solids density and subsequent pulp dilution with water to 25% solids. The best separation of carbonate fluorapatite from calcite and dolomite occurred at pH 8.5 and microemulsion dose between 0.9 and 1.5 kg/Mg, 1.5 min conditioning time and 2 minutes of flotation time. The obtained flotation concentrates using 1.5 kg/Mg of collector contained 84% carbonate fluorapatite (34% P_2O_5) with 84% recovery. The 84/84 separation efficiency in terms of grade-recovery indices points to promising results which can be obtained for real phosphate ores.

Keywords: phosphates, flotation, microemulsion, separation

Introduction

Ores and other raw materials can be processed by different methods including gravity, hydraulic, magnetic, electric and other separations as well as by coagulation, oil agglomeration and flotation (Wills and Napier-Munn, 2006). Among beneficiation methods, flotation is used the most often because of its superior efficiency in many application (Drzymala, 2007). There are different modifications of flotation because it responses well to variation of operational variables and applied reagents. As a result, there is a constant search for flotation improvements. One of recent modifications is a direct contact of particles with flotation reagents in the form of microemulsions or similar structures (Ahmed, 2005; Ahmed and Drzymala, 2004, 2012) and subsequent

flotation after dilution of the pulp with water. This method differs from the traditional approach in which the particles are brought into contact with aqueous solutions or emulsions of the flotation reagents. The direct contact approach tends to overcome the problem of insufficient adsorption of flotation reagents, especially in the case when oil is used as the flotation collector or extender and the surface of particles is not able to absorb it. It happens for instance in the flotation of oxidized coal because the adsorption of oil on hydrophilic coal surfaces is significantly reduced. To increase the chance of oil and other flotation reagents to be adsorbed, it was proposed to change the procedure of flotation. In this approach, particles are contacted with reagents either in the absence of water or with reagents forming with water special structures such as microemulsion or liquid crystals. Next, the pulp is diluted with water to slurry density typical in froth flotation. It was proved that this modification works very well for highly oxidized coals (Ahmed and Drzymala, 2012) because there was no flotation when the flotation reagents were added to the aqueous suspension and very good coal flotation in the case of the direct contact approach. In this paper the separation efficiency using the direct contact technique and flotation will be investigated for a model carbonate fluorapatite-calcite-dolomite system while in another paper, part 2 of this paper, the case of phosphate ores will be presented. Phosphates were selected for investigations because they are a global resource of phosphorus, an essential element for plant and animal nutrition (Negm and Abouzeid, 2008). However, there is a constant depletion of the high-grade phosphates (Negm and Abouzeid, 2008), so there is a need to optimize the available mineral processing technologies, to maximize the benefits of the low-grade phosphate resources in a more efficient manner, and to minimize the associated wastes. This can be achieved by looking for new processing technologies or adaptation of recent innovations in the classical upgrading techniques including flotation. However, flotation has its limitation in treating low grade phosphate ores in addition to the high price of some reagents used. Therefore, this paper aims at modifying the classical flotation technique to improve flotation of low grade phosphate ore. We will test the approach of direct contact of flotation reagents with particles before flotation for separation of carbonate fluorapatite from the calcite and dolomite gangue.

Experimental

Minerals

Carbonate fluorapatite (francolite, $Ca_5(PO_4)_{2.5}(CO_3)_{0.5}F$), dolomite ($CaCO_3·MgCO_3$) and calcite ($CaCO_3$) were investigated. Carbonate fluorapatite was obtained from Ma'aden Company while dolomite and calcite from Saudi Carbonate Co. Ltd. Their identity and purity was checked by the X-ray analysis. The minerals were dry crushed in a jaw crusher and wet ground in a ball mill to get the size fraction below 0.25 mm.

Reagents

For the direct contact (conditioning) stage we used microemulsion ME1 (Fig. 1) consisting of collector (Custafloat AR27, a blend of fatty acid soaps and sulfates), oil (extender, fuel oil #5) and water. The phase diagram of the Custafloat AR27 - fuel oil #5 - water system is presented in Fig. 1. It was constructed using a water titration method at ambient temperature. The mixtures of oil and collector, at certain weight ratios, were mixed with water added as drops, under moderate stirring with a magnetic bar. After being equilibrated at ambient temperature for 24 hours, the system was visually analyzed under strong light to detect microemulsions, emulsions and other structures. The finding were confirmed by measuring transmittance using a Digital D-801 Photocon colorimeter at the 570–590 nm wavelength (Chen et al., 2004).
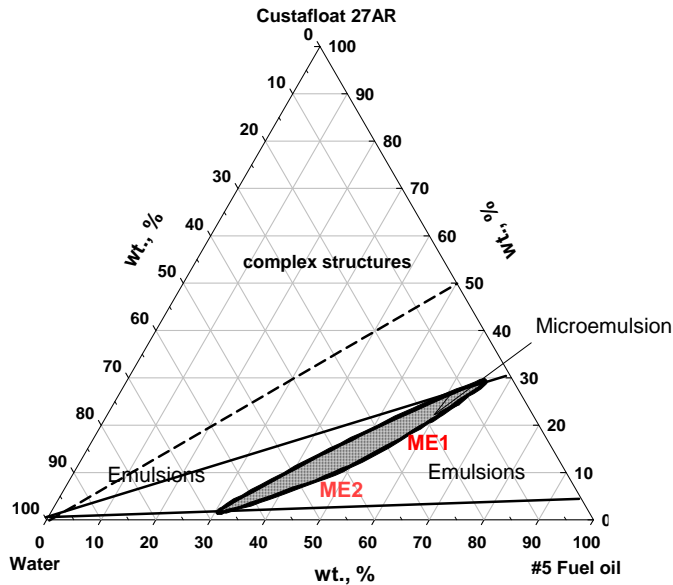
Fig. 1. Ternary collector-oil-water phase diagram showing used in experiments
microemulsion ME1 region and composition

The phase diagram shows that the investigated collector-fuel oil-water system is able to form microemulsions. The shape of the microemulsion area is like a lens. The lower boundary of the lens is represented by a line having collector-to-fuel oil ratio of approximately 1:19, while the upper boundary is determined by the collector-to-fuel oil ratio of 1:2.33. The lens is oriented from the bottom towards the higher water content and from the top towards the lower water content. This indicates that the microemulsion, called ME2, starts to form at low collector concentrations and high water content. This can be attributed to the fact that in the presence of water, the

collector starts to act as a surfactant which accumulates at the water-oil interface leading to more stable droplets. On the other hand, microemulsion ME1 is formed at low water concentrations (top head of the lens), but at a higher collector amount. In our investigation we will use ME1 because of smaller amount of water in its structure. Preliminary tests with carbonate fluorapatite showed superiority of ME1 over ME2. The weight fractions of ME1 were 20% collector, 55% oil and 25% water with a collector-to-oil ratio of 20:55, which is equivalent to 1:2.75.

The phase diagram also shows that at the collector concentration less than 30% an emulsion is formed, while higher concentrations of the collector lead to the formation of a complex reagents structure. Usually these complex structures hamper flotation as it was observed by Ahmed (2005) during oxidized coal flotation.

Flotation tests

Flotation tests were carried out in a D-12" Denver flotation cell equipped with a 1 dm^3 flotation tank. Tap water was used in all the tests. After establishing the collector-oil-water phase diagram (Fig. 1), the flotation tests were performed using a special procedure. In this procedure the flotation reagents in the form of microemulsion were added to a single, binary or tertiary pure mineral(s)-water system and conditioned at a high solid percent equal to 70%. The reagentized pulp was diluted to the targeted solid/liquid ratio and aerated for initiation of flotation. The different obtained products were collected, dried and weighted. In the case of binary and ternary pure minerals mixtures, they were subjected either to mineralogical or chemical analyses for determination of flotation performance. In single pure mineral flotation in the presence of microemulsions, different parameters such as conditioning time, conditioning pH, flotation pulp solids content and microemulsion dosage were investigated. The determined optimum conditions were applied for binary or ternary pure mineral systems as simulation of real ore flotation. It is worth mentioning that the aeration rate and flotation time were kept constant for the entire test program. The impeller speed was 1200 rpm in all the tests.

Results and discussion

Pure minerals flotation using a direct contact with microemulsion ME1

The first parameter that has been taken into consideration when using ME1 for flotation of pure minerals is the microemulsion conditioning time with pure single minerals. This was so because the conditioning time is an important parameter in determining the amount of microemulsion to be adsorbed on the mineral surface. The results of this series of experiments along with some additional process parameters (conditioning pulp density 70%, natural pH, microemulsion dosage of 0.5 kg/Mg) are given in Fig. 2. It shows that at the applied microemulsion dose, the carbonaceous gangue yield is small and is not highly affected by the conditioning time. On the other

hand, the carbonate fluorapatite recovery to the concentrate is affected by the conditioning time and varies from 70 to approximately 98% with maximum at 1.5 min of conditioning. The reduced recovery at a short conditioning time may be attributed to incomplete adsorption of microemulsion on the carbonate fluorapatite surface. With increasing conditioning time, the adsorption increases, leading to an increase in the carbonate fluorapatite recovery. Longer conditioning times result in decreasing carbonate fluorapatite recovery. This effect can be attributed to mechanical removal of microemulsion from the carbonate fluorapatite surface and decomposition of the microemulsion by cations coming from the carbonate fluorapatite surface into the solution. The obtained result indicates that the 1.5 min conditioning time is sufficient and it will be used in the subsequent experiments.
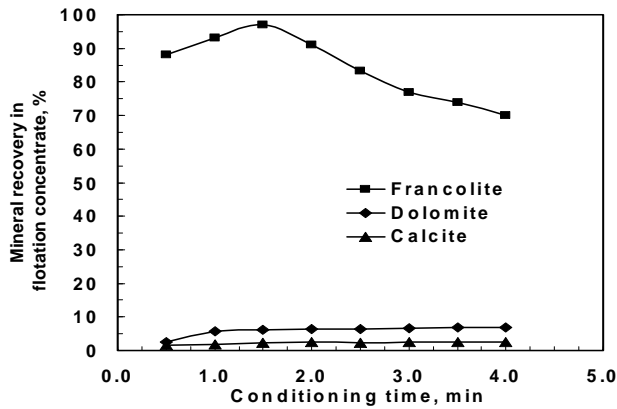

Fig. 2. Effect of conditioning time on single mineral flotation recovery
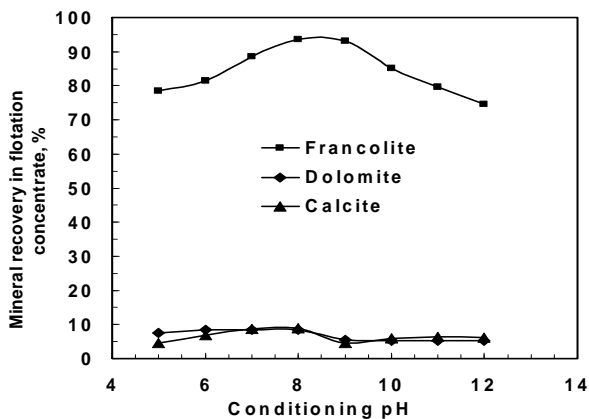using 0.5 kg/Mg of ME1 (pH = 8.5, solids density: conditioning 70%, flotation 25%)

Fig. 3. Effect of conditioning pH on single mineral flotation recovery
using 0.5 kg/Mg of ME1 (conditioning: time 1.5 min, solids density 70%;
flotation: time 2 min, pH 8.5, solids density 25%)

Another important parameter which controls reagents adsorption on the solid surface is conditioning pH. The conditioning pH was changed from 5 to 12 and the obtained results are plotted in Fig. 3. According to Fig. 3 the optimum conditioning pH is 8.5. In fact, this supports the interpretation of the pH effect in the case of conditioning time optimization previously assumed.

The next studied parameter was solid content in the pulp (Fig. 4). It can be seen that the solid content providing the best recovery of carbonate fluorapatite is about 25%.
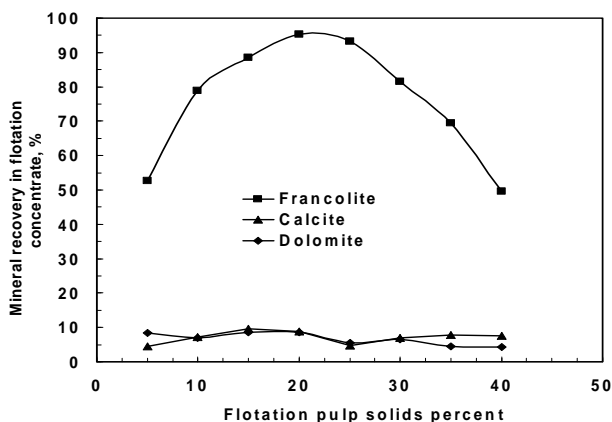
Fig. 4. Effect of flotation pulp solids content on single mineral flotation recovery using 0.5 kg/Mg of the ME1 (conditioning: time 1.5 min, solids density 70%, pH = 8.5; flotation time: 2 min, pH 8.5, solids density variable)

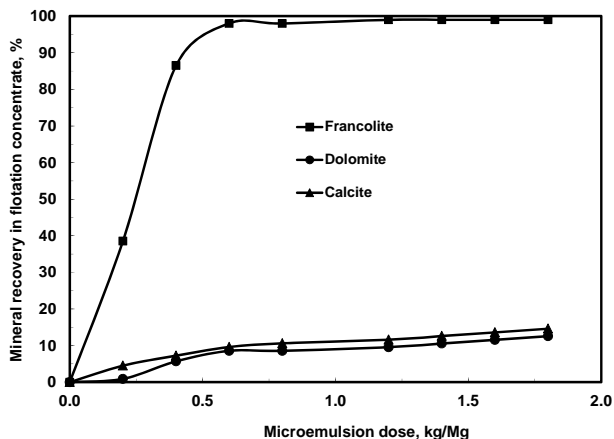Fig. 5. Effect of microemulsion dose on single mineral flotation recovery using ME1 (conditioning: time 1.5 min, solids density 70%, pH = 8.5, emulsion dose variable; flotation: time 2 min, pH 8.5, solids density 25%)

The hitherto determined favorable conditions were used to determine the dose of the microemulsions. The dose was changed from 0.1 to approximately 1.8 kg/Mg. The obtained results are shown in Fig. 5. The figure shows that the carbonate fluorapatite recovery increases sharply up to about 0.6 kg/Mg when the recovery is almost complete.

Two pure minerals mixtures flotation using microemulsion ME1

In this set of experiments, two separate mixtures were formed. The first mixture was composed of pure carbonate fluorapatite mixed with pure dolomite while the second mixture was made of pure carbonate fluorapatite mixed with pure calcite. The carbonate fluorapatite-to-dolomite ratio of the first mixture was 1:1 by weight while the carbonate fluorapatite-to-calcite ratio in the second mixture was 2:1 by weight. These ratios of mixing were selected to simulate the mineralogical ratios observed in many phosphate ores (Al-Wakeel, 2005).

The effect of microemulsion dose on flotation of carbonate fluorapatite either from the carbonate fluorapatite-dolomite mixture or carbonate fluorapatite-calcite mixture was investigated. In both sets of experiments, the operating conditions were kept constant as previously determined for single pure minerals flotation (conditioning: time 1.5 min, pH = 8.5, solids density 70%; flotation: time 2 min, pH 8.5, solids density 25%) for carbonate fluorapatite-to-dolomite ratio as 1:1. Figure 6 shows the flotation response with microemulsion ME1 for the carbonate fluorapatite-dolomite mixture while Fig.7 for the carbonate fluorapatite-calcite mixture.

Fig. 6. Effect of microemulsion (ME1) dose on carbonate fluorapatite flotation from carbonate fluorapatite-dolomite binary mixture (conditioning: time 1.5 min, pH = 8.5, solids density 70%; flotation: time 2 min, pH 8.5, solids density 25%) (carbonate fluorapatite: dolomite ratio 1:1)

It can be seen in Figs 6 and 7 that the recovery of minerals in both systems increases with the dose of microemulsion and the recovery of francolite reaches 95% while for dolomite and calcite the recovery is about 15%. Thus, the separation of carbonate fluorapatite by flotation from binary mixtures with either dolomite or calcite is very efficient.
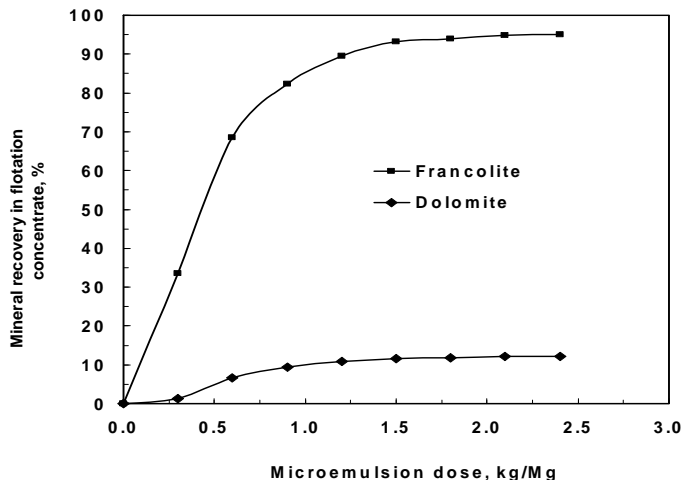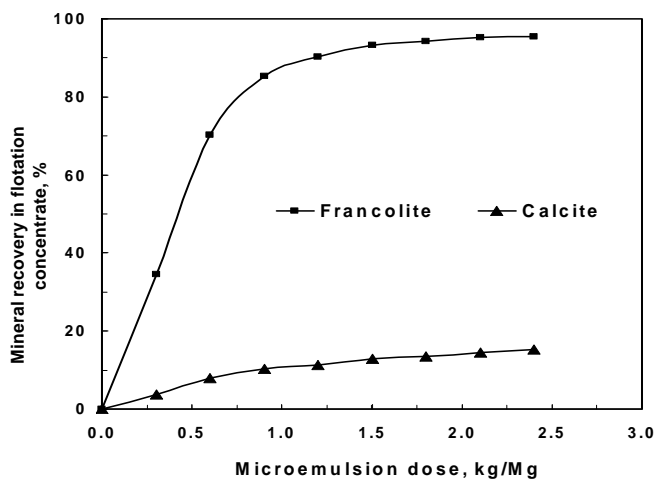

Fig. 7. Effect of microemulsion ME1 dose on carbonate fluorapatite flotation
from carbonate fluorapatite-calcite binary mixture (conditioning: time 1.5 min, pH = 8.5,
solids density 70%; flotation: time 2 min, pH 8.5, solids density 25%)
at carbonate fluorapatite-to-calcite ratio equal to 2:1

It can be noticed that the plateau at 95% recovery of carbonate fluorapatite from the binary mixture using microemulsions is lower than that in the case of single pure mineral flotation using the same microemulsion ME1 because the recovery is 99% (Fig. 5). This may be attributed to some microemulsion consumption by dolomite and calcite.

Three pure minerals mixture flotation using microemulsion ME1

In a trial to simulate a real phosphate ore, a synthetic mixture of carbonate fluorapatite, dolomite and calcite were made. The minerals ratios in the artificial mixture were as 2:2:1 by weight of carbonate fluorapatite, dolomite and calcite, respectively. Flotation of carbonate fluorapatite from this mixture was tried using different doses of microemulsion ME1. The operating conditions were as follows: conditioning: time 1.5 min, pH = 8.5, solids density 70%; flotation: time 2 min, pH 8.5, and solids density 25%. The obtained results are presented in Fig. 8.

According to Fig. 8 a good separation of carbonate fluorapatite from the ternary mixtures by flotation occurs at the microemulsion dose from 0.9 to 1.5 kg/Mg. At 1.5 kg/Mg the concentrate contains 83.6% carbonate fluorapatite. Microemulsion dosages lower than 0.9 kg/Mg provided less favorable results.
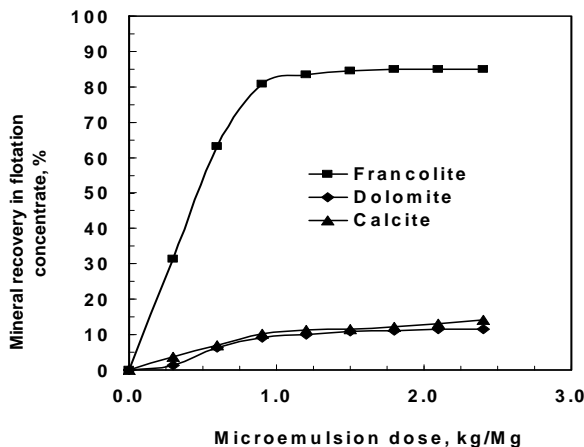
Fig. 8. Effect of microemulsion ME1 dose on carbonate fluorapatite flotation from carbonate fluorapatite-dolomite-calcite (2:2:1) ternary mixture (conditioning: time 1.5 min, pH=8.5, solids density 70%; flotation: time 2 min, pH 8.5, solids density 25%)

The results from Fig. 8 were replotted as the grade-recovery Halbich upgrading curve to see better the possible separation results for phosphate ores containing carbonate fluorapatite using the approach of the direct contact of flotation reagents forming microemulsion and interacting with particles at high solids densities, and subsequent flotation after dilution of the slurry to typical densities. Figure 9 shows that this approach provides high quality concentrates (above 33% of P_2O_5) with reasonable P_2O_5 recovery of about 85%. The calculations are based on the assumption that the investigated carbonate fluorapatite (francolite) contains 40% of P_2O_5 (Melike et al., 2011).

The results obtained in this study indicate a possibility of using microemulsion for upgrading phosphates. The noticeably shortcoming of special concern is a relatively high dose of microemulsion needed. A dose of 0.6 kg/Mg of microemulsion was enough to recover more than 90% of carbonate fluorapatite when it was floated alone. This dose has increased to approximately 0.8 kg/Mg to recover about 85% of carbonate fluorapatite when floated from binary mixtures containing dolomite or calcite and now the dose has increased to above 0.9 kg/Mg. The high dose required in this case may be attributed to the fact that the mixture was not deslimed. This may lead to a high surface area requiring a high dose of microemulsions for surface coverage and flotation. One more reason is that the high surface area of the carbonaceous minerals may lead to a noticeable increase in Ca^{2+} ions concentration in the solution and thus disturb the microemulsion droplets.
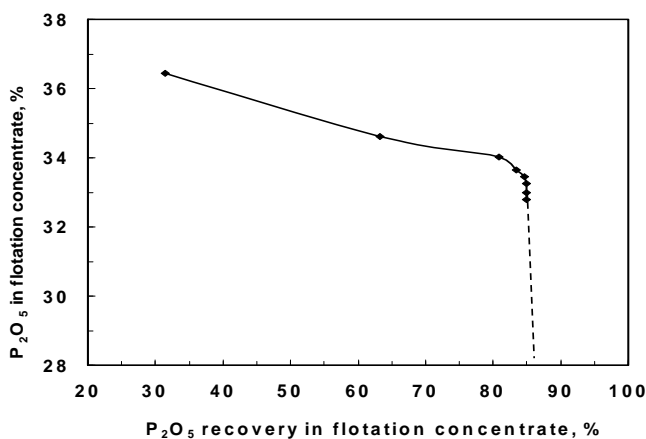
Fig. 9. Carbonate fluorapatite (francolite) separation from tertiary carbonate fluorapatite–dolomite–calcite
model mixtures by flotation after a direct contact of flotation reagents forming microemulsion
and reacting with particles at 70% solids density and subsequent dilution to 25% solids density
in terms of the Halbich grade (P_2O_5)-recovery (P_2O_5) upgrading curve

Conclusions

It results from the flotation tests conducted at pH 8.5 on a model carbonate fluorapatite-dolomite–calcite system that a direct contact of the flotation reagents forming microemulsion and consisting of 20% of collector, 55% oil, and 25% water with particles at solids density 70% and subsequent dilution of the system with water to form flotation aqueous suspension of 25% density, provide high quality carbonate fluorapatite concentrates containing for instance 83.6% carbonate fluorapatite with 84.6% carbonate fluorapatite recovery when the microemulsion dose of the microemulsion is 1.5 kg/Mg. Negligible separations were achieved when the microemulsion-particles direct contact stage was eliminated. The 84/84 separation efficiency, in terms of the francolite content in concentrate - francolite recovery, points to promising results which can be expected during beneficiation of real phosphate ores. Therefore, the obtained results will be verified with a low quality phosphate ore.

References

ABOUZEID M. Abdel-Zaher, 2008. *Physical and thermal treatment of phosphate ores – An overview International Journal of Mineral Processing*, Vol. 85, Issue 4, 59–84.

AHMED A.M.H., 2005. *Application of microemulsion for upgrading difficult-to-float materials*. Ph.D. thesis, Faculty of Mining Geoengineering and Geology, Wroclaw University of Technology, Poland.

AHMED A.M.H., DRZYMALA J., 2012. *Upgrading difficult-to-float coal using microemulsion*, Minerals & Metallurgical Processing, Vol. 29, No. 2: 75–83.

AHMED A.M.H., DRZYMALA J., 2004. *Effect of flotation procedure and composition of reagents on yield of a difficult-to-float coal*, Physicochemical Problems of Mineral Processing, 38, 53–63.

AL-WAKEEL M. I., 2005, *Effect of mechanical treatment on the mineralogical constituents of Abu-Tartour phosphateore, Egypt*, International Journal of Mineral Processing, Vol. 75, Issues 1–2, 101–112.

CHEN H., CHANG X., WENG T., ZHAO X., GAO Z., YANG Y., XU H., YANG, X., 2004. *A study of microemulsion systems for transdermal delivery of triptolide*. J. Control. Rel. 98: 427–436.

DRZYMALA J., 2007. *Mineral Processing. Foundations of theory and practice of minerallurgy*, Oficyna Wyd. PWr., Wroclaw, 507 pages, http://www.dbc.wroc.pl/Content/2070/Drzymala.pdf

MELIKE SINIRKAYA, A. KADIR ÖZER, M. SAHIN GÜLABOGLU, 2011. *Investigation of the changes of P_2O_5 content of phosphate rock during simultaneous calcination/sulfation*, Powder Technology, Vol. 211, Issue 1, 72–76.

NEGM A.A., ABOUZEID A.Z.M., 2008. *Utilization of solid wastes from phosphate processing plants*, Physicochemical Problems of Mineral Processing, 42, 5–16

WILLS B.A., NAPIER-MUNN T.J., 2006. *Wills; Mineral Processing Technology*, Elsevier, Amsterdam.

CHARACTERIZATION AND BENEFICIATION OF IRANIAN LOW-GRADE MANGANESE ORE

Akbar MEHDILO, Mehdi IRANNAJAD, Mohammad Reza HOJJATI-RAD

[*] Department of Mining and Metallurgical Eng., Amirkabir University of Technology, Tehran, Iran
iranajad@aut.ac.ir

Abstract: The mineralogical studies indicated that the Charagah ore deposit contains approximately 17% pyrolusite, 78% calcite and 3–4% quartz. Pyrolusite as a main valuable mineral is found in the forms of coarse and fine pyrolusites. The coarse grains pyrolusite with simple texture is liberated at 180 micrometers. Another kind of pyrolusite with particle size finer than 10 μm is disseminated inside gangue phases. This kind of pyrolusite has important effect in beneficiation processes and can affect the manganese grade of the concentrate and its recovery negatively. By jigging machine a pre-concentrate with 20% MnO and a final tailing with about 13% manganese loss are obtained. Using tabling technique or wet high intensity magnetic separation (WHIMS) and also their combination with jigging machine, production of a final pyrolusite concentrate with suitable grade but average recovery is possible. By jigging-tabling a concentrate with – 500+45 μm size fraction, 44.3% MnO and 61.3% recovery is obtained while jigging-WHIMS produces a concentrate containing 52.6% MnO with a recovery up to 56.6% and d_{80} = 180 μm.

Introduction

Manganese is used mainly in steel production, directly in pig iron manufacture and indirectly through upgrading ore to ferroalloys. Globally, the most of (90 to 95%) Mn is used in the metallurgical industry as a requisite deoxidizer and desulfurizer in steel making and as an important alloy component. Various amounts of Mn commonly are added to the steel for industrial use, making low or high Mn alloys. High grade ores (Mn content more than 42%) are usually used in metallurgical application. The remainder of the Mn (5 to 10%) is used in the chemical industry, light industry, production of dry cell batteries, in plant fertilizers and animal feed, and as a brick colorant (Fan and Yang, 1999; Lasheen et al., 2009). The world annual production of the total manganese alloys passed 10.3 million MT and it will increase (Lasheen et al., 2009).

The main manganese minerals are the oxide types, such as pyrolusite MnO_2, hausmannite Mn_3O_4 and manganite $MnO(OH)$. Manganese is also found in several minerals, such as pink rhodochrosite ($MnCO_3$), rhodonite ($MnSiO_3$), wad and alabandite (MnS) (Fuerstenau et al., 1986; Fan and Yang, 1999; Corathers and Machamer, 2006). Minerals such as rhodochrosite, rhodonite and hausmannite are often replaced by pyrolusite. Pyrolusite containing 63.2% Mn is the most common manganese mineral) (Zhang and Cheng, 2007). Manganese ores may accumulate in metamorphic rocks or as sedimentary deposits, frequently forming nodules on the sea floor (Jessica et al., 2006).

The main sources of manganese come from the former U.S.S.R, Brazil, South Africa, Australia, Gabon and India. Russia and South Africa produce about 85% of the world's pyrolusite. Manganese nodules or ferro-manganese concretions, usually containing 30–36% Mn, have been found on ocean floors (Jessica et al., 2006; Mohapatra et al. 2009) and could provide another source of manganese. These nodules are found in both the Atlantic and Pacific Oceans, but principally in the Pacific Ocean. Although the primary interests in deep sea nodules are nickel, copper, and cobalt values, the large quantities of manganese could also be of future importance. As a result, much research work has been devoted to recovering not only nickel, copper and cobalt but also manganese as well (Zhang and Cheng, 2007).

Each type of a manganese deposit is a problem by itself in the matter of selection of a proper method of concentration, depending on the manganese minerals and their gangue constituents. Beneficiation technology as applied to manganese ores is similar to that for iron ores. Most ores are crushed and screened, with the lump product (+6 mm) generally being smelted and the fine product (–6 mm) used as feed for chemical and/or electrolytic processing. Sink-float, jigging, tabling, flotation and high-intensity magnetic separation are usually used to upgrade fine manganese ore. Physical separation technologies such as flotation and roasting, and chemical separation process such as leaching have been developed for beneficiation lower grade and more refractory resources (Abeidu, 1972; Fuerstenau et al., 1986; Rao et al., 1988; Mohapatra et al., 1995; Jessica et al., 2006; Zhang and Cheng, 2007; Ito et al., 2008; Mishra et al., 2009).

With increasing the steel production in Iran, exploration and processing of the manganese ores in the country is necessary. There are some manganese mines (venarch mine) and deposits in Iran. The Charagah ore deposit locating in the 82 km at the North-West of Tabriz, is one of the new indexes (Mehdilo et al., 2010; Hojjati-rad and Irannajad, 2011). The characterization of Charagah ore from process mineralogical viewpoint and its upgrading are the main purposes of this article.

Materials and methods

Around one megagram of representative sample, collected from different trenches of deposit, was prepared according Fig. 1 and used for characterization and upgradation

experiments. The detailed characteristics of the sample are presented in section 3-1. The corresponding polished thin sections were studied for ore and rock-forming minerals and their textural relationships by reflected and transmitted light microscopy. The chemical and mineralogical composition of different samples carried out by X-ray fluorescence (XRF) and X-ray diffraction (XRD). The Philips scanning electron microscopy (model: XL30) equipped with WDX (wave length dispersive X-ray) was used for description of texture and determination of valuable mineral. The microspec WDX (model: 3pc) was used for X-ray mapping analysis.

ASTM standard screens were used in sieve analysis. The gravity separation tests were performed using the laboratory jigging machine, shaking table and some heavy liquids. Methylene iodide (density 3.32 g/cm^3) and bromoform (density 2.89 g/cm^3) were used in heavy liquid experiments. The wet high intensity magnetic separation tests were carried out using a Boxmag separator.
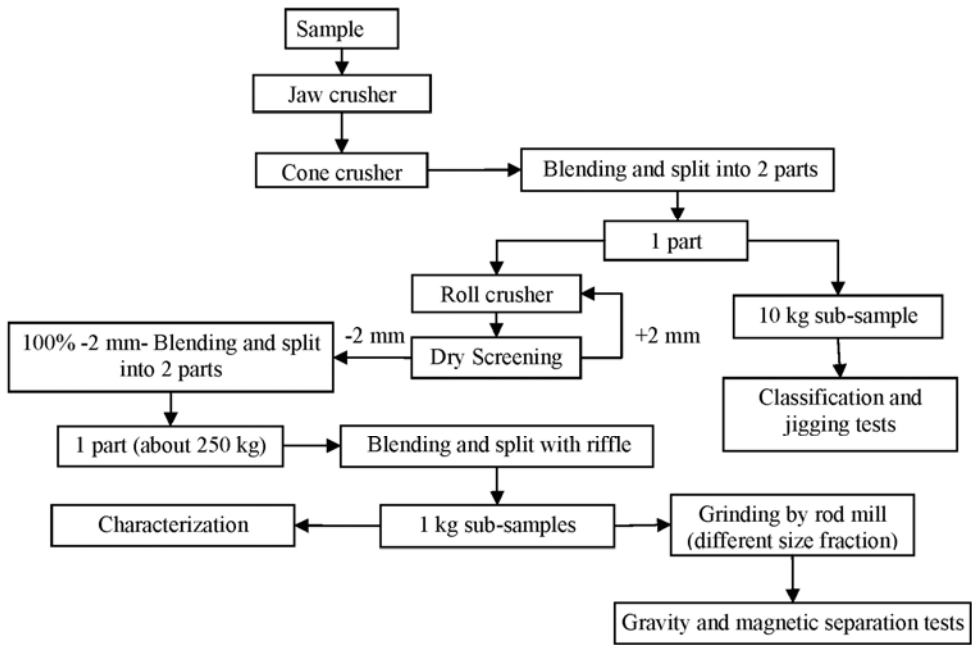

Fig. 1. The procedure of sample preparation

Results

Ore characterization

Chemical and mineralogical composition

According to the X-Ray diffractography (Fig. 2), the ore consist of pyrolusite as the main valuable mineral of manganese and calcite as well as quartz as gangue minerals.

The chemical composition of a representative sample analyzed by XRF is shown in Table 1. The studied ore sample by average grading of 13.8% MnO which implies about 17% pyrolusite (by considering 81.6% theoretical MnO for pyrolusite), is one of the low grade deposits in the world. Based on XRD and XRF analysis, the amounts of calcite and quartz of the ore are about 79% and 2–3%, respectively.

Microscopical studies

Based on the results obtained from transmitted-light microscopy studies, the coarse and fine grains of ore minerals are surrounded by gangue minerals containing calcite and quartz. The interlocking of ore and gangue minerals is shown in Fig. 3. The study of polished sections by reflected-light microscopy showed that pyrolusite (about 12–15 vol %) is the main ore mineral (Fig. 4). The small amount of hematite is also found in the samples.

The studies by scanning electron microscopy indicated that the mineralization of pyrolusite is occurring in two forms. The coarse grains pyrolusites with size about 200 µm have simple interlocking with gangue minerals (Fig. 5a and 5b). Another kind of pyrolusites with complicated texture and interlocking are even finer than 10 micrometers sizes (Fig. 5g). In fact, these very fine pyrolusites are disseminated inside gangue minerals. The distribution or X-Ray mapping of manganese (Mn) as demonstrator of pyrolusite is shown in Figs 5c, 5e and 5h. The small amount of barite particles is also observed in this part of study which is evidenced by analysis using WDX (X-Ray mapping of Ba in Fig. 5f).
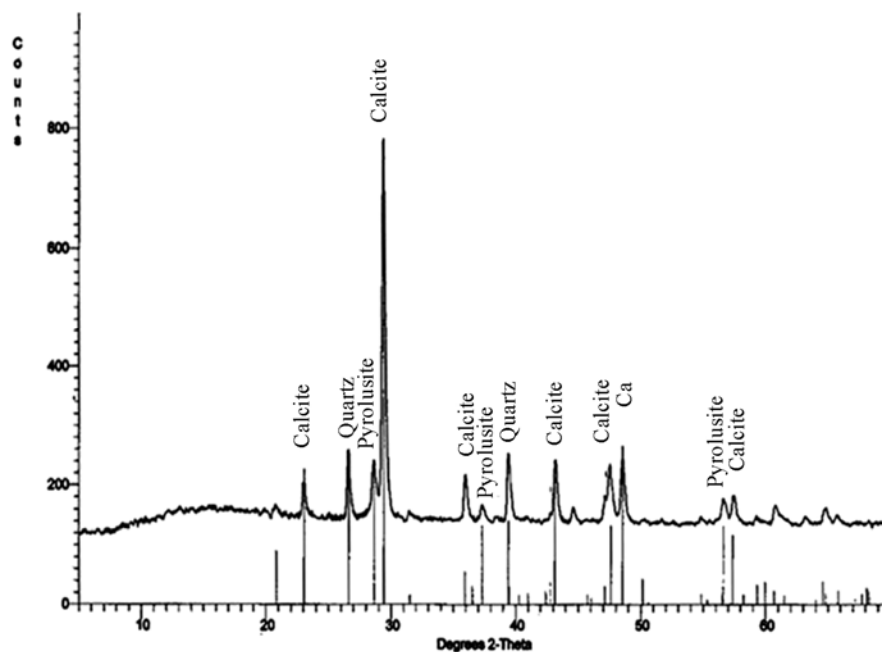
Fig. 2. X-ray diffraction pattern of representative sample

Table 1 the chemical composition of representative sample
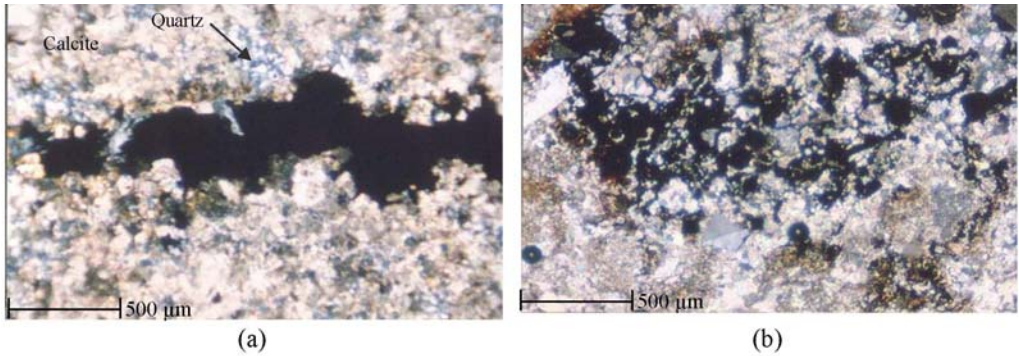
Fig. 3. Study by transmitted light microscopy
(a) Interlocking of calcite, quartz and coarse grains of ore minerals (pyrolusite)
(b) Fine grains mineralization surrounded by gangue minerals
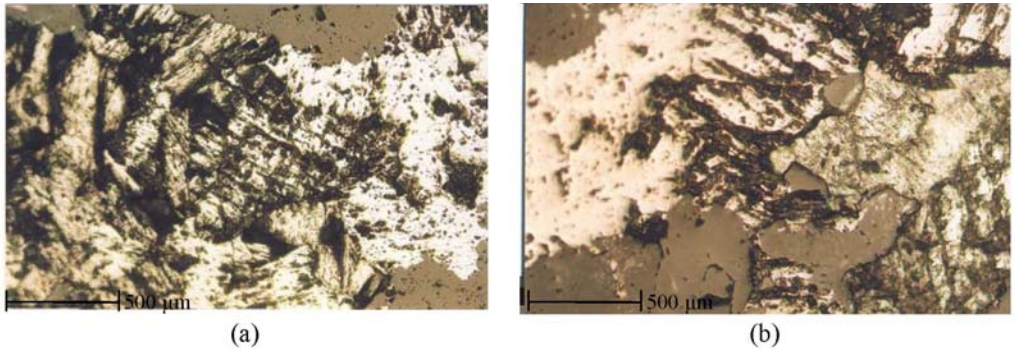
Fig. 4. Study by reflected light microscopy (interlocking of pyrolusite and gangue minerals)
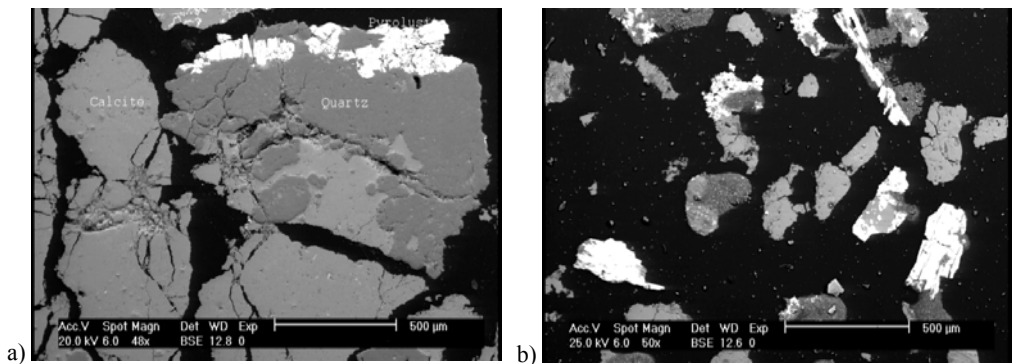
Fig. 5
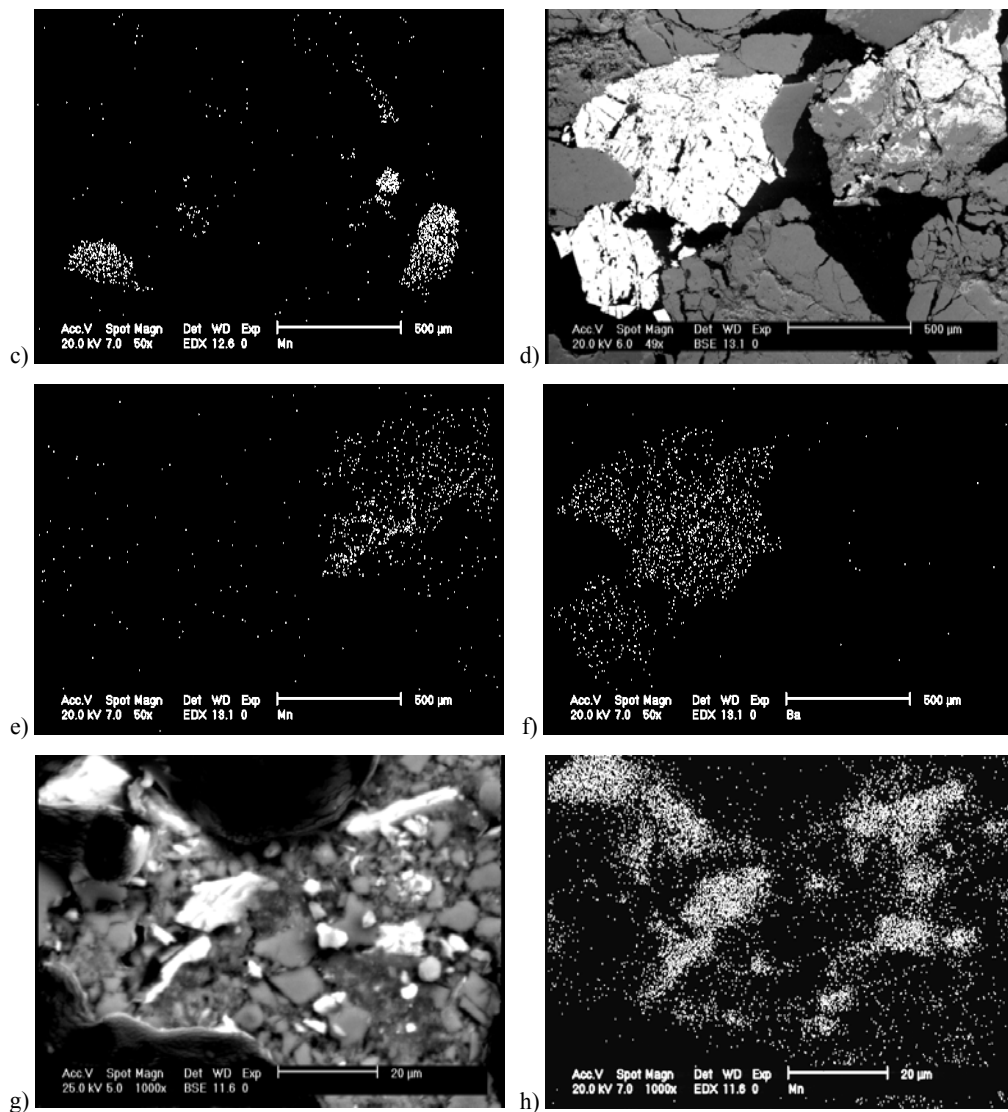
Fig. 5. BSE (Backscattered Electron) images taken by Scanning Electron Microscopy (SEM) and WDX X-Ray mapping: (a) Interlocking of coarse grains of pyrolusite and gangue minerals containing calcite and quartz (–1190+600 μm size fraction); (b) Interlocking of coarse grains of pyrolusite and gangue minerals containing calcite and quartz (–180+150 μm size fraction); (c) X-Ray mapping of manganese (Mn) as demonstrator of pyrolusite in Fig. 5b; (d) Interlocking of coarse grain pyrolusite and barite with gangue minerals containing calcite and quartz (–1190+600 μm size fraction); (e) X-Ray mapping of manganese (Mn) as demonstrator of pyrolusite in Fig. 5d; (f) X-Ray mapping of barium (Ba) as demonstrator of barite in Fig. 5d; (g) Interlocking of fine grains of pyrolusite and gangue minerals containing calcite and quartz; (h) X-Ray mapping of manganese (Mn) as demonstrator of pyrolusite in Fig. 5g

Liberation degree

One of the 1 kg samples was sieved and a representative polished section was prepared from each of eight sieve fractions. BSE (Backscattered Electron) images were taken from different parts of each polished section. In all images of each section the surface area of liberated and locked pyrolusites were measured by using JMicroVison software. Then, the percent of liberation degree is calculated by using Eq. 1 for different fractions. The results, as percent of liberation degree versus size fraction, are shown in Fig. 5. Based on these results the liberation degree of pyrolusite

$$LD(\%) = \frac{S_{LP}}{S_{LP} + S_{IP}} \cdot 100 \tag{1}$$

is determined as 180 micrometers, where S_{LP} is the total surface area of liberated pyrolusites in all images of each polished section and S_{IP} is the surface area of interlocked pyrolusites in all images of each polished section.
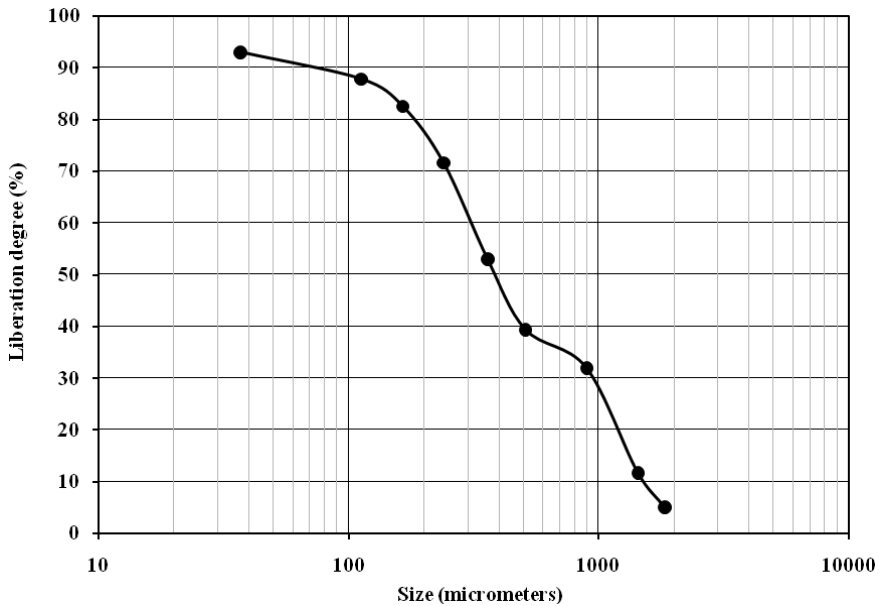
Fig. 5. Liberation degree of pyrolusite, determined using JMicroVison

The laboratory grinding of 1 kg samples with size distribution according Table 2 showed that about 90% of the sample is entered to −180 μm size fraction after grinding for 15 and 9.5 minutes by rod and ball mill, respectively.

Sieve and chemical analysis

After crushing the sample under 2 mm according Fig. 1, a 1 kg representative sample was subjected to sieve analysis using ASTM standard screens and each fraction is

chemically analyzed by XRF. The results of size and chemical analysis of fractionated materials are shown in Table 2. By decreasing the size fraction, the MnO content is increased but the CaO content is decreased gradually. The size and chemical analysis of a sample (-2000 μm) ground by the rod mill for 15 min is presented in Table 3. The results show that the distribution of MnO and CaO in all the size fractions of mill product (Table 3) is almost more uniform than mill feed materials (Table 2). Based on the obtained results, it is clear that pyrolusite is ground more easily than calcite and quartz and also its distribution in fine size fractions is more than coarse size fractions. These fine particles could have negative effects on physical separation processes

Table 2. The size and chemical analysis of a sample crushed under 2000 μm

Size (μm)	Weight (%)	Cumulative passing (%)	MnO			CaO			SiO$_2$		
			%	Distribution		%	Distribution		%	Distribution	
				(%)	Cumulative		(%)	Cumulative		(%)	Cumulative
−2000+1680	10.4	100	10.4	7.9	100	48.1	10.7	100	4.4	15.2	100
−1680+1190	22.8	89.6	12.2	20.3	92.1	47.9	23.4	89.3	3.3	25.1	84.8
−1190+600	33.3	66.8	12.4	30.1	71.8	48.1	34.4	65.9	2.7	30.0	59.7
−600+425	7.2	33.5	12.8	6.7	41.7	47.8	7.4	31.5	2.6	6.2	29.7
−425+300	4.4	26.3	14.1	4.5	35.0	47.7	4.5	24.1	1.7	2.5	23.5
−300+180	5.0	21.9	16.2	5.9	30.5	44.5	4.8	19.6	2.8	4.7	21.0
−180+75	3.5	16.9	20.7	5.3	24.6	41.0	3.0	14.8	4.6	5.3	16.3
−75	13.4	13.4	19.8	19.3	19.3	40.8	11.8	11.8	2.4	11.0	11.0
Bulk	100	–	13.7	100	–	46.6	100	–	3.0	100	–

Table 3. Size and chemical analysis of a sample ground by rod mill for 15 min

Size (μm)	Weight (%)	Cumulative passing (%)	MnO			CaO			SiO$_2$		
			%	Distribution		%	Distribution		%	Distribution	
				(%)	Cumulative		(%)	Cumulative		(%)	Cumulative
−300+210	4.1	100	7.5	2.2	100	45.9	4.2	100	12.2	8.3	100
−210+150	15.1	95.9	9.9	10.6	97.8	47.5	16.1	95.8	6.55	16.5	91.7
−150+75	24.5	80.8	13.0	22.6	87.2	45.5	25.1	79.7	6.96	28.4	75.2
−75+38	17.5	56.3	15.6	19.3	64.6	43.1	17.0	54.6	6.05	17.6	46.8
−38	38.8	38.8	16.4	45.3	45.3	43.0	37.6	37.6	4.45	29.2	29.2
Bulk	100	–	14.1	100	–	44.4	100	–	6.0	100	–

Beneficiation tests

Jigging tests

Some jigging tests were performed on different size fractions including –9500+4750, –4750+2000 and –2000+1180 μm to remove some gangue minerals as a clean tailing with minimum content of MnO and a suitable pre-concentrate. The results shown in Table 4 indicated that the tailing with the minimum grade and recovery is obtained using the feed material by sizing of –9500+4750 μm the produced pre-concentrate in this size fraction with 20% MnO is favorable for other separation techniques such as tabling, magnetic separation and flotation.

Table 4. The results of jigging tests

Size fraction (μm)	product	Weight (%)	MnO (%)	Recovery (%)
–9500+4750	Concentrate	50.3	20.0	77.4
	Tailing	49.7	6.2	22.6
–4750+2000	Concentrate	40.2	23.7	65.2
	Tailing	59.8	8.5	34.8
–2000+1180	Concentrate	36.4	22.4	56.7
	Tailing	63.6	10.3	43.3

Heavy media separation studies

The –180+75 μm size fraction sample was subjected to sink and float studies using methylene iodide (density, γ, 3.32 g/cm^3) and bromoform (γ = 2.89 g/cm^3) as medium. The results of the studies are presented in Fig. 6 and the chemical analysis of the products is shown in Table 5. The results show that using a medium with γ=3.32 g/cm^3, a pyrolusite concentrate containing 71.7% MnO and about 88% purity is produced. This product contains 76% of the manganese. By separating the float product of medium with γ = 3.32 g/cm^3 in bromoform solution another concentrate (sink in γ 2.89 g/cm^3) with 32% MnO and 14.5% recovery is obtained. The SiO_2 content in the sink product of bromoform is relatively high and this can be due to unliberated hard quartz. The float product of the medium with γ= 2.89 g/cm^3 is a final tailing with 68.6% weight percent which contains only 2.86% MnO. This indicates that most of the gangue minerals are present in the liberated form. It is also observed (Table 6) that BaO content is increased in sink products which related to minor amount of barite mineral in the ore sample.

Tabling tests

The representative sample was ground to below 1190μm size and classified into four fractions viz. –1190+425 μm, –425+180 μm, –180+75 μm and –75 μm. These fractions were subjected to tabling studies and results are shown in Table 6 and Fig. 7.
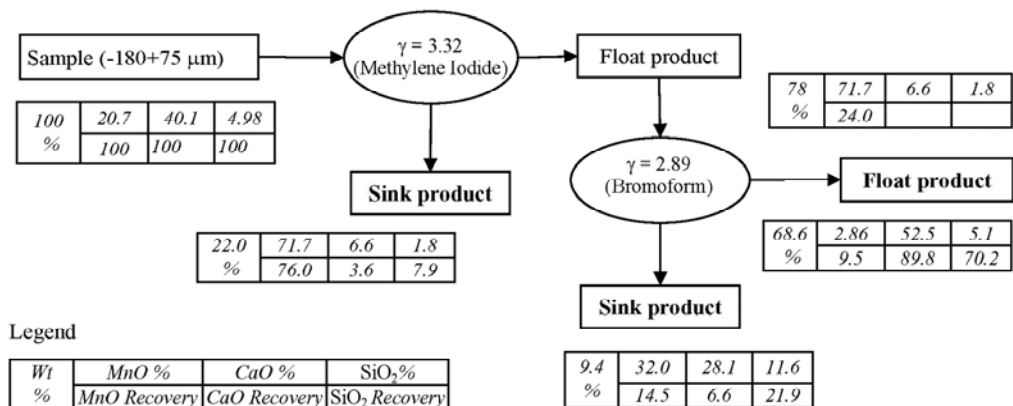
Sample (-180+75 μm) → γ = 3.32 (Methylene Iodide) → Float product

100	20.7	40.1	4.98
%	100	100	100

78	71.7	6.6	1.8
%	24.0		

Sink product

22.0	71.7	6.6	1.8
%	76.0	3.6	7.9

γ = 2.89 (Bromoform) → Float product

68.6	2.86	52.5	5.1
%	9.5	89.8	70.2

Sink product

9.4	32.0	28.1	11.6
%	14.5	6.6	21.9

Legend

Wt	MnO %	CaO %	SiO₂%
%	MnO Recovery	CaO Recovery	SiO₂ Recovery

Fig. 6. Procedure and results of heavy liquid tests

Table 5. Chemical analysis of the sink floats products

Composition (%) / Product	MnO	CaO	SiO$_2$	Fe$_2$O$_3$	Al$_2$O$_3$	MgO	BaO	SO$_3$	L.O.I	Others
Sink in 3.32	71.7	6.6	1.8	0.81	0.0	0.81	2.46	0.6	13.2	2.02
Sink in 2.89	32.1	28.1	11.6	1.05	0.36	0.71	1.06	0.46	22.96	1.6
Float in 2.89	2.98	52.5	5.1	0.52	0.66	0.74	0.083	0.087	36.84	0.51

Table 6. Results of tabling tests on different size fractions

Size fraction (μm)	product	Weight (%)	MnO (%)	Recovery (%)
−1180+425	Concentrate	27.4	29.2	59.6
	Middling	36.4	11.2	30.4
	Tailing	36.2	3.7	10.0
−425+180	Concentrate	19.4	42.8	52.1
	Middling	34.8	13.1	28.6
	Tailing	45.8	6.7	19.3
−180+75	Concentrate	15.3	47.8	41.1
	Middling	42.3	15.6	37.0
	Tailing	42.4	9.2	21.9
−75	Concentrate	10.4	57.6	32.2
	Middling	42.3	16.9	38.4
	Tailing	47.3	11.6	29.4

These results indicate that by decreasing the particle size a concentrate with high MnO content is obtained but the recovery is also decreased. The –425+75 μm size fraction (mixture of –425+180 μm and –180+75 μm fractions) is selected as suitable feed for

separation by tabling which could result in a concentrate containing more than 44% MnO with about 50% recovery.

After removing –30 μm particles as slime, the tabling test was performed on –180+30 μm size fraction and a concentrate having 66% MnO with 40.4% recovery and a tailing with 10.1% MnO are obtained. The size distribution of the concentrate and tailing according Fig. 8 showed that the average particle size of the concentrate (d_{80} = 134 μm) is finer than tailing (d_{80} = 163 μm). These results confirm that it is more easily to grind pyrolusite than gangue minerals and its distribution in fine size fractions.

Magnetic separation

The representative sample for wet high intensity magnetic separation (WHIMS) tests was prepared according Fig. 9. The feed material (d_{80} = 0.18 mm) was subjected to magnetic separation at different magnetic intensities (1.2, 1.5 and 1.77 tesla). The results are presented in Table 7. The results show that the weight percent of magnetic product and recovery of MnO increase with increasing of magnetic intensity while the MnO grade is decreased slightly. As seen from Halbich upgrading curves presented in Fig. 10, the better separation is achieved at higher intensity (1.77 Tesla) which results in more selectivity index f ($f = \beta \cdot \sum \varepsilon / 100$ (Drzymala, 2007)) value in comparing with that's of two other options. It is possible to get a product with 52.6% MnO by recovering 64.6% MnO. The loss of MnO in non-magnetic fractions has also been reduced at higher intensity. About 90% of CaO and 84% of SiO_2 are concentrated in the non-magnetic product or tailing fraction.
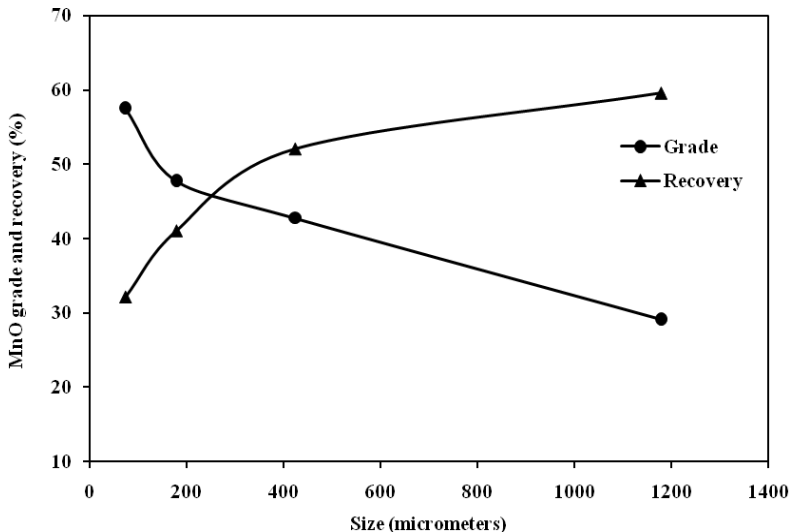

Fig. 7. MnO grade and recovery as a function of size fraction in tabling tests
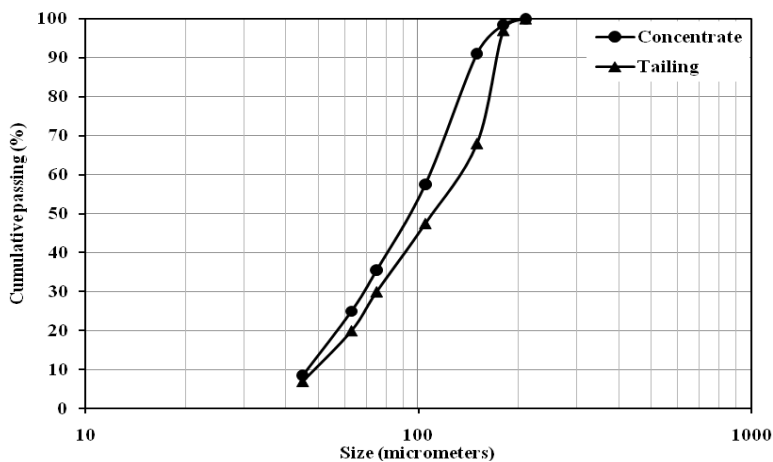
A. Mehdilo, M. Irannajad, M. R. Hojjati-rad

Fig. 8. The size distribution of concentrate and tailing of tabling test on −180+30 μm size fraction
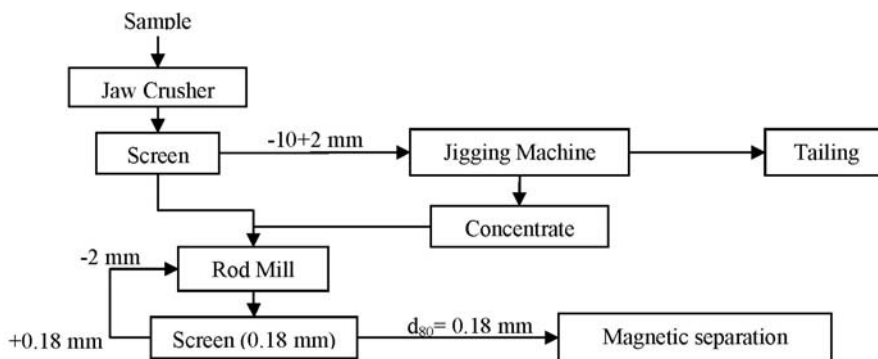
Fig. 9. The procedure of sample preparation for wet high intensity magnetic separation tests

Table 7. The results of magnetic separation tests at different intensities

Intensity (tesla)	Product	Weight (%)	Grade (%)			Recovery (%)		
			MnO	CaO	SiO$_2$	MnO	CaO	SiO$_2$
1.2	Concentrate	18.1	53.5	15.9	5.8	52.3	7.9	13.8
	Tailing	81.9	10.8	40.9	8.0	47.7	92.1	86.2
	Feed	100	18.5	36.4	7.6	100	100	100
1.5	Concentrate	21.6	52.1	16.6	6.5	60.4	9.5	17.1
	Tailing	78.4	9.4	43.5	8.7	39.6	90.5	82.9
	Feed	100	18.6	37.7	8.2	100	100	100
1.77	Concentrate	22.6	52.6	16.2	6.5	64.6	9.8	16.1
	Tailing	77.4	8.4	43.5	9.9	35.4	90.2	83.9
	Feed	100	18.4	37.3	9.1	100	100	100

Fig. 10. The Halbich upgrading curves for magnetic separation at different intensities

Fig. 11. Procedure and results of jigging-WHIMS combination
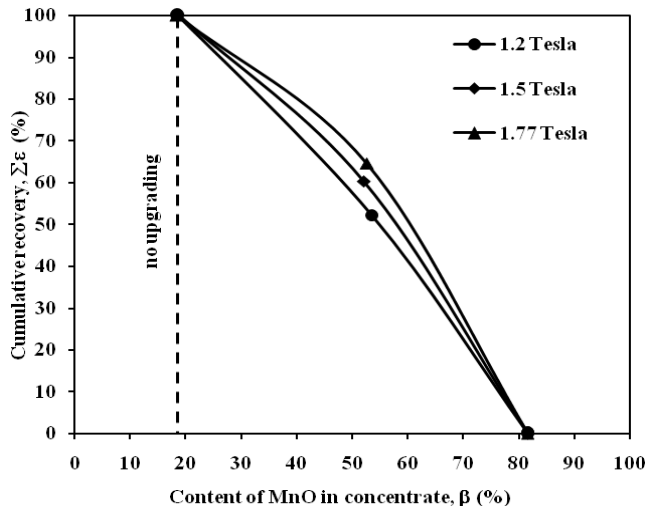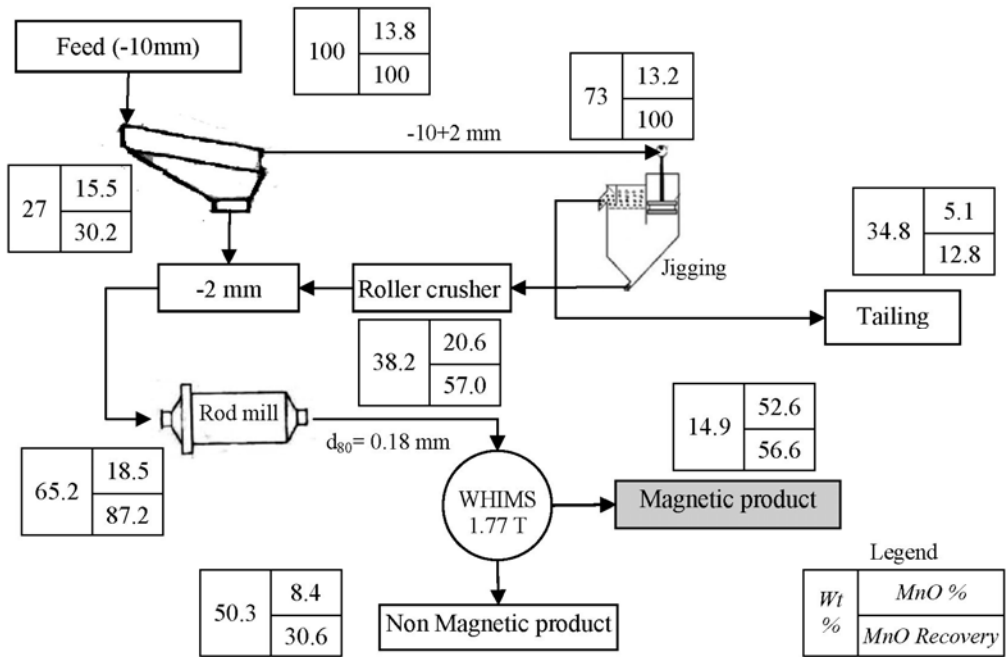
Combination of gravity and magnetic separation methods

Based on the results obtained from gravity and magnetic separation tests, different combinations of them were also examined. The procedure and results of two suitable

combination including jigging-WHIMS and jigging-tabling are shown in Fig. 11 and Fig. 12, respectively. By combination of jigging-WHIMS a concentrate (magnetic product) with 52.6% MnO and 56.6% recovery is obtained. But, the combination of jigging-tabling produces a concentrate containing 44.3% MnO with 61.3% recovery. The separation efficiency (SE) was calculated 49.83% and 48.5% for jigging-WHIMS and jigging-tabling, respectively. The Halbich upgrading curves were also displayed for both combinations in Fig. 13. These curves showed that the selectivity index (f) for jigging-WHIMS combination is always higher than jigging-tabling one. However, the selection of the best flowsheet depends on the technical and economical condition but from separation efficiency (SE) and selectivity index (f) point of view, the Jigging-WHIMS combination is a little better than jigging-tabling alternative.

Discussion

The Charagah ore by average grading of 13.8% MnO which implies about 17% pyrolusite (by considering 81.6% MnO for pyrolusite) as main valuable is one of the low grade deposits in the world. Mineralogical studies indicated that the ore contains about 79% calcite and 3–4% quartz as gangue minerals. The amount of other minerals such as barite and hematite which were observed in microscopical studies is negligible. So, pyrolusite and calcite are two major phases and the ore mineralization is mainly occurred in limestone. Pyrolusite is found in the forms of coarse and fine pyrolusites. The coarse grains pyrolusite with simple texture is liberated in 180 micrometers. Another kind of pyrolusite is very fine particles which have been disseminated inside the gangue phase.

Two major phases, pyrolusite and calcite, differ significantly in respect of their densities (4.7 and 2.7 g/cm^3, respectively). With efficient density of 2.2 g/cm^3, it is expected that the upgradation of the ore will be possible easily. This matter is well demonstrated in the heavy liquid separation studies using bromoform (2.89 g/cm^3) as the separating media. The results of this study clearly demonstrate upgrading of Mn-value up to 59% MnO with 90.5% recovery at –180+75 μm size fraction. Using jigging separation, considerable amount of gangue minerals is removed as tailing with about 13% manganese loss. This tailing is very important in decreasing energy consumption in the later milling process. The results of tabling experiments revealed that a concentrate containing 44% MnO with about 52% recovery is obtained in the size fraction of –425+180 μm. With reduction of the size, the MnO content of the concentrate is increased (47.8% for –180+75 μm and 57.6% for –75 μm) but the recovery is decreased significantly. The lower grade of the manganese in the coarse fractions is due to finely disseminated pyrolusite, which takes the locked gangue minerals into the concentrate. The decreasing recovery in the fine fractions is related to entrance of very fine liberated pyrolusites into the tailing. As an alternative, wet high intensity magnetic technique was employed on -180 μm size fraction to find out
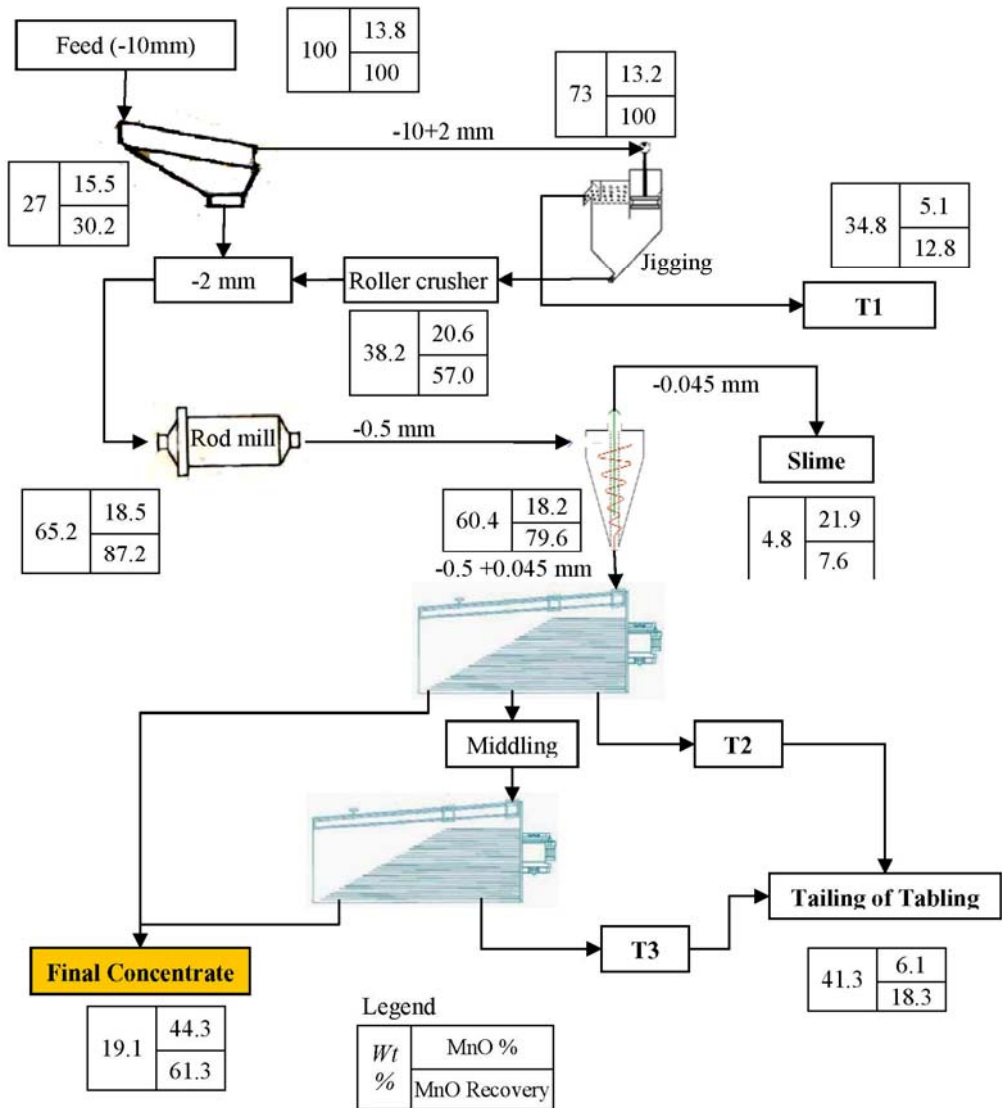
Fig. 12. Procedure and results of jigging-tabling combination

the possibility of pyrolusite separation from gangue minerals. Pyrolusite is a para-magnetic mineral and can easily be separated from calcite and quartz as diamagnetic minerals using high intensity magnetic separators. By increasing magnetic intensity, the recovery of manganese is increased significantly while the MnO grade is decreased slightly. Using WHIMS the fine particles of pyrolusite are recovered more efficiently than the tabling technique.

Fig. 13. The Halbich upgrading curve for the two examined combinations

Conclusion

The ore mainly contains pyrolusite and calcite with significant difference in their densities and magnetic susceptibilities. It is expected that the concentration of the ore can be done easily. Some mineralogical features of pyrolusite can affect the manganese grade and recovery in the concentrate of the physical separation techniques negatively. These features are dissemination of very fine pyrolusites inside gangue minerals and distribution of the most of py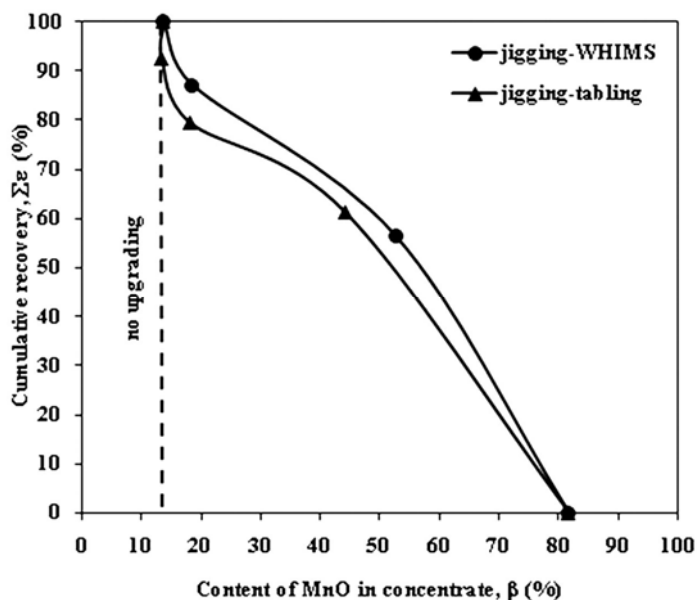rolusites in fine size fractions (-75 μm) in the grinding process to achieve the determined liberation degree (180 μm). Nevertheless, using jigging-tabling or jigging-WHIMS, production of a concentrate with suitable grade (44–53% MnO) and average recovery (56–62%) is possible.

References

ABEIDU A. M., 1972. *The feasibility of activation of manganese minerals flotation*. Trans. JIM 14, 45–49.

DRZYMALA J., 2007. *Mineral processing, foundations of theory and practice of minerallurgy*. Wroclaw University of Technology.

FAN D., YANG P., 1999. *Introduction to and Classification of Manganese Deposits of China*. Ore Geology Reviews 15, 1–13.

FUERSTENAU M. C., Han K. N., Miller J. D., 1986. *Flotation Behavior of Chromium and Manganese Minerals*, In Proceedings of the Arbiter Symposium, Advances in Mineral Processing, March. SME/AIME, 289–307.

HOJJATI-RAD M. R., IRANNAJAD M., 2011. *Mineral processing studies on Charagah Manganese deposit*, M.Sc Thesis, Amirkabir University of Technology, Tehran, Iran.

ITO M., TSUNEKAWA M., YAMAGUCHI E., SEKIMURA K., KASHIWAYA K., HORI K., HIROYOSHI N., 2008, *Estimation of degree of liberation in a coarse crushed product of cobalt-rich ferromanganese crust/nodules and its gravity separation*. International Journal of Mineral Processing 87, 100–105.

JESSICA E. K., NIKHIL C. T., JAMES M. B., STANLEY T. K., 2006. *Industrial Minerals & Rocks: Commodities, Markets, and Uses*, SME, 7th edition, 631-–637.

LASHEEN T. A., EL-HAZEK M. N., HELAL A. S., EL-NAGAR W., 2009. *Recovery of manganese using molasses as reductant in nitric acid solution*. Int. J. Miner. Process. 92 109–114

MEHDILO A., HOJJATI-RAD M. R., IRANNAJAD M., 2010. *Process Mineralogical Studies of Charagah Manganese ore*. International Mining Congress and Exhibition, 18–21 October, Tehran, Iran.

MISHRA P. P., MOHAPATRA B. K., MAHANTA K., 2009. *Upgradation of Low-Grade Siliceous Manganese Ore from Bonai-Keonjhar Belt*, Orissa, India. Journal of Minerals & Materials Characterization & Engineering 8 (1), 47–56.

MOHAPATRA B. K., RAO D. S., SAHU R. K., 1995. *Characterisation and magnetic separation studies on chikla manganese ore*, Maharastra. Ind. Min Eng. J., July 1995, 37–41.

MOHAPATRA B. K., MISHRA P. P., SINGH P. P., RAJEEV, 2009. *Manganese ore deposits in Koira-Noamundi province of Iron Ore Group, north Orissa, India*: In the light of geochemical signature. Chemie der Erde - Geochemistry 69, 377–394.

RAO, G. V., MOHAPATRA B. K., TRIPATHY A. K., 1988. *Enrichment of the manganese content by wet high intensity magnetic separator from chikla manganese ore, India*. Magnetic and Electrical Separation 9, 69–82.

ZHANG W., CHENG C. Y., 2007. *Manganese Metallurgy Review, Part I: Leaching of Ores/Secondary Materials and Recovery of Electrolytic/Chemical Manganese Dioxide*. Hydrometallurgy 89, 137–159.

THE EFFECT OF ROTATIONAL SPEED OF THE DRUM ON PHYSICAL PROPERTIES OF GRANULATED COMPOST FERTILIZER

Yousef GHASEMI, Mohammad Hossein KIANMEHR, Amir Hossein MIRZABE, Behnam ABOOALI

Department of Agrotechnology, University of Tehran, College of Abouraihan, Tehran, Iran, Corresponding author, a_h_mirzabe@ut.ac.ir (A. H. Mirzabe)

Abstract: Granulation is one of the fundamental operations in particulate processing which has an ancient history and a widespread use. Compost fertilizer was granulated using drum granulation method under different level of drum rotational speed. Rotational speed of the drum (ω) ranged from 40 to 60 rev min^{-1} (40, 45, 50, 55 and 60 rev min^{-1}). The effect of rotational speed of the drum (ω) on some physical properties of granulated compost fertilizer including: useful granules, granules size, fracture force, mass of the granules, bulk density, angle of friction and angle of repose are investigated in the present study. Results indicated that with the increasing drum rotational speed the percentage of useful granules, fracture force, bulk density, angle of friction and angle of repose increase from 69.91% to 80.88%, 34.35 N to 35.23 N, 743.23 to 765.08 kg m^{-3}, 26.50 to 28.01º and 10.83 to 12.88º, respectively. Also the average size of granules decreases from 10.15 to 7.05 mm.

Keywords: drum granulation, compost fertilizer, drum .rotational speed, fracture force, granule size, granule mass

Introduction

High moisture content, high volume and non-uniformity of the materials in manure are the factors that limit the usage of the manure in agriculture. Normally, because of low specific gravity the transportation of manure fertilizers is difficult and expensive (Ghadernejad et al., 2012). Biomass is very difficult to handle, transport, store and utilize in its original form (Sokhansanj et al., 2005). On the other hand governments are looking for ways to dispose of municipal, mineral, industrial, and agricultural wastes. Spreading these wastes on agricultural land is perceived as the most appropriate solution if the wastes can be used to support plant production (Allaire and Parent, 2004). These wastes were spread directly on agricultural land. When the

wastes are combined with mineral fertilizers, the mineral part may compensate for the lack of certain nutrients in the wastes while the organic matter could improve the efficiency of the mineral fertilizers (Allaire and Parent, 2004).

One method to get easy storage, transportation, dispose of agricultural wastes and to decrease the costs is to reduce the volume of the manure by compression in granule form. The compressed manure can be used as the fertilizer in agricultural farms. This also eliminates the need for manure plants and reduces the cost of manure (Adapa et al., 2003). The agglomeration of fertilizer granules in storage, known as caking or bag set, is a significant quality assurance problem for the fertilizer industry. The agglomeration of fertilizer granules can take place over weeks or months in storage (Walker et al., 1999).

Granulation is one of the fundamental operations in particulate processing and has an ancient history and a widespread use. Much fundamental particle science has developed over the last few years to help understand the underlying phenomena. Yet, until recently the development of granulation systems was mostly based on popular practice (Cameron et al., 2005).

While a lot of research concerning granulation processes and physical and mechanical properties of granules in chemistry and pharmacy sciences have been made, a limited number of published literature are available about physical and mechanical properties of fertilizer granule. The mechanisms for granule growth (granulation) including nucleation, growth, random coalescence, pseudo-layering and crushing and layering were studied by Sastry and Fuerstenau (1973). Coalescence agglomeration occurs when two or more particles adhere together using a liquid as the binding agent. In industrial processes, binding liquids include water, water-based solutions and melts. Coalescence is random if the rate of agglomeration is size independent or preferential if agglomeration is size dependent (Walker et al., 2000). Litster and Liu (1989) in their research on the granulation of fertilizers have found that coalescence is the most probable mechanism for low temperature fertilizer granulation using a feed with a broad particle size distribution.

In the operation of drum granulation systems there are a number of process parameters that will affect the extent of size enlargement and physical properties of the final granulate. One of the important parameters is drum rotational speed. With low rotation speed, the granulate slides about the bottom of the drum with little agitation of the granules, with increasing drum speed the granule begins to roll, cascading occurs and the probability of agglomeration increases (Sherrington and Oliver, 1981). It has been suggested that the optimum drum speed is half the critical speed, where the critical speed is defined as the speed at which the dry material will be carried around the drum by centrifugal force (Walker et al., 2007). Effect of the viscosity of binder solution, flight arrangement and critical speed on fertilizer granulation procedure were studied by Walker et al. (2000).

The effect of the granulation parameters on physical properties of the granules is one of the most important factors in optimal granulation conditions. Therefore the

objective of the present work is to investigate the effect of rotational speed of the drum (ω) on some physical properties of granulated compost fertilizer including: useful granules, granules size, fracture force, mass of the granules, bulk density, angle of friction and angle of repose.

Materials and method

Production of granules

The powder used in the production of the granules was multicomponent fertilizer powder supplied by Moshaver Haseb Company. The granules were produced in a no internal flights drum granulation. Production of the granules for each batch was repeated three times. A schematic diagram of the experimental set up is shown in Fig. 1. Drum (3) was driven by electromotor (5) by means of a belt transmission and a clutch. A change of rotational velocity of the drum was obtained by means of inverter (6). The granular bed placed in the drum was wetted drop-wise by means of sprinkler (4), which was introduced axially to the device that ensured a uniform liquid supply. The sprayer was mounted on stand (8), which was independent of the granulator. The wetting liquid (Sugar beet molasses) was supplied from reservoir (1), placed at the height of 300cm from the drum axis and its constant flow rate ($Q = 10^{-6}$ m³/sec) was fixed by means of rotameter (2). During the experiment a constant liquid level was kept in the tank, which guaranteed a constant pressure of supplied liquid. The granular bed was wetted until the material got over-moist which caused that the bed stuck to the inner wall of the granulator (Obraniak and Gluba, 2012).
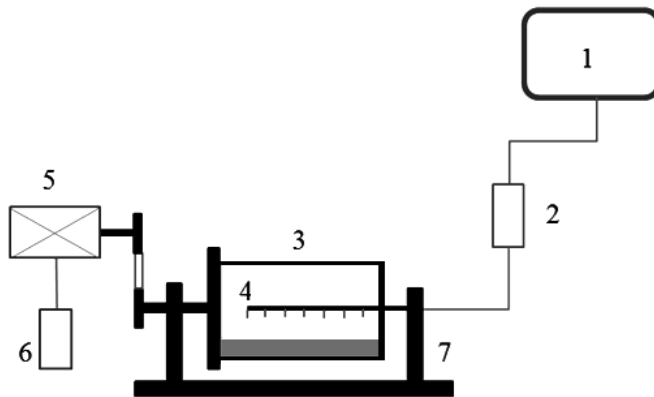

Fig. 1. A schematic diagram of the experimental set up

In the present work the following parameters were used: drum diameter $D = 200$ mm; drum length $L = 380$ mm, filling of the drum with granular material $\varphi = 7.5\%$. The solution to solid phase ratio, defined as the ratio of volume of liquid phase to that

of solid phase in the granule and is given by the equation 1 cited by Walker et al. (2000):

$$y = \frac{M(1-S)\rho_s}{(1-MS)\rho_L} \tag{1}$$

where y is solution to solid phase ratio, M is the moisture content, S is the fertilizer solubility, ρ_s is the solid fertilizer density and ρ_L is the liquid fertilizer density. For each granulation system, the fertilizer liquid and solid densities must remain constant.

Rotational speed of the drum (N) ranged from 40 rev min⁻¹ to 60 rev min⁻¹ (40, 45, 50, 55 and 60). The range change of drum angular velocity is selected in such a way to provide cascading – the typical feed movement for drum tumbling granulators (Obraniak and Gluba, 2012).

The critical rotational speed within drums is the speed at which material can be just carried around the drum by centrifugal action. In terms of the Froude number describing the ratio of inertial to gravitational forces, the critical rotational speed can be defined as:

$$\omega_{cr} = \frac{42.4}{\sqrt{D}} \tag{2}$$

where: ω_{cr} is the critical rotational speed (rev min⁻¹) and D is the drum diameter (m).

In practice, good granulation can be achieved in drums containing no internal flights when rotational speed (ω) ranged from $0.3\omega_{cr}$ to $0.5\omega_{cr}$. In the present work critical speed $\omega_{cr} = 94.81$ rev min⁻¹ is calculated using equation 2.

After granulation processes, wet granules were left in the atmosphere to dry. After being dried in the atmosphere, the granules were collected for measuring their physical properties.

Physical properties of granules

Physical properties of produced granules and effect of the granulation parameters on physical properties of the granule is one of the most important factors in optimal granulation conditions. Effect of the drum rotational speed on some physical properties of produced granules including: useful granules, granules size, granules fracture resistance, granules mass, bulk density, coefficient of friction and angle of repose of granules were studied in the present work.

Useful granules

For the purpose of the present work granules in the size range 5 to 10 mm were required. It was therefore necessary to optimize the process to ensure that the larger fraction of the granules from each batch would be within this size range. Any granules that are larger than 4 mm are regarded as oversize and these would need to be crushed in a continuous granulation circuit. Any granules passing through 5 mm were

classified as fines and these could be recycled by reintroducing them into the granulation process. The efficiency of the process, η, is defined as the percentage of the product which meets the size requirement (Mangwandi et al., 2012):

$$\eta = \frac{M_{\text{Target}}}{M_{\text{Total}}} \cdot 100 \tag{3}$$

where M_{Target} is mass of useful granules and M_{Total} is mass of the batch granules. The mass of the useful granules batch using sieving was measured. Determination of the percentage of the useful granules was repeated three times.

Granules size

The size distribution of the produced granules for each batch was determined using sieving. The stack of sieves with the granules was placed on an orbital sample shaker. Retsch sieves (Retsch GmbH, Germany) were used in the size analysis and the aperture sizes are as follows; 850, 1000, 1180, 1700, 2360, 3350, 4750, 12700 and 19050µm. The duration of sieving was adjusted according to size of the sample. The sieving times for the 500 g batches were 22 min respectively at a speed of 180 rpm. The masses of granules retained on the sieves to determine the size distribution of the granules were used. Determination of the average of the granule size was repeated three times.

Granules fracture force

To investigate fracture force, for each rotational speed of the drum, 20 granules in the shape close to spherical were taken from the bulk sample, and next each granule was placed separately between parallel compressing plates (mobile and immobile). The test lasted until the moment when the granule was destroyed between the compressing plates. Pneumatics press for measuring fracture force of the granules was used (Fig. 2).
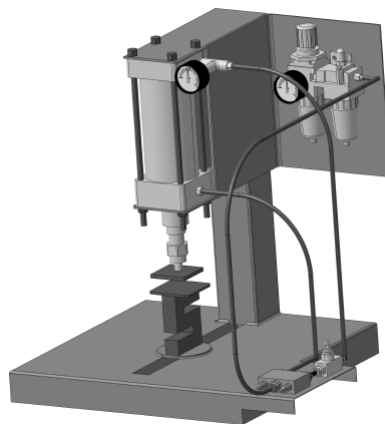

Fig. 2. Schematic of the pneumatics press

Bulk density

One of significant parameters that describe the properties of granular materials is bulk density. For the determination of bulk density, the bulk material (granules) was put into topless cylindrical container with known weight, height (150 mm) and volume (500 dm^3) from a height of 150 mm at a constant rate (Dash et al., 2008; Singh et al., 1996; Sacilik et al., 2003). Bulk density (ρ_b) was calculated from the mass of bulk granules divided by volume containing the mass. Measurement of the bulk density was repeated ten times.

Mass of the granules

In order to determine the effect of the drum speed on mass of the single granule, 100 granules were selected from the bulk samples, quite randomly. Then mass of the granules was measured. From bulk sample 300 granules were selected quite randomly; then granules were divided into three bins so that in each bin 100 seeds were placed. Bin weight was measured and multiplied by 10 to give mass of 1000 granules. The mass of the single granule and 1000 granules mass were measured using a digital balance with an accuracy of 0.01g.

Mass of granules distribution was modelled using log-normal probability density functions. The probability density functions $f(x)$ and cumulative frequency functions ($F(x)$) for Log normal distribution are showed in equation 4 and 5.

$$f(x) = \frac{1}{(x-\gamma)\sigma\sqrt{2\pi}} \exp\left[-\frac{1}{2}\left(\frac{\ln(x-\gamma)-\mu}{\sigma}\right)^2\right] \tag{4}$$

$$F(x) = \varphi\left(\frac{\ln(x-\gamma)-\mu}{\sigma}\right), \quad \varphi(x) = \frac{1}{\sqrt{2\pi}}\int_0^x e^{\frac{-t^2}{2}} dt \tag{5}$$

According to the equation 4 and 5, for the log-normal distribution, μ is scale parameter, σ is shape parameter and γ is location parameter. Whenever γ is equal to zero log-normal distribution is called two parameters distribution, otherwise it is called three parameters distribution. Whenever γ is equal to zero and μ equals one the log-normal distribution is called standard log-normal distribution (Mirzabe et al., 2012). In this study, Log-normal distribution with two parameters was used.

Angle of friction

The coefficient of external static friction, using iron sheet, was determined. A topless and bottomless metallic box with known dimensions (length 100 mm, width 100 mm and height 50 mm) was put on the surface. The box was filled by granules. The surface was gradually raised by the screw. Both horizontal and vertical height values were measured using a rule and digital caliper when the seeds started sliding over the surface and, the coefficient of static frication was calculated using the following equation (Burubai et al, 2007):

$$\mu_s = \tan A_F \tag{6}$$

where: μ_s is coefficient of static friction; A_F is angle of static friction. Measurement of the angle of friction was repeated ten times.

Angle of repose

Static angle of repose of granules was measured by the use of pouring method (Fraczek et al., 2007). The angle of repose was determined using a topless and bottomless metallic cylinder of 250 mm height and 150 mm diameter. The cylinder was placed at the iron surface and was filled with bulk material. The cylinder was raised very slowly. The height and diameter of the cone was measured using digital caliper and the static angle of repose was calculated using the following equation cited by Mirzabe et al. (2012):

$$A_R = \arctan\left(\frac{H}{R}\right) \tag{7}$$

where: A_R is angle of repose; H is height of the cone; R is radius of the cone. Measurement of the angle of repose was repeated ten times.

Results and discussion

The effect of rotational speed of the drum (ω) on some physical properties ofgranulated compost fertilizer including: useful granules, granules size, fracture force, mass of the granules, bulk density, angle of friction and angle of repose were investigated in present study.

Useful granules

The effect of rotational speed of the drum on percentage of the produced useful granules (η) is illustrated in Fig. 3. According to Fig. 3 with increasing drum rotational speed from 40 rev min^{-1} to 60 rev min^{-1}, percentage of the produced useful granules was increased from 69.9% to 80.9%. For the purpose of present work granules in the size range 5 to 10 mm were required. Therefore maximum percentage of the useful granules was produced when the rotational speed of the drum was equal to60 rev min^{-1}.

Granules size

The effect of drum rotational speed on average of produced granule size (D_{50}) is illustrated in Fig. 4. According to Fig. 4 with increasing drum rotational speed from 40 rev min^{-1} to 60 rev min^{-1}, average size of the produced granules was decreased from 10.15 mm to 7.05 mm. The effect of drum rotational speed on average size of produced granule of potassium nitrate was investigated by Rojas et al. (2005). Result

indicated that, when the rotational speed increased from 4 to 7 rev min^{-1} (RPM) average size of the produced granules decreased.
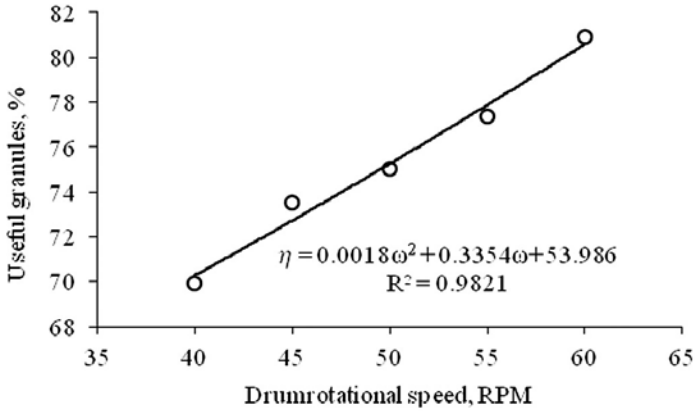
Fig. 3. Effect of drum rotational speed on percentage of useful granules

Fig. 4. Effect of drum rotational speed on average of size

Fracture force

The effect of drum rotational speed on fracture force of the produced granules (F) is illustrated in Fig. 5. According to Fig. 5 with increasing drum rotational speed from 40 rev min^{-1} to 60 rev min^{-1}, fracture force of produced granules was increased and then decreases from 34.35 N to 35.23 N.
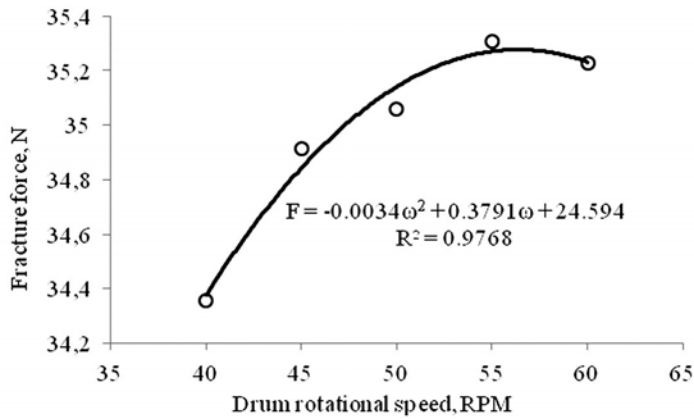
Fig. 5. Effect of drum rotational speed on fracture force

Bulk density

The effect of drum rotational speed bulk density of produced granules (ρ_b) is illustrated in Fig. 6. According to Fig. 6 with increasing drum rotational speed from 40 rev min^{-1} to 60 rev min^{-1}, bulk density of the produced granules was increased from 743.23 kg m^{-3} to 765.08 kg m^{-3}. The effect of rotational speed on bulk density of produced granules of bentonite was investigated by Heim et al. (2005). The results indicated that the effect of relative rotational speed appeared to be very small and could be considered negligible.
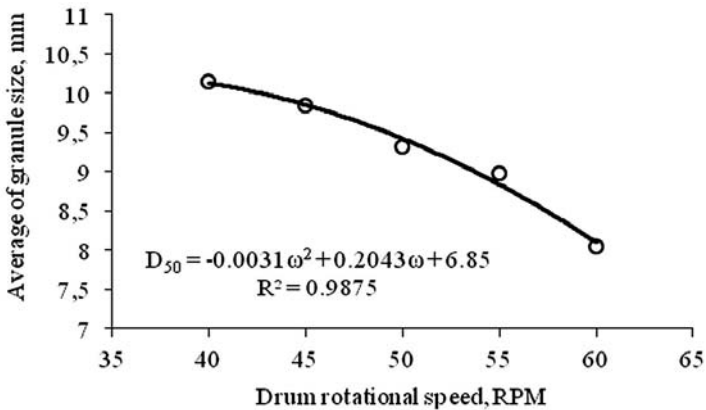

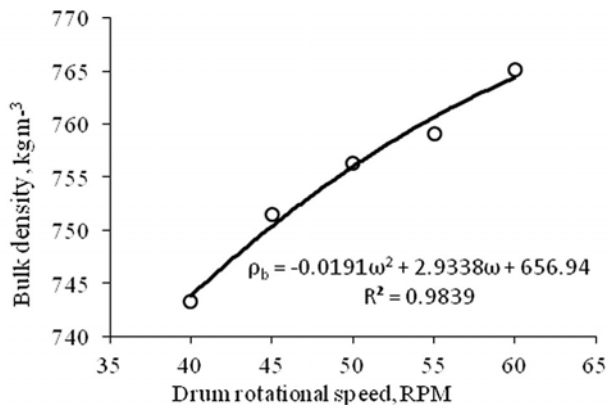Fig. 6. Effect of drum rotational speed on bulk density

Mass of the granules

The effect of drum rotational speed on mass of the produced granules (M_1) is illustrated in Fig. 7. According to Fig. 7 with the increaseof the drum rotational speed

from 40 rev min^{-1} to 50 rev min^{-1}, mass of the produced granules increased from 0.486 g to 0.639 g; but with the increaseof drum rotational speed from 50 rev min^{-1} to 60 rev min^{-1} mass of the produced granules decreased from 0.639 g to 0.548 g.

$$M_1 = -0.0012\omega^2 + 0.1216\omega - 2.496$$
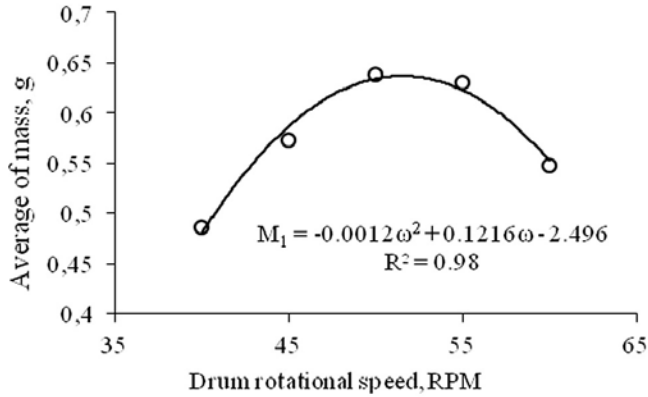$$R^2 = 0.98$$

Fig. 7. Effect of drum rotational speed on mass of granules

The distribution of mass of granules was modeled using log-normal probability density functions. The value of the log location parameter, log scale parameter, mean of log-normal distribution, variance of log normal distribution and log likelihood for each rotational speed were calculated (Table 1). The probability density functions of log-normal distributions for all rotational speed are showed in Fig. 8.

Table 1. Parameters of log normal distributions for mass of the granules

Rotational speed (rev min^{-1})	Log location parameter	Log scale parameter	Mean of distribution	Variance of distribution	Log likelihood
40	−1.012	0.892	0.540	0.355	−14.082
45	−0.797	0.814	0.628	0.371	−20.329
50	−0.655	0.681	0.655	0.253	−18.481
55	−0.661	0.761	0.690	0.373	−23.746
60	−0.854	0.849	0.610	0.393	−19.548

Angle of friction

The effect of drum rotational speed on angle of friction of produced granules (A_F) is illustrated in Fig. 9. According to Fig. 9 with increasing drum rotational speed from 40 rev min^{-1} to 60 rev min^{-1}, angle of friction of the produced granules was decreased from 26.50º to 28.01º.
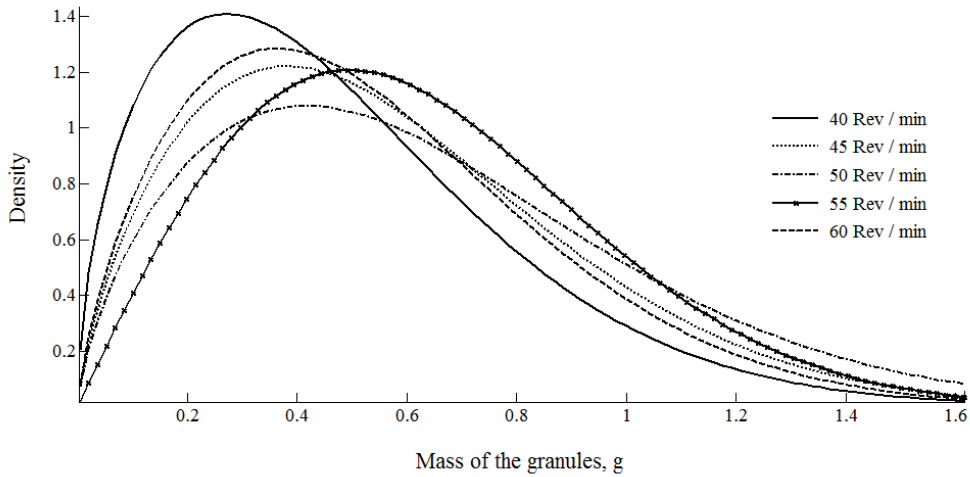
Fig. 8. Probability density function of Log normal distributions for all rotational speed

$$A_F = 0.0019\omega^2 - 0.118\omega + 28.128$$
$$R^2 = 0.995$$
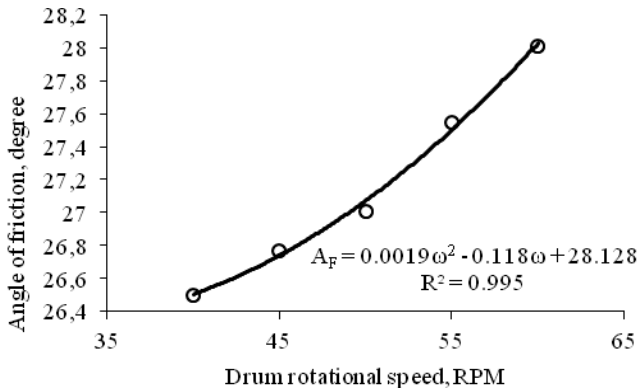
Fig. 9. Effect of drum rotational speed on angle of friction

Angle of repose

The effect of drum rotational speed on the angle of repose of produced granules (A_R) is illustrated in Fig. 10. According to Fig. 10 the angle of repose of the produced granules decreased from 10.8º to 12.9º with increasing drum rotational speed from 40 rev min^{-1} to 60 rev min^{-1}. Results of the angle of friction indicated that, with increasing drum rotational speed, angle of repose of the produced granules increased. Perhaps, with increasing drum rotational speed internal friction coefficient between granules increased, therefore with increasing coefficient of friction, angle of repose of the produced granules increased. Also increase in the value of the angle of repose with the increase in drum rotational speed can be caused by the size and shape of the granules.

Fig. 10. Effect of drum rotational speed on angle of repose

Conclusions

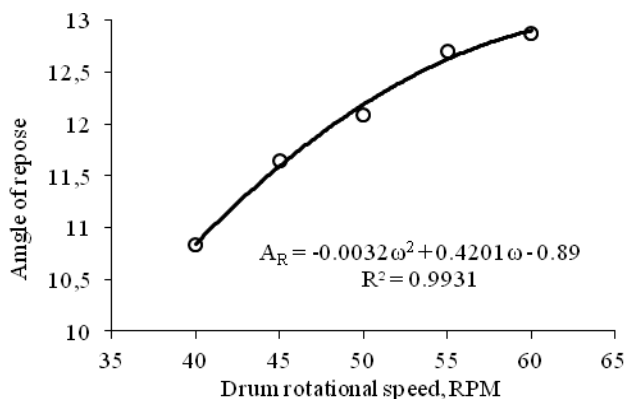In present study the effect of drum rotational speed (ω) on useful granules, granules size, fracture force, mass of the granules, bulk density, angle of friction and angle of repose of granulated compost fertilizer were investigated. The result indicated that, when the rotational speed increased from 40 to 60 rev min^{-1}:

1. percentage of the produced useful granules increased,
2. average size of the produced granules decreased,
3. fracture force of produced granules increased,
4. bulk density of the produced granules increased,
5. speed mass of the produced granules increased,
6. speed angle of friction of the produced granules decreased,
7. speed angle of repose of the produced granules decreased.

Acknowledgements

References

ADAPA P., BUCKO J., TABIL JR L., SCHOENAU G., SOKHANSANJ S, 2003, *Pelleting characteristics of fractionated suncure and dehydrated Alfalfa grinds*, The society for in agricultural, food, and biological systems, 192−207.

ALLAIRE S. E., PARENT L. E, 2004, *Physical properties of granular organic-based fertilizers, Part 1: Static Properties*, Biosystems Engineering, 87 (1), 79–87.

BURUBAI W., AKOR A. J., IGONI A. H., PUYATE Y. T, 2007, *Some physical properties of African nutmeg (Monodoramyristica)*, Int. Agrophysics, 21, 123-126

CAMERONA I. T., WANGA F. Y., IMMANUELB C. D., STEPANEKB F, 2005, *Process systems modeling and applications in granulation: a review*, Chemical Engineering Science, 60, 3723 – 3750.

DASH, A. K., PRADHAN, R. C., DAS, L. M., NAIK, S. N, 2008, *Some physical properties of simarouba fruit and kernel*, International Agrophysics, *22*(2), 111.

FRACZEK J., ZŁOBECKI A., ZEMANEK J, 2007, *Assessment of angle of repose of granular plant material using computer image analysis*, Journal of Food Engineering, 83: 17–22

GEZERMAN A. O, 2012, *Design of a Fluidized Drum Granulator for Ammonium Nitrate Production*, International Journal of Modern Engineering Sciences, 1(2), 88-96

GHADERNEJAD K., KIANMEHR M. H., ARABHOSSEINI A, 2012, *Effect of moisture content and particle size on energy consumption for dairy cattle manure pellets*, AgricEngInt: CIGR Journal, 14(3), 125−130.

HEIM A, OBRANIAK A, GLUBA T, 2005, *Changes of Feed Bulk Density During Drum Granulation of Bentonite,* Physicochemical Problems of Mineral Processing. 39, 219–228

LITSTER J. D., LIU, L. X ,1989, *Population balance modelling of fertilizer granulation*, Proc 5th International Symposium on Agglomeration, Sept 25-27, Brighton UK, 611-621.

MANGWANDI C., ALBADARIN A. B., AL-MUHTASEB A H., ALLEN S.J., WALKER G M, 2012*, Optimisation of high shear granulation of multicomponent fertiliser using response surface methodology*, Powder Technology, article in press.

MIRZABE A.H., KHAZAEI J., CHEGINI G.R, 2012*, Physical properties and modeling for sunflower seeds*, AgricEngInt: CIGR Journal, 14(3) 190−202.

OBRANIAK A., GLUBA T, 2012, *Model of energy consumption the range of nucleation and granule growth in drum granulation of Bentonite*, Physicochemical Problems of Mineral Processing. 48(1), 121–128.

SACILIK K., OZTURK R., KESKIN R, 2003. *Some physical properties of hemp seed*, Biosystems Engineering, 86 (2), 191–198.

SASTRY. K. V. S., D.W. FUERSTENAU, 1973, *Mechanisms of Agglomerate Growth in Green Pelletization*, Powder Technol, 7, P97–P105.

SHERRINGTON P. J., OLIVER R, 1981,*Globulation processes, in granulation*, Heyden and Son ltd, London, 118−140.

SINGH K. K., GOSWAMI T. K, 1996, *Physical properties of cumin seed*, Journal of Agricultural Engineering Research, 64 (2), 93–98.

SOKHANSANJ S., MANI S., BI X., ZAINI P., TABIL L. G, 2005, *Binderlesspelletization of biomass*, ASAE Annual International Meeting, Tampa Convention Centre, Tampa, Florida July 17-20, Paper Number 056061, 2950 Niles Road, St. Joseph, MI 49085–9659, USA.

WALKER G. M., HOLLAND C. R., AHMAD M. N, 1999, *Granular fertilizer agglomeration in accelerated caking tests*, Ind. Eng. Chem, Res, 38, 4100–4103.

WALKER G. M., HOLLAND C. R., AHMAD M. N., FOX J. N., KELLS A. G, 2000*, Drum granulation of NPK fertilizers*, Powder Technology, 107, 282–288.

WALKER, G. M,2007*, Chapter 4: Drum Granulation Processes*, Handbook of Powder Technology, 11, 219–254.

PREDICTION OF ON-LINE FROTH DEPTH MEASUREMENT ERRORS IN INDUSTRIAL FLOTATION COLUMNS: A PROMISING TOOL FOR AUTOMATIC CONTROL

Fardis NAKHAEI[*], Mehdi IRANNAJAD[**]

[*]   Department of Mining & Metallurgical Engineering, Amirkabir University of Technology, Tehran, Iran,
     fardis_nakhaei@aut.ac.ir
[**] Department of Mining & Metallurgical Engineering, Amirkabir University of Technology, Tehran, Iran,
     iranajad@aut.ac.ir

Abstract: The pulp-froth interface position is important from a metallurgical point of view because it determines the relative importance of the cleaning and the collection zones. The pulp-froth interface position is measured based on variations of specific gravity, temperature or conductivity between the two zones to locate the pulp froth interface position. In this study, the pressure measurements are used to calculate the values of the froth layer height. These two meters are installed in the upper part of the column at 1.4 m and 2.4 m respectively, from the top of the column. Methods using pressure gauges are commonly used in industrial operations Even though their accuracy is limited (due to assumptions of uniformity of the pulp and froth density), and they always have some error. In the Sarcheshmeh copper industrial plant (Iran), a float was installed near the column with 2.5 m height that was calibrated to 5 cm intervals in order to determine the more exact forth height and compare it with the recorded froth height in control room. In this paper, an algorithm based on Kalman Filter is presented to predict on-line froth height errors using two pressure gauges. This research is based on the industrial real data collection for evaluating the performance of the presented algorithm. The quality of the obtained results was very satisfied. The RMS errors of prediction froth height errors was less than 0.025 m.

Keywords: *prediction; accuracy; froth height; Kalman filter; error*

Introduction

Nowadays column flotation is an important mineral processing unit. Figure 1 presents a simplified scheme of a flotation column that consists of two principal zones: the collection zone (less than 20% of air) and the froth zone (more than 70% of air). The pulp feed (15–40% solids) enters near the top of the collection zone. Hence, particles

are contacted counter-currently with air bubbles generated near the bottom of the column. Hydrophobic particles collide and adhere to the bubbles and they move upwards to the pulp/froth interface. The froth zone is a mobile bubble bed, approximately 1 m in froth depth, which is contacted counter-currently with wash water (added near the overflow level).

Level control in flotation columns is an important factor that influences the recovery and grade of concentrate from the column. A flotation column is a nonlinear, multi-variable problem with changeable parameters that traditional methods have difficulty controlling.

When the pulp level is too high the concentrate overflows too much and the grade of the concentrate is reduced. When the pulp level is too low the concentrate yield may be reduced, which also results in a reduction in the recovery.
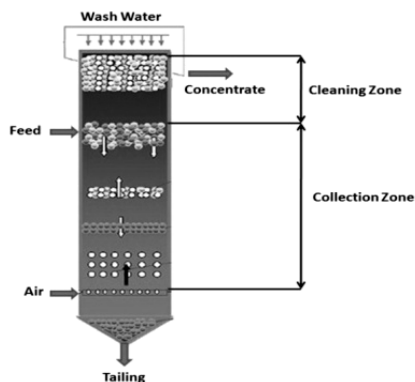
Fig. 1. Flotation column

Many techniques have been proposed in the past for the froth depth measurement. The most common were summarized by Finch and Dobby (1990) and some further developments were presented by Bergh and Yianatos (1995) and Del Villar et al. (1999). All these methods use the difference in physical characteristic, such as specific gravity, temperature or conductivity, between the pulp and the froth to locate the pulp froth interface position. Even though the principles behind these methods are fairly simple, some of them have encountered important operating problems that limit their accuracy. Nevertheless, methods based on the use of a float or pressure gages (one to three) are commonly used and seem to be precise enough for day-to-day process supervision.

Some experimental works, for example Hyma and Salama (1993) as well as Pal and Masliyah (1991), discussed and tested the control of the froth layer height by manipulating the non-floated flow rate in a pilot plant using PI controllers. Del Villar et al. (1999) designed and implemented a distributed PI controller in which the bias and the froth layer height were controlled by manipulating the wash water flow rate and the non-floated flow rates, respectively.

More recently, artificial neural network (ANN) based system identification and model predictive control of a flotation column has been reported by Mohanty (2009). The ANN is an empirical modeling tool, which is analogous to the behaviour of biological neural structures. ANNs are very powerful to effectively represent complex non-linear systems. It is also considered as a non-linear statistical identification technique. He describes the design of a ANN based model predictive controller for controlling the interface level in a flotation column.

The pulp level in a floatation column changes frequently during operation because of changes to the nature of the pulp and the varying discharge rate. Methods using pressure gauges are commonly used in industrial operations even though their accuracy is limited (due to assumptions of uniformity of the pulp and froth density), and they always have some error.

Until now, most studies have focused in importance of froth height system accuracy in floatation operation, and there are not any report in the field of prediction and correction of errors in this system.

This paper aims at presenting a new method to get prediction of froth depth measurement errors using Kalman Filter (KF) on the pressure profile along the column upper section. A KF is an algorithm for obtaining a minimum mean square error point estimate of a random process. In this study, the Kalman Filter method was done using data from case study on CISA flotation column at the Sarcheshmeh copper plant in Iran.

Industrial plant

The Sarcheshmeh copper ore body which may rank as third or fourth largest in the world contains 1 billion tones (1 petagram) averaging 0.90% copper and 0.03% molybdenum. The process consists of grinding circuit with their associated flotation circuits. Figure 2 shows the flotation circuit of the Sarcheshmeh concentrator plant.

The flotation circuit consists of rougher, cleaning and column flotation stages. The rougher flotation bank consists of 8 cells (130 m^3) and the regrind mill is a 3.962 m by 5.791 m ball mill. The cleaner, scavenger banks each have 3 (50 m^3), 5 (50 m^3) cells, respectively. The single stage column flotation operation is composed of a Metso Minerals CISA column with 4 m internal diameter, 12 m height and associated instruments (Fig. 3). A final product with an average grade of 28–30% Cu (chalcopyrite and chalcocite) and 0.7–0.8% Mo are obtained after flotation stages.

The primary objectives are column recovery and concentrate grade, which represent the indices of process productivity and product quality. Common practices to control secondary objectives, such as pH at the feed, froth depth, air flow rate and wash water flow rate. These are usually implemented as local controllers or under Distributed Control Systems (DCS). Ideally, when primary objectives are measured, the control strategy is to change the set points of the controllers under DCS, in order to achieve a good process performance.
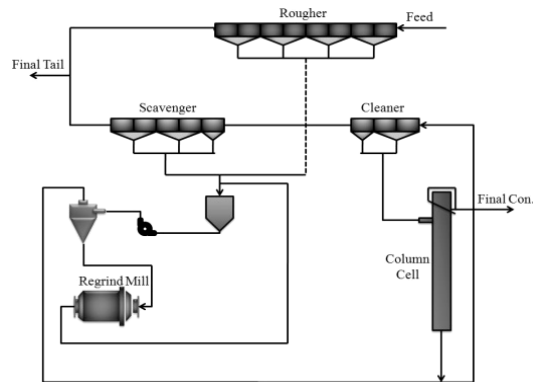
Fig. 2. The flow sheet of flotation circuit of the Sarcheshmeh industrial plant

Fig. 3. Sarcheshmeh industrial plant flotation column

Figure 4 illustrates simplified flotation column instrumentation with all of the variables included. The wash water flow rate is measured by means of an electromagnetic flow meter and controlled by a pneumatic valve. The air flow rate is measured by a mass flow meter and controlled by a pneumatic valve. The pulp feeding is controlled by means of a peristaltic pump with variable speed. Since the non-floated fraction flow rate is not directly measured, it must be inferred from the signal sent to the corresponding frequency inverter. The use of a peristaltic pump to control this flow rate requires special attention, due to the pressure variation at the pump inlet during the operation.

The instruments and the actuators (pumps and valves) are all connected to a data acquisition system which takes care of the analog-to-digital conversion of the output variables and of the digital-to-analog conversion of the manipulated variables.

The pressure measurements (P_1 and P_2 taken, respectively, by LT) are used to calculate the values of the air hold up in the recovery zone and of the froth layer height. These two meters are installed in the upper part of the column at H_1 and H_2, respectively, at 1.4 m and 2.4 m from the top of the column. Each sensor required to 12–53 DC volt energy source and transfer 4–20 mA flow to control system. A real

time data acquisition system was used to store the operating variables on a PC computer hard disk. The ultimate objective of automatic control is to continuously adjust process operation to maintain the best profitability despite disturbances and uncertainties while respecting constraints such as safety and environmental issues. To achieve this goal, a hierarchical indirect optimization structure is often selected.
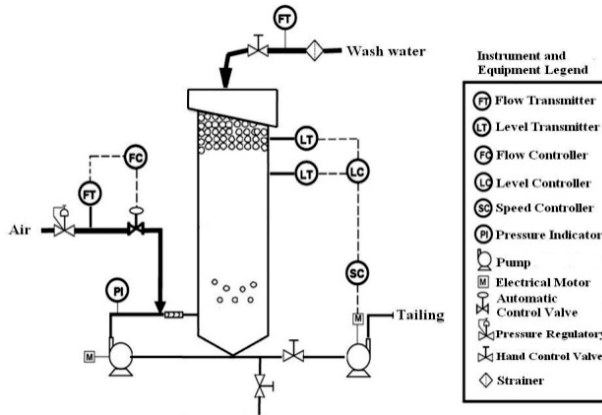
Fig. 4. Schematic diagram of the flotation column and associated instrumentation

Froth height

Interface position is important from a metallurgical point of view, because it determines the relative importance of the cleaning and collection zones. Many techniques have been proposed in the past for froth depth measurement. All these methods use the difference in a physical characteristic, such as specific gravity, temperature or conductivity, between the pulp and the froth to locate the pulp-froth interface position. Nevertheless, methods based on the use of a float or pressure gauges (one to three) are commonly used. The approach privileged in this work is based on the use of two pressure gauges and a float (Fig. 5). The relationships between the pressure values and the process variables can be expressed by:

$$P_1 = (H_1 - H_f)\rho_c g + H_f \rho_f g \tag{1}$$

$$P_2 = (H_2 - H_f)\rho_c g + H_f \rho_f g \tag{2}$$

$$\rho_c = \frac{P_2 - H_f \rho_f g}{(H_2 - H_f)g} \tag{3}$$

The froth layer height is inferred from the measured pressures and is given by equation (4):

$$H_f = \frac{\dfrac{(P_2 - P_1)H_1}{H_2 - H_1} - P_1}{\dfrac{P_2 - P_1}{H_2 - H_1} - g\rho_f} \tag{4}$$

where P_1 and P_2 are the pressure measured values (Pa), $H_1 = 1.4$ m and $H_2 = 2.4$ m (pressure meters distance from the top of the column) and ρ_f and ρ_c are the average value of the froth layer density and pulp in collection zone (kg/m^3), respectively.
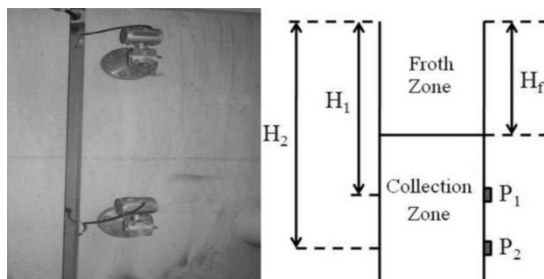
Fig. 5. Two pressure gauges are installed in the upper part of the column

The plant sensors provide raw measurement of secondary variables. Since measurements may be corrupted by bias, noise and even sensor failures, an observer is essential. Observation and data reconciliation, supervised by process and sensor fault detection and diagnosis techniques, extract consistent and reliable information from raw measurements, can infer unmeasured process states or temporarily replace defective sensors, etc. In the Sarcheshmeh copper plant, a float was installed near the column with 2.5 m height which is calibrated to 5 cm intervals, in order to, determine the accurate forth height and compare it with the recorded forth height in control room (measured froth height by two pressure gages) that is observable continuously by camera (Fig. 6).

Fig. 6. Installed float near the column

Research method

Kalman Filter formulation

The KF is an optimal estimation technique that minimizes the estimation error in a well-defined statistical sense. As a linear filter using a recursive algorithm which processes measurement information sequentially in time, the KF involves two main steps: filtering and prediction. Filtering is the estimation of the state vector at the current epoch based on all previous measurement information.

Prediction involves the estimation of the state vector X at a future time (Simon, 2006). The KF system state vector (dynamic model) which evolves with time can be written as:

$$X_{k+1} = \phi_k X_k + W_k .$$ (5)

corresponding to the measurement vector (measurement model):

$$Z_k = H_k X_k + V_k$$ (6)

where $W_k \sim N_k(0, Q_k)$ and $V_k \sim N_k(0, R_k)$ are the system and measurement noises which are mutually uncorrelated vectors. Subscript k refers to the epoch of time. The processes W and V are independent, zero mean Gaussian proportional to σ_ω^2 and σ_v^2 variances. σ_ω^2 coefficient and also β_1, β_2 are estimated using autocorrelation equations as described below (Mosavi et al., 2010):

$$\sigma_\omega^2 = R_{SS}(0) - \beta_1 R_{SS}(1) - \beta_2 R_{SS}(2)$$ (7)

$$\beta_1 = \frac{R_{SS}(0)\, R_{SS}(1) - R_{SS}(1)\, R_{SS}(2)}{R_{SS}^2(0) - R_{SS}^2(1)}$$ (8)

$$\beta_2 = \frac{-R_{SS}^2(1) + R_{SS}(0)\, R_{SS}(2)}{R_{SS}^2(0) - R_{SS}^2(1)}$$ (9)

$$\hat{R}_{SS}(k) = E\{X(n)X(n+k)\}, \quad k = 0,\ 1,\ 2$$ (10)

where ϕ is the transition matrix. A KF requires that the system model to be in state-space form. In this modeling, the transition matrix can be obtained by using the time-varying Auto-Regressive (AR) model. AR is a famous model, which is used in a discrete-time stochastic process. A time varying AR model of second-order is mathematically described by:

$$y(k) = -a_1(k)y(k-1) - a_2(k)y(k-2) + e(k)$$ (11)

where $y(k-i)$ demonstrates the output of the model and $e(k)$ describes the noise value of the system at time k for $k = 1, 2....$ $a_i(k)$ for $i = 1, 2$ is the sets of parameters which describes the model structure. To identify the system, the parameters α_i should be calculated in a way that summation of square errors gets the minimum value. The parameter matrix θ_k may be estimated using the least-squares (LS) method as shown by Mosavi et al., 2002:

$$\theta_k = (F_k^T F_k)^{-1} F_k^T Y_k \tag{12}$$

where matrices F_k and Y_k are calculated as follows:

$$F_k = \begin{bmatrix} y(k-1) & y(k-2) \\ y(k) & y(k-1) \end{bmatrix} \tag{13}$$

$$Y_k = \begin{bmatrix} y(k) \\ y(k-1) \end{bmatrix}. \tag{14}$$

Once the model parameters $a_i(k)$ are known, the value of function $y(k)$ for an arbitrary k can be computed as follows:

$$y(k) = -a_2 y(k-1) - a_1 y(k-2). \tag{15}$$

In order to generate state-space some AR differential equations should be used as the sequence of equations below show:

$$\begin{aligned} x_1(k) &= y(k-2) \\ x_2(k) &= x_1(k+1) = y(k-1) \end{aligned} \tag{16}$$

or

$$\begin{aligned} x_1(k+1) &= x_2(k) \\ x_2(k+1) &= -a_2(k)x_2(k) - a_1(k)x_1(k). \end{aligned} \tag{17}$$

Finally, we are led to the following canonical controllable state-space representation:

$$\begin{bmatrix} x_1 \\ x_2 \end{bmatrix}_{k+1} = \begin{bmatrix} 0 & 1 \\ -a_1 & -a_2 \end{bmatrix}_k \begin{bmatrix} x_1 \\ x_2 \end{bmatrix}_k \tag{18}$$

in which, the transition matrix ϕ_k is resulted from:

$$\phi_k = \begin{bmatrix} 0 & 1 \\ -a_1 & -a_2 \end{bmatrix}_k . \tag{19}$$

In the KF formulation, H is the measurement connection matrix. Elements of H are the partial derivatives of the predicted measurements with respect to each stage and must be computed for every epoch.

The respective Kalman filtering algorithm involves Kalman gain (K), covariance update (P_k) and prediction (P_{k+1}^-), in the time update and measurement update steps. The brief description of second-order KF algorithm is as follows (Mosavi et al., 2006):

Step 1: Initialize KF parameters

$$R = [\sigma_\omega^2] \tag{20}$$

$$Q = \begin{bmatrix} 0 & 0 \\ 0 & \sigma_\omega^2 \end{bmatrix} \tag{21}$$

$$P_0^- = \begin{bmatrix} 1 & 0 \\ 0 & 1 \end{bmatrix} \tag{22}$$

$$\hat{X}_0^- = \begin{bmatrix} 0 \\ 0 \end{bmatrix} \tag{23}$$

$$H = [0 \quad 1] \tag{24}$$

Step 2: Calculate Kalman gain

$$K_k = P_k^- H_k^T (H_k P_k^- H_k^T + R_k)^{-1} \tag{25}$$

Step 3: Update the estimation process

$$\hat{X}_k = \hat{X}_k^- + K_k(Z_k - H\hat{X}_k^-) \tag{26}$$

Step 4: Update the error covariance

$$P_k = (I - K_k H_k)P_k^- \tag{27}$$

Step 5: Project the state ahead

$$X_{k+1}^- = \phi_k \hat{X}_k \tag{28}$$

Step 6: Project the error covariance ahead

$$P_{k+1}^- = \phi_k P_k \phi_k^T + Q_k.$$ (29)

Data collection

The data for this study were collected during the normal operation of the Sarcheshmeh concentration plant. Flotation column is operated under distributed control of froth depth, and chemical reactive dosages, to collect operation data at steady state. In order to collect real data to assess efficiency of suggested method, 300 observations of froth height were provided in 60-hours simultaneously with float and tow pressure gauges, i.e. that during the measurement period (12 minutes), the froth height was measured at the same time twice, one by pressure gauges and the other by float. Field instrumentation was installed and calibrated, and data signals communicated to a PC computer.

Results and Discussion

The previous section provided the algorithm for the KF and the means for estimating the quantities needed to start the filter. In this section the implementation of the KF for use in predicting the error of the two pressure gages will be described. Figure 7 shows the comparison plots of the measured froth height by pressure gages and the actual froth height for 60-hours data set. The prediction of froth height error by using KF was estimated by the MATLAB software. The results are shown in Fig. 8 and Tables 1.

The performances of the models developed in this study have been assessed using various standard statistical performance evaluation criteria. The statistical measures considered have been correlation maximum, minimum average and root mean square (RMS) error. The RMS criteria is calculated according to the following equation:

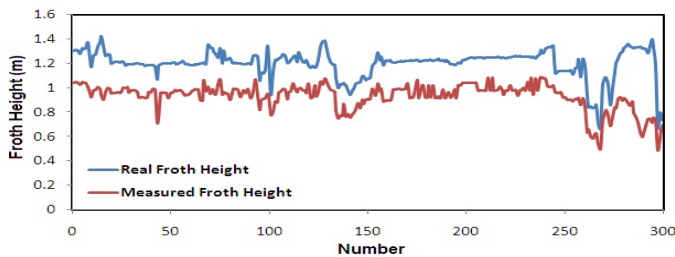$$RMS = \left[\frac{1}{n} \sum (X-Y)^2 \right]^{\frac{1}{2}}$$ (30)

Fig. 7. Comparison of real froth height values
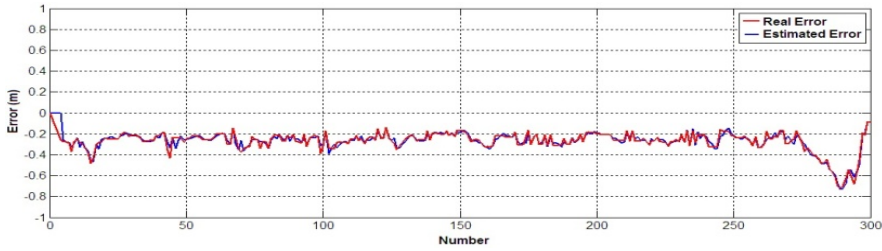in column flotation floatation with measured values

Fig. 8. Comparisonof predicted results using the KF model
with actual errors values for froth height in the flotation column

Table 1. Maximum, minimum, average and RMS errors in the prediction
froth height errors in the column flotation using KF

Parameters	Measured froth height error prediction error (m)
Maximum	0.099
Minimum	–0.1131
Average	0.0002
RMS	0.025

Table 1 presents the error values in the prediction of froth height errors in the column flotation by using KF when RMS is lower than 0.025 m. From these results, a KF model which can be used to predict the error of a sensor with an acceptable error. Also, the result from a test of real data shows that the KF method will guarantee access to more accurate froth height by prediction and correction of sensor measurement errors.

Conclusion

In this paper, we have provided a summary and improvements of the most common techniques used in the flotation column for measurement of froth height. We have shown that the standard implementation of the Kalman filter provides proper forecast of random error. It is able to provide an efficient analysis when measurements are available. The method described in this paper is based on KF using real data from industrial scale in order to predicate measured froth height errors of the Sarcheshmeh copper complex. The quality of the obtained results was very satisfied. The RMS errors of prediction froth height errors were less than 0.025 m. Moreover, with correction of predicted errors, it can be possible to reduce RMS errors in on-line analyzers. Therefore, the implementation of estimators such as Kalman Filter could significantly improve the measuring of the froth depth and as well as the column metallurgical performance. This could lead to great possibilities for plant optimization of the flotation column process.

Acknowledgments

References

BERGH L., YIANATOS J., ACUA C., 1995. Hierarchical Control Strategy for Flotation Columns. Minerals Engineering, 8(12), 1583-1591.

DEL VILLAR R., GREGOIRE M., POMERLEAU A., 1999. Automatic Control of a Laboratory Flotation Column. Journal of Minerals Engineering, 12(3), 291–308.

FINCH J. A., DOBBY G. S., 1990. *Column Flotation*. Pergamon Press.

HYMA D., SALAMA A. I. A., 1993. Design and Implementation of a Process Control System for Column Flotation", Vol.86, No.973, CIM Bulletin, 50–54.

MOHANTY S., 2009. Artificial Neural Network Based System Identification and Model Predictive Control of a Flotation Column. Journal of Process Control, 19(6), 991–999.

MOSAVI M. R., 2006. Comparing DGPS Corrections Prediction using Neural Network, Fuzzy Neural Network, and Kalman Filter. Journal of GPS Solution 10 (2), 97–103.

MOSAVI M. R., MOHAMMADI K., REFAN M. H., 2002. Time Variance ARMA Processing on GPS Data to Improve Positioning Accuracy. The Asian GPS Conference, 125–128.

PAL R., MASLIYAH J. 1991.Process Dynamics and Control of a Pilot Flotation Column", Canadian Metallurgical Quaterly, Vol.30, No. 2, 87–94.

SIMON D., 2006. *Optimal State Estimation Kalman and Nonlinear Approaches*. John Wiley.

Professor Jerzy Sablik, Ph.D., D.Sc.

a tribute on his 80th birthday

Jerzy Sablik was born on 20 May 1933. In 1951, in Cieszyn, he received a secondary school certificate. In 1954 he graduated with a B.Sc. degree in chemistry from the Higher School of Pedagogy (WSP) in Katowice (presently the University of Silesia). Over the next 12 years he worked for the Centre of Teaching Education (Zakład Kształcenia Nauczycieli) and in the Medical Secondary School. In 1956 he started to continue his education at the Jagiellonian University and in 1959 he graduated with a M.Sc. degree in chemistry. In 1960 he was awarded a doctoral scholarship from the Polish Ministry of Education and started his Ph.D. under supervision of prof. Zbigniew Kwapniewski. In 1966 he received the Ph.D. degree after defending his dissertation entitled "Analiza estrów fosforowych inozytolu metodą elektroforezy bibułowej w komorze wilgotnej". In 1965–1966 he worked as a volunteer at WSP Katowice, Department of Organic Chemistry. In 1967 he started his work in the Central Mining Institute in Katowice, where he spent the rest of his scientific life. He received the degree of *doctor habilitatus* (D.Sc.) in technical science in 1987 after submitting the thesis entitled "Własności powierzchniowe węgli kamiennych i stymulatory ich aktywności flotacyjnej". The President of Poland conferred on him the title of Professor of Engineering Sciences in 1999.

Jerzy Sablik worked in the Central Mining Institute in Katowice as a technician, assistant professor, associate professor, professor and academic consultant, respec-

tively. He was a head of the Laboratory of Flotation, a vice head of the Department of Mineral Processing and Waste Management, and a leader of scientific area of "Clean coal technologies". He was also an expert in coal preparation and physicochemical and technological properties of the fine coal particles. Prof. J. Sablik retired on January 1, 2007.

Prof. Jerzy Sablik has published 165 research papers (32 in English) in national and foreign journals, more than 50 papers at national and foreign conferences, congresses and symposiums, 23 patents and 7 standards. He is an author of several monographs including "Flotacja węgli kamiennych" 1998, "Fizykochemiczne właściwości powierzchniowe węgli kamiennych", 2007, and a co-author (with Marek Lenartowicz) of "Energetyczne właściwości powierzchniowe ziaren w produktach przemysłowej flotacji węgla", 2007.

Prof. Jerzy Sablik was a supervisor of 5 and reviewer of 12 doctoral dissertations. He reviewed 6 applications for the position and title of professor, and 4 for the title of *doctor habilitatus*.

Professor Jerzy Sablik was a chairman of several national and international organizing committees, seminars and scientific meetings, including:

- Scientific Industry Seminars of Coal Flotation (1978–1993) (Naukowo-przemysłowe seminaria flotacji węgla w ramach "Dni Techniki ROW"), acting as an editor of eight proceedings volumes
- Technical Committees of Standardization for the Natural Solid Fuels and for the Mechanical Processing of Coal (1993–2007) (within Polish Standardization Committee)
- the chairman of Polish delegation to the Technical Committee of ISO/TC27 "Natural Solid Fuels" (1995, Beijing, China; 1997, Cape Town, RSA; 1999, Norfolk, USA; 2001, Szczyrk, Poland). He was an editor of the Flotation section of the International Coal Preparation Congress held in 1994 in Cracow
- the International Conference on Clean Coal, Regional Direction of Sustainable Energy Production (2001) (Czysty węgiel, racjonalny kierunek zrównoważonego rozwoju produkcji energii), which was organized in co-operation with the Energy Committee in the European Commission of Economy ONZ.

Professor Jerzy Sablik is a member of Mineral Resources Beneficiation Section of Mining Committee of Polish Academy of Sciences and Mining Commission (Mineral Processing Section) as well as Chemical Science Commission of Polish Academy of Sciences (Katowice Branch).

Jerzy Sablik was an expert of the Polish Association of Mining Engineers and Technicians in the field of mechanical processing of coal. He was a founding member of the Polish Mineral Engineering Society, vice-president in 1996–1999 and president in 2000. He is a member of editorial boards of the Journal of the Polish Mineral Engineering Society Inzynieria Mineralna, Physicochemical Problems of Mineral Processing, and a member of committee of the Scientific Papers of Central Mining Institute (Prace Naukowe Głównego Instytutu Górnictwa).

Initially, his research interests included issues related to the use of thin-layer chromatography and electrophoresis for analysis of selected organic compounds. In the Central Mining Institute he focused on theoretical and technological properties of coal preparation, especially physicochemical aspects of upgrading, including:

- determination of impact of various technological parameters on coal flotation
- new method of wetting surface tension measurement for coal covered with different flotation reagents
- determination of wetting surface tension at zero contact angle
- determination of surface properties of different types of coal with native surface and surface covered with different flotation reagents to optimize flotation process
- study of new groups of flotation reagents called promoters and an explanation of their activity mechanism
- study of the three-phase flotation foams properties to determine flotation and drain processes
- foundations of steam coal flotation
- construction of new machines and devices for physicochemical methods of upgrading
- purification of contaminated soil using mineral oils used in mineral processing
- presence of organic sulfur in coal and its desulfurization
- application of statistics for prediction and evaluation of coal preparation.

He and his team developed 18, implemented in industry, technologies, including:
- standard flotation technology of coal
- flotation technology of coal with low concentration of solid
- steam coal flotation technology
- column flotation technology in the FLOKOB column
- new groups of flotation reagents called promoters
- modification of the three–phase flotation foams to improve drain process
- conditioning technology of coal slurry in the UFOZ device.

For his community work Professor Sablik has received dozens of awards, medals and distinctions in Poland, including the Knight's and Officer's Crosses of Polonia Restituta, the Silver and the Gold Crosses of Merit, the Gold Badge of Merit Mining, and others. He is a General Director of Mining (grade III).

Prof. Sablik was married with Daniela (she died in 2009). In 2004 the President of Poland honored him the "Medal for long-term marital status". He is a father of two sons, Krzysztof and Bogdan, a grandfather of Michal, Tomasz, Anna and Wojciech and a great-grandfather of Witold.

He likes classical music, skiing, swimming, hiking and travelling. He was the organizer of many hiking and camping groups.

List of publications

1. Kwapniewski Z., Gliwiński K., Sliwiok M., Szulik J., John A., Sablik J., Kozakiewicz M.: *Chromatografia bibułowa i cienkowarstwowa barwników sudanowych*. Zeszyty Naukowe WSP, Katowice, 6. s. 15–21, 1965.

2. Kwapniewski Z., Sablik J.: *Próba analizy soli sodowej kwasu inozytosześciofosforowego oraz produktów jej hydrolizy metodą chromatografii cienkowarstwowej*. Zeszyty Naukowe WSP, Katowice, Sekcja chemii 7, s. 45–49, 1967.

3. Kwapniewski Z., Sliwiok M., Sablik J.: *Teoretyczne wyznaczenie współczynników Rf dla szeregu homologicznego wyższych kwasów tłuszczowych w metodzie chromatografii bibułowej*. Zeszyty Naukowe WSP, Katowice, Sekcja chemii 7, s. 7–15, 1967.

4. Sablik J., Kwapniewski Z.: *Próba rozdziału estrów fosforowych inozytolu metodą elektroforezy cienkowarstwowej w komorze wilgotnej*. Zeszyty Naukowe Uniwersytetu Śl., Katowice, Sekcja chemii 8/41, s. 55–59, 1968.

5. Sablik J., Kwapniewski Z.: *Rozdział kilku produktów hydrolizy kwasu fitynowego oraz ilościowe oznaczenie fosforu metodą chromatografii cienkowarstwowej*. Zeszyty Naukowe Uniwersytetu Śl., Katowice, Sekcja chemii nr. 8/41, s. 49–53.

6. Kwapniewski Z., Sablik J., Przybyla H., Niziurska M.: *Zastosowanie chromatografii cienkowarstwowej oraz jonoferezy do badania czystości związków fitynowych*. Zeszyty Naukowe Politechniki Krakowskiej, Chemia Z–1, nr.2, s. 25–31, 1968.

7. Kwapniewski Z., Sablik J.: *Rozdział estrów fosforowych inozytolu metodą jonoferezy bibułowej w komorze wilgotnej*, Czasopismo Techniczne Politechniki Krakowskiej Z-4M /126/ s. 26–28, 1969.

8. Orczyk M., Sablik J.: *Wykorzystanie zasolonych wód dołowych w zakładach przeróbki mechanicznej węgla*. Gospodarka wodna 2, s. 51–53, 1969.

9. Sablik J., Czarkowski R.: *Magnetyczna obróbka wody dla celów przeróbki mechanicznej kopalin*. Rudy i metale nieżelazne 3, s. 165–169, 1969.

10. Czarkowski R., Orczyk M., Sablik J.: *Wpływ zasolenia wód na przebieg flotacji*. Prace GIG, Komunikat nr 473, Katowice, 1969.

11. Sablik J.: *Magnetyczne przygotowanie wody – nowy czynnik intensyfikujący niektóre procesy związane z przeróbką mechaniczną kopalin*. Przegląd Górniczy 10, s. 484–488, 1969.

12. Czarkowski H., Sablik J.: *Zastosowanie metody Boxa i Wilsona do badania przemysłowej komory flotacyjnej Z-1*. Przegląd Górniczy 6, s. 284–287, 1970.

13. Sablik J., Czerw B.: *Surface energy structure of coal and its floatability*. Central Mining Institute Annual Report. s. 86–87, 1970/71.

14. Sablik J.: *O możliwości uzdatniania wody działaniem pola magnetycznego*. Gospodarka Wodna 7, s. 266–272, 1970.

15. Kwapniewski Z., Sablik J.: *Planowanie i ocena doświadczeń chemicznych metodą Boxa i Wilsona*. Czasopismo techniczne Politechniki Krakowskiej, Z-4 i 6M, s. 57–61, 1970.

16. Sablik J., Czarkowski R.: *Kinetyka flotacji węgla w wodach przygotowanych w polu magnetycznym*. Przegląd Górniczy 12 s. 575–578, 1970.

17. Sablik J.: *Kinetyka flotacji węgla kop. Anna w zasolonych wodach dołowych*. Gospodarka wodna 1, s. 22–24, 1971.

18. Sablik J.: *Zastosowanie metod statystycznych do planowania i oceny wyników flotacji węgla*. Zeszyty Naukowe AGH Kraków 277, G–27, s. 47–72, 1971.

19. Czerw B., Sablik J.: *Wpływ struktury węgla na proces flotacji*. Prace GIG, Komunikat nr 547, Katowice 1972.

20. Szczypa J., Neczaj-Hruzewicz J., Sablik J.: *Some properties of slime coatings in coal-gangue system*. Trans. Inst. of Min. Met. nr 802, seetion C, s. 167–169, 1973.

21. Czarkowski R., Sablik J.: *Wpływ zagęszczenia nadawy na flotację węgla*. Wzbogacanie i Utylizacja Kopalin 5, s. 13–19, 1973.

22. Sablik J., Makula K.: *Wpływ odczynnika ze stymulatorem na przebieg procesu flotacji węgla w świetle badań laboratoryjnych i przemysłowych*. Wzbogacanie i Utylizacja Kopalin 6, s.20–24, 1973.

23. Szczypa J., Jurkiewicz K., Jańczuk B., Sablik J.: *Badania nad trwałością agregatów węgla i skały płonnej z pęcherzykiem powietrza w procesie flotacji*. Chemia stosowana 1, s. 109–116, 1974.

24. Brzezina R., Romańczyk E., Sablik J.: *Stosowanie pneumatycznych maszyn flotacyjnych do wzbogacania mułów węglowych*. Wzbogacanie i Utylizacja Kopalin 2, s. 3–8, 1974.

25. Sablik J.: *Nowa koncepcja technologii dwustopniowej flotacji mułów węglowych w zastosowaniu do wzbogacania węgla kop. Nowa Ruda – Pole Słupiec*. Wzbogacanie i Utylizacja Kopalin 5, s. 16–21, 1974.

26. Sablik J., Gabzdyl W.: *Petrograficzne kryterium prawidłowego flotowania mułów węglowych*. Archiwum Górnictwa 1 1975.

27. Brzezina R., Sablik J.: *Optymalizacja parametrów technologii flotacji na przykładzie kop. 1 Maja*. Prace GIG, Komunikat nr 664, Katowice 1976.

28. Sablik J., Olszówka J.: *Flotation applied for desulphurising the smallest coal grain classes*. Central Mining Institute "Annual Raport" s. 54–55, 1976.

29. Pape`e J., Sablik J.: *Przegląd kierunków projektowania flotacji węgla w aspekcie dużych wydajności*. Projekty Problemy, Budownictwa Węglowego 6, s. 8–15, 1976.

30. Sablik J., Bednarska J., Olszówka J.: *Technologiczna analiza warunków wzbogacania metodą flotacji mułów polskich węgli gazowych i energetycznych*. Przegląd Górniczy 1, 1977.

31. Makula K., Sablik J., Olszówka J.: *Odczynniki flotacyjne w projektowaniu węzła flotacji węgla*. Projekty Problemy, Budownictwa Węglowego 1, 1977.

32. Brzezina R., Sablik J.: *Heavy duty pneumatic-mechanical flotation machine type IZ–12 used for concentration of coal slurries*. Central Mining Institute "Annual Raport" s.69–71 1977.

33. Brzezina R., Sablik J.: *Conditions for use of type IZ pneumomechanical flotation machines for concentration of coal slurries*. Central Mining Institute "Annual Raport", s. 58–59, 1978.

34. Sablik J., Pawlik J.: *The influence of the finest coal and mineral grains on the properties of threee–phase froth in the flotation process*. Central Mining Institute "Annual Report", s. 59–61, 1978 /udział własny 50%/, /także w wersji językowej rosyjskiej/.

35. Brzezina R., Sablik J.: *Zastosowanie maszyny flotacyjnej IŻ-12 do wzbogacania mułów węglowych*. Projekty Problemy – Budownictwo Węglowe 3, s. 14–19, 1978.

36. Sablik J.: *Ewolucja technologii flotacji węgla jako efekt wdrożenia w przemyśle wyników prac naukowo-badawczych*. Projekty Problemy, Budownictwo Węglowe 12, 1978.

37. Sablik J., Makula K., Olszówka J.: *Odczynniki flotacyjne jako elementy technologii flotacji węgla*. Prace GIG, seria dodatkowa, Katowice 1979.

38. Pawlik J., Sablik J.: *Zależność własności pian flotacyjnych od niektórych parametrów zawiesiny mułowej we flotacji węgla*. Projekty Problemy, Budownictwo Węglowe 3, s. 18–22, 1979.

39. Sablik J.: *Foundations and methods in the Central Mining Institute*. Document ISC/TC–27/ SC 1/WG–4/N,10. 1979.

40. Sablik J., Olszówka J.: *Stan prac badawczych nad flotowaniem mułów węgli energetycznych*. Projekty Problemy, Budownictwo Węglow 10, 1980.

41. Sablik J., Pawlik J.: *Kondycjonowanie zawiesiny mułowej jako istotny czynnik intensyfikujący proces flotacji węgla*. Prace GIG, Komunikat nr 713, Katowice 1980.

42. Sablik J.: *Flotowalność polskich węgli kamiennych jako funkcje stopnia ich uwęglenia*. Prace GIG, seria dodatkowa Katowice 1980 (monografia).

43. Sablik J., Brzezina R.: *Wzorcowa technologia flotacji mułów węglowych oraz ocena możliwości jej stosowania w zakładach wzbogacających węgle koksowe*. Przegląd Górniczy 5, 1981.

44. Sablik J., Trybała M.: *Zależność koncentracji części stałych w koncentratach flotacyjnych węgla od wybranych parametrów technologicznych procesu flotacji*. Projekty Problemy, Budownictwo Węglowe 4–5, 1982.

45. Sablik J.: *Pojęcie i miara flotowalności mułów węglowych*. Prace GIG, Komunikat nr 725, Katowice 1982.

46. Sablik J.: *The grade of metamorphizm of Polish coals and their natural and activated floatability*. INT.J. of Min. Proc. 9 s. 245–257, 1982.

47. Sablik J.: *Flotacja węgla. Kolejne naukowo-przemysłowe seminarium*. Projekty Problemy, Budownictwo Węglowe s, 1982.

48. Sablik J., Pawlik J.: *The influence of the finest coal partieles on frothability of some theree–phase systems*. Powder Technology 36, nr 1 s. 21–24, 1983.

49. Sablik J.: *The effect of a promoter on the floatability of low rank coals*. Archiwum Górnictwa 29, 1, s. 11–23 1984.

50. Sablik J.: *Flotacja węgla. IV seminarium poświęcone problemom wzbogacania mułów węglowych*. Budownictwo Węglowe. Projekty Problemy 11, 1984.

51. Sablik J., Kozłowski Cz., Brzezina R.: *Technologia bezpośredniej flotacji węgla z wody obiegowej*. Budownictwo Węglowe, Projekty Problemy 10, 1984.

52. Sablik J., Makula K.: *Wyznaczanie granicznego kąta zwilżania węgla poprzez pomiar ciśnienia kapilarnego*. Aparatura Naukowo Dydaktyczna 6, 1984.

53. Sablik J.: *Free surface energy of coals of highest hydrophobicity*. Polish Journal of Chemistry 4, 1985.

54. Kozłowski Cz., Sablik J.: *Technologiczna efektywność wzbogacania mułów węglowych metodami klasyfikacji hydraulicznej i flotacji*. Budownictwo Węglowe, Projekty, Problemy 7, 1985.

55. Sablik J., Pawlik J.: *Certain Properties of three-phase Flotation Froth formed during the Coal Flotation Process*. Powder Technology 45, 1986.

56. Sablik J.: *Własności powierzchniowe węgli kamiennych i stymulatory ich aktywności flotacyjnej*. Prace GIG, seria dodatkowa. Katowice 1986 (monografia).

57. Sablik J., Wierzchowski K.: *Podstawy i technologiczna prognoza flotowania węgli kamiennych o najmniejszym stopniu zmetamorfizowania*. Przegląd Górniczy 5, s. 15, 1987.

58. Sablik J.: *Rezultaty technologiczne wzbogacania mułu węgla gazowopłomiennego metodami aglomeracji sferycznej lub flotacji*. Przegląd Górniczy 2, 1988.

59. Sablik J., Wierzchowski K.: *Zależność współczynnika flotowalności mieszanin mułów węglowych od współczynników flotowalności mułów wchodzących w skład tych mieszanin*. Budownictwo Węglowe, Projekty Problemy 3, 1988.

60. Sablik J.: *50 lat flotacji węgla w Polsce*. Przegląd Górniczy 1, s. 10, 1989.

61. Sablik J.: *FK collector for coal flotation*, Polish Technical Review 1, s. 27, 1989 /cztery wersje językowe/.

62. Sablik J., Wierzchowski K.: *Estry dwukarboksylowych kwasów organicznych jako odczynniki zbierające do flotacji węgla*. Przemysł Chemiczny 69, 2, 1990.

63. Sablik J.: *Rola odczynnika flotacyjnego w procesie zwiększania efektów technologicznych flotacji węgla koksowego na przykładzie wzbogacania mułów z kop. Morcinek*, Budownictwo Węglowe – Projekty Problemy 9, 1989.

64. Sablik J.: *Wpływ polarnego odczynnika pianotwórczego na aktywność flotacyjną węgla kamiennego*. Przegląd Górniczy 10, 1989.

65. Sablik J.: *Zależność aktywności flotacyjnej węgli koksowych od chemicznego składu odczynnika zbierającego*. Fizykochemiczne problemy mineralurgii 21, 1989.

66. Sablik J.: *Contact angle, isoelectric point and standard floatability as functions of oxygen content in coal*. Fizykochemiczne Problemy Mineralurgii 22, s. 110–126, 1990.

67. Sablik J.: *Relation between flotation response of coal and presence of double bonding / electrons/ in the chemical structures of collectors and promoters*. Proceedings of the VII th International Pittsburgh Coal Conference, Clean Coal Technology meeting Energy and Environmental Needs. Pittsburgh 1990.

68. Wierzchowski K., Sablik J.: *2-ethylohexanole used as a frothing agent for flotation of a coking coal*, Central Mining Institute , Annual Report 1990.

69. Sablik J.: *Wpływ obecności podwójnych wiązań w chemicznej strukturze kolektorów i stymulatorów na aktywność flotacyjną węgla*. Przegląd Górniczy 3, 1991.

70. Sablik J.: *Technologia czystego węgla – amerykański program przeciwdziałania skażeniu powietrza powstającego w wyniku utylizacji węgla w energetyce*. Przegląd Górniczy 5, 1991.

71. Sablik J., Brzezina R., Wierzchowski K.: *Wpływ stopnia zmetamorfizowania węgla na wielkości ziarn podlegających wyniesieniu do piany w procesie flotacji węgla*. Fizykochemiczne Problemy Mineralurgii 24, s. 67–74, 1991.

72. Wierzchowski K., Sablik J.: *Wartości krytyczne swobodnej energii powierzchni polskich węgli kamiennych określone metodą "film flotation"*. Fizykochemiczne Problemy Mineralurgii 24, s. 173–178, 1991.

73. Brzezina R., Sablik J.: *Zastosowanie flotacji kolumnowej do wzbogacania mułów węglowych*. Fizykochemiczne Problemy Mineralurgii 24, s. 57–68, 1991.

74. Brzezina R., Sablik J.: *Pneumatic Column Flotation Machine FLOKOB-4 – An Industrial Scale Model*. Proceedings of the International Conference an Column Flotation "Column 91" Sadbury 1991 /Canada/.

75. Sablik J., Brzezina R.: *Aktywność flotacyjna mułów węglowych w warunkach standardowych i technologicznie optymalnych*. Przegląd Górniczy 48, 4/22–28/ 1992.

76. Sablik J., Wierzchowski K.: *Evaluation of the influence of flotation reagents on the hydrophobicity of coal using the film flotation method*. Fuel 71, 4/474–475/ 1992.

77. Sablik J., Brzezina R., Wierzchowski K.: *Improving quality of power coals by flotation*, Colliery quardian 240, 3/90–94/ 1992.

78. Wierzchowski K., Sablik J.: *Wpływ metyloizobutylokarbinolu na energię powierzchniową zwilżania różnych węgli*. Fiz-chem. Problemy Mineralurgii 25, s.41–46, 1992.

79. Wierzchowski K., Sablik J.: *Energia powierzchniowa ziarn w mułach węgli o różnym stopniu zmetamorfizowania*. Prace naukowe GIG No 775 Katowice 1993.

80. Sablik J., Wierzchowski K.: *Effect of a polar wetting agent on the adhesion of air bubbles to various types of coal*, J. Adhesion Sei. Technol. 7, 5 435–439 1993.

81. Sablik J.: *The use of MDB reagent as a collector or promoter in the flotation of metallurgical Coals*. Fizykochemiczne Problemy Mineralurgii 27, 89–98, 1993.

82. Kurczabiński L., Sablik J.: *Działalność Głównego Instytutu Górnictwa w zakresie przeróbki mechanicznej węgla* /wersje językowe polska i angielska/. Wiadomości Górnicze, 5–6, /123–126/ 1994.

83. Sablik J.: *Selected Problems in the Research Programme Implemented at the Flotation Laboratory of the Central Mining Institute*, Gospodarka Surowcami Mineralnymi 1994, 10 2,/315–330/.

84. Sablik J., Nicol S.K.: *Recent Scientific and Technological Advances in Coal Flotation,* New Trends in Coal Preparation Technologies and Equipment, 12 Int. Coal Preparation Congress Cracow May 1994 /1129–1144/.

85. Wierzchowski K., Sablik J.: *Dependence of Natural and Reagent Activated Standard Coal Flotation Response on the Surface Energy*, New Trends in Coal Preparation Technologies and Equipment, 12 Int. Coal Preparation Congress Cracow May 1994 /953–959/.

86. Brzezina R., Sablik J.: *The "FLOKOB" Column Flotation Machine*, New Trends in Coal Preparation Technologies and Equipment, 12 Int. Coal Preparation Congress Cracow May 1994 /1219–1228/.

87. Olszówka J., Wierzchowski K., Sablik J.: *Wyniki badań przemysłowych nowych odczynników do flotacji węgla*. Przegląd Górniczy 7–8, s. 31–38, 1994.

88. Sablik J., Brzezina R., Cieślak W., Targański A., Klimek Z.: *Ocena efektywności technologicznej maszyny kolumnowej FLOKOB–40 wzbogacającej muły węglowe w Zakładzie Przeróbczym kop. "Szczygłowice"*. Przegląd Górniczy 7–8, s. 37–40, 1994.

89. Wierzchowski K., Sablik J.: *Wpływ stymulatora Rokacet 07 na energię powierzchniową węgli*. Zbiór referatów na XXVI Krakowską Konferencję Naukowo Techniczną Przeróbki Kopalin nt.: Techniki i technologie w procesach wzbogacania surowców mineralnych i odpadowych (s. 13–18) AGH Kraków, Centrum PPGSMiE PAN Kraków, Ustroń, wrzesień 1994.

90. Sablik J., Brzezina R.: *Wpływ sposobu aeracji zawiesiny w kolumnie „FLOKOB" na efektywność wzbogacania mułu węglowego*. Zbiór referatów na XXVI Krakowską Konferencję Naukowo Techniczną Przeróbki Kopalin nt.: „Technika i technologia w procesach wzbogacania surowców mineralnych i odpadowych" (s. 5–12) AGH Kraków Centrum PPGSMiE PAN Kraków, SITG 20 Kraków, Ustroń, wrzesień 1994.

91. Sablik J., Wierzchowski K.: *The Effect of Pre–Wetting With Flotation Reagents on the Surface Energy of Coals*. Coal Preparation 1994 Vol 15, s. 1–10.

92. Sablik J., Piwowarczyk J.: *Odolejanie gleb i wód z wykorzystaniem metody flotacji*. Zbiór referatów na Międzynarodowe Sympozjum: „Usuwanie zanieczyszczeń naftowych z gruntów i wód podziemnych. Metodyka oceny zagrożeń. MOSZNiL i PZiTS, Krajowa Rada Ekologiczna. Poznań, czerwiec 1994.

93. Kurczabiński L., Sablik J.: *State and Prognosis of Power Coal Smalls Upgrading Development in Poland*, Proceedings of "The Interational Conference on Environment, Energy, and Society" SIU at Carbondale, TUMM Ostrawa, NCKU Taiwan, Schaumburg III., Carbondale III. August–September 1994.

94. Sablik J., Wierzchowski K.: *The film flotation method applied to determine surface energy of coal wettred with flotation reagents*. Archives of Mining Sciences Vol. 40 1995 nr 1.

95. Piwowarczyk J., Sablik J.: *Technologia oczyszczania gleb i wód z zastosowaniem mułów węglowych jako sorbenta (Badania skuteczności procesu w skali półtechnicznej. Założenia do projektu instalacji komercyjnej)*. Międzynarodowe Sympozjum Szkoleniowe „Usuwanie zanieczyszczeń naftowych z gruntów i wód podziemnych – rezultaty". Arka Konsorcjum, MOSZNiL, WAT, Poznań, czerwiec 1995.

96. Wierzchowski K., Sablik J.: *Effect of Storage on Surface Energy of Bituminous Coals*, Proceedings of the 1 st UBC –McGill Bi–annual Int. Symp.: Processing of Hydrophobic Minerals and Fine Coals. CIM, ed J.S. Laskowski and G.W. Poling, Vancouver B.C. 1995.

97. Sablik J., Róg L.: *Refleksyjność i energia powierzchniowa węgli kamiennych*, Fizykochemiczne problemy mineralurgii 29 (1995), (39–46).

98. Sablik J., Brzezina R., Wierzchowski K.: *Możliwości zwiększenia zawartości części stałych w koncentratach w procesie flotacji węgli energetycznych*. Zbiór referatów na I Międzynarodową Konferencję

Przeróbki Kopalin: Technika i technologia w procesach wzbogacania surowców mineralnych i odpadowych. AGH, Pol. Śląska, CPPGSMiE PAN. Zakopane 1995.

99. Sablik J.: *Wpływ temperatury na stopień oczyszczania w procesach aglomeracji olejowej lub flotacji gruntów skażonych substancjami ropopochodnymi*. Fizykochemiczne Problemy Mineralurgii 30, 1996, 57 – 62.

100. Róg L., Sablik J.: *Charakterystyka petrograficzna i refleksyjność frakcji węglowych o różnej krytycznej energii powierzchniowej*. Fizykochemiczne Problemy Mineralurgii 30, 1996, 41–48.

101. Sablik J., Wierzchowski K.: *Surface energy of coal and pyrite wetted with reagents and their flotation response*. Engineering Foundation International Conference on: "Application of surface science to advancing flotation technology" Naantali, Finlandia, sierpień 1996.

102. Piwowarczyk J., Sablik J.: *Technologia dekontaminacji gleby bazująca na sorpcji ropopochodnych na mułach węglowych. Właściwości metody określone badaniami w skali półtechnicznej*. Międzynarodowa konferencja "Analiza i utylizacja zaolejonych odpadów" AUZO'96, Gdańsk, wrzesień 1996.

103. Sablik J., Wierzchowski K.: *Wpływ wybranych odczynników flotacyjnych na energię powierzchniową węgla i pirytu i ich flotowalność.*: II Międzynarodowa Konferencja Przeróbki Kopalin nt.: Nowoczesne technologie i urządzenia przeróbki kopalin i odpadów.Ustroń listopad 1996.

104. Sablik J.: *Metody wzbogacania kopalin i węgiel w procesach oczyszczania gruntów skażonych ropopochodnymi*. II Międzynarodowa Konferencja Przeróbki Kopalin nt.: Nowoczesne technologie i urządzenia przeróbki kopalin i odpadów.Ustroń listopad 1996.

105. Brzezina R.,Sablik J.: *Kolumna flotacyjna „FLOKOB" z podwójnym napowietrzeniem zawiesiny*. Przegląd Górniczy. 12, 1996.

106. Wierzchowski K. Sablik J.: *Zmiany energii powierzchniowej węgla pod wpływem odczynników stosowanych do flotacji*. Prace Naukowe GIG No 821 Katowice 1996.

107. Sablik J.: *Flotowalność mułów węglowych jako funkcja krytycznej energii powierzchniowej zwilżania węgla*, Fizykochemiczne Problemy Mineralurgii 31, 1997, 235–240.

108. Sablik J., Róg L., Wierzchowski K.: *Selected properties of different coal types in the light of their critical surface tension*, Proceedings of the 5th Southern Hemisphere Meeting of Mineral Technology, Buenos Aires, Intemin–Segemar, Argentyna 1997.

109. Brzezina R., Sablik J.: *Investigation of two stage aeration of coal slurries in column flotation*, Proceedings of the XX Int. Min. Proc. Congress V–3, Aachen Germany 1997.

110. Kurczabiński L., Sablik J.: *Activities and achivments of the Central Mining Institute in Katowice in the area of coal preparation*, Proceedings of the XX Int. Min. Proc. Congress, V–1, Aachen, Germany 1997.

111. Sablik J., Wawrzynkiewicz W.: *Siarka organiczna w węglach pokładów Górnośląskiego Zagłębia Węglowego*, Gospodarka Surowcami Mineralnymi,13, 1997 Zeszyt specjalny.

112. Sablik J.: *Międzynarodowa Konferencja Komitetu Technicznego ISO/TC 27 Naturalne Paliwa Stałe*, Normalizacja 2, 1997, 18 – 21.

113. Sablik J.: *Flotacja węgli kamiennych*. Monografia, wyd. GIG Katowice 1998.

114. Sablik J.: *14 Międzynarodowa Konferencja Komitetu Technicznego ISO/TC 27 "Paliwa Stałe"*, Normalizacja, 3, 1998.

115. Wierzchowski K., Sablik J.: *Uzysk siarki pirytowej w węglowych koncentratach flotacyjnych w zależności od wielkości ziarn pirytu*. Fizykochemiczne Problemy Mineralurgii, XXXV Sympozjum 1998. Wyd. Komitet Górnictwa PAN, Pol. Wrocławska.

116. Wawrzynkiewicz W., Sablik J.: *Organic Sulphur Content in Coal Beds of the Vistula River Coal Area in Poland*. Gospodarka Surowcami Mineralnymi, Wyd. IGSMiE PAN 1998.

117. Wawrzynkiewicz W., Sablik J.: *Wpływ siarki organicznej zawartej w węglu energetycznym na emisję SO2 do atmosfery*. IV Międzynarodowa Konferencja Przeróbki Kopalin 1998. Zeszyty Naukowe Pol. Śląskiej, Górnictwo nr 238 Wyd. Pol. Śląskiej.

118. Sablik J., Wawrzynkiewicz W.: *Dependence of coal quality on organic sulphur content in steam coals*. Proceedings of the Int. Conference "Clean Coal 2000" Prague 1999.

119. Sablik J., Cieślak W., Pyka I.: *Direction of clean coal technologies implementation in Poland*. Proceedings of the Int. Conference "Clean Coal 2000" Prague 1999.

120. Sablik J., Róg L., Wierzchowski K.: *Critical Surface Tension and Selected Properties of Different Types of Coal*. Gospodarka Surowcami Mineralnymi t.15. 1999, IGSMIE PAN.

121. Sablik J.: *Niejednorodność krytycznego napięcia powierzchniowego zwilżania w zbiorze bardzo drobnych ziarn węglowych*. Inżynieria Mineralna 2000 vol 1, 1.

122. Sablik J.: *Fizykochemiczne metody wzbogacania węgla – flotacja*. Prace Naukowe GIG, seria konferencje nr 34. Wybrane problemy przeróbki kopalin, Sekcja Wykorzystania Surowców Mineralnych Komitetu Górnictwa PAN Katowice 2000.

123. Sablik J.: *Flotacja i inne fizykochemiczne metody wzbogacania*. I Szkoła Inżynierii Mineralnej nt.:Przeróbka węgla kamiennego. Brenna 2000.

124. Pyka I., Brzezina R., Sablik J., Aleksa H., Dyduch F.: *Technologiczne i ekonomiczne uwarunkowania zmniejszania ilości drobnoziarnistych odpadów w procesach wzbogacania węgla energetycznego w Polsce*. Międzynarodowa Konferencja Naukowo Techniczna KOMEKO 2000 nt.: Produkcja surowców mineralnych z uwzględnieniem ochrony środowiska, KOMAG, Szczyrk 2000.

125. Wierzchowski K., Lenartowicz M., Sablik J.: *Napięcie powierzchniowe zwilżania ziarn węglowych wzbogaconych w procesie flotacji*. Fizykochemiczne Problemy Mineralurgii, Prace Naukowe Instytutu Górnictwa Politechniki Wrocławskiej, nr 88 2000.

126. Wawrzynkiewicz W., Sablik J.: *Prawidłowości charakteryzujące występowanie siarki organicznej w węglach GZW*. Zeszyty Naukowe Pol. Śląskiej. Górnictwo Z 245 2000.

127. Sablik J., Wierzchowski K.: *Charakterystyka właściwości powierzchniowych węgli metodą frakcjonowanej flotacji powierzchniowej*. Zeszyty Naukowe Pol. Śląskiej. Górnictwo zrównoważonego rozwoju. Górnictwo Z 246 2000.

128. Martyniak J., Sablik J., Kalemba J., Brzezina R., Wycisk H.: *Naturalne uwarunkowania statystycznych metod kontrolnych w procesie wzbogacania węgla*. Prace Naukowe GIG Nr844 Katowice 2001.

129. Cieślak W., Sablik J., Martyniak J., Wycisk H.: *Analysis of potential risk in a Polish coal preparation plant*. International workshop on "Clean coal use – a reliable option for sustainable energy" Proceedings V1 , Central Mining Institute Szczyrk Poland 2001.

130. Sablik J.: Wawrzynkiewicz W.: *Wpływ siarki organicznej na jakość węgli energetycznych*. Inżynieria Mineralna II 1(3), 2001.

131. Lenartowicz M., Sablik J.: *Napięcie powierzchniowe zwilżania ziarn węgli z frakcji wydzielonych w procesie flotacji metodą Della*. Gospodarka Surowcami Mineralnymi. T 17, Zeszyt specjalny 2001.

132. Sablik J., Wierzchowski K.: *Characteristic of hard coals surface properties using film flotation*. Inżynieria Mineralna II 2(4) 2001.

133. Sablik J.: *Przyroda go nie skąpi.. Technologia czystego węgla – geneza i rozwój*. Ekoprofit nr 1, (61), 2002.

134. Cieślak W., Sablik J., Martyniak J., Wycisk H.: *Analiza ryzyka eksploatacyjnego w zakładach wzbogacania węgla*. Inżynieria Mineralna nr1 (5) 2002 (wersja polska i angielska).

135. Sablik J., Lenartowicz M.: *Zależność oporu właściwego filtracji zawiesin węglowych od energetycznej charakterystyki powierzchni ziaren*. Prace Naukowe Instytutu Górnictwa Politechniki Wrocławskiej nr 35, 2002.

136. Wawrzynkiewicz W., Sablik J.: *Organic sulphur in the hard coal of the stratygraphic layers of the Upper Silesian coal basin*. Fuel, 81 (2002) 1889–1895.

137. Sablik J.: *Problematyka Komitetu Technicznego ISO/TC27 „Paliwa Stałe" w działalności normalizacyjnej w Polsce*, Inżynieria Mineralna 2 (6) 2002 (wersja polska i angielska).

138. Jaroń-Kocot M., Sablik J.: *Wpływ odpadowego wapna pokarbidowego na właściwości technologiczne hydromieszanin lokowanych w zrobach*. Przegląd Górniczy 3, 2003.

139. Sablik J., Wierzchowski K.: *Wpływ odczynników stosowanych w analizie gęstościowej na krytyczną energie powierzchniową zwilżania węgla*, Inżynieria Mineralna, Zeszyt specjalny S.3 (10), 2003.

140. Jaroń-Kocot M., Sablik J.: *Minimalizacja skażeń wód dołowych związkami chromu w procesie podziemnego lokowania popiołów lotnych*; WUG. Bezpieczeństwo pracy i ochrona środowiska w górnictwie, 10 (110) 2003.

141. Sablik J., Wierzchowski K.: *Krytyczne napięcie powierzchniowe zwilżania różnych typów węgla wzbudzone odczynnikami stosowanymi w analizie gęstościowej i flotacji*, Prace naukowe GIG, Górnictwo i Środowisko 3, Katowice 2003.

142. Jaroń-Kocot M., Sablik J.: *Wpływ odpadowego wapna lokowanego w zrobach na stan środowiska wodnego*. WUG. Bezpieczeństwo pracy i ochrona środowiska w górnictwie, 11 (111) 2003.

143. Jaroń-Kocot M., Sablik J.: *Wpływ gazów toksycznych emitowanych z hydromieszanin podsadzkowych z udziałem wapna pokarbidowego na środowisko pracy w kopalni*. Przegląd Górniczy 12, 2003.

144. Sablik J.: *Zależność między granicznym kątem zwilżania a średnim krytycznym napięciem powierzchniowym węgli o różnym stopniu zmetamorfizowania* (The relationship between contct angle and mean critical surface tension of coals of different rank), Inżynieria Mineralna, Vol IV, nr 2 (11) 2003.

145. Sablik J., Wierzchowski K.: *Wpływ odczynników technologicznych na wartości granicznych kątów zwilżania węgla w zbiorze ziaren mułowych*. Górnictwo i Geoinżynieria, Zeszyt 2/1 2004. Wyd. AGH.

146. Sablik J.: *Wartości zerowe flotowalności i granicznych kątów zwilżania w funkcji napięcia powierzchniowego zwilżania* (Zero values of flotation response and contact angle of coals in the function of their critical surface tension of wetting), Inżynieria mineralna. Vol V, nr1 (12) 2004.

147. Jaroń-Kocot M., Sablik J.: *Odpadowe wapno pokarbidowe jako składnik hydromieszanin lokowanych w pustkach poeksploatacyjnych na dole kopalń*. Prace naukowe GIG, Górnictwo i Środowisko 4, Katowice 2004.

148. Sablik J., Aleksa H., Dyduch F.: *Rozwój systemu paliwowo energetycznego w Polsce*, w: „Model ekologicznego i ekonomicznego prognozowania wydobycia i użytkowania węgla" tom I „Bazy i prognozy gospodarki surowcami energetycznymi oraz strategie i kierunki rozwoju sektora paliwowo–energetycznego". Praca zbiorowa pod redakcją J. Sablika, Główny Instytut Górnictwa, Katowice 2004.

149. Sablik J., Aleksa H., Dyduch F.: *Prognozy gospodarki paliwami pierwotnymi*, w: "Model ekologicznego i ekonomicznego prognozowania wydobycia i użytkowania węgla" tom I "Bazy i prognozy gospodarki surowcami energetycznymi oraz strategie i kierunki rozwoju sektora paliwowo–energetycznego". Praca zbiorowa pod redakcją J. Sablika, Główny Instytut Górnictwa, Katowice 2004.

150. Sablik J., Aleksa H., Pyka I.: *Strategie i kierunki rozwoju sektora paliwowo energetycznego w świecie i Unii Europejskiej – implikacje dla Polski*, w: "Model ekologicznego i ekonomicznego progno-

zowania wydobycia i użytkowania węgla" tom I "Bazy i prognozy gospodarki surowcami energe-tycznymi oraz strategie i kierunki rozwoju sektora paliwowo–energetycznego". Praca zbiorowa pod redakcją J. Sablika, Główny Instytut Górnictwa, Katowice 2004.

151. Jaroń-Kocot M., Sablik J: *Charakterystyka odpadowego wapna pokarbidowego w aspekcie jego gospodarczego wykorzystania*, Przemysł Chemiczny 84/4 (2005), 267 – 272.

152. Lenartowicz M. Sablik J.: *Rozkład napięcia powierzchniowego zwilżania ziaren węglowych w pro-duktach wzbogacania maszyny flotacyjnej typu IŻ*, Zeszyty Naukowe Politechniki Śląskiej, Górnic-two Z 266, 2005.

153. Sablik J.: *Fizykochemiczne właściwości powierzchniowe węgli najdrobniej uziarnionych*, Przegląd Górniczy, 9 2005.

154. Sablik J., Czaplicka K., Bojarska-Kraus M., Aleksa H.: *Ocena wpływu wzbogacania węgla na ob-ciążenie środowiska naturalnego metodą analizy cyklu życia* (Assessment of the effects of coal upgrading on the charge of natural environment using the LCA method) Inżynieria Mineralna nr 1 2005.

155. Czaplicka K., Sablik J.: *Zagrożenia ekologiczne w cyklu życia węgla energetycznego*, Przegląd Górniczy, 2, 2006, 16–23.

156. Lenartowicz M., Sablik J.: *Ocena pracy maszyn flotacyjnych IŻ 12 na podstawie pomiarów napięcia powierzchniowego zwilżania*, w: Innowacyjne systemy przeróbcze surowców mineralnych, Konfe-rencja KOMEKO, KOMAG, Zakopane marzec 2006.

157. Lenartowicz M., Sablik J: *The hydrophilic particles in washing products of trough pneumo – me-chanical flotation machine*, 10th Conference on Environment and Mineral Processing, Part I, TSB–TU Ostrava 2006, Czech Republic.

158. Lenartowicz M., Sablik J.: *Ziarna hydrofilowe w przemysłowym procesie flotacji węgli o różnym stopniu uwęglenia*, Górnictwo i Geoinżynieria,. 2006 Z.3/1 Rok 30, Wyd. AGH Kraków.

159. Lenartowicz M., Sablik J.: *Ocena pracy maszyn flotacyjnych IŻ-12 na podstawie pomiarów napię-cia powierzchniowego zwilżania*, Maszyny Górnicze 2, 2006.

160. Sablik J.: *Fizykochemiczne właściwości powierzchniowe węgli kamiennych*, Wyd. Główny Instytut Górnictwa, Katowice 2007 (monograph).

161. Sablik J.: *Energy characteristics of finest coal particles surfaces versus their upgrading using flota-tion*, Physicochemical Problems of Mineral Processing 41 (2007) 67–78.

162. Sablik J., Lenartowicz M.: *Energetyczne właściwości powierzchniowe ziaren w produktach przemy-słowej flotacji węgla*, Prace Naukowe – Monografie CMG KOMAG, 2007.

163. Lenartowicz M., Sablik J.: *Zastosowanie frakcjonowanej flotacji powierzchniowej do oceny techno-logii wzbogacania mułów węglowych metodą flotacji*. KOMEKO 2011, Innowacyjne i przyjazne dla środowiska techniki i technologie przeróbki surowców mineralnych. Bezpieczeństwo – Jakość – Efektywność, Instytut Techniki Górniczej KOMAG, Gliwice 2011, 175–183.

164. Lenartowicz M., Sablik J.: *Assessment of operation of neumo-mechanical flotation machines using film flotation method*. Arch. Min. Sci., Vol. 56 (2011), No 3, 477–488.

165. Sablik J., Lenartowicz M.: *Wykorzystanie frakcjonowanej flotacji powierzchniowej do oceny tech-nologii flotacji węgla*. Przegląd Górniczy 2011 nr 7–8, 94–98.

Jan Drzymala

(translation by Przemyslaw B. Kowalczuk)